

**THE GEOLOGY OF BEN NEVIS, SOUTH-WEST HIGHLANDS,  
SCOTLAND**

**Rodney Michael Burt**

**A Thesis Submitted for the Degree of PhD  
at the  
University of St Andrews**



**1994**

**Full metadata for this item is available in  
St Andrews Research Repository  
at:**

**<http://research-repository.st-andrews.ac.uk/>**

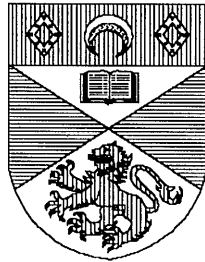
**Please use this identifier to cite or link to this item:**

**<http://hdl.handle.net/10023/9766>**

**This item is protected by original copyright**

# **The Geology of Ben Nevis, Southwest Highlands, Scotland**

**Rodney Michael Burt**



**Department of Geology  
University of St. Andrews**

**Thesis presented in partial fulfilment of the  
Degree of Doctor of Philosophy,  
May 1994**

TL  
B552

Read me a lesson, muse and speak it loud  
Upon the top of Nevis blind in mist !  
I look into the Chasms and a Shroud  
Vaprous doth hide them; just so much I wist  
Mankind do know of Hell: I look o'erhead  
And there is a sullen mist, even so much  
Mankind can tell of heaven: Mist is spread  
Before the Earth beneath me - even such  
Even so vague is Man's sight of himself  
Here are the craggy Stones beneath my feet;  
Thus much I know, that a poor witless elf  
I tread on them; that all my eye doth meet  
Is mist and crag - not only on this height  
But in the world of thought and mental might.

J. Keats (1818)

The base of Ben Nevis is covered with soil; grass, shrubs, and trees climb up its sides to a considerable height, but its lofty summit is composed of grey rocks that seem to leave vegetation below. The north side of the mountain may be said to be hung with terrors. Perpendicular and projecting rocks, gulphy glens and awful precipices, gloomy and tremendous caverns, the vast repositories of snow from age to age, these with blue mists guazing the grey rocks of the mountain and terrible cataracts thundering from Ben Nevis, made altogether a scene sublimely dreadful.

T. Wilkinson (1824)

## Declaration

I, Rodney Michael Burt, hereby certify that this thesis has been composed by myself, that it is a record of my own work, and that it has not been accepted in partial or complete fulfilment of any other degree or professional qualification.

Signed

Date 27 APRIL 94

I was admitted to the Faculty of Science of the University of St. Andrews under Ordinance General No. 12 on 1st October 1990 and as a candidate for the Degree of Ph.D. on the 1st October 1991.

Signed

Date 27 APRIL 94

I hereby certify that the candidate has fulfilled the conditions of the Resolution and Regulations appropriate to the Degree of Ph.D.

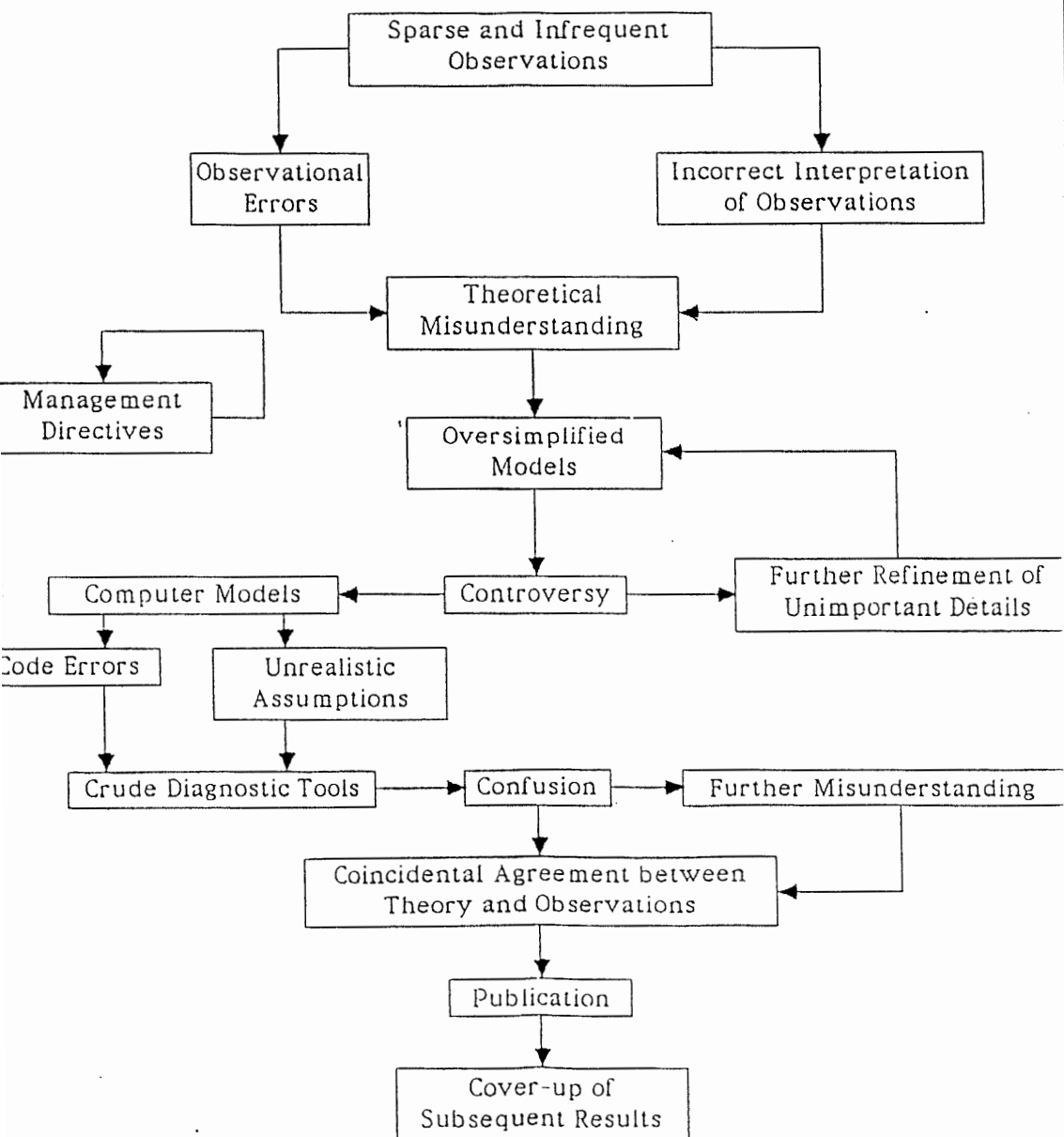
Signed

Date 27 April 94

## Copyright

In submitting this thesis to the University of St Andrews I understand that I am giving permission for it to be made available for use in accordance with the regulations of the University Library for the time being in force, subject to any copyright vested in the work not affected thereby. I also understand that the title and abstract will be published and a copy of the work will be made available to any *bona fide* library or research worker.

# The Course of Science



## Acknowledgements

I wish to thank the technicians at St Andrews namely; Jim Allen, Richard Batchelor, Angus Calder, Colin Cameron, Donald Herd, Andie Mackie, Graham Sandeman and Stuart Allison; thanks go also to the staff at that most idyllic of locations East Kilbride (S.U.R.R.C.), and in particular Vincent Gallagher and Anne Kelly.

This thesis has benefited from useful discussion with my supervisors Peter Brown and Ed Stephens at St Andrews and Graeme Rogers at East Kilbride. Many thanks to Matthew Thirlwall for making available his unpublished analyses from the volcanic pile of Ben Nevis and to Henry Haslam for the loan of his thesis, also to Peter Kokelaar, John Mendum and Bruce Paterson for their help with volcanology, the Grampian terrane and isotope geology respectively.

My thanks go also to the warden of the Youth Hostel in Glen Nevis, who knows what he thought when I started to move Ben Nevis bit by bit into his car park. I am very grateful to Bob Richardson and the S.M.C. for use of the CIC hut situated below the North Face. I wish to thank the nurse in Ft. William hospital for removing large chunks of Ben Nevis from my knee, not after an especially daring escapade on the North Face but, after tripping on the Tourist Path not 200m from the Youth Hostel. I am grateful to Noel Williams and the Lochaber Mountain Rescue Team for their advice, conversation and company in the Nevis Bank Hotel. My thanks to that most unwitting member of the human race, the tourist, for a never ending source of amusement during the course of my research.

To my friends including: Nigel and Catherine Botting, Suzie Clarke, Justin Dix, Ros Gash, Judith Jensen, Richard McCoyd, Richard Moseley, Jon Seedhouse, Richard Shepherd, Lindsay Stother, Iain Sutherland, Silke Wewetzer and Elen Williams, many thanks for your friendship and companionship on the hills and in more civilised locations (as well as East Kilbride). Thanks to my fellow Nightliners, good luck in the future.

For the carriage of a few rock samples, thanks go to Dave Scurrah and to Adam Bumby who also was 'privileged' to spend a week on Ben Nevis rock climbing at the department's expense; in the cause of science of course.

Last, but very definitely not least, I wish to acknowledge the support of my parents.

## Abstract

The Ben Nevis volcanic-plutonic Complex was intruded into garnet grade Precambrian metasediments in the Southwest Highlands of Scotland towards the end of the Caledonian Orogeny. A variety of techniques have been applied to the Ben Nevis Complex in order to model its volcanic and plutonic evolution; these include: field mapping, petrography, mineral chemistry, whole rock major and trace element geochemistry and a combined study of the isotopes of neodymium and strontium.

Rocks of the volcanic pile are subdivided into the following formations; the Allt a' Mhuillinn formation, the Coire na Ciste formation, the Ledge Route formation and the Summit formation, and these overlie a basement of Dalradian schist. Fine grained metasediments of the Allt a' Mhuillinn formation were deposited in a lacustrine basin into which entered a series of non-volcanic mass flow units. Non-volcanic deposition was terminated with the entry of the first volcanoclastic lahars of the Coire na Ciste formation into the Ben Nevis basin. Block and ash flows, lava flows and sills are also found in this formation. The Ledge Route formation testifies to a complex period of quiescence, airfall deposition and mass flow movement after which localised flows of lava dominate the overlying Summit formation. A single felsite dyke is found intruding the volcanic pile and is correlated with early members of the Ben Nevis dyke swarm in the northern area of the Ben Nevis Complex.

Plutonic rocks of the Ben Nevis Complex are subdivided into the Fine Quartz Diorite, Sgurr Finnisg-aig Quartz Diorite, Coarse Quartz Diorite, Porphyritic Outer Granite and Inner Granite; these were intruded to a high level in the crust. A dextral stress regime operated during the intrusion of the plutonic rocks. Each of the above units was intruded as a series of pulses.

Mass balance and qualitative trace element vector modelling (Rayleigh crystallisation) is able to model the geochemical evolution of the Porphyritic Outer Granite using plagioclase, amphibole, biotite and magnetite as the fractionating assemblage. Pyroxene is found as a phenocryst and as a groundmass phase in the quartz diorites with calcic amphibole found mainly as a replacement mineral after pyroxene; however, trace element modelling identifies amphibole as a fractionating phase.

Isotopic modelling of the Ben Nevis Complex indicates the involvement of at least three components; these being a mantle source, a lower crustal source with similar isotopic characteristics to the Islay-Colonsay-Basement and, of lesser importance, Dalradian metasediments. No single parental magma can explain the geochemical and isotopic variation of the Ben Nevis Complex.

# Contents

i	Declaration
ii	Acknowledgements
iii	Abstract
iv	Contents page
viii	List of Figures
xviii	List of Photos
xxiv	List of Tables

## **1 INTRODUCTION TO THE BEN NEVIS COMPLEX**

1	1.1 <u>Introduction</u>
1	1.1.1 General Statement
1	1.1.2 Names
1	1.2 <u>Physiography</u>
1	1.2.1 Location
3	1.2.2 Climate
4	1.2.3 Terrain
6	1.3 <u>Aims &amp; Objectives</u>
10	1.4 <u>Methodology</u>
10	1.5 <u>Thesis Format</u>

## **2 GEOLOGICAL SETTING**

11	2.1 <u>Introduction</u>
11	2.1.1 General statement
11	2.2 <u>Regional Geology</u>
11	2.2.1 Stratigraphy and sedimentology
13	2.2.2 Structure and Deformation
17	2.2.3 Metamorphism
17	2.3 <u>Caledonian Magmatic Activity</u>
17	2.3.1 Younger Basic magmatism
17	2.3.2 Older Granites
19	2.3.3 Alkaline intrusions of the NW Highlands
19	2.3.4 Newer Granites
20	2.3.5 Old Red Sandstone Lavas
21	2.4 <u>The Closure of Iapetus</u>
23	2.5 <u>Ben Nevis</u>
23	2.5.1 Intrusive members of the Ben Nevis Complex
23	2.5.2 Extrusive members of the Ben Nevis Complex

## **3 THE VOLCANIC PILE**

28	3.1 <u>Introduction</u>
28	3.1.1 General statement
29	3.1.2 Volcanological Terminology
29	3.1.3 Introducing Calderas
32	3.2 <u>Terrain</u>
35	3.3 <u>Previous Research</u>
35	3.4 <u>Relative age of the Volcanic Pile</u>
36	3.5 <u>Stratigraphy</u>
36	3.5.1 The Dalradian Basement
38	3.5.2 The Allt a' Mhuillinn Formation

40	3.5.3	The Coire na Ciste Formation
47	3.5.4	The Ledge route Formation
50	3.5.5	The Summit Formation
52	3.6	<u>Intrusions within the Volcanic Pile</u>
53	3.7	<u>The Fault Facies</u>
58	3.8	<u>Interpretation</u>
58	3.8.1	The Allt a' Mhuillin Formation
59	3.8.2	The Coire na Ciste Formation
63	3.8.3	The Ledge route Member
65	3.8.4	The Summit Formation
67	3.8.5	Subaqueous deposition
68	3.8.6	Fault facies
68	3.9	<u>Model</u>
73	<b>4</b>	<b><u>FIELD GEOLOGY OF THE INTRUSIVE MEMBERS OF THE BEN NEVIS COMPLEX</u></b>
73	4.1	<u>Introduction</u>
73	4.1.1	General statement
79	4.1.2	Terrain
80	4.1.3	Previous research
82	4.2	<u>The Outer Granite</u>
82	4.2.1	Introduction
84	4.2.2	Field Geology
91	4.2.3	Conclusions - subdividing the Outer Granite
92	4.3	<u>Intrusion Breccias</u>
94	4.4	<u>Inner exposures of Quartz Diorite</u>
94	4.4.1	Previous interpretation
94	4.4.2	Allt a' Mhuillin
95	4.4.3	Allt Daimh
95	4.5	<u>Xenoliths and Enclaves</u>
95	4.5.1	Xenoliths
96	4.5.2	Enclaves
96	4.6	<u>The Inner Granite</u>
98	4.7	<u>Minor Intrusions</u>
98	4.7.1	Dykes
99	4.7.2	Sheets
99	4.7.3	Appinites
100	4.8	<u>Structural geology</u>
100	4.8.1	Granite Structure
100	4.8.2	Absence of fabrics in the Outer & Inner Granites
101	4.8.3	Structural geology of the Ben Nevis complex
104	4.8.4	Depth of intrusion
107	4.8.5	Intrusion mechanism
110	4.9	<u>Mineralisation</u>
112	4.10	<u>Conclusion</u>
114	<b>5</b>	<b><u>PETROLOGY AND MINERALOGY</u></b>
114	5.1	<u>Introduction</u>
114	5.1.1	General statement
114	5.2	<u>Petrography of the Ben Nevis Complex</u>
120	5.2.1	Fine Quartz Diorite, Sgurr Finnisg-aig Quartz Diorite and Coarse Quartz Diorite

120	5.2.3	Porphyritic Outer Granite
122	5.2.4	Inner Granite
123	5.2.5	Volcanic Pile
124	5.2.6	Pyroxene to calcic amphibole transition
125	5.2.7	Clots
126	5.3	<u>Mineralogy of the Ben Nevis Complex</u>
126	5.3.1	Corrections for Ferric and Ferrous iron
127	5.3.2	Biotite
135	5.3.3	Amphiboles
141	5.3.4	Pyroxenes
142	5.3.5	Plagioclase
144	5.4	<u>Conclusions</u>
145	<b>6</b>	<b><u>THE GEOCHEMISTRY OF THE BEN NEVIS COMPLEX</u></b>
145	6.1.	<u>Introduction</u>
145	6.1.1	General statement
145	6.1.2	Methodology
146	6.1.3	Previous research
147	6.2	<u>Composition and Classification of the Ben Nevis Complex</u>
147	6.2.1	SiO <sub>2</sub> as an index of fractionation
147	6.2.2	Harker Diagrams
156	6.2.3	Classification of the Ben Nevis Plutonic rocks
164	6.2.4	Tectonic discrimination from granitoid chemistry
166	6.2.5	Classification of the Ben Nevis volcanic rocks
169	6.3	<u>Comparison with experimental studies on Granite systems</u>
170		
179	6.4	<u>Spidergrams</u>
179	6.5	<u>Fractional crystallisation and differentiation of the Ben Nevis Complex</u>
179	6.5.1	Introduction
181	6.5.2	Mass Balance
182	6.5.3	Qualitative vector modelling
188	6.5.4	Conclusion
191	6.6	<u>Relationship of the Ben Nevis Complex to subduction</u>
193	6.7	<u>Conclusion</u>
194	<b>7</b>	<b><u>ISOTOPE GEOLOGY</u></b>
194	7.1	<u>Introduction</u>
194	7.1.1	General statement
195	7.2	<u>Isotope Geochemistry</u>
195	7.2.1	Rubidium - Strontium
196	7.2.2	Samarium - Neodymium
197	7.2.3	Uranium - Lead
197	7.2.4	Oxygen
197	7.3	<u>Summary of the literature</u>
197	7.3.1	Newer Granites
205	7.3.2	The Lower Crust
208	7.3.3	Old Red Sandstone Volcanics
210	7.4	<u>Isotope Geology of the Ben Nevis Complex</u>
210	7.4.1	Introduction
211	7.4.2	Selection of samples

212	7.4.3	The age of the Ben Nevis Complex
213	7.4.4	Strontium isotope results
214	7.4.5	Neodymium Isotope Results
215	7.4.6	Discussion of the Sr isotope results
219	7.4.7	Discussion of Nd isotope ratios for the Ben Nevis Complex
221	7.4.8	Combined Sr and Nd Isotope Results
225	7.5	<u>Source compositions</u>
225	7.5.1	Mantle Source Compositions
235	7.5.2	The Lower Crust
237	7.6	<u>Discussion</u>
238	7.6.1	Composition of the Mantle Source
240	7.6.2	The Summit Trend
241	7.6.3	The trend of BN366 and BN400
245	7.7	<u>Summary and Model for the evolution of the Ben Nevis Complex</u>
247	<b>8</b>	<b><u>CONCLUSIONS</u></b>
247	8.1	<u>Introduction</u>
247	8.1.1	General Statement
247	8.2	<u>The evolution of the Volcanic Pile - a tale of many breccias</u>
251	8.3	<u>Granite Intrusion</u>
253	8.4	<u>Petrogenesis</u>
256	8.5	<u>The Silurian-Devonian magmatic event</u>
256	8.5.1	I and S-type granite formation
257	8.5.2	Lamprophyres and Appinites
258	8.5.3	Subduction
262	8.5.4	Conclusions
262	8.6	<u>Further Research</u>
264		REFERENCES
288	Appendix #1	Location of samples
290	Appendix #2	Mineral analyses + Analytical Methods
309	Appendix #3	Whole rock and modal analyses + Analytical Methods
322	Appendix #4	Analytical Methods

## List of Figures

### Chapter 1 General Introduction

Fig. 1.1 The geographical location of low-lying slabby exposures within the outcrop of the Ben Nevis volcanic pile referred to in the text.

Fig. 1.2 The main geographical features of the Ben Nevis Complex (Geology from Bailey & Maufe 1960).

Fig. 1.3 The location of the main topographical features on the North Face of Ben Nevis, and the line of the climbing routes attempted during this study.

Fig. 1.4a The North Face of Ben Nevis (see Photo 1.4a).

Fig. 1.4b The northern wall of Coire na Ciste and the location of Ledge Route (see Photo 1.4b).

### Chapter 2 Geological Setting

Fig. 2.1 Structural geology of the South-central Highlands, adapted from (Thomas 1974).

Fig. 2.2 Structural cross-section through the west Central Highlands, adapted from Thomas (1979).

Fig. 2.3 Distribution of ORS lavas and Newer Granite suites in Scotland.

Fig. 2.4 Cartoon reconstructions to illustrate the Silurian closure of Iapetus, and the presence of micro-plates and multiple subduction zones, adapted from Soper et al. (1992).

Fig. 2.5 Geological Survey map of the Ben Nevis Volcanic-plutonic Complex (Bailey & Maufe 1916).

Fig. 2.6 The Geology around the Ben Nevis Volcanic-plutonic Complex, adapted from Glover (1993).

Fig. 2.7 Geological Survey Model for the evolution of the Ben Nevis Volcanic-plutonic Complex.

### Chapter 3 The Volcanic Pile

Fig. 3.1 TAS diagram for the Ben Nevis volcanic pile. The majority of samples are not andesitic but trachydacite to dacite. The miscellaneous group includes intrusions within the volcanic pile and clasts from volcanic breccias. The diagram also illustrates that the sediments are compositionally similar to the volcanic rocks suggesting a large volcanic ash content.

Fig. 3.2 Cartoon of an idealised cross section through a caldera.

Fig. 3.3a The North Face of Ben Nevis (see also Photo 1.4a).

Fig. 3.3b The location of the main topographical features, climbing routes and exposures mentioned in the text.

Fig. 3.4 Geographical distribution of lithostratigraphic formations of the Ben Nevis volcanic pile.

Fig. 3.5 Cartoon logs of the two Allt a' Mhuillin formation exposures. Extreme lateral heterogeneity characterises this formation.

Fig. 3.6 Close up of the Allt a' Mhuillin formation outcrop.

Fig. 3.7 Active erosion and channelisation within the Coire na Ciste Formation during deposition of this formation. Channel erosion occurred between deposition of the sediments and VBb. The presence of baked mudstone clasts in the base of VBc suggests that this unit eroded and entrained part of the underlying sedimentary sequence and was emplaced hot.

Fig. 3.8 Contact relationships between the Coire na Ciste fm., the Trident member and the Ledge route member in the area between Coire na Ciste and No. 5 gully. North of No. 5 gully, the Trident member is not observed and the Ledge route member overlies an andesitic unit which may have formed the margin of the Trident member sedimentary basin.

Fig. 3.9 Field geology and interpretation of BN185/BN204. Repetition of volcanic pile/Inner Granite contact caused by renewed movements along Fault 2. This later activity, was a largely brittle process with negligible addition of new material.

Fig. 3.10 The generation of pyroclastic flows, adapted from Sato et al. (1992).

Fig. 3.11 Model for the evolution of a pyroclastic pumiceous flow on entering the marine environment, adapted from Cas & Wright (1988).

Fig. 3.12 Simplified cartoons depicting the evolution of the Volcanic pile.

## Chapter 4 Field Geology of the Intrusive Members of the Ben Nevis Complex

Fig. 4.1. Geological Survey map of the Ben Nevis Volcanic-plutonic Complex (Bailey & Maufe 1916).

Fig. 4.2a. Geology of the Outer Granite in part of the northern area according to Anderson (1935). Contrast the geology of the Allt Daimh section with that of Haslam (1965) displayed in Fig. 4.3.

Fig. 4.2b. Geology of the Outer Granite in the eastern area according to Anderson (1935).

Fig. 4.3 Map of Haslam (1965).

Fig. 4.4 New interpretation for the subdivision of the Outer Granite, minor intrusions removed for the sake of clarity.

Fig. 4.5 Localities and exposures mentioned in the text.

Fig. 4.6 Cartoon illustration of the Geological Survey Ring dyke model.

Fig. 4.7 Graph illustrating the difference in geochemistry between the Sgurr Finnisg-aig Quartz Diorite and the other members of the Outer Granite.

Fig. 4.8a Subdivisions according to Haslam (1965).

Fig. 4.8b Geochemistry of the subdivisions presented in this thesis.

Note the marked difference in chemistry of BN412, the intrusive sheet, from the main field of quartz diorite data. The recognition of BN418 and BN420 as chilled variants of the Porphyritic Outer Granite is illustrated by the greater similarity of these samples to Porphyritic Outer Granite than to Coarse Quartz Diorite. Anomalous behaviour of BN366 due to extensive assimilation of Dalradian metasediments.

Fig. 4.9 Similarity between Basic Inner Granite and Fault Facies samples is illustrated in this diagram.

Fig. 4.10 Cartoon illustrations of stress vector data obtained from the Ben Nevis dyke swarm. All illustrated examples are sinistral, adapted from Morris & Hutton (1993).

Fig. 4.11 Structural data from the Ben Nevis Complex. In general the data indicates relative compression acting in WNW-ESE and relative extension acting NNE-SSW. Note the change in stress data at the northern margin interpreted as a forceful magmatic push.

Fig. 4.12 Decline in temperature of the contact metamorphic aureole of the Ben Nevis Complex. Data from Webb (1977).

## Chapter 5 Petrology and Mineralogy

Fig. 5.x Mineral stability in the Ben Nevis Complex. Where an arrowhead is depicted this represents the minimum or maximum whole rock chemical range and no data is available for the minimum/maximum whole rock SiO<sub>2</sub> content at which crystallisation of the mineral started/ceased.

Fig. 5.1 Localities and samples mentioned in the text along with the location of probe samples and photomicrographs.

Fig. 5.2 Comparison of measured and recalculated pyroxene and amphibole data from Haslam (1968).

Fig. 5.3 Perfect relationship between Al<sup>(iv)</sup> and Si in the biotites. These two cations are the only ones present in the tetrahedral sheet.

Fig. 5.4 Comparison of Al<sup>(iv)</sup> against Ti for biotite highlighting the low Ti contents of biotite from BN68b.

Fig. 5.5 Composition of the biotites in the Fe-Mg-(Al)<sup>iv</sup> plane.

Fig. 5.6a High total Al and Al<sup>(iv)</sup> of BN68b biotites relative to the main bulk of Ben Nevis biotite data.

Fig. 5.6b Comparison of Fe<sup>2\*</sup> for the biotites, showing relatively high Fe contents in BN68b relative to the rest of the Ben Nevis data.

Fig. 5.7a Increasing Ti with decreasing Fe+Mg for the biotites.

Fig. 5.7b Decreasing Fe+Mg with increasing vacancy in the octahedral site for biotite from Ben Nevis.

Fig. 5.7c Decreasing Fe+Mg with increasing Al<sup>(iv)</sup> for the biotites with the exception of BN68b where a weak positive correlation is observed.

Fig. 5.8 Near perfect correlation between Fe<sup>2\*</sup> and Mg for biotite. Note the relatively low Mg content of BN68b.

Fig. 5.9a Decreasing whole-rock MnO with increasing fractionation (whole-rock SiO<sub>2</sub>) for the Ben Nevis Complex.

Fig. 5.9b Indiscriminate scatter between Mn and Al<sup>(iv)</sup> in biotite. Biotite did not cause the fractionation of MnO observed in Fig. 5.9a

Fig. 5.10a Discrimination diagram for amphiboles derived from the plutonic rocks. Based on Fig. 3.a of Leake (1978).  $(Na+K)A < 0.50$ ,  $Ti \leq 0.50$ .

- Fig. 5.10b Discrimination diagram for amphiboles derived from the volcanic pile. Based on Fig. 3.c of Leake (1978).  $(\text{Na}+\text{K})\text{A} \geq 0.50$ ,  $\text{Ti} \leq 0.50$   $\text{Fe}^{3+}$ .
- Fig. 5.11  $(\text{Al})_{\text{iv}}$  against  $\text{Mg}/(\text{Mg}+\text{Fe})$ . Note the two trends apparent in the plutonic amphibole data, within-pulse and within-pluton.
- Fig. 5.12 In the volcanic amphiboles, substitution of  $(\text{Al})_{\text{iv}}$  is balanced by the entry of  $(\text{R}3+)_{\text{vi}}$  into the M1-M3 sites and increasing A-site occupancy. Minor entry of Na into M4 balances deviation from the perfect 1:1 trend.
- Fig. 5.13  $\Sigma[(\text{Al})_{\text{iv}}+(\text{Fe}^{3+})_{\text{iv}}]$  against  $\Sigma[\text{A-site occupancy}+\text{Fe}^{3+} + \text{Ti}]$  for the plutonic amphiboles.
- Fig. 5.14  $(\text{Al})_{\text{iv}}$  substitution into the tetrahedral site of plutonic amphiboles is not related to the level of A-site occupancy which remains  $\approx$  constant.
- Fig. 5.15 Composition of pyroxene from the Ben Nevis complex in the pyroxene quadrilateral.
- Fig. 5.16 Variation in plagioclase composition throughout the Ben Nevis Complex.
- Fig. 5.17 General decrease in amphibole Mn with increasing fractionation.

## Chapter 6 The Geochemistry of the Ben Nevis Complex

- Fig. 6.1a Location of intrusive rocks analysed for their major and trace element compositions. Those samples prefixed with 82 or 83 or 84 were collected by Dr W. E. Stephens.
- Fig. 6.1b The location of volcanic samples analysed for major and trace elements. Samples prefixed by 83 are from the collection of Dr W. E. Stephens.
- Fig. 6.2 Harker diagrams for  $\text{TiO}_2$ ,  $\text{Al}_2\text{O}_3$ ,  $\text{FeO}^*$ , MnO, MgO, CaO,  $\text{K}_2\text{O}$  and  $\text{Na}_2\text{O}$ . Fields depicted in  $\text{K}_2\text{O}$  are from Le Maitre et al. (1989) and Rickwood (1989).
- Fig. 6.2(continued) Harker diagrams for  $\text{P}_2\text{O}_5$ , Nb, Zr, Y, Sr, Rb, Pb and Th.
- Fig. 6.2(continued) Harker diagrams for Ga, Zn, Ni, Ce, Sc, V, Ba and La.
- Fig. 6.3 Harker diagrams for  $\text{TiO}_2$ ,  $\text{Al}_2\text{O}_3$ ,  $\text{FeO}^*$ , MnO, MgO, CaO,  $\text{K}_2\text{O}$  and  $\text{Na}_2\text{O}$ . Fields depicted in  $\text{K}_2\text{O}$  are from Le Maitre et al. (1989) and Rickwood (1989).
- Fig. 6.3(continued) Harker diagrams for  $\text{P}_2\text{O}_5$ , Nb, Zr, Y, Sr, Rb, Pb and Th.
- Fig. 6.3(continued) Harker diagrams for Ga, Zn, Ni, Ce, Sc, V, Ba and La.
- Fig. 6.4 The AFM diagram for the Ben Nevis Complex which defines a typical Calc-alkaline trend with no iron enrichment.
- Fig. 6.5a R1-R2 multication diagram for the plutonic rocks.
- Fig. 6.5b R1-R2 multication diagram for the volcanic rocks.
- Fig. 6.6 Corundum and Diopside normative compositions for the plutonic rocks of the Ben Nevis Complex.
- Fig. 6.7 A/CNK for the Ben Nevis Complex. An A/NCK value of 1.1 is approximates to a Corundum normative values of 1%. The mainly I-Type composition of the Ben Nevis Complex is again illustrated.
- Fig. 6.8  $\text{K}_2\text{O}$  v  $\text{Na}_2\text{O}$  for the plutonic rocks. Fields for I-Type and S-Type compositions from Norman et al. (1992).

Fig. 6.9 Shand's Index. The peralkaline field fall below  $A/NK = 1$ . The Ben Nevis Complex is mildly S-type and the Inner Granite is peraluminous.

Fig. 6.10 High Ga abundance is illustrated for those samples of the Porphyritic Outer Granite and Inner Granite with anomalously high  $Na_2O$ .

Fig. 6.11 Normative compositions for the intrusive members of the Ben Nevis Complex are plotted on the QAPF classification scheme of Le Bas & Streckeisen (1991). The modal analyses of Haslam (1968) are plotted for comparison.

Fig. 6.12 Classification of the Ben Nevis plutonic rocks on Barker's (1979) modification of O'Conner (1965). CIPW norms are also plotted for the samples of Haslam (1968).

Fig. 6.13a & 6.13b Tectonic discrimination of the Ben Nevis plutonic rocks according to the discrimination diagrams of Pearce et al. (1984).

Fig. 6.14a and 6.14b. Tectonic discrimination of the Ben Nevis plutonic rocks according to the discrimination diagrams of Maniar & Piccoli (1989). In 6.14a, the plutonic rocks have  $FeO^* < 10\%$  and therefore fall within the orogenic field with no overlap into other tectonic fields. In 6.14b, the plutonic rocks overlap slightly with the post-orogenic field.

Fig. 6.15 Total alkali vs  $SiO_2$  classification diagram for the volcanic rocks of the Ben Nevis Complex. Field boundaries are from Le Maitre et al. (1989).

Fig. 6.16 Two of the classification diagrams of Winchester & Floyd (1977) and applied to the volcanic rocks of the Ben Nevis Complex.

Fig. 6.17 Diopside and corundum normative compositions of the volcanic pile. Compare with the same diagram for the plutonic rocks (Fig. 6.8).

Fig. 6.18 The Ben Nevis plutonic rocks trend toward the 1Kbar minimum composition. Experimental data from Schairer & Bowen (1935), Tuttle & Bowen (1958), Steiner et al. (1975), Luth et al. (1964) and Huang & Wyllie (1975).

Fig. 6.19a Spidergrams for the quartz diorites of the Ben Nevis Complex normalised against MORB composition of Pearce (1983).

Fig. 6.19a Spidergrams for the Porphyritic Outer Granite of the Ben Nevis Complex normalised against MORB composition of Pearce (1983).

Fig. 6.19a Spidergrams for the Inner Granite of the Ben Nevis Complex normalised against MORB composition of Pearce (1983).

Fig. 6.19a Spidergrams for the minor intrusions of the Ben Nevis Complex normalised against MORB composition of Pearce (1983).

Fig. 6.19a Spidergrams for the appinites and lamprophyres of the Ben Nevis Complex normalised against MORB composition of Pearce (1983).

Fig. 6.19a Spidergrams for the andesites of the Ben Nevis Complex normalised against MORB composition of Pearce (1983).

Fig. 6.19a Spidergrams for the miscellaneous members of the Ben Nevis Complex normalised against MORB composition of Pearce (1983).

Fig. 6.19b Averaged spidergrams for the Ben Nevis Complex normalised against MORB composition of Pearce (1983).

Fig. 6.20a and 6.20b indicate that feldspar fractionation was continuous during the evolution of the Ben Nevis Complex. 6.20a illustrates the high Albite content of the plagioclase in the Inner Granite.

Fig. 6.21 Variation in Sr and Rb within the plutonic rocks of the Ben Nevis Complex. Mineral vectors superimposed. Bi = Biotite, Am = Amphibole, Ksp = K-feldspar, Pl = plagioclase and Cpx = clinopyroxene.

Fig. 6.22 The relationship between K<sub>2</sub>O and Rb in the plutonic rocks, and illustrating the magmatic and pegmatite-hydrothermal trends of Shaw (1968).

Fig. 6.23 Variation in Ba and Rb within the plutonic rocks of the Ben Nevis Complex. Mineral vectors superimposed. See Fig. 6.21 for key to mineral symbols

Fig. 6.24 Variation in CaO and Y within the plutonic rocks of the Ben Nevis Complex. Mineral vectors superimposed. See Fig. 6.21 for key to mineral symbols

Fig. 6.25 Variation in Ce and Y within the plutonic rocks of the Ben Nevis Complex. Mineral vectors superimposed. See Fig. 6.21 for key to mineral symbols

Fig. 6.26 Variation in V and Ni within the plutonic rocks of the Ben Nevis Complex. Note the compositional overlap between the Porphyritic Outer Granite and the Fine Quartz Diorite and Coarse Quartz Diorite. Mineral vectors superimposed. See Fig. 6.21 for key to mineral symbols

Fig. 6.27 Variation in TiO<sub>2</sub> and Zr within the plutonic rocks of the Ben Nevis Complex. Mineral vectors superimposed. See Fig. 6.21 for key to mineral symbols.

Fig. 6.28 Variation in Y and Zr within the plutonic rocks of the Ben Nevis Complex. Mineral vectors superimposed. See Fig. 6.21 for key to mineral symbols.

Fig. 6.29 Variation in V and TiO<sub>2</sub> within the plutonic rocks of the Ben Nevis Complex. Mineral vectors superimposed. See Fig. 6.21 for key to mineral symbols.

Fig. 6.30a Variation in V and Ni within the plutonic and volcanic rocks of the Ben Nevis Complex. Mineral vectors superimposed. For key to mineral symbols see Fig. 6.21.

Fig. 6.30b Variation in Ce and Y within the plutonic and volcanic rocks of the Ben Nevis Complex. Mineral vectors superimposed. See Fig. 6.21 for key to mineral symbols.

Fig. 6.31 Variation in Rb/Zr and Nb in the Cairngorm, South of Scotland and Argyll Suites. Published data from Halliday & Stephens (1984).

Fig. 6.32 Variations in Rb/Zr and Nb for the ORS lavas of Scotland. Data from Thirlwall (1983).

## Chapter 7 Isotope Geology

Fig. 7.1 Contamination of high Sr content Lorne Plateau Lava (L-56 Thirlwall 1982) by low Sr content Dalradian Schist (A561 Dempster 1985). Initial ratios remain low <0.71 until >80% assimilation of Dalradian Schist. Mixing Equation from Faure (1986) = Equation 9.21.

Fig. 7.2 Evolution of <sup>143</sup>Nd/<sup>144</sup>Nd (expressed in εNd units) with time for several model reservoirs. Model ages calculated relative to depleted mantle (T<sub>DM</sub>) for the Lorne Plateau Lavas are identical to ≈1.3Ga continental crust. If the Lorne Plateau Lavas are derived from

LREE-enriched mantle then  $T_{DM}$  ages for these magmas are meaningless. CHUR values from Jacobsen & Wasserburg (1980) and DM from Liew & Hofmann (1988).

Fig. 7.3 Locations of the main granitoid intrusions, Old Red Sandstone Lavas, Mid-Grampian Line and key xenolith localities in Scotland.

Fig. 7.4 Pb isotope data for K-Feldspars from Newer Granites. (Data from Blaxland et al. 1978 and van Breemen et al. 1979) and for Lewisian Samples (Data from Chapman & Moorbath 1977) plotted relative to two-stage Earth Evolution Curve (Stacey & Kramers 1975). Alkali feldspar from the Newer Granite is more radiogenic than alkali feldspar from the Lewisian, but tends to become more Lewisian-like closer to the area of Lewisian outcrop, e.g. Mull.

Fig. 7.5  $\delta^{18}O$  vs  $(^{87}Sr/^{86}Sr)_{425}$  for the Newer Granites with fields for upper crustal rocks at 425Ma. SULPS = Southern Uplands Lower Palaeozoic Sediment. Adapted from Harmon (1984).

Fig. 7.6  $\epsilon Nd_t$  vs  $\delta^{18}O$  for the Newer Granites. Similar  $\delta^{18}O$  but different  $\epsilon Nd_t$  reveals the presence of two separate contaminants, one of which contains ancient zircons, the other does not. Adapted from Halliday (1984).

Fig. 7.7  $\epsilon Sr_t$  vs  $\epsilon Nd_t$  for Newer Granites at time of emplacement and crustal fields calculated at 425Ma. No simple two component mix can explain the distribution of the Newer Granite data set. Data from Frost & O'Nions (1985), Thirlwall (1982, 1983, 1986 & 1988), Tindle (1982), Thirlwall & Bluck (1984), Taylor et al. (1984), Waters et al. (1990), Whitehouse (1990, 1989, 1988), Marcantonio et al. (1988), Morton & Taylor (1991), Thirlwall & Burnard (1990), Fowler (1992) Dempster & Bluck (1991), Halliday (1984), Holden et al. (1987) & Clayburn (1988).

Fig. 7.8  $\epsilon Nd_t$  vs  $\epsilon Sr_t$  for enclaves and granites from Strontian and Criffell.  $\epsilon Nd_t$  for enclaves displaced to higher (more primitive) values. Data from Holden et al. (1987).

Fig. 7.9 LIPSB profile across Northern Britain (Bamford 1979).

Fig. 7.10  $\epsilon Nd_t$  vs  $\epsilon Sr_t$  for Old Red Sandstone (ORS) lavas and the Mantle array. Numbers 1-3 refer to Thirlwall's (1982) three source compositions, 1=Southwest Highland mantle, 2=Depleted mantle and 3=Subducted slab. Data from Frost & O'Nions (1985) and Thirlwall (1982, 1983 & 1986).

Fig. 7.11a The location of intrusive samples analysed for Nd and Sr isotopes.

Fig. 7.11b The location of volcanic samples analysed for Nd and Sr isotopes.

Fig. 7.12a  $(^{87}Sr/^{86}Sr)$  measured vs Rb/Sr for Ben Nevis Complex. Note position of BN170 (appinite) relative to rest of data. Field of Thirlwall unpublished data. Published results from Hamilton et al. (1980) and Harmon & Halliday (1980).

Fig. 7.12b  $\epsilon Sr_t$  vs Rb/Sr for Ben Nevis Complex. Field of Thirlwall unpublished data. Published results from Hamilton et al. (1980) and Harmon & Halliday (1980).

Fig. 7.13  $SiO_2$  vs  $\epsilon Sr_t$ . Initially variable but generally decreasing  $\epsilon Sr_t$  with fractionation followed by increasing  $\epsilon Sr_t$  with fractionation.

Fig. 7.14a Rb vs  $SiO_2$  for the Ben Nevis intrusive lithologies along with the field for Dalradian Schists. Data for Dalradian from Lambert et al. (1982) and Hickman & Wright (1983). Miscellaneous group incorporates the minor intrusions of the Ben Nevis Complex.

Fig. 7.14b Sr vs SiO<sub>2</sub> for the Ben Nevis intrusive lithologies along with the field for Dalradian Schists. Data for Dalradian from Lambert et al. (1982) and Hickman & Wright (1983). Miscellaneous group incorporates the minor intrusions of the Ben Nevis Complex.

Fig. 7.15 εSr<sub>425</sub> vs Rb/Sr for Ben Nevis magmas and Dalradian Schists. Dalradian samples have significantly higher εSr<sub>t</sub> than Ben Nevis. Minor contamination may therefore have a noticeable effect on the Sr isotope ratios of the BNC. Dalradian data from Dempster (1985), Lambert et al. (1982), O'Nions et al. (1983) & Frost & O'Nions (1985).

Fig. 7.16a A plot of Nd vs SiO<sub>2</sub> for the Ben Nevis Complex and showing no correlation.

Fig. 7.16b A plot of Sm vs SiO<sub>2</sub> for the Ben Nevis Complex and showing no correlation.

Fig. 7.16c A plot of Sm/Nd vs SiO<sub>2</sub> for the Ben Nevis Complex and showing moderate correlation between the two parameters. Note the highly variable Sm/Nd ratio exhibited by the summit andesites at ≈ constant SiO<sub>2</sub>.

Fig. 7.16d A plot of εNd<sub>t</sub> vs SiO<sub>2</sub> for the Ben Nevis Complex and showing no correlation.

Fig. 7.17 εNd<sub>t</sub> vs εSr<sub>t</sub> shows no simple overall correlation between the two isotopic systems. Secondary contamination, although represented by a single arrow is likely to occur at any point along the Summit trend depending on the isotopic composition of the sample on entering the upper crust. Note the position of BN170.

Fig. 7.18 εNd<sub>t</sub> vs Sr/Nd. The summit trend is defined by decreasing εNd<sub>t</sub> and increasing Sr/Nd ratios. A combination of plagioclase fractionation and crustal contamination disperses the other samples off the summit trend.

Fig. 7.19 Sr/Nd vs SiO<sub>2</sub>. Vertical trend of the Summit samples is not the result of fractional crystallisation.

Fig. 7.20 εNd<sub>t</sub> vs εSr<sub>t</sub> for the Permo-Carboniferous lavas of Scotland (Smedley 1986, 1988a & b), and εNd<sub>300</sub> vs εSr<sub>300</sub> data for Scottish mantle xenoliths (Menzies & Halliday 1988, Menzies et al. 1987 and Halliday et al. 1993). The data indicate the presence of extreme LREE-enriched mantle in the NW of Scotland, whereas further south in the Midland Valley, the data for mantle xenoliths are comparable to depleted mantle or Ocean Island Basalt source mantle and overlap strongly with the Scottish Permo-Carboniferous lavas. K+A = Permo-Carboniferous from Kintyre and Arran. MVS = Midland Valley. Data points labelled Loch Roag also include those from Duncansby Ness.

Fig. 7.21 MORB normalised spidergrams for mantle xenoliths from the Midland Valley and Loch Roag + Duncansby Ness. The samples from the Midland Valley also show Nb depletion and are comparable to Duncansby Ness. The data are from Halliday et al. (1993) and are presented by these authors as 'representative xenolith compositions' from these localities.

Fig. 7.22 Vertical stratification of the upper mantle across Northern Britain at 410Ma. Diagram from Thirlwall (1982).

Fig. 7.23 Log Sm/Ce vs log Sr/Ce for samples from the ORS lavas of the Midland Valley (MVS) and the Lorne Plateau. Increasing Sr/Ce is believed by Hawkesworth & Powell (1980) to be the trace element analogue of increasing εSr. This is not the case in for the Lorne samples where high Sr/Ce correlates with low εSr and the high Sr/Ce of the LPL is a feature of the source region. Also included are the high Ni (>60ppm) samples from the Ben Nevis Complex. Fractional crystallisation drives the data to lower Sr/Ce at approximately

constant Sm/Ce. The BNC data lie within the field for the Lorne Plateau suggesting that any involvement of DM (Frost & O'Nions 1985) was minimal. Data from Thirlwall (1986, 1983 & 1982).

Fig. 7.24  $\epsilon\text{Sr}_t$  vs  $^{206}\text{Pb}/^{204}\text{Pb}$ . Data from Thirlwall (1986) and Frost & O'Nions (1985). Lorne trend to increasing  $\epsilon\text{Sr}$  is not caused by the same contaminant which is affecting the Etive Pluton.

Fig. 7.25  $\epsilon\text{Nd}_t$  vs  $\epsilon\text{Sr}_t$  data for Loch Borrallan and Glen Dessary (Thirlwall & Burnard 1990 and Fowler (1992) and xenolith data (see Fig. 7.20 for references). Enriched Hebridean type mantle cannot be the source for the alkaline intrusions.

Fig. 7.26 The Summit trend of the Ben Nevis Complex could be explained by contaminating SWH mantle melts with Islay-Colonsay Basement crustal material. The overlap in isotopic composition between the Ben Nevis Complex and the Etive Complex is demonstrated in this diagram. Data from Marcantonio et al. (1988), Frost & O'Nions (1985) and the references for the Lorne samples can be found in Fig. 7.25.

Fig. 7.27 Model for the evolution of the Ben Nevis Complex plumbing system with time. Increasing maturity of the system reduces the potential for wall-rock contamination during passage of the magmas through the crust. Later increases in  $\epsilon\text{Sr}_t$  with  $\text{SiO}_2$  reflect moderate AFC processes in the upper crustal magma chamber (Fig. 7.29).

Fig. 7.28 Model age ( $T_{\text{DM}}$ ) data for Caledonide magmas. The LPL, although believed to be largely primitive mantle melts have  $T_{\text{DM}} > 1300\text{Ma}$ . Magmas derived wholly or partially from SWH mantle parent melts will also have high  $T_{\text{DM}}$ . It may be significant that the BNC and Argyll suite (Stephens & Halliday 1984) granite data plot between the LPL and ICB data sets. South of Scotland suite granites plot with  $T_{\text{DM}} = 1000\text{Ma}$  consistent with a Depleted mantle + SULPS origin for these magmas (Halliday et al. (1980).

## Chapter 8 Conclusions

Fig. 8.1  $\text{SiO}_2$  vs  $\epsilon\text{Sr}_t$ . Initially variable but generally decreasing  $\epsilon\text{Sr}_t$  with fractionation followed by increasing  $\epsilon\text{Sr}_t$  with fractionation.

Fig. 8.2 Comparison of data from the Lorne Plateau lavas (Thirlwall 1986, 1983 & 1982) with the lamprophyres of Caledonian age from Lismore, Ardgour. Normalised against average Calc-alkaline lamprophyre (Rock 1991).

Fig. 8.3 Cartoon reconstructions to illustrate the Silurian closure of Iapetus, and the presence of micro-plates and multiple subduction zones, adapted from Soper et al. (1992).

Fig. 8.4 Comparison of the Lorne Plateau lavas (Thirlwall 1986, 1983 & 1982) with high Mg# basalts from Baja California (Rogers & Saunders 1989) and from the Antarctic Peninsula (Hole 1988). MORB values from Pearce (1983).

Fig. 8.5 Sr/Y vs Y. Data from the Lorne Plateau fall within the field of adakites (bajaites) and those from south of the Highland Boundary Fault fall within the 'normal' arc basalt field. Field boundaries from Defant et al. 1991. Lorne data from Thirlwall (1986, 1983 & 1982).

## List of Photographs

### Chapter 1 General Introduction

- Plate 1 Photo 1.1 View of the northern portion of the Ben Nevis Complex from the B8004 Corpach - Gairlochy Rd.
- Plate 1 Photo 1.2 Approaching Tower Gap from the Great Tower.
- Plate 2 Photo 1.3 Aerial view of the North Face of Ben Nevis (copyright A. Gillespie).
- Plate 2 Photo 1.4 View of Ledge route from the base of NE Buttress (see Fig. 1.4b for names).
- Plate 3 Photo 1.5 Panorama of the North Face of Ben Nevis (see Fig.1.4a for names).

### Chapter 3 The Volcanic Pile

- Plate 4 Photo. 3.1 Dalradian basement to the volcanic pile, intensely folded metapelite and semi-pelite. BN198 (NN170, 720)
- Plate 4 Photo. 3.2 View of Five Fingers Gully looking north. The exposures of Dalradian metasediments are located in the gully forming the middle ground of the photograph.
- Plate 5 Photo. 3.3 Alteration and staining of the felsite sill in Five Fingers Gully. BN362 (NN152 711)
- Plate 5 Photo. 3.4 Offshoot of the felsite sill intruding into the volcanic pile. The white rock in the centre of the picture represents an offshoot of the felsite which is located in the foreground of the photograph.
- Plate 6 Photo. 3.5 View of the volcanic pile/Inner Granite/felsite contact in Five Fingers Gully looking south towards the col between Carn Dearg (SW) and Ben Nevis. The prominent gully below the col is due to faulting and the preferential erosion of the Tertiary dyke. The volcanic pile is on the left hand side of the photograph and the contact with the Inner Granite and Felsite dyke effectively follows the line of rocky exposure until meeting the prominent gully where the contact climbs steeply to gain the col thus pinching out the Felsite.
- Plate 6 Photo. 3.6 Conglomeratic breccia of the Allt a' Mhuillin formation. White clasts are quartzite with the remainder of the clast population composed of contemporaneous sediments and Dalradian schists. BN197 (NN169 720)
- Plate 7 Photo. 3.7 Contact between Dalradian basement and the conglomeratic breccia of the Allt a' Mhuillin formation (right hand side). Note the fine grained base to the breccia (below the lens cap) and the predominance of quartzite clasts in contrast to the local pelitic basement lithology (Photo3.1) that forms the left hand side of the photograph. BN197 (NN169 720)
- Plate 7 Photo. 3.8 Rhythmic layering in the mudstones of the Allt a' Mhuillin formation. The basal andesite forms the rounded exposures towards the top right corner of the photograph. BN197 (NN169 720)

- Plate 8 Photo. 3.9 Photomicrograph of mudstone from the Allt a' Mhuillinn formation. Note the layering depicted by small crystals of Fe-Ti oxide and the extremely fine grained nature of these sediments. (BN197S \* 21) (NN169 720)
- Plate 8 Photo. 3.10a Eutaxitic ignimbrite clast from the CIC hut boulder. Dark green grey clasts represent flattened pumice and are set in a matrix of lithic fragments and ash? predominantly andesite (NN167 723)
- Plate 9 Photo. 3.10b Eutaxitic ignimbrite clast from the CIC hut slabs. Note the lithic clast in the centre of the photograph around which the fiamme have been deformed. BN207 (NN166 723)
- Plate 9 Photo. 3.11 Photomicrograph of an eutaxitic ignimbrite clast, pale yellow band in the centre of the photograph is a flattened crystal rich clast of pumice. (BN140 \* 12). CIC hut Boulder (NN167 723)
- Plate 10 Photo. 3.12 Sheared base to volcanic breccia, base of flow is towards the bottom of the photograph and the shear direction is parallel with the base of the Plate. Clasts are of andesite. BN230 (NN165 721)
- Plate 10 Photo. 3.13 Well exposed volcanic breccia (Hammer 40cm in length), angular to sub-rounded clasts of andesite showing clast and matrix support. BN249 (NN167 721)
- Plate 11 Photo. 3.14 Thin volcanic breccias exposed at the base of the Tower slabs. (NN 166 720)
- Plate 11 Photo. 3.15 The two light coloured patches represent the maximum lateral extent of a rhyolite bearing volcanic breccia sandwiched between an andesite on the left hand side and a volcanic breccia on the left hand side. The volcanic succession in this locality has been overturned during collapse of the volcanic pile. BN207 (NN169 722)
- Plate 12 Photo. 3.16a Slope morphology of the Coire na Ciste slabs (view to south toward Tower Ridge); the slope is composed of volcanic and andesitic breccias.
- Plate 12 Photo. 3.16b Slope morphology of the Ledge route and the Gt. Buttress of Carn Dearg (view to north).
- Plate 13 Photo. 3.17 Rhythmic fining up cycles in the sediments of BN205. Note the coarser andesitic bands. Each cycle is between two and four cm thick. (NN166 720)
- Plate 13 Photo. 3.18 Photomicrograph of fining up cycles (BN205 \* 12). (NN166 720)
- Plate 14 Photo. 3.19 Deformed calcareous sediments of BN142. (NN162 719)
- Plate 14 Photo. 3.20 Sediments and conglomeratic breccias within the Coire na Ciste Formation. The lithologies in the photograph are overlain by VBc of Fig 3.7. Green coloured rock is fine grained sediments, that with the abundant white fragments is the sedimentary breccia and the upper part of the photograph is

- composed of brecciated andesite forming the base of an andesite lava. BN271 (NN165 722)
- Plate 15 Photo. 3.21 Sediments exposed between VBa and VBb of Fig 3.7. BN271 (NN165 722)
- Plate 15 Photo. 3.22 Baked mudstone clasts in the base of VBc. BN271 (NN165 722)
- Plate 16 Photo. 3.23 Photomicrograph of deformed micaceous Dalradian fragments (white patches in the photograph) and mica crystals around lithic (andesite) fragments and feldspar crystals. (BN268 \* 12) (NN167 716)
- Plate 16 Photo. 3.24 Photomicrograph of NE Buttress sample, note the range of andesite/matrix contacts in this photograph illustrating that the andesite was still largely molten during formation of the rock (NE Buttress \* 12). (NN170 714)
- Plate 17 Photo. 3.25 View of fine grained mudstones forming the Trident Member. Note the large degree of soft sediment deformation and small scale faulting. BN215 (NN162 731)
- Plate 17 Photo. 3.26 Transition zone between the Ledge route Member and the Trident member. 'White' bands in the photograph represent early Ledge Route Member volcanic breccias sandwiched between fine grained sediments of the Trident Member. BN215 (NN162 731)
- Plate 18 Photo. 3.27 Fallen block of transition zone rich lithologies in the mudstones of the Trident Member. Note the deformation at the base of this block and the large quartzite clast in the right hand corner of the block. BN215 (NN162 731)
- Plate 18 Photo. 3.28 Hand specimen photograph of the Ledge route Member. BN215 (NN162 731)
- Plate 19 Photo. 3.29 Sheared fine grained base to the Ledge route Member. Sheared base is located in the green grey bands such as that found beneath the lens cap. BN215 (NN162 731)
- Plate 19 Photo. 3.30 Sediment splurge of the Trident Member forced into the Ledge route Member, the injected sediments curve round to a position above the head of Noel Williams. Note the sharp contact between mudstones of the Trident Member and breccias of the Ledge route Member. Escape pipe of Photo 3.31 is located along the feature to the left of Noel Williams. BN215 (NN162 731)
- Plate 20 Photo. 3.31 Escape pipe found within the Ledge route Member, note the fine grained nature of the entrained material suggesting that it originated in the Trident Member. BN215 (NN162 731)
- Plate 20 Photo. 3.32 View south from Ledge route across Coire na Ciste to the summit region of Ben Nevis. Sky-line ridge is the North East Ridge, that in the middle ground is Tower ridge with the Gt. Tower forming an obvious projection. A number of faint  $\approx$  horizontal lines are apparent in the Summit

Formation, these are believed to represent contacts between different andesite units.

- Plate 21 Photo. 3.33 Monolithologic volcanic breccia (Nuées ardentes ?) of the Summit Formation. Ice axe is 55cm long. Blue colour is an artefact of the copying process and the rock is really a dark purple-grey  
BN130 (NN158 719)
- Plate 21 Photo. 3.34 Typical andesite, note crude alignment of plagioclase and hornblende/pyroxene phenocrysts from top right to bottom left.  
(Castle Ridge NN157 725)
- Plate 22 Photo. 3.35 Photograph shows stringers of autobrecciated andesite intruding into the volcanic breccia. Flow movement from bottom left to top right.  
BN249 (NN167 721)
- Plate 22 Photo. 3.36 Autobrecciated andesite. BN277/1 (NN162 721)
- Plate 23 Photo. 3.37 Mechanical brecciation of andesite lava. Flow movement from right to left. Semi-solid to solid clasts of andesite are being sheared and broken up during movement of the surrounding andesite.  
BN234 (NN165 717)
- Plate 23 Photo. 3.38 Contact between volcanic breccia (top) and autobrecciated andesite (bottom). Slight darkening at the base of the volcanic breccia. The base of the andesite lava is shown in the above photo (3.37)  
BN234 (NN165 717)
- Plate 24 Photo. 3.39 Intrusion Type 1 showing small scale offshoots from the main vein. Host rock is an andesite sill. BN249 (NN167 721)
- Plate 24 Photo. 3.40 Surface spaghetti-like texture to intrusion Type 1.  
BN249 (NN167 721)
- Plate 25 Photo. 3.41 The photomicrograph displays a number of clast types forming the fill in the No. 4 gully vent. The pale clast on the left hand side with dark speckling is a rounded fragment of Dalradian schist whereas the majority of the slide is formed of andesitic clasts and a fine grained igneous matrix. Note the euhedral pyroxene pseudomorphs in the clast forming the top right of the photograph. (BN220 \* 3) (NN161 717)
- Plate 25 Photo. 3.42 Intrusion Type 4, fine grained (ash ?) brown coloured pipes.  
BN234 (NN165 717)
- Plate 26 Photo. 3.43 Fresh surface exposure of the Fault facies. Flow banded rhyolite is clearly depicted in this photograph and not rock which has been sheared.  
BN242 (NN171 713)
- Plate 26 Photo. 3.44a Contact between Fault facies and Volcanic pile. Fault facies is found in the bottom of the photograph. BN239 (NN165 725)
- Plate 27 Photo. 3.44b Contact between Fault facies and Inner Granite. Inner Granite forms the left hand side of the photograph. BN239 (NN165 725)

- Plate 27 Photo. 3.45 Photomicrograph of reworked Fault facies. The slightly darkened band in the middle of the photograph represents the line along which the Fault facies was reworked. (BN185b \*21) (NN 168 722)
- Plate 28 Photo. 3.46a Type locality of the 'flinty crush rock'. The author's right foot is on the Inner Granite and the left foot rests on Fault facies. The extreme right margin of the photo is comprised of Allt a' Mhuillin Formation sediments. BN184 (NN169 721)
- Plate 28 Photo. 3.46b Close up of the flinty crush rock type locality. The grey-brown streak to the right of the lens cap is in reality the chocolate-brown Flinty Crush Rock of Bailey & Maufe (1916). This streak is found within the Fault Facies and is not observed at the contact between the Inner Granite and the volcanic pile indicating that it is a fine grained variant of the Fault facies and not a product of shearing. BN184 (NN169 721)
- Plate 29 Photo 3.47 Photomicrograph of Fault facies, note the flattening of biotite and amphibole crystals around larger feldspar fragments (BN242 \* 21).
- Plate 29 Photo. 3.48 Photomicrograph of contact between sediments of the volcanic pile and the Fault facies. Note the wavy/irregular chilled margin of the Fault facies indicating the existence of a large temperature difference between the two rocks types. There is no sign of shearing in this thin section. (BN240 \* 21) (NN155 726)

#### Chapter 4 Field geology of the Intrusive Members of the Ben Nevis Complex

- Plate 30 Photo. 4.1 Example of contact observed in the fine grained quartz diorites of Allt Daimh. Fine grained quartz diorite on the left hand side has a sharp contact with fine-medium grained quartz diorite on the right hand side. OBN11 (NN171 771)
- Plate 30 Photo. 4.1 Examples of contact observed in the fine grained quartz diorites of Allt Daimh. Fine grained quartz diorite in the lower half has a sharp contact with fine-medium grained quartz diorite towards the top of the photograph. OBN13 (NN172 770)
- Plate 31 Photo. 4.2a Photomicrograph of fine grained quartz diorites of Allt Daimh, compare with Plate 4.2b; in particular note the in-equigranular grain size of 4.2a compared to the equigranular grain size of 4.2b. Phenocrysts of orthopyroxene and plagioclase are found in 4.2a (OBN11e \* 21 XPL).
- Plate 31 Photo. 4.2b Photomicrograph of fine grained quartz diorites of Allt Daimh, compare with Plate 4.2a. (OBN11d \* 21 XPL)
- Plate 32 Photo. 4.3 Internal contact within the Porphyritic Outer Granite, granite towards the bottom of the photograph has a higher mafic content than that towards the top of the photograph Line of contact has been exploited by late stage fluids/magmas. (Exposure in the Allt Daimh NN186 726).

- Plate 32 Photo. 4.4 Contact between the Porphyritic Outer Granite and the Dalradian in the Nameless Burn. Photographer is standing on the Porphyritic Outer Granite which has compressed the Dalradian metasediments in this area forming a conjugate set of thrust faults. BN394 (NN182 764)
- Plate 33 Photo. 4.5 View of the eastern margin. The left hand side is Locality 1 (Fig. 4.5) where erosion has failed to expose the underlying granite. The ridge on the right hand side is formed of Dalradian metasediments and represent remnants of the magma chamber wall. The stream in the middle of the photograph has cut down through the Dalradian, exposing the underlying granite.
- Plate 33 Photo. 4.6 Contact between fine grained red granite and Dalradian metasediments on the col between Aonach Mor and Stob an Cul Choire. This granite intrusion is similar to those found in An Cull Choire and was previously interpreted as part of the Outer Granite (Anderson 1935 and Haslam (1965). (NN197 730)
- Plate 34 Photo. 4.7 Granite vein within the Dalradian metasediments. (NN196 735)
- Plate 34 Photo. 4.8a Intrusion breccias in the vicinity of Aonach Mor. Note the small scale movements exhibited by blocks on the lower photograph and the granitic matrix to the breccia. (NN196 735)
- Plate 35 Photo. 4.8b Intrusion breccias in the vicinity of Aonach Mor. Note the small scale movements exhibited by individual clasts and the granitic matrix to the breccia. (NN196 735)
- Plate 35 Photo. 4.9 Xenolith laden dyke in the Nameless Burn. Core of the dyke (bottom left hand side) dominated by Dalradian clasts, margins (top right hand side) dominated by quartz diorite clasts. BN384 (NN181 766)
- Plate 36 Photo. 4.10 Photomicrograph of a volcanic xenolith. Conspicuous phenocryst is Oxy-hornblende. (OBN37e \* 107 PPL) (NN123 724)
- Plate 36 Photo. 4.11 Back injection of the Inner Granite. Thickness of vein  $\approx$ 40cm. Injection is cross-cut by late stage aplite veins and the contact between injection and Inner Granite has also been exploited by these veins. (NN165 702)
- Plate 37 Photo. 4.12 Contact exposed at BN421. Porphyritic Outer Granite forms the top left hand side, Inner Granite forms the right hand side and can be traced underwater from right to left, passing into an aplitic vein. (NN185 727)
- Plate 37 Photo. 4.13 Obvious line formed by the outcrop of a diorite sheet/sill (BN431).
- Plate 38 Photo. 4.14 'Appinite' of the Red Burn locality. Thin hornblende rich margin to the Porphyritic Outer Granite separates the igneous rock on the left hand side from the Ballachulish Limestone Formation on the right hand side. The blue colour is an artefact of the copying process and the hornblende

imparts a dark olive green colour to both the 'appinite' and the limestone.  
BN134 (NN136 717)

- Plate 38 Photo. 4.15 Intrusive contact relationships between appinitic magmas (darker colour) and the Coarse Quartz Diorite.
- Plate 39 Photo. 4.16a Pre-full crystallisation fabric within the Porphyritic Outer Granite. Pen is orientated parallel to fabric.
- Plate 39 Photo. 4.16b Pre-full crystallisation fabric within the Sgurr Finnisg-aig Quartz Diorite, fabric orientation is approximately horizontal in this photograph.
- Plate 40 Photo. 4.17 'Nick' in the hillside revealing the contact between the Porphyritic Outer Granite and Dalradian metasediments. Grassy areas in the foreground cover the intrusive red granite sheets of BN412. Aonach Beag is the mountain in the background.
- Plate 40 Photo. 4.17b Close up of the 'nick'. Contact metamorphosed Dalradian schists form the overhang and the granite obscured by vegetation. (NN195 722)
- Plate 41 Photo. 4.18a Example of structural data provided by the Ben Nevis dyke swarm; en-echelon dyke segments revealing dextral fabrics. (NN177 746)
- Plate 41 Photo. 4.18b Example of structural data provided by the Ben Nevis dyke swarm; small sinistral shears offsetting the thin dyke. (NN177 746)
- Plate 42 Photo. 4.19a Molybdenite and quartz intergrowths along a fault plane (M5). Thickness of vein  $\approx$ 4cm. (NN186 733)
- Plate 42 Photo. 4.19b Extreme alteration along/adjacent to faults in the Ben Nevis Complex. (NN185 734)

## Chapter 5 Petrology and Mineralogy

- Plate 43 Photo. 5.1 OBN10 Strong preferential alignment of the Fine Quartz Diorite in contact with the Dalradian country rocks in the Allt Daimh area of the Ben Nevis Complex. Minerals include plagioclase, ortho and clinopyroxene, biotite with minor Fe ore, quartz and alkali feldspar.  
\*21 XPL (NN171 721)
- Plate 43 Photo. 5.2 OBN11d Corrosion of a plagioclase feldspar phenocryst in the bottom half of the photograph by alkali feldspar in the centre of the photograph. \*43 XPL (NN171 771)
- Plate 44 Photo. 5.3 OBN11d Relatively well preserved pyroxene crystals (groundmass and phenocrysts). A thin actinolitic rim partially mantles the pyroxenes and is in turn partially mantled/replaced by biotite. Note the corroded opaque oxide in the centre top of the photograph.  
\*43 PPL (NN171 771)
- Plate 44 Photo. 5.4 BN87 The amphibole crystal in the centre of the photograph is a pseudomorph after pyroxene. Late stage poikilitic outgrowth of amphibole

- into the groundmass. Note the absence of opaque oxides in the biotites.  
\*43 PPL (NN159 765)
- Plate 45 Photo. 5.5 OBN18f Zoned pyroxene showing partial replacement by biotite.  
\*43 PPL (NN172 766)
- Plate 45 Photo. 5.6 OBN5 Corroded orthopyroxene core to a clinopyroxene rim which  
in turn passes into calcic amphibole. Plagioclase can be found as a phenocryst  
and as a groundmass phase in the photograph. \*107 PPL (NN132 735)
- Plate 46 Photo. 5.7 BN172 Biotite replacing pyroxene without, or after consuming,  
an intervening amphibole stage. \*107 PPL (NN140 756)
- Plate 46 Photo. 5.8 BN68b Euhedral foxy-red biotite crystals with pleochroic  
haloes having formed around apatite and occasionally zircon.  
\*43 PPL (NN155 764)
- Plate 47 Photo. 5.9 BN174 Foxy-red biotite intergrown/replacing amphibole.  
Alteration of biotite to chlorite is also a feature of this slide. Plagioclase  
shows much sericitisation. \*43 PPL (NN141 756)
- Plate 47 Photo. 5.10 OBN11a Well preserved pyroxene crystals ranging in size from  
microphenocrysts in the centre of the photograph (2mm) to examples in the  
groundmass. Note the corroded opaque oxides in the centre of the biotite  
crystals on the right hand side of the photograph. \*21 PPL (NN171 771)
- Plate 48 Photo. 5.11 BN378b Euhedral magmatic amphiboles in the Sgurr Finnisg-  
aig Quartz Diorite. \*107 XPL (NN194 763)
- Plate 48 Photo. 5.12 BN418 Subhedral amphibole showing corrosion by alkali  
feldspar located above and below the amphibole crystal.  
\*107 XPL (NN192 729)
- Plate 49 Photo. 5.13 BN157 'Hybrid' rock. Euhedral plagioclase, biotite and  
amphibole are enclosed within a single alkali feldspar which occupies the  
entire field of view. A number of the mafic minerals show signs of corrosion  
by the alkali feldspar. \*21 XPL (NN177 765)
- Plate 49 Photo. 5.14 BN366 Biotite - feldspar patches/clots interpreted as small  
xenoliths. Note the occurrence of muscovite in the lower right of the  
photograph. \*43 XPL (NN198 730)
- Plate 50 Photo. 5.15 BN328 Typical Inner Granite; note the zoned and corroded  
plagioclase phenocryst in the centre of the field of view and the low  
proportion of mafic (biotite) minerals. \*43 XPL (NN151 743)
- Plate 50 Photo. 5.16 BN324 The mafic Inner Granite with pale green ragged  
amphibole crystals. Also visible in this photograph are albite rich rims to  
the plagioclase. \*21 XPL (NN177 745)
- Plate 51 Photo. 5.17 BN210 Corroded euhedral hornblende in the volcanic  
pile. \*43 PPL (NN166 723)
- Plate 51 Photo. 5.18 BN199 Corroded pseudomorphs after amphibole.  
\*21 XPL (NN172 716)

## List of Tables

### Chapter 3 The Volcanic Pile

- 29 Table 3.1a. Non-Genetic classification of volcanoclastic rocks (adapted from Cas & Wright 1988).
- 30 Table 3.1b. Grainsize limits for proven pyroclastic fragments and pyroclastic aggregates (adapted from Fisher 1961, 1966).
- 31 Table 3.2. Commonly used terms and their definitions (based on Cas & Wright 1988).

### Chapter 4 Field geology of the Intrusive Members of the Ben Nevis Complex

- 73 Table 4.1 Comparison of different schemes for the subdivision of the plutonic members of the Ben Nevis Complex.
- 84 Table 4.2 The range in silica content for the plutonic members of the Ben Nevis Complex.
- 107 Table 4.3 Aluminium in hornblende geobarometry.

### Chapter 5 Petrology and Mineralogy

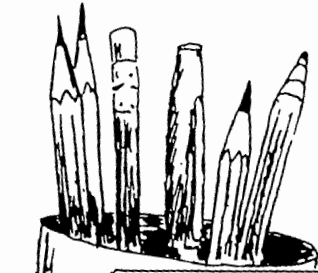
- 114 Table 5.1 Textural Criteria used to define magmatic biotite (adapted from Speer 1984).
- 142 Table 5.2 Average pyroxene compositions.

### Chapter 6 The Geochemistry of the Ben Nevis Complex

- 146 Table 6.1 A comparison of I-Type and S-Type Granitoids.
- 182 Table 6.2 Major element composition of the parent magma, daughter magma and mineral phases used in mass balance modelling.
- 183 Table 6.3 Results of mass balance modelling for the Porphyritic Outer Granite.

### Chapter 7 Isotope Geology

- 213 Table 7.1 Radiometric Ages for the Ben Nevis Complex in the literature.
- 213 Table 7.2 Sr and Nd Isotope Results for the Ben Nevis Complex.
- 213 Table 7.3 Characteristics of possible source rock compositions for the Ben Nevis Complex.



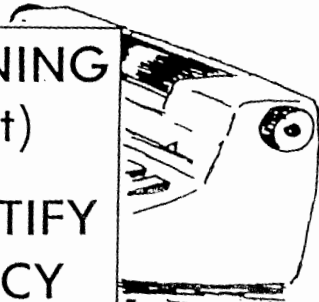
**LACK OF PLANNING**

(on your part)

**DOES NOT JUSTIFY**

**AN EMERGENCY**

(on my part)



# CHAPTER 1

## GENERAL INTRODUCTION

### 1.1 Introduction

#### 1.1.1 General Statement

Before describing the geology of Ben Nevis (The Ben), it is worth stepping back from a strictly academic study, and looking at the Ben as a physical entity rather than shading on a geological map.

#### 1.1.2 Names

Spellings of place names referred to in this thesis are as used by the Ordnance Survey and in particular in "Mountainmaster of Ben Nevis, the Grey Corries and Mamores" Outdoor Leisure Sheet 32. Names applied to features on the northern cliff line of Ben Nevis are those used in "Scrambles in Lochaber" (Williams 1985) and in "Rock Climbing in Scotland" (Howett 1990). In addition, the following names are first defined in this thesis for: Coire na Ciste slabs, Scramble slabs, CIC hut slabs, Buttress slabs and are applied to the area between Tower Ridge and the Great Buttress of Carn Dearg (Fig. 1.1).

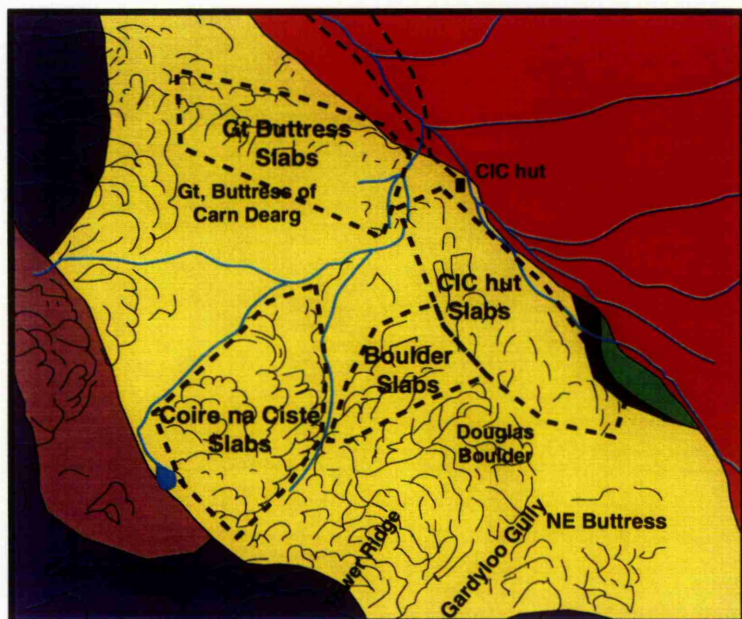
### 1.2 Physiography

#### 1.2.1 Location

The Ben Nevis group of mountains (Ben Nevis, Carn Mor Dearg and Aonach Mor) form an area of high ground, rising to 1000m+, on the southern side of the Great Glen some 2km from the northeastern end of Loch Linnhe (sea level). Fort William is the nearest population centre (refuge) and exceptional fell runners can run from the outskirts of Fort William to the summit of Ben Nevis and back, a distance of 12miles, in under 90mins; lesser mortals average 7hours.

The outer margins of the Ben Nevis volcanic-plutonic Complex, hereafter termed the Ben Nevis Complex, form the first area of high ground south of the Great Glen. Strontian, situated on the northern side of the Great Glen, is 30km to the southwest and the Etive volcanic-plutonic Complex is less than 10km to the south. The so-called Fort William Slide outcrops along the northeastern margin of the granite.

Two smaller granitoid plutons, Coille Lèanachain to the north and Mullach nan Coirean to the south, outcrop immediately next to the Ben Nevis pluton. The quartz diorites of Coille Lèanachain are petrographically and chemically similar to those of Ben Nevis (Anderson 1935). Mullach nan Coirean is only partially unroofed and is petrographically similar to the Meall Odhar granite phase of the Etive Complex (Bailey & Maufe 1960). The proximity of the three plutons lends itself to the suggestion that they are genetically related



- |   |  |
|---|--|
| <span style="display: inline-block; width: 15px; height: 10px; background-color: green; border: 1px solid black;"></span> Dalradian Basement.   | <span style="display: inline-block; width: 15px; height: 10px; background-color: red; border: 1px solid black;"></span> Ledge Route Fm.          |
| <span style="display: inline-block; width: 15px; height: 10px; background-color: black; border: 1px solid black;"></span> Allt a' Mhuillinn Fm. | <span style="display: inline-block; width: 15px; height: 10px; background-color: darkblue; border: 1px solid black;"></span> Summit andesite Fm. |
| <span style="display: inline-block; width: 15px; height: 10px; background-color: yellow; border: 1px solid black;"></span> Coire na Ciste Fm.   |  |

0.5 Km.

Fig. 1.1 The geographical location of low-lying slabby exposures within the outcrop of the Ben Nevis volcanic pile referred to in the text.

in some manner; however, the nature of such a relationship does not fall into the remit of this thesis.

### 1.2.2 Climate

Quite simply the summit of Ben Nevis is the wettest place in the United Kingdom. The operation of three observatories at the turn of the century (Fort William, Half Way and Summit) has considerably increased our knowledge of the weather on Ben Nevis, but raw scientific data alone cannot put over the sheer volume of water that cascades onto Ben Nevis each year. Sir John Carr (1907) describes the weather on Ben Nevis thus, "I was now in a region of rain, which descended with little intermission during my stay at Maryburgh (now Fort William), with a copiousness which I have not often beheld. Rain, which continues in this neighbourhood for nine or ten weeks together, is called by the natives by the gentle name of a shower."

For a detailed account of life at the observatory and its operation, the reader is referred to Crocket (1990) and to "Ben Nevis and its Observatory" (1983).

Although the observatory failed in its primary mission, that of weather prediction, it was whilst working in the observatory that Wilson designed the 'Wilson Cloud Chamber' and enabled scientists for the first time to observe the motion of sub-atomic particles. Wilson was awarded a Nobel Prize for this discovery in 1927. Just in case the reader is mistaken into believing that government apathy towards scientific research is a relatively recent phenomenon, the Ben Nevis observatory was closed in 1904 when government funding was insufficient to enable its continued operation.

Mean annual rainfall on the summit is 4.08m, in contrast, Fort William at sea level receives just over half this amount. Mean monthly temperatures are below freezing from October to May, and the average yearly temperature is just 0.3°C, 9°C colder than Fort William. Consequently, snow never completely disappears from the mountain except in exceptionally warm years. In 21 years of operation, the observatory was in sunlight for  $\frac{1}{6}$ th of the possible time; it was not uncommon for early ascensionists to record in the Observatory's visitors book "Missed the view, but viewed the mist".

Volunteers manning the observatory came to know the mountain well during their month long stints. An article on the operation of the observatory (Paton 1954) praises the usefulness of J. Miller in the following manner, "There are other local conditions where his (Miller's) knowledge would be invaluable, e.g. there is a large mass of rock not far from the top which is strongly magnetised and deflects your compass so much that in a mist you are guided in a circle. This rock is not far away from the precipitous cliff and is a source of great danger". Unfortunately no location is mentioned despite the acknowledged hazard that such a rock would present during whiteout or fog. Crocket (1990) speculates that the 'mass' is a meteorite, certainly there is no mechanism in the model presented in chapter 3 that could account for the existence of a large magnetic body. However, despite several days of

work on the summit plateau, no trace of such a mass could be found. Conversations with members of the local Mountain Rescue Team, who know the hazards of the mountain better than anyone, yielded no further information on the existence of this 'mass'. In fact one team member was heard to say, "That's a good excuse I'll have to remember that one". The Mountain Rescue Team uses a large scale map of The Ben onto which compass bearings have been printed. Noel Williams, the designer of the map, has no knowledge of an iron rich rock and it appears that the existence of such a rock is doubtful. One possible explanation is that Miller walked over an object buried in the snow, such as a large mass of iron or the Telegraph cable during operation, which deflected his compass. Alternatively, Miller had a drop too much of the 'Dew of Ben Nevis' !.

### 1.2.3 Terrain

Ben Nevis is the highest mountain in the United Kingdom (1344m), and along with its associated mountains forms a testing training ground for Munro-basher and Himalayan Mountaineer alike. In an average year, six people die on Ben Nevis and the Lochaber Mountain Rescue Team vies with the Glencoe team for the unenviable distinction of being the busiest rescue team in Scotland.

As well as including the highest mountain in the U.K., the Ben Nevis Complex has two U.K. geological records to its name. These are, the lowest exposure of Outer Granite in Glen Nevis and the highest on Aonach Mor represent a height difference of over 1,350m (3,900ft) making this intrusion the largest vertical thickness of granitic rock exposed anywhere in the U.K. Secondly, Aonach Beag is the highest mountain in the U.K. formed of metamorphic rock.

The Ben Nevis Complex is bounded to the north by the Great Glen and to the south and west by Glen Nevis. Both of these glacial troughs allow easy access to their respective sides of the Complex. In contrast the western margin, despite the building of the Aonach Mor gondola station, is relatively inaccessible. The summit of Aonach Mor is still 2,000ft of ascent and 1 to 2 hours away from the gondola top station. Needless to say, the most interesting exposures of country rock-granite contact can be found in this area.

Three glacial valleys, running north-south, transect the Ben Nevis Complex, and subdivide the area into 7 units. These are from west to east: (Photo 1.1 & Fig. 1.2)

1. Glen Nevis
2. Ben Nevis (1344m) and Meall an t Suidhe (711m)
3. Allt a' Mhuillin
4. Carn Mor Dearg (1220m), Carn Dearg Meadhonach (1179m) and Carn Beag Dearg (1010m)
5. Allt Daim and Allt Coire Giubhsachan
6. Aonach Mor (1221m) and Aonach Beag (1234m)
7. Allt Choille-rai (Killiechonnate Forest)

---

Plate 1 Photo 1.1 View of the northern portion of the Ben Nevis Complex from the  
B8004 Corpach - Gairlochy Rd.

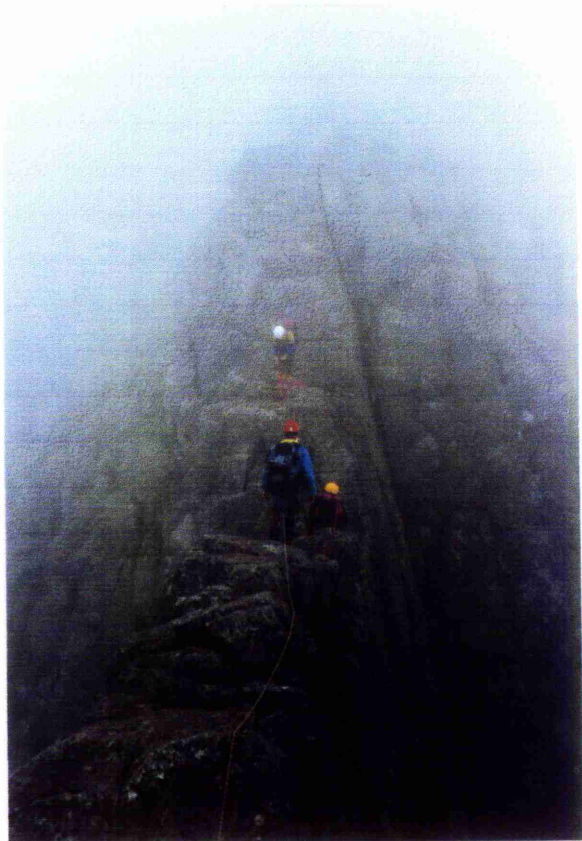
---

---

Plate 1 Photo 1.2 Approaching Tower Gap from the Great Tower.

---

PLATE 1



East-west movement off the areas of high ground is usually difficult and often dangerous, with the exception of the western slopes of Carn Mor Dearg.

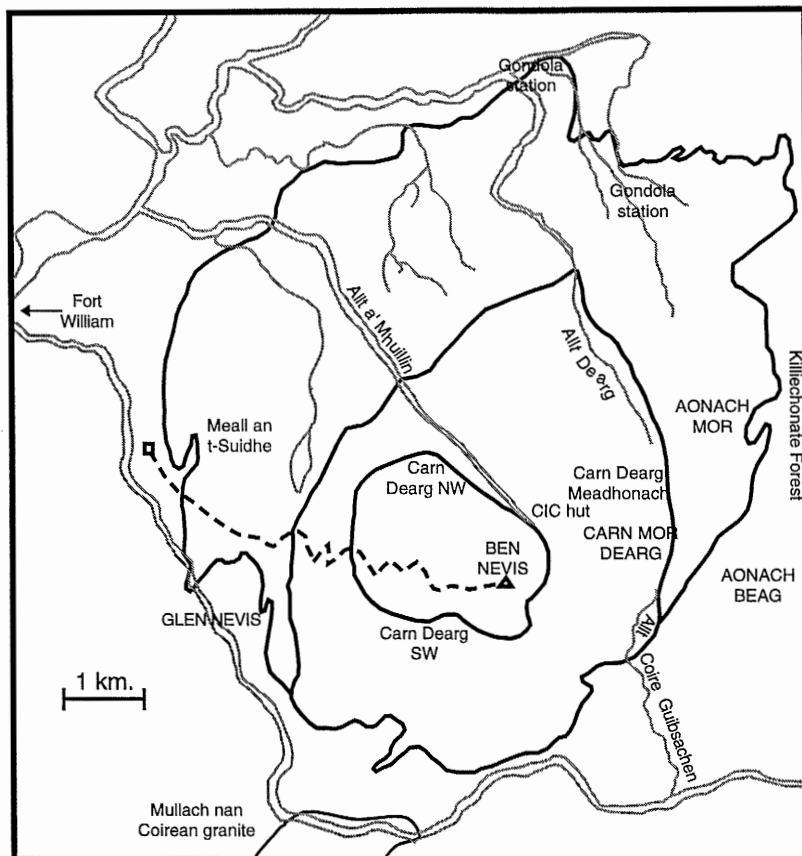


Fig. 1.2 The main geographical features of the Ben Nevis Complex.

The most obvious topographical feature within the area studied is the North Face of Ben Nevis and it is in this area that the volcanic pile outcrops. These cliffs are up to 2,000ft in height and the difficulties of studying such terrain should not be underestimated. Study of the volcanic pile was greatly aided with the purchase of "Scrambles in Lochaber" (Williams 1985) and "Rock Climbing in Scotland" (Howett 1990). Geologically, 'Ledge Route' (Fig. 1.4b) is superb and relatively easy to traverse. However, the description of any particular area within the Ben Nevis Complex does not mean that access to the area described is recommended (e.g. Five Fingers Gully). Five rock routes were completed with the aim of tracing gross geological features across the northern cliffs. Detailed mapping was obviously not possible. These routes are North East Buttress (Diff.), The Long Climb (Severe), Observatory Buttress (Diff), Tower Ridge (Diff.) (Photo 1.2) and Castle Ridge (Mod.); the grades of each route are given in parenthesis. For detailed route descriptions the reader is referred to Richardson (1994) and Williams (1984). Tower Ridge is the longest rock route

in the U.K. and was climbed via the Douglas Boulder. These routes are not recommended without climbing gear and some knowledge of basic rock climbing techniques. The location and line of these routes are depicted in Photos 1.3, 1.4 and 1.5 and in Figs. 1.3, 1.4a and 1.4b.

Active scree slopes are found across much of Ben Nevis; this presents certain difficulties when examining rock outcrop at the side of these slopes. Fortunately, in May and June hard compacted snow covers much of the scree and it is much easier to map these areas at this time, assuming that crampons and an ice axe are to hand.

### 1.3 Aims & Objectives

The Ben Nevis Complex was last studied in detail in the mid-late 1960's (Haslam 1965). Subsequently, Ben Nevis has only been studied within regional isotopic and chemical surveys, e.g. Thirlwall (1979), Hamilton et al. (1980) and Harmon & Halliday (1980). Modern geochemical and isotopic techniques have greatly complicated early models for the generation of igneous melts, e.g. the recognition of more than one mantle reservoir. In addition, one of the difficulties in summarising previous results from the literature is that each group of workers have tended to concentrate on one component of British Late Caledonide magmatism, e.g. lavas (Thirlwall), Granites (Halliday) and lamprophyres (Rock). No single study has looked at all the components and consequently inconsistencies between the different groups occur, e.g. Lorne Plateau Lavas have been proposed as representative of the mantle source from which lamprophyres and appinites were derived (Pitcher 1993, Yarr 1992). Thirlwall (1988 and refs. therein) suggests that the mantle source for the Lorne Plateau Lavas is distinct from that of the Midland Valley and Southern Uplands, yet lamprophyres are found in all the tectonic zones of the British Caledonides. The data presented in this thesis can assist in the development of a unified model for the South-west Highlands Caledonide magmatism, because lavas, granites and appinites/lamprophyres outcrop within the Ben Nevis Complex.

Apart from a brief one-page description in the B.G.S. Memoir (Bailey & Maufe 1960), the field geology of the volcanic pile has received scant attention. Geochemical studies have included samples from the volcanic pile (Haslam 1965 and Thirlwall 1979) but previous researchers have been content to acknowledge the existence of volcanic rocks on Ben Nevis and possibly sample the more accessible localities, but no volcanological interpretation has been made.

Subsequent to publication of both editions of the B.G.S. Memoir (Bailey and Maufe 1915 & 1960), the field of volcanology has advanced considerably. The recognition of calderas and modern theories of eruption mechanics and depositional processes have important implications for the interpretation of the volcanic pile and a model for its evolution is presented here.

---

Plate 2 Photo 1.3 Aerial view of the North Face of Ben Nevis (copyright A. Gillespie).

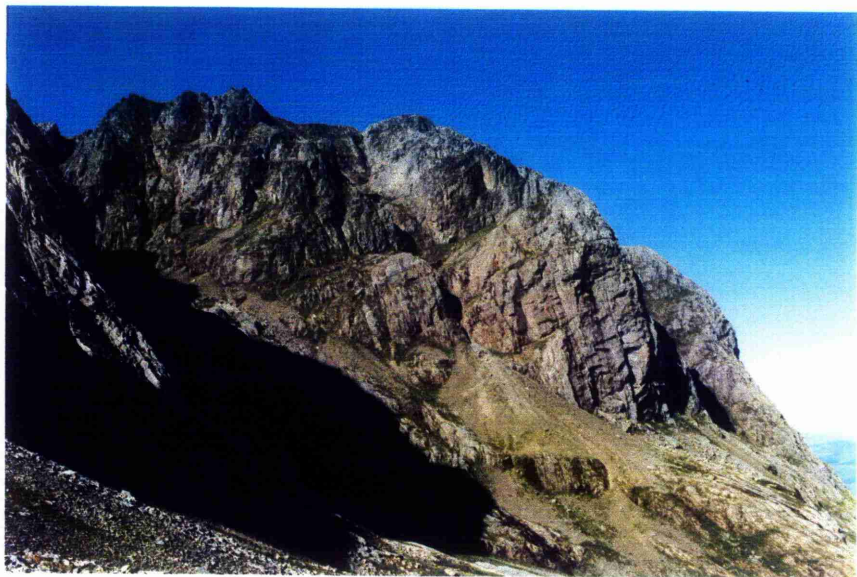
---

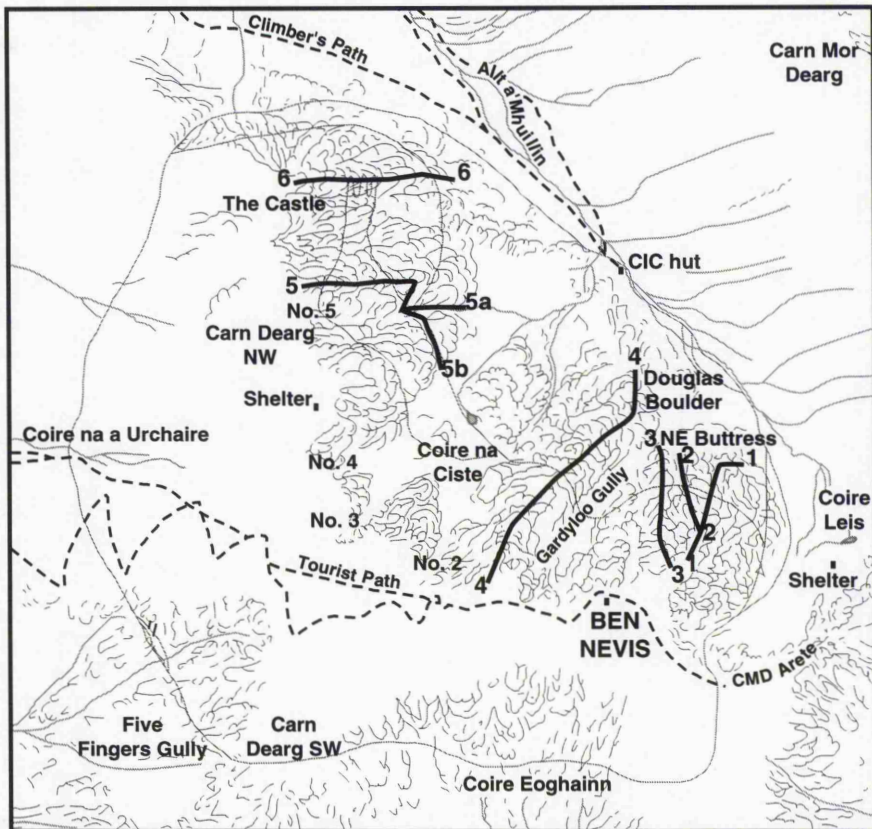
---

Plate 2 Photo 1.4 View of Ledge route from the base of NE Buttress (see Fig. 1.4b for names).

---

PLATE 2



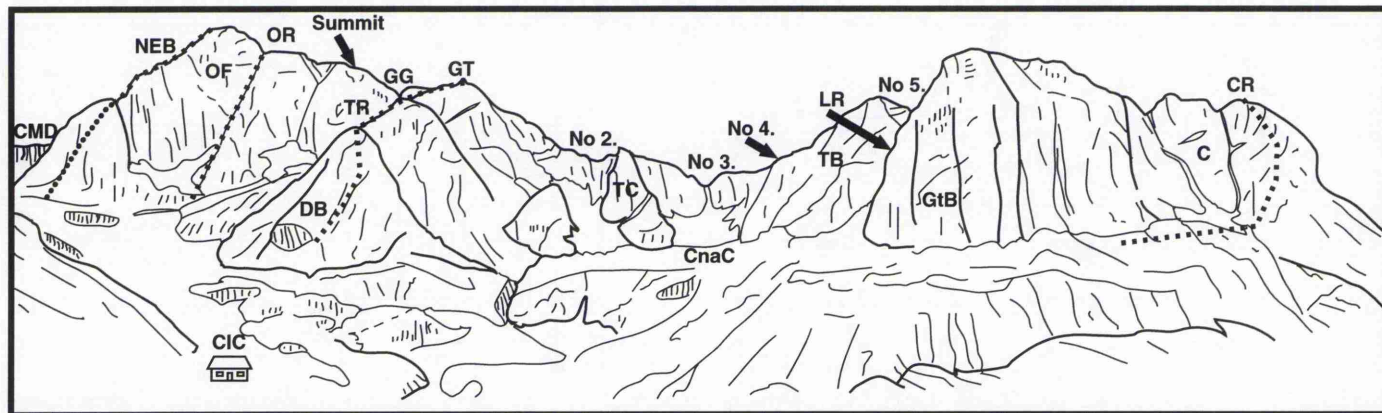


Key

- |                       |   |
|-----------------------|---|
| 1. NE Buttress.       | 5a. Ledge Route No.5 Gully variation.     |
| 2. Long Climb.        | 5b. Ledge Route Coire na Ciste variation. |
| 3. Observatory Ridge. | 6. Castle Ridge.                          |
| 4. Tower Ridge.       | No. 2 - No. 2 Gully.                      |

0.5 km

Fig. 1.3 The location of the main topographical features on the North Face of Ben Nevis, and the line of the climbing routes completed during this study.



CMD = Carn Mor Dearg Arete  
 NEB = North-east Buttress  
 OF = Orion Face  
 OR = Observatory Ridge  
 CIC = CIC hut  
 DB = Douglas Boulder

TR = Tower Ridge  
 GG = Gardylloo Gully  
 GT = Great Tower  
 TC = The Comb  
 CnaC = Coire na Ciste  
 TB = Trident Buttress

GtB = Great Buttress of Carn Dearg  
 C = The Castle  
 CR = Castle Ridge  
 No 2. = Number 2 Gully  
 LR = Ledge Route (see Fig 1.4b)  
 .... = Route of Climb

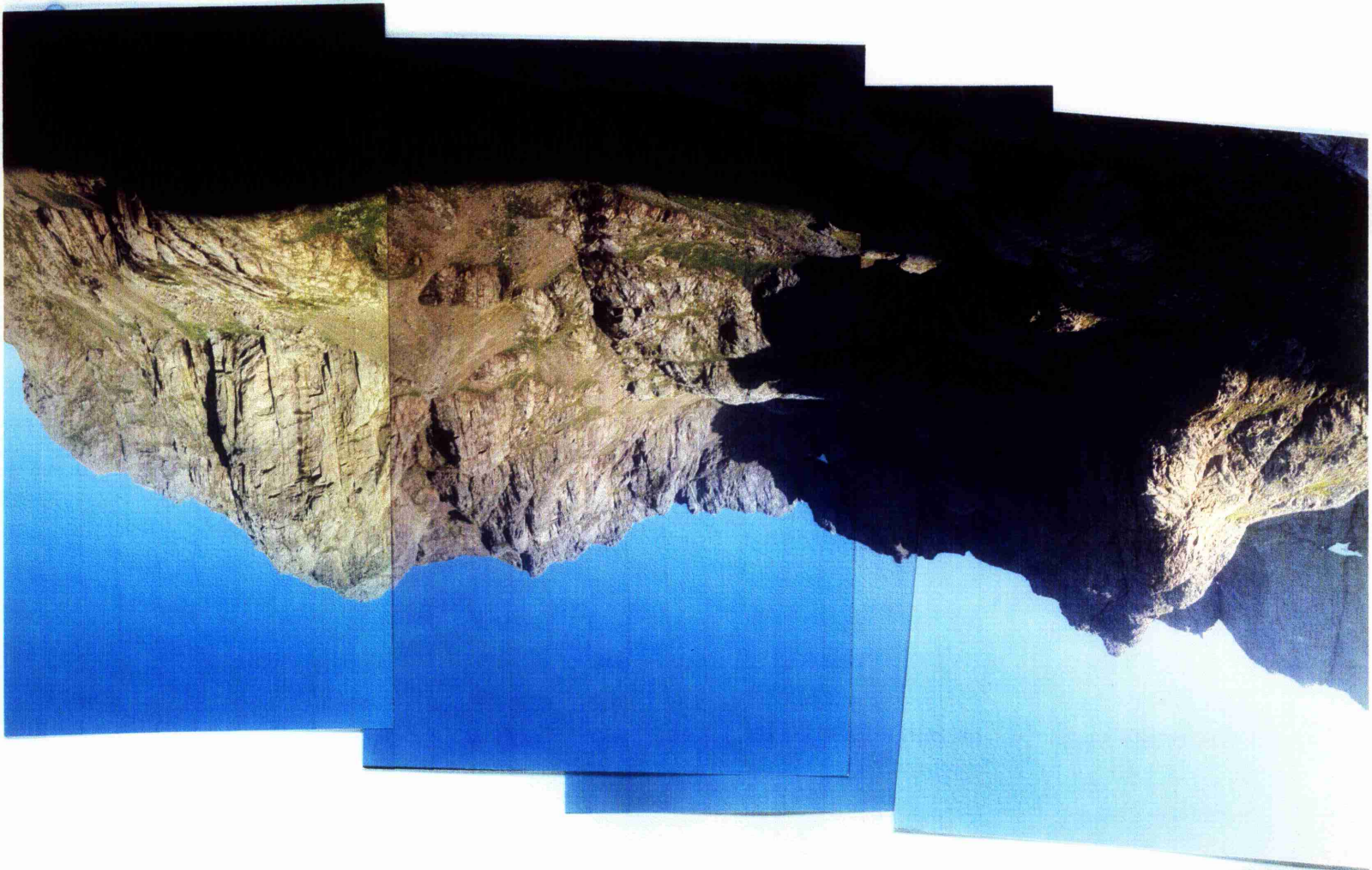
Fig. 1.4a The North Face of Ben Nevis (see also Photo 1.5).

---

Plate 3 Photo 1.5 Panorama of the North Face of Ben Nevis (see Fig.1.4a for names).

---

r



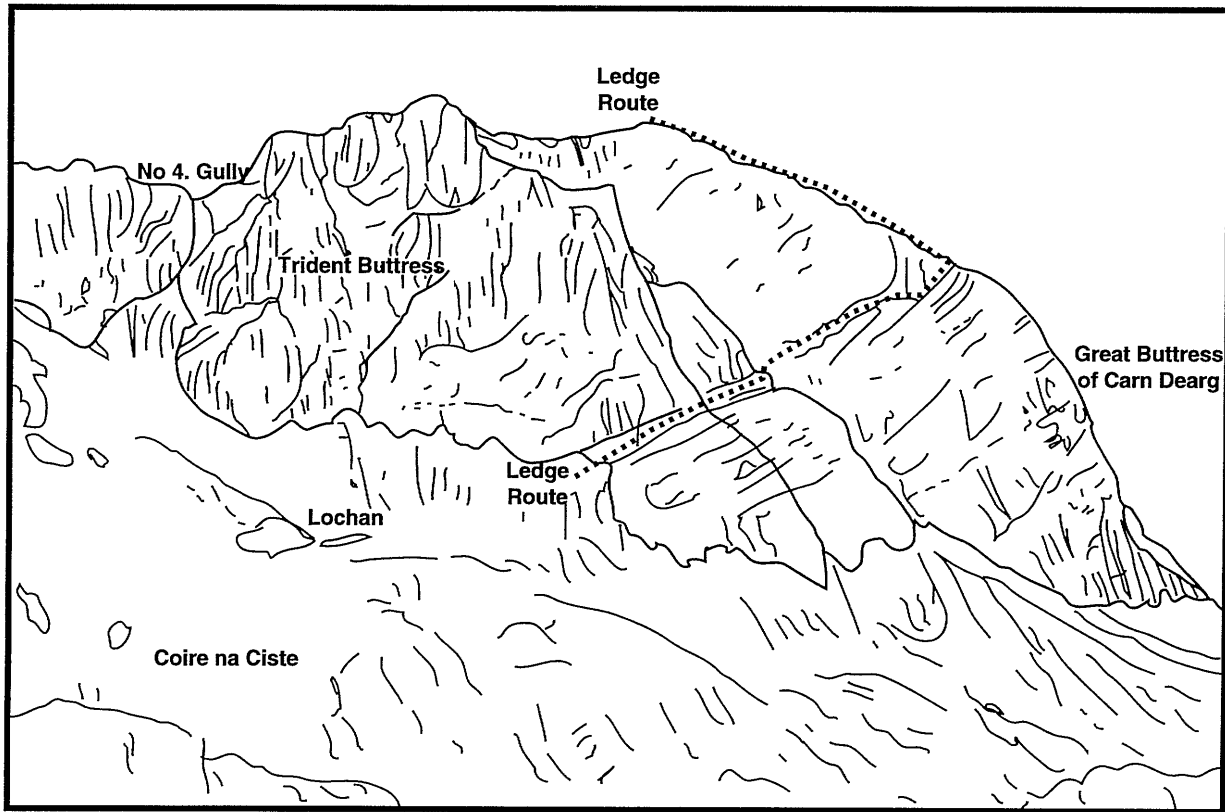


Fig. 1.4b The northern wall of Coire na Ciste and the location of Ledge Route.

To summarise the aims of this thesis are:

- 1) To produce a model for the development of the volcanic pile.
- 2) To identify the magma source composition(s) and how these changed during the evolution of the Ben Nevis Complex.
- 3) To develop an integrated model for the evolution of the Ben Nevis Volcanic-Plutonic Complex and apply this to the South-west Highlands in general.

#### 1.4 Methodology

Geochemical and isotopic analysis are of little use without adequate field control and to this end the entire complex was mapped on a scale of 1:10,000. Parts of the volcanic pile were studied in greater detail at 1:5,000 and 1:2,500. It is only in recent years that the complexity of ancient volcanic terrains has begun to be unravelled. Studies in the English Lake District have shown that pyroclastic flows, lava flows, sills and sediments outcrop over short distances (Branney 1988). To sample the volcanic pile as part of a geochemical or isotopic study without first unravelling the field relationships between the different components, would hide its underlying complexity.

Thin section, XRF and EMPA techniques were used to investigate the relationships between different components of the Ben Nevis Complex. Sm-Nd and Rb-Sr isotopes were obtained from a subset of samples analysed by XRF.

#### 1.5 Thesis Format

This thesis is laid out in the following manner:

Chapters 1 and 2: Background information on the geology of Ben Nevis and the surrounding area.

Chapter 3: Field based research on the volcanic pile is discussed and a new model for the development of this part of the Ben Nevis Complex is presented.

Chapter 4: Field based research for the plutonic rocks of the Ben Nevis Complex is discussed and a scheme for sub-dividing the Outer Granite is put forward along with an alternative intrusion mechanism based on new structural data.

Chapter 5: Petrographic and mineralogical data are presented for the plutonic and volcanic rocks.

Chapter 6: Geochemical data are presented for the plutonic and volcanic rocks and the suitability of fractional crystallisation as a model for the evolution of the igneous rocks is discussed.

Chapter 7: New isotope data for the Ben Nevis Complex are presented. Results from previous isotopic studies of the British Caledonides are discussed in the light of the new Ben Nevis data.

Chapter 8: A unifying model tying together all of the above is put forward. The end of the Caledonian Orogeny and the nature of late Caledonian magmatism in Northern Britain are discussed.



The Last Revision!

## CHAPTER 2

### GEOLOGICAL SETTING

#### 2.1 Introduction

##### 2.1.1 General statement

The metasediments and igneous rocks of the Caledonian Orogenic Belt are amongst the most intensely studied rocks in the world. Over a period of 600Ma (1000Ma-400Ma), the entire range of tectonic and magmatic activity affected the rocks forming Northern Britain today. Consequently, the geological history of this region is extremely complex and the following chapter can only be a brief summary of the current state of knowledge. Stratigraphic subdivision of the orthotectonic Caledonides is based on Johnson (1992) and Harris & Johnson (1992). Division is used here in the sense of Johnstone et al. (1969).

#### 2.2 Regional Geology

##### 2.2.1 Stratigraphy and sedimentology

The metamorphic rocks of the Central Highlands comprise units referred to as the Central Highland Division, Grampian Group and Dalradian Supergroup.

##### 2.2.1.i The Central Highland Division

The Central Highland Division is composed of migmatitic gneisses, predominantly semipelite and pelite with minor psammite and rare limestones, representing deposition on a shallow, occasionally intertidal, shelf (Piasecki 1980).

The Central Highland Division is separated from the Grampian Group by the Grampian slide zone, a 200m thick sequence of intensely tectonised metasediments. Movement along the slide coincided with local D<sub>3</sub> in the underlying Central Highland Division, and the slide is itself folded by D<sub>1</sub> of the Dalradian (Piasecki 1980).

Johnstone (1975) correlated the Central Highland Division, also referred to as the Younger Moine, with the Moine of the Northern Highlands and did not distinguish the Central Highland Division from the Loch Eil Group of the Moine Supergroup. Piasecki (1980) preferred a Glenfinnan Group correlation. The age of the Central Highland Division is poorly constrained and the base of the sequence is nowhere seen. In the Grampian Slide zone at Ord Ban, a migmatitic granite gneiss forms part of a tectonic slice of the Central Highland Division. Piasecki & van Breemen (1983) quoted a maximum Rb-Sr age of  $\approx 1300$ Ma for this gneiss which was correlated with Grenvillian age gneisses intruding the Moine Supergroup (e.g. West Highland Granite Gneiss). Muscovites obtained from pegmatites within the Grampian slide zone yield Rb-Sr ages of between 780Ma and 730Ma and

represent the minimum age of the Central Highland Division (Piasecki & van Breemen 1983). These authors cite similar ages for pegmatites within the Moine as evidence of an orogenic event between the Grenvillian and the Caledonian orogenies. In the Moine this event is known as the Morarian (Lambert 1969).

Soper & Hutton (1984) question the validity of the Morarian as an orogenic event drawing attention to the dilational geometry of the pegmatites upon which evidence for the Morarian rises or falls. The authors go on to suggest that the pegmatites are evidence of enhanced heat flow and crustal stretching, possibly during the early evolution of the Dalradian Basin.

#### 2.2.1.ii The Grampian Group

This monotonous series of psammites and semipelites is often placed within the Dalradian Supergroup (Harris & Pitcher 1975), but the Grampian Group sedimentary basin apparently subsided and filled before regional subsidence and the onset of Dalradian sedimentation (Glover & Winchester 1989). It is therefore considered to be a separate sedimentary sequence from the Dalradian (Glover & Winchester 1989).

The age and stratigraphic position of the Grampian Group is unclear. A sedimentary transition between Grampian Group and Dalradian Supergroup metasediments is recognised in the River Leven inlier (Treagus 1974). Further west, in the area around Fort William, a sharp boundary between the two sequences is recognised. Previously believed to be tectonic and known as the Fort William Slide (Bailey 1910, 1916, 1960), recent research has re-interpreted this boundary as an unconformity (Glover 1993).

Hickman (1975) has shown that the predominantly feldspathic and quartzofeldspathic sandstone lithologies of the Grampian Group are typical of intertidal or shallow coastal depositional environments. Infrequent dropstone horizons are interpreted as evidence of glaciation (Glover 1993).

#### 2.2.1.iii The Dalradian Supergroup

The age of the Dalradian Supergroup, subdivided into Appin, Argyll and Southern Highland Groups (Harris & Pitcher 1975), is uncertain as is the nature of tectonic events affecting this group of rocks, and even the position of the Dalradian sedimentary basin in palaeotectonic reconstructions has recently been questioned (Bluck & Dempster 1991). A Rb-Sr date of  $668 \pm 23$  Ma (Pringle 1973) has been obtained from the Varanger Tillite (Norway) which is correlated with the Port Askaig Tillite at the base of the Argyll Group. Acritarchs in the Bonahaven dolomite Formation (Argyll Group) are Vendian in age and those within the Tayvallich Limestone Formation (top of Argyll Group), previously thought to be of lower Cambrian age (Downie et al. 1971), are now recognised as having a much longer range that extends into the Precambrian (Downie pers. comm. to Harris 1989). Mafic volcanics from Tayvallich at the base of the Southern Highland Group yield U-Pb zircon ages

of  $597 \pm 4$  Ma (Halliday et al. 1989; error re-calculated to  $2\sigma$ ) and the entire Dalradian sequence is now known to have been deposited in the Precambrian (Rogers et al. 1989). The top of the sequence is nowhere seen.

Early shallow water deposits of the Appin Group are overlain by widespread glacial deposits of the Port Askaig Tillite Formation. Forty-seven tillite horizons are recognised (Spencer 1971) and yet the Argyll Group also contains sediments that require tropical conditions, e.g. the Aberfeldy baryte deposit and the Bonahaven dolomite Formation. Clearly, this period of glaciation must have covered much of the globe. Boulders within the Port Askaig Tillite Formation have been tentatively correlated with basement gneisses exposed on Islay and Colonsay (Fitches et al. 1990).

A succession of deepening and shallowing cycles is recorded in the sediments of the Argyll Group, which includes tillite, dolomite, quartzite, pelite, and towards the top of this group, abundant mafic volcanics. Although the sedimentary environments are complex, the overall trend is towards deepening of the Dalradian basin; each outburst of igneous activity coinciding with renewed extension and subsidence (Fettes et al. 1986). Graham & Bradbury (1981) suggest that the chemistry of mafic volcanics within the Dalradian is indicative of the failed development of oceanic crust. Argyll Group sedimentation was increasingly affected by tectonic activity and deposition is locally controlled by block faulting along NE-SW and NW-SE trending faults (Anderton et al. 1979).

The Southern Highland Group is comprised of turbiditic grits, greywackes and muds, deposited in a deep-sea fan type environment. Mafic (Tayvallich volcanics) volcanics at the base of this group represent the culmination of igneous activity initiated in the Argyll Group.

## 2.2.2 Structure and Deformation

Structurally the Grampian Highlands are extremely complex and major differences of opinion are found between different groups of workers, compare Lindsay et al. (1989) with Highton (1992). After the work of Johnson (1963), four deformation events are recognised in the Dalradian Supergroup although there is some disagreement e.g. Treagus (1974).

Lambert & McKerrow (1976) defined the Grampian orogeny as "the set of events... which caused the deformation and metamorphism of the Dalradian sediments". The term Caledonian orogeny was restricted to events after the Grampian orogeny and during the late Ordovician - mid Devonian i.e. Grampian events correlate with  $D_1$ - $D_2$  structures and the Caledonian with  $D_3$ - $D_4$  in the model of Lambert & McKerrow (1976).

The Ben Vuirich granite intrudes Neoproterozoic Dalradian metasediments in the Central Highlands of Scotland and cross-cuts  $D_1$ - $D_2$  structures (Bradbury et al. 1976).  $D_1$ - $D_2$  were thought to have been the major crustal thickening events in the Dalradian,

whereas peak metamorphism was believed to have coincided with D<sub>3</sub> (Harte et al. (1984). A U-Pb zircon age of 514±7Ma (Pankhurst & Pidgeon 1976) from Ben Vuirich, provided an important time marker in the evolution of the Grampian terrane. However, in recent years the above interpretation of Dalradian geology has been shown to be incorrect.

A precise, concordant U-Pb zircon age of 590±2Ma (Rogers et al. 1989) from Ben Vuirich has been confirmed by a SHRIMP ion microprobe U-Pb zircon age of 597±11Ma (Pidgeon & Compston 1992); consequently, all Dalradian sediments must have been deposited in the Precambrian. New interpretations of the structural position of Ben Vuirich (Tanner & Leslie 1994), and of the Older Granites outcropping in Glen Clova/Glen Isla (Robertson 1994), have shown that they are post-D<sub>1</sub> pre-D<sub>2</sub> intrusions and not post-D<sub>2</sub> pre-D<sub>3</sub> as stated by Bradbury et al. (1976). D<sub>1</sub> must have occurred between eruption of the Tayvallich volcanics, which have a U-Pb zircon age of 594±5Ma (Halliday et al. 1989, error re-calculated to 2σ), and intrusion of Ben Vuirich with a U-Pb zircon age of 590±2Ma (Rogers et al. 1989). D<sub>1</sub> gave rise to a series of upright folds under greenschist facies conditions (Treagus 1987). In the area around Ben Vuirich, the main structural event associated with porphyroblast growth was D<sub>2</sub> and not D<sub>3</sub> (Tanner & Leslie 1994). The age of D<sub>3</sub> (≈490Ma) is relatively well constrained by radiometric dates obtained from the Newer Gabbros which were intruded during and after D<sub>3</sub>, which is also coincident with peak metamorphism (Rb-Sr ages of Pankhurst 1970 and the mean <sup>207</sup>Pb/<sup>206</sup>Pb age from six magnetic fractions of discordant zircon, Jagger et al. 1988). Robertson (1994) has shown that D<sub>2</sub> and D<sub>3</sub> are linked by related mineral growth stages and fabric development, and it has been suggested that D<sub>2</sub> preceded D<sub>3</sub> by <10-20Ma (Tanner & Leslie 1994); consequently, D<sub>2</sub> is believed to have occurred between 510-490Ma and with D<sub>3</sub> at 490Ma.

There is no record of deformation along the Laurentian continental margin during the time span in which D<sub>1</sub> is thought to have occurred (599-588Ma, from the maximum analytical errors of Halliday et al. (1989) for Tayvallich and Rogers et al. (1989) for Ben Vuirich), leading to the proposal of Bluck & Dempster (1991) that the Dalradian basin was located on the margin of Gondwana and not Laurentia. In this location the Dalradian terrane underwent deformation associated with the Pan African 1 orogeny, before rifting from Gondwana and inclusion within the British Caledonides as an exotic terrane.

Figs. 2.1 and 2.2 are interpretations of the structural geology of the western Central Highlands after Thomas (1979). Webb (1977) presented a structural synthesis of the part of the Ben Nevis aureole. In this interpretation, an upright almost isoclinal synform, the Aonach Beag synform, represents regional D<sub>1</sub>, subsequent deformation, equivalent to D<sub>2</sub>-D<sub>3</sub>, produced minor folds and a crenulation cleavage; D<sub>4</sub> in this area is represented by kink bands. Mica growth coincides with D<sub>1</sub>-D<sub>2</sub> and the main metamorphic episode is associated with D<sub>3</sub>. In Fig. 2.1 however, the Stob Ban synform, a composite regional D<sub>2</sub> structure, is found in the same location as the Aonach Beag synform.

Key to structural abbreviations in Fig. 2.1.

AA	Ardrishaig Anticline	CS	Croftnagowan Synform
ACA	Allt Culaibh Antiform	DS	Dochard Synform
AHA	Airds Hill Anticline	ES	Errochty Synform
AN	Atholl Nappe	GCA	Glen Creran Synform
AS	Appin Syncline	GS	Garry Synform
BA	Bohespic Antiform	IBS	Iltay Boundary Slide
BaS	Ballachulish Slide	KA	Kinlochleven Anticline
BCA	Beinn Chuirn Anticline	KAf	Kinlochleven Antiform
BDS	Bealach Dubh Synform	KS	Kinlochleven Syncline
BIA	Blackwater Antiform	LAS	Loch Awe Syncline
BLA	Beinn na Lap Antiform	MA	Mamore Anticline
BLF	Ben Lui Fold	MBS	Meall Buidhe Synform
BUS	Beinn Udlaidh Syncline	MS	Mamore Syncline
CA	Clunes Antiform	OA	Glen Orchy Antiform
CCA	Cam Chreag Antiform	SBS	Stob Ban Synform
CCS	Creag Ghuanach Syncline	TA	Toaig Anticline
CMA	Creag A' Mhadaidh Antiform	TM	Trinafour Monoform

In the context of Fig. 2.1, the Ben Nevis Complex intrudes rocks deformed by the D<sub>1</sub> structures of the Appin syncline and the Kinlochleven anticline exposed in the western limb of the D<sub>2</sub> Stob Ban synform. To the northwest, the outermost exposures of the Ben Nevis Complex cross-cut the Fort William Slide, variously interpreted as a lag (Bailey & Maufe 1916 & 1960), an extensional listric fault (Soper and Anderston 1984) and an unconformable contact between Grampian Group and Dalradian Supergroup metasediments (Glover 1993).

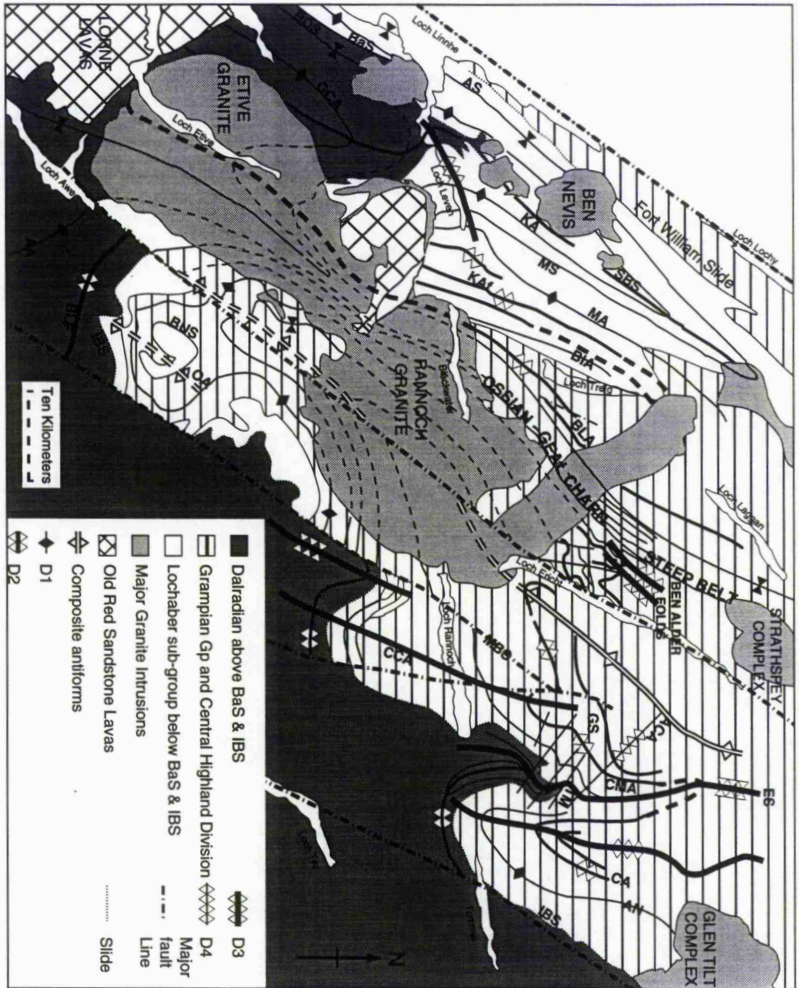


Fig 2.1 Structural geology of the South-central Highlands, adapted from (Thomas 1979).

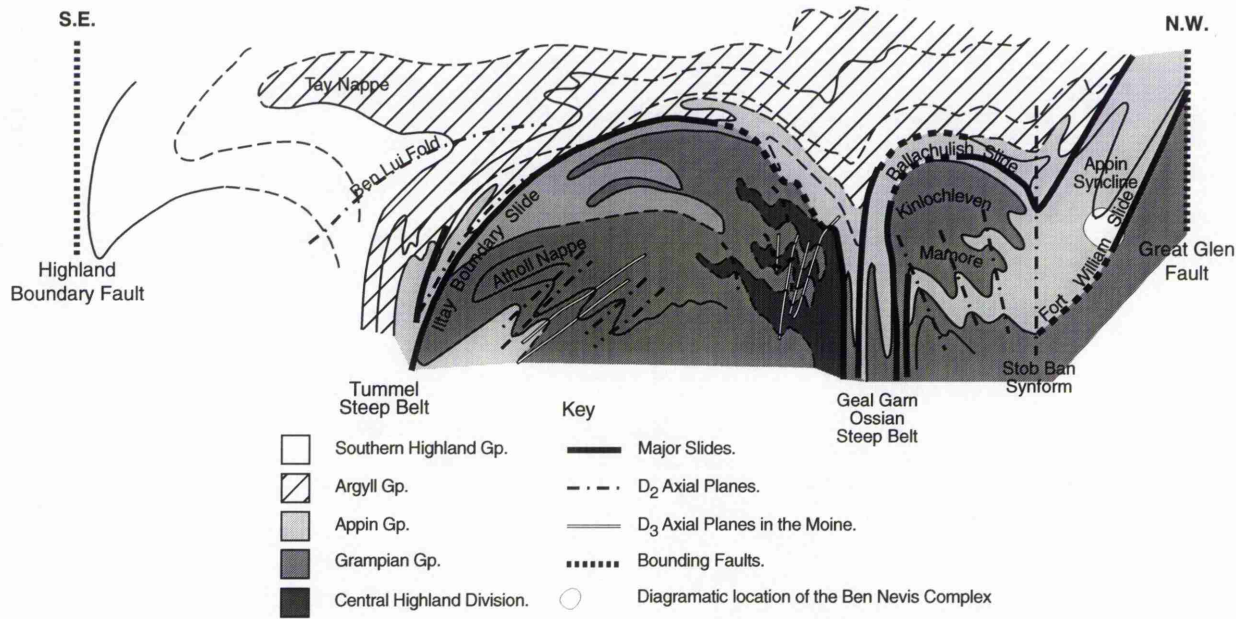


Fig. 2.2 Structural cross-section through the west Central Highlands, adapted from Thomas (1979).

### 2.2.3 Metamorphism

The metasediments of the Central Highlands are historically significant in that Barrow (1893 & 1912) developed his scheme of index minerals in this region. Regional metamorphic grade increases from greenschist facies in the SW to upper amphibolite in the NE. The metasediments of the Dalradian Supergroup and the Grampian Group around the Ben Nevis Complex are of garnet grade (Fig. 2.1), and were buried to a depth equivalent to 5kbars (Harte 1988).

Detailed work on part of the Dalradian Supergroup has revealed that burial and uplift was localised and discontinuous rather than regional and uniform (Dempster 1985). Harte (1988) refined Dempster's (1985) conclusions into a model where the evolution of the Dalradian Basin was controlled by major crustal lineaments subdividing the basin into a number of discrete domains or provinces. Variations in the rates of burial, uplift, cooling and heat conductivity resulted in the development of different PTt paths for each fault controlled domain.

## 2.3 Caledonian Magmatic Activity

Igneous activity accompanying the development of the Caledonian mountain belt has been grouped by Read (1961) into pre, syn and post-tectonic episodes. For a detailed discussion of all the various aspects of Caledonian magmatic activity in Northern Britain, the reader is referred to Read (1961), Stephens (1988) and Brown (1992). The granitoid intrusions and the Old Red Sandstone lavas of Scotland are displayed in Fig. 2.3.

### 2.3.1 Younger Basic magmatism

A series of basic intrusions was emplaced within the Dalradian Supergroup during peak metamorphism (Fettes 1970). Contact metamorphic aureoles are preserved (Droop & Charnley 1985) and structural interpretations indicate a syn-post D<sub>3</sub> age (Fettes 1970).

### 2.3.2 Older Granites

Granites that intrude previously deformed Caledonian sediments, but are themselves deformed and metamorphosed by subsequent regional metamorphism and deformation outcrop at Ben Vuirich (590 ±2Ma), Dunfallandy Hill, Meall Gruaim and Glen Tilt. These intrusions post-date D<sub>1</sub> and have tectonic fabrics imposed by D<sub>2</sub> (Robertson 1994 and Tanner & Leslie 1994). Also included within the Older Granite group are outcrops of augen gneiss at Portsoy. Pankhurst (1974) interpreted a whole-rock Rb-Sr age of 655±10Ma as the age of intrusion, Sturt et al. (1977) argued that these and other migmatitic gneisses represent basement rocks tectonically emplaced in the Dalradian cover.

Key to locations in Fig. 2.3.

1. Strath Halladale
2. Ben Loyal
3. Helmsdale
4. Lairg-Rogart
5. Borralan
6. Migdale
7. Fearn
8. Carn Chuinneag
9. Ratagain
10. Abriachan
11. Cluanie
12. Glen Dessary
13. Strontian
14. Ross of Mull
15. Ballachulish
16. Etive
17. Glencoe
18. Ben Nevis
19. Rannoch Moor
20. Strath Ossian
21. Strathspey
22. Foyers
23. Glen Kyllachy
24. Findhorn
25. Moy
26. Ardclach
27. Grantown
28. Ben Rinnes
29. Aberchirder
30. Longmanhill
31. Strichen
32. Peterhead
33. Kennethmont
34. Bennachie
35. Monadhliath
36. Cairngorm
37. Glen Cairn
38. Lochnagar
39. Ballater
40. Hill of Fare
41. Skene complex
42. Aberdeen
43. Auchlee
44. Kincardine (Mt Battock)
45. Comrie
46. Garabal Hill
47. Arrochar
48. Distinkhorn
49. Cairnsmore of Cairnsphairn
50. Loch Doon
51. Cairnsmore of Fleet
52. Criffell-Dalbeattie

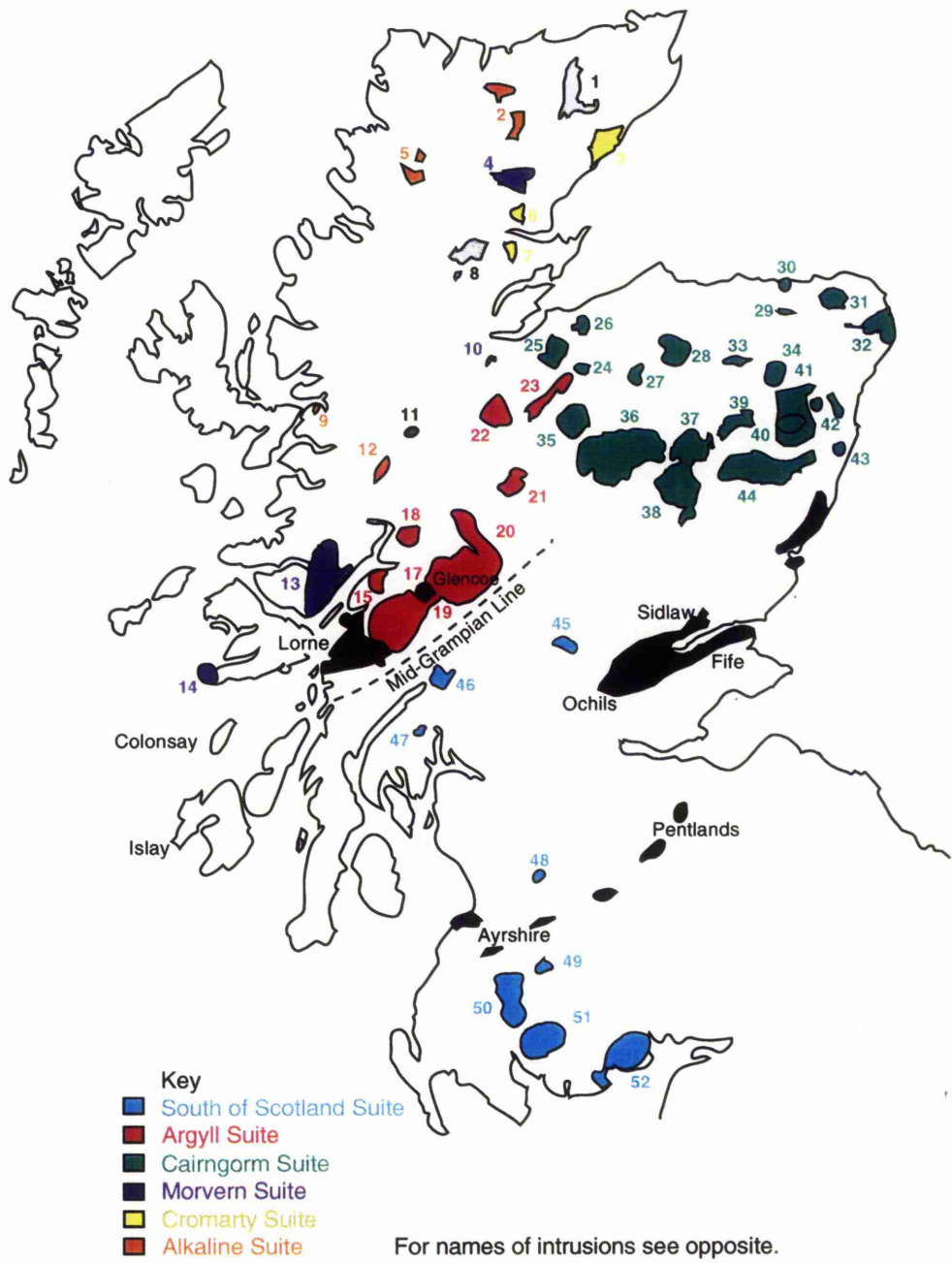


Fig. 2.3 Distribution of ORS lavas and Newer Granite suites in Scotland.

### 2.3.3 Alkaline intrusions of the NW Highlands

In the NW Highlands, alkaline magmatic activity spans a period of 25-30Myrs and constrains the age of movements along the Moine Thrust. (Halliday et al. 1987 and van Breemen et al. 1979 a&b). Isotopic and chemical modelling of individual plutons has developed a series of models that are discussed in chapter 7.

A single exposure of carbonatite has been observed in the vicinity of the Loch Borrallan pluton (B. Young pers. comm. to Brown 1992).

### 2.3.4 Newer Granites

The Siluro-Devonian suite of granite plutons in the British Caledonides, known as the Newer Granites (Read 1961), together with coeval Old Red Sandstone (ORS) volcanics are amongst the most intensively studied examples of calc-alkaline magmatism anywhere in the world. Although often referred to as granite, Newer Granite plutons also contain substantial volumes of diorite, tonalite, granodiorite and adamellite and should be properly referred to as granitic or granitoid. By the far the greatest number of Newer Granite plutons are found within the Central Highlands.

Enrichments in Na, Ba and Sr are considered to be characteristic of the Newer Granite province (Halliday & Stephens 1984). Stephens & Halliday (1984) divided the Newer Granite province into a number of suites based on variations in trace element chemistry. The geographic distribution of these suite is shown in Fig. 2.3. The authors believed that variations between the different suites are generated by differences in magma source and melting conditions.

Various workers have applied the I & S-type classification scheme (Chappell & White 1974) to the Newer Granite suite. The majority of plutons are I-type and very few are strongly peraluminous. Cairnsmore of Fleet and part of the Criffell pluton, are notable exceptions with O and Sr isotope characteristics tending to S-type (Stephens & Halliday 1984) These two plutons are chemically more closely related to those Newer Granites outcropping south of the Iapetus suture than to other granitic plutons in the South of Scotland.

Early regional major element studies (Nockolds & Mitchell 1946, Nockolds & Allen 1953 and Mercy 1963 ) and later geochemical studies on individual plutons (e.g. Strontian - Sabine 1968, Ben Nevis - Haslam 1965) revealed no distinct differences in chemical composition between the Older and Newer Granites and the origin of both granite groups was attributed to crustal anatexis and subsequent fractional crystallisation. This hypothesis, although compatible with estimated Dalradian P-T indicators (Richardson & Powell 1976), was questioned on geophysical, trace element and isotopic grounds and a substantial lower crustal or mantle input to the Newer Granite magmas was proposed (Pankhurst 1979, Plant

et al. 1983 and Brown & Locke 1979). The geochemical and isotopic geology of the Newer Granite province is discussed more fully in chapter 7.

### 2.3.5 Old Red Sandstone Lavas

Calc-alkaline volcanic rocks of Old Red Sandstone (ORS) age are found throughout Northern Britain, including, Shetland, Orkney, Lorne, Glencoe, Ben Nevis, Sidlaw and Ochills Hills, Pentland Hills and in the Cheviots. All are associated with continental sediments of the ORS, which is usually regarded as Devonian in age, but in fact extends from the Wenlock (Thirlwall 1988 and Marshall 1991) into the Dinantian (Paterson & Hall 1986). The overwhelming majority of ORS volcanism is Silurian (Thirlwall 1983). ORS sedimentation and volcanism on Ben Nevis and in Glencoe are discussed in chapter 3.

#### 2.3.5.i Shetland and Orkney

Three distinct volcanic sequences are recognised in the Shetland ORS (Mykura 1976), spores extracted from interleaved sediments are of middle Devonian age (Marshall pers. comm. to Thirlwall 1984). The rocks are transitional from calc-alkaline to tholeiitic and the final ORS volcanic episode in Scotland, the Hoy lavas of Orkney, includes alkali olivine-basalts and hawaiites heralding the onset of Carboniferous volcanism (Thirlwall 1979).

Geochemically, Shetland and Orkney volcanics have trace element patterns consistent with subduction.

#### 2.3.5 ii Lorne

The lavas of the Lorne plateau cover an area of 300km<sup>2</sup> and attain a thickness of 800m (Groome & Hall 1974) above a Dalradian basement. Although basalt and andesite dominate the succession, rhyolite and two tuff horizons are also found (Kynaston 1903). Groome and Hall (1974) reported that, whereas the basalts and andesite are closely related, the rhyolites are not part of the same fractionation series. The ignimbrites of Glencoe have been correlated with the two tuff horizons of the Lorne Plateau (Roberts 1974), which Kynaston (1903) described as the "product of showers of minute glassy particles ejected from a volcanic orifice by discharge of a highly explosive character". This interpretation was written prior to the recognition of nuées ardentes or calderas. Andesites chemically similar to those of Lorne are found in the Glencoe caldera.

Chemically and isotopically the basaltic lavas of the Lorne Plateau have primitive subduction related patterns (Thirlwall 1981) and, relative to ORS volcanics of Shetland and the Midland Valley, are enriched in Ba, K and Sr.

### 2.3.5.iii Sidlaw, Ochills and Pentland Hills

In the northern part of the Midland Valley, up to 2,400m of basalt and andesite with rare rhyolite are exposed, but no base is seen. In the south of the Midland Valley, 300-2,000m of basalt, andesite and rhyolite are conformable with Silurian sediments that show progressive shallowing from deep marine to continental facies. Substantial volumes of andesite, dacite and rhyolite are found as clasts within the ORS sandstones of the Northern Midland Valley and it is inferred that eruption of these rocks along or to the north of the Highland Boundary Fault was followed penecontemporaneously by erosion. There is evidence of caldera activity from ignimbrites recognised near Dunkeld (Paterson & Harris 1969). Vent agglomerates near Maybole and Dalmellington provide evidence for local eruptive centres in the Pentland Hills.

### 2.3.5.iv Cheviots

Volcanic rocks in the Cheviots hills form a 900m thick pile of two pyroxene andesites resting unconformably on Wenlock turbidites. They are at least 10Ma younger than those ORS volcanics outcropping further north (Thirlwall 1988), and also show marked chemical and isotopic differences from the northern exposures, although a subduction signature is still noticeable despite the fact that the Cheviot volcanics span the trace of the Iapetus suture in Northern Britain and could not therefore, be generated by subduction of Iapetus either northwards beneath Scotland, or southwards beneath England and Wales.

## 2.4 The closure of Iapetus

The Caledonian mountain belt was formed in response to the closure of the Iapetus Ocean. Early models for the closure of Iapetus invoked orthogonal E-W closure between two ancient continents; Gondwana and Laurentia and dextral strike-slip along the British sector (e.g. Dewey 1969 and Phillips et al. 1976). But Soper (1986) stated that "Insurmountable problems of distribution and timing arise when attempts are made to relate the magmatic activity (late Caledonian) as a whole to a traditional two-plate collision model for the orogeny".

Watson (1984) suggested that active subduction was not the primary mechanism for the generation of late Caledonian magmas and a two-stage process was put forward. Fluids emanating from a subducting slab metasomatised the overlying mantle wedge, subsequent post-subduction movement of basement blocks triggered partial melting of 'pickled' mantle and resulted in the emplacement of magmas with subduction zone characteristics.

Soper and his fellow workers advocated active subduction as the primary mechanism, but along a number of subduction zones rather than just one centred along the Solway Line

(Fig. 2.4). Three collision events affecting Northern Britain are described in Soper et al. (1992), namely:

1) Oblique collision between Greenland (then part of Laurentia) and Baltica during the Scandian orogeny (Ordovician- Silurian) led to crustal scale imbrication in the Scottish Caledonides with final closure of the intervening ocean  $\approx 420$ Ma. Docking of Western Avalonia with previously accreted Dunnage and Gander terranes on the western margin of Laurentia also occurred at this time.

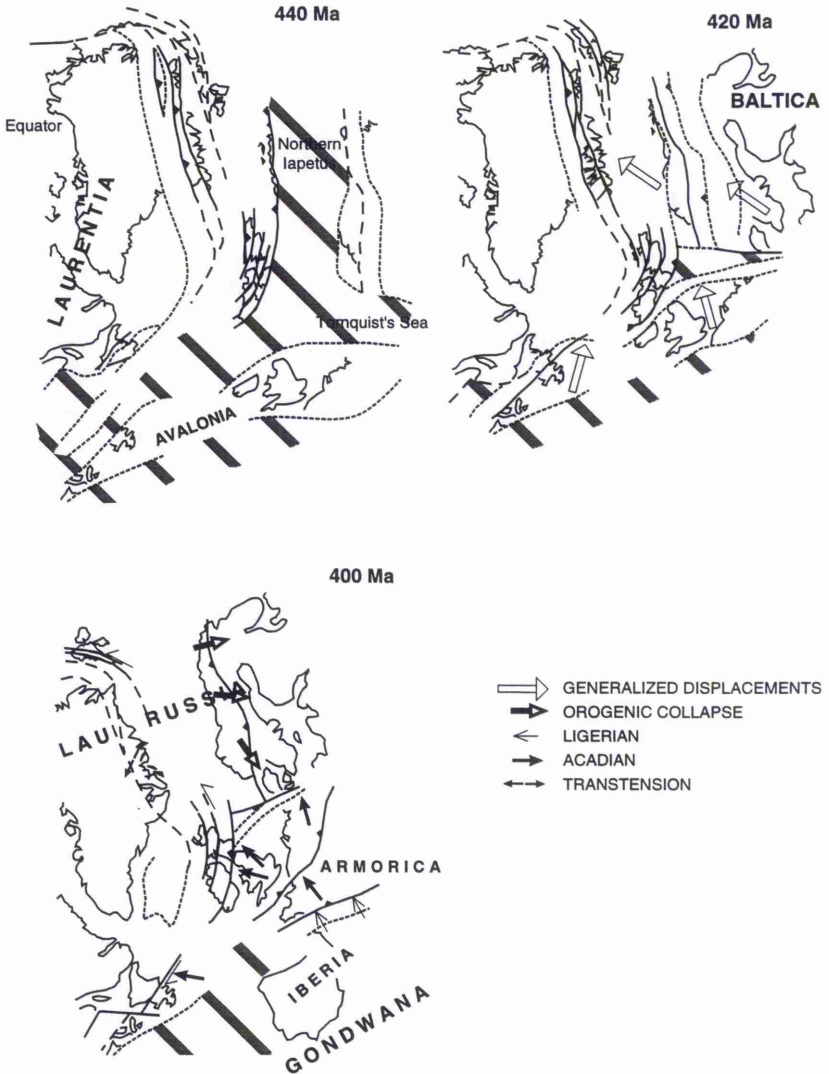


Fig.2.4. Cartoon reconstructions to illustrate the Silurian closure of Iapetus, and the presence of micro-plates and multiple subduction zones, adapted from Soper et al. (1992).

2) Soft collision of Eastern Avalonia and anticlockwise rotation against the Scottish corner of Laurentia led to progressive west to east closure of a wedge shaped remnant of Iapetus. Closure was largely complete by  $\approx 430\text{Ma}$  in Ireland and  $\approx 420\text{Ma}$  in Northern Britain (Soper & Woodcock 1990).

3) A collision between Armorica & Iberia with Eastern Avalonia & Baltica during the early Devonian ( $\approx 400\text{Ma}$ ) was invoked by Soper et al. (1992) to account for deformation within the slate belts of Northern Britain, and a change in cleavage orientation across Northern Britain from a NE-SW Appalachian trend to a ESE-WNW Tornquist trend of the Mid European Caledonides (Soper et al. 1987).

Soper et al. (1992) extend the use of 'Acadian' from Devonian deformation in the northern Appalachians to broadly contemporaneous deformation (event 3 above) in the slate belts of Northern Britain. Sinistral transpression accompanied both event 2 and event 3 (Hutton & McErlean 1991), and many of the faults that were active during these collision events are thought to have played a fundamental role during the intrusion of the Newer Granites (Hutton 1988a, Rogers & Dunning 1991, Pitcher 1993 and Jacques & Reavy in press).

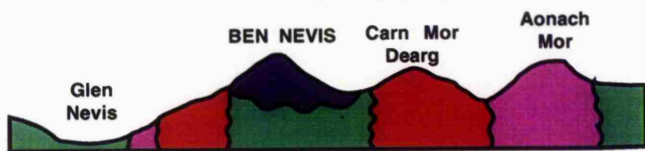
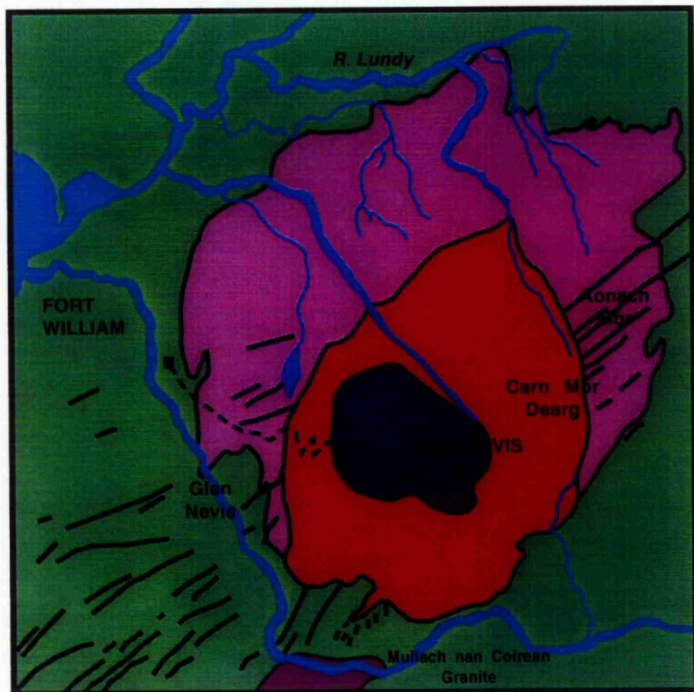
Thirlwall (1988) argued for the closure of Iapetus in the early Devonian based on the eruption of lavas with subduction related signatures north of the Southern Uplands Fault, but there is abundant geophysical (Klemperer et al. 1991), sedimentological (Soper & Woodcock 1990) and palaeontological (Cocks & Fortey 1990) evidence for closure in the Silurian.

## 2.5 Ben Nevis

The Ben Nevis volcanic-plutonic Complex consists of a central core of volcanic rocks resting unconformably on a Dalradian basement and completely enclosed by the Inner Granite that is in turn partially enclosed, along two thirds of its circumference, by the Outer Granite (Fig. 2.5). These units form an oval-shaped area of  $\approx 45\text{km}^2$  with a N-S long axis of 9km and an E-W axis of 7km. Fig. 2.6 shows the Ben Nevis Complex in terms of the surrounding geology.

### 2.5.1 Intrusive members of the Ben Nevis Complex

The evolution of early geological theories for the origin of Ben Nevis, which range from layer cake oceanic chemical precipitates (Macknight 1811 & 1821) to the recognition of the granites as igneous intrusions (Macculloch 1817) and of the volcanics first as intrusions (von Oeynhausien & von Dechen 1830) and then extrusions (Bryce 1864 and Judd 1874), is summarised in both editions of the Geological Survey memoir (Bailey & Maufe 1916 & 1960). Ben Nevis is omitted from Geikie (1897) and Glen Coe is described merely as an outlier of the Lorne Series.



Key

- |   |   |
|---|---|
|  Metamorphic   |  Volcanic Pile |
|  Outer Granite |  Ben Nevis     |
|  Inner Granite |  Dyke Swarm    |

Fig 2.5. Geological Survey map of the Ben Nevis volcanic-plutonic Complex (Bailey & Maufe 1916).

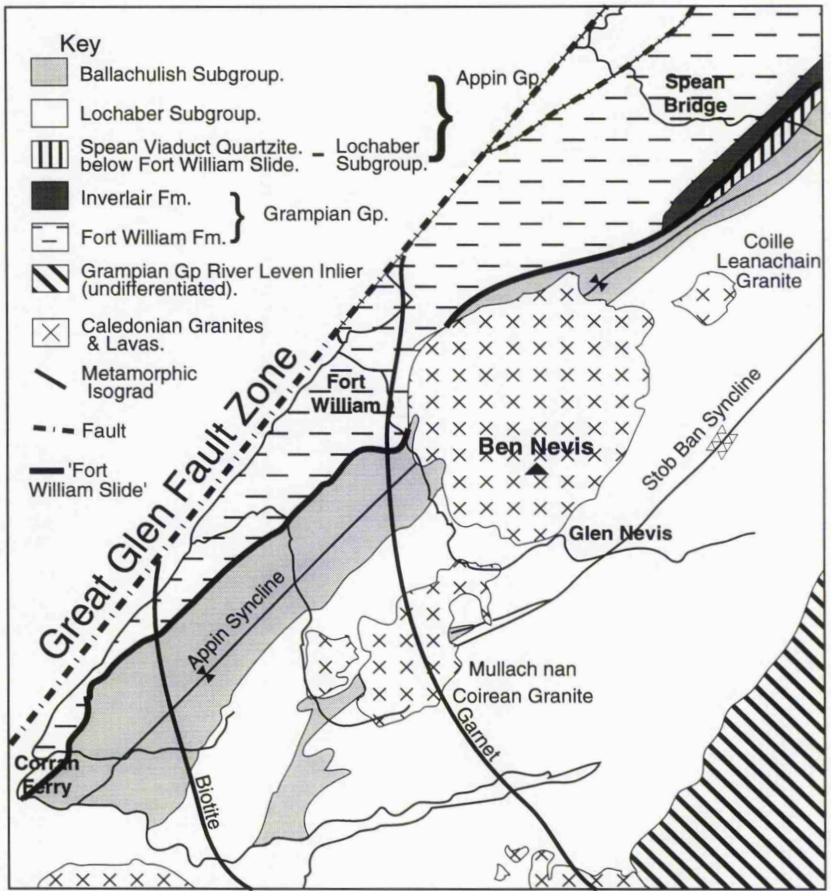


Fig. 2.6. The Geology around the Ben Nevis Volcanic-plutonic Complex, adapted from Glover (1993).

Most of the Geological Survey mapping of Ben Nevis was carried out by E. Wilson at the turn of the twentieth century, but it was left to Maufe (1910) to publish the results after largely re-mapping the area. Maufe recognised three units within the Ben Nevis Complex which he termed the Outer Granite, the Inner Granite and the volcanic pile. Maufe recognised a basic non-porphyrific margin to the Outer Granite, but no further data were presented on the nature of this margin due to the lack of time.

An account of the geology within the BAA hydroelectric tunnel stretching from Loch Treig to Fort William, and running in part through the Outer Granite, was presented by Peach (1930). This account stimulated Anderson (1935) to study the Outer Granite in more detail.

Anderson (1935), as well as subdividing the Outer Granite, also observed that the non-porphyrific margin became more acidic on the easternmost and highest granite outcrops. It was suggested that the increase in silica content from E-W was due to gravitational differentiation. Haslam (1965) tried to pursue this idea further, but was unable to because of the complexity of the non-porphyrific margin. Both Anderson (1935) and Haslam (1965) believed that the units making up the Outer Granite formed a once continuous ring which was removed in part by the subsequent intrusion of the Inner Granite.

The main thrust of Haslam's thesis (1965) and the accompanying paper (Haslam 1968) was a study of the chemistry of the Ben Nevis granites, their mineralogy and the conditions under which they crystallised. The absence of primary magmatic hornblende in all but the most acidic units was attributed to intrusion high into the crust. In the place of hornblende, primary magmatic pyroxene crystallised. During further cooling, pyroxene became unstable and was partially or wholly replaced by secondary low alumina hornblende.

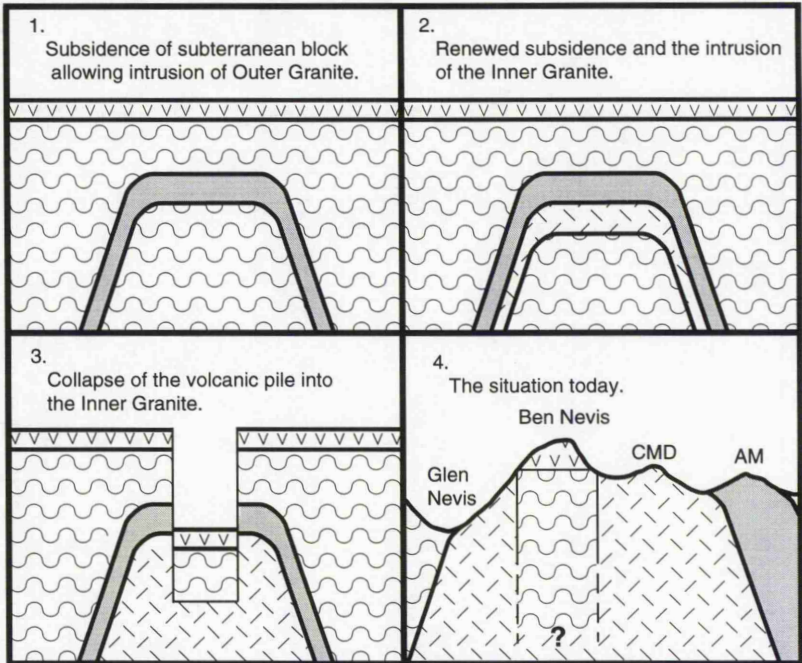
Haslam (1965) also noted that the ferromagnesian minerals in the more acidic rocks contained more magnesium than the more basic rocks. This phenomenon, which is the reverse of normal magmatic trends, was attributed to an unusually high and constant partial pressure of oxygen, possibly derived in part from an atmospheric connection.

Haslam(1970) described appinites exposed at the surge chamber (NN 134 750) and in the Red Burn (NN 134 716) which he considered to be the reaction products between the outer granite margin and the adjacent Ballachulish Limestones.

#### 2.5.2 Extrusive members of the Ben Nevis Complex

The only detailed account of the volcanic pile is found in Bailey & Maufe (1916) and is essentially unchanged in the second edition of the memoir (Bailey & Maufe 1960). The Geological Survey documents the inter-stratification of 'agglomerate' with andesite and recognises the difficulty in differentiating between 'agglomerate' and autobrecciated andesite. The base of the volcanic pile rests on Dalradian schists, presumably Leven Schist,

and is exposed along two sections of the volcanic pile/Inner Granite margin (Fig. 2.5). Immediately between the Dalradian basement and the first volcanic rocks is a thin sequence of finely laminated muds and massive conglomerates. Small exposures of mudstone are scattered throughout the volcanic pile. The volcanic pile has a basin-like structure with steeply dipping margins and a gently dipping to flat core, Maufe (1910) believed that this feature was due to friction with the adjacent Inner Granite during subsidence of the volcanic pile. No dykes were observed in the volcanic pile and the classic Survey model for the evolution of the Ben Nevis Complex is shown in Fig. 2.7.



### KEY

-  Plateau Lavas
-  Inner Granite
-  Outer Granite
-  Dalradian Schists
- CMD - Carn Mor Dearg
- AM - Aonach Mor

Fig. 2.7 The Geological Survey model for the evolution of the Ben Nevis volcanic-plutonic Complex.



# CHAPTER 3

## THE VOLCANIC PILE

### 3.1 Introduction

#### 3.1.1 General statement

During the period of Lower Old Red Sandstone deposition an extensive cover of lava and volcanic breccia was formed above a basement of crystalline schists and contemporaneous sediments. Of this once extensive cover, only relatively minor exposures remain within the Scottish Highlands, these being: the Lorne Plateau lavas, the Glencoe caldera and the volcanic pile of Ben Nevis. This chapter presents the first detailed field study of the Ben Nevis volcanic pile since the early part of the twentieth century when the area was mapped on behalf of the then Geological Survey Office by E.B. Maufe.

Geochemical and mineralogical data for the volcanic pile will be discussed in chapters 5 and 6. Although, the majority of the andesites sampled fall within the fields of trachydacite - dacite on a TAS (total alkalis vs silica) diagram (Fig. 3.1), the field term andesite will be used throughout this chapter in keeping with previous work.

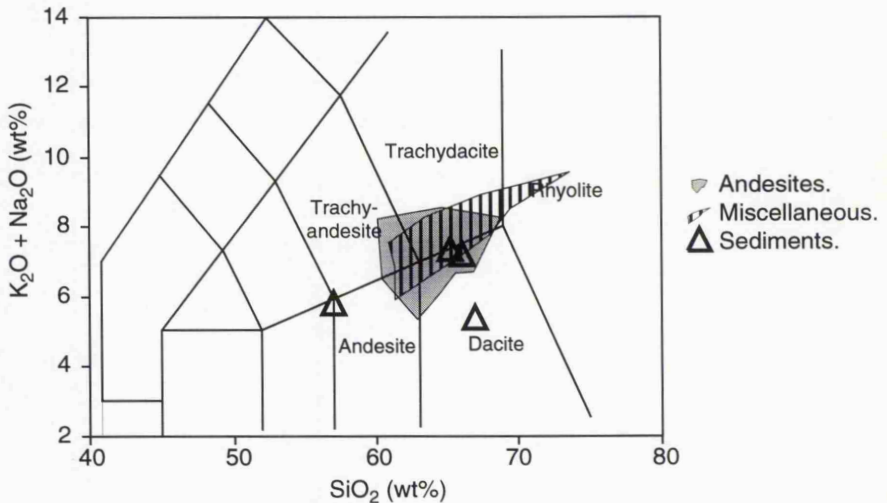


Fig. 3.1 TAS diagram for the Ben Nevis volcanic pile. The majority of samples are not andesitic but trachydacite to dacite. The miscellaneous group includes intrusions within the volcanic pile and clasts from volcanic breccias. The diagram also illustrates that the sediments are compositionally similar to the volcanic rocks suggesting a large volcanic ash content.

### 3.1.2 Volcanological Terminology

There is no unique approach to classifying modern or ancient volcanic successions Cas & Wright (1988). For this reason the following section presents the classification system used throughout this thesis, and is largely based on Cas & Wright (1988) and Schmid (1981) to which the reader is referred for a more detailed discussion. Two separate classification systems are applied to ancient volcanic terrains; a genetic classification and a lithological classification. Cas & Wright (1988) stated that the genetic classification can only be rigorously applied to modern volcanic terrains. A lithological classification is primarily descriptive and records the major characteristics of a deposit and its constituent fragments. These features may indicate a particular process and provide some evidence for the genesis of a deposit. Table 3.1a (Cas & Wright 1988) provides a useful starting point for the classification of ancient volcanic rocks; if a pyroclastic origin can be established then Table 3.1b can be applied. Table 3.2 is a list of terms commonly used in this chapter along with a brief description.

### 3.1.3 Introducing calderas

Maufe (1910) and Bailey & Maufe (1916 & 1960) describe the Ben Nevis volcanic sequence as "...hornblende-andesite lavas with a fair proportion of agglomerate; a few thin bands of sediment are also found...". No volcanological interpretation was attempted. The similar chemistry of andesites from Glencoe, the Lorne plateau and Ben Nevis led Bailey & Maufe (1916 & 1960) to suggest that the three areas were extruded contemporaneously. It

Table 3.1a

Non-Genetic classification of **volcaniclastic** rocks (Adapted from Cas & Wright 1988).

Volcanic breccia - essential angular fragments	
closed framework	
open framework	
non-cohesive, granular matrix,	
cohesive mud-sized matrix	
Volcanic conglomerate - essential rounded fragments.	
closed framework	
open framework	
non-cohesive, granular matrix,	
cohesive mud-sized matrix	
2 mm -----2 mm	
Volcanic sandstone	
0.0625 mm-----0.0625 mm	
Volcanic mudstone	
Volcanic siltstone	
if sufficiently well sorted and volcanic origin is clear	
Volcanic claystone	

---

Table 3.1b

Grainsize limits for proven pyroclastic fragments and  
pyroclastic aggregates (Adapted from Fisher 1961, 1966).

Grain size (mm)	Pyroclastic fragments		Name of unconsolidated aggregate	Lithified equivalent
		Round and <u>fluidally shaped</u>		
		<u>Angular</u>		
256-----	coarse bombs	blocks	Agglomerate (bombs) or pyroclastic breccia	Agglomerate (bombs) or pyroclastic breccia
64-----			lapilli deposit	lapillistone
2-----	lapilli coarse			
1/16-----	ash fine		ash deposit	tuff

was stated that the Glencoe and Ben Nevis sites were not merely outliers of the Lorne plateau, but were sites of local volcanic activity that may have been contiguous with the Lorne lavas. Subsequently, a number of authors have quoted Bailey & Maufe (1916 & 1960) as believing that Glencoe and Ben Nevis were northerly remnants of the Lorne plateau (e.g. Mykura 1992).

These early geologists developed the following model for the preservation of volcanic rocks on Ben Nevis. After intrusion of the Outer Granite and Inner Granite "...a subaerial cauldron-subsidence developed, for the roof of the subterranean cauldron gave way, and a block of schists, with its burden of lavas subsided into still liquid Inner Granite. The motion developed a streaky flow-structure in the magma, which itself became chilled against the cool descending mass. The latter, during its subsidence, buckled into its basin shape by reason of the friction on its walls". The juxtaposition of the volcanic pile directly against the Inner Granite led Bailey & Maufe (1916 & 1960) to propose that Ben Nevis is analogous to Glencoe, but eroded to a deeper level. In Glencoe, the volcanic rocks of the subsided block are separated from the surrounding metamorphic rock by a thin sliver of granite, deemed the fault intrusion. Bailey & Maufe (1916 & 1960) regard the fault intrusion as "...an advance guard of the Cruachan granite".

Table 3.2

Commonly used terms and their definitions (based on Cas & Wright 1988),

**Volcaniclastic** - Any fragmental aggregate of volcanic parentage, regardless of origin. Non-genetic.

**Pyroclastic** - Fragmental aggregate formed by explosive volcanic activity and transported solely by processes directly related to this activity. Genetic.

**Epiclastic** - Fragmental aggregate, fragmented and/or transported by normal surface processes involving weathering and erosion. Genetic.

**Volcanic breccia** - Essential angular clasts, >64mm diameter which are predominantly volcanic in origin. Non-genetic.

**Nuées ardentes** - Often used as a blanket term for pyroclastic flows but should be restricted to small volume block-and-ash flows produced by the collapse of an actively growing lava flow or dome (La Croix 1904). Genetic.

**Ignimbrite** - Again often used as a blanket term. Following Sparks et al. (1973), ignimbrite is defined by Cas & Wright (1988) as: the rock or deposit formed from pumiceous pyroclastic flows irrespective of the degree of welding or volume. Ash flow tuff is often used for ignimbrites in American literature (after Smith et al. 1960) but the grain size in many deposits is in the lapilli or bomb size range. Genetic.

**Tuff** - Lithified equivalent of an ash deposit, grain size <2mm. Genetic.

**Eutaxitic** - a foliation in a pyroclastic flow, due to flattening of glass shards and pumice fragments by compaction immediately following deposition. Genetic.

**Debris flow** - Moving mass of mud and rock fragments, where very coarse to fine grain sediment is involved (mud flow - coarse material absent). Typically involves cohesive mud as the lubricating fluid and with sufficient strength to support large clasts. Genetic.

**Lahar** - Lahars are volcaniclastic rich debris flows that may or may not be generated as a direct result of volcanic activity (Crandell 1971). Lapidus (1987) restricts the term to hot volcaniclastic material but Cas & Wright (1988) include any debris flow dominated by volcaniclastic material regardless of hot or cold emplacement. In keeping with the other terms in this chapter, the scheme of Cas & Wright (1988) is adopted. Genetic.

In Clough et al. (1909) the volcanic sequence and its metamorphic basement played an essentially passive role during cauldron subsidence. More recent models, beginning with the work of Taubeneck (1967) and Roberts (1974), and culminating in that of Moore (pers. comm.), have presented a much more dynamic picture for the Glencoe cauldron. In Moore's model, the Group 2 and Group 3 lithologies of the volcanic sequence are intimately related to several episodes of caldera collapse. The Group 2 rhyolite is now generally regarded as a rheomorphic ignimbrite; Moore suggests that the eruption of this ignimbrite resulted in the formation of a caldera. Oversteepening of the caldera walls induced failure and the deposition of the Group 3 breccias. Sediments found within Groups 4 - 7 have been interpreted as caldera lake deposits.

There are two end-member scenarios for the evolution of the volcanic pile. Firstly, the volcanic pile represents a sequence of volcanic rocks unrelated to subsidence into the Inner Granite. The second scenario requires an active role for the volcanic deposits during formation of a caldera at the land surface. The validity of both these scenarios is discussed in section 3.7.

Typically, a caldera produces four products, these being:

- (i) A central block, that subsides into the underlying chamber and is bounded by a ring fault that may or may not contain remnants of the erupted magma.
- (ii) An ash flow tuff (or ignimbrite) which may pond into the depression caused by the subsidence of the central block, as well as flowing away from the centre of eruption.
- (iii) A large eruption column with juvenile magma being the dominant component.
- (iv) Oversteepening and slumping of the caldera walls results in megabreccias being incorporated within and above the syn-caldera collapse deposits.

For a typical caldera, the sequence shown in Fig. 3.2 would be expected.

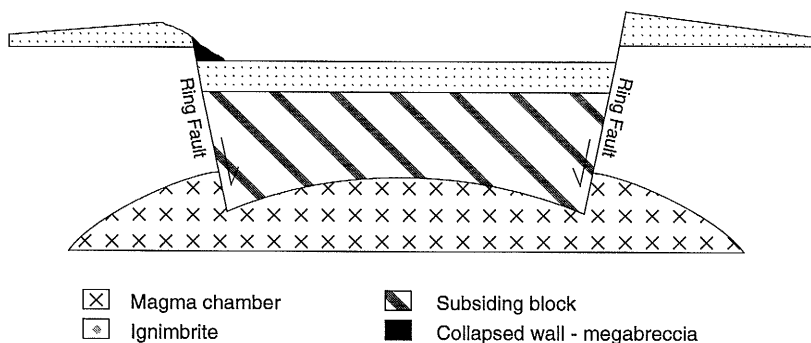
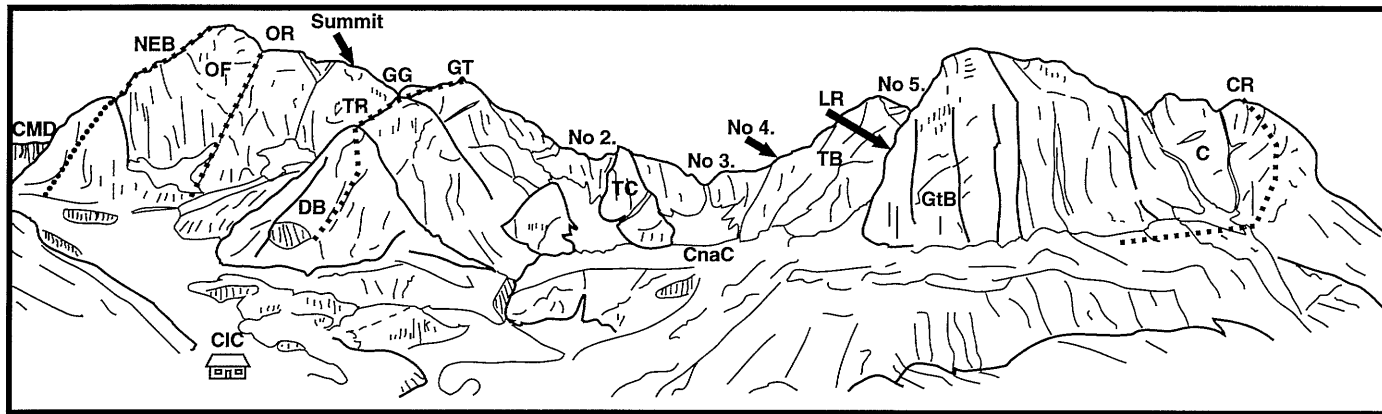


Fig. 3.2 Cartoon of an idealised cross section through a caldera.

When the roof of the chamber fails, the confining pressure is removed and volatiles flash out of solution. Explosion of gas bubbles fragments the magma producing large quantities of fine grained ash and pumice. As the fragmentation level descends deeper into the chamber, the overlying lava + gas mixture is explosively vented onto the surface. The resultant ejecta is dominated by glass shards that are recognised by concave bounding surfaces. Welding of ignimbrites is common, along with post eruption crystallisation and the development of hexagonal columnar jointing patterns. The formation of a welded ignimbrite is almost always related to caldera collapse (Cas & Wright 1988).

### 3.2 Terrain

Some 650m of mainly volcanic rock, underlain by an unknown thickness of Dalradian schist, is enclosed entirely within the Inner Granite and forms the summit of Ben Nevis. The area of outcrop is 3.5km<sup>2</sup>, much of which is covered by an extensive boulder field (the summit plateau) or rendered inaccessible by precipitous cliffs. Fortunately, the cliff line is broken by Coire na Ciste which affords relatively easy access to much of the volcanic succession. Localities mentioned in the text are displayed in Figs. 3.3a and 3.3b, see also Photos 1.4a, 1.4b and 1.5.

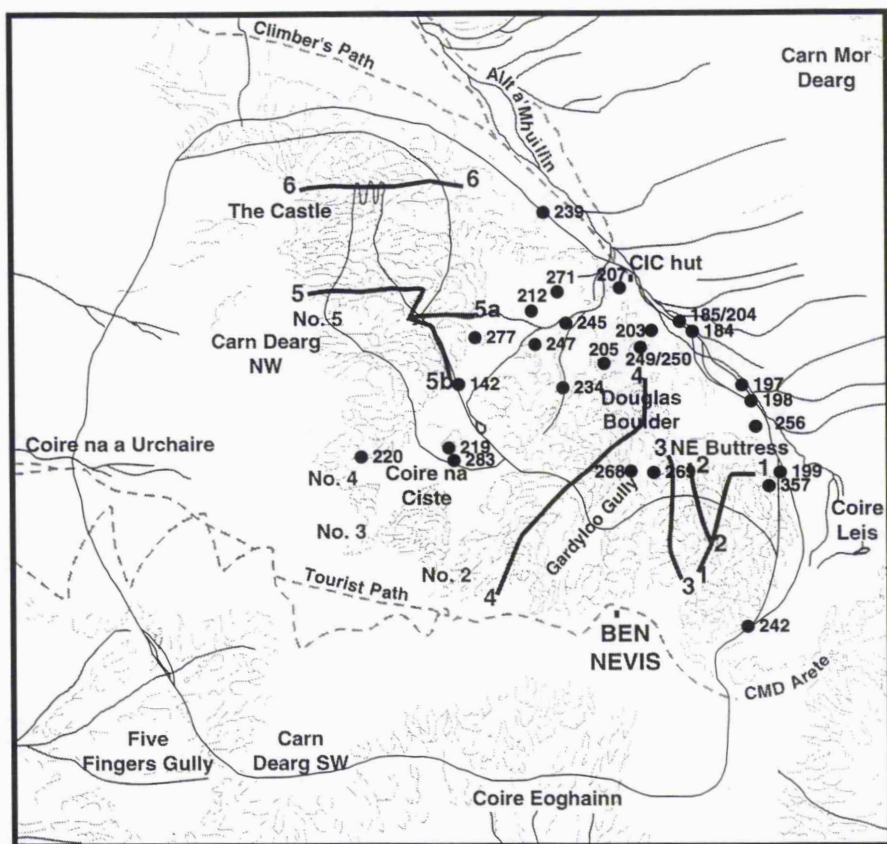


CMD = Carn Mor Dearg Arete  
 NEB = North-east Buttress  
 OF = Orion Face  
 OR = Observatory Ridge  
 CIC = CIC hut  
 DB = Douglas Boulder

TR = Tower Ridge  
 GG = Gardylloo Gully  
 GT = Great Tower  
 TC = The Comb  
 CnaC = Coire na Ciste  
 TB = Trident Buttress

GtB = Great Buttress of Carn Dearg  
 C = The Castle  
 CR = Castle Ridge  
 No 2. = Number 2 Gully  
 LR = Ledge Route (see Fig 1.4b)  
 .... = Route of Climb

Fig. 3.3a The North Face of Ben Nevis (see also Photo 1.4a).



Key

- |                      |  |
|----------------------|--|
| 1. NE Buttress       | 5a. Ledge Route No.5 Gully variation     |
| 2. Long Climb        | 5b. Ledge Route Coire na Ciste variation |
| 3. Observatory Ridge | 6. Castle Ridge                          |
| 4. Tower Ridge       | No. 2 - No. 2 Gully                      |

● 242 Locality referred to in the text.

0.5 km

Fig. 3.3b The location of the main topographical features, climbing routes and exposures mentioned in the text.

Problems with the identification of ancient volcanic products are highlighted by Krauskopf (1948). If the lava field of Paracutin were buried and then exhumed, Krauskopf (1948) suggested that " ... it would be difficult to trace the boundaries between one (lava) flow and the next, since different tongues of the same flow would overlap with one another and since some flows would have moved under an older one. Massive lava and several different kinds of breccia would be intricately interlayered".

### 3.3 Previous research

Bryce (1864) first recognised that the 'porphyry' of Ben Nevis was a succession of lava sheets separated by masses of agglomerate. Teall (1888) described a specimen of lava from the summit as hornblende andesite.

Mackie (1907) sectioned a sample of what he believed to be flow brecciated andesite and found it to be an air fall tuff (lithified ash). This conclusion is equivocal because no tuffs were found *in situ* on Ben Nevis during the present study; the sample studied by Mackie (1907) was obtained from a boulder by the side of the tourist path and could conceivably have once been a tuffaceous clast contained within a volcanic breccia.

The most detailed account of the volcanic pile is found in Bailey & Maufe (1916 & 1960). This account is the first to mention the existence of Dalradian schists at the base of the volcanic pile and the authors also note that volcanic pile has a basin-like structure. Minor contact metamorphism of the volcanic pile at the contact with the Inner Granite, coupled with intense chilling and 'crushing' of the Inner Granite, led Maufe (1910) to the conclusion that the volcanic pile had collapsed into the Inner Granite by a process known as cauldron collapse (Clough et al. 1909) (see Fig. 2.7).

### 3.4 Relative age of the volcanic pile

Brown (1972) obtained three whole rock K-Ar ages for the volcanic rocks, these are listed below. In addition, Brown (1972) published a whole rock Rb-Sr age for the volcanics and this is also listed below; no grid references or geochemical data accompanied this information.

K-Ar Whole rock -  $411 \pm 6$ Ma

K-Ar Whole rock -  $416 \pm 5$ Ma

K-Ar Whole rock -  $390 \pm 5$ Ma

Rb-Sr Whole rock -  $413 \pm 5$ Ma. Three samples analysed, one of which is described as a lithic tuff.

The volcanic rocks of the Ben Nevis Complex rest on Dalradian schists and are intruded by flow banded rhyolite veins (intrusion type 1; see section 3.6) which are believed to have been injected from the Inner Granite/Fault facies. Bailey & Maufe (1916 & 1960) believe that the volcanics are of comparable age to the Glencoe caldera on the basis of

similar sediment lithologies. No dykes were found by the authors within the volcanic pile and this was attributed to occurrence of the volcanic pile above the level of dyke injection (Bailey & Maufe 1916) or injection of the dyke swarm from a ring dyke of greater radius than the present outcrop of the volcanic pile (Bailey & Maufe 1960). During the current study a felsite dyke was found intruding the Summit Formation in Five Fingers Gully. Elsewhere within the Ben Nevis Complex, felsite dykes are only found in Allt Coire an t-Sneachda and in a nameless burn immediately to the east of Allt Coire an t-Sneachda. These dykes are cross-cut by, or are intruded into the earliest pulses of the Outer Granite and therefore represent one of the earliest magmas within the plutonic sequence. Consequently, the volcanic pile is believed to have formed before or during the intrusion of the earliest granitic magmas.

### 3.5 Stratigraphy

The volcanic pile can conveniently be sub-divided into four formations (Fig. 3.4), these being in ascending order:

- 1) The Allt a' Mhuillin Formation
- 2) The Coire na Ciste Formation
- 3) The Ledge route Formation
- 4) The Summit Formation

The Allt a' Mhuillin Formation rests unconformably on a basement of Dalradian schist which is correlated with the Leven Schist Formation (Bailey & Maufe 1916 & 1960).

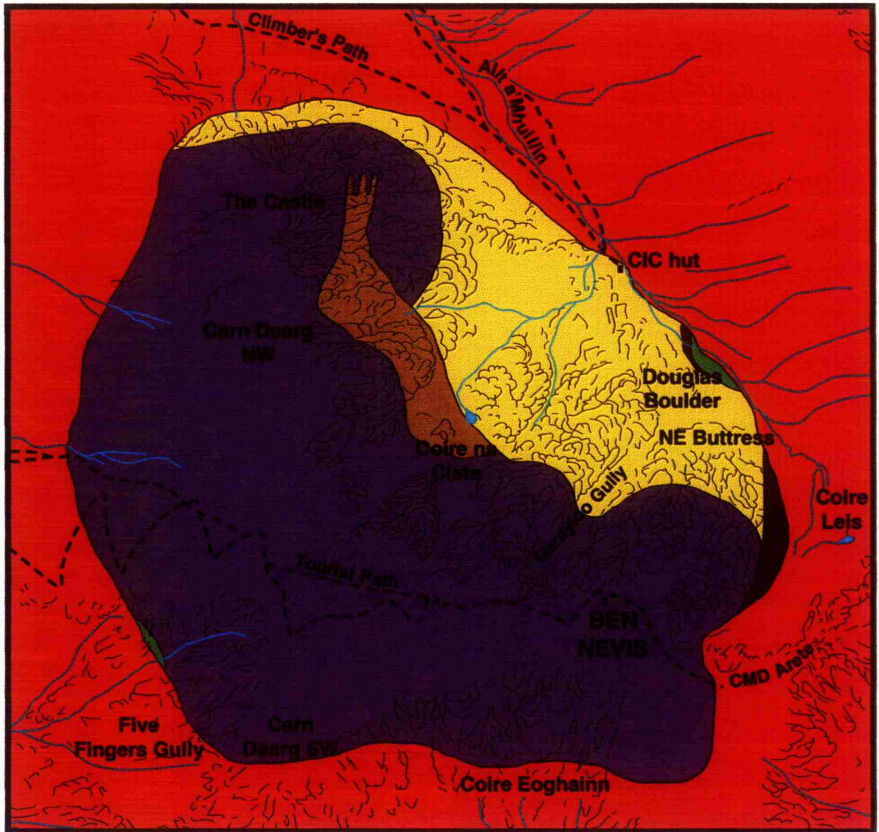
#### 3.5.1 The Dalradian Basement

Two exposures of Dalradian basement are found at the base of the volcanic pile.

##### 3.5.1.ii Allt a' Mhuillin Dalradian exposure

Exposed in the stream bed and on the west bank of the Allt a' Mhuillin, 200m upstream from the CIC hut, are a number of exposures of Dalradian pelite and semi-pelite. These form an outcrop area never more than 15m wide (measured perpendicular to the volcanic pile/Inner Granite contact), and exposed for 150m parallel to the contact. Immediately at the contact with the Inner Granite, the Dalradian has suffered much fracturing and alteration from the passage of fluids along the fractured zone. Normally underwater, but exposed during longer dry spells, a small patch (<20cm diameter) of quartzite is exposed beneath metapelite.

Two styles of deformation can be identified within the schists. An earlier fold dominated style (Photo 3.1), presumably related to regional Caledonian events, followed by a later brittle faulting episode that is related to the collapse of the volcanic pile into the Inner Granite.



Key

Extent of Dalradian in Five Fingers Gully is exaggerated.

- |  |  |
|--|--|
| <span style="display: inline-block; width: 15px; height: 10px; background-color: #388e3c; border: 1px solid black; margin-right: 5px;"></span> Dalradian Basement. | <span style="display: inline-block; width: 15px; height: 10px; background-color: #8b4513; border: 1px solid black; margin-right: 5px;"></span> Ledge Route Fm.     |
| <span style="display: inline-block; width: 15px; height: 10px; background-color: #2e2e62; border: 1px solid black; margin-right: 5px;"></span> Alt a' Mhuillin Fm. | <span style="display: inline-block; width: 15px; height: 10px; background-color: #4b2c82; border: 1px solid black; margin-right: 5px;"></span> Summit andesite Fm. |
| <span style="display: inline-block; width: 15px; height: 10px; background-color: #f1e025; border: 1px solid black; margin-right: 5px;"></span> Coire na Ciste Fm.  |  |

Fig. 3.4 Geographical distribution of lithostratigraphic formations of the Ben Nevis volcanic pile.

Two andesitic breccia 'veins' intrude the pelites at BN198 (NN 1698 7018). One end of the larger of these two veins (0.5m thick) can be seen to terminate within the area of Dalradian outcrop. The andesite breccia becomes progressively more contaminated by Dalradian fragments before passing into a zone of deformed metasediments. These 'veins' are similar in character to the first andesite unit of the Coire na Ciste Formation, exposed above the Allt a' Mhuillin Formation in the banks of the Allt a' Mhuillin, and may therefore represent the feeder pipes to this andesite.

#### 3.5.1.ii Five Fingers Gully (Coire Ghaimhnean) Dalradian exposure

Poor exposures of Dalradian metasediment can be found in Five Fingers Gully (Photo 3.2). Relationships between the Dalradian and the volcanic pile in this area are obscured by hydrothermal alteration. Fault related fracturing has provided numerous pathways for the percolation of Mn and Fe rich fluids (Photo 3.3). Fracturing and mineralisation (hematite staining) occurred after solidification of the Inner Granite. The orientation of this zone of alteration ( $120^{\circ}/300^{\circ}$ ) is parallel to that of a series of *en echelon* Tertiary basalt dykes exposed in the Tourist Path and in Five Fingers Gully. It is possible that the alteration and mineralisation is related to the intrusion of these Tertiary dykes. The Dalradian pelites in Five Fingers Gully are only exposed where small streams running off Ben Nevis have cut down into the contact and consequently the exposure is much more limited than the BGS map suggests.

This locality has the only example of the Ben Nevis dyke swarm exposed within the volcanic pile. A felsite dyke is exposed for  $\approx 200\text{m}$  and outcrops parallel to the contact between the Inner Granite and the volcanic pile. At the present day the dip of this contact is vertical to steeply dipping and the felsite has a horizontal orientation. Correcting for the tilt of the volcanic pile brings the felsite dyke into a vertical attitude. At the northern termination several offshoots of the felsite cut up into the volcanic pile (Photo 3.4) for a short distance and provide conclusive proof that the felsite is intrusive. At the southern end of the Felsite dyke outcrop the exposure is pinched out when the Inner Granite/volcanic pile contact rises to gain the col between Ben Nevis and Carn Dearg (SW) (Photo 3.5).

#### 3.5.2 The Allt a' Mhuillin Formation

Unconformably overlying Dalradian basement schists in the Allt a' Mhuillin, and also exposed at the base of the cliffs between the NE Buttress and Brenva Face (Fig. 3.3a), is a sequence of mudstone and siltstone, interbedded with poorly sorted non-volcanic conglomeratic breccias, hereafter referred to as the Allt a' Mhuillin Formation. No sediments were found above the Dalradian in the area of Five Fingers gully. In the Allt a' Mhuillin stream bed, a sedimentary breccia overlies the Dalradian and is in turn overlain by mudstones and siltstones. The exposure at the foot of the cliffs is dominated by mudstone and siltstone with three conglomeratic breccia horizons. In between these two areas, the Coire na Ciste Formation is exposed in contact with the Inner Granite. Sedimentary logs of the Allt a'

---

Plate 4 Photo. 3.1 Dalradian basement to the volcanic pile, intensely folded meta-  
pelite and semi-pelite. BN198 (NN170, 720)

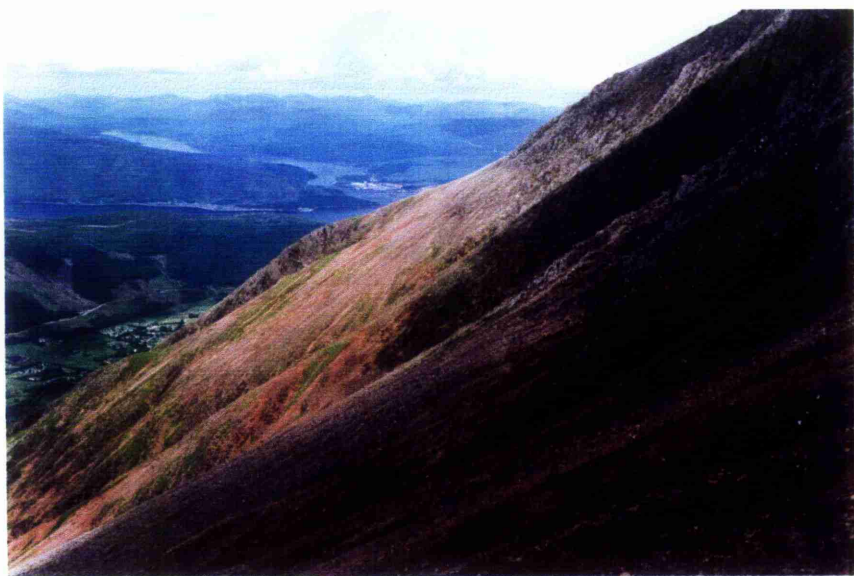
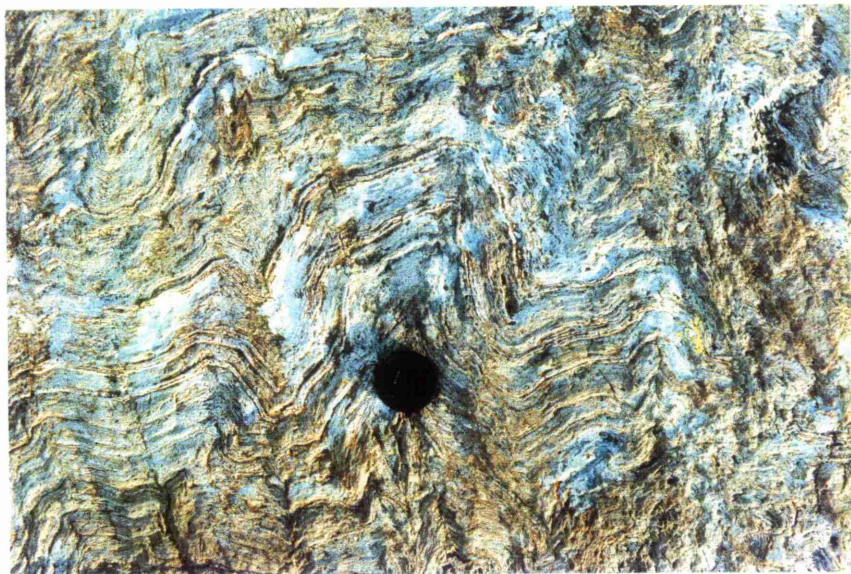
---

---

Plate 4 Photo. 3.2 View of Five Fingers Gully looking north. The exposures of  
Dalradian metasediments are located in the gully forming the middle ground of  
the photograph.

---

PLATE 4



---

Plate 5    Photo. 3.3    Alteration and staining of the felsite sill in Five Fingers Gully.  
BN362 (NN152 711)

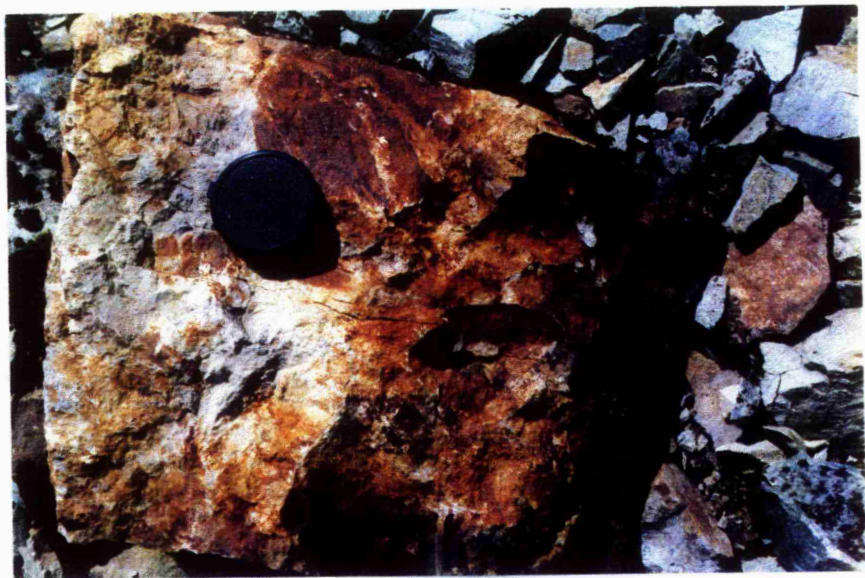
---

---

Plate 5    Photo. 3.4    Offshoot of the felsite sill intruding into the volcanic pile. The  
white rock in the centre of the picture represents an offshoot of the felsite  
which is located in the foreground of the photograph.

---

PLATE 5



Mhuillin Formation in the area of the Allt a' Mhuillin and of the NE Buttress can be found in Fig. 3.5. The Allt a' Mhuillin Formation provides the first evidence of lateral variation that characterises all the formations of the volcanic pile.

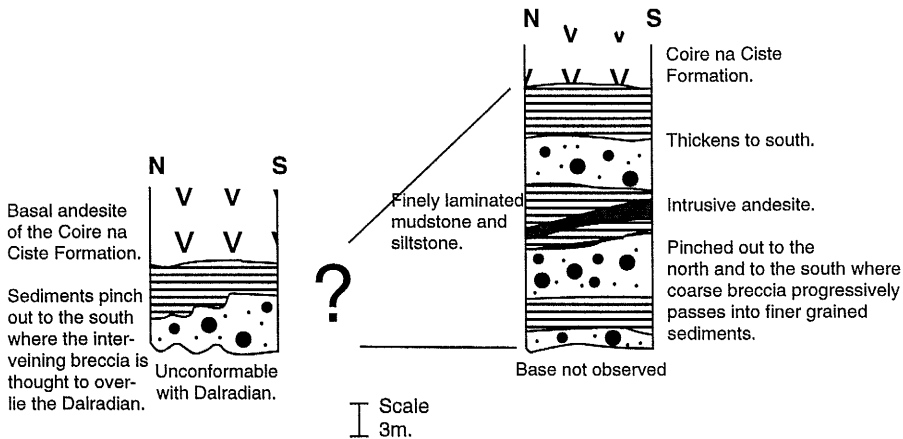


Fig. 3.5 Cartoon logs of the two Allt a' Mhuillin Formation exposures. Extreme lateral heterogeneity characterises this formation.

### 3.5.2.i Conglomeratic breccias

#### Clasts

The most obvious clast type in this lithology is sand to large cobble sized (0.1cm - 20cm), angular to sub-rounded quartzite fragments. Numerous clasts of pelite and semi-pelite tend to be more angular and smaller in size (0.1-15cm). These pelitic clasts are difficult to distinguish from contemporaneous fine grained sediments in hand specimen. Fragments of igneous rock are absent.

#### Textures

Both clast and matrix support fabrics are found within each conglomeratic breccia horizon, and a weak preferred alignment is often observed (Photo 3.6). The matrix tends to be mud-sand grade material. A fine grain base is occasionally observed. Each individual conglomeratic breccia horizon is massive and texturally and compositionally immature.

#### Contact relationships

In the Allt a' Mhuillin, a conglomeratic breccia rests unconformably on Dalradian pelites (Photo 3.7) and thickens in a southerly direction (upstream), from 0.3m to 2.5m. The upper contact is hummocky and irregular. Those conglomerates exposed beneath the NE Buttress have distorted and deformed the underlying sediments and may contain clasts ripped up from the underlying sediments. None of the conglomeratic breccias exposed

---

Plate 6    Photo. 3.5    View of the volcanic pile/Inner Granite/felsite contact in Five Fingers Gully looking south towards the col between Carn Dearg (SW) and Ben Nevis. The prominent gully below the col is due to faulting and the preferential erosion of the Tertiary dyke. The volcanic pile is on the left hand side of the photograph and the contact with the Inner Granite and Felsite dyke effectively follows the line of rocky exposure until meeting the prominent gully where the contact climbs steeply to gain the col thus pinching out the Felsite.

---

---

Plate 6    Photo. 3.6    Conglomeratic breccia of the Allt a' Mhuillin formation. White clasts are quartzite with the remainder of the clast population composed of contemporaneous sediments and Dalradian schists. BN197 (NN169 720)

---

PLATE 6



beneath the cliff-line are laterally extensive, the middle horizon CB(b) is exposed for a distance of 50m, and forms a lens of breccia 'enclosed' within the surrounding sediments. At either end CB(b) tails into a thin conglomeratic horizon before passing into sandstone some 2-3m from the main body. Towards the base of the exposure beneath the cliffs, a thin conglomeratic band, 5cm thick, and comprising quartzite and mudstone clasts up to 1cm in diameter, probably represents the 'terminal' zone of a fourth conglomeratic breccia horizon.

### 3.5.2.ii Mudstone and siltstone

Where these sediments are best preserved, a rhythmic 2-3cm scale fining upwards cycle (Photo 3.8), occasionally broken by thicker (5-8cm) coarse sandstone horizons, is observed. No other depositional features are recognised. In the exposures beneath the cliffs, the maximum observed thickness of mudstone reaches  $\approx 30$ m, but the base of this exposure is not found. A thickness of 30m is considerably thicker than the exposure of conglomerate and mudstone in the Allt a' Mhuillin ( $\approx 5$ m). Small scale folds and brecciated mudstone horizons sandwiched between undeformed sediments indicate soft sediment deformation; dewatering structures are also observed. Photo 3.9 is a photomicrograph of the mudstone and illustrates the very fine grained nature of the sediments, Small crystals of Fe-Ti oxides define discrete layers. A monolithologic hornblende-biotite andesite breccia sill intrudes the Allt a' Mhuillin Formation beneath the cliff line.

### 3.5.3 The Coire na Ciste Formation

#### 3.5.3.i The intervening breccia

Between the Allt a' Mhuillin Formation exposed in the Allt a' Mhuillin and at the base of the NE Buttress, a sediment bearing but andesite rich breccia is exposed in contact with the Inner Granite; this breccia is hereafter referred to as the intervening breccia in order to distinguish it from the volcanic breccias at the base of the Coire na Ciste Formation in the vicinity of the CIC hut.

#### Clasts

This breccia differs from other volcanic breccias in the Coire na Ciste Formation in that it contains a significant fraction of metamorphic and sedimentary clasts, up to 10%. Non-volcanic clast types are rare (<1%) within the other Coire na Ciste volcanic breccias. The proportion of country rock clasts decreases with distance from the Inner Granite contact, and probably reflects swamping of the country rock source area by volcanic material. The proportion of individual clast types, listed below, is extremely variable.

Small, baked mudstone clasts <1cm diameter sub-rounded to rounded

Dalradian quartzite and pelite fragments, up to 10cm diameter, angular to sub-rounded

---

Plate 7 Photo. 3.7 Contact between Dalradian basement and the conglomeratic breccia of the Allt a' Mhuillin formation (right hand side). Note the fine grained base to the breccia (below the lens cap) and the predominance of quartzite clasts in contrast to the local pelitic basement lithology (Photo 3.1) that forms the left hand side of the photograph. BN197 (NN169 720)

---

---

Plate 7 Photo. 3.8 Rhythmic layering in the mudstones of the Allt a' Mhuillin formation. The basal andesite forms the rounded exposures towards the top right corner of the photograph. BN197 (NN169 720)

---

PLATE 7

CONTACT



CONTACT



Various andesitic clasts (forms the majority of unit) up to 15cm diameter sub-angular to rounded. A number of the larger andesite clasts have crenulate margins implying hot emplacement. This has important implications for the genetic origin of these deposits.

#### Textures

Those clasts with one axis significantly longer than the others, define a weak preferred alignment. It is likely that this unit is made up of a number of individual 'beds'. Texturally, this unit is very similar to the conglomeratic breccias of the Allt a' Mhuillin Formation, but, unlike the Allt a' Mhuillin Formation examples, it is dominated by andesite clasts which show evidence of hot emplacement. For these reasons it is included within the Coire na Ciste Formation.

#### Contact relationships

The thickness and lateral extent of this horizon is unclear; it forms a large part of the NE Buttress, but is largely absent from Tower Ridge and is not observed between the CIC hut and Coire na Ciste. Unfortunately, the contact with the remainder of the Coire na Ciste Formation is buried under a boulder field. The northernmost exposure of the Dalradian basement is just 0.3m from the first exposures of the intervening breccia (Fig. 3.6). No sediments are observed *in situ* between the two exposures. Between BN256 (intervening breccia) and BN199 (fine grained sediment), BN357 represents an important line of evidence. At this exposure, monolithologic andesite breccia with poorly developed flow folds and containing rare quartzite xenoliths passes rapidly into the intervening breccia. The base of the intervening breccia is often confused, and hollows in the surface of the andesite were infilled and then left 'stranded' as the movement surface migrated upwards to a mechanically more efficient flat surface. The underlying andesite breccia can be traced into a more massive core and is continuous with the monolithologic andesite breccia overlying the sediments in the Allt a' Mhuillin (Fig. 3.6). The intervening breccia is therefore contemporaneous with the earliest members of the Coire na Ciste Formation.

#### 3.5.3.ii Volcanic breccias

##### Clasts

In contrast to the underlying conglomeratic breccias of the Allt a' Mhuillin Formation, the Coire na Ciste volcanic breccias are almost exclusively composed of andesite, with subordinate rhyolite and eutaxitic ignimbrite clasts. Sedimentary and metamorphic clasts are rare (<1%). Although a variety of fine-grained hornblende-biotite and hornblende andesite clasts are present in all volcanic breccia horizons, typically one andesite type will dominate an individual horizon. Those volcanic breccias exposed towards the base of the Coire na Ciste Formation tend to include a greater variety of clasts than those higher in the sequence. In particular, the lower volcanic breccias include eutaxitic ignimbrite clasts (Photo 3.10a and 3.10b); good examples of which can be found in the

---

Plate 8 Photo. 3.9 Photomicrograph of mudstone from the Allt a' Mhuillin formation. Note the layering depicted by small crystals of Fe-Ti oxide and the extremely fine grained nature of these sediments. (BN197S \* 21). (NN169 720)

---

---

Plate 8 Photo. 3.10a Eutaxitic ignimbrite clast from the CIC hut boulder. Dark green grey clasts represent flattened pumice and are set in a matrix of lithic fragments and ash? predominantly andesite (NN167 723)

---

PLATE 8



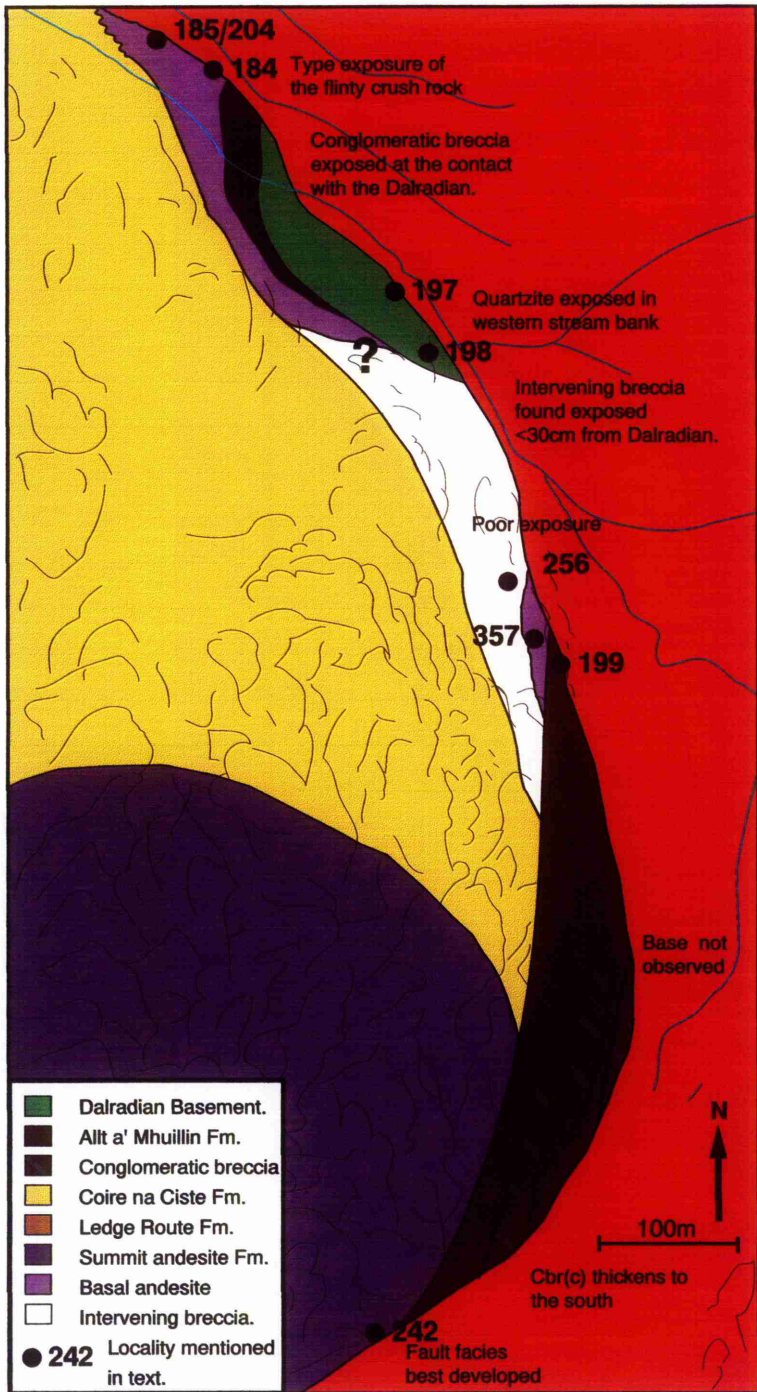


Fig 3.6 Close up of the Allt a' Mhuillinn formation outcrop.

obvious large boulder just north of the CIC hut and *in situ* in the adjacent CIC slabs (Fig. 1.1). Preferential erosion of fiamme has led to the development of a characteristic elongate pitted surface. In two dimensions, individual fiamme are 2-5cm \* 0.5-1cm in size. Fiamme are difficult to identify in thin section (Photo 3.11) and tend to merge with the surrounding matrix. All of the ignimbrite clasts examined contain large numbers of lithic fragments (Photo 3.10b), these include volcanoclastic material, andesitic and rhyolitic clasts, together with whole or fragmented euhedral plagioclase, biotite and hornblende crystals. The matrix is comprised of a fine grained mesostasis of feldspar, mica and phyllosilicate minerals, and presumably represents altered devitrified glass.

A number of volcanic breccias throughout the Coire na Ciste Formation include pinkish red clasts of fine grained rhyolite. These volcanic breccias provide useful marker bands. A weak structure to these clasts is defined by aligned micro-phenocrysts of feldspar and biotite. The groundmass is very poorly preserved and is represented by a cryptocrystalline mesostasis of felsic and minor mafic minerals. Leaching of iron from Fe-Ti oxide phenocrysts and deposition in the adjacent groundmass has developed Fe enriched coronas around the oxide minerals.

A range of andesite clasts are found within the Coire na Ciste volcanic breccias; most show trachytic and/or trachyoid textures. Phenocryst phases include feldspar, hornblende, Fe-Ti oxide  $\pm$  biotite  $\pm$  pyroxene  $\pm$  quartz. Alteration has affected these rocks to varying degrees, mafic minerals being replaced by chlorite, epidote and titanite. Plagioclase is generally less altered and the groundmass is often extensively altered. Vesicles are generally not observed.

#### Matrix

The matrix is micro to cryptocrystalline and has suffered significant alteration; consequently no textures are observed within the matrix of the volcanic breccia in hand-specimen, thin section or with the Electron Microprobe. It is not therefore possible to unambiguously distinguish between an epiclastic origin and a pyroclastic origin for the matrix. Pumice/fiamme are not found and vitroclastic textures, if originally present, have not survived a combination of devitrification, contact metamorphism against the Inner Granite and subsequent alteration and weathering. The matrix consists of a fine-grained mesostasis of feldspar, sericite, chlorite, titanite, epidote, carbonate, biotite and Fe-Ti oxide.

#### Textures

An inversely graded and often strongly sheared zone can be found at the base of a number of volcanic breccias and may extend up to 30cm above the base of the breccia (Photo 3.12). The rest of the volcanic breccia horizon is comprised of massive, unsorted and texturally immature breccia. The dominant clast type within the volcanic breccias is sub-

---

Plate 9    Photo. 3.10b Eutaxitic ignimbrite clast from the CIC hut slabs. Note the lithic clast in the centre of the photograph around which the fiamme have been deformed. BN207 (NN166 723)

---

---

Plate 9    Photo. 3.11 Photomicrograph of an eutaxitic ignimbrite clast, pale yellow band in the centre of the photograph is a flattened crystal rich clast of pumice. (BN140 \* 12). CIC hut Boulder (NN167 723)

---



PLATE 9



rounded to angular non-vesicular andesite (Photo 3.13). Both matrix and clast support can be found in individual horizons.

#### Contact relationships

The Coire na Ciste Formation rests on the Allt a' Mhuillin Formation. The upper contact of this formation is less obvious. On the northern margin of Coire na Ciste, the top of the Coire na Ciste Formation is overlain by the Ledge route Formation. Elsewhere within the volcanic pile, the contact between the Coire na Ciste Formation and the overlying Summit Formation is taken as the point where autobrecciated andesite begins to dominate the succession. North of No. 5 gully this occurs beneath the Ledge route Formation (Fig. 3.4), consequently, the contacts between the Ledge route and Coire na Ciste Formations, the Coire na Ciste and Summit Formations and the Ledge route and Summit Formations are believed to be diachronous. In complex volcanic terrains, lithostratigraphic subdivisions are unlikely to follow a simple layer cake geometry (Cas & Wright 1988).

Individual volcanic breccia horizons vary from 0.25m (Photo 3.14) to thicknesses of 30m+. Lateral variations are considerable; for example, a 30m thick rhyolite bearing volcanic breccia exposed at the southern end of the Coire na Ciste slabs cannot be traced into the Douglas Boulder or into the Great Buttress and No. 5 gully. A second rhyolite bearing volcanic breccia is exposed in the CIC slabs, and terminates at the northern end of these exposures. Two isolated patches of rhyolite bearing volcanic breccia represent the maximum lateral extent of this breccia (Photo 3.15).

Contacts between individual volcanic breccia horizons are irregular on the scale of a few metres, and local palaeo-topography is the prime control on the location of individual volcanic breccias (see the description of BN212 below).

Present day topography within Coire na Ciste is controlled to some extent by individual volcanic breccia horizons, contacts between different horizons can be identified from breaks in slope morphology even if the contact is not physically exposed (Photo 3.16a & 3.16b).

#### 3.5.3.iii Sediments within the Coire na Ciste Formation

Thin, laterally discontinuous sediments are exposed within the Coire na Ciste Formation. These fall into three categories.

##### 1) Fine grained sediments. BN205, BN245, BN247, BN271

Although deformed and fragmented, it is possible to recognise a sequence of 2-5cm scale rhythmic fining up cycles (Photo 3.17) and these sediments are therefore comparable to those of the Allt a' Mhuillin Formation. At BN205, thin, <2cm thick, fining-up pebbly sandstone bands punctuate the finer grained succession (Photo 3.17). Clasts within the pebbly sandstones are of rounded to sub-angular andesite, with minor mudstone and

---

Plate 10 Photo. 3.12 Sheared base to volcanic breccia, base of flow is towards the bottom of the photograph and the shear direction is parallel with the base of base of the Plate. Clasts are of andesite. BN230 (NN165 721)

---

---

Plate 10 Photo. 3.13 Well exposed volcanic breccia (Hammer 40cm in length), angular to sub-rounded clasts of andesite showing clast and matrix support. BN249 (NN167 721)

---

PLATE 10



---

Plate 11 Photo. 3.14 Thin volcanic breccias exposed at the base of the Tower slabs.  
(NN 166 720)

---

---

Plate 11 Photo. 3.15 The two light coloured patches represent the maximum lateral extent of a rhyolite bearing volcanic breccia sandwiched between an andesite on the left hand side and a volcanic breccia on the left hand side. The volcanic succession in this locality has been overturned during collapse of the volcanic pile. BN207 (NN169 722)

---



---

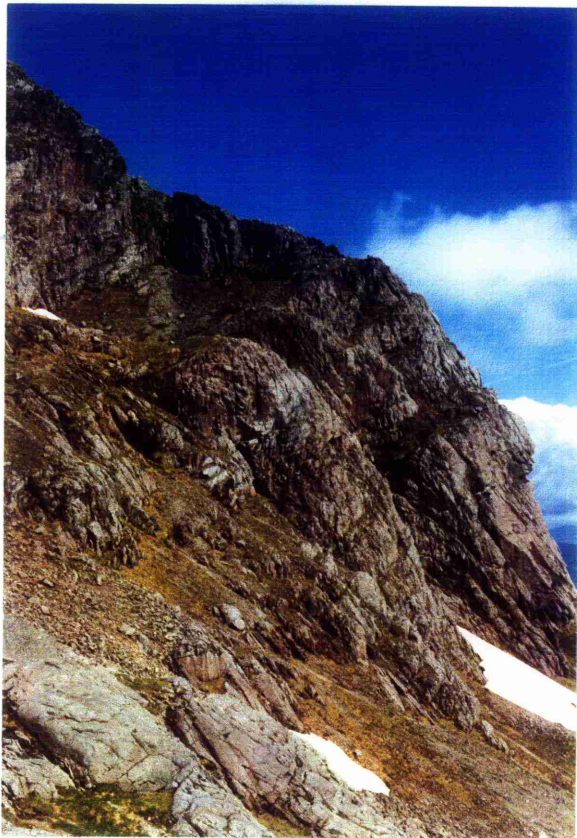
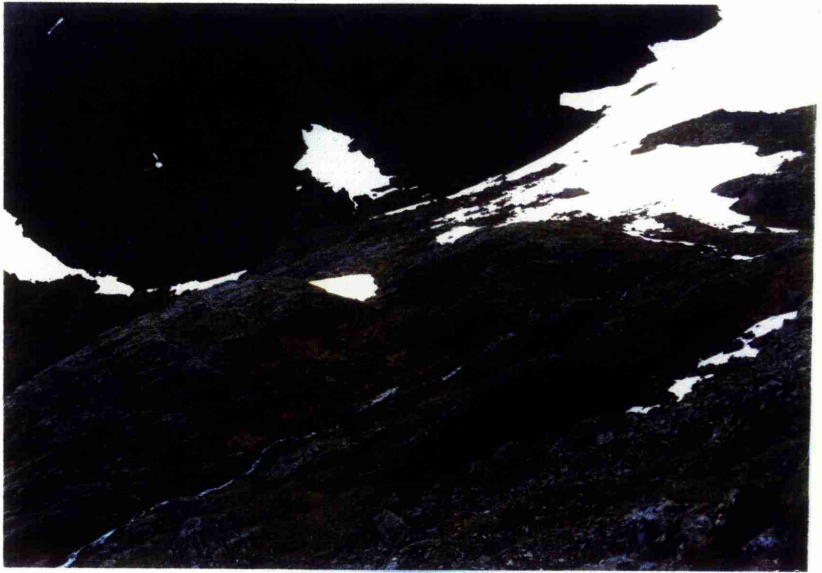
Plate 12 Photo. 3.16a Slope morphology of the Coire na Ciste slabs (view to south toward Tower Ridge); the slope is composed of volcanic and andesitic breccias.

---

---

Plate 12 Photo. 3.16b Slope morphology of the Ledge route and the Gt. Buttress of Carn Dearg (view to north).

---



siltstone. These coarser 'events' are interspersed at irregular intervals throughout exposure BN205. The maximum thickness of BN205 is 8m, but just 30m along strike the sedimentary horizon has faded out.

The coarse component of a fining up cycle includes feldspar fragments, with rarer zoned euhedral crystals, Fe-Ti oxide minerals and quartz enclosed within a finer grained groundmass (Photo 3.18). A sharp contact is obvious between the coarse base of one fining up cycle and the fine grained top of an earlier cycle. Geochemically, these sediments are little different from andesite lava (Fig. 3.1) and are believed to be comprised primarily of altered ash.

## 2) Calcareous sandstones. BN142, BN212, BN271

Several thin (<0.5m) calcareous sandstone horizons are found at the northern end of the Coire na Ciste slabs in the vicinity of Lochan Coire na Ciste (BN142). A single band is situated within the Gt. Buttress slabs (BN212 & BN271), and passes down into the sediments of group i).

The sediments of BN142 have undergone considerable soft sediment deformation (Photo 3.19). In hand specimen, these rocks are a pale lime-green colour and in thin section the rock is comprised of pale green tremolite, minor feldspar and titanite. Tremolite is not a primary mineral and is observed replacing feldspar. The rock has suffered low grade metamorphism and the original mineralogy of the calcareous sediments is obscured, feldspar is the only mineral for which even vestigial traces remain.

## 3) BN142, BN212, BN247

Associated with the above sediment groups are thin (<0.5m) conglomeratic breccias. Significantly, quartzite is the dominant clast type within these matrix and clast supported sediments (Photo 3.20). Although finer of grain size, a strong similarity with the conglomeratic breccias of the Allt a' Mhuillin Formation is observed and it is believed that these breccias were formed by similar processes to those of the Allt a' Mhuillin Formation.

### 3.5.3.iv Andesites within the Coire na Ciste Formation

Several andesite breccia units are found within the volcanic breccias. These andesites are of similar type and geochemistry to those of the Summit Formation and are therefore discussed in the section dealing with the Summit Formation (section 3.5.5).

### 3.5.3.v Key exposures within the Coire na Ciste Formation

Base of the Coire na Ciste Formation, CIC slabs. BN185, BN203, BN207

These exposures are of the lowest horizons of volcanic breccias within the volcanic pile. The stratigraphic relationship between these breccias and the intervening breccia at

---

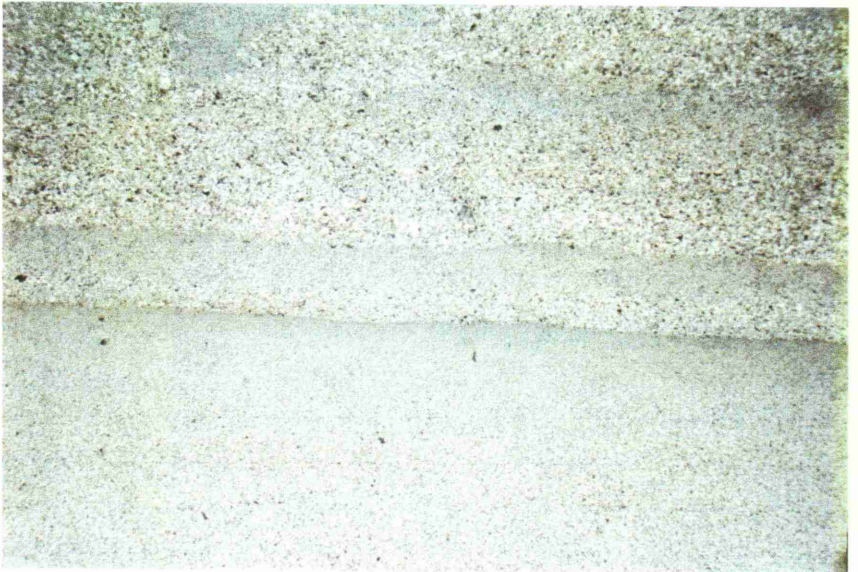
Plate 13 Photo. 3.17 Rhythmic fining up cycles in the sediments of BN205. Note the coarser andesitic bands. Each cycle is between two and four cm thick. (NN166 720)

---

---

Plate 13 Photo. 3.18 Photomicrograph of fining up cycles (BN205 \* 12). (NN166 720)

---



---

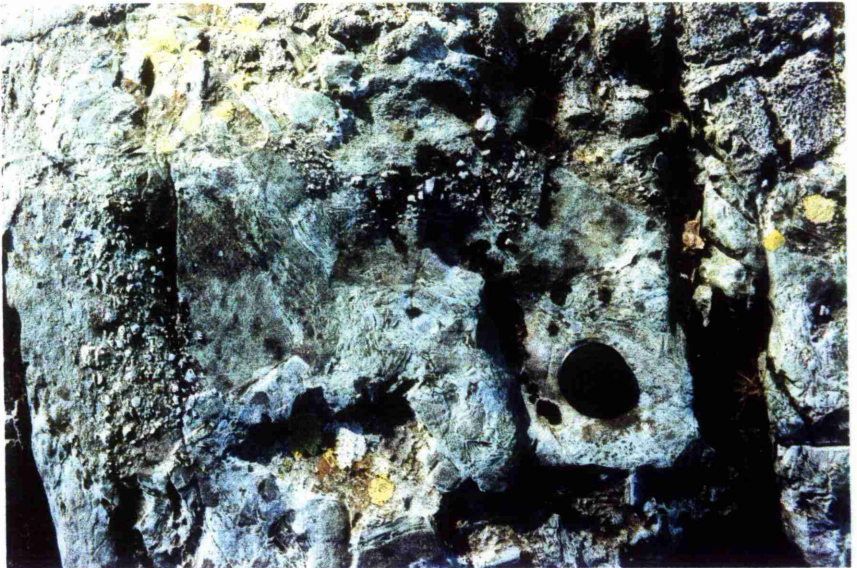
Plate 14 Photo. 3.19 Deformed calcareous sediments of BN142. (NN162 719)

---

---

Plate 14 Photo. 3.20 Sediments and conglomeratic breccias within the Coire na Ciste Formation. The lithologies in the photograph are overlain by VBC of Fig 3.7. Green coloured rock is fine grained sediments, that with the abundant white fragments is the sedimentary breccia and the upper part of the photograph is composed of brecciated andesite forming the base of an andesite lava. BN271 (NN165 722)

---



the top of the Allt a' Mhuillin Formation is unclear, both are known to overlie the monolithologic andesite breccia (BN197) which overlies the sediments of the Allt a' Mhuillin Formation.

Clasts of rhyolite and eutaxitic ignimbrite are found within these exposures. Rhyolite, other than syn-collapse intrusions (see section 3.6), and eutaxitic ignimbrites are not found *in situ* on Ben Nevis, the volcanic breccias must therefore be derived from a source external to the current area of outcrop of the volcanic pile.

#### Great Buttress slabs. BN271

The contact relationships in this area indicate that erosion accompanied deposition and that local topography played an important role in the location of individual volcanic breccia horizons. In Fig. 3.7 and Photo 3.21, three volcanic breccia units are marked. VBa, terminates within the field of view and is overlain by mudstone and siltstone which pass up into calcareous sandstone and then into a quartzite bearing conglomeratic breccia. The mudstone and siltstones are sandwiched between VBa and VBb. VBb is overlain by and has a similar range of clast types to VBc which also overlies the sediments above VBa. A thin shear band and fining up sequence marks the contact between VBb and VBc, The base of VBc, above the sediments includes small (<2cm) mudstone clasts (Photo 3.22). These are preferentially aligned and show baked margins indicating that the volcanic breccia was hot when emplaced.

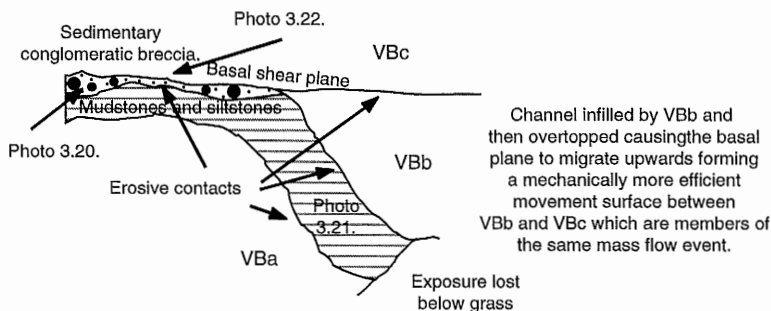


Fig. 3.7 Active erosion and channelisation within the Coire na Ciste Formation during deposition of this formation. Channel erosion occurred between deposition of the sediments and VBb. The presence of baked mudstone clasts in the base of VBc suggests that this unit eroded and entrained part of the underlying sedimentary sequence and was emplaced hot.

The following sequence of events is proposed to explain the above exposure.

- i. Emplacement of VBa
- ii. Erosion of a  $\approx 4\text{m}$  deep depression within VBa, alternatively a topographic low ( $\approx 4\text{m}$  deep) could have been present in the top of VBa
- iii. Deposition of mudstones, siltstones, calcareous sandstones and quartzite bearing conglomeratic breccias

---

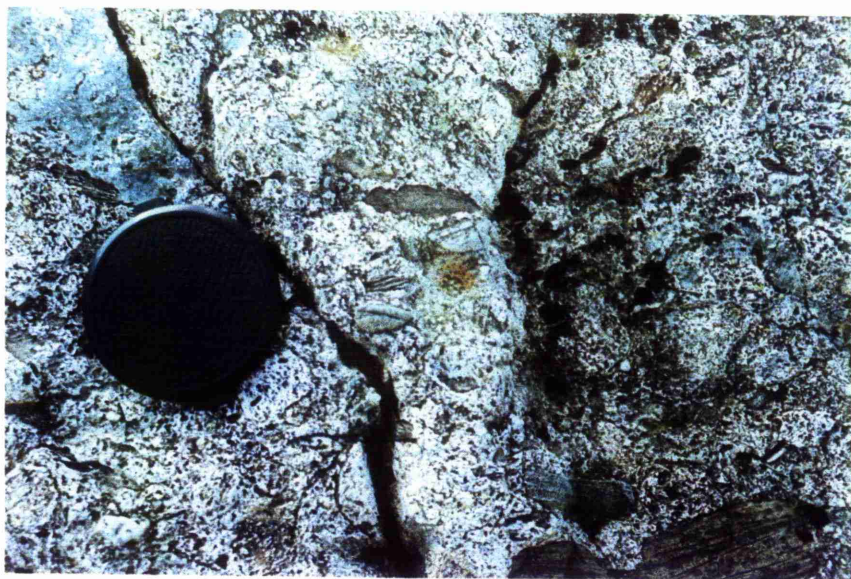
Plate 15 Photo. 3.21 Sediments exposed between VBa and VBb of Fig 3.7. BN271  
(NN165 722)

---

---

Plate 15 Photo. 3.22 Baked mudstone clasts in the base of VBc. BN271 (NN165 722)

---



#### IV. Erosion of the sediments deposited in iii.

vi. Emplacement of VBb. The volume of this volcanic breccia exceeded that of the available channel and the breccia overtopped the local topography, it then became mechanically more efficient for the volcanic breccia to flow along a flat surface and consequently, the base of the active flow migrated out of the channel resulting in the formation of the shear band between VBb and VBc. Both VBb and VBc were part of the same mass flow unit and were emplaced hot.

#### Gardyloo Gully. BN268

The volcanic breccia (sedimentologically a pebbly mudstone) exposed at BN268 is comprised of 2-4cm rounded-subangular clasts of andesite, rhyolite and Dalradian, supported in a fine grained massive matrix that forms 40-50% of the rock unit.

In thin section, there is evidence that this unit was emplaced hot. Some of the larger feldspar clasts (>1mm) have been corroded and infilled by the matrix. Mica and micaceous Dalradian fragments are deformed and folded around feldspar crystals or lithic fragments (Photo 3.23). The same stress field caused a number of feldspar crystals to fracture, and the fracture lines have been preferentially corroded by the matrix.

#### NE Buttress, thin section

Two components make up the slide, a fine grained ashy matrix and an andesite 'clast'. A range of boundary contacts can be seen between the two components from straight, sharp boundaries to blurred and indistinct. From Photo 3.24, it can be seen that the ashy matrix penetrates the andesite clast and that fragments of andesite within the matrix are similar in petrology to this clast. It is believed that these contact relationships indicate hot emplacement of this volcanic breccia and that, in this case at least, there is a genetic relationship between clast and matrix (ash).

#### 3.5.4 The Ledge route Formation

The Ledge route Formation is particularly well exposed on Ledge route, in No. 5 gully in much of the Trident Buttress and in the upper parts of Castle Ridge and Castle Corrie. The formation is sub-divided into two members, the Trident Member and the Ledge route Member. Much of the Orion Face is also comprised of a similar lithology to the Ledge route Member, but the litho-stratigraphical position of the Orion Face exposures is unclear. Lithologies similar to the Ledge route Member are not found on the NE buttress or on Tower Ridge and the Orion Face exposures are apparently isolated from the Ledge route outcrop.

##### 3.5.4.i The Trident Member

At the start of Ledge route (Coire na Ciste variation, 5a in Fig. 3.3a), a band of fine grained sediments attains a maximum thickness of  $\approx 20\text{m}$ , and is hereafter referred to as the

---

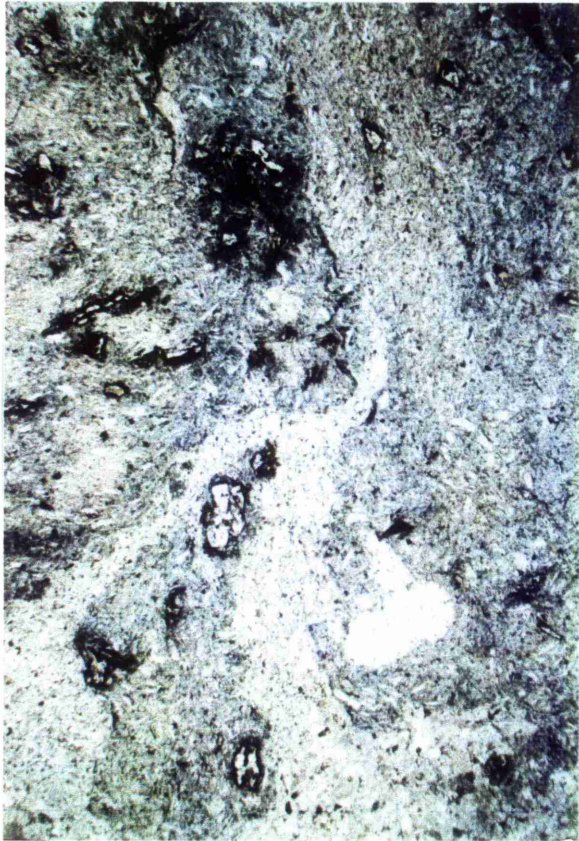
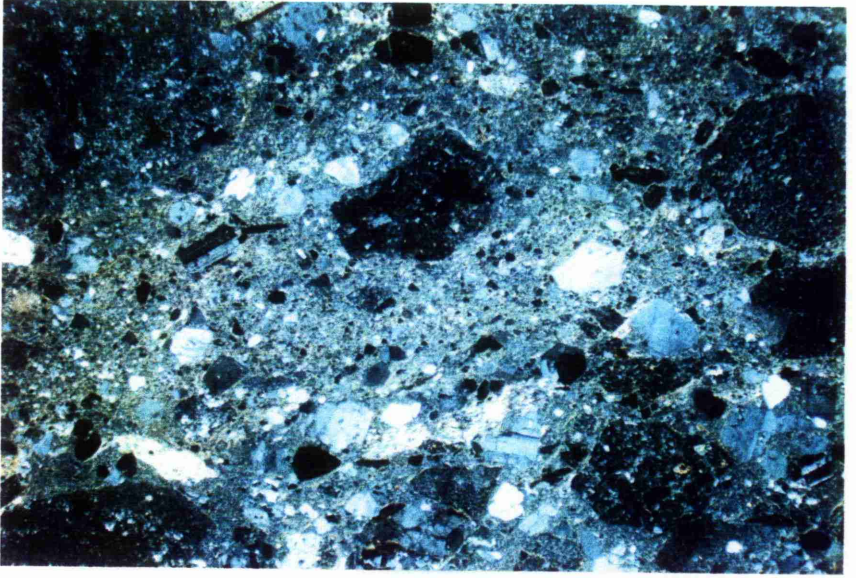
Plate 16 Photo. 3.23 Photomicrograph of deformed micaceous Dalradian fragments (white patches in the photograph) and mica crystals around lithic (andesite) fragments and feldspar crystals. (BN268 \* 12) (NN167 716)

---

---

Plate 16 Photo. 3.24 Photomicrograph of NE Buttress sample, note the range of andesite/matrix contacts in this photograph illustrating that the andesite was still largely molten during formation of the rock (NE Buttress \* 12). (NN170 714)

---



Trident Member. The Trident Member is not found within Coire na Ciste or on the northern side of No. 5 gully.

Cross bedding and other current structures are not observed and the sediments represent a finely bedded succession of mudstone and siltstone sediments (Photo 3.25) passing into a transition zone between the Trident Member and the Ledge route Member, where mudstone is interbedded with early precursors of the Ledge route Member (Photo 3.26). The mudstones and siltstone are extensively deformed by small scale folding and faulting (Photo 3.25).

The contact with the underlying Coire na Ciste Formation is not seen, but the sediments must overlie the volcanic breccia exposed just 20cm below the lowest mudstone exposure. Local palaeo-topographic variations, and slumping related to movement of the overlying Ledge route Member (see section 3.5.4.ii), have developed a complex set of field relationships between the Coire na Ciste Formation, the Trident Member and the Ledge route Member (Fig. 3.8). The southernmost exposure of the Trident Member occupies a small depression in the surface of the underlying volcanic breccia. No transition zone is observed in this area and the contact with the overlying Ledge route Member is sharp, except where the sediments have been squeezed up into the Ledge route Member (see section 3.5.4.ii).

Photo 3.27 is of an isolated triangular block ( $\approx 75\text{cm}$ ) of sediments within the Trident Member. Deformation structures in the underlying sediments indicate that the block has fallen into its current location. This block was not emplaced ballistically during a volcanic eruption as no volcanic block or bombs are found within Trident Member, therefore the block must have fallen from a local topographic high. A large clast of quartzite (8cm) is visible within the block. Quartzite clasts are occasionally found within the Ledge route Member, but are relatively scarce.

#### 3.5.4.ii The Ledge route Member

The Ledge route Member is comprised of moderately well sorted volcanic breccias. Sub-rounded to angular andesite clasts, typically 2-3cm in diameter, although the maximum size is exceptionally 10cm, form a strong clast supported framework. Clasts of non-volcanic material are rare. Photo 3.28 is of a typical example of the Ledge route Member. Interbedded with the volcanic breccias in Coire na Ciste and in No. 5 gully are a number of mudstone horizons (up to 20m thick). The thickness and frequency of these sediment horizons decreases northwards from a maximum number of five in Coire na Ciste (max. thickness 20m), through two in No. 5 gully (max. thickness 8m), to zero on Ledge route above the Great Buttress of Carn Dearg. On Castle Ridge, the Ledge route Member is found interbedded with andesite lavas. No internal contacts were observed within the volcanic breccias. Above the Great Buttress of Carn Dearg, the thickness of the Ledge route Member is >200m and thins southwards, across No 5 Gully and the Trident Buttress, to less than 50m on the northern flank of Coire na Ciste.

---

Plate 17 Photo. 3.25 View of fine grained mudstones forming the Trident Member.  
Note the large degree of soft sediment deformation and small scale faulting.  
BN215 (NN162 731)

---

---

Plate 17 Photo. 3.26 Transition zone between the Ledge route Member and the Trident member. 'White' bands in the photograph represent early Ledge Route Member volcanic breccias sandwiched between fine grained sediments of the Trident Member. BN215 (NN162 731)

---



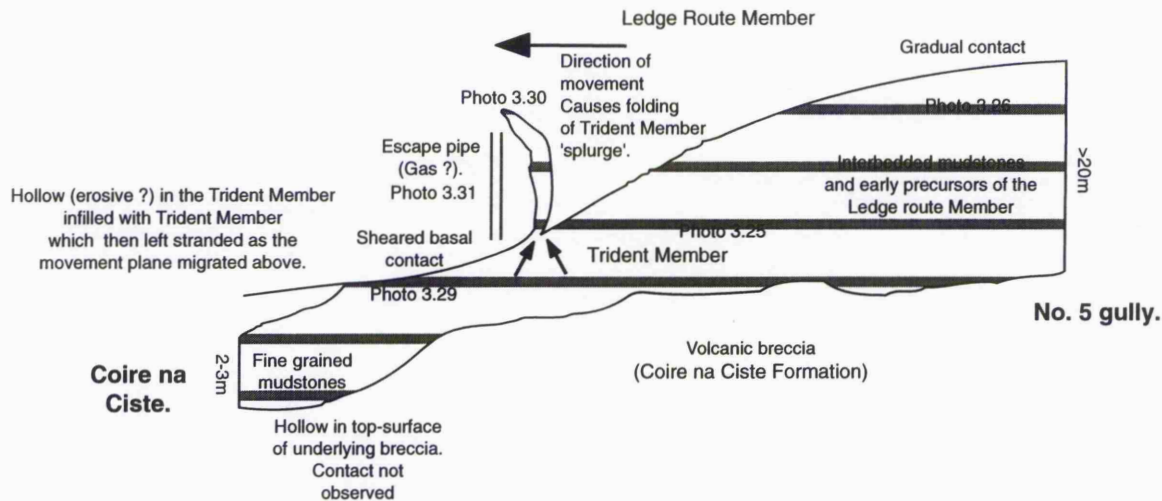


Fig. 3.8 Contact relationships between the Coire na Ciste Formation, the Trident Member and the Ledge route Member in the area between Coire na Ciste and No. 5 gully. North of No. 5 gully, the Trident Member is not observed and the Ledge route Member overlies an andesitic unit which may have formed the margin of the Trident Member sedimentary basin.

---

Plate 18 Photo. 3.27 Fallen block of transition zone rich lithologies in the mudstones of the Trident Member. Note the deformation at the base of this block and the large quartzite clast in the right hand corner of the block. BN215 (NN162 731)

---

---

Plate 18 Photo. 3.28 Hand specimen photograph of the Ledge route Member. BN215 (NN162 731)

---



In thin section, the strong clast supported fabric is clearly visible. Post depositional compaction has deformed single mica crystals around whole or fragmented feldspar crystals. The matrix is comprised of a cryptocrystalline mesostasis of felsic and phyllosilicate minerals.

Three lines of evidence indicate that the Ledge route Member flowed into its current location. Firstly, there is a weak preferred orientation to clasts of the Ledge route breccias which indicates a period of laminar flow. Secondly, the base of the Ledge route Member, at the southern end of the Coire na Ciste Ledge, is represented by a zone of shearing (Photo 3.29). Thirdly, also at the southern end of the Coire na Ciste Ledge several 'injections' of Trident Member sediment penetrate up to 6m into the Ledge route Member (Photo 3.30). The injections are formed of coherent blocks of sediment and appear to have been squeezed up into the Ledge route Member. Sediments of the Trident Member at the contact with the Ledge route Member have been fragmented by passage of the Ledge route Member. A possible explanation for the absence of the transition zone in this locality is that it has been removed as the Ledge route volcanic breccias flowed over the top. Localised topography, depicted in Fig. 3.8, was overtopped. The movement plane then migrated to a mechanically efficient flat surface resulting in the development of a thin shear band within the Ledge route Member.

Sometime after the cessation of movement an escape structure (Photo 3.31) rose up through the Ledge route Member. No base to the structure was exposed. The escape structure is dominated by fine-grained material in contrast to gas or fluid escape structures where fine-grained material is preferentially removed. This suggests that the escape structure originated within or below the sediments of the Trident Member. Also the contact between the escape pipe and the volcanic breccias is sharp suggesting that the Ledge route Member was relatively coherent and resisted invasion of the escaping fluid.

### 3.5.5 The Summit Formation

#### 3.5.5.i General description of the Summit Formation

The andesite breccias of the Ben Nevis Complex form much of the summit plateau and the uppermost sections of the cliffs in Coire Leis and Coire na Ciste (Photo 3.32). It is believed that the underlying Allt a' Mhuillin, Coire na Ciste and Ledge route Formations are essentially absent in Five Fingers Gully and the Summit Formation rests unconformably on the Dalradian basement in this locality.

A substantial volume of the Summit Formation (est. at 10-40%) is comprised of volcanic breccias comparable to those of the Coire na Ciste Formation (Photo 3.33). Below the summit and in the vicinity of NE Buttress, the proportion is  $\approx$ 40%. On Castle Ridge, and along the northern outcrop of the Summit Formation, the volume of volcanic breccia is  $\approx$ 10%.

---

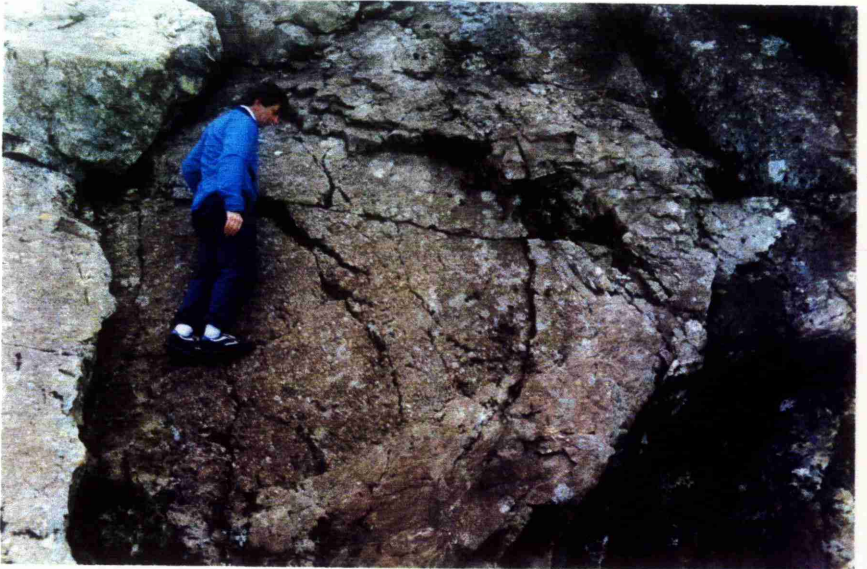
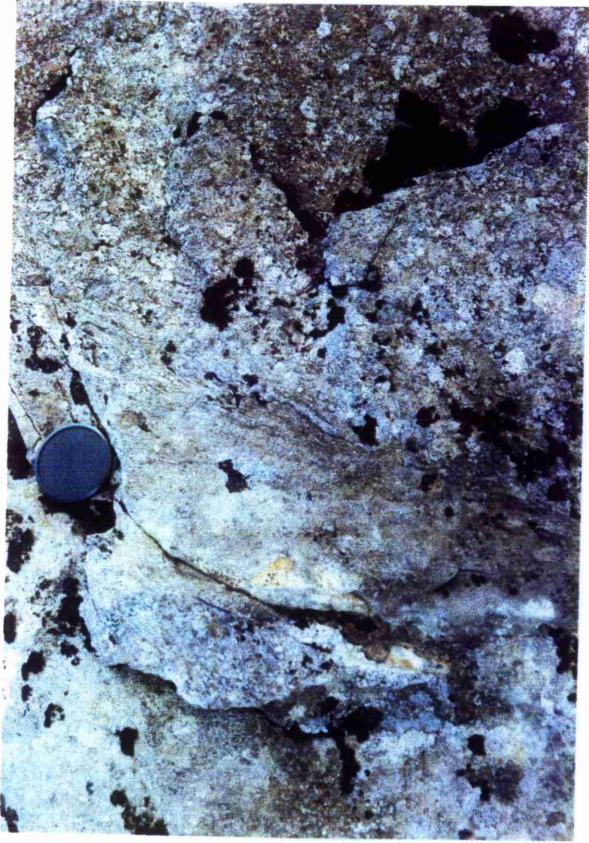
Plate 19 Photo. 3.29 Sheared fine grained base to the Ledge route Member. Sheared base is located in the green grey bands such as that found beneath the lens cap. BN215 (NN162 731)

---

---

Plate 19 Photo. 3.30 Sediment splurge of the Trident Member forced into the Ledge route Member, the injected sediments curve round to a position above the head of Noel Williams. Note the sharp contact between mudstones of the Trident Member and breccias of the Ledge route Member. Escape pipe of Photo 3.31 is located along the feature to the left of Noel Williams. BN215 (NN162 731)

---



---

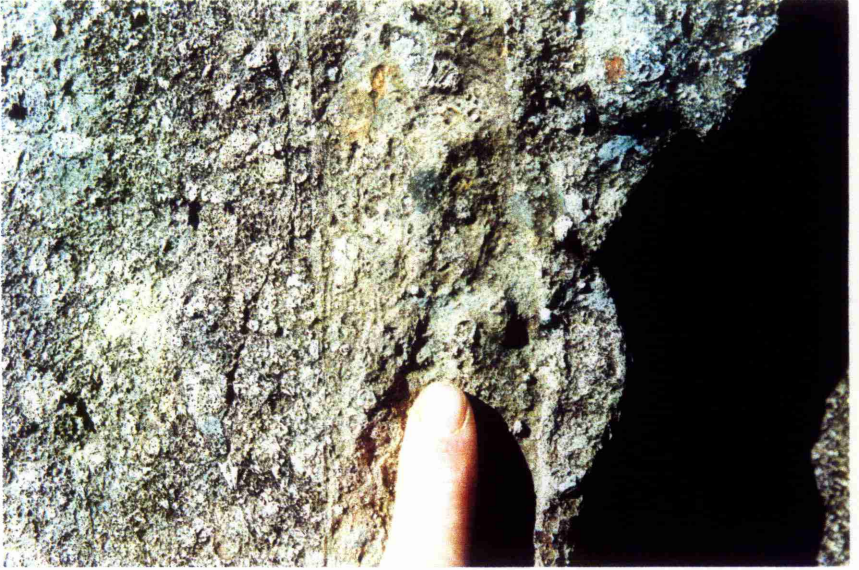
Plate 20 Photo. 3.31 Escape pipe found within the Ledge route Member, note the fine grained nature of the entrained material suggesting that it originated in the Trident Member. BN215 (NN162 731)

---

---

Plate 20 Photo. 3.32 View south from Ledge route across Coire na Ciste to the summit region of Ben Nevis. Sky-line ridge is the North East Ridge, that in the middle ground is Tower ridge with the Gt. Tower forming an obvious projection. A number of faint  $\approx$  horizontal lines are apparent in the Summit Formation, these are believed to represent contacts between different andesite units.

---



Like the other formations of the volcanic pile, lateral variation is significant. A distinctive hornblende andesite outcrops within Gardyloo gully but cannot be traced on Tower Ridge or on Observatory Ridge and must therefore have a lateral outcrop width of <400m.

In the field, the andesites appear very similar, being medium grey in colour and brecciated to a greater or lesser extent. Minerals found as phenocryst phases are plagioclase + hornblende + Fe-Ti oxide  $\pm$  biotite  $\pm$  pyroxene (Photo 3.34). Individual andesite bodies range in thickness from <5m (e.g. BN277) to several tens of metres (Observatory and Tower Ridge). Vesicles are rare and where observed are infilled with epidote and quartz. Xenoliths are rarely observed. Jointing is chaotic and columnar jointing is not a feature of the Ben Nevis andesites. One flow fold was observed *in situ* (BN219), although individual blocks within the volcanic breccias and in the summit boulder fields often exhibit flow-like textures. Autobrecciation of the andesites is common; this typically occurs throughout the entire thickness of an individual horizon.

In thin section, the groundmass is represented by a micro-cryptocrystalline mesostasis of mafic and felsic minerals. Very few phenocrysts, especially the mafic phases, have not suffered some degree of alteration. Brown hornblende crystals have coronas of opaque oxides and often show the effects of corrosion by the matrix. Haslam (1965 & 1968) believed that green hornblende crystals replace ortho and clinopyroxene phenocrysts (but see chapter 5). Plagioclase is typically strongly zoned and in a number of slides shows signs of corrosion by the groundmass.

Bailey & Maufe (1916 & 1960) describe the andesites as autobrecciated lavas however, there is evidence that a number of the andesite bodies are in fact sills. Although this evidence is obtained from the andesite breccias outcropping within the Coire na Ciste Formation, there is no *a priori* reason why sills are not found within the Summit Formation. In the volcanic breccias of the Coire na Ciste Formation the contrast between heterolithic volcanic breccia and monolithic andesite breccia, coupled with essentially flat lying and relatively accessible exposures, allow the identification of extrusive vs intrusive contact relationships more readily than within the largely inaccessible Summit Formation.

#### 3.5.5.ii Key exposures of the Summit Formation

CIC slabs. BN249 & BN250

Both BN249 and BN250 are exposures of the same brecciated andesite body, separated by a distance of  $\approx$ 30m. At BN250 the andesite is  $\approx$ 20m thick with upper and lower contacts against a heterolithic eutaxitic ignimbrite and rhyolite bearing volcanic breccia. At BN249 the andesite terminates; there is no evidence that the volcanic breccias exposed above and below the andesite body form two separate volcanic breccia horizons. Injections of andesite can be found within the volcanic breccia above the main body of

---

Plate 21 Photo. 3.33 Monolithologic volcanic breccia (Nuées ardentes ?) of the Summit Formation. Ice axe is 55cm long. Blue colour is an artefact of the copying process and the rock is really a dark purple-grey  
BN130 (NN158 719)

---

---

Plate 21 Photo. 3.34 Typical andesite, note crude alignment of plagioclase and hornblende/pyroxene phenocrysts from top right to bottom left.  
(Castle Ridge NN157 725)

---



andesite (Photo 3.35). Both of these features indicate that the andesite intrudes a single volcanic breccia horizon.

South of No 5. gully. BN277

In Photo 3.36, the monolithologic and brecciated nature of this andesite horizon is apparent. In thin section andesite clasts merge into the 'matrix'. Petrographically, there is very little difference between clast and 'matrix', indicating that autobrecciation has fragmented that lava and not pyroclastic or epiclastic processes.

Base of Coire na Ciste slabs. BN234

Photo 3.37 is of BN234 and shows a number of clasts of andesite being stretched and pulled apart as the surrounding andesite matrix flowed from right to left (north to south). The contact with the overlying volcanic breccia can be seen in the top left of the photograph and also in Photo 3.38.

### 3.6 Intrusions within the volcanic pile

Those rocks identified as intrusive fall into five groups listed below:

1) Fine grained pink to pink brown rhyolitic veins penetrate the volcanic pile and are especially concentrated close to the contact with the Inner Granite. Individual veins vary between 0.01m and 2m and can be traced for over 100m. Each vein may diverge into several offshoots (Photo 3.39a) that may or may not link up again further into the volcanic pile. At the contact with the host rock, a thin fine grained dark grey band, up to a 1cm thick is often found.

Streaky flow banding (Photo 3.39b), phenocrysts of plagioclase, xenoliths of Dalradian schist and of contemporaneous sediments define a strong fabric similar to that observed in the Fault facies (section 3.7). At least one example of this group can be seen to pass into the Fault facies and the two rock units are intimately related. In thin section, the veins are similar to the Fault facies (compare Photo 3.40 with Photo 3.47).

2) Semi-conformable rhyolite lenses, attaining thicknesses of 1-2m and up to 10m wide, have been preferentially eroded to form shallow hollows in the cliffs of Ben Nevis. In No. 5 gully, a number of these lenses are linked by a dyke-like intrusion of rhyolite located along the line of No. 5 gully. Petrographic and geochemical evidence suggests that this group represent thicker lateral intrusions of group 1) rhyolite veins.

3) On the north side of No 4. gully (BN220, NN 161,717), a 15m by 20m ellipsoidal vent intrudes the Summit Formation. In contrast to the near horizontal Summit Formation, a strong vertical fabric is observed within the vent. In thin section (Photo 3.41), rounded clasts of Dalradian quartzite and phyllite can be identified along with a

---

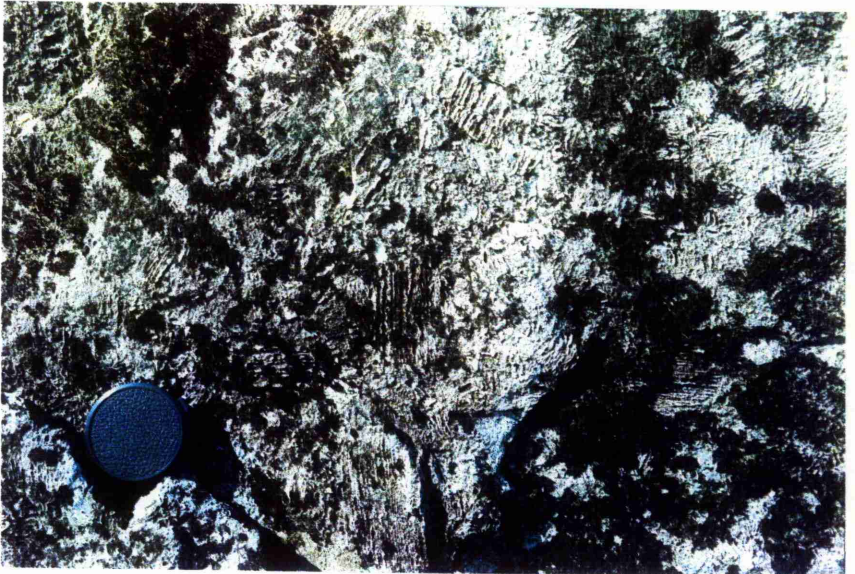
Plate 22 Photo. 3.35 Photograph shows stringers of autobrecciated andesite intruding into the volcanic breccia. Flow movement from bottom left to top right.  
BN249 (NN167 721)

---

---

Plate 22 Photo. 3.36 Autobrecciated andesite. BN277/1 (NN162 721)

---



---

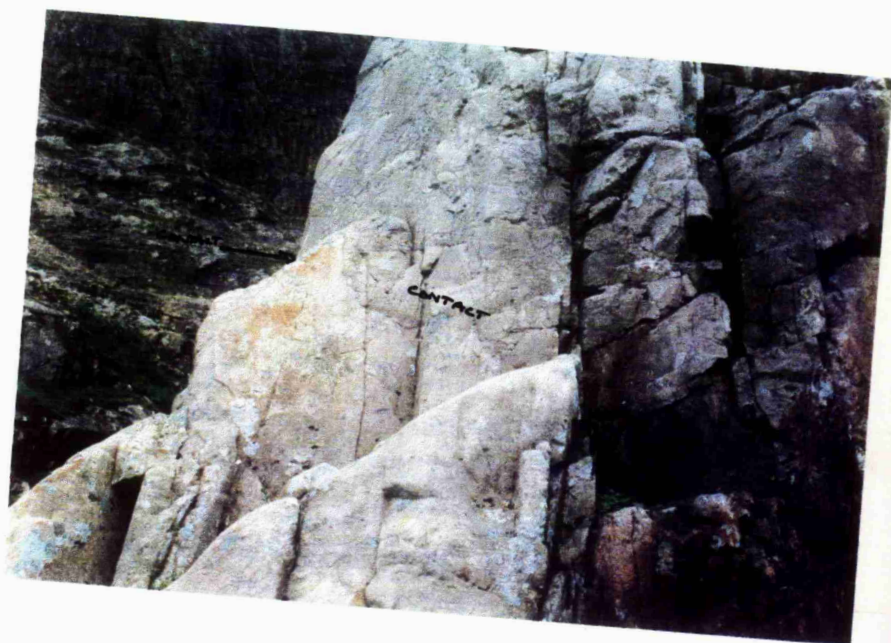
Plate 23 Photo. 3.37 Mechanical brecciation of andesite lava. Flow movement from right to left. Semi-solid to solid clasts of andesite are being sheared and broken up during movement of the surrounding andesite.  
BN234 (NN165 717)

---

---

Plate 23 Photo. 3.38 Contact between volcanic breccia (top) and autobrecciated andesite (bottom). Slight darkening at the base of the volcanic breccia. The base of the andesite lava is shown in the above photo (3.37)  
BN234 (NN165 717)

---



---

Plate 24 Photo. 3.39 Intrusion Type 1 showing small scale offshoots from the main vein. Host rock is an andesite sill. BN249 (NN167 721)

---

---

Plate 24 Photo. 3.40 Surface spaghetti-like texture to intrusion Type 1. BN249 (NN167 721)

---



variety of rounded andesite fragments and supported within a cryptocrystalline matrix containing phenocrysts of plagioclase and rarer mafics.

BN220 may link in with a 20m by 0.75m exposure (BN283, NN 1635,7168) in the floor of Coire na Ciste and having similar characteristics.

4) In Gardyloo Gully (BN269, NN 1675,7162) and at the entrance to the steep-sided gorge defining the southern limit of the Coire na Ciste slabs, brown pipes, 5-25cm thick, intrude the volcanic breccias (Photo 3.42). Prior to tilting of the margins of the volcanic pile, these pipes would have had a near vertical orientation. Strong fabrics are visible in both exposures and neither exposure can be traced onto the opposite wall of the gully/gorge or laterally for any distance hence the use of the term pipe.

In thin section, the pipes at both locations are dominated by a cryptocrystalline matrix, supporting small (<0.8cm) rounded clasts of andesite and fragments of plagioclase. It is believed that these pipes were feeders to small surface eruptions.

5) On Ledge route below the summit of Carn Dearg (SW), a 12m thick by 50m wide, andesite cryptodome intrudes the Ledge route Formation. This dome is extremely well exposed and three feeder pipes have been found. Dalradian fragments entrained within the dome define a fabric parallel to its margin.

In thin section, small microlaths of plagioclase define a strong trachytic texture. Phenocrysts of plagioclase, green hornblende, biotite and Fe-Ti oxides are aligned parallel to the trachytic fabric. A number of feldspar phenocrysts are cracked and have suffered from corrosion.

### 3.7 The Fault facies

#### 3.7.1.i Previous research

Bailey & Maufe (1916 & 1960) described a "Marginal zone of fine grain rhyolite, with small scattered phenocrysts of feldspar and biotite, and with a strong streaky flow structure parallel to the vertical junction (between Inner Granite and volcanic pile), along which a seam of flinty crush rock is developed. This flinty crush rock erodes the rhyolite, as has been described at Glencoe (p163 Bailey & Maufe 1960). The flow structure of the rhyolite is even more apparent than that of the neighbouring andesite lavas." (p181 Bailey & Maufe 1960). The authors contrasted the chilled internal margin of the Inner Granite to that of the outer margin where chilling is only slight.

Clough et al. (1909) described the flinty crush rock of Glencoe thus "It can be shown here, as elsewhere, dark flinty or tachylitic rocks with perfect flow structure have been produced by the shearing of various types of rock, quite independently of igneous action of any sort." (p630, underlining added for this thesis). More recent interpretations of the Glencoe flinty crush rock are described in section 3.8.6.

---

Plate 25 Photo. 3.41 The photomicrograph displays a number of clast types forming the fill in the No. 4 gully vent. The pale clast on the left hand side with dark speckling is a rounded fragment of Dalradian schist whereas the majority of the slide is formed of andesitic clasts and a fine grained igneous matrix. Note the euhedral pyroxene pseudomorphs in the clast forming the top right of the photograph. (BN220 \* 3) (NN161 717)

---

---

Plate 25 Photo. 3.42 Intrusion Type 4, fine grained (ash ?) brown coloured pipes. BN234 (NN165 717)

---



↑ PIPE ↑

### 3.7.1.ii The Fault facies

Intermittently exposed around the margin of the volcanic pile is a flow banded rhyolite, hereafter termed the Fault facies. A strong contact parallel vertical fabric, defined by colour/flow banding, preferred orientation of xenoliths and of plagioclase phenocrysts can clearly be identified in hand specimen (Photo 3.43). Occasionally the fabric exhibits flow folding and can veer to a sub-horizontal orientation. Traditionally this rock has been interpreted as a marginal modification of the Inner Granite caused by the subsidence of the volcanic pile into the Inner Granite (Bailey & Maufe 1916 & 1960).

### 3.7.1.iii Key exposures of the Fault facies

#### BN239. Climbers path

Approximately 100m north of the CIC hut, a flat exposure of the Inner Granite/volcanic pile contact can be examined some 20-30m west of the Climber's path. At this locality, two contacts are visible. A sharp contact (Photo 3.44a) is observed between the volcanic pile and the Fault facies and a second sharp contact occurs between the Fault facies and Inner Granite (Photo 3.44b). In contrast to the strong fabric of the Fault facies, the Inner Granite has a weak fabric. Bailey & Maufe (1916 & 1960) described the flow banded rhyolite at the contact as a modification of the Inner Granite with which it gradually passes into, but the evidence from this locality (BN239) indicates that the chilled flow banded rhyolite is a separate body from the Inner Granite.

#### BN185/204. Allt a' Mhuillin

Approximately 150m south of the CIC hut, the Allt a' Mhuillin falls over a short (2m high) waterfall. Just below this waterfall four rock types are exposed at the contact (Fig. 3.9). Thin sections were made of each of the four rock types, and the following interpretation is applied.

BN204a. Thin sliver of chilled Inner Granite. In thin section, signs of incipient fragmentation are observed.

BN204b Volcanic breccia typical of that found near the base of the Coire na Ciste Formation

BN204c Fault facies, flow banded rhyolite containing fragments of andesite and of Dalradian schists.

BN204d Dalradian basement and the Allt a' Mhuillin Formation

BN185b Reworked Fault facies. Rounded fragments of Fault facies flow banded rhyolite, Dalradian schist and mudstones found within this unit (Photo 3.45).

The contact between the Inner Granite and the Fault facies is repeated twice at this locality (BN204c & BN185d), and it is suggested that there have been two phases of movement along the Fault facies/Inner Granite contact.

---

Plate 26 Photo. 3.43 Fresh surface exposure of the Fault facies. Flow banded rhyolite is clearly depicted in this photograph and not rock which has been sheared. BN242 (NN171 713)

---

---

Plate 26 Photo. 3.44a Contact between Fault facies and Volcanic pile. Fault facies is found in the bottom of the photograph. BN239 (NN165 725)

---



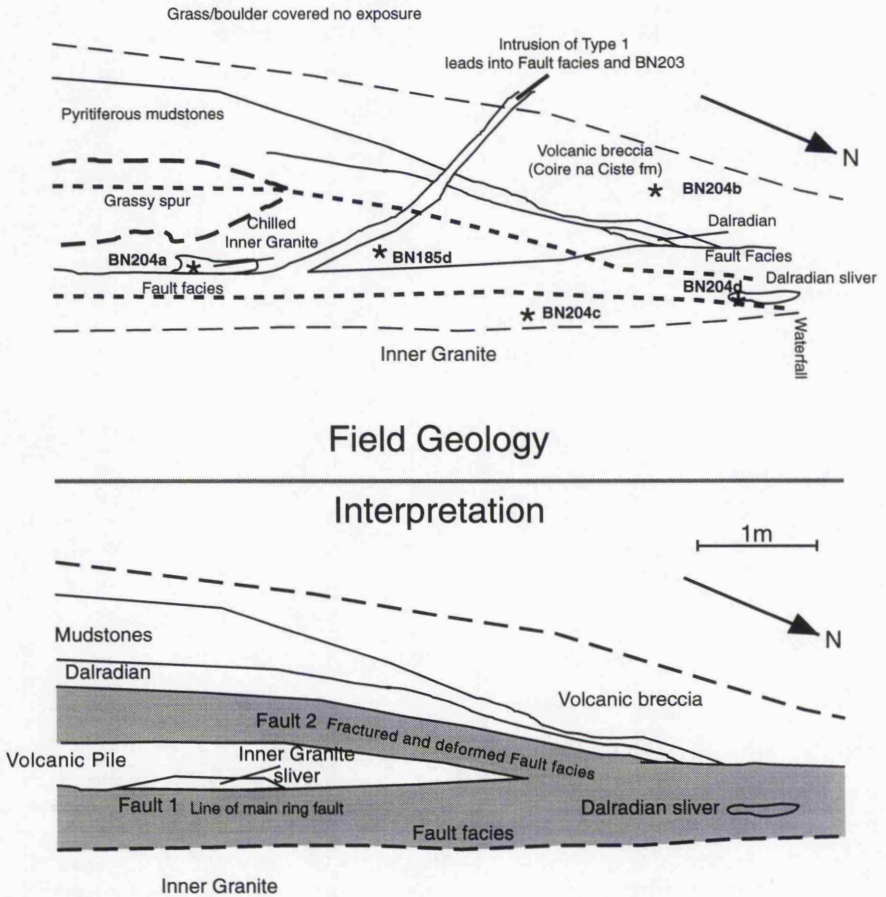


Fig. 3.9 Field geology and interpretation of BN185/BN204. Repetition of volcanic pile/Inner Granite contact is caused by renewed movements along Fault 2. This later activity was a largely brittle process with negligible addition of new Fault facies material. This locality can be found in the bed of the Allt a' Mhuillin (flow from left to right) at Grid. ref. NN168 722.

---

Plate 27 Photo. 3.44b Contact between Fault facies and Inner Granite. Inner Granite forms the left hand side of the photograph. BN239 (NN165 725)

---

4.

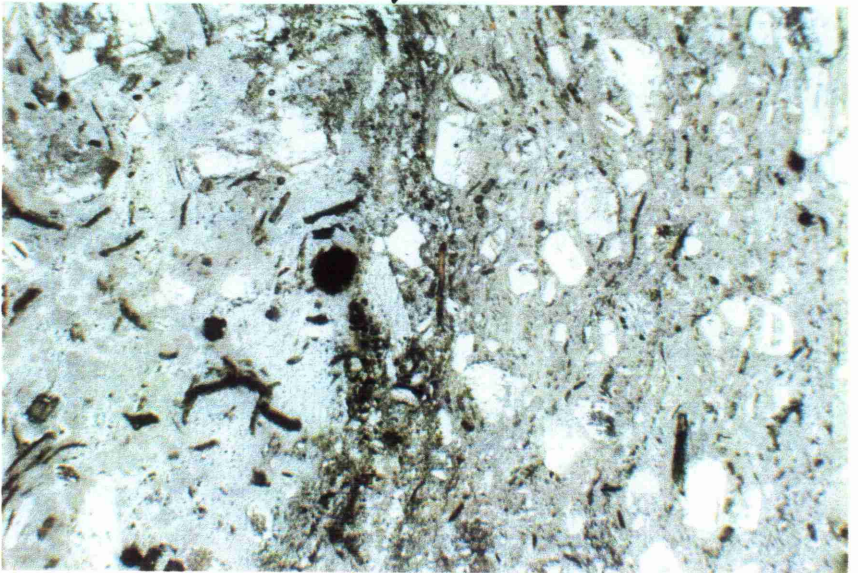
---

Plate 27 Photo. 3.45 Photomicrograph of reworked Fault facies. The slightly darkened band in the middle of the photograph represents the line along which the Fault facies was reworked. (BN185b \*21) (NN 133 702)

---



REWORKED FAULT FACIES



Phase 1 (BN204c) is associated with intrusion of the Fault facies along the Inner granite/volcanic pile contact. Phase 2 (BN185d) reworked the Phase 1 contact and excavated fragments of Fault facies, Dalradian schist and mudstone to form a coarse fault breccia. In thin section, the breccia is made up of a large proportion of these fragments (85%), and the matrix includes whole and partial crystals of plagioclase, biotite and quartz within a cryptocrystalline 'groundmass'. The mudstone clasts have a thin baked margin implying that the matrix represents relatively hot material.

The model of Bailey & Maufe (1916 & 1960) cannot account for the field relationship and structures of BN204/BN185. There is no evidence of shear induced melting, rather the Fault facies has flowed into its current position entraining fragments of the adjacent wall rock en route. Baked mudstone clasts require a hot Fault facies matrix and later brittle faulting has reworked the contact between the Fault facies and the Inner Granite in this locality.

#### BN184. Allt a' Mhuillin

BN184 is the type locality for the flinty crush rock of Bailey & Maufe (1916 & 1960). In Photo 3.46a & 3.46b, a fine grained chocolate-brown band represents the flinty crush rock. If this band has been formed by shear melting at the contact between the volcanic pile and Inner Granite, then it should be located at the contact, but, it is in fact found entirely within the Fault facies. An alternative interpretation for the chocolate-brown band, is that it represents a fine grained phenocryst poor band of the Fault facies.

#### BN242. Coire Leis

Photo 3.43 and 3.47 are hand specimen and thin section photographs of the Fault facies from this locality. The Fault facies attains its maximum apparent thickness (8m) at this exposure, true thickness is probably 5-6m. On weathered surfaces the Fault facies has a spaghetti-like texture comparable to that observed within group i) intrusions. Locally the fabric of the Fault facies tends to a sub-horizontal orientation. On fresh surfaces (Photo 3.43), a strong flow banding is obvious. In thin section (Photo 3.47), biotite is bent around phenocrysts of plagioclase and small xenoliths. This feature is indicative of a flattening strain and not of shearing.

Xenoliths include fragments of Dalradian metasediments and of andesite. If the Fault facies simply represents an *in situ* chilled margin to the Inner Granite then, like the Inner Granite, it should contain no xenoliths. Additionally, Bailey & Maufe (1916 & 1960) state that the flinty crush rock erodes the Inner Granite of Ben Nevis; therefore if this mechanism is correct, xenoliths from the volcanic pile should not be found within the chilled margin of the Inner Granite. The occurrence of fragments of the volcanic pile within the Fault facies and the absence of Inner Granite fragments, provides crucial evidence on the nature of the contact. Clearly the Fault facies has eroded fragments from the volcanic pile, the absence of Inner Granite fragments can be explained if the Fault facies represents

---

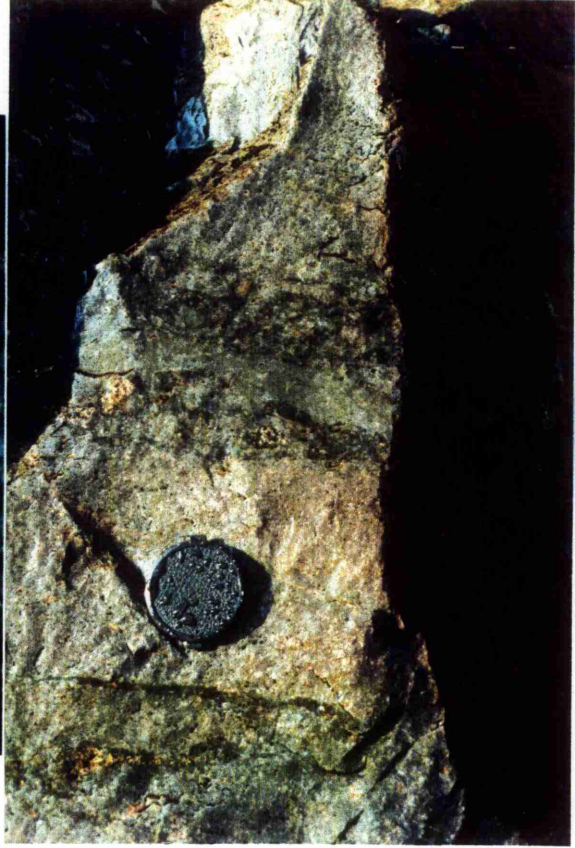
Plate 28 Photo. 3.46a Type locality of the 'flinty crush rock'. The author's right foot is on the Inner Granite and the left foot rests on Fault facies. The extreme right margin of the photo is comprised of Allt a' Mhuillin Formation sediments. BN184 (NN169 721)

---

---

Plate 28 Photo. 3.46b Close up of the flinty crush rock type locality. The grey-brown streak to the right of the lens cap is in reality the chocolate-brown Flinty Crush Rock of Bailey & Maufe (1916). This streak is found within the Fault Facies and is not observed at the contact between the Inner Granite and the volcanic pile indicating that it is a fine grained variant of the Fault facies and not a product of shearing. BN184 (NN169 721)

---



molten Inner Granite forced up from deeper levels in the magma chamber by the descending volcanic pile.

#### BN240. Castle Ridge

In thin section the Fault facies at this location has a crenulate chilled margin against a mudstone band in the volcanic pile (Photo 3.48). Deformation of, and partial intrusion of the Fault facies into the mudstone is observed. The Fault facies has a 0.1 cm thick chilled margin against the mudstone. This suggests that the Inner Granite was sufficiently hot to be chilled against the volcanic pile. No shearing at the contact is recognised and it is believed that the Fault facies was molten and not heated by friction during collapse of the volcanic pile.

The model of Bailey & Maufe (1916 & 1960) for the development of the flinty crush rock and marginal modification of the Inner Granite by friction and cooling during the collapse of the volcanic pile cannot explain the features observed at the contact during this field study, specifically:

1) It is mechanically difficult for a molten magma such as the Inner Granite, to cross an active shear zone and yet numerous intrusions (Type 1) with textures comparable to that of the Fault facies are found within the volcanic pile. The simplest explanation for this feature is that the Fault facies represents magma displaced by the subsiding block, some of which was injected into fractures that opened in the block during subsidence.

2) Both group i) intrusions and the Fault facies contain biotite crystals bent around feldspar crystals and lithic fragments. One interpretation of this structure is that the Fault facies and veins of group i) represent the remnants of an expanded fluidised magma. Cessation of intrusion and loss of volatiles resulted in partial collapse of the magma conduit and flattening of the enclosed magma (Wolff 1986).

3) Contacts between the Fault facies and the Inner Granite indicate that the two are separate intrusions.

4) Fabrics within the Fault facies are indicative of flow rather than shearing.

5) The chocolate brown band of BN184, the type locality of the flinty crush rock (Bailey & Maufe 1916 & 1960), is found entirely within the Fault facies (Photo 3.46b) and cannot have been formed by shearing at the contact between the Inner Granite and the volcanic pile. Shearing within the Inner Granite would have to be invoked, yet Bailey & Maufe (1916 & 1960) believed that Inner Granite was largely molten during collapse of the volcanic pile.

6) The model of Bailey & Maufe (1916 & 1960) does not address the problem of space. In this model the volcanic pile represents part of the magma chamber roof which collapsed into the underlying Inner Granite. The minimum amount of subsidence can be

---

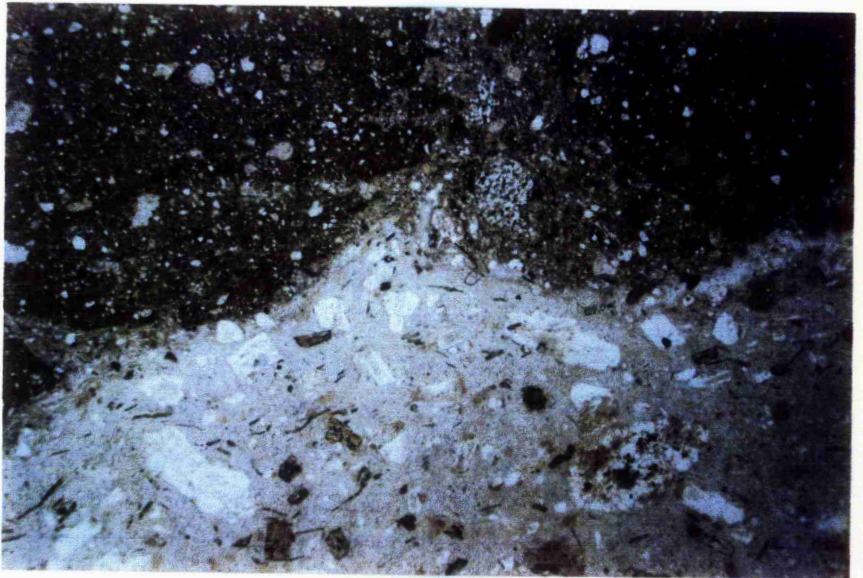
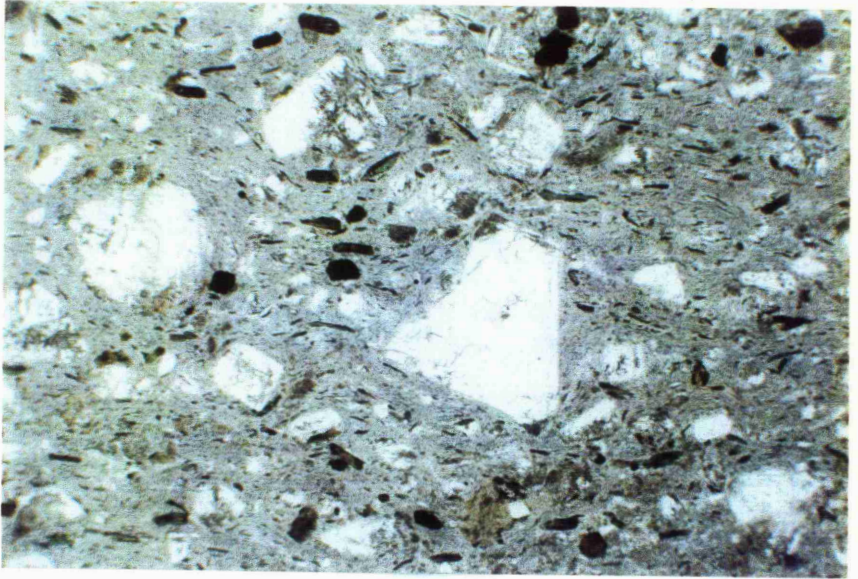
Plate 29 Photo 3.47 Photomicrograph of Fault facies, note the flattening of biotite and amphibole crystals around larger feldspar fragments (BN242 \* 21).

---

---

Plate 29 Photo. 3.48 Photomicrograph of contact between sediments of the volcanic pile and the Fault facies. Note the wavy/irregular chilled margin of the Fault facies indicating the existence of a large temperature difference between the two rocks types. There is no sign of shearing in this thin section.  
(BN240 \* 21) (NN155 726)

---



estimated from the difference in altitude between the lowest exposure of the volcanic pile and the highest exposure of the Inner Granite and is  $\approx 650\text{m}$ . Multiplying this estimate by the area of the volcanic pile ( $3.5\text{km}^2$ ) obtains a volume of  $2.3\text{km}^3$ . This volume of magma needs to have been removed to create space for the volcanic pile during subsidence. The most efficient mechanism for moving large amounts of magma is to erupt the magma onto the surface. The strongly flow banded Fault facies is believed therefore, to represent a pathway by which material from below the subsiding block was vented onto the land surface.

### 3.8 Interpretation

#### 3.8.1 The Allt a' Mhuillinn Formation

Summary of main features;

- 1) Fine grained laminated mudstones and siltstones with conglomeratic breccias
- 2) Apart from a 2-5cm scale rhythmic fining up cycle, the mudstones lack cross-bedding, ripples and other current related structures
- 3) Conglomerates breccias are clast and matrix supported
- 4) Clasts within the conglomerates breccias often exhibit a preferred orientation
- 5) Considerable lateral variation in the distribution of conglomeratic breccias
- 6) Absence of marine fossils and bioturbation
- 7) Lack of macroscopic volcanic detritus

##### 3.8.1.i Fine grained sediments

The contrast in grain size between mudstones and conglomeratic breccias reveals the operation of two separate depositional processes. Deposition of mudstone and siltstone point to a freshwater lacustrine environment; there is no evidence, such as marine fossils, bioturbation etc, of a marine environment. Branney (1988) uses similar arguments to support a freshwater lacustrine environment for the parallel laminated sandstones in the Borrowdale Volcanic Group. Periodic failure of sediment accumulations on the lake margins or flash flood events generated low volume fine grained turbidites and are preserved as 2-5cm scale fining-up sequences.

##### 3.8.1.ii Conglomeratic breccias

Bailey & Maufe (1916 & 1960) describe the conglomeratic breccias as locally derived basement breccias, but, although the conglomeratic breccia exposed in the Allt a' Mhuillinn stream bed rests on Dalradian metasediments, those exposed below the North-east Buttress are found resting on mudstones of the Allt a' Mhuillinn Formation. In addition, the volume of local Dalradian pelitic basement clasts is outweighed by the volume of quartzite clasts and consequently, the conglomeratic breccias cannot be considered as basement breccias.

Matrix supported deposits, such as the conglomeratic breccias, require the simultaneous deposition of both clast and matrix, the lack of internal structure within individual conglomeratic breccias indicates deposition as a single flow unit. These features indicate that each conglomeratic breccia was emplaced as a gravity flow. Leeder (1982) defines four end-member gravity flow types, these being: grain flows, debris flows, liquefied flows and turbidity flows. Grain flows tend to be restricted to aeolian environments or to small-scale ripple structures. Deposits from liquefied flows are characterised by abundant water escape structures. Turbidity currents are unlikely to contain such coarse and unstratified detritus. Debris flows are represented by massive unsorted and unstratified material with a range of clast sizes from fine mudstone to large boulders. A fine grained component is essential to debris flows, providing the flow with the ability to transport coarse material, however the volume of this component can be as little as 1%. Leeder (1982) suggests that plug flow is the dominant transport mechanism for debris flows, producing a massive unsorted deposit resting on a sheared, fine grained base. Consequently, except at the basal shear zone, clasts within a debris flow will not exhibit a preferred orientation, but Fisher (1971) and Enos (1977) described debris flow deposits with a preferred orientation. Enos (1977) further stated that coarse grained unsorted deposits with preferred orientations are characteristic of debris flow deposits. The conglomeratic breccias of the Allt a' Mhuillin Formation are therefore interpreted as debris flow deposits.

Lateral variation in the distribution of each conglomeratic breccia demonstrates either confinement within some form of channel or that each conglomeratic breccia flowed as a coherent body over a relatively flat surface. No evidence of channelling could be found within the Allt a' Mhuillin Formation and the latter mechanism is preferred.

The debris flows of the Allt a' Mhuillin Formation flowed under water. Mixing between the water column and the margins of conglomeratic breccia CB(b) resulted in turbulence and sorting at the margin explaining the rapid transition from unsorted debris flow into more texturally mature and finer deposits that culminates in a fine grained sandstone.

Hampton (1972) suggests that sub-aqueous debris flows can grade into turbidity currents, providing sufficient water can be added to the matrix in order to decrease the yield strength and viscosity of the flow such that turbulence is allowed to develop. It could therefore be envisaged that the fine grained low volume turbidites represent the distal component of the conglomeratic breccia debris flows. However, the absence of any intermediate stage deposit suggests that this is not the case. Mullineaux & Crandell (1962) traced individual lahar deposits over distances of up to 40km from the source. The debris flows and lahars of the Allt a' Mhuillin Formation may similarly have travelled large distances prior to entering the Ben Nevis sedimentary basin.

### 3.8.2 The Coire na Ciste Formation

#### Summary of main features:

- 1) Dominated by massive unsorted volcanic breccias
- 2) Contains clasts of eutaxitic ignimbrite and rhyolite which are not found *in situ*
- 3) Andesitic clasts are gas/vesicle poor and exhibit a range of boundary relationships with the matrix
- 4) Baked mudstone clasts are present in at least one volcanic breccia
- 5) Structurally, the volcanic breccias are comparable to the conglomeratic breccias of the Allt a' Mhuillinn Formation; volumetrically, however, the volcanic breccias tend to be larger.
- 6) The outcrop pattern in Coire Leis suggests that volcanic breccias pond into a topographic low and there is evidence of channelisation
- 7) Andesite lavas/sills and sediment bands can be found within the Coire na Ciste Formation

Modern volcanoclastic deposits are often analysed and described on the basis of grain size distributions. This technique cannot be applied to the Ben Nevis volcanic pile because the volcanic breccias are now solid rock and not the unconsolidated deposits of modern day volcanic terrains.

#### 3.8.2.i Possible modes of origin for volcanic breccias

Large silicic stratovolcanoes can generate volcanic breccias with similar compositions and textures via a number of different mechanisms. Epiclastic lahars and pyroclastic block and ash flows in particular, are easily confused. It is likely that a number of volcanic breccias in the volcanic pile of Ben Nevis, are lahars; particularly those with heterolithic clast compositions, however interpretations based on clast heterogeneity alone should be treated with caution. Early papers from Mount Pelée by Roobol & Smith (1975 & 1976) described monolithologic breccias as block and ash flows and heterolithic breccias as lahars. Later papers by the same authors (Smith & Roobol 1990) stated that this method is ambiguous because of the variable lithic content of some block and ash flows especially close to the vent (i.e. lag breccias in the sense of Druiitt & Sparks (1982) and lithic breccias in the sense of Walker (1985) and Roobol et al. (1987)). Instead, evidence for hot or cold emplacement was used to distinguish between block and ash flow deposits and lahar deposits. Roobol & Smith (1990) suggested that the presence of gas escape pipes and carbonized wood distinguish block and ash flows from lahars, but lahars can contain carbonised wood either as a primary feature or as an entrained clast (Mullineaux & Crandell 1962). Gas pipes have not been observed in lahars and may represent an unambiguous genetic marker, but it is possible that post depositional compaction and alteration can obscure these pipes.

A single volcanic eruption is capable of producing vesicle poor lava blocks and/or bombs, ash, glass and pumice (Cas & Wright 1988). Such variation in products from a

single volcanic eruption complicates diagnostic methods based on the homogeneity or otherwise of the volcanic breccias.

Fisher & Heiken (1982) describe block and ash flows from Mount Pelée as topographically controlled, unsorted and massive deposits with an ash matrix and containing large, generally non-vesicular cognate lithics up to 5m in diameter. Lithic clasts within block and ash flows are derived from three sources (Cas & Wright 1988); these being slow cooled and crystallised magma rinds, rocks excavated from conduit walls and rock fragments entrained during flow. Individual block and ash flows can contain up to 50% lithics (Rose et al. 1976) and individual clasts are angular to sub-angular.

Large volcanic debris avalanches can generate deposits structurally and compositionally similar to lahars and pyroclastic flows. If sufficient water is picked up along route, then debris avalanches can grade into lahars. Poorly sorted brecciated debris, often with a jigsaw fit to fragmented clasts characterise debris avalanche deposits. In general, the average clast size decreases with distance from the source. Individual clasts can be up to several hundred metres in diameter (Siebert 1984). These large megablocks, where present, characterise debris avalanche deposits, but not all debris avalanches contain megablocks and Siebert (1984) also documented avalanche deposits with a maximum grain size of a few metres. The absence of fragmented jigsaw fit clasts within the Coire na Ciste volcanic breccias suggests that they are not debris avalanche deposits, although this is not conclusive evidence.

Although Cas & Wright (1988) describe block and ash flows as having non-juvenile material rarely exceeding 5%, Siebert (1984) suggests that there is a continuous series between 100% juvenile block and ash flows and 0% juvenile volcanic debris avalanches if, as at Mount St Helens, the mechanism leading to the eruption of block and ash flows is the catastrophic failure of part of the volcanic cone exposing the underlying magma chamber.

Mullineaux & Crandell (1962) used the presence or absence of older rocks types to distinguish between lahars and pyroclastic flows. The authors studied Mount St Helens, an active stratovolcano with a well constrained 'volcano-stratigraphic' succession and where they could trace individual deposits along drainage channels to their point of origin up to 40km away. The small area of volcanic exposure on Ben Nevis renders this method unusable, and field geology combined with thin section work is used to identify block and ash flows from lahars.

#### 3.8.2.i The intervening breccia

The textures in the intervening breccia are identical to those of the conglomeratic breccias with the exception that the intervening breccia contains volcanic and baked mudstone clasts. Baking of mudstone clasts shows that the flow was relatively hot and it is suggested that the intervening breccia represents a sequence of lahars generated during or shortly after a volcanic eruption.

### 3.8.2.iii A pyroclastic origin ?

Lahars and block and ash flows generate very similar deposits; both are topographically controlled, unsorted and are generally massive with an essential fine grained component. Lahars generated by contemporaneous volcanic activity can be monolithologic and contain fresh andesitic glass. Post depositional alteration and lithification can further blur differences between the two mass flow types (Cas & Wright 1988).

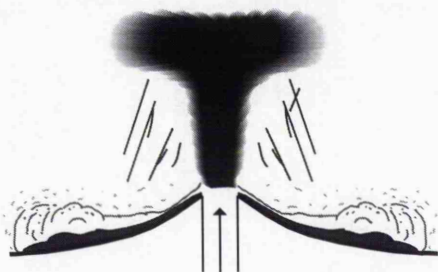
A pyroclastic origin is preferred for those volcanic breccias dominated by one andesite clast type and in thin section show evidence that these clasts were hot when emplaced and that the matrix contains a similar suite of phenocrysts. These deposits are topographically controlled and were therefore generated by pyroclastic flows. Absence of pumice and scoria combined with a very low vesicle content of the andesite clasts define these deposits as block and ash flows. A number of mechanisms have been put forward for the generation of block and ash flows (Fig. 3.10). From the low gas/vesicle content of the Ben Nevis examples, it is evident that the volatile content of the magma was not the main mechanism for the formation of these deposits. Sato et al. (1992) described numerous block and ash flows from the repeated collapse of a dacite lava dome being formed on the Unzen volcano. Frames obtained from a videotape depict the formation of one such block and ash flow from the failure of a lava flow front. The authors suggested that the trigger for fragmentation of this flow may have been the sudden reduction in confining pressure or landing shock as fragments fractured on hitting the ground or a combination of both these processes. Similar mechanisms are proposed for the generation of block and ash flow deposits on Ben Nevis.

Pyroclastic surge deposits are intimately related with pyroclastic flows (Smith & Roobol 1990), but none are observed within the Ben Nevis volcanic pile. There are three possible explanations:

1) All the volcanic breccias are lahars, but this is not thought likely given the clast/matrix boundary relationships described above (3.5.5.ii).

2) Unlike pyroclastic flows, pyroclastic surges possess sufficient energy to surmount all but the steepest terrain. It is possible that pyroclastic surges were decoupled from the underlying pyroclastic flow when the combined flow/surge body encountered high ground that the pyroclastic surge was able to surmount but the pyroclastic flow had to go around.

3) Outcropping intermittently throughout the volcanic pile are a number of fine grained sediments; these reveal the presence of a standing body of water. Cas & Wright (1988) stated that the mechanism by which a pyroclastic flow interacts with a body of water is controlled by the density of the flow. Their model is based on pumice flows. If the density of the flow is  $> 1.0 \text{ gcm}^{-3}$  then it can enter the water column. A gas-particulate

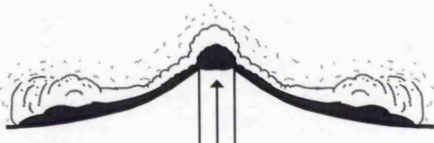


Eruption column collapse.

(Soufriere Type).

$$P_e > T_s$$

Where  $P_e$  = excess pore pressure  
and  $T_s$  = tensile strength of lava.



Low pressure 'boiling' over.

(Merapi Type).

$$P_e \leq T_s \text{ (locally } P_e > T_s)$$



Directed blast or dome collapse.

(Pelean Type).

$$P_e < T_s$$

Fig. 3.10 The generation of pyroclastic flows, adapted from Sato et al. (1992).

such as a pumice flow, would be destroyed by violent phreato-magmatic eruptions and pass into an ash turbidite, but the effect of the water column on a dense (up to  $2.0 \text{ gcm}^{-3}$ , Cas & Wright 1988) coherent block and ash flow is likely to be somewhat different. Sparks et al. (1980a & b) modelled the passage of pyroclastic flows into the water column with reference to a block and ash flow erupted on Dominica. Having a high yield strength and a low gas content, the block and ash flow maintained its integrity on entering the sea and flowed along the basin floor. Low density ( $<1.0 \text{ gcm}^{-3}$ ) pyroclastic surges are likely to override the water surface and settle out as fine ash (Fig. 3.11). At Mount Pelée, the block and ash flow entered the sea whilst the associated pyroclastic surge flowed out across the water (Anderson & Flett 1903 and La Croix 1904).

### 3.8.3 The Ledge route Member

Summary of main features:

- 1) Moderately well sorted volcanic breccias
- 2) Strongly clast supported
- 3) Weak preferred orientation visible in some localities
- 4) Local topography evident from contact with underlying Trident Member

5) Thins towards Coire na Ciste where the volcanic breccias are interbedded with fine grained sediments

7) Deformed underlying Trident Member sediments

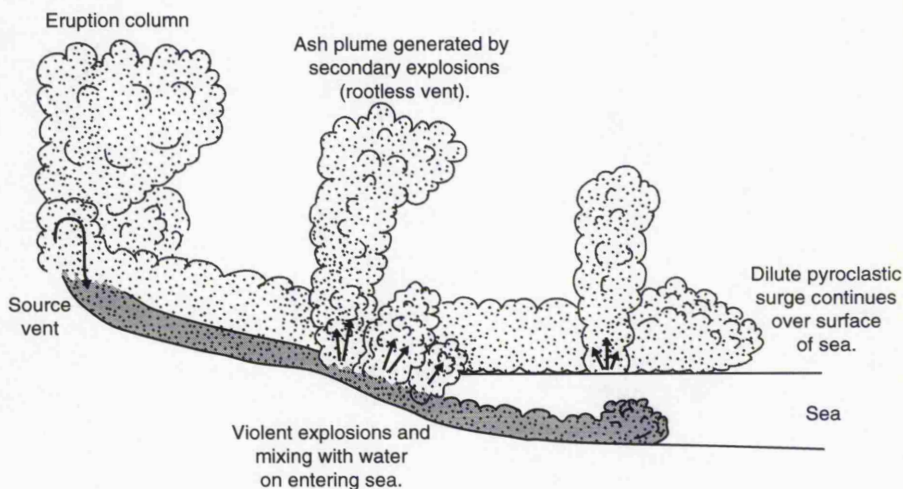


Fig. 3.11 Model for the evolution of a pyroclastic pumiceous flow on entering the submarine environment, adapted from Cas & Wright (1988).

Two features of the Ledge route Member are apparently anomalous, these are: evidence that the Ledge route Member flowed into its current location with sufficient energy to deform the underlying sediments and that the clasts are moderately well sorted. Two mechanisms are required to explain these features; a mechanism for sorting the clasts and a mechanism by which the volcanic breccias flowed into the Trident Member basin.

In Castle Coire the Ledge route Member is associated with andesite breccias; in Coire na Ciste the Ledge route Member is found interbedded with sediments. In addition, the thickness and frequency of these sediments decreases northwards towards Ledge route. A period of time is required for the deposition of the mudstones and the Ledge route Member must therefore be formed from a number of similar volcanic breccia horizons. The source for these deposits is believed to be from the north where the Ledge route Member volcanic breccias are interbedded with a number of andesite breccia horizons. Because the sediments with which the volcanic breccias are interbedded show no form of current related structure, it is proposed that the Ledge route Member represents a proximal airfall deposit which was subsequently reworked by mass flow processes. Substantial local topography is indicated by the presence of the fallen block within the transition zone between Trident Member and Ledge route Member deposits. Rapid build-up of tephra on this local topography would rapidly form oversteepened and unstable slopes that then failed and flowed into the Trident Member sedimentary basin.

### 3.8.4 The Summit Formation

Summary of main features;

- 1) Dominated by autobrecciated andesite
- 2) Brecciation most commonly extends throughout a single andesite horizon
- 3) Vesicle/gas poor
- 4) Laterally discontinuous
- 5) A number of andesite horizons are sills
- 6) Interbedded with monolithologic volcanic breccias
- 7) Require degassing prior to eruption

With the possible exception of some basic and ultrabasic magmas, most subaerially erupted magmas potentially contain sufficient volatiles to generate explosive eruptions especially given the availability of meteoric water. Consequently, the majority of subaerial silicic volcanic successions are dominated by pyroclastic and epiclastic deposits (Cas & Wright 1988). For coherent silica rich lavas to be erupted at the surface, the magma must have undergone a period of degassing. This can be achieved by either the direct escape of exsolving volatiles (gradually through the vent, hydrothermal springs and fumarole activity or more rapidly by episodic hydrothermal explosions) or by degassing during an earlier or contemporaneous episode of pyroclastic activity during which most of the volatiles within the magma chamber are removed. This suggests that the extrusion of lava represents the terminal phase of many volcanic eruptions, e.g. Mount St Helens (Swanson et al. 1987). Volcanologists now believe that the efficiency of magma degassing is the primary control on eruption style (Sato et al. 1992 and Fink 1991).

The Summit Formation is dominated by autobrecciated andesite lava; monolithologic volcanic breccia (block and ash flows ?) form a relatively minor component (10-40%) of this formation. Consequently, direct exsolution of volatiles is believed to be the main mechanism by which volatiles were lost from the magma chamber. Alternatively, it is also possible that the volcanic breccias of the Coire na Ciste Formation and the andesites of the Summit Formation represent different eruptive products from a single large magma chamber that was later degassed by pyroclastic activity prior to extrusion of andesitic lava of the Summit Formation. But, isotopic data do not support the existence of a single large magma chamber, rather a small volume magma chamber that was repeatedly replenished during the formation of the volcanic pile. As each fresh pulse of magma into the chamber would require degassing, a single period of pyroclastic activity early in the history of the volcanic pile is not a tenable mechanism for generating the andesites of the Summit Formation.

Degassing increases the viscosity and yield strength of the magma, which would in turn affect the length and thickness of a lava flow (Walker 1973a). Although the small area of exposure can yield no detailed evidence of flow length, because of the low volatile content

(absence of vesicles), brecciated character and silicic chemistry, it is suggested that the summit andesites are near source lavas.

Subaerial silicic lava flows are typically described as having a brecciated base that passes into a massive core and then into a brecciated upper surface (Krauskopf 1948, Segerstrom 1950, Suthren 1977 and Sigurdsson 1981). Internally, behind the flow front, andesitic lavas are usually massive with columnar or blocky jointing. Aligned phenocrysts indicate laminar flow. The Ben Nevis andesites, however, are brecciated throughout their entire thickness. Vincents et al. (1989) described similar lava flows from Paleao-Pelée. Volcanic breccias of their "Tombeau Caraïbe" type are well lithified (form high ridges) and form a succession of coarse disorganised matrix to clast supported flow units separated by ill-defined contacts. Flow units range between a few metres and twenty metres in thickness and are poorly graded. Clasts are mainly sub-rounded acid andesites and are slightly to non-vesicular. Boundaries between clast and matrix show a complete gradation from sharp clear contacts to more progressive transitions. Some clasts show features consistent with progressive disintegration. Vincent et al. (1989) believed that these breccias result from the progressive mechanical brecciation during movement of the lava and not pyroclastic activity. This is believed to have occurred at source vent or in the magma conduit. Massive andesite lavas are relatively scarce in Paleao-Pelée, as they are on Ben Nevis. Suthren (1977) believed that subaerial lavas that are autobrecciated throughout are formed by the sinking of individual blocks from the brecciated lava 'roof'. The main problem with this model is that the buoyancy contrast between clast and lava is negligible and, given the viscosity of andesitic lava, an individual clast is unlikely to sink. The presence of even a small vesicle component to individual clasts would render them less dense than the underlying magma.

The "Tombeau Caraïbe" type deposits are described from areas less than 10km from the source vent. Unfortunately, no paleaogeographic interpretation is presented. Given the existence of standing bodies of water during the deposition of the Allt a' Mhuillin Formation, Coire na Ciste Formation and Ledge route Formation, it is conceivable that the summit andesites were also erupted under or flowed into water. Furnes et al. (1980) described andesite lavas frequently brecciated throughout and with no flow banding or vesicles as having been erupted into the water column; a similar conclusion was reached by Busby-Spera (1986) for andesites lavas brecciated throughout in a submarine caldera complex.

Cas (1978) described deep water silicic lava flows with phenocrysts of feldspar and quartz set in a fine grained crystalline (recrystallised ?) mosaic of quartz, feldspar, phyllosilicate minerals and epidote. Fragmentation yielded clasts with planar to curvilinear surfaces and these are unlikely to have been generated by gas bubbles.

Both the descriptions of Furnes et al. (1980) and Cas (1978) could equally be applied to the Ben Nevis andesite breccias, and it is possible that the andesites were erupted under or flowed into a body of water.

### 3.8.5 Subaqueous deposition

In the above discussion a subaqueous environment was put forward in order to explain a number of features within different formations of the volcanic pile. The literature lacks detailed descriptions of subaqueous silicic lava flows and subaqueous high density pyroclastic flows. In a recent discussion of active lava flows, Kilburn & Luongo (1993) presented a bibliography for those volcanologists wishing to look at subaqueous lava flows. This list does not contain any example of subaqueous silicic magmatism. Cas & Wright (1991) reviewed the literature with respect to subaqueous pyroclastic flows and ignimbrites and they state that "...very few examples of subaqueous pyroclastic deposits with evidence for hot emplacement and of being wholly submerged have been described". The authors go on to document just seven examples where they believed that the evidence for subaqueous pyroclastic flow was unequivocal, but unfortunately none of these examples includes pyroclastic block and ash flows.

Evidence for the presence of water during the evolution of the Ben Nevis volcanic pile is based on the occurrence of fine grained clastic mudstones and siltstones at the base of the succession and sporadically throughout the volcanic pile. It is unlikely that the volcanic eruptions only occurred when a large body of standing water was not present in the palaeo-Ben Nevis area.

Cas & Wright (1988) suggested that certain evidence must be present before classifying a pyroclastic flow as subaqueous. Firstly, the facies characteristics of the host sediments in immediate contact with the pyroclastic flow should be fully documented and provide incontrovertible evidence of subaqueous deposition. Secondly, evidence for hot emplacement (welding, gas escape structures, columnar jointing) must be convincing. The authors recognised that application of these criteria to an ancient tectonised and altered succession can be problematic. In addition, block and ash flows are rarely welded, gas escape pipes are not common and columnar jointing is not a feature of block and ash flows (Cas & Wright 1988). Given the high yield strength and the high density of block and ash flows Sparks et al. (1980) suggested that block and ash flows will undergo very little alteration during entry into the subaqueous environment and it can reasonably be assumed that the same can be said for lahars and debris avalanche deposits.

Whilst the evidence for any single horizon having flowed under the water is equivocal, it is probable that a number, if not all of the volcanic breccias and lava flows of the Ben Nevis pile entered or were formed under a standing body of water.

Cas et al. (1981) placed a similar interpretation on the Lower Devonian volcanoclastics of the northeastern Lachlan Fold Belt. In this sequence, a mudstone facies represents background deep marine sedimentation, and a volcanoclastic facies association interrupts the mudstone facies with various forms of mass flow. Both facies were deposited

in relatively deepwater and represent a submarine volcanic apron, probably developed around the newly emergent volcanic Bindook Complex.

### 3.8.6 Fault facies

Summary of main features;

- 1) Sharp contact with the Inner Granite
- 2) Flow fabric of igneous origin
- 3) Outcrops between the volcanic pile and the Inner Granite

The Fault facies outcrops between the Inner Granite and the volcanic pile, this indicates that it has an intimate relationship with whatever process is envisaged to have juxtaposed the volcanic pile against the Inner Granite. Textures observed within the Fault facies are consistent with partial collapse of a magma conduit after magmatic flow had ceased. As stated by Bailey & Maufe (1916 & 1960), the volcanic pile is metamorphosed by the Inner Granite and the Inner Granite exhibits chilling at the contact with the volcanic pile. The simplest explanation for these features is that the volcanic pile collapsed into the still molten Inner Granite. The fact that the volcanic pile is comprised of extrusive igneous rocks suggests that the magma forced out of the way by the subsiding block was forced out onto the surface. The volcanic pile therefore represents a pre-caldera sequence. Aramaki & Yamasaki (1963) demonstrated a relationship between the volume of ejected magma and the mechanism by which it was erupted. Using this relationship, the volume of ejected magma ( $\approx 2.3\text{km}^3$ ) falls into the field of caldera collapse.

The Fault facies represents the remnants of magma forced out of the magma chamber and onto the land surface. This erupted magma has subsequently been removed by erosion. A similar interpretation has been proposed, using similar arguments, for the flinty crush rock and fault intrusion of the Glencoe caldera (Roberts 1966, Taubeneck 1967 and Moore & Kokelaar pers. comm.)

### 3.9 Model

It has been suggested that the sediments and volcanic breccias of the Allt a' Mhuillinn and Coire na Ciste Formations represent a post-caldera collapse breccia (Kokelaar pers comm.). In this context, the exposures of Dalradian schist represent large megablocks within the collapse breccia. This hypothesis is criticised on the following grounds,

- 1) The Fault facies and its associated group of intrusions (type 1 and possibly type 2) clearly post-date the volcanic breccias and andesites of the volcanic pile. Unless two episodes of caldera formation are invoked, not improbable given the occurrence of multiple intrusions (Anderson 1935, Haslam 1965 and chapter 4), the volcanic breccias cannot represent a collapse breccia.

2) With the exception of small clasts within the breccias, the only outcrops of Dalradian basement are found at the lowest exposures of the volcanic pile. It is remarkable, if a caldera collapse origin is believed, that these exposures are not only the largest blocks present within the volcanic pile, but that they are also only found at the lowest exposed level of the volcanic pile.

3) The Dalradian exposures in the Allt a' Mhuillin, are overlain by a well developed succession of fine grained sediments and conglomeratic breccias. This succession must also be a part of the Dalradian megablock, but the contacts between conglomeratic breccia, mudstone and Dalradian basement would provide natural lines of weakness along which such a block could fragment.

4) A number of fine grained mudstone and siltstone horizons are found throughout the volcanic pile. These fill hollows and depressions within the underlying volcanic breccias and indicate periods of low energy deposition. A caldera lake setting is a possible interpretation, but the structures within these sediments (fining up cycles etc) are identical to those of the sediments above the Dalradian basement indicating a similar depositional environment.

5) There is abundant evidence of topographic control and substantial periods of time must have elapsed between the deposition of volcanic breccias separated by sediment horizons. This is unlikely to have occurred if the volcanic breccias represent collapse breccias.

6) The presence of non-volcanic conglomeratic breccias within the volcanic breccia sequence requires a source capable of generating debris flows formed entirely of non-volcanic clasts. It is unlikely that such a source could be found in the caldera wall given the overwhelming dominance of volcanic clasts within the volcanic breccias. Few country rock clasts are found in the volcanic breccias and no igneous clasts are found in the conglomeratic breccias; it is difficult to see how collapse of the caldera wall could generate volcanic and conglomeratic breccias with no mixing between clasts from the two types of source. In addition, these conglomeratic breccias are found at the top of mudstone horizons and could therefore be interpreted as the first depositional event of a fresh period of volcano-tectonic upheaval after a period of relative quiescence.

7) The volcanic breccias of BN268, are formed from a number of mass flow units. Phenocrysts show evidence of corrosion by the matrix and are indicative of hot emplacement. It is difficult to envisage a mechanism by which the collapse of a caldera wall could generate such deposits.

8) The simplest explanation for the volcanic pile and the Fault facies exposed today on Ben Nevis is that the volcanics represent a pre-caldera sequence that fell into the underlying Inner Granite generating the Fault facies. The alternative hypothesis is based solely on the presence of ignimbrite clasts within the volcanic breccias of the Coire na Ciste

Formation. and the interpretation of exposures of Dalradian metasediments as large megablocks.

For the above reasons, a caldera collapse origin for the Allt a' Mhuillin and Coire na Ciste Formations is not thought possible and a cartoon model for the evolution of the Ben Nevis volcanic pile is presented in Fig. 3.12 with the volcanic pile representing a pre-caldera sequence.

The Ben Nevis volcanic pile was formed in a low-lying region that, for at least some of the time and probably for all, was the site of a large lake-like body of standing water. Flash flood events or periodic failure of sediment accumulations on the lake margins, possibly during tectonic activity and movements along the nearby Great Glen Fault generated low volume turbidity currents. Much larger debris flows entered the lake basin at irregular intervals; these may have originated subaerially before entering the lake basin. Whilst soft sediment deformation, and possibly generation of turbidity currents, indicate an active tectonic environment, there is no macroscopic evidence of volcanic activity in the lowest horizons of the Allt a' Mhuillin Formation.

The size of the depression is unknown, sediment accumulations within the volcanic pile, locally reach thickness of 20m+, implying a fairly substantial body of water. G. Rogers (pers. comm.) mentioned the existence of standing bodies of water trapped behind natural dams formed from lava or mass flow deposits in the volcanic deposits of NW. Mexico. The preservation potential of these deposits, however, is likely to be limited, but it is possible that the sediments of the Ben Nevis volcanic pile represent the settling of fine grained detritus into similar small localised standing bodies of water. However, the absence of the Allt a' Mhuillin and Coire na Ciste Formations in Five Fingers Gully indicates that some 300m of the volcanic succession is missing in this area. The presence of turbidity currents in the lake basin suggests the existence of a fairly major depression. Taubeneck (1967) believed that local topography in the northern section of the Glencoe caldera exceeded 2,000ft (650m). It is therefore believed that Ben Nevis occupies the former site of a large lacustrine basin.

An autobrecciated andesite represents the first local volcanic event. From this point at the base of the Coire na Ciste Formation block and ash flow and lahar deposition dominate the geology of the volcanic pile until generation of the Ledge route and Summit Formations.

The volcanic breccias of the Coire na Ciste Formation contain clasts of rhyolite and eutaxitic ignimbrite. These are not found *in situ*, and the lahars and block and ash flows must therefore have been generated from outside of the Ben Nevis basin; presumably from a major volcanic centre. How far away this source was located is unknown, modern lahar and block and flows have been traced for distances of at least 40km (Mullineaux & Crandell 1962). Glencoe, Rannoch Moor, Etive, Strontian, Ballachulish, Mullach nan Coirean, Coille

Hypothetical volcanic source.

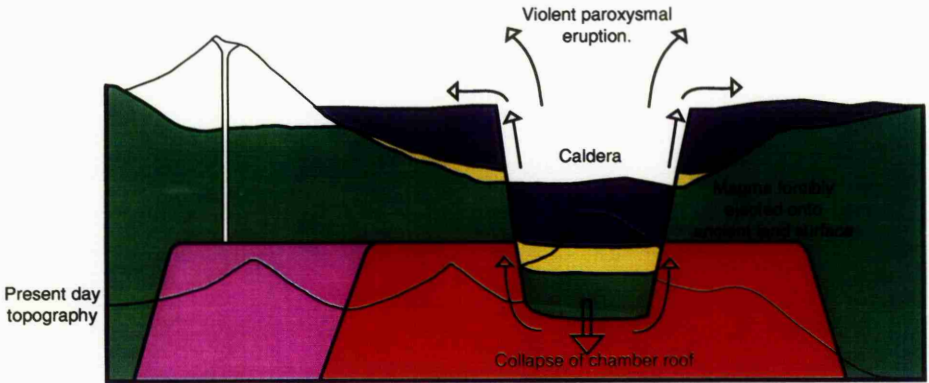
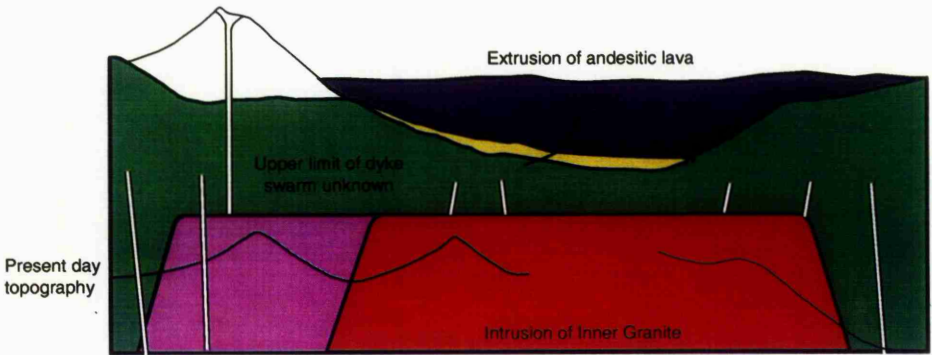
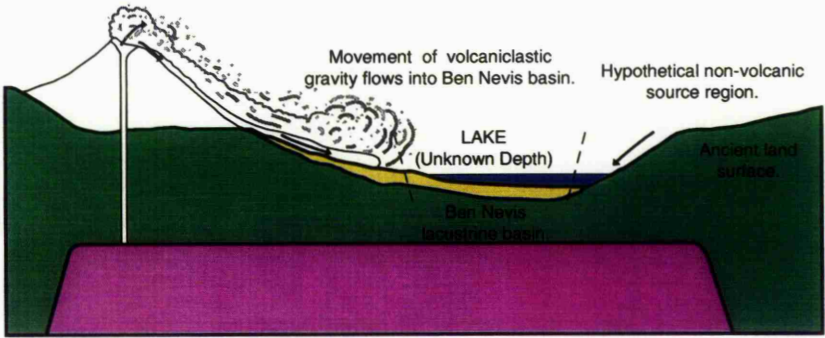


Fig. 3.12 Simplified cartoons depicting the evolution of the Volcanic pile.

Lèanachain and Strath Ossian are all possible sources; alternatively the marginal intrusions of Ben Nevis are equally likely to represent the source magma chamber.

Periodic andesitic sill injection and lava extrusion during deposition of the Coire na Ciste Formation indicates the presence of a local magmatic plumbing system. Background lacustrine sedimentation continued and is preserved in minor accumulations of sediment. Small debris flows with no macroscopic volcanic detritus and dominated by quartzite clasts indicate the presence of a non-volcanic sediment source.

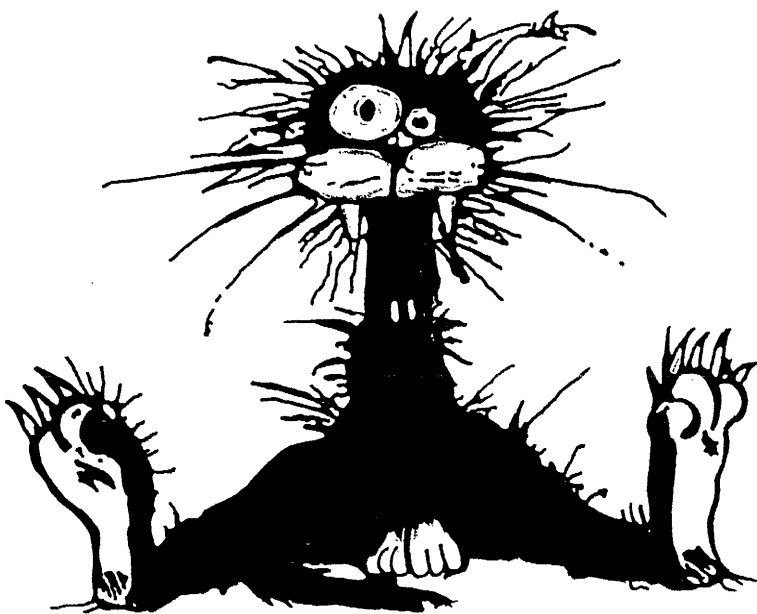
A relatively long period of mudstone deposition (Trident Member) was terminated by localised pyroclastic activity which rapidly formed a large thickness of loose unconsolidated deposits. Periodic slope failure caused these air fall deposits to flow down slope distorting and deforming the underlying mudstones on at least one occasion. The source vent for this activity was located north of Castle Ridge, but is not preserved. Non eruptive periods during the life-time of this vent allowed renewed deposition of fine grained sediments. Andesite lavas exposed within the Ledge route Formation on Castle Corrie may have been extruded during these quieter episodes with each overlying tephra deposit representing the input of fresh volatile rich magma into the underlying magma chamber.

The final episode recorded in the geology of the volcanic pile is represented by autobrecciated andesite lavas and sills which top the volcanic pile today. Minor pyroclastic activity accompanied this last episode. The source which generated the lahars and block and ash flows of the underlying Coire na Ciste Formation appears to have died out (rhyolite and eutaxitic ignimbrite clasts are not found in the volcanic breccias of the Summit Formation).

How thick the volcanic pile was prior to collapse is unknown.

Intrusion of the Inner Granite weakened the roof of the magma chamber inducing failure and collapse of the volcanic pile into the Inner Granite. Magma was vented explosively onto the surface and the Fault facies represents the only preserved remnant.

The size of the resultant caldera would have been greater than the size of the volcanic pile today. The sides of the volcanic pile have been upturned during descent of the volcanic pile into the Inner Granite and estimates of the area of the pre-collapse volcanic pile are consequently on the low side.



# "STRESS"

THE CONFUSION CREATED WHEN  
ONE'S MIND OVERRIDES THE  
BODY'S BASIC DESIRE TO CHOKE  
THE LIVING SHIT OUT OF SOME  
ASSHOLE WHO DESPERATELY  
NEEDS IT !

## CHAPTER 4

# FIELD GEOLOGY OF THE INTRUSIVE MEMBERS OF THE BEN NEVIS COMPLEX

### 4.1. Introduction

#### 4.1.1 General statement

The granitic rocks of the Ben Nevis volcanic-plutonic Complex occupy an area of  $\approx 45\text{km}^2$  in the Southwest Highlands of Scotland. They are intruded into garnet grade metamorphic schists of the Grampian group and Dalradian Supergroup (Glover 1993) and a contact metamorphic aureole extends up to 1.5km from the granite margin (Webb 1977).

This chapter is concerned with the field geology of the plutonic members of the Ben Nevis Complex and the Ben Nevis dyke swarm (Fig. 4.1). Previous workers (Anderson 1935 and Haslam 1965) have attempted to subdivide the granitic rocks into a number of separate units (Fig. 4.2 and Fig. 4.3 respectively, see also Table 4.1). These early schemes fit the geology of the Ben Nevis Complex poorly and a new scheme is presented in this chapter and is used throughout this thesis.

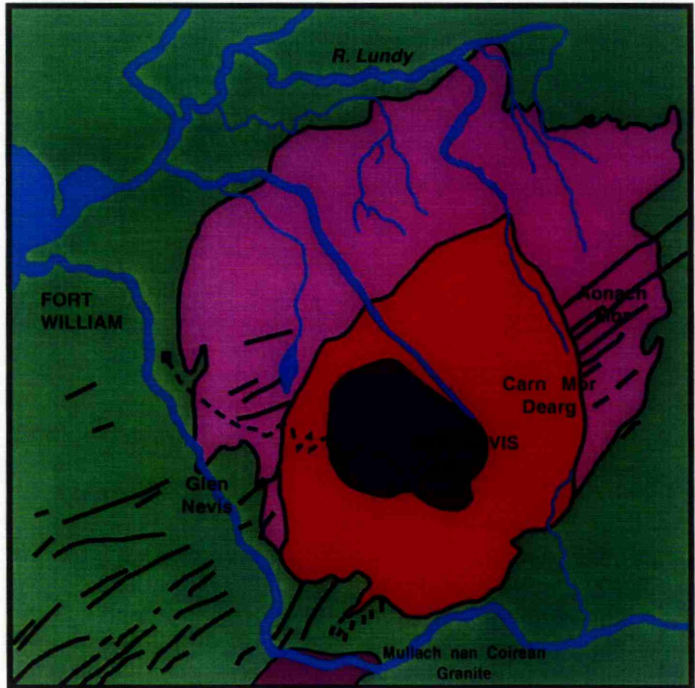
Table 4.1 Comparison of different schemes for the subdivision of the plutonic members of the Ben Nevis Complex.

Author.				
Subdivisions	Maufe (1910)	Anderson (1935)	Haslam (1965)	Burt (this thesis)
		Fine Type	Outer QD	Fine QD
	Outer Granite	Medium Type		Sgurr Finnisg-aig QD
		Coarse Type	Inner QD	Coarse QD
		Porphyritic Type	Porphyritic OG	Porphyritic OG
	Inner Granite	Inner Granite	Inner Granite	Inner Granite

QD - Quartz Diorite      OG - Outer Granite.

The Medium Type of Anderson (1935) is incorporated into the Outer and Inner Quartz Diorites of Haslam (1965). Some of the Medium Type forms the Sgurr Finnisg-aig Quartz Diorite in this thesis and the rest is included within the Fine and Coarse Quartz Diorites. The table merely lists the various components that each author has identified in the Ben Nevis Complex; it is not a direct correlation between the different schemes.

Field relationships are described only where pertinent information on the plutonic complex is obtained. The map of the Ben Nevis Complex (Fig. 4.4) is essentially that of Haslam (1968) with a few minor modifications and additions. In particular, the outcrop of Inner Quartz Diorite (Fig. 4.3, or Coarse Type Fig. 2b) in the eastern area is placed within the Porphyritic Outer Granite (Fig. 4.4) and a new magma type, the Sgurr Finnisg-aig Quartz Diorite is defined.



Key

- |   |   |
|---|---|
| <span style="display: inline-block; width: 15px; height: 15px; background-color: green; border: 1px solid black; margin-right: 5px;"></span> Metamorphic  | <span style="display: inline-block; width: 15px; height: 15px; background-color: darkblue; border: 1px solid black; margin-right: 5px;"></span> Volcanic Pile |
| <span style="display: inline-block; width: 15px; height: 15px; background-color: pink; border: 1px solid black; margin-right: 5px;"></span> Outer Granite | <span style="display: inline-block; width: 15px; height: 15px; border: 1px solid black; margin-right: 5px;"></span> Ben Nevis                                 |
| <span style="display: inline-block; width: 15px; height: 15px; background-color: red; border: 1px solid black; margin-right: 5px;"></span> Inner Granite  | <span style="display: inline-block; width: 15px; height: 15px; border: 1px solid black; border-style: dashed; margin-right: 5px;"></span> Dyke Swarm          |

Fig. 4.1. Geological Survey map of the Ben Nevis volcanic-plutonic Complex (Bailey & Maufe 1916).

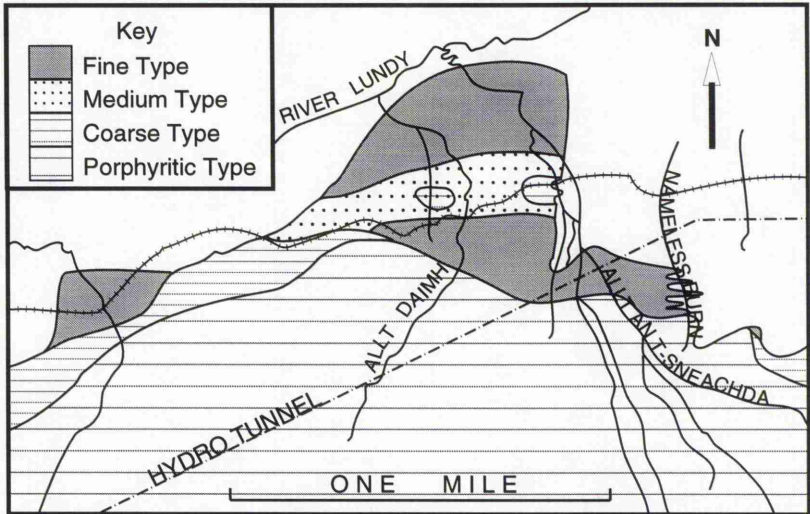


Fig. 4.2a. Geology of the Outer Granite in part of the northern area according to Anderson (1935). Contrast the geology of the Allt Daimh section with that of Haslam (1965) displayed in Fig. 4.3.

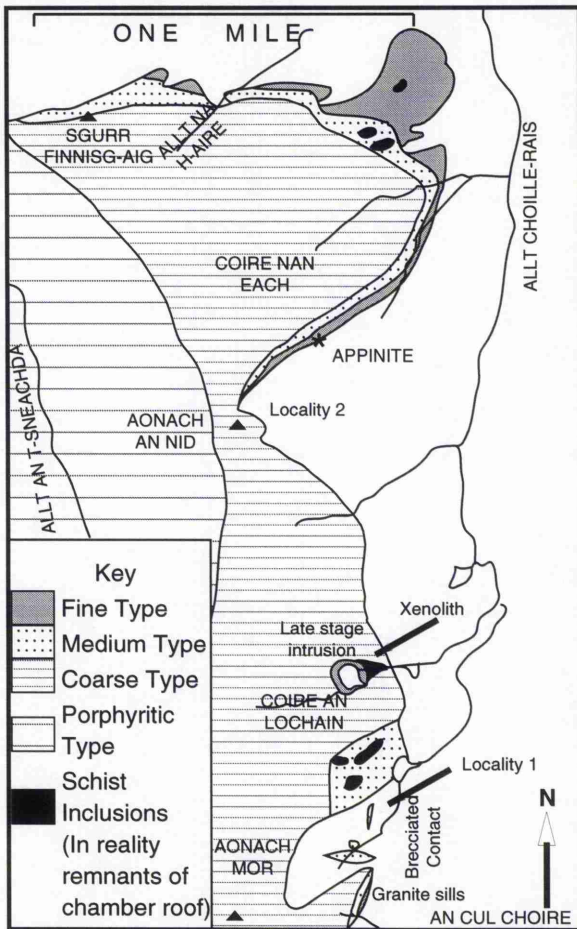
The following chapter may well appear to be little more than a criticism of earlier work (Anderson 1935 and Haslam 1965); however, the evidence presented in this chapter illustrates that schemes for subdividing the Outer Granite presented by these earlier workers are oversimplified and inconsistent. Their work is used as a basis for describing the geology of the Outer Granite before a new scheme is presented.

With regard to discussing individual segments of the Ben Nevis Complex, the author follows Anderson (1935) in defining four geographical areas (Fig. 4.5), these being:

- 1) The northern area lies between the BAA hydroelectric pipeline and the Nameless Burn (first burn east of Allt an t-Sneachda).
- 2) The eastern area lies between the Nameless Burn and the southern limit of the Outer Granite outcrop in Coire Giubhsachan.
- 3) The southern area is that area where the Inner Granite is found in direct contact with Dalradian schists.
- 4) The western area lies between the southern limit of the Outer Granite in Glen Nevis, and the BAA hydroelectric pipeline.

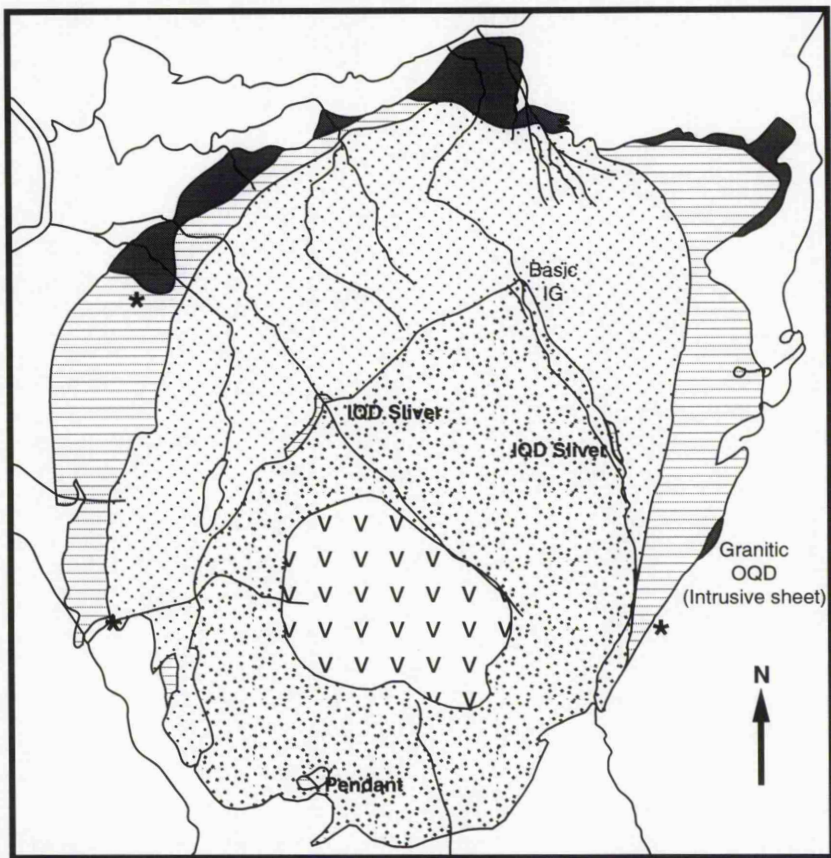
High levels of Mo, Cu, Pb and Zn are found in sediments obtained from streams draining the eastern part of the Ben Nevis Complex. The origin of these high levels is discussed in this chapter.

A small unnamed burn east of Allt an t-Sneachda has exposed several crucial outcrops, this burn is hereafter referred to as the Nameless Burn (Fig. 4.5)



Lower case labels refer to new interpretations text for explanation.  
 The contact geometry of Locality 1 & 2 discussed in section 4.2.2.v.

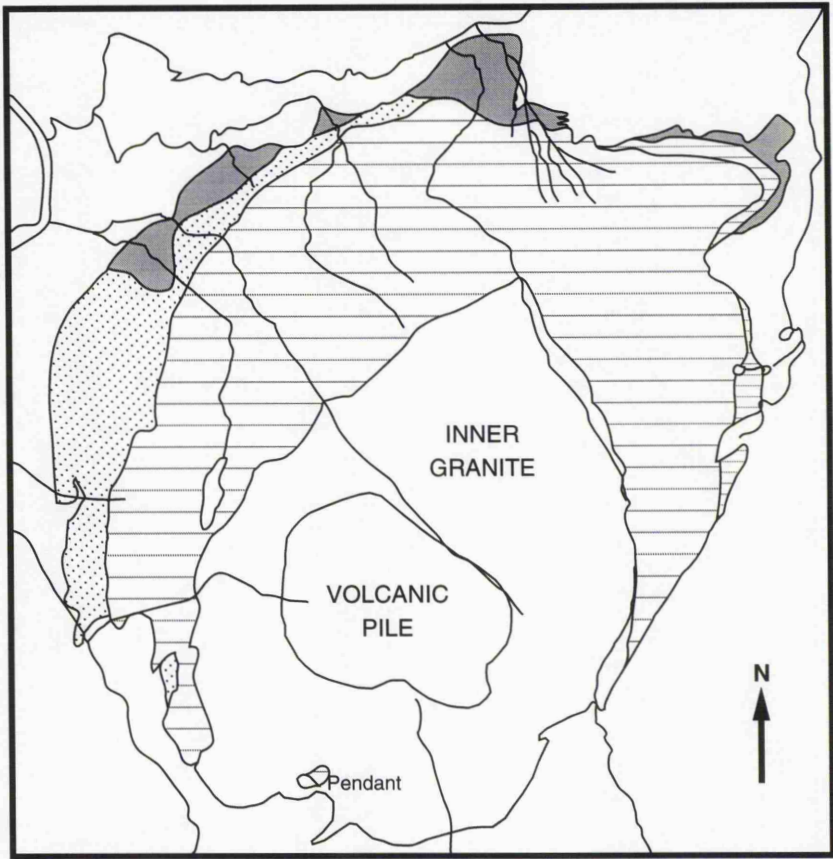
Fig 4.2b. Geology of the Outer Granite in the eastern area according to Anderson (1935).



**KEY**

- |   |                           |   |                   |
|---|---------------------------|---|-------------------|
|    | Outer quartz diorite      |    | Inner Granite     |
|  | Inner quartz diorite      |  | Volcanic pile     |
|  | Porphyritic Outer Granite |  | Appinite locality |

Fig 4.3 Map of Haslam (1965).



**KEY**

- |   |                                  |  |                           |
|---|----------------------------------|--|---------------------------|
|   | Fine quartz diorite              |  | Porphyritic Outer Granite |
|  | Sgurr Finnisg-aig quartz diorite |  |                           |
|  | Coarse quartz diorite            |  |                           |

Fig. 4.4 New interpretation for the subdivision of the Outer Granite, minor intrusions removed for the sake of clarity.

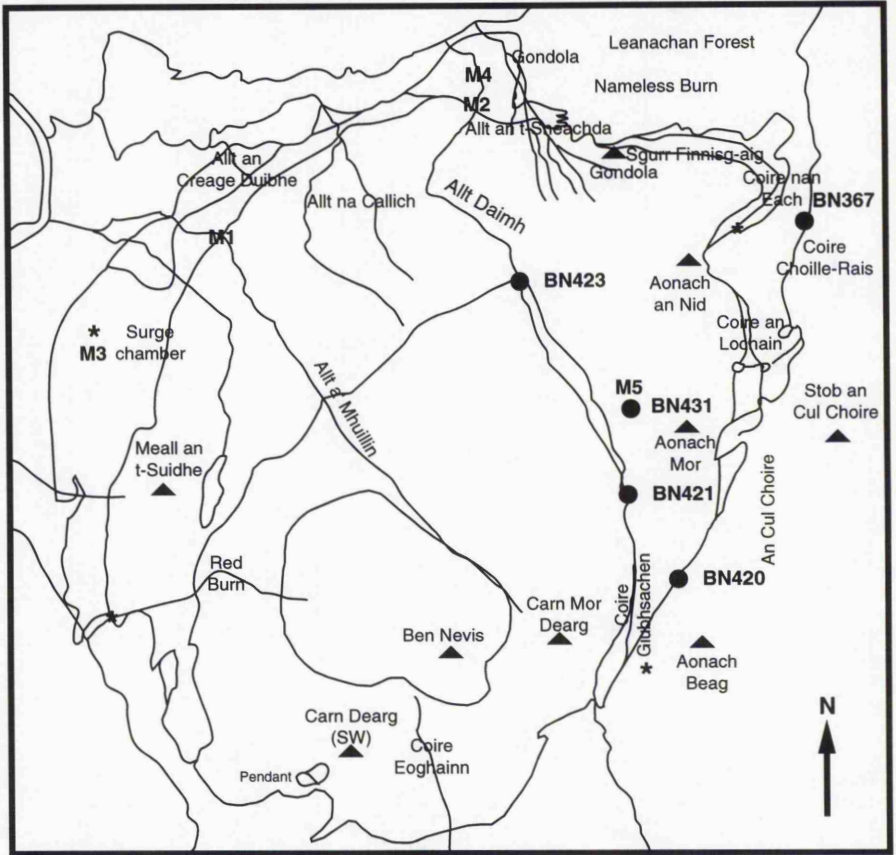


Fig. 4.5 Localities and exposures mentioned in the text.

#### 4.1.2 Terrain

The nature of the terrain, particularly in the northern area, has changed significantly since the work of Maufe (1910), Anderson (1935) and even Haslam (1965) was published. In particular, the BAA hydroelectric scheme has deprived stream channels below the intake points of much of their water for over 60 years. Consequently, vegetation has begun to encroach onto the abandoned stream margins. Construction of the Aonach Mor Gondola has improved access to the eastern area of the complex; unfortunately the popular myth that gondola extends to the summit of Aonach Mor must here be dispelled. The gondola stops near the summit of Sgurr Finnisg-aig some 650m below the summit of Aonach Mor. The area enjoys/endures the highest rainfall in the U.K., run-off is rapid and large volumes

of sediment are moved each year. Leanachan Forest, planted in the 1930's, has in part been harvested and replanted, and in part remains as mature coniferous plantation. The forest, whether harvested or not, is largely inaccessible not least because of the large numbers of midge which thrive in the damp environment, though what they eat when they can't get succulent geologist remains a mystery.

#### 4.1.3 Previous research

##### 4.1.3.i Subdivisions of the plutonic complex

Pre-1900 interpretations of the Ben Nevis Complex are described in chapter 2; post-1900 field based research is here discussed in greater detail.

Maufe (1910) recognised three components to the Ben Nevis Complex (Fig. 4.1) which he termed the Outer Granite, the Inner Granite and the volcanic pile. Although Maufe recognised a basic non-porphyrific margin to the Outer Granite, no further data were presented on the nature of this margin due to the lack of time.

Anderson (1935) recognised four units within the Outer Granite (Table 4.1), these are;

- 1) Fine-grained Non-porphyrific Marginal Type or Fine Type
- 2) Medium-grained Non-porphyrific Marginal Type or Medium Type
- 3) Coarse-grained Non-porphyrific Marginal Type or Coarse Type
- 4) Porphyritic Marginal Type or Porphyritic Type

These subdivisions are based on variations in texture (particularly grain size) and Anderson (1935) believed that they are significant to the evolution of the Outer Granite.

Contacts between individual units are gradational unless one or more of the sequence is missing in which case the contact appears as a "sharp intrusive junction" (Anderson 1935). Prior to publication of Anderson (1935), Bailey (in Bailey & Maufe 1960) had the opportunity to verify Anderson's conclusions in the field with Anderson himself, and largely agreed with a fourfold subdivision.

Wright (in Bailey & Maufe 1960 p177) had difficulty in recognising three distinct non-porphyrific marginal types and suggested that there was too much variation and intermingling of types to allow definite boundaries to be drawn with confidence. Consequently, BGS sheet 62E shows the non-porphyrific margin of the Ben Nevis Complex in one colour and the Porphyritic marginal type in another.

Haslam (1965 & 1968) also had difficulty in identifying three non-porphyrific marginal types, and his map (Fig. 4.3) subdivides the Ben Nevis Complex into the Outer Quartz Diorite, Inner Quartz Diorite, Porphyritic Outer Granite, Inner Granite and volcanic pile (Table 4.1). The Medium Type of Anderson (1935) was abandoned, and exposures

formerly of this type were assigned to either the Outer Quartz Diorite or Inner Quartz Diorite depending on local field relationships.

Each plutonic unit of the Ben Nevis Complex was believed by Haslam (1965 & 1968) to represent a single intrusion of magma. Variations within an individual unit were attributed to differences in cooling rate, contamination, water content,  $fO_2$ , etc.

#### 4.1.3.ii Intrusion mechanism

The structure of the Ben Nevis Complex was compared, by Bailey & Maufe (1916 & 1960), to the Etive and Glencoe igneous centres. The evidence which led the authors to develop cauldron subsidence as a mechanism for granite intrusion was presented in detail by Clough et al. (1909), to which the reader is referred.

Bailey & Maufe (1916 & 1960) noted that the outcrop of the Ballachulish Limestone formation is cross cut for a short distance by the Ben Nevis Complex. It appears again well to the northwest of its expected location, and when traced along strike, the limestone band swings back to regain its normal course. The authors suggested that the deflection "is undoubtedly linked with the emplacement of the granite", but were unable to decide if a downward sag or an outward magmatic push or a combination of these two mechanisms was the cause.

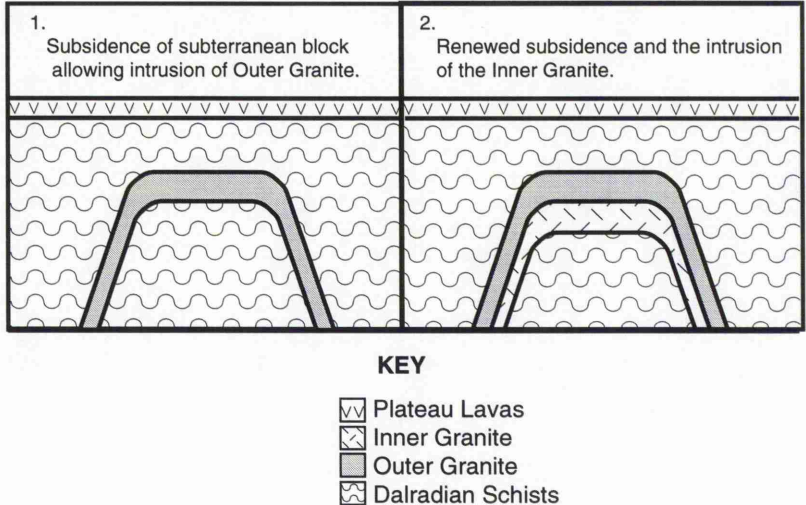


Fig. 4.6 Cartoon illustration of the Geological Survey Ring dyke model.

Maufe (1910), Anderson (1935) and Haslam (1965 & 1968) all agreed that the Outer Granite formed a once continuous ring (Fig. 4.6), the southern part of which was removed during intrusion of the Inner Granite. A large xenolith or pendant mass of Inner

Quartz Diorite and Porphyritic Outer Granite is found within the Inner Granite south of Carn Dearn (SW) (Fig. 4.3). Haslam (1965 & 1968) believed that this mass provides conclusive evidence that the Outer Granite was intruded as a complete series of ring dykes and its present form is the result of partial removal of the Outer Granite by intrusion of the Inner Granite.

In addition to the granite intrusions, a contemporaneous NE-SW trending dyke swarm and several minor intrusions are associated with the Ben Nevis Complex. The majority of dykes were intruded in the period between intrusion of the Outer Granite and the Inner Granite (Bailey & Maufe 1916 & 1960). Bailey & Maufe (1916) suggested that the dykes may have been injected from a subterranean ring dyke which accounts for their rare occurrence within the Inner Granite and volcanic pile.

In addition to its main outcrop, the Inner Quartz Diorite is also found in two localities (Fig. 4.3) forming a narrow band between the Porphyritic Outer Granite and the Inner Granite (Haslam 1965 & 1968). Its presence in this location could be explained by the suggested sequence of intrusion of the Outer Granite. The Inner Quartz Diorite, following intrusion of the Outer Quartz Diorite, was intruded as a large ring dyke. Solidification proceeded from both chamber walls to the core of the intrusion but, prior to complete crystallisation, the Porphyritic Outer Granite was intruded and it exploited the line of weakness formed by the strip of still molten Inner Quartz Diorite left between solidified margins. Much of the inner segment of the Inner Quartz Diorite was removed by subsequent intrusion of the Inner Granite.

In the northeastern outcrop of the Inner Granite, along the course of the Allt Daimh, a small outcrop of granite texturally comparable to the Inner Granite, but slightly more basic and bearing hornblende is recorded by Haslam (1965 & 1968). On the basis of textural similarity, Haslam (1965 & 1968) assigned this granite outcrop to the Inner Granite although a sharp contact is recorded between the two varieties.

## 4.2 The Outer Granite

### 4.2.1 Introduction

#### 4.2.1.i Terminology

Although, geochemically speaking, the Outer Granite ranges in composition from diorite through granodiorite to hornblende biotite adamellite (Haslam 1965), the terms quartz diorite and porphyritic outer granite, as used by Haslam (1965), are retained for the sake of continuity with the literature.

Anderson (1935) presented a four-fold subdivision of the Outer Granite (4.1.3.i), and mention of a rock type suffixed by 'Type', i.e. Fine Type, implicitly refers to the interpretation of Anderson (1935). Similarly a rock unit prefixed by either Inner or Outer refers to the work of Haslam (1965). The use of either scheme does not necessarily mean

that the author agrees with these classifications; they merely provide a useful starting point for discussion. Both Anderson (1935) and Haslam (1965) largely agreed on the location and extent of the Porphyritic Outer Granite (Porphyritic Type of the former). Essentially the Inner Quartz Diorite is synonymous with the Coarse Type and Outer Quartz Diorite is synonymous with the Fine Type. Medium Type is only recognised by Anderson (1935). These early classifications can be compared with each other, and the new interpretation presented in this chapter, in Table 4.1.

#### 4.2.1.ii Rationale

There are a number of different schemes for subdividing the Outer Granite, the purpose of the following section is to provide a framework into which geochemical and petrological data can be placed. The earlier schemes do not allow detailed comparisons to be made between different units of the Outer Granite because the schemes are based solely on textural variations, in particular grain size. This results, for instance, in chilled Porphyritic Outer Granite, bearing no large alkali feldspars being placed in the Coarse Type (Anderson 1935) or Inner Quartz Diorite (Haslam 1965).

The following features, described by Anderson (1935) and/or Haslam (1965), of the Outer Granite require an explanation:

1) The Outer Granite is not a single homogenous intrusion; as gradual merging contacts and hybridisation (Anderson 1935 and Haslam 1965) can be found within it.

2) Chemically, the Outer Granite (regardless of type) becomes more siliceous from east to west such that the most acidic samples of the Outer Granite are found in the vicinity of Aonach Mor (Anderson 1935 and Haslam 1965).

3) Haslam (1965) and Wright (in Bailey & Maufe 1960), both recognised the complexity of the non porphyritic margin and noted considerable variation in the Outer Granite often over distances of a few tens of metres.

4) The contact between the Inner Quartz Diorite and the Porphyritic Outer Granite in the northern area is characterised by a sharp junction or by a 3m thick zone of what Haslam (1965) believed was hybridisation between the two units. In the eastern area both Anderson (1935) and Haslam (1965) described a gradual contact over a distance of a few tens of metres between the Coarse Type or Inner Quartz Diorite and the Porphyritic Outer Granite. On the western side of the Ben Nevis Complex, the contact between the two units is represented by a rapid transition from Inner Quartz Diorite to Porphyritic Outer Granite over a distance of a few metres.

5) In the Allt Carnach the Outer Quartz Diorite is extensively veined by the Inner Quartz Diorite and slightly upstream (deeper into the Inner Quartz Diorite) abundant xenoliths of the Outer Quartz Diorite are found.

6) Haslam (1965) noted that variations within individual intrusions are greater than variations between intrusions. Considerable overlap in SiO<sub>2</sub> content occurs between the various units (Table 4.2).

Table 4.2 The range in silica content for the Outer Granite.

Lithology	Silica range
Fine Quartz Diorite	58.0 - 62.2
SF Quartz Diorite	63.1
Coarse Quartz Diorite	53.0 - 61.7
Miscellaneous	61.3 - 74.8
Porphyritic Granite	63.7 - 70.9

SF - Sgurr Finnisg-aig  
 Miscellaneous includes; dykes, sheets/sills and appinites

#### 4.2.2 Field Geology

##### 4.2.2.i The Allt Daimh

In the Allt Daimh (Fig. 4.5), Anderson (1935) recorded the following sequence (Fig. 4.2a), Dalradian schists, Fine Type, Medium Type, Fine Type, Porphyritic Outer Granite. In a small unnamed stream to the west of Allt Daimh, an outcrop of the Coarse Type is found within that of the Medium Type (Fig. 4.2a). Haslam (1965) includes the whole area in his Outer Quartz Diorite unit (Fig. 4.3).

The outcrop of Medium (or Coarse) Type was not found during the current study; however on a traverse along the bed of the Allt Daimh, no less than five contacts between different types of fine grained quartz diorite were identified (Photo 4.1). Bedrock is exposed for ≈60% of the length of the Allt Daimh between the Dalradian schist and the Porphyritic Outer Granite; it is therefore likely that there are further contacts hidden beneath glacial and fluvial drift. Clear differences between adjacent exposures of quartz diorite are also recognised in thin section (compare Photo 2a with 2b).

Harry & Richey (1963) cast doubt on the general assumption that individual plutonic units are emplaced in a single intrusive event. The lack of internal contacts within a single plutonic unit does not prove this assumption, merely that the conditions during intrusion did not allow the formation of internal contacts, one reason for which may be the intrusion of the pluton in a single event. Three types of pulse-pulse contact were described by Harry & Richey (1963), these being:

- 1) Sharp contacts - solidification of each pulse was completed prior to intrusion of the following pulse.
- 2) Merging contacts - each pulse had only partially crystallised before its successor was intruded.
- 3) Cryptic contacts - each pulse was intruded before significant crystallisation of the previous pulse allowing mingling between the two pulses.

---

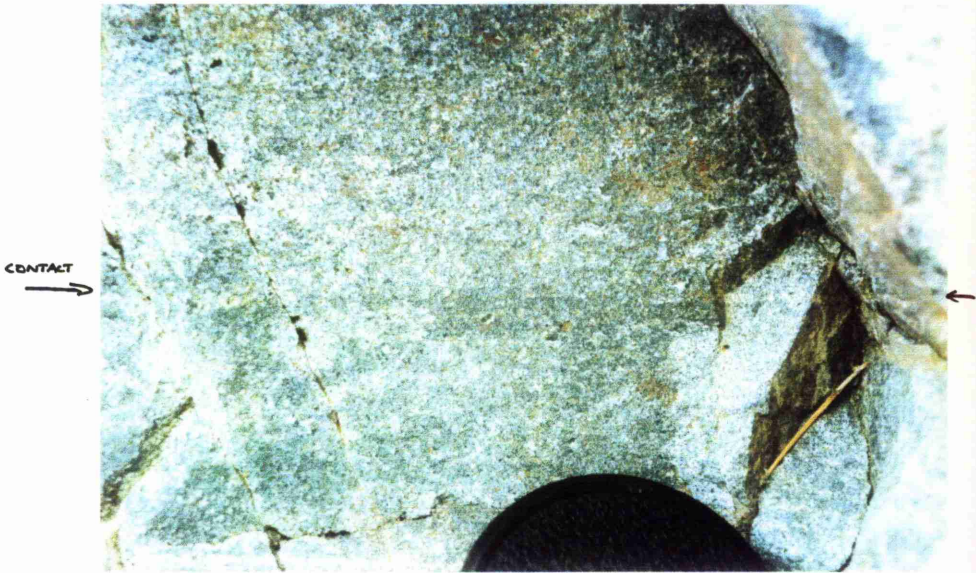
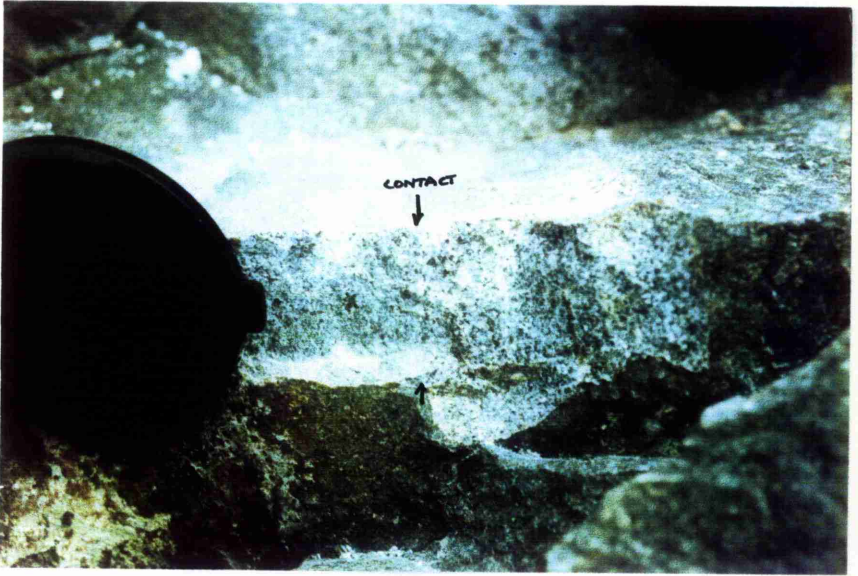
Plate 30 Photo. 4.1 Example of contact observed in the fine grained quartz diorites of Allt Daimh. Fine grained quartz diorite on the left hand side has a sharp contact with fine-medium grained quartz diorite on the right hand side.  
OBN11 (NN171 771)

---

---

Plate 30 Photo. 4.1 Examples of contact observed in the fine grained quartz diorites of Allt Daimh. Fine grained quartz diorite in the lower half has a sharp contact with fine-medium grained quartz diorite towards the top of the photograph.  
OBN13 (NN172 770)

---



---

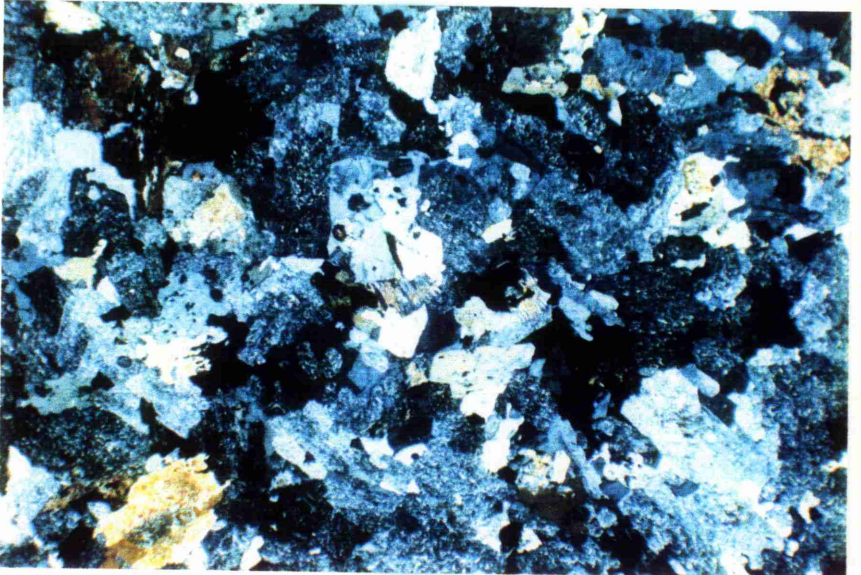
Plate 31 Photo. 4.2a Photomicrograph of fine grained quartz diorites of Allt Daimh, compare with Plate 4.2b; in particular note the in-equigranular grain size of 4.2a compared to the equigranular grain size of 4.2b. Phenocrysts of orthopyroxene and plagioclase are found in 4.2a (OBN11e \* 21 XPL).

---

---

Plate 31 Photo. 4.2b Photomicrograph of fine grained quartz diorites of Allt Daimh, compare with Plate 4.2a. (OBN11d \* 21 XPL)

---



Part of Harry & Richey's (1963) evidence was obtained from previously published research on the Ben Nevis Complex. The authors believed that Maufe (1910) had described the Outer Granite as a single intrusion (in fact, Maufe had insufficient time to subdivide the Outer Granite, hence its description as a single plutonic body, Bailey & Maufe 1960), whereas Anderson (1935) had presented evidence for the existence of four intrusions forming the Outer Granite. This, they believed, was evidence for the intrusion of the Outer Granite pluton not in a single event, but as a series of four magma pulses.

The recognition of sharp clearly defined contacts between quartz diorites of differing mineralogy and texture indicate that the Allt Daimh exposures are made up of a number of magma pulses. The type of internal contact is dependent on variations in chemical composition and cooling rate; if the pluton as a whole is cooling relatively rapidly then sharp contacts are likely to form between successive pulses, such as those found in the Allt Daimh stream section. Small variations in geochemistry within the Coarse Quartz Diorite and the Porphyritic Outer Granite (Fig. 4.8b), along with the rare observation of an internal contact (Photo 4.3), suggest that the rate of cooling was the primary control on the nature of pulse-pulse contacts in the Ben Nevis Complex. When the rate of cooling was relatively slow, and successive pulses were of broadly similar composition internal contacts, are often cryptic. The number of pulses within the Outer Granite is unknown; however, from the number of internal contacts in the Allt Daimh, the number is significantly larger than the four pulses of Harry & Richey (1963).

#### 4.2.2.ii Sgurr Finnisg-aig

Around Sgurr Finnisg-aig (Fig. 4.5), a distinctive fine-medium grained quartz diorite outcrops between a fine grained xenolith rich diorite and coarse grained quartz diorite assigned to the Inner Quartz Diorite (Fig. 4.3) by Haslam (1965) (but see section 4.2.2.iv and Fig. 4.4). This distinctive type is hereafter referred to as the Sgurr Finnisg-aig quartz diorite and has sharp contacts with both the adjacent rock types. It is likely the Sgurr Finnisg-aig Quartz Diorite represents the Medium Type (Anderson 1935) in this area (Fig. 4.2b); Haslam (1965) assigned the Medium Type in this area to either the Outer Quartz Diorite or Inner Quartz Diorite (it is not clear which). From field relationships, it is clear that three different intrusions are found in this area, the fine grained diorite, the Sgurr Finnisg-aig Quartz Diorite and the coarse grained quartz diorite.

Exposures of Sgurr Finnisg-aig Quartz Diorite can be found as dykes intruding the fine grained quartz diorite, hereafter referred to as the Fine Quartz Diorite, in the Allt an t-Sneachda and the Nameless Burn. Sgurr Finnisg-aig Quartz Diorite is also exposed intermittently along the eastern margin of the Ben Nevis Complex and a thin sliver is found between the Porphyritic Outer Granite and the Fine Quartz Diorite in Allt an t-Sneachda. In this area, veins of Porphyritic Outer Granite can be found cross-cutting the Sgurr Finnisg-aig Quartz Diorite indicating the earlier intrusion of the latter rock type.

In hand specimen, thin section and geochemically (Fig. 4.7), the Sgurr Finnisg-aig Quartz Diorite bears little resemblance to other types of quartz diorite exposed in the Ben Nevis Complex. Neither Anderson (1935) or Haslam (1965) treat the Sgurr Finnisg-aig Quartz Diorite as separate from the rest of the Outer Granite despite its consistent variation from the typical quartz diorite succession such as that exposed in the northern and western areas (Fig. 4.2a & 4.3). In this thesis it is regarded as a separate unit of the Ben Nevis Complex.

The geometry of the Ben Nevis Complex in the vicinity of the gondola line is intricate (Fig. 4.2a). Linear dyke-like intrusions of the Sgurr Finnisg-aig Quartz Diorite are found in the low lying area close to the gondola base station, but as 'ring dyke' intrusions at higher levels on Sgurr Finnisg-aig and at the contact with the Porphyritic Outer Granite in the stream bed of Allt an t-Sneachda (a height difference of  $\approx 350\text{m}$ ). The contact between Fine Type and Dalradian country rocks in Allt an t-Sneachda is  $\approx 100\text{m}$  above sea level, whereas the contact on Sgurr Finnisg-aig is exposed at a height of  $\approx 650\text{m}$ . Between the two localities, the non-porphyritic margin is absent and Porphyritic Outer Granite is exposed in contact with the Dalradian (Photo 4.4 and Fig. 4.2a).

It is believed that the Sgurr Finnisg-aig Quartz Diorite intruded the Fine Quartz Diorite as dykes in the lower levels of the Ben Nevis Complex (i.e. Allt an t-Sneachda and the Nameless Burn), but ponded against the roof of the magma chamber at higher levels (i.e. Sgurr Finnisg-aig) where it solidified prior to the intrusion of the Porphyritic Outer Granite.

#### 4.2.2.iii Coire nan Each

In the extreme northeastern corner of the Ben Nevis Complex (Fig. 4.2b), the outer contact is extremely irregular. Small sheet-like projections of Fine Quartz Diorite bud off from the main outcrop and locally extend the granite margin into the Dalradian schists; dyke like projections are also much in evidence along the margin between Coire nan Each and Sgurr Finnisg-aig. These are best exposed below the prominent waterfall of Allt na h-Aire. Abundant brecciation is observed at the contact with the Dalradian schists; the mechanism for this feature is discussed in section 4.3.

#### 4.2.2.iv Aonach Mor

In the vicinity of Aonach Mor (Fig. 4.5), a thick band of Inner Quartz Diorite (or Coarse Type) separates the Porphyritic Outer Granite from the Dalradian schists. Anderson (1935) recognises that the Coarse Type in this area is noticeably different from that exposed elsewhere in the Ben Nevis Complex, being of "more acid aspect and it is considerably closer in appearance to the Porphyritic Type than to the normal Coarse Type".

The contact between the Coarse Type and the Porphyritic Type in this area is gradual, occurring over a distance of several tens of metres. On a traverse from Porphyritic Outer

---

Plate 32 Photo. 4.3 Internal contact within the Porphyritic Outer Granite, granite towards the bottom of the photograph has a higher mafic content than that towards the top of the photograph Line of contact has been exploited by late stage fluids/magmas. (Exposure in the Allt Daimh NN186 726).

---

---

Plate 32 Photo. 4.4 Contact between the Porphyritic Outer Granite and the Dalradian in the Nameless Burn. Photographer is standing on the Porphyritic Outer Granite which has compressed the Dalradian metasediments in this area forming a conjugate set of thrust faults. BN394 (NN182 764)

---



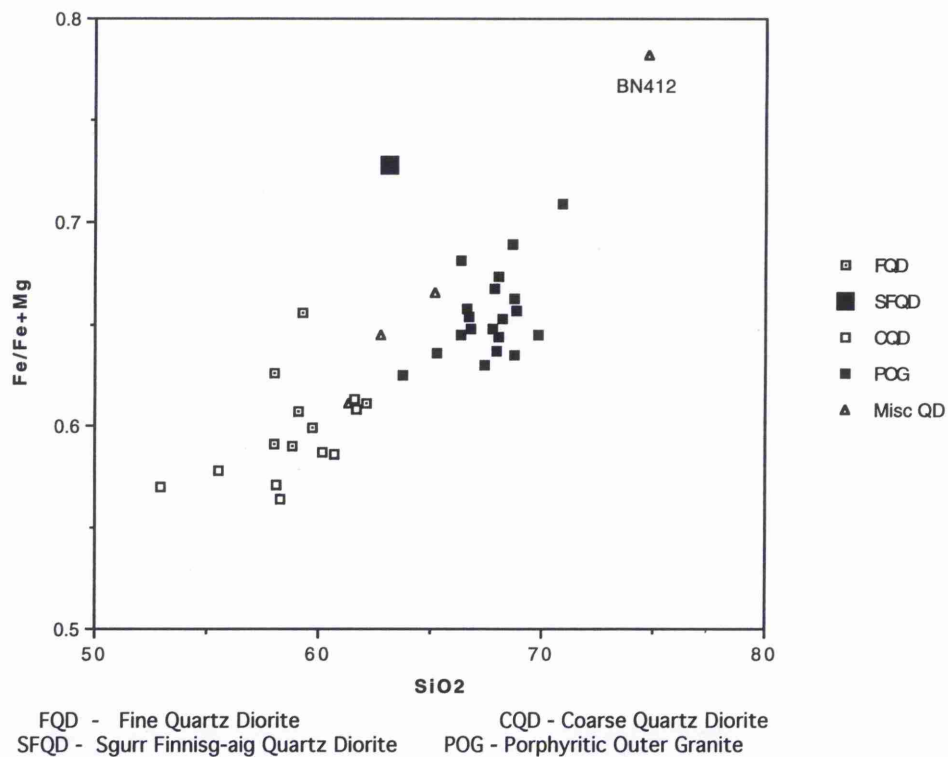


Fig. 4.7 Graph illustrating the difference in geochemistry between the Sgurr Finnisg-aig Quartz Diorite and the other members of the Outer Granite.

Granite to Dalradian schist, the frequency and size of the conspicuous alkali feldspars of the Porphyritic Outer Granite gradually decreases until individual crystals no longer stand out from the medium-coarse grained groundmass. Plagioclase phenocrysts mirror the behaviour of the alkali phenocrysts. Clearly this contact between the Coarse Type and the Porphyritic Outer Granite is very different from that exposed in the northern area where hybridisation and magma mingling have occurred (Haslam 1965).

A zone of hybridisation, found in the Allt an Creige Duibh (Fig. 4.5) between the Coarse Type and Porphyritic Outer Granite, was first documented by Haslam (1965). However, although petrographic evidence points to a hybrid origin for this 3m wide band of granodiorite, the contacts between the hybrid and adjacent magmas are sharp (i.e. intrusive). If the granodiorite is a hybrid, then hybridisation did not occur *in situ*. Whether the granodiorite represents mixing between the Porphyritic Outer Granite and Inner Quartz Diorite at depth or is a separate pulse of magma to these two units of the Ben Nevis Complex is unclear.

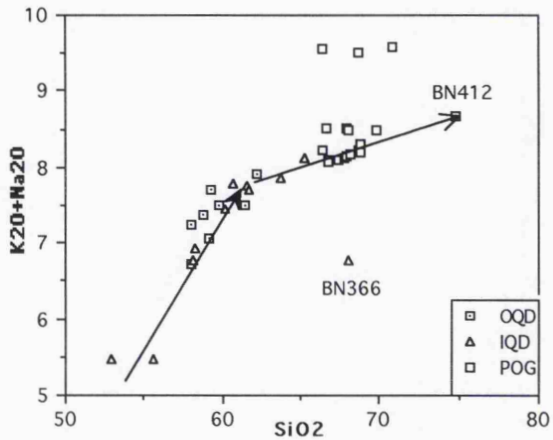
Given the transitional nature of the Porphyritic Outer Granite/Coarse Type contact in the vicinity of Aonach Mor, and the recognisable difference between Coarse Type in this area and Coarse Type in the northern and western areas, Anderson's (1935) subdivisions can be re-interpreted such that the Coarse Type in the eastern area forms a chilled modification of the Porphyritic Outer Granite and is not part of the Coarse Type. The wide outcrop of the chilled Porphyritic Outer Granite, relative to that in the western area, can be explained by the closer proximity of the magma chamber roof (see section 4.2.2.v) and the greater cooling effect that this would cause.

Recognition the Coarse Type in the eastern area as a chilled variant of the Porphyritic Type reduces the degree to which SiO<sub>2</sub> increases from west to east. Geochemically, these chilled margin magmas are more readily assigned to the Porphyritic Type than the Coarse Type (compare Fig. 4.8a with 4.8b and see section 4.2.3).

#### 4.2.2.v The geometry of the eastern margin

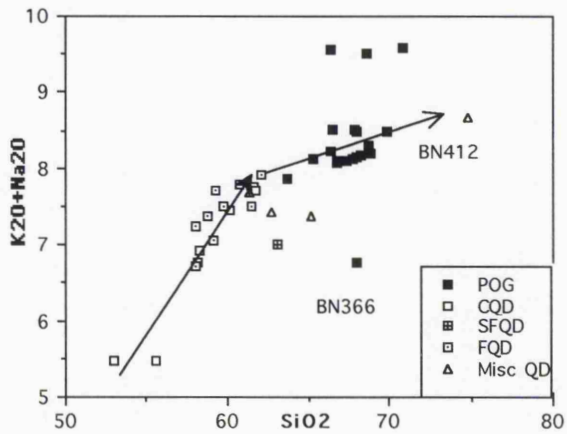
In Fig. 4.2b, a number of isolated exposures of Dalradian schist are visible in the Outer Granite (Photo 4.5). Anderson (1935) believed these exposures to be xenoliths; however, an alternative explanation, that the exposures represent remnants of the magma chamber wall or roof, as argued below, is more likely.

Erosion has failed to expose the Ben Nevis Complex at two localities along the eastern margin (Locality 1 and Locality 2, Fig. 4.2b) and the outcrop of Dalradian schist 'projects' into that of the Ben Nevis Complex. At Locality 1 Dalradian schists are found just a few metres below the summit plateau of Aonach Mor (Fig. 4.5). A similar but less pronounced projection, Locality 2, is found just south of Aonach an Nid, where Dalradian schists are found for a short distance outcropping on the summit plateau. At both these localities (Fig. 4.2b), the presence of Dalradian schist is represented topographically by the presence of a



OQD - Outer Quartz Diorite      POG - Porphyritic Outer Granite  
 IQD - Inner Quartz Diorite

Fig. 4.8a Subdivisions according to Haslam (1965).



FQD - Fine Quartz Diorite      CQD - Coarse Quartz Diorite  
 SFQD - Sgurr Finnis-aig Quartz Diorite      POG - Porphyritic Outer Granite

Fig. 4.8b Geochemistry of the subdivisions presented in this thesis. Note the marked difference in chemistry of BN412, the intrusive sheet, from the main field of quartz diorite data. The recognition of BN418 and BN420 as chilled variants of the Porphyritic Outer Granite is illustrated by the greater similarity of these samples to Porphyritic Outer Granite than to Coarse Quartz Diorite. Anomalous behaviour of BN366 due to extensive assimilation of Dalradian metasediments.

ridge leading from Allt Choille-rai to the summit plateau of Aonach Mor. The overall sense of the contact in this area is of a steeply dipping plane that closely follows the topographic gradient. At Aonach an Nid (Fig. 4.5), the dip of the contact decreases dramatically until

Dalradian schists with a horizontal contact against the underlying granite are found on summit plateau. Xenoliths exposed north of Coire an Lochain are continuous with the orientation of the Dalradian-granite contact and are therefore better interpreted as isolated remnants of the magma chamber wall. No granite is found overlying these schist outcrops and a weak ridge is defined by the southern pair (Fig. 4.2b and Photo 4.5). Within Locality 1 (Photo 4.5), small streams running off the summit plateau have cut down through the schists and exposed the underlying granite. It is not difficult to envisage that further erosion and excavation of Locality 1, by these streams, would leave a series of isolated blobs similar to those described as xenoliths by Anderson (1935) and depicted in Fig. 4.2b.

Those blobs exposed in the northeastern corner (Fig. 4.2b) are topographically much lower than the summit plateau of Aonach Mor; however, the geometry of the quartz diorites in this area indicates a thin sheet of the Fine Quartz Diorite intruding Dalradian schists that have largely been removed by erosion with the exception of these small remnant blobs.

An exception to this new interpretation is to be found where the xenolith exposed at the outlet of the upper of the two small lochans in Coire an Lochain (Fig. 4.5), is clearly over and underlain by granite.

#### 4.2.2.vi Coire an Lochain

Anderson described an outcrop of the Fine Type around the upper lochan in Coire an Lochain (Fig. 4.5) as "...a pink fine grained rock extensively veined by the Coarse pink Type". The Coarse pink Type in this locality is re-interpreted as Sgurr Finnisg-aig Quartz Diorite and the field evidence indicates that it is intruded by the fine grained pink rock and not vice versa. The Sgurr Finnisg-aig Quartz Diorite shows no sign of chilling whereas the fine grained pink rock is extremely inhomogeneous varying from coarse to fine grained, and is often chilled against the Sgurr Finnisg-aig Quartz Diorite. Veins of pink rock intrude the Sgurr Finnisg-aig Quartz Diorite, the larger veins (30-40cm wide) grade from coarse pink granite to fine almost aplitic granite. Inclusions of the Sgurr Finnisg-aig Quartz Diorite are found within the pink rock. The pink granite was intruded into the Sgurr Finnisg-aig Quartz Diorite whilst it was still semi-molten and plastic deformation of the Sgurr Finnisg-aig Quartz Diorite is observed. No exposure could be found where fine grained pink granite was veined by the Sgurr Finnisg-aig Quartz Diorite. The exposures described above have recently been uncovered by small landslides affecting the western margin of the upper lochan.

The origin of the fine grained pink granite is unclear; most likely it represents a late stage fluid/magma from the Porphyritic Outer Granite or even from Sgurr Finnisg-aig Quartz Diorite. High fluid pressures are indicated by rapid grain size variations.

#### 4.2.2.vii An Cul Choire

In An Cul Choire (Fig. 4.5), both Anderson (1935) and Haslam (1965) (Figs. 4.2b & 4.3 respectively) recorded the presence an outcrop of Fine Type + Medium Type (or Outer Quartz Diorite) between the Coarse Type (that is now recognised as a chilled variant of the Porphyritic Outer Granite) and the Dalradian. This outcrop is re-interpreted as a fine grained intrusive sheet of red granite. Actually, two sheets are found in this locality, one intruding Dalradian schists and the other, Porphyritic Outer Granite, a third sheet is found on the col between Aonach Mor and Stob an Cul Choire (Photo 4.6). No exposure of Fine Type + Medium Type could be found in this area; Anderson (1935) described the 'Fine Type' in this area as "...here pink in colour and rather acid in composition" indicating that the intrusive sheets described here were misidentified by Anderson (1935) and assigned to the Outer Granite. Recognition of this outcrop as an intrusive sheet invalidates Haslam's (1965) statement that the greatest amount of chemical variation can be found in the Outer Quartz Diorite, as this new interpretation removes the high silica analysis (74.8%) of this outcrop from the Outer Quartz Diorite (now the Fine Quartz Diorite) into the miscellaneous group.

#### 4.2.3 Conclusions - subdividing the Outer Granite

The scheme outlined below is primarily designed to aid in geochemical analysis rather than describing in detail the intrusion history of the Outer Granite. Earlier schemes (Anderson 1935 and Haslam 1965 & 1968) have oversimplified the geology and in some cases clear ambiguities exist. These early schemes also described each separate unit of the Outer Granite as a single intrusion. From field evidence obtained along the Allt Daimh it is clear that individual units are not single intrusions (*sensu stricto*), but are made up of a number of smaller magmata pulses.

In the northern and western areas the subdivisions of Haslam (1965 & 1968) are retained (compare Fig. 4.3 with 4.4), but the names are changed in order to emphasise the average crystal grain size rather than the location of an individual unit within the Ben Nevis Complex. In fact, the use of Inner and Outer is misleading; in Glen Nevis for instance, the Outer Quartz Diorite is missing and Inner Quartz Diorite is found on the outside of the Ben Nevis Complex. Therefore, in this account, Fine Quartz Diorite replaces Outer Quartz Diorite, Coarse Quartz Diorite replaces Inner Quartz Diorite while Porphyritic Outer Granite is retained (Table 4.1).

In the eastern area the situation is more complex. A characteristic quartz diorite first identified during current research on Sgurr Finnisg-aig and therefore referred to as the Sgurr Finnisg-aig Quartz Diorite replaces the Medium Type (Fig. 4.2b) of Anderson (1935) and is found intermittently along the eastern margin of the Ben Nevis Complex (Fig. 4.4). Between the Dalradian and the Sgurr Finnisg-aig Quartz Diorite in this area, a fine grained quartz diorite is exposed; this unit is included within the Fine Quartz Diorite. The absence of coarse grained diorite comparable with the Coarse Quartz Diorite, has led to the

---

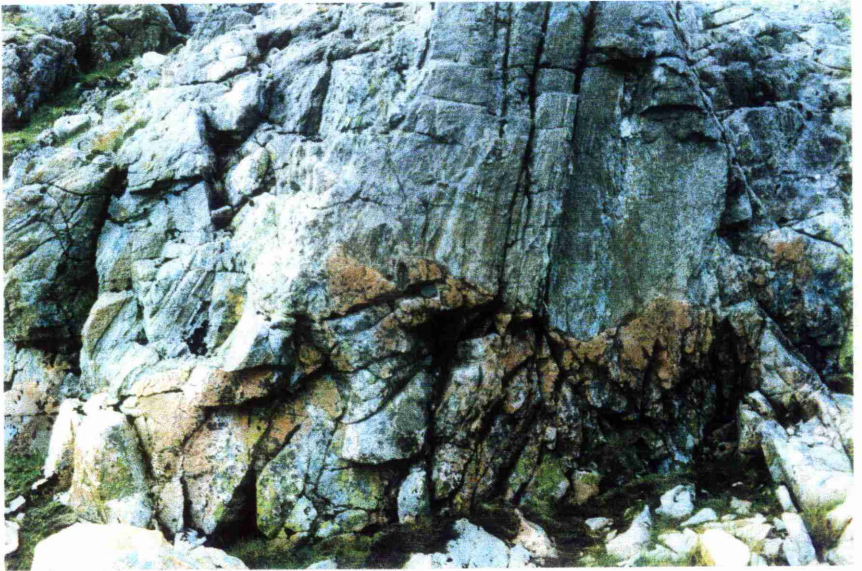
Plate 33 Photo. 4.5 View of the eastern margin. The left hand side is Locality 1 (Fig. 4.5) where erosion has failed to expose the underlying granite. The ridge on the right hand side is formed of Dalradian metasediments and represent remnants of the magma chamber wall. The stream in the middle of the photograph has cut down through the Dalradian, exposing the underlying granite.

---

---

Plate 33 Photo. 4.6 Contact between fine grained red granite and Dalradian metasediments on the col between Aonach Mor and Stob an Cul Choire. This granite intrusion is similar to those found in An Cull Choire and was previously interpreted as part of the Outer Granite (Anderson 1935 and Haslam (1965). (NN197 730)

---



removal of Inner Quartz Diorite or Coarse Type in the eastern area, and in its place the field of the Porphyritic Outer Granite is expanded to include outcrops formerly assigned to the Coarse Type/Inner Quartz Diorite (Fig. 4.4).

Haslam (1965) attempted to expand on Anderson's (1935) hypothesis that the higher silica values in the eastern area were related to the higher altitude of this area (600-1200m vs 0-400m). However, a vertical traverse revealed no correlation between altitude and geochemical variation, several explanations were put forward, but Haslam (1965) could find no satisfactory model which explained all the features of the chemical variation in the eastern area. One explanation, suggested that the Outer and Inner Quartz Diorites in the eastern margin were separate intrusions from those of the northern and western margins. The reason that this explanation was discarded was, that both the Outer and Inner Quartz Diorites showed similar increases in  $\text{SiO}_2$ ; however, increasing  $\text{SiO}_2$  of the Outer Quartz Diorite was based on the exposure of this rock type in An Cul Choire (Fig. 4.5) that is now recognised as a post-Porphyritic Outer Granite intrusive sheet (section 4.2.2.vii) and not part of the Outer Granite.

Recognition of the Sgurr Finnisg-aig Quartz Diorite and the chilled marginal variant of the Porphyritic Outer Granite, greatly reduce the significance of the eastward increase in  $\text{SiO}_2$  reported by both Anderson (1935) and Haslam (1965). Whereas expansion of the Porphyritic Outer Granite field results in a greater geochemical spread for this field, examination of the trends marked on Figs. 4.8a and 4.8b, reveals that the geochemical variation within the new Porphyritic Outer Granite field and the new Coarse Quartz Diorite field is more consistent with the new scheme than the old. Both of these new groups shows similar behaviour with respect to  $\text{K}_2\text{O} + \text{Na}_2\text{O}$  vs  $\text{SiO}_2$ .

In terms of their relative age, the following sequence was deduced from field relationships between members of the dyke swarm and plutonic rocks exposed along the Nameless Burn and in Allt an t-Sneachda. Some overlap probably exists between Fine Quartz Diorite, Sgurr Finnisg-aig Quartz Diorite and Coarse Quartz Diorite in terms of the timing of intrusion.

Porphyritic Outer Granite (youngest)	
Coarse Quartz Diorite + appinites (including xenolith bearing dyke)	
Sgurr Finnisg-aig Quartz Diorite and associated dykes	
Lamprophyres and microdiorite dykes	
Fine Quartz Diorite	}Felsite dykes
Early lamprophyres and members of the dyke swarm (oldest)	

### 4.3 Breccias

Three areas of breccia (Fig. 4.5) are recognised in the Ben Nevis Complex, these being: in Allt an Creige Duibhe between the Fine Quartz Diorite and Coarse Quartz Diorite, between Fine Quartz Diorite and Dalradian country rocks in the vicinity of Aonach an Nid, and the most extensive and best exposed area along the contact between the Porphyritic Outer

Granite and Dalradian schists between Coire an Lochan and An Cul Choire on the eastern side of the Ben Nevis Complex. This latter area is now discussed in greater detail with the aim of providing a model for the formation of all three breccia zones.

The contact between Dalradian country rock (Leven schist formation) and Porphyritic Outer Granite in the eastern area is markedly different from that exposed elsewhere in the Ben Nevis Complex where it is usually sharp and little interaction between granite and country rock is observed. In the eastern area, the contact is strongly brecciated and veined; the close relationship between brecciation and veining suggests that the two features are intimately related. Veins from a few mm to several metres in width (Photo 4.7) can be found up to 100m from the main contact throughout much of the eastern area. Brecciation is typically confined to discrete zones up to 20m+ from the main contact. The matrix of the breccia zones is granitic and broadly comparable to chilled Porphyritic Outer Granite. Dismemberment of the schist has been accompanied by rotation and small scale movements of individual blocks; transport distances are <5m and often much less. Clasts within the breccia zones are often strongly veined. Cavities and metalliferous mineralisation are not observed within the breccia zones. Migmatization is not observed and the main granite body shows no noticeable increase in xenolith numbers relative to other areas of the Ben Nevis Complex.

Similar exposures have been described from an area of the Etive Complex. It was suggested by Brown (1972) that the breccias in this area are found on the floor of the Etive magma chamber and represent the accumulation of rock fragments 'stopped' from the walls and roof. This interpretation cannot be applied to the Ben Nevis Complex because the exposures of breccia are located in the roof/walls of the magma chamber. Neither can intensive stoping be the explanation as the Porphyritic Outer Granite in this locality is not noticeably enriched in xenoliths; the breccia zones are confined to discrete zones within the roof and wall rock exposures. The breccias do not contain exotic fragments but are comprised of the local Dalradian lithology (Leven schist formation - Photo 4.8) and must have therefore been formed *in situ*.

Walker (1928) presented a model for the development of breccia pipes where an initial gas explosion fragments the adjacent rock, generating broken fragments and void space that may then be permeated by magma. Continued intrusion of magma leads to the formation of discrete pipes of magma within the breccia zone and eventually a solid mass of magma will develop after transport of the country rock from the zone of brecciation to higher levels in the crust. He concluded that "An intrusive mass of igneous rock with near-vertical walls from a few hundred yards to three miles in diameter and roughly circular, oval or elliptical in plan merits consideration as a possible volcanic plug or stock occupying an earlier explosion breccia pipe and if around its periphery, some residual patches of indurated pre-intrusive breccia remain this possibility may be recognised as approaching a certainty."

---

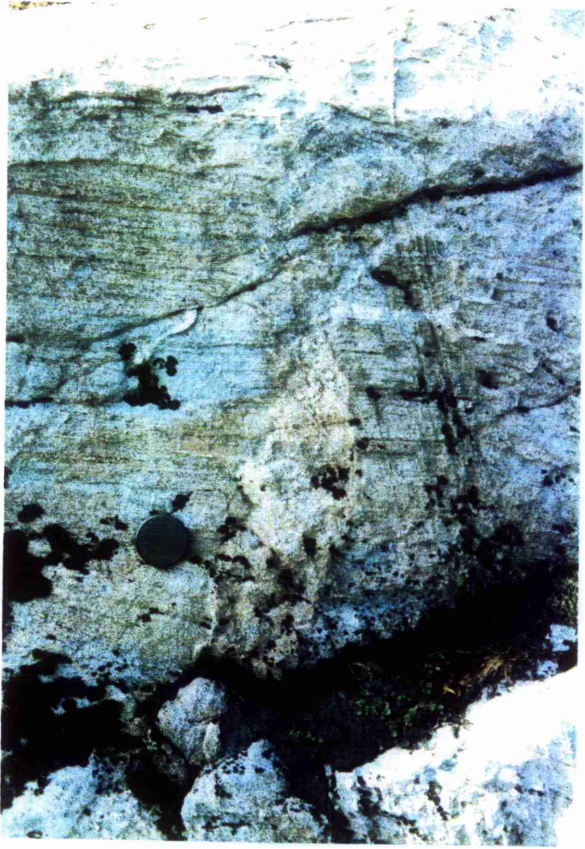
Plate 34 Photo. 4.7 Granite vein within the Dalradian metasediments. (NN196 735)

---

---

Plate 34 Photo. 4.8a Intrusion breccias in the vicinity of Aonach Mor. Note the small scale movements exhibited by blocks on the lower photograph and the granitic matrix to the breccia. (NN196 735)

---



At first sight, the Ben Nevis Complex appears to fit the model of Walker (1928), but granite forming the veins in, and matrix of, the breccia is continuous with the Porphyritic Outer Granite and therefore contemporaneous, implying that the cause of brecciation and veining must be found within the Porphyritic Outer Granite and not ascribed to some earlier event. In addition, the presence of veins within individual breccia clasts indicates that veining occurred before or during brecciation and not after as in the Walker (1928) model.

Harker (1908) described similar exposures where "the Newer rock has sometimes penetrated the older in a network of ramifying veins and this enclosed detached blocks of it, of all sizes, also veined. The junction is thus not a line but a zone which may have a width of a hundred yards or more. Such a zone of mechanical admixture may be termed for convenience an intrusion breccia." From this description it is clear that the intrusive rocks are believed to vein/intrude the country rock and where this is sufficiently intense, blocks of the country rock become detached and included within the granite to form Harker's intrusion breccia.

During crystallisation, volatiles become concentrated in the roof zone of a magma chamber; gradual build of pressure results and numerous veins intrude the adjacent country rock. If the zone of veining reaches the land surface, explosive loss of volatiles and magma is accompanied at depth by the rapid volume expansion of magma and a drop in magmatic pressure results in fragmentation of the wall/roof to form a zone of brecciated rock. A similar mechanism has been proposed for the net-veined and brecciated quartz dolerite ring dyke of Intrusion Centre 2 Ardnamurchan (Wells 1954).

It is unlikely that this zone of brecciation represents the roots of a volcanic vent which erupted material now forming the Ben Nevis volcanic pile because a large number of schist xenoliths would be found in the ejecta and no such horizon is found within volcanic pile.

#### 4.4 Inner exposures of Quartz Diorite

##### 4.4.1 Previous interpretation

At two locations along the Porphyritic Outer Granite/Inner Granite contact (Fig. 4.3), Haslam (1965) recorded the existence of coarse grained quartz diorite slivers that he believed were part of the Inner Quartz Diorite. According to the interpretation of Haslam (1965), the Porphyritic Outer Granite intruded the largely molten core of the Inner Quartz Diorite, subsequent intrusion of the Inner Granite removed much of the inner portion of the Inner Quartz Diorite; such that only two exposures reveal the presence of this inner band, these being along the Allt Daimh and the Allt a' Mhuillin (Fig. 4.3).

##### 4.4.2 Allt a' Mhuillin

The Allt a' Mhuillin sliver is much veined by fine grained pink Inner Granite and therefore predates intrusion of the Inner Granite. Hornblende crystals show multiple twinning and feldspars are cloudy, features which are interpreted as the effects of contact

metamorphism by the Inner Granite. Phenocrysts in the Porphyritic Outer Granite decrease in size towards the contact with the sliver and it can therefore be stated that the sliver predates intrusion of the Porphyritic Outer Granite and that the model of Haslam (1965) is viable for this locality.

#### 4.4.3 Allt Daimh

On re-examining the Allt Daimh exposure, it was found that whilst the northern outcrop of the sliver was situated at the contact between Porphyritic Outer Granite and Inner Granite as recorded by Haslam (1965), the southern outcrop was located entirely within Porphyritic Outer Granite. The shape of the sliver is not that of a thin band, but more akin to a teardrop with its tail pointing deeper into the Porphyritic Outer Granite (Fig. 4.4). Large alkali feldspar phenocrysts are observed in the Porphyritic Outer Granite right up to the contact with the teardrop. In the Allt Daimh stream-bed a dyke trending  $245^{\circ}/065^{\circ}$  is found intruding the Porphyritic Outer Granite; if its trend is extrapolated then it should cross cut the teardrop exposures; this is not the case and it is believed that the teardrop post-dates dyke injection.

The upper contact between the Porphyritic Outer Granite and the teardrop is characterised by mingling between the two rock types. Rapid and frequent grain size variations are noted in the teardrop, as is a strong contact parallel fabric. Phenocrysts in the Porphyritic Outer Granite are slightly deformed and this may be the result of intrusion of the teardrop. The evidence indicates that the teardrop was intruded after the Porphyritic Outer Granite and at least one member of the post-Porphyritic Outer Granite dyke swarm. On the basis of such evidence, the sliver model of Haslam (1965) is no longer valid and the exposure of quartz diorite in the Allt Daimh is better explained as a minor intrusion within the Ben Nevis Complex.

### 4.5 Xenoliths and Enclaves

#### 4.5.1 Xenoliths

Xenoliths are rarely observed in the Outer Granite, with the exception of the breccia zones mentioned earlier (section 4.3). Those xenoliths which are observed are often found in discrete sheets, dykes and pods/patches. Up to 60%+ of the volume of granitic rock in these zones may be taken up by xenoliths. These discrete xenolith rich exposures are only observed in the quartz diorites and are particularly associated with the Coarse Quartz Diorite. It is suggested that these exposures, which are often intrusive, are intimately associated with appinitic/lamprophyric magmatism and are not a feature typical of the Outer Granite in general. Xenoliths are dominated by metalimestone and quartzite, individual clasts are sub to well rounded and rarely exceed 10cm in diameter. In the Nameless Burn, a xenolith rich dyke (Photo 4.9) includes abundant xenoliths of metalimestone and quartzite in the centre of the dyke, whereas the margins show high concentrations of quartz diorite xenoliths. It

---

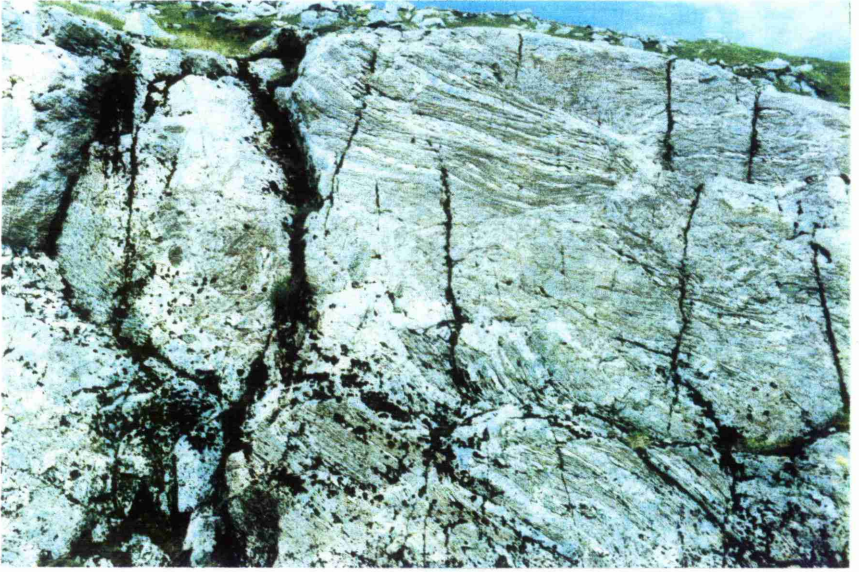
Plate 35 Photo. 4.8b Intrusion breccias in the vicinity of Aonach Mor. Note the small scale movements exhibited by individual clasts and the granitic matrix to the breccia. (NN196 735)

---

---

Plate 35 Photo. 4.9 Xenolith laden dyke in the Nameless Burn. Core of the dyke (bottom left hand side) dominated by Dalradian clasts, margins (top right hand side) dominated by quartz diorite clasts. BN384 (NN181 766)

---



therefore appears that the dyke has entrained country rock xenoliths prior to intruding a quartz diorite and excavating clasts from this lithology.

In the Allt a' Mhuillin (NN 145 754) abundant calc-silicate xenoliths are found in a sub-horizontal sheet below the large waterfall downstream of the BAA road bridge. Contact metamorphism has developed a dark green hornblende rich rim to a number of entrained clasts.

A number of discrete patches rich in xenoliths are found sporadically throughout the Fine Quartz Diorite and Coarse Quartz Diorite in the northern area. It is suggested that volatile charged magma first excavated and then transported these xenoliths into their present location. This process may well be akin to that suggested for the intrusion breccias on Aonach Mor, these patches representing the pipe between an intrusion breccia at depth and a vent on the surface. A similar model was developed by Platten (1982 & 1984) for breccia pipes in the South-west Highlands. An emplacement pressure of between 0.5 and 1.0 kbars was calculated for the South-west Highland examples (Platten 1984), highlighting the shallow level of the Ben Nevis Complex (section 4.8.4).

Larger xenoliths up to several metres in diameter are occasionally found throughout the Outer Granite. Examples include that exposed below the outlet of the upper lochan in Coire an Lochan. A number of xenoliths are also found along the tourist path, notably just above the second aluminium bridge. One complicated xenolith exposure contains occasional oxy-hornblende phenocrysts (Photo 4.10). Conversion of hornblende to oxy-hornblende has been achieved on heating hornblende in air to 800°C. Deer et al. (1992) state that most oxy-hornblendes crystallised initially as common hornblende in volcanic rocks, such as andesite, and were oxidised after eruption during the later stages of lava consolidation. The occurrence of oxy-hornblende in a xenolith leads to the conclusion that at least part of the magma chamber roof was comprised of volcanic rocks.

#### 4.5.2 Enclaves

Mafic Microgranular Enclaves (MME) are scattered throughout the Outer Granite and are especially common in the quartz diorites. Their shape is uniformly spherical and little flattening is observed. Exceptionally large numbers of MME can be found associated with xenoliths swarms described above (section 4.5.1) and in this situation they have almost certainly been excavated from the Ben Nevis Complex, rather than brought up from deep levels in the crust.

### 4.6 The Inner Granite

The Inner Granite is a medium to coarse grained biotite granite and is relatively homogenous throughout its entire outcrop. Slight chilling is visible along the outer contact; more extensive chilling is observed along the inner contact. Here, a zone of up to 50m reveals the effects of the collapse of a large cold block (the volcanic pile) into the Inner

Granite. There is a progression from normal Inner Granite, to strongly chilled Inner Granite at the contact with the Fault facies (see chapter 3). Coarse quartz - alkali feldspar granophyric intergrowths are the first discernible effects of chilling. With increasing proximity to the inner contact, crystal size decreases and a preferred alignment of the phenocryst phases is observed. Fenn (1986) reproduced graphic intergrowth textures in a series of experiments. Intergrowths were formed when growth rates were faster than diffusion rates (of silica) and undercooling was a significant feature of the melt. Coarse granophyric intergrowths are therefore interpreted as the result of slight chilling of the Inner Granite and the effects of cooling rapidly achieved greater significance closer to the volcanic pile.

In Coire Eoghainn an intrusive sheet is found within the Inner Granite (Photo 4.11); this feature is attributed to back injection of a slightly more basic variant of the Inner Granite during collapse of the volcanic pile.

Haslam (1965 & 1968) documented the existence of a basic hornblende bearing variant of the Inner Granite in the northern extremity of the Inner Granite outcrop. He reported sharp contact with both the Porphyritic Outer Granite and the normal Inner Granite. Chemically, the basic Inner Granite is comparable to the Porphyritic Outer Granite, but texturally it is more akin to the Inner Granite, although significantly less altered by hydrothermal fluids.

The contact against the Porphyritic Outer Granite in this northern area is sharp; in addition a second contact internal to the basic Inner Granite is observed  $\approx 1\text{m}$  from the Porphyritic Outer Granite/basic Inner Granite contact. The band of basic Inner Granite between the two contacts is subtly different from that of the main outcrop in that it is slightly more mafic and a weak pre-full crystallisation (PFC) fabric contrasts with the strong fabric of the main body close to the internal contact. The strong PFC fabric dies out less than 20cm from the contact. Both the basic Inner Granite and the Porphyritic Outer Granite are cross cut by aplitic veins. Upstream of this location (BN423 - Fig. 4.5), normal Inner Granite is found in contact with the Porphyritic Outer Granite (BN421 - Fig. 4.5). At this locality a vein of Inner Granite intrudes the Porphyritic Outer Granite where it rapidly passes into aplite (Photo 4.12). If the aplite veins in the basic Inner Granite and the Porphyritic Outer Granite are of the same generation as this Inner Granite generated vein, then it can be stated that the basic Inner Granite predates generation of aplite veins from the Inner Granite.

The Fault facies is geochemically almost identical to the basic Inner Granite (Fig. 4.9) and it is suggested that the Inner Granite magma chamber was partially zoned prior to collapse of the volcanic pile. Basic magma from a lower level was forced toward the surface, either along the contact between the volcanic pile and the Inner Granite or in this northern area.

---

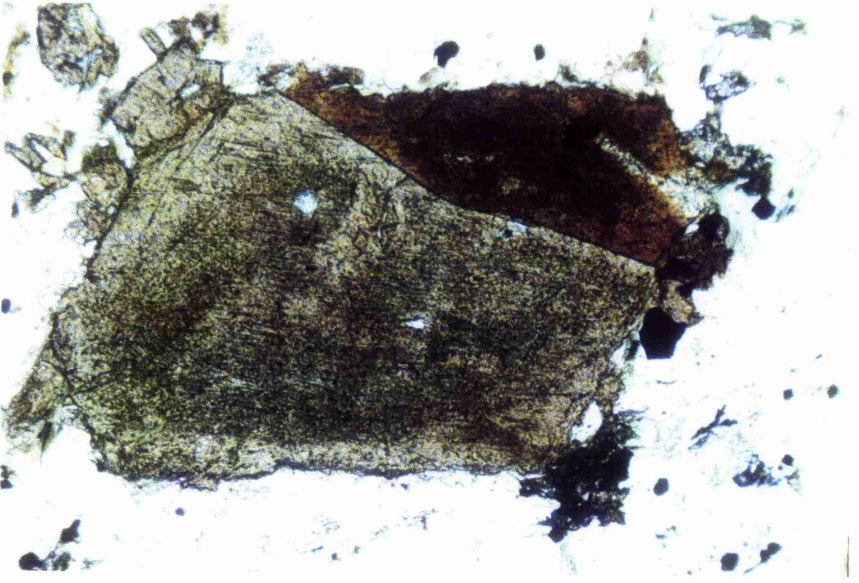
Plate 36 Photo. 4.10 Photomicrograph of a volcanic xenolith. Conspicuous phenocryst is Oxy-hornblende. (OBN37e \* 107 PPL) (NN123 724)

---

---

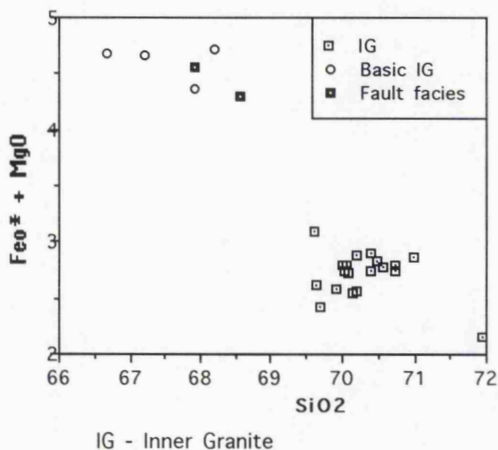
Plate 36 Photo. 4.11 Back injection of the Inner Granite. Thickness of vein  $\approx$ 40cm. Injection is cross-cut by late stage aplite veins and the contact between injection and Inner Granite has also been exploited by these veins. (NN165 702)

---



## 4.7 Minor Intrusions

Minor intrusions related to the Ben Nevis Complex take the forms of dykes, sills/sheets and appinite pipes. Intrusions erroneously assigned in previous studies (Anderson 1935 and Haslam 1965) to members of the Outer Granite have already been described and are not discussed in this section.



A small number of dykes pre-date the intrusion of the Outer Granite; in particular the felsites dykes outcropping in the Nameless Burn and Allt an t-Sneachda are found cross cutting and cross-cut by early members of the Fine Quartz Diorite. Evidently these dykes were intruded early in the history of the Ben Nevis Complex. Additionally, as already mentioned, a number of dykes in this complex north-eastern margin are intimately related to the intrusion of the Sgurr Finnisg-aig Quartz Diorite.

#### 4.7.2 Sheets

In addition to the fine grained pink granite sheets in the vicinity of An Cul Choire (section 4.2.2.vii), two fine grained quartz diorite sheets are found within the Ben Nevis Complex. The first sheet (BN367 - Fig. 4.5) is found in a riverside cliff exposure along the Allt Choille-Rais. The second (BN431 - Fig. 4.5) is found on the western slopes of Aonach Mor and forms a conspicuous line (clearly visible from the summit of Ben Nevis) in the slopes of this mountain (Photo 4.13). Both appear to have been intruded relatively late in the history of the dyke swarm. From field relationships exposed in a small stream running off Aonach Mor, it is apparent that the second sheet is fed by dykes from below and feeds dykes above, therefore forming one rung of a ladder intrusion.

#### 4.7.3 Appinites

The origin of the Ben Nevis appinites will be discussed in greater detail in chapters 5, 6 and 7. The discussion below is merely concerned with aspects of their field geology.

Anderson documents the occurrence of three appinite localities (Fig. 4.4). These are: a thin hornblende rich margin to the Porphyritic Outer Granite in the Red Burn (Photo 4.14) first recorded by Bailey & Maufe (1916), "a tiny irregular boss" exposed on the hillside just below the surge chamber of the BAA hydro scheme and a number of appinitic veins within the schists near the igneous margin on the slopes of Aonach Beag. In addition to these three localities, a previously unrecorded appinite pipe was found below the summit of Aonach an Nid (Fig. 4.4).

The surge chamber appinite is described by Haslam (1968) as "An area is described in which the main rock type is a variable dioritic rock, thought to have been formed by the expulsion of the residual acidic liquid from a largely crystalline quartz-diorite magma. It contains numerous xenoliths of pyroxenite and appinite... ..they are considered to be the reaction products of the outer margin of a magma and the adjacent calcareous country rock." Although Haslam (1970) describes the appinites as xenoliths, a number of small appinite pipes occur in this area; these are clearly intrusive, are less than 30cm in diameter and have contacts consistent with a intrusive origin (Photo 4.15).

The Aonach an Nid locality exhibits a crude reverse zonation with the most mafic compositions being situated in the core of this 10m by 8m subcircular outcrop. Appinite at the margin of this pipe is characterised by short stubby crystal of hornblende, whereas the

---

Plate 37 Photo. 4.12 Contact exposed at BN421. Porphyritic Outer Granite forms the top left hand side, Inner Granite forms the right hand side and can be traced underwater from right to left, passing into an aplitic vein.  
(NN185 727)

---

---

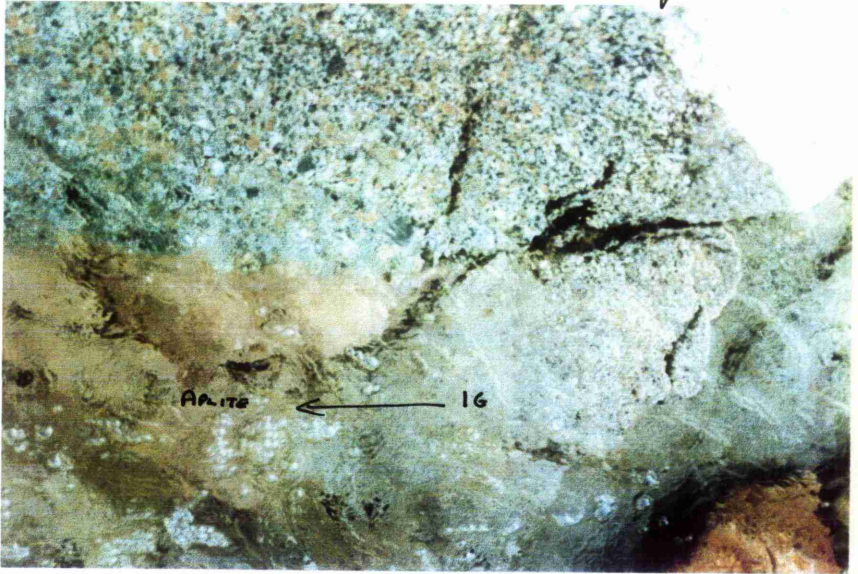
Plate 37 Photo. 4.13 Obvious line formed by the outcrop of a diorite sheet/sill  
(BN431).

---

PLATE 37

POG ↓ 16

POG  
→  
ARITE



---

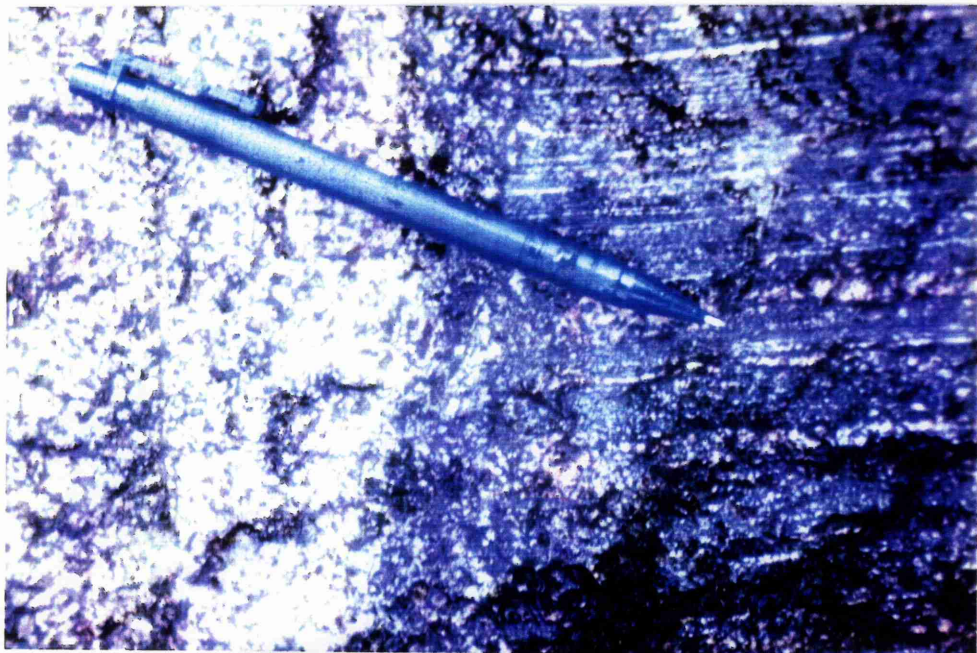
Plate 38 Photo. 4.14 'Appinite' of the Red Burn locality. Thin hornblende rich margin to the Porphyritic Outer Granite separates the igneous rock on the left hand side from the Ballachulish Limestone Formation on the right hand side. The blue colour is an artefact of the copying process and the hornblende imparts a dark olive green colour to both the 'appinite' and the limestone. BN134 (NN136 717)

---

---

Plate 38 Photo. 4.15 Intrusive contact relationships between appinitic magmas (darker colour) and the Coarse Quartz Diorite.

---



core contains needles of hornblende up to 2cm long. The pipe is intruded into the contact zone between the Fine Quartz Diorite and Leven schist.

## 4.8 Structural geology

### 4.8.1 Granite Structure

In general, the granites of the Ben Nevis Complex are uniformly lacking in any form of pre-full crystallisation (PFC) or crystal plastic strain (CPS) fabric (nomenclature of Hutton 1988b). Those fabrics which are observed are almost always found against the outer margin of the Ben Nevis Complex and have a vertical contact-parallel orientation. In particular, the Sgurr Finnisg-aig Quartz Diorite usually exhibits a strong PFC fabric with aligned plagioclase phenocrysts (Photo 4.16a). The Porphyritic Outer Granite also reveals a moderately strong fabric (Photo 4.16b) particularly where the large alkali feldspar phenocrysts are not well developed.

On the col between Aonach Mor and Aonach Beag, a strong fabric is observed in the chilled marginal variant of the Porphyritic Outer Granite well inboard of the outer contact. Again the fabric is approximately contact parallel and in the vertical plane. In this area (BN420 - Fig. 4.5), alkali feldspar phenocrysts slowly increase in size with distance from the contact. The contact is located on the eastern side of the col and a very obvious nick is found in the hillside (Photo 4.17a & 4.17b). Moving deeper into the Ben Nevis Complex from the contact involves crossing the col and then descending sharply into Coire Giubhsachan. Phenocrysts of alkali feldspar become visible on the col a little distant from the contact itself. Once over the col and into the descent, a sudden jump in phenocryst size is observed and the Porphyritic Outer Granite changes in character from a chilled variant with small (<1cm diameter) phenocrysts to typical Porphyritic Outer Granite with phenocrysts up to 2cm in diameter. This occurs over a distance of 2-3m. Both the chilled Porphyritic Outer Granite and normal Porphyritic Outer Granite have strong PFC and CPS fabrics. Both feldspar types show preferred alignment and small shears deform these phenocryst phases. The fabric in the normal Porphyritic Outer Granite dies away rapidly from this location and the best explanation of this exposure is that the Porphyritic Outer Granite was subjected to deformation at a late stage in its crystallisation history, resulting in the juxtaposition of the chilled marginal Porphyritic Outer Granite and normal Porphyritic Outer Granite. What caused this late stage movement is unclear; movement of magma below the present surface is one possibility.

### 4.8.2 Absence of fabrics in the Outer and Inner Granites

The absence of PFC or CPS fabrics in the plutonic rocks of the Ben Nevis Complex may not be a result of the lack of strain imposed on the granites during their emplacement, as there are numerous indicators of syn-plutonic strain (faults, dykes and the shape of the plutons), but may be due to either a low crystal volume during intrusion or to low aspect ratios of the crystal phases.

---

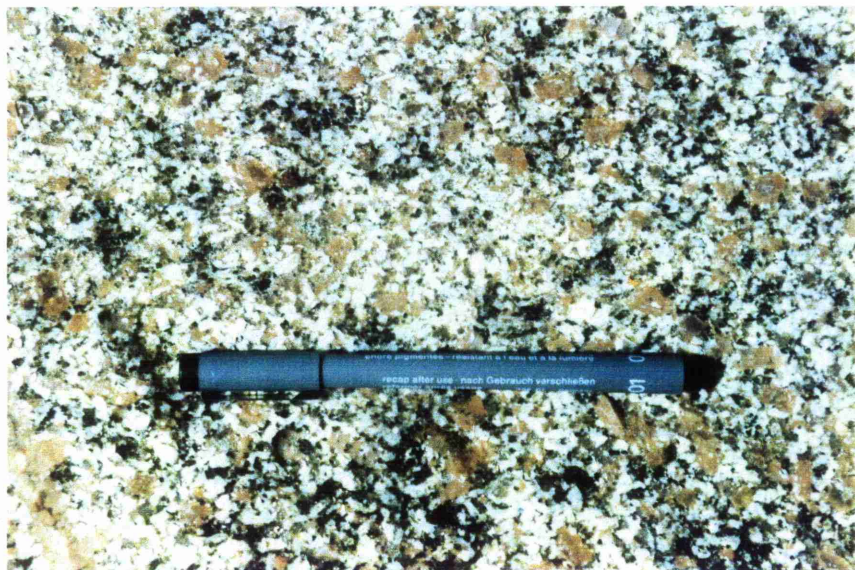
Plate 39 Photo. 4.16a Pre-full crystallisation fabric within the Porphyritic Outer Granite. Pen is orientated parallel to fabric.

---

---

Plate 39 Photo. 4.16b Pre-full crystallisation fabric within the Sgurr Finnisg-aig Quartz Diorite, fabric orientation is approximately horizontal in this photograph.

---



---

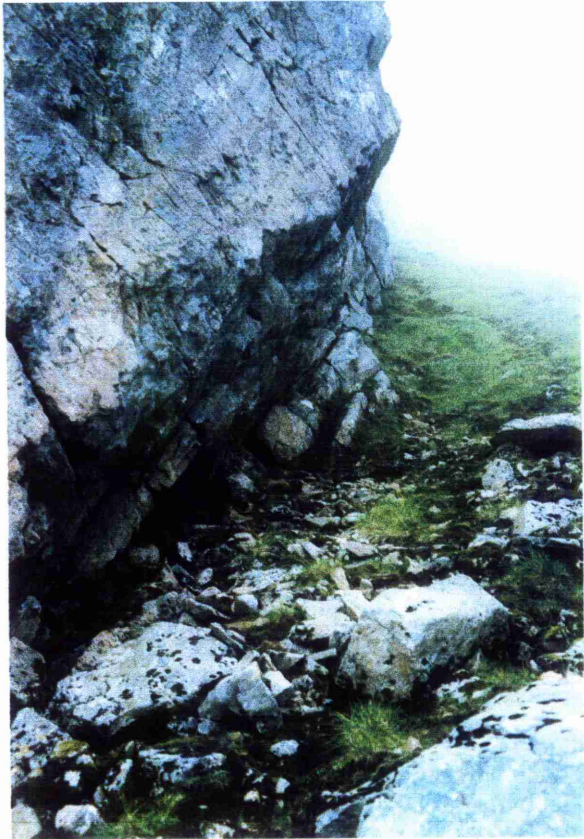
Plate 40 Photo. 4.17 'Nick' in the hillside revealing the contact between the Porphyritic Outer Granite and Dalradian metasediments. Grassy areas in the foreground cover the intrusive red granite sheets of BN412. Aonach Beag is the mountain in the background.

---

---

Plate 40 Photo. 4.17b Close up of the 'nick'. Contact metamorphosed Dalradian schists form the overhang and the granite obscured by vegetation. (NN195 722)

---



Strong contact parallel vertical fabrics are also observed in the Coarse Quartz Diorite exposed in the area of the surge chamber appinite. The association of this fabric with the appinite suggests that it is caused by intrusion of numerous small appinite pipes and volatile streaming associated with the appinite.

The Porphyritic Outer Granite reveals CPS and PFC fabrics where large alkali phenocrysts are not well developed; this is associated with proximity to the outer contact and therefore chilling of the magma. Hornblende and plagioclase phenocrysts are also much reduced in size and it is suggested that the Porphyritic Outer Granite was intruded with a substantial melt volume. Rapid cooling at the chamber margin during intrusion of the Porphyritic Outer Granite decreased the volume of melt until individual crystals began to interact with each other and show preferential alignment. The largely molten interior remained essentially fluid until the strains imposed on the Ben Nevis Complex had diminished. It is suggested that the strains imposed on the chilled margin were imposed by the intrusion of later pulses of magma forming the main body of the Porphyritic Outer Granite.

#### 4.8.3 Structural geology of the Ben Nevis Complex

Despite the general lack of PFC or CPS fabric data from the plutonic rocks, useful structural data can be gleaned from the overall shape of the complex, syn-plutonic faults and from stress field indicators within the Ben Nevis dyke swarm.

##### 4.8.3.i Shape

The Inner Granite is oval in shape, being 7km (NNE-SSW) by 4km (ESE-WNW). Jacques & Reavy (in press) believe that the shape of the Cruachan and Starav granites indicate *in situ* ballooning whilst undergoing sinistral transpression. The orientation of the long axis of these granites is ENE-WSW and, according to Jacques & Reavy (in press) relative extension is acting in this direction, whereas relative compression is acting in the same orientation as the short axis (WNW-ESE). The shape of the Inner Granite of Ben Nevis (Fig. 4.11) implies relative extension to the NNE-SSW, giving a dextral shear sense in contrast to the sinistral sense of the Etive Complex. Because the structural grain runs NE-SW, elongation of the Ben Nevis Complex cannot be related to the grain of the country rock, and must therefore be an intrinsic feature of the stress field operating during intrusion.

The shape of the Outer Granite is distorted by extension due to intrusion of the Ben Nevis dyke swarm (up to 17%, Anderson 1935) and its areal extent has been truncated by the Inner Granite; consequently it is not considered here.

##### 4.8.3.ii Faults

A number of obvious steep sided gullies are visible from Glen Nevis on the flanks of Meall an t-Suidhe and Ben Nevis/Carn Dearg (SW). Where the bedrock is visible in the floor of these gullies, faults with a dextral sense of movement can be identified. Dip of the fault plane

varies between 60° NW to 60° SE and they strike 040° or 220° ± 20°. However later reactivation has confused the shear sense data and a number of sinistral displacements are also observed. These later movements post-date intrusion of the dyke-swarm and their age relative to the Ben Nevis Complex is not clear.

Movements along fault planes have been shown to be contemporaneous with magma emplacement elsewhere in the British Caledonides; Strontian (Hutton 1988a), Ratagain (Hutton & McErlan 1991) Strath Ossian (Key et al. 1993), Glencoe (Morris & Hutton 1993) and Etive (Jacques & Reavy in press).

#### 4.8.3.iii Dykes

The earliest members of the Ben Nevis dyke swarm predate, or are intimately associated with, the plutonic complex; however the majority of the dyke swarm was intruded during the period between intrusion of the Outer and Inner Granites. Bailey & Maufe (1916 & 1960) suggested that the Ben Nevis swarm was contemporaneous with the Etive dyke swarm. The Ben Nevis dyke swarm is orientated NE-SW and the average dyke thickness is ≈3m (Anderson 1935).

The majority of dyke exposures yield no tectonic/strain data due to their having parallel or planar contacts but a number of dykes show features which can be related to the local stress regime. These features are depicted in Fig. 4.10 and representative examples are displayed in Photo 4.18.

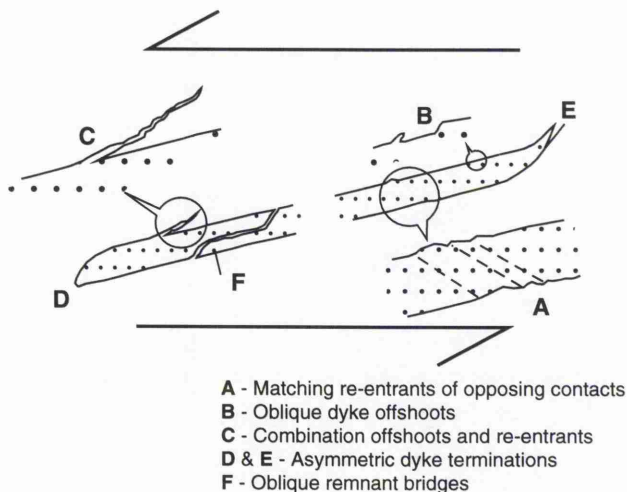


Fig 4.10 Cartoon illustrations of stress vector data obtained from the Ben Nevis dyke swarm. All illustrated examples are sinistral, adapted from Morris & Hutton (1993).

---

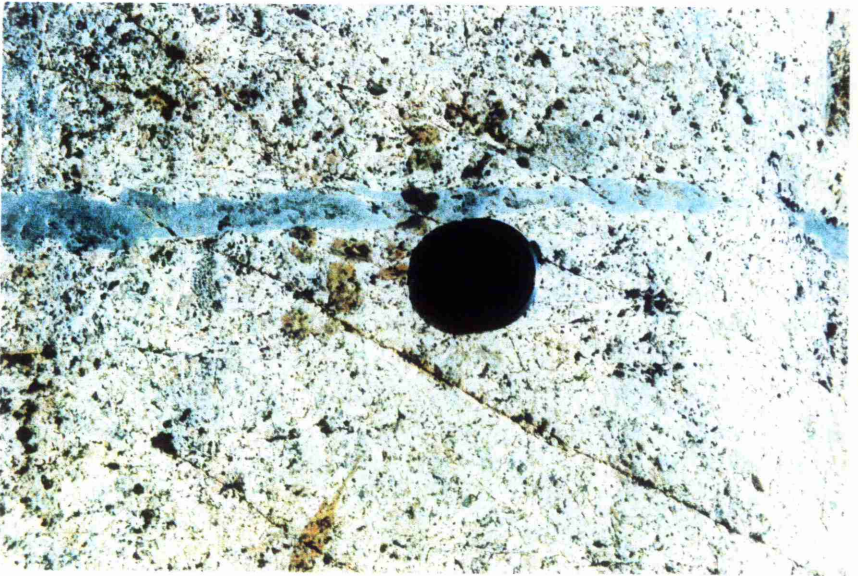
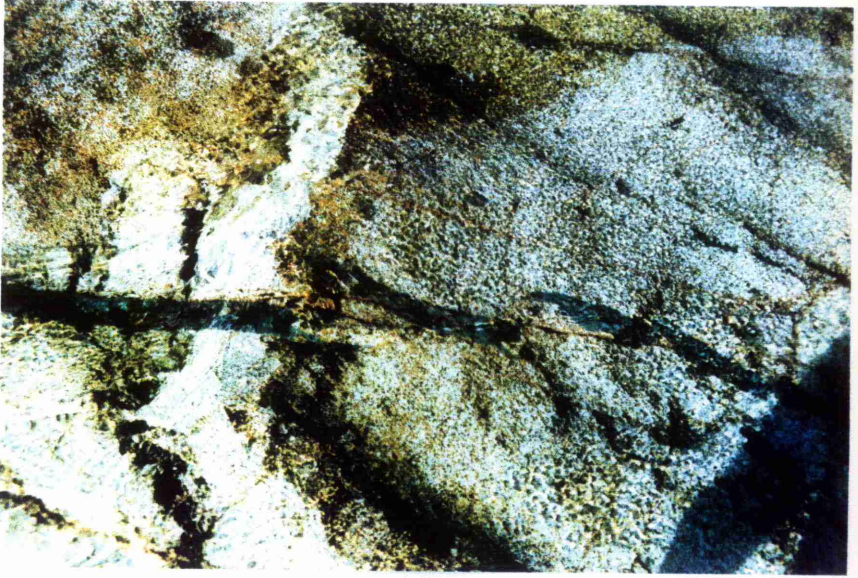
Plate 41 Photo. 4.18a Example of structural data provided by the Ben Nevis dyke swarm; en-echelon dyke segments revealing dextral fabrics. (NN177 746)

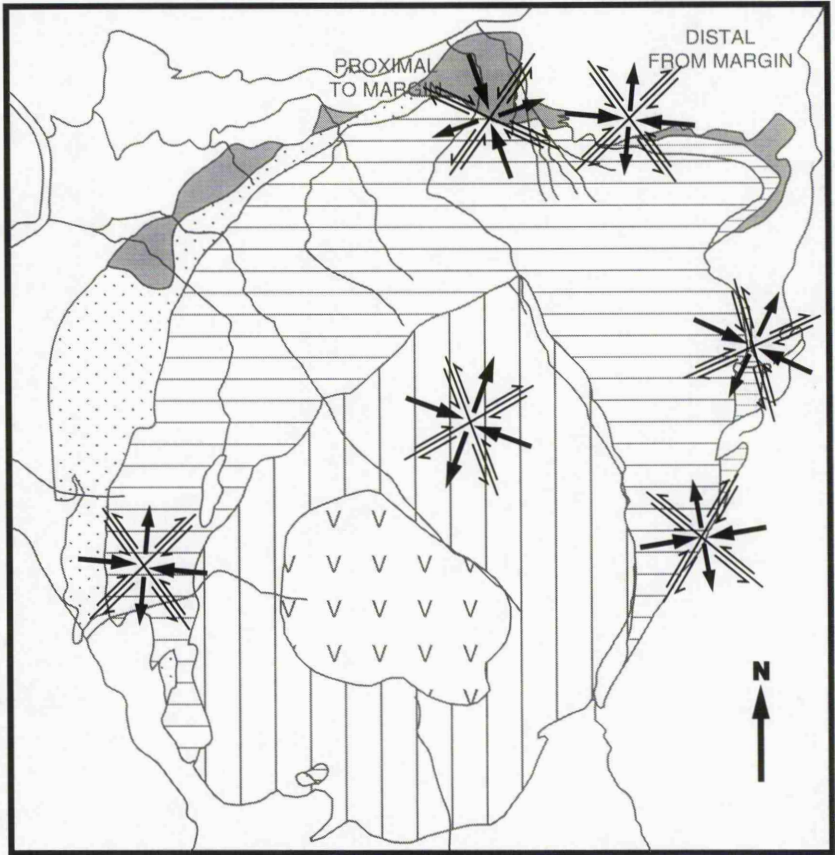
---

---

Plate 41 Photo. 4.18b Example of structural data provided by the Ben Nevis dyke swarm; small sinistral shears offsetting the thin dyke. (NN177 746)

---





**KEY**

- |   |                                  |   |                                   |
|---|----------------------------------|---|-----------------------------------|
|  | Fine Quartz Diorite              |  | Inner Granite                     |
|  | Sgurr Finnisg-aig Quartz Diorite |  | Volcanic Pile                     |
|  | Coarse Quartz Diorite            |  | Shear sense                       |
|  | Porphyritic Outer Granite        |  | Relative compression or extension |

Fig. 4.11 Structural data from the Ben Nevis Complex. In general the data indicate relative compression acting in WNW-ESE and relative extension acting NNE-SSW. Note the change in stress field orientation at the northern margin, interpreted as a forceful magmatic push.

In common with the Inner Granite, the majority of shear sense data derived from the dyke swarm indicate relative NNE-SSW extension and ENE-WSW compression (Fig. 4.11). Close to the contact with the Porphyritic Outer Granite (<100m) in Allt an t-Sneachda and the Nameless Burn, the stress regime reverses and relative compression is orientated approximately N-S. The rotation of the stress field is backed by syn-plutonic (Porphyritic Outer Granite) faults (Photo 4.4) that also indicate approximately N-S compression. Because this occurs within a few tens of metres from the contact between Porphyritic Outer Granite and Dalradian schists, it is believed that this change in stress field orientation reflects compression caused by the intrusion of the Porphyritic Outer Granite as it created space for itself.

#### 4.8.3.iv Conclusions

Morris & Hutton (1993) examined part of the Etive dyke swarm and from those dykes which yielded shear sense information, concluded that they were intruded into a sinistral stress field. This conclusion, they suggested, was supported by large scale counter-clockwise (sinistral) rotations in the orientation of dykes depicted on the BGS map (Sheet 53). From the fragments of the BGS map presented with the Morris & Hutton (1993) paper, a number of left-stepping en-echelon bends and clockwise (dextral) rotations are also apparent; it is not obvious whether counter-clockwise or clockwise rotations dominate the dyke swarm. From Sheet 53, an area to the south of the Etive Complex shows clear large clockwise (dextral) rotation of members of the Etive dyke swarm intruding the Lorne plateau lavas and the southern margin of the Cruachan granite.

The Etive and Ben Nevis dyke swarms, if taken in a regional context, indicate relative extension to the NW-SE and compression to the NE-SW (Anderson 1936). This fits with a sinistral sense of shear for the Grampian Highlands during intrusion of the Newer Granites as suggested by Watson (1984), Soper & Hutton (1984), Hutton & McErlan (1991), Key et al. (1993), Morris & Hutton (1993) and Jacques & Reavy (in press).

The Ben Nevis data, supported by data from Strontian (Hutton 1988a), from dykes within the Lorne plateau and from late Caledonian movements along faults within the Dalradian (Treagus 1991), indicate a dextral shear sense. This suggests that the stress regime during intrusion of the Newer Granites was more complex than previously believed (Watson 1984, Soper & Hutton 1984, Hutton & McErlan 1991, Key et al. 1993, Morris & Hutton 1993 and Jacques & Reavy in press) and both dextral and sinistral regimes may have operated towards the end of the Caledonian Orogeny.

#### 4.8.4 Depth of intrusion

The plutonic rocks of the Ben Nevis Complex are regarded as high level intrusions (Read 1961, Mercy 1965 and Bailey & Maufe 1916 & 1960) on the basis that, like Glencoe (pressures for the Etive Complex, calculated from the contact aureole, lie within the range 1-2kbars approximately 3-6km Droop & Treloar 1981), it is closely associated with

extrusive magmatic products and terrestrial sediments. There are a number of lines of evidence which back this supposition.

Combined fluid inclusion analysis of quartz veins and calcite-dolomite geothermometry of the associated calc-silicate country rock yields a 5.5km (1.5kbar) depth for a late stage thermal event affecting metasediments exposed in the vicinity of Spean Bridge (Powell & Smith 1973), approximately 7km north of the Ben Nevis Complex. According to Webb (1977), the most likely cause of this thermal event was intrusion of the Ben Nevis Complex. On the assumption that no differential uplift has occurred between Spean Bridge and the Ben Nevis Complex the plutonic rocks of the Ben Nevis Complex were intruded between 4.5 and 5.5km below the surface (Webb 1977).

A marginal variant of the Mullach nan Coirean granite (<2km from the Ben Nevis Complex) contains 1.5% modal andalusite (Haslam 1971), a low pressure form of  $Al_2SiO_5$ . Haslam (1971) argues that in this case, andalusite is a primary magmatic mineral and not a xenocryst or a replacement mineral. The granite in which it is found is corundum normative and therefore has Al in excess of that required to combine with Ca, K, and Na in order to form feldspar. Excess Al is usually reflected in granites by the presence of muscovite and the occurrence of andalusite reveals that the pressure was below that at which muscovite forms a stable phase. Haslam (1971) stated that the Mullach nan Coirean granite was intruded below 3kbars of pressure and probably below 2kbars.

Garnet is not found in the metamorphic aureole but low pressure minerals such as andalusite and cordierite are. Experimental work on the stability of almandine garnet (Hsü 1968) demonstrated that garnet is stable at low pressures (0.5 - 3kbars), at temperatures of 600 - 800°C and where  $fO_2$  was below the fayalite-magnetite-quartz buffer. The extension of the biotite-cordierite field at the expense of the almandine stability field, however, is considered to be a feature of low pressure metamorphism (Webb 1977) and almandine is absent in low pressure aureoles because of the formation of biotite and cordierite unless the rock is unusually rich in iron.

Further geothermal calculations led Webb (1977) to model the decline in temperature from the granite margin (Fig. 4.12) and to calculate the regional geotherm ( $70^\circ C km^{-1}$ ) and background temperature (480°C) during intrusion of the Inner Granite.

Haslam (1968) placed on record the presence of primary magmatic pyroxene and Al-poor amphibole in all but the most siliceous magmas. This contrasts with most other granite intrusions which typically contain aluminous hornblende. Textural evidence was used to show that pyroxene crystallised directly from the magma, whilst Al-poor hornblende was formed by the replacement of pyroxene at near solidus temperatures. Experimental studies (Yoder & Tilley 1962) indicated that hydrous silicate melts crystallising under high pressures favour the formation of hornblende, whereas those at lower temperatures favour the formation of pyroxene. Haslam (1968) therefore concluded that the Ben Nevis granites crystallised under low pressures.

Further experimental work by Piwinski & Wyllie (1968) and Robertson & Wyllie (1971) found that clinopyroxene would crystallise in water-saturated magmas at pressures below 1.7kbars and at higher temperatures than hornblende. Above 1.7kbars, hornblende would crystallise without the appearance of pyroxene. Under anhydrous conditions, pyroxene would always form at any pressure; increasing water activity increases the field in which hornblende will form. Robertson & Wyllie (1971) further showed that in any magma with sufficient water to crystallise biotite and hornblende, pyroxene would only appear at pressures below 2kbars. Webb (1977) therefore concluded that the Ben Nevis granites most probably crystallised at pressures <2kbars (<7km).

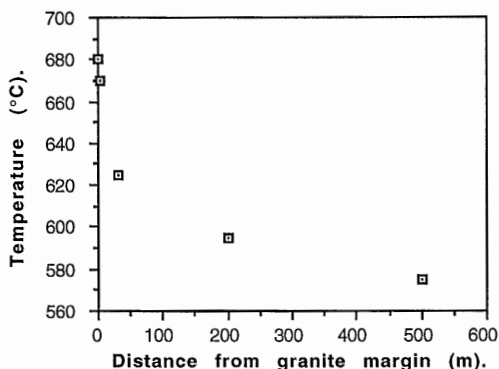


Fig. 4.12 Decline in temperature of the contact metamorphic aureole of the Ben Nevis Complex. Data from Webb (1977).

Differences in the Al content of calcic amphiboles are directly related to the depth of crystallisation (Hammarstrom & Zen 1986). Several amphibole geobarometric equations have been published; these are listed in Table 4.3 along with the results obtained for the most extreme amphibole compositions obtained from the Porphyritic Outer Granite. Blundy & Holland (1990) suggested that temperature is the most important control on the Al content of calcic amphiboles and presented a combined plagioclase and hornblende geothermometer. The correlation between  $Al^t$  (total Al of hornblende) and pressure, according to Blundy & Holland (1990), reflects variations in the granite solidus with varying temperatures. However, this hypothesis is criticised by Schmidt (1992), Hammarstrom & Zen (1992) and Johnson & Rutherford (1992) and it is generally accepted that the Al content of amphibole is controlled by the depth of magma emplacement (Barth 1990), although Pitcher (1993) suggested that pressure estimates derived from the Al in hornblende method fall on the low side because of late to post-magmatic crystallisation of hornblende.

Table 4.3 Aluminium in hornblende geobarometry.

Authors	Equation	Result for $Al^{\dagger} = 0.791$	Result for $Al^{\dagger} = 0.622$	Error
Johnson & Rutherford (1989)	$-3.46+4.23Al^{\dagger}$	-0.11407	-0.82894	$\pm 0.5\text{kbar}$
Schmidt (1992)	$-3.01+4.76Al^{\dagger}$	0.75516	-0.04928	$\pm 0.6\text{kbar}$
Hammarstrom & Zen (1986)	$-3.92+5.03Al^{\dagger}$	0.05873	-0.79134	$\pm 3.0\text{kbar}$
Hollister et al. (1987)	$-4.76+5.64Al^{\dagger}$	-0.29876	-1.25192	$\pm 1.0\text{kbar}$

None of the Al in hornblende geobarometric equations so far published have been calibrated to pressures below 2kbars. If the Al content in hornblende falls below a threshold value (0.79 in the Hammarstrom & Zen 1986 equation) a negative pressure is derived (an interesting physical problem). Leake (1978) reports that igneous hornblende typically has an Al content  $> 0.5$ . The mineral assemblage required for application of the Al in hornblende geobarometer is plagioclase + hornblende + biotite + quartz + alkali feldspar + magnetite + ilmenite + titanite  $\pm$  epidote. The Porphyritic Outer Granite is the only composition in the Ben Nevis Complex for which these phases were crystallising in equilibrium. Hornblende from the quartz diorites was not analysed because of the difficulty in defining primary magmatic hornblende from that replacing pyroxene. The hornblende crystals selected from the Porphyritic Outer Granite may also be replacement crystals, but those analysed were idiomorphic phenocrysts up to 2mm in size and it is not thought that such crystals could form by the replacement of pyroxene.  $Al^{\dagger}$  is greater than 0.5 for these amphiboles thus complying with Leake (1978).

Results obtained for the Ben Nevis Complex, although variable, consistently yield negative pressures or values below 2kbars (i.e. below the calibrated range of the equation). The only constraint that the Al in hornblende thermometer can therefore provide, is that the Ben Nevis magmas crystallised outside the range of the geobarometer (i.e. below 2kbars). If the equation of Schmidt (1992) was calibrated to below 2kbars then the depth of emplacement of the Ben Nevis granite was  $2.7\pm 2.2\text{km}$  (crustal density  $\approx 2.75\text{gcm}^{-3} = 3.6\text{km per kbar}$ ).

There is good field and geochemical evidence that the Ben Nevis granites were intruded below 2kbars and probably below 1kbar of pressure. Clearly the intrusion was emplaced at a shallow level in the crust, but an accurate estimate of intrusion depth must wait until the development of geobarometers which remain valid at low pressures. High volatile/fluid pressures in this environment may make this objective unattainable.

#### 4.8.5 Intrusion mechanism

The Outer and Inner Granites differ noticeably from each other; the Outer Granite shows variation in geochemistry, has an irregular margin, contains xenoliths and enclaves and is intimately associated with dyke injection. In contrast, the Inner Granite is compositionally and texturally homogenous (other than where the effects of the volcanic pile

come into play) and has a sharp regular and well defined outer contact with the exception of the Inner Granite/Dalradian contact, where local planes of weakness in the schists have controlled the local contact geometry (Webb 1977). This variation between the two granite bodies suggests that two separate intrusion mechanisms acted at different times during the formation of the Ben Nevis Complex.

Granite emplacement is a function of the interaction between magma buoyancy forces and ambient tectonic forces (Hutton 1988b). However, even where magma intrusion is apparently intimately associated with space created by movement along faults/shear zones, the rate of tectonic movement is several orders of magnitude too slow to be considered as the sole intrusion mechanism (Paterson & Fowler 1993a). Fault movement rates range from a few millimetres to a few centimetres per year. Rock strengths are too weak and lithostatic pressures too great to maintain large voids, and tectonic space creation must be balanced by magma influx. With slow rates of movement/space creation, numerous small injections would be required to form large plutons. These small injections would cool rapidly and form sheeted plutons and dyke swarms and not the elliptical shapes common to many granite plutons (Paterson & Fowler 1993b). Some local or regional extension may occur during the intrusion of a pluton, but other mass transfer processes must dominate during granite emplacement.

The Ben Nevis Complex has traditionally been considered as a classic example of subterranean cauldron subsidence (Maufe 1910). Both the Outer and Inner Granites are believed to have been intruded into the space created by the gravitational sinking of a subterranean block into the underlying magma (Fig. 4.6). However, the Outer Granite is not easily reconciled with a cauldron subsidence model. Clarke (1992) lists the diagnostic features of cauldron subsidence as; country rocks are structurally undisturbed, have suffered contact metamorphism and have sharp to diffuse contacts with the granite. Abundant country rock xenoliths are found within the margins of the granite.

The xenoliths (and enclaves) of the Outer Granite are not concentrated at the margins of the granite, but are found concentrated in large numbers into appinitic dykes, sheets small pods/pipes or into explosion breccias, suggesting that the volatile content of the magma was the fundamental control on xenolith location and not magma emplacement. The recognition of dykes within the Nameless burn and Allt an t-Sneachda, with similar chemistry, mineralogy and texture to the Sgurr Finnisg-aig Quartz Diorite leads to the conclusion that these dykes formed feeders to the Sgurr Finnisg-aig Quartz Diorite and that it was not emplaced by passive upwelling around a subsiding block. Deflection of the line of strike of the Ballachulish Limestone formation around the Ben Nevis Complex, and the recognition of compressional stress perpendicular to the contact in the Nameless Burn, indicate that the intruding granite pushed aside the Dalradian metasediments in order to create space for itself.

Cauldron subsidence does not solve the problem of space creation; a large body of magma is required beneath the subsiding block prior to subsidence. Cauldron subsidence merely removes the problem of space creation to a deeper level in the crust. Isotopic and geochemical evidence points to the presence of a small magma chamber beneath the Ben Nevis Complex where batches of additional melt caused substantial variations in isotopic and chemical composition during the life time of the Outer Granite. For cauldron subsidence, the underlying magma chamber must have the same areal dimensions as the Outer Granite chamber, the small volume required by the geochemistry requires a chamber of large areal extent but relatively thin, and therefore prone to rapid cooling and also blockage of the magma conduit during subsidence (Marsh 1982).

Hutton (1988b) distinguishes between forceful emplacement mechanisms, where tectonic extension (space creation) is less than magmatic compression (space destruction) and passive emplacement, where tectonic extension is greater than magmatic compression. This approach has been criticised (Paterson and Fowler 1993a) because tectonic forces cannot approach the rates required for the intrusion of a large elliptical pluton; however, the fact remains that a number of granite plutons appear to have passively infilled space created for them, whereas others appear to have forced their way in. Given the fact that the Ballachulish Limestone formation is deflected around the Ben Nevis Complex, and that compressional strain immediately adjacent to the plutonic margin has been identified, it is clear that the Outer Granite has created some space for itself by pushing aside the Dalradian schists. Structures found within the granite are concentrated at the margin and again suggest compression due to flattening in the vertical plane. The absence of PFC or CPS fabrics within the main outcrop of the Outer Granite argues neither for or against passive or forceful emplacement. Ramsay (1989) believed that flattening of xenoliths can only occur after the host magma has largely solidified. Pitcher (1979a) stated that "...granites often show a remarkable homogeneity of fabric and only develop strong preferred mineral orientations under special conditions". This statement was based on the findings of Nickel et al. (1967) who showed that lineations in granites can only form outside the Newtonian flow domain when crystallisation neared completion. Paterson et al. (1989) believed that fabrics will develop in granitic melts only when the volume of melt falls below 30% and interference between crystals begins. Thus ductile deformation can occur at the chilled and solid margin of a pluton whereas its core remains essentially liquid. If, on complete solidification, further stresses affect the granite, then fabrics will develop in all parts of the pluton placed under stress. Clearly, in the case of Ben Nevis, post crystallisation stresses were insufficient to deform solid granite.

It has been shown that the Ben Nevis Complex was emplaced to a high level in the crust (section 4.8.4); at such a level the effects of the unconstrained land surface become important during magma emplacement and strain within the envelope is at a minimum (Stevens 1959, Barrière 1977 and Pitcher 1979a).

The Outer Granite is geochemically zoned, with silica increasing with distance from the margin. Normal zoning, according to Castro (1987) is evidence of a ballooning emplacement mechanism. Intrusion of more evolved magma compositions into the centre of the pluton gives rise to ballooning and lateral expansion of the intrusion. In the case of Ben Nevis, space is most likely to have been created by uplift of the magma chamber roof with only minor compression of the laterally adjacent country rock. It is possible that the centre of magma intrusion migrated southwards with time so that the southern exposures of the Porphyritic Outer Granite are in contact with Dalradian metasediments and the northern exposures are in contact with the earlier quartz diorites (Fig. 4.4).

In contrast to the Outer Granite, the Inner Granite has a clearly defined contact and where it is found in contact with Dalradian schists, local planes of weakness have controlled the local rock relationship (Webb 1977). Against the Outer Granite, the Inner Granite has a sharp, well defined and regular contact reflecting the structurally isotropic nature of the Outer Granite. These contact relationships indicate an essentially passive emplacement mechanism, and cauldron subsidence is the preferred emplacement mechanism for the Inner Granite.

Walker (1975) modelled diapirs, ring complexes, cone sheets and cauldron subsidence; however his model requires a substantial body of basic magma beneath the Ben Nevis Complex. Not only are rocks of basic composition conspicuously lacking in the British Caledonian Granite province (Halliday & Stephens 1984), regional gravity surveys have shown that the Newer Granites are associated with negative gravity anomalies (Brown 1979) and not the positive anomaly associated with the Tertiary volcanic province ring complexes on which Walker (1975) based his model.

From the above evidence, it has been shown that the Ben Nevis Complex progressed from forceful emplacement, through a period of extension allowing repeated dyke injection, to passive emplacement. Oldershaw (1974) reached similar conclusions regarding the emplacement of the Lochnagar granite ring complex.

Slight chilling of the Inner Granite is observed at the contact with the Outer Granite, implying that a period of time had elapsed between intrusion of the two granite bodies. It is now recognised that the Glen Sanda Granodiorite of the Strontian plutonic Complex was intruded between 3 and 11Myrs after intrusion of the Loch Sunart granodiorite (Paterson et al. (1993). Earlier it was noted that the Ben Nevis Complex was structurally comparable to the dextral regime of Strontian. It is therefore possible that the two intrusive complexes were formed during the same magmatic events and that the Inner Granite may be as much as 10Myrs younger than the Outer Granite.

#### 4.9 Mineralisation

Disseminated molybdenite was first recognised within the outer margin of the Porphyritic Outer Granite by Haslam (1965). Two localities where molybdenite could be

found *in situ* were described (Haslam pers. comm. to Gallagher et al. 1971), these being: hybrid rocks in the Allt a' Mhuillinn (NN 145 754) and in a pegmatitic vein associated with hybridisation in the Allt Daimh (NN 170 763). Both hybrid localities (M1 & M2 respectively, in Fig. 4.5) are associated with the contact between the Porphyritic Outer Granite and the Inner Quartz Diorite (nomenclature of Haslam 1965).

Stream sediment sampling (Haslam 1986) identified high values of Mo, Cu, Pb and Zn in streams draining the outer contact of the Porphyritic Outer Granite on the steep western slopes of Aonach Mor. High concentrations of Cu, Mo, Zn were also found in close association with the surge chamber appinite (M3 in Fig. 4.5). Here abundant xenoliths of appinite (Haslam 1970 but see section 4.7.3) and Dalradian schist are enclosed in diorite that is typically more altered than normal Inner Quartz Diorite (terms of Haslam 1970). Copper concentrations of 0.3% were identified in one sample, but the mineralised area was deemed too low grade and too localised to have any potential economic value (Haslam 1986)

In addition to the occurrences noted by Haslam (1965 & 1986), disseminated pyrite was found within a single pulse of the Fine Quartz Diorite exposed in the Allt Daimh (M4 in Fig. 4.5). This occurrence is associated with clots of biotite. Pyrite, chalcopyrite and molybdenite are found throughout the Fine Quartz Diorite and are probably primary minerals in the same manner as disseminated pyrite found in the diorites of Ballachulish (Haslam 1986).

The high concentrations of Mo, Cu, Pb and Zn noted by Haslam (1986) in streams draining Aonach Mor are almost certainly due to mineralisation along fault planes cutting the Porphyritic Outer Granite. Mineralisation in these veins (M5 in Fig. 4.5) is associated with open space growth (Photo 4.19a & 4.19b). Faults with a similar sense of movement and the same orientation to the one in the photograph are recognised as syn-plutonic and fault movements appear to span the period of dyke injection.

Absence of high metal contents in the eastern area may reflect the fact that this area is more deeply eroded than the western area. However the exposure of molybdenite in the Allt Daimh occurs at less than 200m, and it is likely that the absence of mineralisation in the western area is a feature of poor exposure and the difficult nature of the terrain. Hematite staining is found associated with the Tertiary dyke (in fact a number of en-echelon dykes) and probably reflects local hydrothermal circulation initiated by intrusion of this basaltic dyke (M6 in Fig. 4.5).

Webb (1977) stated that geochemical reactions in the metamorphic aureole of the Ben Nevis Complex were essentially isochemical. The action of fluids emanating from the granite was not believed significant, except along local zones of dislocation along which fluids emanating from the granite passed inducing partial melting in the adjacent metasediments.

---

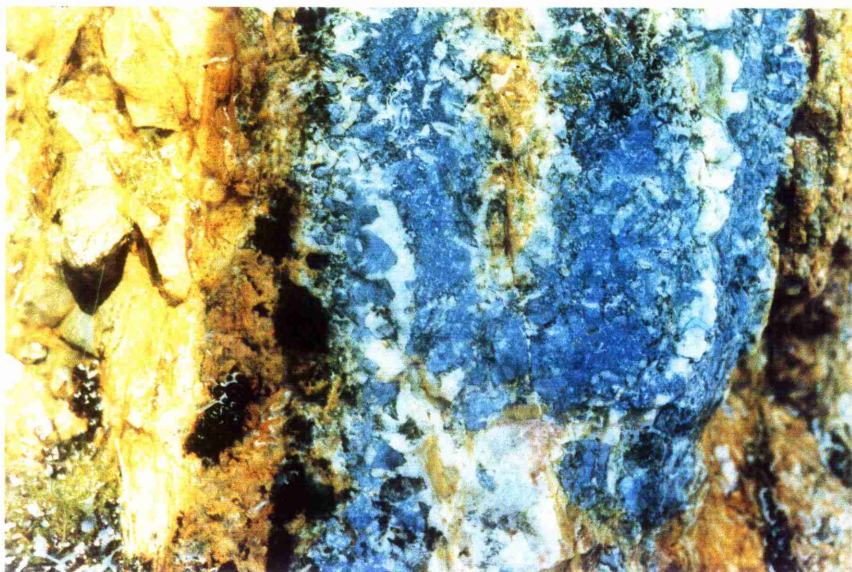
Plate 42 Photo. 4.19a Molybdenite and quartz intergrowths along a fault plane (M5).  
Thickness of vein  $\approx$ 4cm. (NN186 733)

---

---

Plate 42 Photo. 4.19b Extreme alteration along/adjacent to faults in the Ben Nevis  
Complex. (NN185 734)

---



Mineralisation in the Ben Nevis Complex is associated with appinites, pegmatites and faulting. With the exception of faulting, these occurrences are associated with high vapour/fluid pressures. The chalcophile elements are known to concentrate into fluids (Hutchison 1983). It is therefore suggested that the high concentrations of the chalcophile elements in these areas are due to the activity of late stage fluids. Rice & Davies (1979) describe high concentrations of chalcophile elements associated with late stage acid phases of the Lagnaha appinite pipe. Late stage acid pegmatites cross cut the surge chamber appinite and it is believed that the injection of these veins was accompanied by mineralisation in this area.

The occurrence of molybdenite in the fault zone (M5 in Fig. 4.5) must be related to post-intrusion alteration of the Porphyritic Outer Granite in which it is found. Fluids percolating the intrusion after intrusion and subject to local additions of energy during intrusion of the dyke swarm are likely to have scavenged metals from the Porphyritic Outer Granite. Fault planes provide lines of weakness along which these fluids can easily flow. A reduction in fluid pressure associated with the opening of small cavities along the fault plane would cause precipitation of minerals held in solution. That the passage of mineralising fluids accompanied fault movement is apparent from the large number of faults which contain barytes, calcite and quartz mineralisation and which have zones of intense alteration immediately adjacent to the plane of movement (Photo 4.19b).

#### 4.10 Conclusion

The intrusive members of the Ben Nevis Complex were intruded to within a few kilometers of the land surface towards the end of the Caledonian orogeny when end-orogenic uplift and erosion had largely been completed (Watson 1984 and Soper & Hutton 1984).

Units of the Outer Granite (Fine Quartz Diorite - Porphyritic Outer Granite) are not single intrusions, but rather a number of magma pulses. Over time, the geothermal gradient was raised by the intrusion of the earliest members of the Ben Nevis Complex and the rate of cooling of fresh magmatic pulses slowed, allowing individual pulses to mingle/merge.

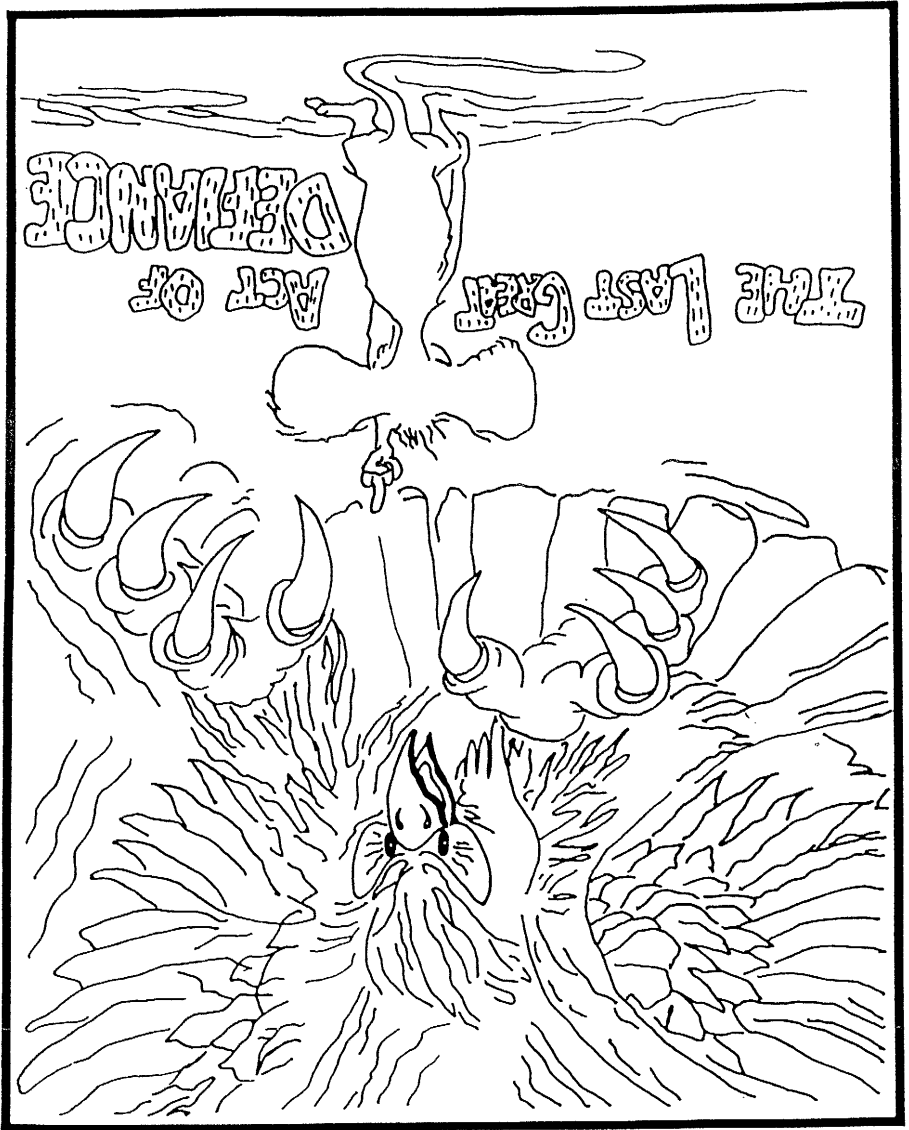
During crystallisation, volatiles collected towards the roof of the magma chamber and extensive but localised veining permeated the adjacent country rock. Magma pressures gradually built up until explosive release, presumably during surface venting, resulting in the formation of discrete zones of brecciated country rock.

The mechanism by which the granitic members of the Ben Nevis Complex were intruded changed with time. The Outer Granite has a number of features consistent with a forceful ballooning style of intrusion and the geology of the Inner Granite fits a cauldron subsidence model.

Intrusion of the Ben Nevis Complex was accompanied by relative extension to the NW-SE. Like Strontian (Hutton 1988a), the shear sense during formation of the Ben Nevis

Complex was dextral. The intrusion of the Outer and Inner Granites may have been triggered by the same events that formed the two components of the Strontian plutonic Complex and the Inner Granite may therefore be between 3 and 11 Myrs younger than the Outer Granite.

Collapse of the volcanic pile into the Inner Granite brought a slightly more basic variety of the Inner Granite closer to the surface; this basic component now forms the fault facies. The existence of a basic Inner Granite with similar chemistry along the Allt Daimh may also be an effect of the volcanic pile. Small scale back-injections within the Inner Granite are also a feature that can be linked to collapse.



## CHAPTER 5

### PETROLOGY AND MINERALOGY

#### 5.1 Introduction

##### 5.1.1 General statement

A combination of thin section petrography and electron microscopic analysis was used to examine the intrusion and crystallisation history of the Ben Nevis Complex. Variations within and between individual pulses are discussed. Locations mentioned in the text are shown in Fig. 5.1. The criteria by which magmatic biotite is distinguished from subsolidus biotite are presented in Table 5.1. Structural formula (Appendix II) were calculated using the computer program of Rock & Carroll (1990) and the formulae for biotite and amphibole were calculated using 22 and 23 oxygen atoms per formula unit respectively to counter uncertainties in the amount of water and halogens present in these minerals. Mineral compositions and analytical procedures are presented in Appendix II .

Table 5.1  
Textural Criteria used to define magmatic biotite  
(adapted from Speer 1984)

grain size comparable to other magmatic minerals  
sharp terminations  
subhedral to euhedral shape  
no reaction - relation textures with other minerals  
relatively abundant  
the host rock is relatively unaltered  
enclosed entirely or partially within a magmatic mineral

#### 5.2 Petrography of the Ben Nevis Complex

##### 5.2.1 Fine Quartz Diorite, Sgurr Finnisg-aig Quartz Diorite and Coarse Quartz Diorite

The principal difference between the Fine Quartz Diorite, Sgurr Finnisg-aig Quartz Diorite and Coarse Quartz Diorite is one of grain size. For this reason the petrology of all the quartz diorites units in the Ben Nevis Complex are described together.

The quartz diorites are the most variable rock types in the Ben Nevis Complex and exhibit a range of petrological textures and mineralogical and whole rock compositions. The major mineral phases are: plagioclase, clinopyroxene, orthopyroxene, biotite and calcic amphibole, with minor amounts of alkali feldspar and quartz. Accessory minerals include opaque oxides, titanite, apatite and zircon.

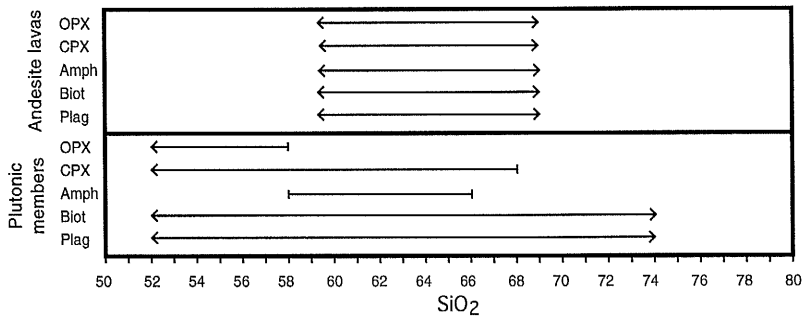
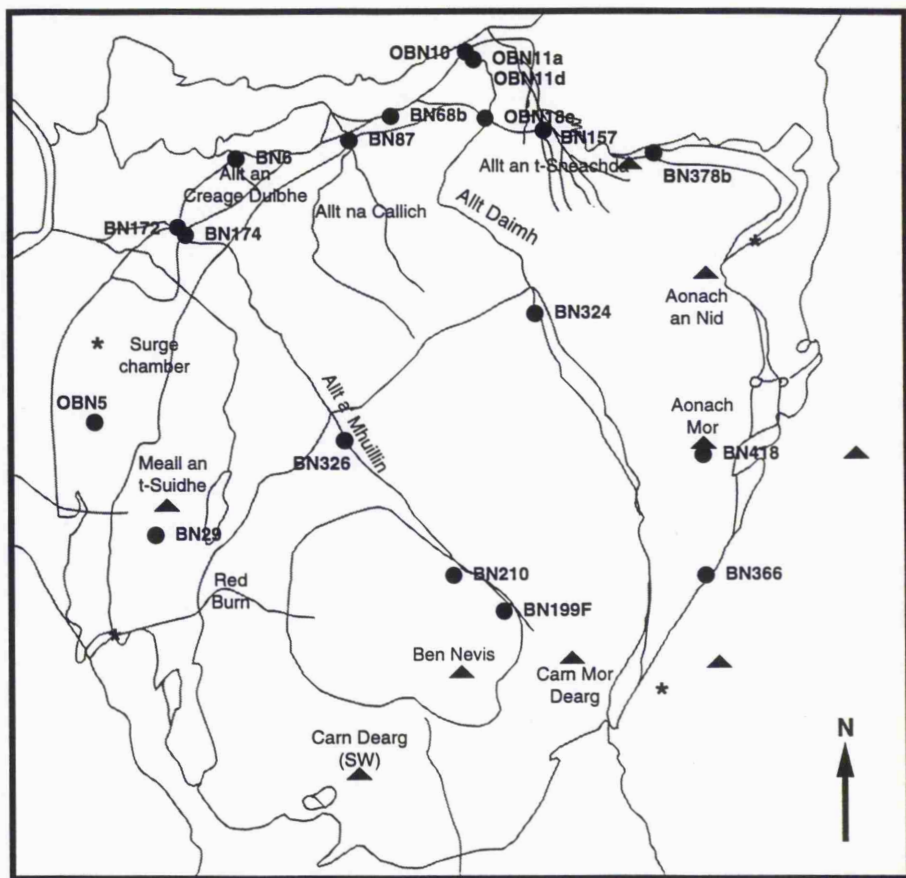


Fig. 5.x Mineral stability in the Ben Nevis Complex. Where an arrowhead is depicted this represents the minimum or maximum whole rock chemical range and no data is available for the minimum/maximum whole rock SiO<sub>2</sub> content at which crystallisation of the mineral started/ceased.



**KEY**

- \* Appinite locality.
- BN174 Location of exposure or photo mentioned in text.

Fig 5.1 Localities and samples mentioned in the text along with the location of probe samples and photomicrographs.

## Plagioclase

Plagioclase is found as phenocrysts and in the groundmass. The finer grained examples of the Fine Quartz Diorite show a greater tendency to an equigranular grain size and, against the Grampian/Dalradian contact, may show strong preferential alignment parallel to the contact (Photo 5.1). Zoning is apparent in all plagioclase phenocrysts and in some cases is extreme ( $An_{10}$ - $An_{55}$  vs  $An_{20}$ - $An_{40}$ ). Often, zoning is highlighted by discrete rings of sericitisation. Patchy zonation is displayed by a number of phenocrysts, particularly in the Coarse Quartz Diorite. Harrison (1987) interpreted similar plagioclase crystals in the Cairngorm pluton as examples of restite. Small inclusions of biotite, pyroxene/amphibole and opaque oxides testify to the early formation of these minerals. Where plagioclase is found adjacent to alkali feldspar it is often corroded (Photo 5.2); elsewhere, plagioclase phenocrysts are observed growing into the groundmass, although a euhedral form is retained.

## Pyroxene

Clinopyroxene and orthopyroxene are found as metastable phases in the quartz diorite. The degree of replacement by calcic amphibole (actinolite to actinolitic hornblende) is variable (see section 5.2.6) from thin amphibole rims (Photo 5.3) to almost complete replacement and pseudomorphism (Photo 5.4). Those pyroxenes that are relatively well preserved have euhedral-subhedral form and zoning is occasionally observed (Photo 5.5).

Both clinopyroxene (diopside & augite) and orthopyroxene (enstatite) are often turbid, with minute inclusions of biotite, amphibole, hematite and most commonly opaque oxides (Photo 5.5). Orthopyroxene is moderately pleochroic (a = pink, b = colourless & g = pale green). In a few examples of the Fine Quartz Diorite, clinopyroxene is found to contain corroded cores of orthopyroxene (Photo 5.6).

## Biotite

Magmatic versus subsolidus formation of biotite is often difficult to identify (Bailey 1984) and the criteria presented in Table 5.1 are used to distinguish between the two types in this thesis.

Biotite is found in three habits within the quartz diorites. Primary magmatic biotite and interstitial subsolidus biotite are found in varying proportions in all samples, but the third habit, that where biotite is replacing calcic amphibole, is only observed in some of the quartz diorites. The Coarse Quartz Diorite contains noticeably more subsolidus biotite than the Fine Quartz Diorite testifying to its slower cooling history. A few biotite crystals were observed with bent cleavage planes. Although three biotite habits are recognised, this does not mean that biotite growth occurred in three discrete episodes; biotite began to crystallise early in the history of individual quartz diorite pulses and growth was probably continuous into the subsolidus. There is no recognisable optical or compositional variation between

---

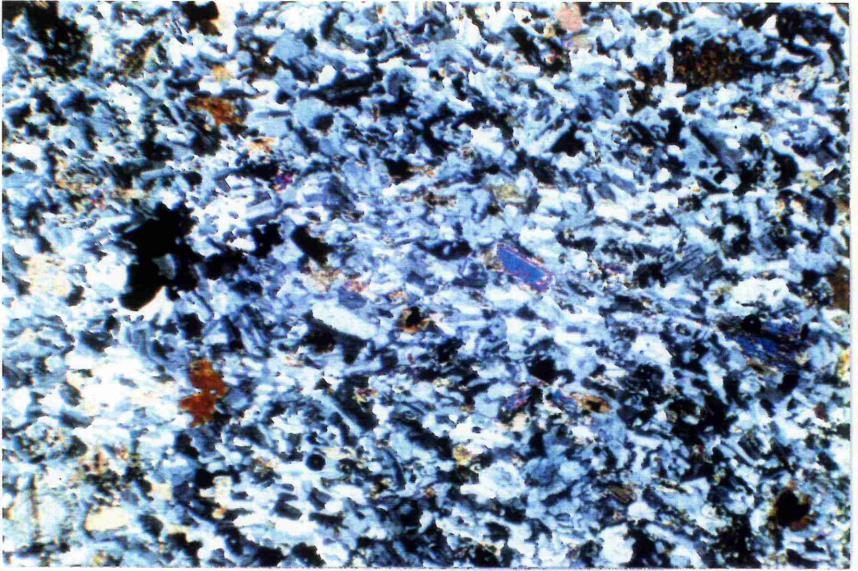
Plate 43 Photo. 5.1 OBN10 Strong preferential alignment of the Fine Quartz Diorite in contact with the Dalradian country rocks in the Allt Daimh area of the Ben Nevis Complex. Minerals include plagioclase, ortho and clinopyroxene, biotite with minor Fe ore, quartz and alkali feldspar.  
\*21 XPL (NN171 721)

---

---

Plate 43 Photo. 5.2 OBN11d Corrosion of a plagioclase feldspar phenocryst in the bottom half of the photograph by alkali feldspar in the centre of the photograph. \*43 XPL (NN171 771)

---



---

Plate 44 Photo. 5.3 OBN11d Relatively well preserved pyroxene crystals (groundmass and phenocrysts). A thin actinolitic rim partially mantles the pyroxenes and is in turn partially mantled/replaced by biotite. Note the corroded opaque oxide in the centre top of the photograph.

\*43 PPL (NN171 771)

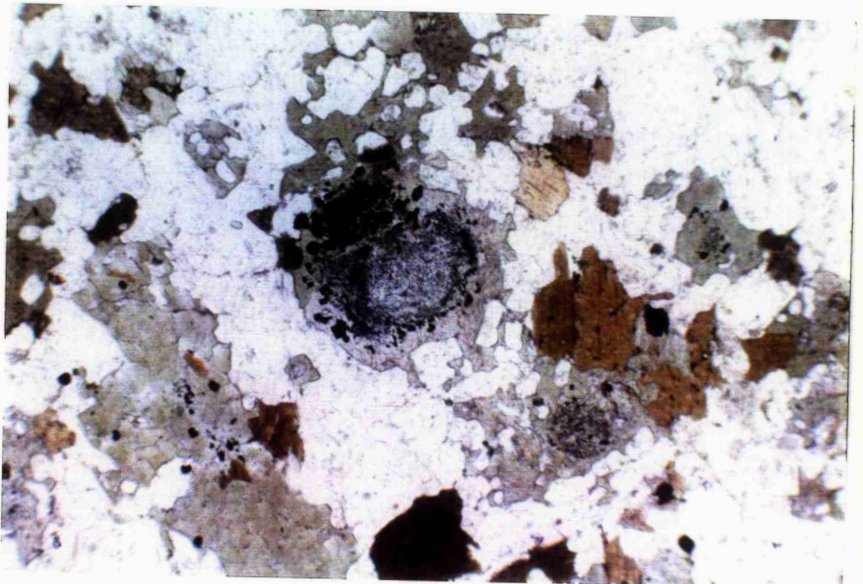
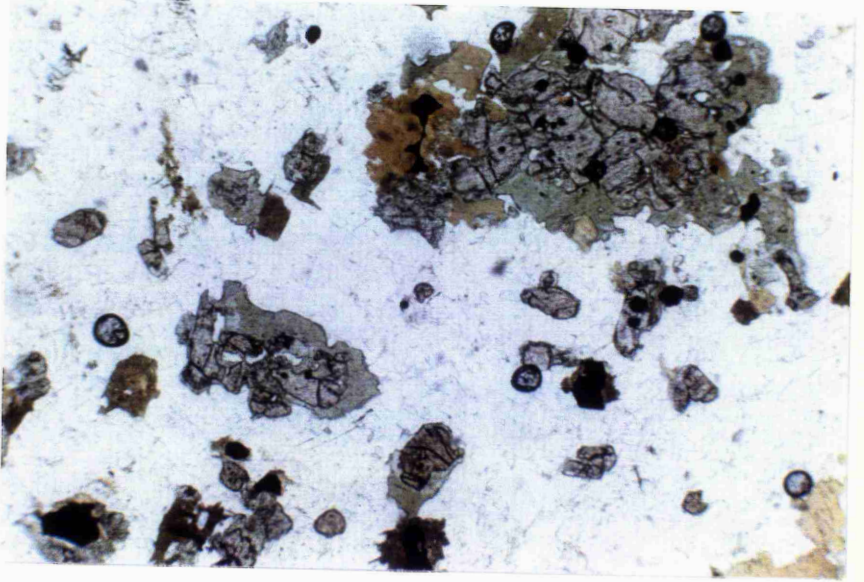
---

---

Plate 44 Photo. 5.4 BN87 The amphibole crystal in the centre of the photograph is a pseudomorph after pyroxene. Late stage poikilitic outgrowth of amphibole into the groundmass. Note the absence of opaque oxides in the biotites.

\*43 PPL (NN159 765)

---



---

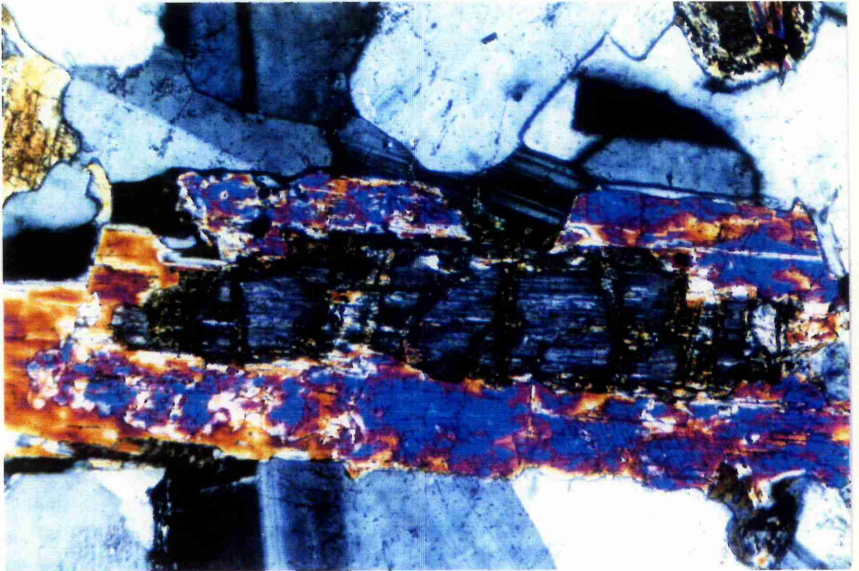
Plate 45 Photo. 5.5 OBN18f Zoned pyroxene showing partial replacement by biotite.  
\*43 PPL (NN172 766)

---

---

Plate 45 Photo. 5.6 OBN5 Corroded orthopyroxene core to a clinopyroxene rim which  
in turn passes into calcic amphibole. Plagioclase can be found as a phenocryst  
and as a groundmass phase in the photograph. \*107 PPL (NN132 735)

---



magmatic and subsolidus biotite within an individual pulse and it is suggested that extensive magmatic and subsolidus equilibration has occurred.

Early formation of biotite is apparent from the presence of small euhedral oikocrysts within a number of plagioclase phenocrysts. Sub to euhedral biotite of comparable grain size to other magmatic mineral phases is also believed to be magmatic (Table 5.1). Late stage sub-solidus growth is recognised by interstitial habit, mantling, reaction textures or ragged appearance. Secondary biotite overgrowths are commonly observed on primary magmatic biotite, as small finger-like extensions protruding from the margins of the original crystal. These overgrowths are chemically and optically indistinguishable from the primary biotite. Where pyroxene is relatively abundant, and amphibole has replaced only the outermost rim of individual pyroxene crystals, biotite is often observed partially replacing amphibole (Photo 5.3); in extreme cases biotite is found directly replacing pyroxene without an intervening amphibole stage (Photo 5.7). Biotite is often observed mantling and partially replacing opaque oxides, particularly where pyroxene is well preserved.

Biotite-quartz intergrowths are sporadically observed throughout the quartz diorites and Haslam (1965) interpreted these as replacement textures, possibly after clinopyroxene (Wones & Eugster 1965).

Alteration is common, particularly in euhedral biotite grains where the conversion of pyroxene to calcic amphibole is near completion. Prehnite and chlorite form discrete lenses along the plane of cleavage. Less frequently, titanite and epidote are observed partially replacing biotite. These alteration effects are comparable to those observed in the volcanic pile. Fluids emanating from the Inner Granite are believed to have been the primary cause of alteration in the volcanic pile (Maufe 1910 and Haslam 1968), and it is suggested that alteration in the early pulses of the Outer Granite is caused by the passage of late stage hydrothermal fluids emanating from later pulses. Late stage fluids are known to have caused extensive alteration along fault planes penetrating the Porphyritic Outer Granite (chapter 4).

A number of biotite crystals show partial replacement by muscovite. This is dominantly observed adjacent to the contact with the country rock, and in particular, where biotite is found in grain-grain contact with alkali feldspar. Harrison (1987) suggested that similar replacement textures in the Cairngorm pluton could be attributed to late-stage interaction between biotite, feldspar and an Al-rich fluid. The fact that in the Ben Nevis pluton these textures are found only along parts of the outer contact suggests that the Al-rich fluid was derived, at least in part, from Grampian/Dalradian metasediments.

Biotites with  $\beta = \gamma$  = foxy red-brown to straw yellow and  $\alpha$  = foxy red brown were identified in two settings; firstly where plutonic rocks are found in contact with Dalradian and Grampian metasediments (Photo 5.8) and secondly, in the area of the BAA surge

---

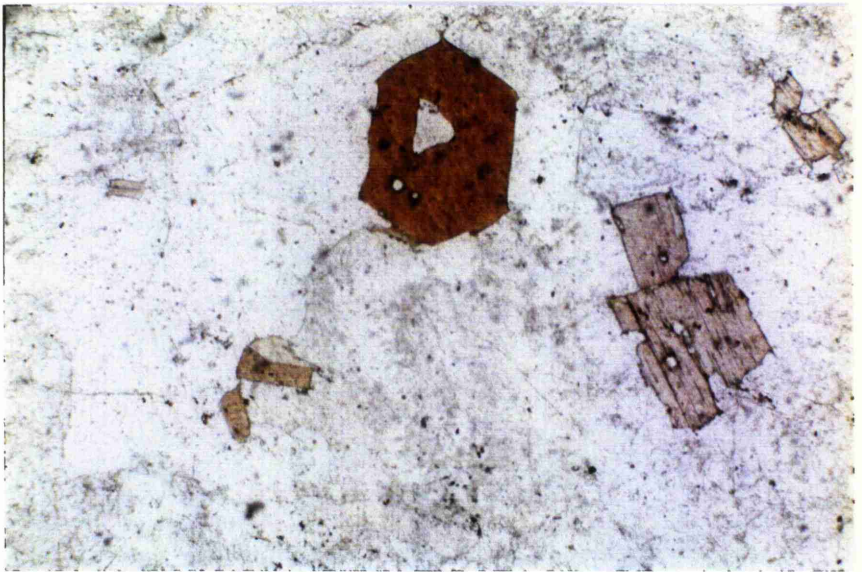
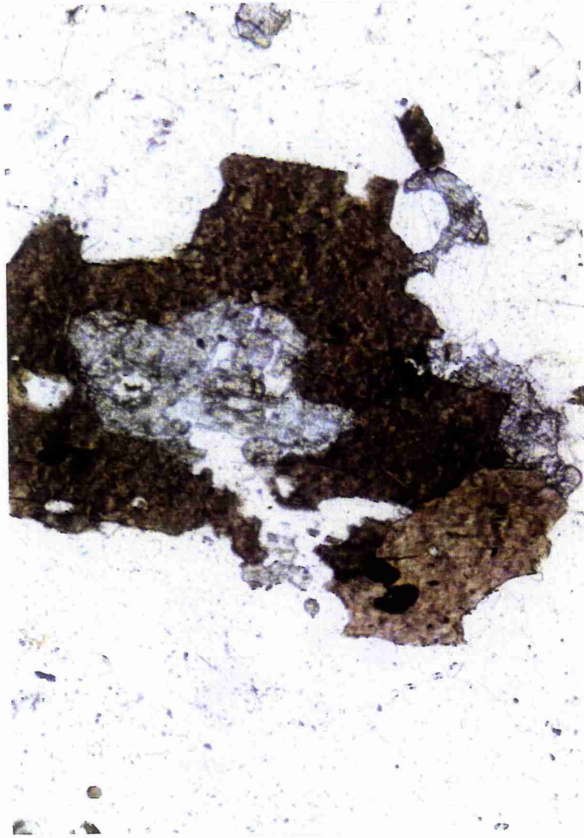
Plate 46 Photo. 5.7 BN172 Biotite replacing pyroxene without, or after consuming,  
an intervening amphibole stage. \*107 PPL (NN140 756)

---

---

Plate 46 Photo. 5.8 BN68b Euhedral foxy-red biotite crystals with pleochroic  
haloes having formed around apatite and occasionally zircon.  
\*43 PPL (NN155 764)

---



chamber where intrusion of appinite occurred simultaneously with the intrusion of the Coarse Quartz Diorite (Photo 5.9).

In the former locality, biotite is usually the sole mafic mineral, hornblende is not common and pyroxene is partially replaced by biotite. Primary sub-euhedral magmatic biotite is often associated with relatively abundant apatite containing high levels of radiogenic elements that form numerous pleochroic haloes (Photo 5.8). Rapid cooling along the margin is indicated by acicular biotite and graphic-granophyric intergrowth textures between alkali feldspar and quartz. Muscovite appears as a subsolidus phase replacing biotite and feldspar.

In the appinite locality biotite partially replaces amphibole, and also forms ragged interstitial partially poikilitic grains indicating that growth occurred below the solidus. The Porphyritic Outer Granite and Fine Quartz Diorite in this area are little different from exposures elsewhere in the Ben Nevis Complex, leading to the conclusion that appinite intrusion occurred during and immediately after intrusion of the Coarse Quartz Diorite.

#### Calcic amphibole

Amphiboles within the quartz diorites of the Outer Granite are almost always formed from the replacement of pyroxene (Photos 5.3 & 5.4). Haslam (1968) argued that the abundance of amphibole is dependent on the extent of pyroxene replacement and believed that clinopyroxene altered directly to green hornblende, whereas orthopyroxene was usually replaced by a 'plexus of cummingtonite crystals', that were then gradually converted, from the margin inwards, to green hornblende. However, probe analyses of Ben Nevis amphiboles all yield  $(Ca+Na)_B > 1.34$  and  $Na_B < 0.67$  (section 5.3.3) which defines them as calcic amphiboles (Leake 1978). The amphibole analyses of Haslam (1968) also fall into the calcic amphibole field, furthermore, no optically negative amphibole (i.e. cummingtonite) was identified in thin section.

In slides where pyroxene is relatively well preserved, grain size ranges from medium grain microphenocrysts (Photo 5.5) to sizes comparable with the rest of the groundmass (Photo 5.10). However, in a number of specimens, pyroxene formation appears to have been arrested at some point and small idiomorphic calcic amphiboles (Photo 5.11) take the place of the smaller pyroxene crystals in the crystallisation sequence. Opaque mineral 'dusts' and/or abundant biotite and/or quartz inclusions characterise the replacement amphiboles; in contrast, idiomorphic amphiboles lack such features and it is suggested that these amphiboles are primary magmatic minerals. Primary amphibole crystallisation is also indicated by the presence of euhedral amphibole overgrowths on pyroxene.

Adjacent to Grampian/Dalradian metasediments, the Coarse Quartz Diorite exhibits relatively large (5mm) acicular needles of calcic amphibole indicative of magma quenching against the cooler metasediments. Late stage amphibole growth is revealed by quartz diorite

---

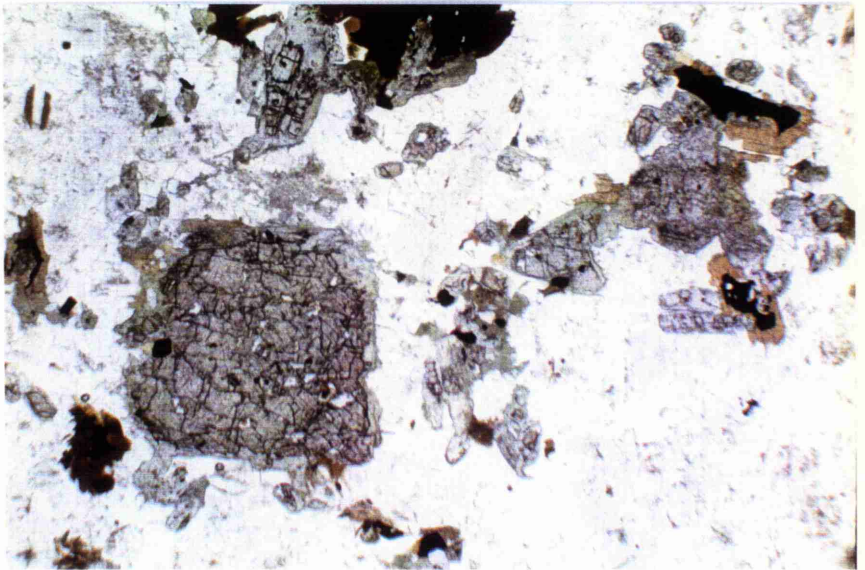
Plate 47 Photo. 5.9 BN174 Foxy-red biotite intergrown/replacing amphibole. Alteration of biotite to chlorite is also a feature of this slide. Plagioclase shows much sericitisation. \*43 PPL (NN141 756)

---

---

Plate 47 Photo. 5.10 OBN11a Well preserved pyroxene crystals ranging in size from microphenocrysts in the centre of the photograph (2mm) to examples in the groundmass. Note the corroded opaque oxides in the centre of the biotite crystals on the right hand side of the photograph. \*21 PPL (NN171 771)

---



samples in the region of Allt Creag Duibhe; here the margin of a number of grains is extended by poikilitic outgrowths (Photo 5.4). This may be aided by concentration of volatiles in this area, prior to brecciation of the Fine Quartz Diorite by the Coarse Quartz Diorite (chapter 4).

#### Alkali Feldspar

The abundance of alkali feldspar appears to be inversely correlated with preservation of pyroxene. Those examples with relatively little amphibole contain only small amounts of interstitial alkali feldspar. Increasing amounts of alkali feldspar correlates with increasing pyroxene to amphibole conversion. The degree of alteration (sericitisation) exhibited by plagioclase is also correlated with intensity of pyroxene replacement/abundance of K-feldspar.

A number of slides show incipient intergrowth textures between alkali feldspar and quartz. The Coarse Quartz Diorite at the contact with Grampian/Dalradian metasediments exhibits much granophyric and graphic intergrowth between alkali feldspar and quartz, a feature which is attributed to rapid chilling at the margin.

Corrosion of plagioclase adjacent to alkali feldspar, testifies to the presence of a late stage potash rich fluid (Haslam 1968). In a number of thin sections, amphibole also shows corrosion when in contact with alkali feldspar (Photo 5.12).

#### Quartz

Quartz is found as an interstitial phase and occasionally forms poikilitic textures. Undulose extinction of quartz is common throughout the quartz diorites.

#### Accessory Minerals

Accessory minerals include opaque oxides, apatite and minor monazite, allanite and zircon. The opaque mineral phases are ilmenite and magnetite, the latter sometimes converted to martite (hematite). Opaque oxide 'dusts' are found in both pyroxenes, and in amphibole replacing pyroxene, and are considered as signs of pyroxene metastability or of the former presence of pyroxene respectively. Apatite is considerably more abundant than zircon, particularly adjacent to the outer contact, both forming pleochroic haloes in biotite. Primary titanite is rarely observed in the quartz diorites except close to the outcrop of the Porphyritic Outer Granite or as an alteration product (after biotite).

Apatite is a common liquidus phase and also remains in the residue during episodes of partial melting. During a study by Watson & Capobianco (1981) it was noted that the saturation level of  $P_2O_5$  in silicic melts is  $\approx 0.14\%$ . Therefore, in a source undergoing partial melting, with as little as  $0.05\% P_2O_5$ , apatite will remain as a stable phase until the melt volume reaches 35%. In source rocks with concentrations of  $P_2O_5$  greater than the melt saturation level, apatite will remain a stable phase at 100% fusion and increase in

---

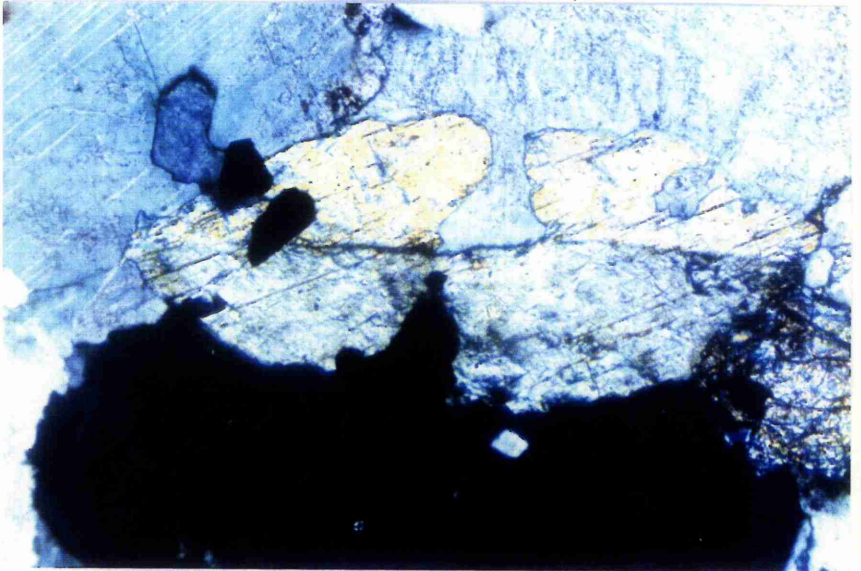
Plate 48 Photo. 5.11 BN378b Euhedral magmatic amphiboles in the Sgurr Finnisg-  
aig Quartz Diorite. \*107 XPL (NN194 763)

---

---

Plate 48 Photo. 5.12 BN418 Subhedral amphibole showing corrosion by alkali  
feldspar located above and below the amphibole crystal.  
\*107 XPL (NN192 729)

---



abundance. It is suggested that much of the apatite in the Outer Granite may be restitic in origin.

### 5.2.3 Porphyritic Outer Granite

In comparison with the other members of the Outer Granite, the Porphyritic Outer Granite is relatively homogeneous, with the exception of the eastern area where the proximity of the magma chamber roof/wall has led to the development of a chilled margin variant (chapter 4). Phenocrysts of plagioclase, alkali feldspar, hornblende, biotite and rare quartz are found within a fine to medium grained groundmass. The coarsest examples of the Porphyritic Outer Granite are found close to the Inner Granite contact in the Allt Daimh where the alkali feldspar forms conspicuous salmon pink crystals up to 2cm in size. Chilled margin Porphyritic Outer Granite contains no obvious phenocryst phases and is a medium to coarse grained granodiorite.

Where the Porphyritic Outer Granite is found in contact with the Coarse Quartz Diorite, potash rich fluids have migrated from the Porphyritic Outer Granite into the Coarse Quartz Diorite that was still semi-molten. Corrosion of the earlier formed phases is common, and interstitial alkali feldspar forms large poikilitic grains. An extreme end-member of this process is represented by the 'hybrids' in the northern region (Haslam 1965). Here, the enclosing chadacrysts are significantly larger than the oikocrysts (5-10mm vs 0.2mm respectively) and form a significant proportion of the rock volume. Invasion of the quartz diorite occurred whilst calcic amphibole + biotite  $\pm$  pyroxene were the main phases crystallising; these remain as euhedral (Photo 5.13) grains enclosed within feldspar and quartz derived from the Porphyritic Outer Granite. The hybridised mass then rose toward the surface, forming intrusive contacts against the Porphyritic Outer Granite and the Coarse Quartz Diorite.

#### Plagioclase

Plagioclase phenocrysts form laths up to 1cm in length and are more numerous than the larger alkali phenocrysts. Composition averages  $\approx$ An<sub>25</sub>, though zoned examples vary between An<sub>40</sub> and An<sub>15</sub>. Cores tend to be euhedral, whereas the margins have grown into the groundmass. Plagioclase is also found within the groundmass assemblage, but here it is subordinate to alkali feldspar.

A number of plagioclase phenocrysts show deformed twin lamellae and sub-grain development, a feature which is also observed in the quartz diorites. This is believed to reflect post-crystallisation strain. Like the quartz diorites, the Porphyritic Outer Granite contains a number of plagioclase grains that display complex patchy twinning and a restitic origin is inferred.

## Pyroxene

The conversion of pyroxene to calcic amphibole is largely completed in the Porphyritic Outer Granite and pyroxene is rarely observed even as relict cores within amphibole crystals. Its former existence is indicated by the presence of opaque oxide 'dusts' in the majority of amphibole grains.

## Biotite

Biotite occurs as euhedral magmatic phenocrysts, as small inclusion in plagioclase phenocrysts and as poikilitic/interstitial subsolidus grains. Phenocrysts commonly show outgrowth into the groundmass giving rise to ragged margins. Biotite is often found as an incomplete rim comprised of a number of individual crystals around the margin of granoblastic amphibole clots (section 5.2.7). Fine grained biotite-feldspar patches (Photo 5.14) are interpreted as small xenoliths and are particularly common in BN366 .

## Calcic amphibole

Haslam (1968) stated that all the amphibole minerals in the Outer Granite were formed at or near the solidus by the replacement of pyroxene. However, the presence of small (<0.5mm) idiomorphic grains of calcic amphibole (Photo 5.12) suggests that, at least in the later stages of crystallisation, amphibole precipitated directly from the melt. Individual crystals are often somewhat ragged. The majority of amphibole is found within amphibole rich clots, where they are associated with interstitial biotite, feldspar and minor quartz. Almost all of the amphibole in these clots contain numerous small opaque oxide inclusions indicative of their former origin as pyroxenes.

## Alkali Feldspar

Alkali feldspar forms conspicuous salmon-pink phenocrysts within the Porphyritic Outer Granite; these commonly reach 2cm in size. Corroded plagioclase is found within a number of alkali feldspar phenocrysts and an albite rich rim separates the two feldspar types. Perthite unmixing is an obvious feature of the alkali feldspar, especially the phenocrysts, and is occasionally coarse enough that twinning of exsolved plagioclase is visible under the microscope. Growth of individual phenocrysts continued into the groundmass. Oikocrysts of groundmass plagioclase, biotite and hornblende indicate that the alkali feldspar, despite its large size, was one of the last mineral phases to form.

## Quartz

Quartz forms rare euhedral phenocrysts and numerous anhedral grains in the groundmass. Undulose extinction is common. Very coarse intergrowth textures are observed in the Porphyritic Outer Granite of the Allt Daimh area.

---

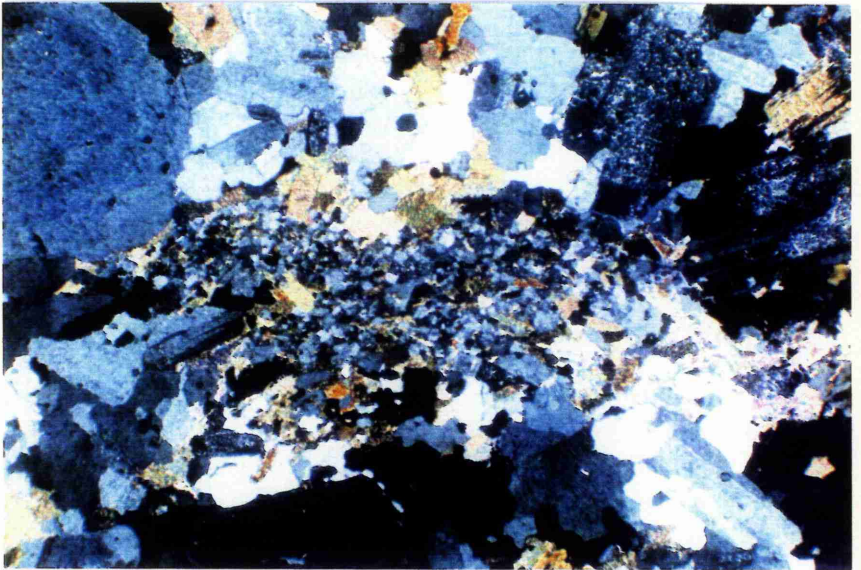
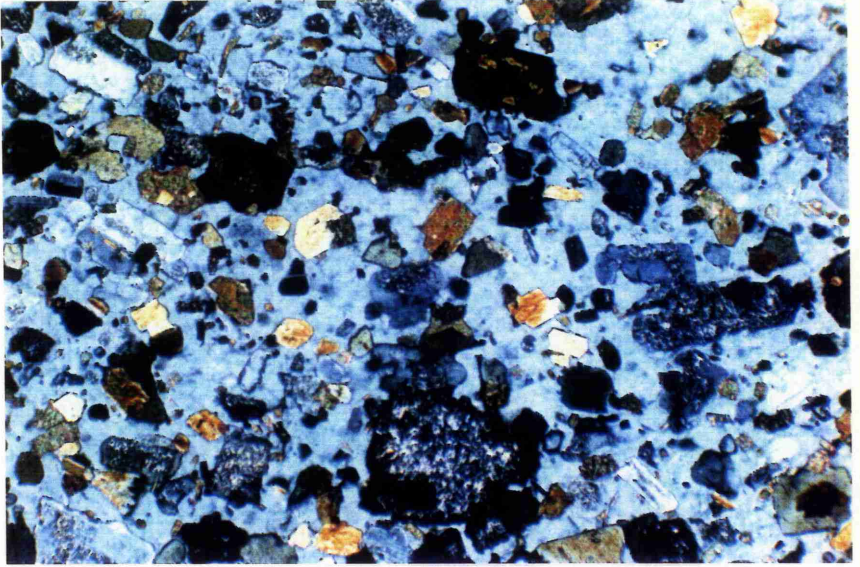
Plate 49 Photo. 5.13 BN157 'Hybrid' rock. Euhedral plagioclase, biotite and amphibole are enclosed within a single alkali feldspar which occupies the entire field of view. A number of the mafic minerals show signs of corrosion by the alkali feldspar. \*21 XPL (NN177 765)

---

---

Plate 49 Photo. 5.14 BN366 Biotite - feldspar patches/clots interpreted as small xenoliths. Note the occurrence of muscovite in the lower right of the photograph. \*43 XPL (NN198 730)

---



## Accessory Minerals

Accessory minerals include opaque oxides, apatite, zircon and titanite. Titanite is occasionally found as euhedral diamonds but is often most observed as interstitial, almost poikilitic, grains.

### 5.2.4 Inner Granite

The Inner Granite is a homogeneous biotite granodiorite (Haslam 1965). Slight chilling is evident at the outer contact and relatively strong chilling is observed at the inner contact. A more basic hornblende bearing variant of the Inner Granite is located in the extreme northeastern corner of the Inner Granite outcrop. This basic variant shows considerably less hydrothermal alteration than the adjacent Inner Granite.

#### Plagioclase

In contrast to the rather elongate plagioclase laths in the Outer Granite, those in the Inner Granite form sub-euhedral strongly zoned stubby laths. The nature, composition and ratio of calcic core to sodic rim are extremely variable suggesting repeated variations in magma chamber chemistry or, given the chemical and isotopic homogeneity of the Inner Granite, active convection within the parent magma chamber. Basic cores are usually  $\approx An_{40}$  and abrupt compositional changes are observed between the core and the rim in a number of individual crystals. Rim compositions range between  $An_{15}$  and  $An_{10}$ . Patchy zoning and complex twinning reveals the presence of relict plagioclase.

Hand specimens of the Inner Granite are pale pink to red in colour, the most prominent geographical feature formed by the Inner Granite is the prominent north-south trending ridge of Carn Mor Dearg - Carn Beag Dearg. The Gaelic for red is dearg and the red colouration of the granite has clearly influenced the naming of these mountains. Red colouration in feldspar is due to the presence of minute grains of hematite formed from late to subsolidus oxidation of iron in the feldspar lattice.

#### Biotite

In normal Inner Granite, biotite is the sole mafic mineral forming euhedral grains and often altered to chlorite and prehnite (Photo 5.15). In the basic variant, titanite is commonly found replacing biotite.

#### Calcic amphibole

Amphibole is only observed in the basic variant of the Inner Granite, and forms pale green ragged prisms often intergrown with biotite (Photo 5.16).

---

Plate 50 Photo. 5.15 BN328 Typical Inner Granite; note the zoned and corroded plagioclase phenocryst in the centre of the field of view and the low proportion of mafic (biotite) minerals. \*43 XPL (NN151 743)

---

---

Plate 50 Photo. 5.16 BN324 The mafic Inner Granite with pale green ragged amphibole crystals. Also visible in this photograph are albite rich rims to the plagioclase. \*21 XPL (NN177 745)

---



## Alkali Feldspar

Microperthite alkali feldspar forms a few subhedral grains, but is dominantly found as interstitial anhedral patches in the groundmass. Mantling of earlier plagioclase is common.

## Quartz

Quartz forms anhedral grains and is often interstitial. Undulose extinction is not common confirming a fundamental difference in the intrusion mechanism between the strained Outer Granite and the unstrained Inner Granite.

## Accessory Minerals

Accessory minerals include opaque oxides, apatite and zircon.

### 5.2.5 Volcanic Pile

In the field, the andesites all appear very similar, being medium grey in colour and often brecciated throughout (chapter 3). Alteration is usually extensive and much is due to the passage of fluids emanating from the Inner Granite (Maufe 1910 and Haslam 1968). Vesicles are rare and where observed are infilled with epidote and quartz. The following petrographic description is concerned solely with the andesites lavas and sills; brief descriptions of the other components (Dalradian basement, volcanic breccias, sediments and minor intrusions) can be found in chapter 3. Once again the term andesite will be used to describe volcanic rocks of Ben Nevis, although the majority of samples fall within the fields of trachydacite - dacite on a TAS (total alkalis vs silica) diagram (Fig. 3.1). Minerals found as phenocryst phases are plagioclase + hornblende + Fe-Ti oxide  $\pm$  biotite  $\pm$  pyroxene.

The groundmass is usually extensively altered and represented by a fine grained micro-cryptocrystalline mesostasis of plagioclase, opaque oxide, an undetermined ferromagnesian mineral, quartz and clay. It is possible that the groundmass of the more acidic specimens represents devitrified glass, but given the altered nature of the groundmass, this conclusion is speculative.

## Plagioclase

Euhedral plagioclase forms the main phenocryst phase in the andesites of Ben Nevis, zoning is common and ranges from An<sub>10</sub> to An<sub>60</sub>. Corrosion is visible in a number of specimens (Photo 5.17). Minute plagioclase laths combine to form trachytic textures in the groundmass.

## Pyroxene

Both orthopyroxene and clinopyroxene are occasionally observed as remnant cores to pale green amphiboles.

## Biotite

Biotite forms euhedral phenocrysts and often exhibits strong resorption. Alteration minerals include chlorite, prehnite and rare epidote and titanite.

## Amphibole

Both brown and green hornblende is found in the andesites. Brown hornblende is usually seen as euhedral prisms, often with a rim of opaque oxide and partially resorbed (Photo 5.17). Green hornblende shows patchy pleochroism, is occasionally cored by pyroxene and reveals no opaque oxide rim or corrosion. Haslam (1968) suggested that all the green hornblende was formed from the replacement of pyroxene, however, most green amphibole is of euhedral form suggesting that it is a primary magmatic phase.

## Accessory Minerals

Accessory mineral include opaque oxides, rare zircon and apatite. Opaque minerals are often found as pseudomorphs after pyroxene (Photo 5.18).

### 5.2.6 Pyroxene to calcic amphibole transition

The extent to which pyroxene has been replaced by calcic amphibole is dependent to a large degree on the phases crystallising early in the evolution of an individual magma pulse. Very often the calcic amphibole is zoned with a core of pale green amphibole passing into a rim of more strongly coloured green amphibole (actinolite passing to actinolitic hornblende). In those few examples which show idiomorphic prisms of calcic amphibole, believed to be primary magmatic phases, the amphibole rim is often euhedral and presumably also magmatic. It is suggested that the water content of the magma reached a level at which amphibole crystallisation was preferred over pyroxene. This lends itself to the suggestion that the conversion of pyroxene to calcic amphibole, where magmatic amphibole is not observed, occurred at or below the solidus.

If biotite formed an early phase, then amphibole almost always completely replaces pyroxene. Should biotite formation be delayed, such that subsolidus biotite growth predominates, pyroxene is normally well preserved with only minor replacement by calcic amphibole (Photo 5.3). The calcic amphibole rim of this latter occurrence is often thin and sandwiched between a core of pyroxene and a rim of biotite. This biotite represents both subsolidus growth and partial replacement of calcic amphibole. Additionally, biotite may also replace directly pyroxene (Photo 5.7).

---

Plate 51 Photo. 5.17 BN210 Corroded euhedral hornblende in the volcanic  
pile. \*43 PPL (NN166 723)

---

---

Plate 51 Photo. 5.18 BN199 Corroded pseudomorphs after amphibole.  
\*21 XPL (NN172 716)

---



Haslam (1968) suggested that cooling was the dominant control on the extent to which pyroxene is replaced. It is here suggested that cooling was a relatively minor control in the quartz diorites, and early mineralogical variations, reflecting slight differences in the magma, were a more important control. If cooling was the prime factor, then the Coarse Quartz Diorite should show a greater degree of conversion to calcic amphibole irrespective of the early mineral assemblage; this is not the case. Furthermore, quartz diorite adjacent to the Grampian/Dalradian contact varies from samples with biotite as the sole mafic mineral (BN68b), through early biotite + converted calcic amphibole (BN6), to pyroxene + minor calcic amphibole and subsolidus biotite (OBN11a). Also, those samples obtained from the chilled Porphyritic Outer Granite/Dalradian contact in Glen Nevis do not show noticeably more pyroxene cores than those obtained from the coarse grained Allt Daimh area.

The presence of corroded plagioclase and amphibole reveals the existence of a late-stage post-pyroxene replacement K and Al-rich fluid/magma which ultimately formed alkali feldspar and quartz. Where biotite formed an early phase, the development of this fluid was inhibited and, as a result, the abundance of alkali feldspar and quartz is also reduced. In those samples where biotite was not a significant early phase, the late stage fluid contributed to growth of late subsolidus biotite, alkali feldspar and quartz. Additionally, earlier formed mineral phases show signs of increased alteration; in the pyroxenes this is evident in conversion first to amphibole and then, as the composition of the parent fluid/magma altered, biotite. Diffusion was probably the limiting factor in conversion, hence the rather thin rims of amphibole around pyroxene. Magmas with biotite forming an early phase either contained more water or varied from the biotite absent pulses in some other parameter. This variation was an intrinsic feature of the melt and replacement pyroxene by amphibole was therefore more efficient.

Euhedral biotite is common within the Porphyritic Outer Granite as is subsolidus growth. Consequently, pyroxene is rarely preserved due to the combined action of both magmatic and fluid conversion processes.

#### 5.2.7 Clots

Amphibole rich polycrystalline clots, of similar size to the larger crystal phases in the host magma, are common throughout the Outer Granite. Individual clots tend to be zoned with a rim developed from a number of individual crystals of biotite and an interior dominated by amphibole with minor interstitial biotite, plagioclase, quartz and opaque oxide. Pyroxene cores are often a feature of the amphiboles, particularly where pyroxene is also found in the host rock, and similar replacement textures are observed.

In a detailed study of clots from Strontian and the Quintana pluton (Hercynian fold belt of Iberia), Castro & Stephens (1992) demonstrated a chemical and textural zonation to individual clots. Whereas the margin showed mineralogical compositions and textures comparable to the host magma indicating partial re-equilibration, the cores showed compositional and textural variations from the host. The core has a granoblastic texture,

that is indicative of a 'foreign' origin, and the authors favoured a restite origin for these clots. Those clots from Ben Nevis are similar to those of Strontian and, similarly, a restitic origin is inferred.

### 5.3 Mineralogy of the Ben Nevis Complex

#### 5.3.1 Corrections for Ferric and Ferrous iron

Wet chemical and Mössbauer spectroscopic analyses testify to the presence of both forms of iron in most of the common rock forming minerals (Deer et al. 1992). Unfortunately, the electron microprobe is unsuited to the determination of the relative abundances of  $\text{Fe}^{2+}$  and  $\text{Fe}^{3+}$  and Fe data are expressed as total FeO ( $\text{FeO}^*$ ).

Numerous schemes for calculating  $\text{Fe}^{3+}$  have been presented (see Droop 1987 for a discussion). For the purposes of this thesis, the general formula developed by Droop (1987) is applied to the mineral analyses from Ben Nevis. The formula is unsuited to minerals such as biotite with vacant cation sites. This is also true for amphiboles, but a number of variations to the basic formula are presented by Droop (1987) in order to correct for site vacancy in amphibole.

The general formula of Droop (1987) is based on stoichiometric criteria, and is described below:

$$F = 2X (1 - T/S) \quad [1]$$

Where F is the number of  $\text{Fe}^{3+}$  cations per X oxygens in the mineral formula, T is the ideal number of cations per formula unit and S is the observed number of cations per X oxygens assuming all iron to be  $\text{Fe}^{2+}$ .

For amphiboles, the following alternatives are presented:

$$F = 46 (1 - T/S) \quad [2]$$

This is suitable only for those amphiboles with full A-sites and is the amphibole version of equation [1].

$$F = 46 (1 - 15/y) \quad [3]$$

Where  $y = \Sigma(\text{Si}, \text{Ti}, \text{Al}, \text{Fe}, \text{Mn}, \text{Mg}, \text{Ca})$  and is based on the assumption that Na and K are confined to the A-site, which may be partially vacant; and on a total of 15 cations in the ideal formula exclusive of Na and K. This is generally true of Fe-Mg amphiboles and coexisting calcic amphiboles.

$$F = 46 (1 - 13/f) \quad [4]$$

Where  $f = \Sigma(\text{Si}, \text{Ti}, \text{Al}, \text{Fe}, \text{Mn}, \text{Mg})$  and based on the assumption that Ca is confined to the M4 site, Na to the M4 and A sites and K to the A-site; and on a total of 13 cations in the ideal formula exclusive of Ca, Na and K. This formula is suited to many calcic amphiboles.

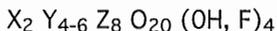
The procedure for implementing the appropriate equations is presented in Droop (1987).

Equation [3] yields the closest comparison for the plutonic amphiboles with data presented by Haslam (1968 & 1970) for which  $\text{Fe}^{2+}$  and  $\text{Fe}^{3+}$  data are available (Fig. 5.2). Haslam's (1968 & 1970) data were obtained using wet chemical analyses of mineral concentrates. In thin section, amphiboles often contain small inclusions of quartz, opaque oxide, biotite and are often cored by remnant pyroxenes; each of these would have an effect on the mineral analyses. Variations from Haslam's (1965) results are also due to the fact that the calculation of Droop (1987) can only provide an indirect estimate of the  $\text{Fe}^{2+}$  and  $\text{Fe}^{3+}$  contents.

Equation [3] gives no  $\text{Fe}_2\text{O}_3$  for amphiboles from the volcanic pile, and yet Haslam (1968) presents data on a brown hornblende from the volcanic pile containing 4.01%  $\text{Fe}_2\text{O}_3$  and 8.42% FeO. This suggests that equation [3] is unsuited to the amphiboles of the volcanic pile. A closer agreement with the sample from Haslam (1968) is obtained by applying the correction of equation [4]. It may be that the reason why equation [3] works for the plutonic and not the volcanic samples, is that pyroxene acts as the coexisting Fe-Mg amphibole. Where amphibole is formed directly from the melt, this is no longer true and consequently equation [4] is better suited.

### 5.3.2 Biotite

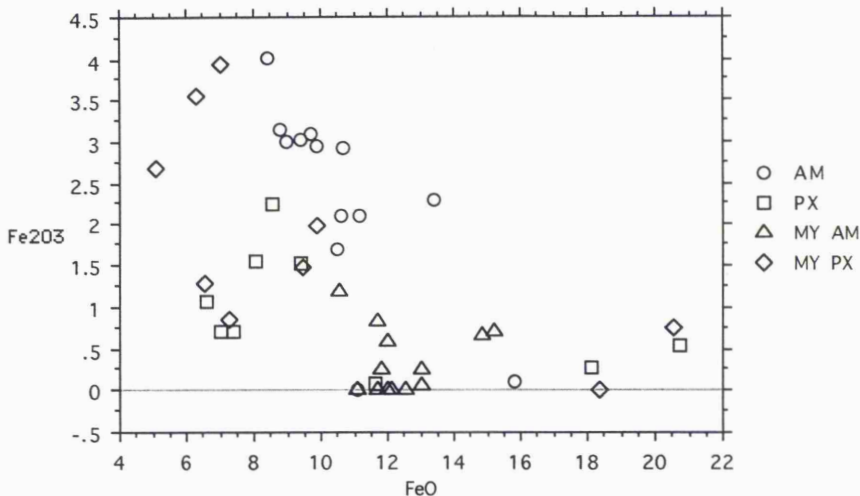
The general formula for mica is ;



In an ideal mica, X should equal two and the Y (octahedral site) contain six cations but spaces are almost always present due to the substitution of  $\text{R}^{3+}$  (R is any cation) or  $\text{R}^{4+}$  ions for  $\text{R}^{2+}$  cations in the Y sheet.

The Z (tetrahedral) sheet contains Si and Al if there is insufficient (Al)<sup>IV</sup> to fill the sheet,  $\text{Fe}^{3+}$  may enter to maintain charge balance. However, in the case of the Ben Nevis biotites,  $\text{Si}+\text{Al} \geq 8$ , biotite is therefore saturated with Al and the Z site is comprised of Si and Al cations only. Consequently the only substitution mechanism in the tetrahedral sheet is the replacement of Si by Al and a perfect 1:1 negative correlation is observed between these two ions (Fig. 5.3).

Biotites from Ben Nevis are saturated with respect to alumina (i.e. the tetrahedral site is comprised solely of Si and Al cations), and analyses occupy positions adjacent to the siderophyllite-phlogopite join (Fig. 5.5). Given the large numbers of substitutions possible in biotites, it is perhaps remarkable that biotite analyses from a single sample plot within a discrete area on any of the diagrams presented. This provides further evidence that intrusion of individual members of the Ben Nevis Complex was achieved by the injection of a number of small magma pulses.



AM = Amphibole analysis of Haslam      PX = Pyroxene analysis of Haslam.  
 MY AM = Recalculated amphibole      MY PX = Recalculated pyroxene.

Fig 5.2 Comparison of measured and recalculated pyroxene and amphibole data from Haslam (1968).

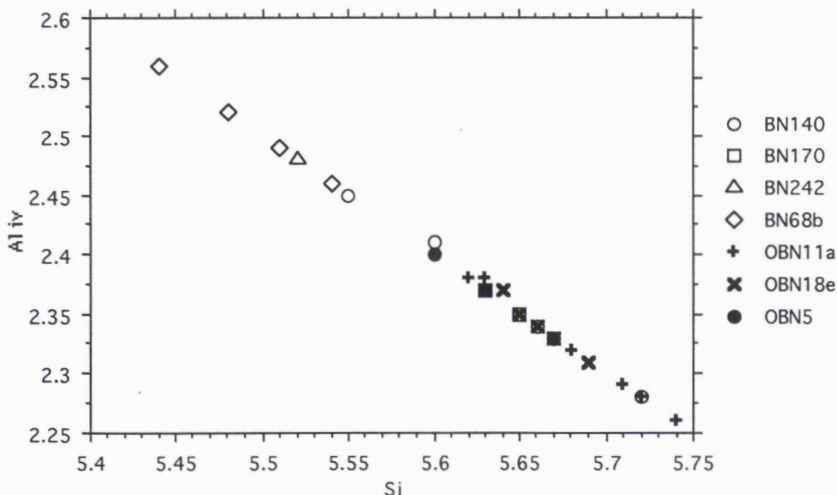


Fig 5.3 Perfect relationship between Al(IV) and Si in the biotites. These two cations are the only ones present in the tetrahedral sheet.

The contrast in biotite composition between BN68b and the rest of the biotite data is readily apparent in a number of plots. The BN68b biotites are enriched in total Al and (Al)<sup>iv</sup> (Fig. 5.6a), in Fe (Fig. 5.6b) and depleted in Ti (see below and Fig. 5.4). Different substitution mechanisms operated in BN68b than those in the main granite body. BN68b is

dominated by the incorporation of Al into the tetrahedral site whereas the majority of samples show strong correlations between (Fe + Mg) - Ti (Fig. 5.7a), (Fe + Mg) - ( $\diamond$ )<sup>vi</sup> (Fig. 5.7b) and (Fe + Mg) - (Al)<sup>iv</sup> (Fig. 5.7c). The following substitution mechanisms are the main controls on elemental substitution in BN68b and the main Ben Nevis group;



Subsolidus replacement between muscovite and biotite occurs close to the contact between quartz diorite and Grampian/Dalradian metasediments. The boundary between biotite and muscovite is sharp, reflecting the 'miscibility' gap between muscovite and biotite minerals. Conversion from biotite to muscovite occurs when (Al)<sup>vi</sup> reaches a critical limit and excess (Al)<sup>vi</sup> can no longer be accommodated by rotation of the crystal lattice (Hewitt & Wones 1975); at this point muscovite replaces biotite. High (Al)<sup>vi</sup> contents are apparent in the contaminated BN68b sample (Fig. 5.6a), but no muscovite is observed, suggesting that BN68b occupies an intermediate position between normal Ben Nevis magma and strongly contaminated magma.

There is a simple negative correlation between Fe and Mg (Fig. 5.8) in all the Ben Nevis biotite analyses, indicating that annite-phlogopite (Al)<sup>vi</sup> free end-member substitutions continued amid more complex interactions between Al, Si, Ti and presumably Fe<sup>3+</sup>.

Hildreth (1981) has shown that Mn tends to become enriched towards the later stages of granite differentiation; however, Miller & Stoddart (1981) have suggested that extensive hornblende fractionation during the early stages of magma evolution will deplete the subsequent melt in Mn; therefore, an absence of hornblende fractionation will lead to a progressively more Mn enriched magma. Enrichment of Mn has not occurred within the Ben Nevis Complex (Fig. 5.9a); in fact, a slight depletion is observed. Rocks such as BN68b, with no mafic phase other than biotite, do not show enrichment of Mn. Biotite can take up Mn, if hornblende is not present, but micas in BN68b do not contain more Mn than samples bearing both biotite and pyroxene. This suggests that Mn depletion was controlled by hornblende fractionation at depth.

#### Foxy-red Biotite

Foxy-red pleochroic colours result from either high Ti contents or high Fe<sup>3+</sup>/Fe<sup>2+</sup> ratios (Deer et al. 1992). Colouration of biotite due to high Ti contents alone will mask the contribution of other elements such that high Ti biotites will always exhibit foxy-red colours. Those biotites analysed from the northern contact (e.g. BN68b) have low Ti values relative to other samples from the Ben Nevis Complex (Fig. 5.4); thus, it is the oxidation state of iron (i.e. Fe<sup>3+</sup> rich) that controls the pleochroic colouration of biotite in this location. These rocks are found adjacent to the country rock contact and it is suggested that

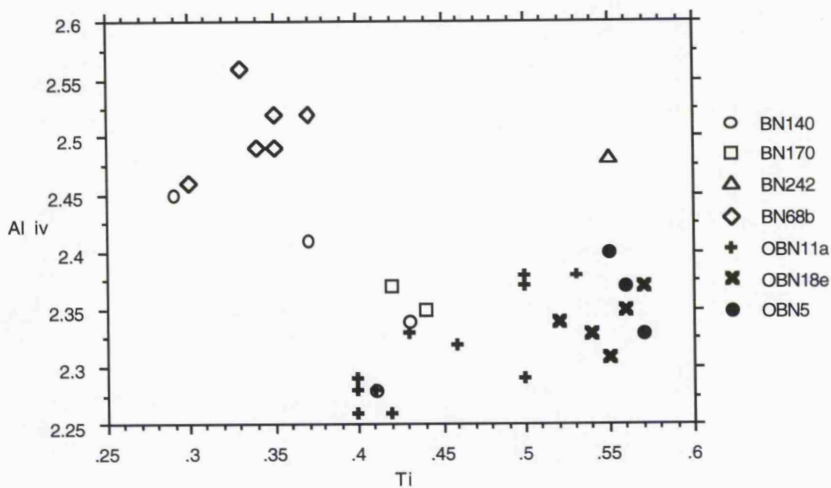


Fig 5.4 Comparison of (Al)iv against Ti for biotite highlighting the low Ti contents of biotite from BN68b.

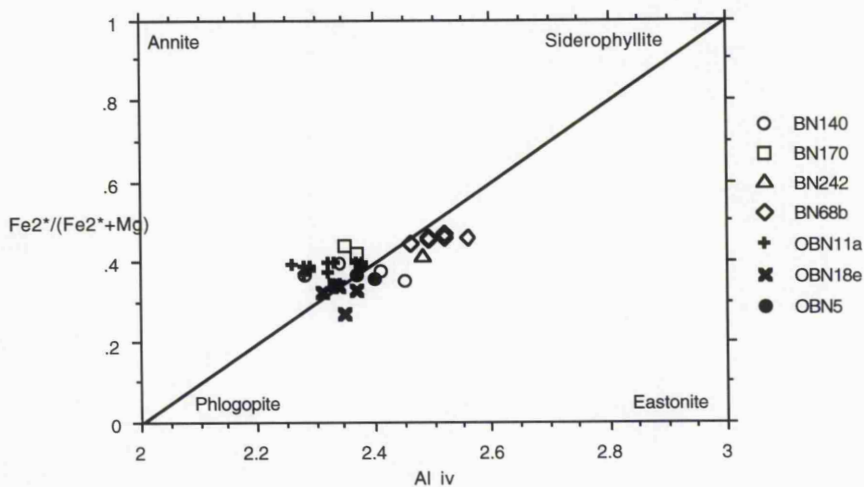


Fig 5.5 Composition of the biotites in the Fe-Mg-(Al)iv plane.

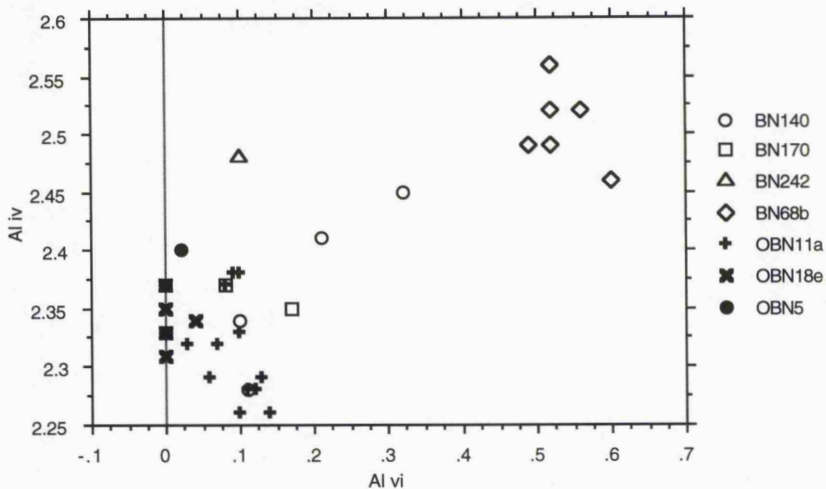


Fig 5.6a High total Al and (Al)<sub>iv</sub> of BN68b biotites relative to the main bulk of Ben Nevis biotite data.

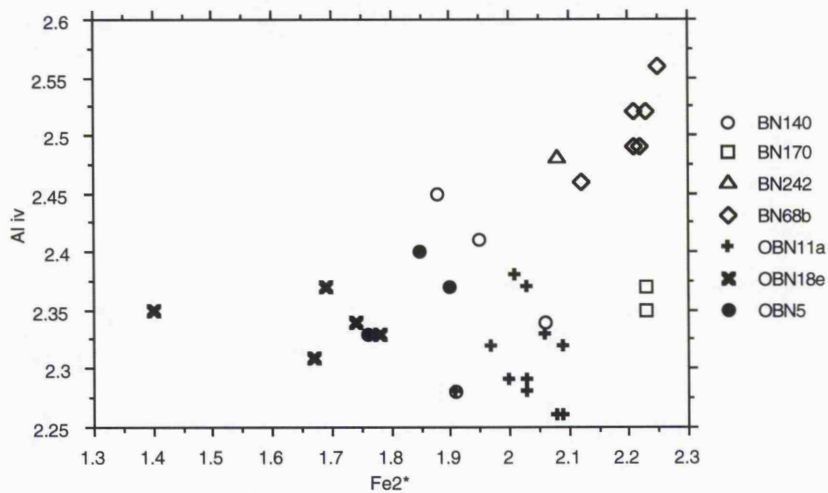


Fig 5.6b Comparison of Fe<sup>2+</sup> for the biotites, showing relatively high Fe contents in BN68b relative to the rest of the Ben Nevis data.

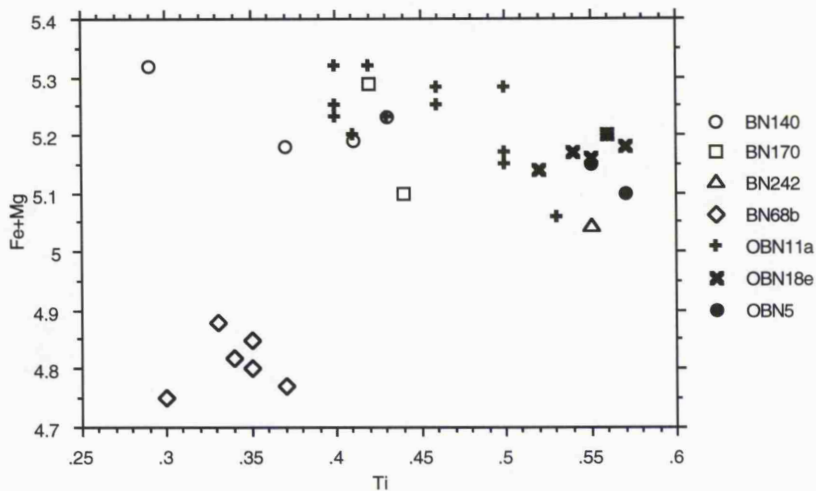


Fig 5.7a Increasing Ti with decreasing Fe+Mg for the biotites.

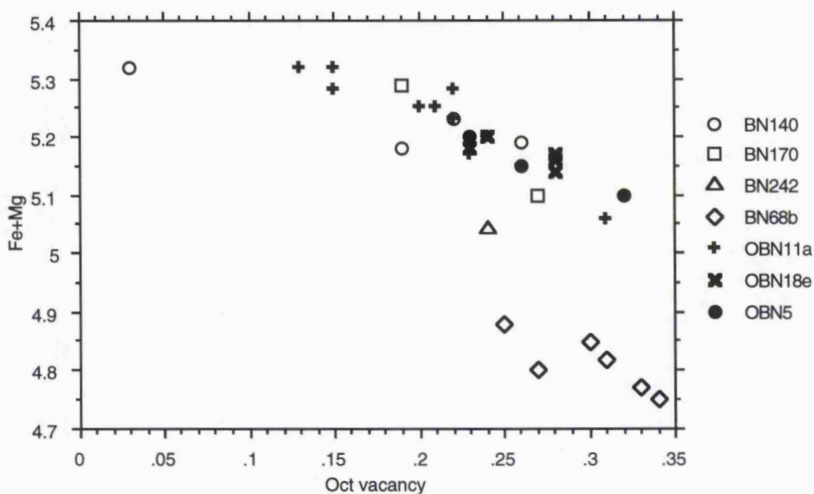


Fig 5.7b Decreasing Fe+Mg with increasing vacancy in the octahedral site for biotite from Ben Nevis.

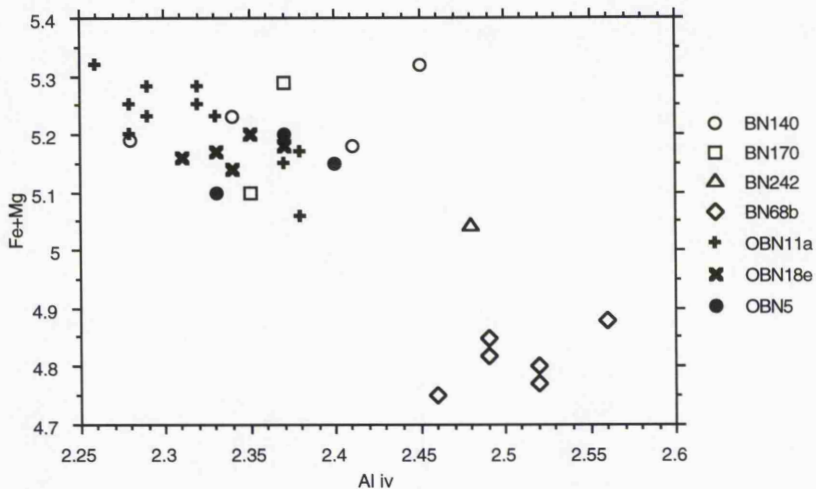


Fig 5.7c Decreasing Fe+Mg with increasing (Al)iv for the biotites with the exception of BN68b where a weak positive correlation is observed.

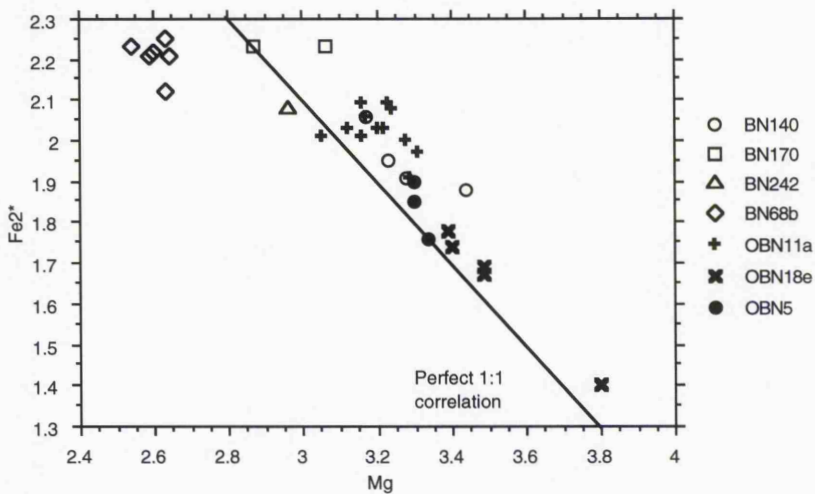


Fig 5.8 Near perfect correlation between Fe2\* and Mg for biotite. Note the relatively low Mg content of BN68b.

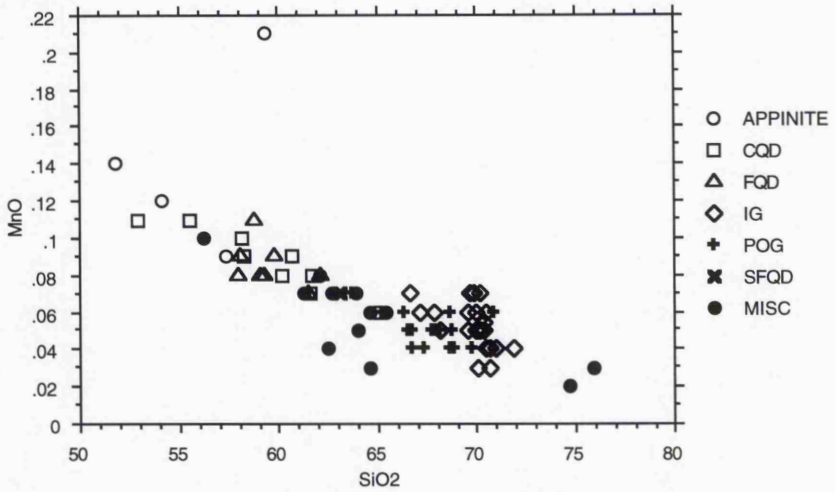


Fig 5.9a Decreasing whole-rock MnO with increasing fractionation (whole-rock SiO<sub>2</sub>) for the Ben Nevis Complex.

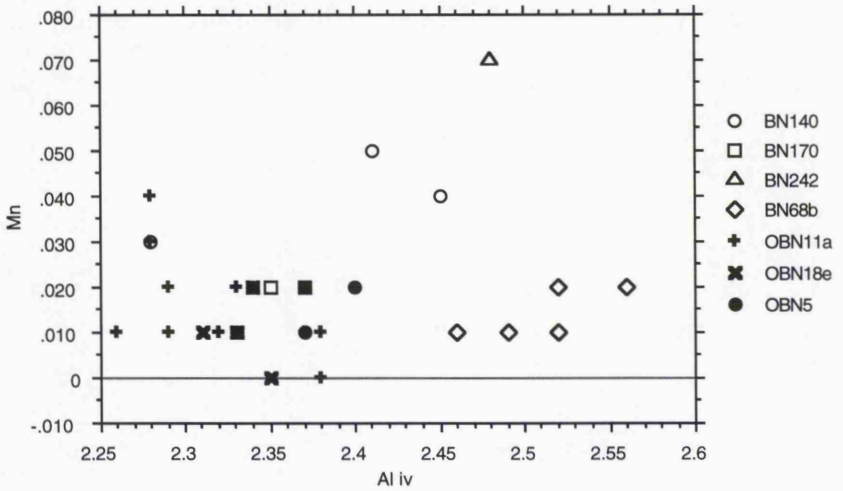


Fig 5.9b Indiscriminate scatter between Mn and (Al)iv in biotite. Biotite did not cause the fractionation of MnO observed in Fig 5.9a.

either assimilation of, or passage of fluids from, the country rock into the granite locally increased  $fO_2$ . BN68b has noticeably different whole rock compositions from the main plutonic rocks and assimilation is preferred.

Foxy-red pleochroic biotites are also found in the vicinity of the appinite intrusions between the Allt a' Mhuillin and the BAA surge chamber. The most basic whole-rock samples are obtained from this area (Haslam 1970 and chapter 6). Haslam (1968 & 1970) suggested that appinite formation and intrusion resulted from the assimilation of the Ballachulish Limestone formation at depth. Whereas this is probably the cause of 'appinitisation' in the Red Burn, it is thought unlikely that such a process could generate the large area of appinite intrusion and altered Coarse Quartz Diorite between the Allt a' Mhuillin and the surge chamber (chapter 4 and Yarr 1991). There is also isotopic evidence that the appinites are magmatic in origin (chapter 7).

Appinites are associated with large volatile contents (Hamidullah & Bowes 1987) and it is suggested that the action of volatile rich fluids emanating from appinite locally altered the  $fO_2$  of the adjacent Coarse Quartz Diorite in this area as biotite was crystallising. The presence of both appinite xenoliths (Haslam 1970) and intrusive contacts between appinitic pipes and the Coarse Quartz Diorite (chapter 4), indicates that the surge chamber appinite was intruded at around the same time as the Coarse Quartz Diorite, thus any volatile fluxing associated with appinite intrusion would have affected the minerals crystallising in the adjacent magma.

### 5.3.3 Amphiboles

The general formula for amphibole is:



In structural terms, the A, B, C and T atoms are represented respectively in A, M4, (M1 + M2 + M3), and T (tetrahedral) sites (Deer et al 1992).

Like biotite, amphiboles are capable of a wide variety elemental substitutions, indeed, amphibole has been termed a 'mineralogical sponge' because of its ability to scavenge a wide variety of elements from a coexisting melt or fluid.

The applicability of Al in hornblende geobarometers to the Ben Nevis Complex has already been discussed in chapter 4, and will not be further mentioned here.

Amphiboles are classified according to the procedure and nomenclature of Leake (1978).  $(Ca+Na)_B$  for all the Ben Nevis examples (Appendix II) exceeds 1.34, also  $(Na)_B < 0.67$  and therefore all the Ben Nevis amphiboles fall into the calcic amphibole group. Amphiboles from the plutonic rocks have  $Ti < 0.50$  and  $(Na + K)_A < 0.5$ , hence the application of discriminant diagram Fig. 5.10a (Fig. 3a of Leake). Amphiboles from the volcanic pile have  $(Na + K)_A \geq 0.50$ ,  $Ti < 0.50$  and  $Fe^{3+} \geq (Al)^{vi}$  and require the application of a separate discrimination diagram (Fig. 5.10b) for these examples (Fig. 3c of Leake 1978).

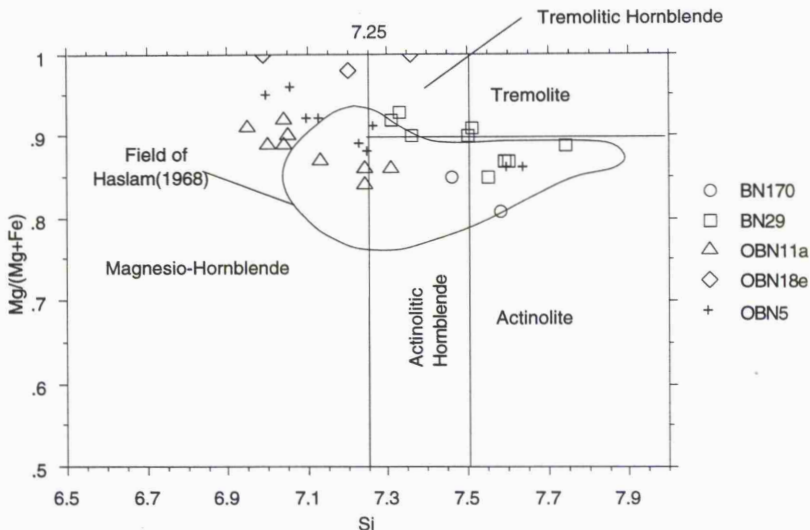


Fig 5.10a Discrimination diagram for amphiboles derived from the plutonic rocks. Based on Fig 3.a of Leake (1978).  $(Na+K)A < 0.50$ ,  $Ti \leq 0.50$ .

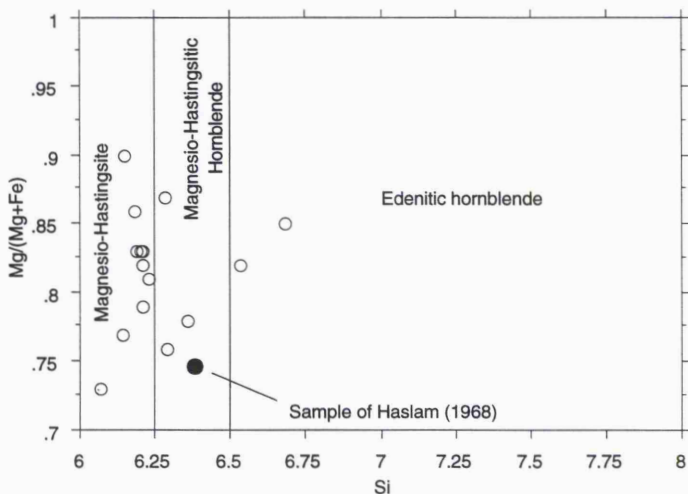


Fig 5.10b Discrimination diagram for amphiboles derived from the volcanic pile. Based on Fig 3.c of Leake (1978).  $(Na+K)A \geq 0.50$ ,  $Ti \leq 0.50$ ,  $Fe^{3+} \geq (Al)_{vi}$ .

Volcanic amphiboles from Ben Nevis range in composition from edenitic hornblende to magnesian-hastingsite (Fig. 5.10a). Those from the plutonic rocks range from actinolite to magnesian-hornblende with occasional samples in the actinolite to actinolitic hornblende field (Fig. 5.10b). The data of Haslam (1968 & 1970) were also plotted as an independent

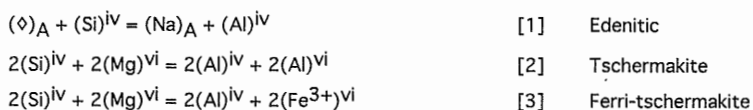
check on the calculations applied to the data. Sample 14 of Haslam (1968) was obtained from the volcanic pile, although it is described by Haslam (1968) as paragasitic hornblende; according to the procedure outlined by Leake (1978), this sample plots as magnesio-hastingsitic hornblende and falls into the same field as the volcanic data presented here ( $Fe^{3+} \geq Al_{VI}$ ).

Haslam (1968) also reports cummingtonite as an intermediate stage between pyroxene and hornblende during replacement of the former by the latter. However, no sample with  $(Ca+Na)_B \leq 1.34$  was identified during the current study or in Haslam's (1968) data set, and the amphiboles from the Ben Nevis Complex are calcic amphiboles of actinolite to magnesio-hornblende compositions (Fig. 5.10a). Again the plutonic data presented here falls within the same set of fields as the published data (Fig. 5.10a), validating the Fe corrections and structural calculations applied to the new data.

The amphiboles from Ben Nevis are often cored by pyroxene and a progression from pyroxene through actinolite to actinolitic hornblende is encountered when moving from core to rim. The ultimate stage in this progression is the presence of a rim of biotite mantling hornblende. In the majority of samples from the Ben Nevis Complex, this occurred at or below the solidus; a few samples exhibit small idiomorphic amphiboles and it is thought that these were formed directly from magma rather than by pyroxene replacement. It was earlier suggested (section 5.2.2) that conversion of pyroxene to amphibole occurred either in the melt phase or by elemental diffusion between pyroxene and a fluid/late stage magma. No geochemical difference is noted between the two types.

From Fig. 5.11, two trends can be identified. A pluton wide trend of decreasing  $(Al)^{IV}$  with increasing fractionation is overprinted by within-pulse trends of increasing  $(Al)^{IV}$  with increasing Mg. Subsolvus substitutions and the conversion of pyroxene to amphibole control this latter trend, whereas the former is controlled by compositional variations in the magma.

The plutonic rocks are undersaturated in Al, and  $Fe^{3+}$  is required to fill the available sites in the tetrahedron; this contrasts with the biotites which are  $(Al)^{IV}$  saturated. Two factors control the degree of  $(Al)^{IV}$  saturation in the Ben Nevis amphiboles; firstly, the Ben Nevis pluton is a high level pluton (<2kbars and probably closer to 1kbar, chapter 4) and it is generally agreed that the quantity of Al in calcic amphibole is proportional to the pressure at which it formed (Hammarstrom & Zen 1986). Secondly, the majority of plutonic amphiboles are formed from the replacement of pyroxene and these are also low in Al (Haslam 1968). The incorporation of  $(Al)^{IV}$  and  $(Fe^{3+})^{IV}$  into the tetrahedral site is accompanied by elemental substitutions in the M1-M3 sites in order to balance mineral charge, the most important of these are;



$2(\text{Si})^{\text{iv}} + (\text{Mg})^{\text{vi}} = 2(\text{Al})^{\text{iv}} + (\text{Ti})^{\text{vi}}$	[4]	Ti-tschermakite
$2(\text{Ca})_{\text{M4}} + 2(\text{Mg})^{\text{vi}} = 2(\text{Na})_{\text{M4}} + 2(\text{Al})^{\text{vi}}$	[5]	Glaucophane
$2(\text{Ca})_{\text{M4}} + 2(\text{Mg})^{\text{vi}} = 2(\text{Na})_{\text{M4}} + 2(\text{Fe}^{3+})^{\text{vi}}$	[6]	Riebeckite
$(\diamond)_{\text{A}} + (\text{Ca})_{\text{M4}} = (\text{Na})_{\text{A}} + (\text{Na})_{\text{M4}}$	[7]	Richterite
$(\diamond)_{\text{A}} + (\text{Mg})^{\text{vi}} + 2(\text{Si})^{\text{iv}} = (\text{Na})_{\text{A}} + (\text{Al})^{\text{vi}} + 2(\text{Al})^{\text{iv}}$	[8]	pargasite

$\diamond$  = Vacancy in the A-site. Note also that in the plutonic rocks  $\text{Fe}^{3+}$  is found in the tetrahedral site as insufficient Al is available.

Amphiboles in the volcanic rocks are chemically (e.g. tetrahedral site is saturated in Al) and optically different to those in the plutonic rocks. Brown et al. (1982) showed that by plotting  $(\text{Al})^{\text{iv}}$  against  $\Sigma[\text{Total A-site occupancy} + (\text{Al})^{\text{vi}} + (\text{Fe}^{3+})^{\text{vi}} + 2(\text{Ti})^{\text{vi}}]$  a 1:1 relationship should be maintained if charge balance is controlled by substitutions [1], [2] and [3]. Fig. 5.12 shows that all the volcanic pile data fall on a line parallel to and below this 1:1 relationship (i.e. they have higher levels of elements in the algebraic expression than can be balanced by  $(\text{Al})^{\text{iv}}$  alone). Consequently the migration of Na into the M4 site according to mechanisms [5] and [6] is invoked. For the volcanic rocks, it can be concluded that the edenitic, tschermakitic and ferri-tschermakitic substitutions dominate the chemistry of the amphiboles, with minor incorporation of Na into the M4 site. Plotting  $(\text{Al})^{\text{iv}}$  against individual components of the above algebraic expression yields only poor correlations indicating that the dominant substitution mechanism varies considerably between and within different samples/crystals.

The plutonic rocks are much more complex. Within-pluton trends are complicated by within-pulse trends (Fig. 5.11). Again, considering the variety of possible substitution mechanisms, the degree of within-sample harmony must be significant. Individual samples plot within discrete fields in any of the plots presented and show similar within-sample gradients indicating that similar substitution mechanisms affected each individual sample. Variations between each sample again emphasise the fact that the Ben Nevis plutonic magmas were intruded as a series of small magma pulses, each with slightly different chemistry from other pulses.

Amphiboles in the Ben Nevis pluton are uniformly low in Al; insufficient Al is available to fill the tetrahedral site and  $\text{Fe}^{3+}$  is required to balance the crystal structure. Those samples with the lowest  $(\text{Al})^{\text{iv}}$  plot closest to the ideal 1:1 relationship between  $\Sigma[(\text{Al})^{\text{iv}}$  and  $(\text{Fe}^{3+})^{\text{iv}}]$  against  $\Sigma[\text{Total A-site occupancy}, (\text{Al})^{\text{vi}}, (\text{Fe}^{3+})^{\text{vi}}$  and  $2(\text{Ti})^{\text{vi}}]$ . Where total Al is greater, the amphibole compositions begin to diverge from the 1:1 line (Fig. 5.13); again this probably reflects increasingly higher levels of Na incorporation into the M4 site.

Total A-site occupancy (Fig. 5.14) shows only a slight increase with increasing  $(\text{Al})^{\text{iv}}$  and remains uniformly low (<0.2). This reveals that the edenitic substitution was relatively unimportant in the plutonic rocks.

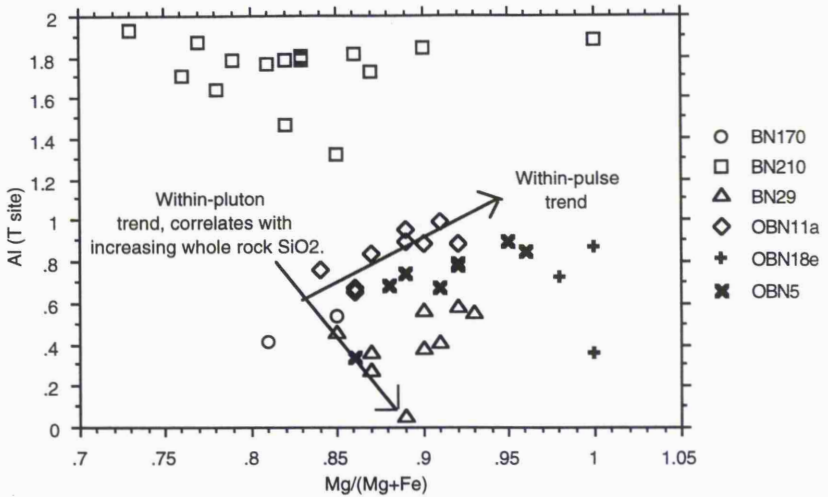


Fig 5.11 (Al)<sub>iv</sub> against Mg/(Mg+Fe). Note the two trends apparent in the plutonic amphibole data, within-pulse and within-pluton.

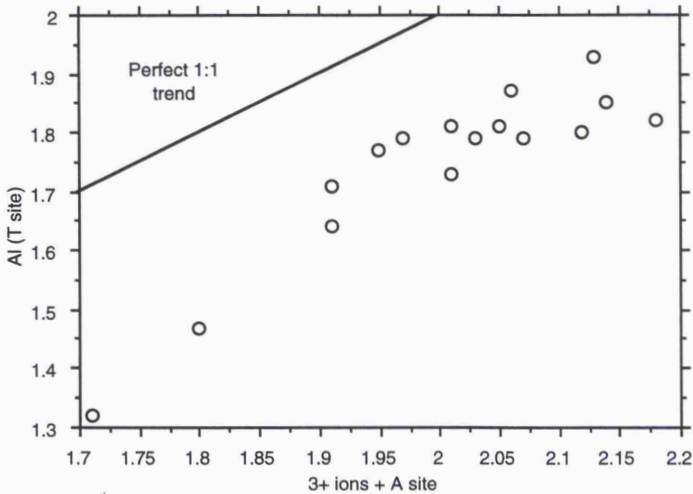


Fig 5.12 In the volcanic amphiboles, substitution of (Al)<sub>iv</sub> is balanced by the entry of (R<sub>3+</sub>)<sub>vi</sub> into the M1-M3 sites and increasing A-site occupancy. Minor entry of Na into M4 balances deviation from the perfect 1:1 trend.

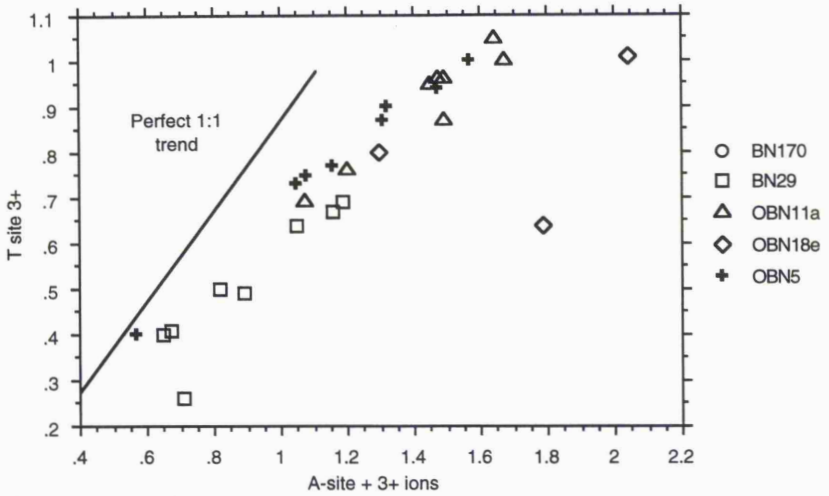


Fig 5.13  $\Sigma[(Al)^{iv}+(Fe^{3+})^{iv}]$  against  $\Sigma[A\text{-site occupancy}+Fe^{3+} + Ti]$  for the plutonic amphiboles.

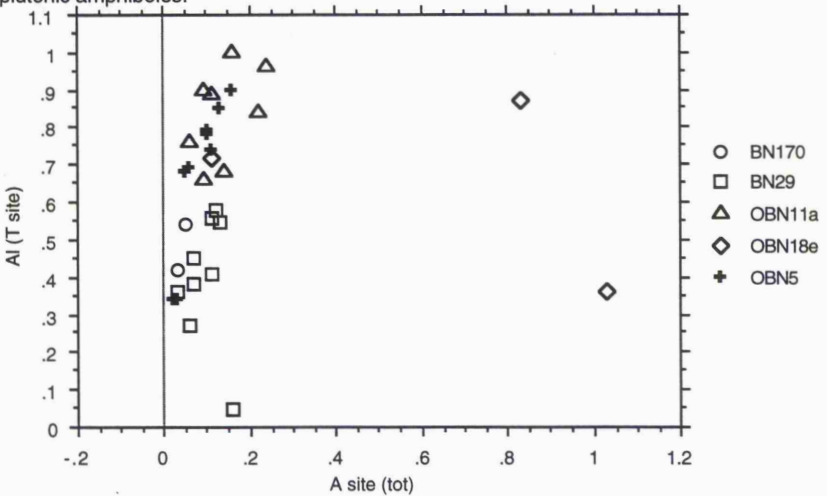


Fig 5.14  $(Al)^{iv}$  substitution into the tetrahedral site of plutonic amphiboles is not related to the level of A-site occupancy which remains  $\approx$  constant.

Both  $(Fe^{3+})^{vi}$  and  $2(Ti)^{vi}$  yield strong positive correlations against  $\Sigma[(Al)^{iv}]$  and  $(Fe^{3+})^{iv}$  and both the Tschermakite and Ferri-tschermakitic substitutions are important in the plutonic rocks.

The overall plutonic trend is one of decreasing  $(Al)^{iv}$  at high  $Mg/(Mg + Fe)$ . There is too much variability in the  $Mg/(Mg+Fe)$  ratio within individual pulses to define starting points accurately enough in order to identify within pluton variations in this ratio, other

than a general increase in  $Mg/(Mg+Fe)$  with increasing host-rock silica (Fig. 5.11). Haslam (1968) reports increasing  $Mg/(Mg+Fe)$  with increasing silica, the opposite of normal fractionation trends. The suggested mechanism put forward to explain this feature by Haslam (1965) was a high and constant partial pressure of oxygen, possibly the result of an atmospheric connection. The data presented by Haslam (1968) were based on wet chemical analyses of mineral separates and therefore within pulse (and within crystal) variation is averaged out, allowing comparison of the  $Mg/(Mg+Fe)$  ratio between different components of the Ben Nevis Complex.

#### 5.3.4 Pyroxenes

The general formula for pyroxene is



Pyroxenes are classified according to the procedure and nomenclature of Morimoto (1988). All the Ben Nevis examples (Appendix II) have  $Q (Ca+Mg+Fe^{2+}) > 1.5$  and  $J (2Na) < 0.5$  thus allowing use of the pyroxene quadrilateral (Fig. 5.15), with end-member compositions; Wollastonite, Enstatite and Ferrosilite, to define their composition. For this plot, Ca, Mg and  $\Sigma(Fe^{2+}+Fe^{3+} \text{ and Mn})$  are normalised to 100%.

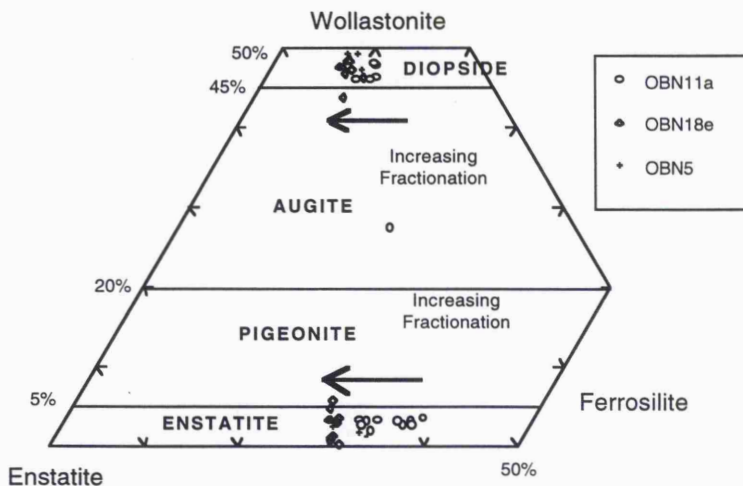


Fig 5.15 Composition of pyroxene from the Ben Nevis complex in the pyroxene quadrilateral.

All orthopyroxenes fall within the enstatite field (Fig. 5.15). Clinopyroxenes fall either side of the divide between diopside and augite. Data from Haslam (1968 & 1970) plot similarly, justifying the Fe correction made according to the formula of Droop (1987). Both pyroxene types plot in a tight group indicating that limited post-magmatic substitution

has occurred. The pyroxenes show a trend of increasing proportion of the enstatite molecule (i.e. increasing Mg) with increasing SiO<sub>2</sub>, in agreement with the increasing Mg/(Mg+Fe) ratios noted for the ferromagnesian minerals by Haslam (1968).

A two-pyroxene thermometer is available in the GPP (Geist et al. 1989) program and based on the work of Kretz (1982); pyroxenes from individual samples were averaged (Table 5.2) and entered into the program. OBN11a and OBN18e yielded temperatures within 6°C of each other at 1053°C and 1059°C respectively. Both these samples are members of the Fine Quartz Diorite. Pyroxenes from the Coarse Quartz Diorite (OBN5) yielded a temperature of 936°C.

Table.5.2

Average pyroxene compositions

Sample	Fe2O3	FeO	CaO	MgO
OBN11a	1.08	21.34	1.44	21.75
OBN18e	1.14	18.20	1.37	24.14
OBN5	0.14	19.75	0.97	23.37
OBN11a	1.73	7.87	20.67	14.76
OBN18e	2.43	5.06	22.28	15.02
OBN5	3.00	5.20	23.05	14.58

Pyroxene data from Sample No1, of Haslam (1968), obtained from the Fine Quartz Diorite, gives a temperature of 1054°C, in close agreement with those temperatures calculated from pyroxenes analysed in the current study. Again the validity of Droop's (1987) Fe correction calculation is confirmed. Pyroxenes from a pyroxenite xenolith situated in the vicinity of the surge chamber appinite (Haslam 1970) give a temperature of 1003°C.

The range of temperatures (1050-930°C) obtained for the Ben Nevis pluton is comparable with those obtained from pyroxene in the quartz diorites of the Ballachulish pluton (Weiss & Troll 1989), which range between 1050°C and 900°C.

### 5.3.5 Plagioclase

Plagioclase is commonly strongly zoned in both volcanic and plutonic rocks. The nature and degree of zoning have been discussed in section 5.1 and the results of microprobe analysis of plagioclase phenocrysts discussed briefly here. In many of the andesite samples, it is unstable and shows signs of corrosion by the matrix (section 5.1). The most calcic examples are found in the Fine Quartz Diorite, with An as high as 60%. Zoning is variable and sericitisation has often picked out discrete basic rings and/or more basic cores. Fig. 5.16 reveals the variation in plagioclase composition throughout the Ben Nevis Complex .

A plagioclase-whole rock geothermometer has been developed by Mathez (1973) and is available within the GPP program. P.H<sub>2</sub>O was estimated at 1kbar under the assumption

that the Ben Nevis magmas crystallised at a high level in the crust. The most extreme plagioclase compositions were placed into the computer along with an average value; the results ranged between 1039°C and 887°C with an average of 956°C for the quartz diorites. Results for the Porphyritic Outer Granite range from 893°C to 766°C with an average of 807°C. The data for the quartz diorites again fall within the range of the Ballachulish quartz diorites (Weiss & Troll 1989). Emplacement of the Porphyritic Outer Granite and crystallisation of plagioclase occurred at temperatures ranging between 900°C and 750°C. These values suggest that plagioclase phenocrysts formed directly from the melt and have undergone little below solidus re-equilibration despite the activity of late stage corrosive K-rich fluids. This suggests that the late stage fluids were confined to the interstices between crystals and the pluton passed through the 'freezing' temperature of these fluids before significant diffusion between fluid and crystal could occur. A similar explanation is invoked for the thin amphibole rims formed where pyroxene has reacted with the interstitial late stage fluid (section 5.2.6). Rapid cooling in the high level environment of the Ben Nevis magma chamber is the most likely cause for preservation of magmatic temperatures. In the deeper (3kbar) Ballachulish pluton, a number of plagioclase analyses record the effects of low temperature (<700°C) subsolidus alteration.

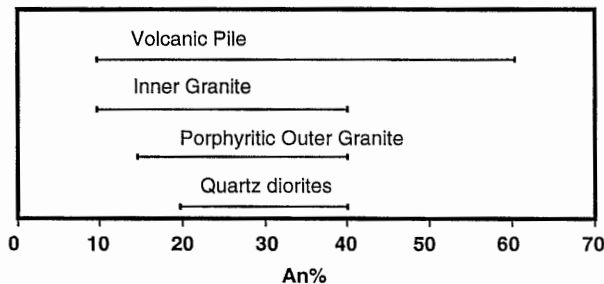


Fig 5.16 Variation in plagioclase composition throughout the Ben Nevis Complex.

From this section evidence, it is known that plagioclase formed an early phase in the crystallisation history of the Ben Nevis Complex. Despite early crystallisation, temperatures obtained from plagioclase are 100-150°C lower than those obtained for the pyroxenes. One explanation for this discrepancy is inter-crystal re-equilibration during progression from calcic core to sodic margin, thus altering the chemistry of earlier formed cores towards compositions compatible with lower temperatures. The presence of crystal zoning indicates that the cores of individual crystal are not in equilibrium with the rims or with the last melt phase.

#### 5.4 Conclusions

The petrography of the Ben Nevis Complex shows considerable variation between individual pulses. Mineralogical variations within-pulse are remarkably coherent and the formation of the Ben Nevis Complex as a series of magma pulses is again confirmed.

Similar substitution mechanisms occur within each pulse, suggesting that once the magmas entered the Ben Nevis chamber, their elemental substitutions continued along similar lines.

Temperatures of intrusion for the Fine Quartz Diorite are estimated at 1050°C with the Coarse Quartz Diorite being somewhat lower at 950°C. Crystallisation proceeded to 800°C or less. Where water contents were high, biotite formed a major early phase and pyroxene converted readily to amphibole. Where water contents were lower, pyroxene remained stable until the formation of a late stage K and Al rich fluid. The end of magmatic activity was marked by the formation of alkali feldspar and quartz prior to the separation of a late fluid phase, that resulted in mineralisation where this fluid was concentrated, such as along fault planes. Passage of this fluid is marked by slight sericitisation of both plagioclase and alkali feldspar; adjacent to fault planes alteration is much greater.

The level of MnO decreases with increasing fractionation within the Ben Nevis Complex (Fig. 5.9a) and neither pyroxene or biotite show a similar trend. Amphibole also shows a gradual decrease in Mn with increasing fractionation (Fig. 5.17) and yet is relatively rare as a primary mineral phase. Decreases in MnO with fractionation cannot be attributed to crystallisation of any of the mineral phases observed in the Ben Nevis Complex. Romick et al. (1992) have demonstrated that the formation of amphibole at depth may control the trace element characteristics of andesitic and dacitic magma erupted at the surface in the Aleutians. The trace element characteristics of these lavas reflect amphibole crystallisation at depth which was then replaced by pyroxene as the magma rose to shallower levels in the crust. A similar process may be invoked for the Ben Nevis Complex, which culminated in the partial replacement of pyroxene by amphibole. At high levels in the crust, pyroxene forms in preference to amphibole (Yoder & Tilley 1962), thus MnO should increase with fractionation in the high level magma chamber and any late stage fluid/magma would become enriched in Mn; it is from this late stage fluid that amphibole is obtaining Mn.

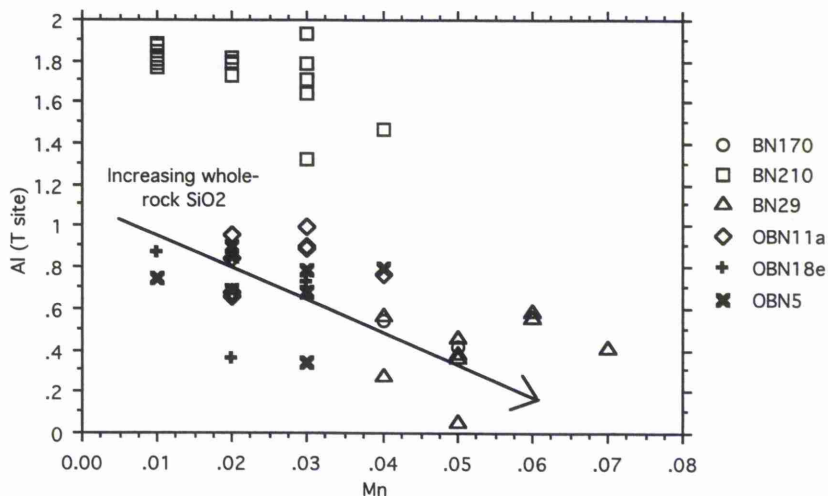
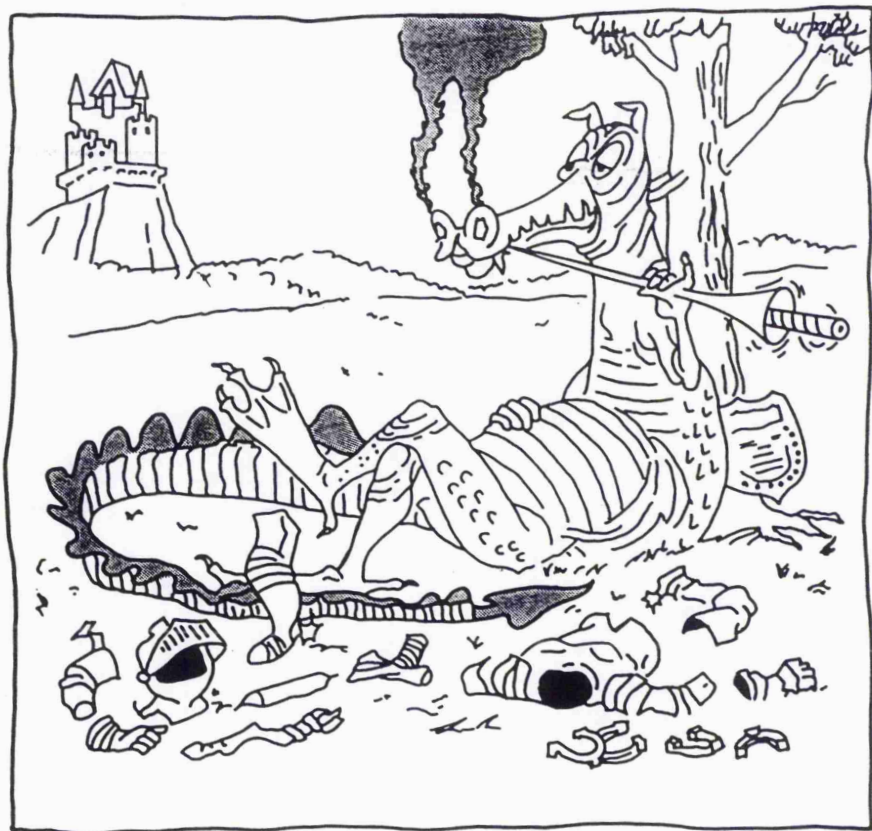


Fig 5.17 General decrease in amphibole Mn with increasing fractionation.

Remember...



Sometimes The Dragon Wins

## CHAPTER 6

### THE GEOCHEMISTRY OF THE BEN NEVIS COMPLEX

#### 6.1. Introduction

##### 6.1.1. General statement

Apart from a limited number of wet chemical analyses from the pre-war period (Bailey & Maufe 1916 and Anderson 1935), published data on the Ben Nevis Complex are effectively confined to the work of Haslam (1965, 1968 & 1970). Analyses presented by Haslam, were obtained using a combination of gravimetric, wet chemical, flame photometry, calorimetric and spectrographic techniques. A few samples of the Ben Nevis Complex have been included in regional surveys (e.g. granites - Stephens & Halliday 1984, volcanics - Thirlwall 1979). Consequently this thesis contains the first detailed study of the geochemical evolution of the Ben Nevis Complex using XRF derived data.

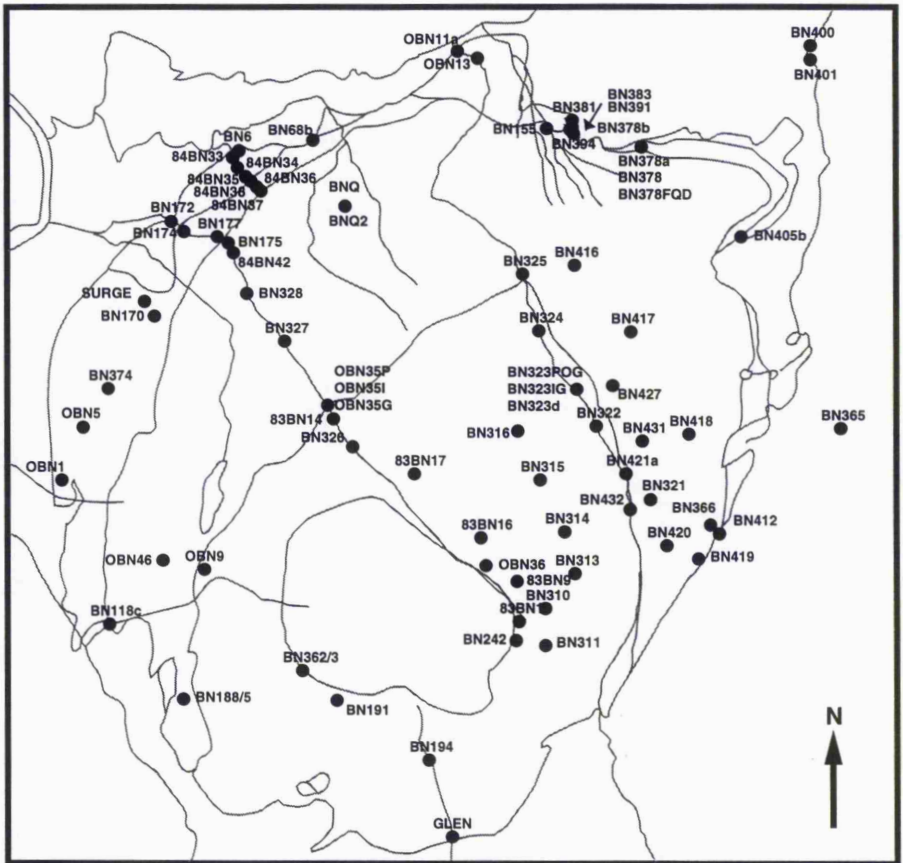
The presence of sharp contacts between individual pulses and units of the Ben Nevis Complex indicates the presence of a number of separate magma pulses. Sharp internal contacts do not, however, preclude differentiation at deeper crustal levels with periodic magma migration to higher crustal levels, tapping successively more fractionated residual magma. The degree to which the separate units of the Ben Nevis Complex can be related by crystal fractionation is examined in section 6.5. At least four separate parent magmas are required to explain the geochemical variations between different units of the Ben Nevis Complex; this conclusion is also supported by new isotope data presented in chapter 7.

Reference is made during this chapter to the I- and S- type classification scheme of Chappell & White (1974). The I- and S-type classification is believed to reflect different source rock compositions (Chappell & White 1974). I-type granites are thought to reflect derivation from the partial melting of an igneous protolith, whereas S-type granites are believed to be partial melts of a sedimentary or metasedimentary protolith that has suffered at least one weathering cycle. The two types of granite have different geochemical characteristics; these are summarised in Table 6.1.

##### 6.1.2 Methodology

A total of 103 samples were collected for XRF analysis during the current study. In addition Dr W.E. Stephens kindly made available his rock collection from Ben Nevis, providing an additional 20 analyses. Sample preparation and XRF operation are described in Appendix III, along with the major and trace element analyses. Sample locations are shown in Fig. 6.1 and listed in Appendix I.

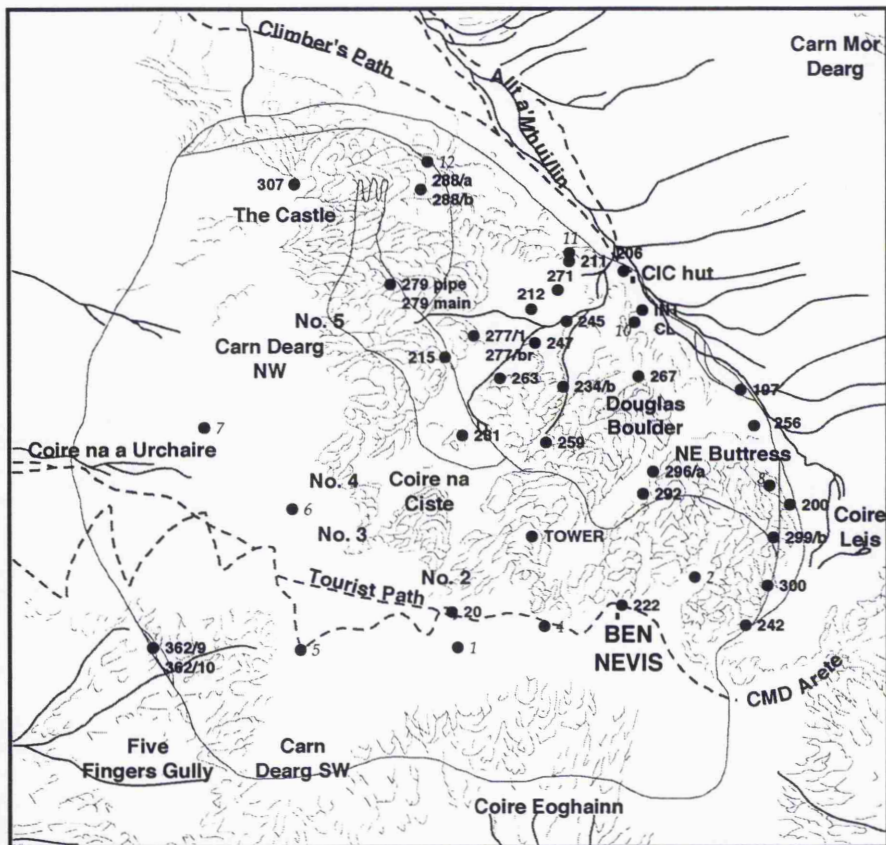
For CIPW norm calculations, the abundance of  $\text{Fe}_2\text{O}_3$  was derived from Irvine & Barager's (1971) formula, where  $\text{Fe}_2\text{O}_3 = 1.5 + \text{TiO}_2$ . The results obtained are comparable



**KEY**

- BN174 Location of exposure or photo mentioned in text.

Fig. 6.1a Location of intrusive rocks analysed for their major and trace element compositions. Those samples prefixed with 82 or 83 or 84 were collected by Dr W. E. Stephens.



Key

● BN242 Location of sample.

0.5 km

Fig 6.1b The location of volcanic samples analysed for major and trace elements. Where mentioned specifically in the text, these samples are all prefixed with BN. Samples numbers in *italics* are from the collection of Dr W. E. Stephens.

to those of Haslam (1968) for which wet chemical analyses of FeO and Fe<sub>2</sub>O<sub>3</sub> are available, verifying the applicability of the Irvine & Barager (1971) formula to the Ben Nevis Complex.

Table 6.1 A comparison of I-Type and S-Type Granitoids.

PARAMETER	I-TYPE	S-TYPE
CaO	Moderate to High (2-10%)	Low <2%
Molar A/CNK	<1.1	>1.1
Norms	Often diopside normative	Corundum normative
Trace element enrichment	Transition (Ni & Cr) and LIL (Ba, Sr etc) elements	Alkali earths (Rb, Li etc) plus U and Th
REE	+ve Eu anomaly LREE enriched	Generally flat pattern or possibly HREE enriched
( <sup>87</sup> Sr/ <sup>86</sup> Sr)	Low (0.704 - 0.706)	High (> 0.708)
δ18O	Relatively low <9‰	Relatively high >10‰
Restite type	Relatively uncommon and mainly in the form of mafic clots	Metasedimentary blocks relatively common
Characteristics of source region	Relatively homogenous and mainly source that has not suffered a previous cycle of crustal residence	Sedimentary source The volume of clay minerals has a strong influence on granite chemistry during melting

Table derived from Chappell & White (1974), Chappell & Stephens (1988), White & Chappell (1988), Chappell & White (1992) and references therein.

### 6.1.3 Previous research

The data of Haslam (1965), with the exception of the basic (appinitic) samples, fall along a coherent trend which was interpreted as a liquid line of descent. Comparisons with data from other South-west Highland Caledonian intrusions revealed similar trends with only minor variations in SiO<sub>2</sub> (1-2% lower) and Na<sub>2</sub>O (0.5% lower). On a triangular diagram (K<sub>2</sub>O-Na<sub>2</sub>O-CaO), the Outer Granite follows a potassic trend whilst the Inner Granite and Mullach nan Coirean Granite were shown to follow a more sodic trend. Scatter was attributed to the late stage movement of potassic fluids.

Haslam (1965) stated that the most acidic and the most basic analyses of the Ben Nevis Complex were obtained from the same intrusion, namely the Outer Quartz Diorite. Anomalously high contents of Cr, V and Ni were noted for the siliceous sample and confirmed his belief that the sampled outcrop was part of the quartz diorite. However, it was shown in chapter 4 that the acidic rock intrudes the Porphyritic Outer Granite and therefore post-dates intrusion of the quartz diorites.

In Anderson (1935), a sample derived from the Coarse Type (nomenclature of Anderson 1935) was the most basic analysed. Nichols (1951) used this as evidence for reverse zoning in the Outer Granites. However, the sample of Coarse Type was derived from the zone of interaction with appinitic magmas in the vicinity of the surge chamber and therefore not representative of the Coarse Type. Such is the variability of the Outer Granite, that no one sample can be considered as representative of an individual unit.

## 6.2 Composition and Classification of the Ben Nevis Complex

### 6.2.1 SiO<sub>2</sub> as an index of fractionation

SiO<sub>2</sub> is used as a fractionation index throughout this thesis. Zr and Zr/element ratios have often been preferred as indices of fractionation (Sceal & Weaver 1971 and Pearce & Norry 1979); however the removal of Zr during fractionation of the Porphyritic Outer Granite and the volcanic andesites results in decreasing Zr with increasing fractionation. In the Inner Granite and quartz diorites, Zr increases; such non-uniform variation renders Zr useless as a fractionation index. Ni is an alternative fractionation index; however its abundance in some of the andesites and in the Inner Granite approaches that of the lower limit of detection. Furthermore, considerable scatter of this element is apparent in the quartz diorites.

Mg# (MgO/(MgO+FeO) or MgO or FeO are sometimes used as fractionation indices for basic rocks; however the plutonic and volcanic rocks of the Ben Nevis Complex range in composition from intermediate to acidic with very few exceptions. SiO<sub>2</sub> remains, with regard to the Ben Nevis Complex at least, the simplest and most easily interpreted fractionation index.

### 6.2.2 Harker Diagrams

Alignments and groupings of data points along Harker diagrams have been variously interpreted as liquid lines of descent (Harker 1909), as proof of fractionation (Walsh & Clarke 1982) or demonstrating bimodal distribution in magmas (Daly 1933). Harker diagrams are used here to demonstrate variations/similarities between different units of the Ben Nevis Complex. Coherent trends along Harker diagrams are often used as evidence of continuous chemical evolution from basic to acidic compositions (e.g. Haslam 1968). In reality, individual samples which fall along a trend represent magmas erupted in a random time sequence, and therefore a single trend represents the average evolutionary pathway of numerous batches of magma from parental magmas of similar composition (Wilson 1989). This is demonstrated admirably in the Ben Nevis Complex by the younger Coarse Quartz Diorite pulses in the bed of the Allt a' Mhuillin that are more basic than the older Fine Quartz Diorite pulses downstream.

#### 6.1.4 Element mobility and alteration.

Element mobility and alteration is particularly important for the samples analysed from the volcanic pile where alteration of the groundmass is ubiquitous. Thirlwall (1979), after comparing mobile (Ca, Mg, Na, K, Rb, Sr & Ba) and immobile (Cr, Zr, Y, Nb, Ti & P) elements, stated that volcanic whole rock samples with loss on ignition values of <2.5% had suffered little removal/alteration of elements after crystallisation. The loss on ignition values for the are presented in Appendix III and are <2.5% for the majority of andesite lavas.

### 6.2.2.i Granites

A silica gap exists between the bulk of the quartz diorites and the bulk of the Porphyritic Outer Granite data (Fig. 6.2), which is partially filled by BN68b and chilled eastern margin variants of the Porphyritic Outer Granite (BN366, BN419 & BN420). BN68b is believed to have been strongly contaminated by the country rock (chapter 5) and the chilled marginal variants of the Porphyritic Outer Granite represent the earliest and least evolved pulses of the Porphyritic Outer Granite, and are not found elsewhere in the Ben Nevis Complex. This point ( $\text{SiO}_2 \approx 63\%$ ) coincides with inflexions in the trend of the data and is indicative of a change in the petrogenetic evolution of the plutonic rocks. In the majority of major element plots, the Inner Granite forms a continuation to the trend of the Outer Granite. Exceptionally, the  $\text{Na}_2\text{O}$  diagram does not follow this general observation, and the Inner Granite is relatively enriched in this element. All the major elements, other than  $\text{Na}_2\text{O}$ , show good correlations with  $\text{SiO}_2$ . The miscellaneous group of analyses (dykes, sills and minor intrusions) tend to have lower  $\text{K}_2\text{O}$  contents with respect to the granitic rocks.

For the Ben Nevis Complex, trace element Harker diagrams rarely show simple correlations with  $\text{SiO}_2$ . Those that do very often also show inflexions at  $\approx 63\%$  (the silica gap). Such elements include Th, Rb, Sr, Ga, Ce, Sc and V. A number of elements change from increasing/decreasing to decreasing/increasing with respect to  $\text{SiO}_2$ ; this is shown in Zr, Nb, Rb, Ce and Ba. Further complications lie in the fact that the Inner Granite does not always continue the trend defined by the Outer Granites; this is exemplified in Zr, Rb, Th, Ce, Ba and La.

According to Goldschmidt (1954), MnO increases with crystal fractionation but the Ben Nevis granites show decreasing MnO with increasing  $\text{SiO}_2$ . Miller & Stoddart (1981) have suggested that extensive hornblende fractionation during the early stages of magma evolution will deplete the subsequent melt in MnO, but amphibole is mainly a replacement mineral in the Outer Granite and cannot therefore, have caused depletion in MnO. Biotite may take up Mn into its structure, but as shown in chapter 5, the MnO content of biotite cannot be related to fractionation. Romick et al. (1992) have demonstrated that the crystallisation of amphibole at depth may control the trace element characteristics of andesite and dacite erupted at the surface in the Aleutians. The trace element characteristics of the Aleutian lavas reflects amphibole crystallisation at depth which was replaced by pyroxene crystallisation as the magma rose to shallower levels in the crust. Such a model is equally applicable to the Ben Nevis Complex and is discussed further in section 6.5.

Peccerillo & Taylor (1976) and Le Maitre et al. (1989) subdivide the subalkaline volcanic rocks according to their concentrations of  $\text{K}_2\text{O}$  and  $\text{SiO}_2$ . The Ben Nevis Complex granites fall into the high-K calc-alkaline series of Peccerillo & Taylor (1976) which is equivalent to the high-K field of Le Maitre et al. (1989). A few samples fall within the shoshonite (ultrapotassic) series of Peccerillo & Taylor (1976), and a few samples fall within the calc-alkaline series. This scatter is caused by the Fine Quartz Diorite and Coarse

Quartz Diorite units only. Haslam (1968) attributed the variation in  $K_2O$  within the Fine Quartz Diorite and Coarse Quartz Diorite to late stage enrichment by potash fluids; however, the quartz diorites also show considerable variation in  $TiO_2$ , Nb, Zr and Y. These elements are considered immobile in aqueous fluids (Pearce & Norry 1977) and consequently, scatter in the quartz diorites is attributed to variations between separate pulses of magma.

In the Inner Granites, both Zr and Y show steep increases in abundance against  $SiO_2$ . The clustering of Inner Granite data off the Outer Granite trend suggests that the two units have different origins and cannot be related by fractional crystallisation processes alone. In particular, highly incompatible elements such as Ba, Rb and Th, that should increase during fractional crystallisation, have lower abundances in the high  $SiO_2$  Inner Granite than in the lower  $SiO_2$  Porphyritic Outer Granite. This feature supports the belief, first expounded in chapter 4, that the Inner Granite and Outer Granites have slightly different parent magmas.

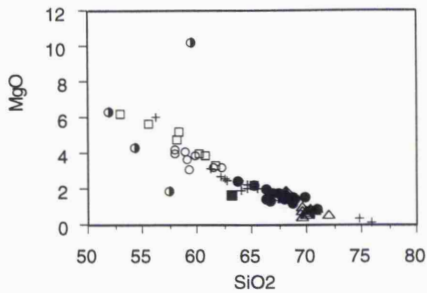
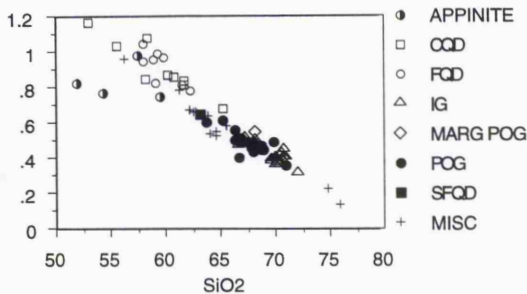
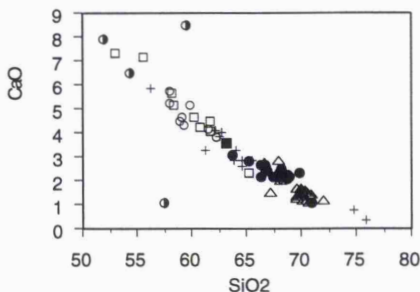
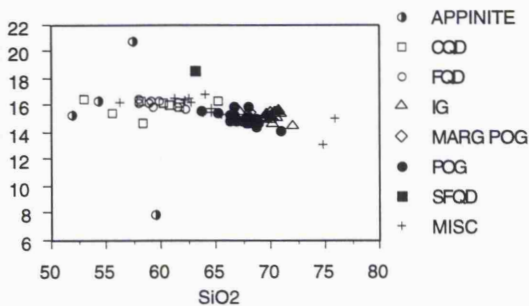
#### 6.2.2.ii Volcanics

The volcanic rocks from the Ben Nevis Complex exhibit a greater degree of scatter in Harker diagrams (Fig. 6.3) than the plutonic rocks. This is not surprising with respect to the miscellaneous group which includes samples from a range of different origins, including sediments, minor intrusions, volcanic breccias, clasts from volcanic breccias and injections from the Fault facies tuffsite. However, a large degree of variation is also evident in the andesites. The bulk of andesitic samples cluster between 63% and 67%  $SiO_2$

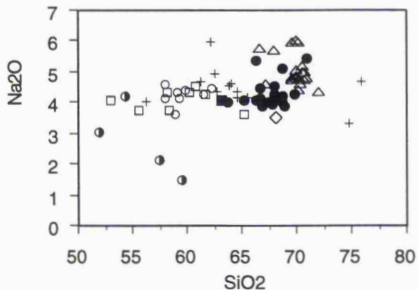
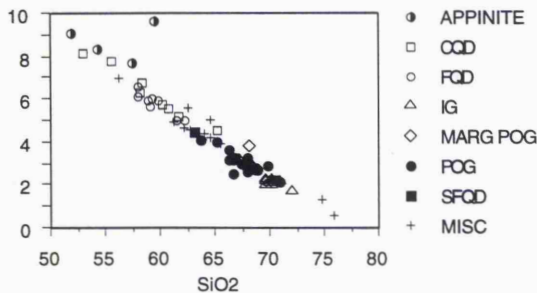
According to the classification schemes of Peccerillo & Taylor (1976) and Le Maitre et al. (1989), the volcanic rocks fall into the same field as the bulk of the plutonic rocks (high-K calc-alkaline series of Peccerillo & Taylor 1976 or high-K field of Le Maitre et al. 1989). Enrichment in K from fluids emanating from the Inner Granite is likely to have caused some of the scatter in this element (Haslam 1968); however, like the quartz diorites, the andesites also show considerable scatter in the elements believed to be immobile in aqueous fluids.

With the exception of BN197, a fine grained mudstone found at the base of the volcanic pile, the miscellaneous group closely follows variations in the andesites indicating the influence of similar petrogenetic processes in the igneous samples and a large quantity of volcanic ash in the sediments.

Reasonably good correlations are found in the following Harker diagrams,  $TiO_2$ ,  $Al_2O_3$ ,  $FeO^*$ , MgO, CaO,  $P_2O_5$ , Ga, Zn, Ni, Sc and V. There is no inflexion or reversal in any of the trends. Scatter is found in immobile and mobile elements e.g. Zr, Y, Rb, Ba, and cannot therefore be related to late stage alteration effects (Pearce & Norry 1977) and must therefore be source related. The andesites show decreasing Zr with increasing  $SiO_2$  and cannot therefore be considered as the direct equivalent of the quartz diorites.

TiO<sub>2</sub>Al<sub>2</sub>O<sub>3</sub>

FeO\*



MnO

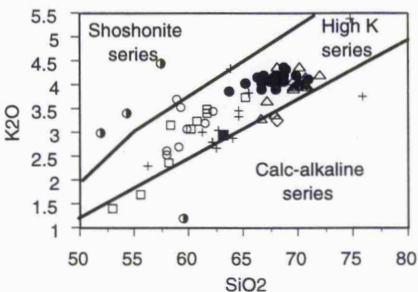
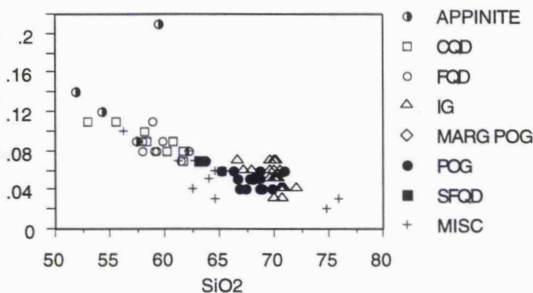


Fig. 6.2 Harker diagrams for TiO<sub>2</sub>, Al<sub>2</sub>O<sub>3</sub>, FeO\*, MnO, MgO, CaO, K<sub>2</sub>O and Na<sub>2</sub>O. Fields depicted in K<sub>2</sub>O are from Le Maitre et al. (1989) and Rickwood (1989).

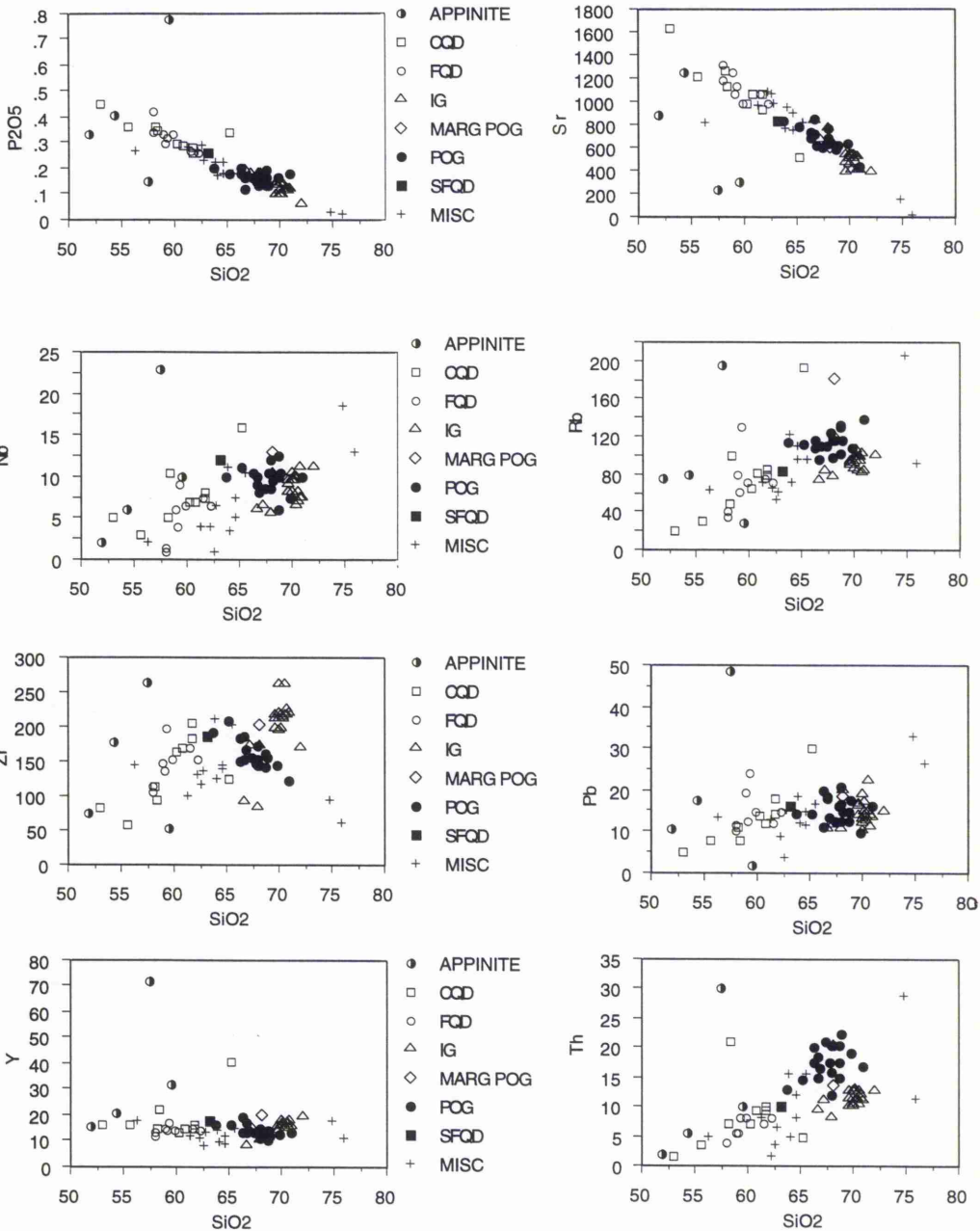


Fig. 6.2(continued) Harker diagrams for P<sub>2</sub>O<sub>5</sub>, Nb, Zr, Y, Sr, Rb, Pb and Th.

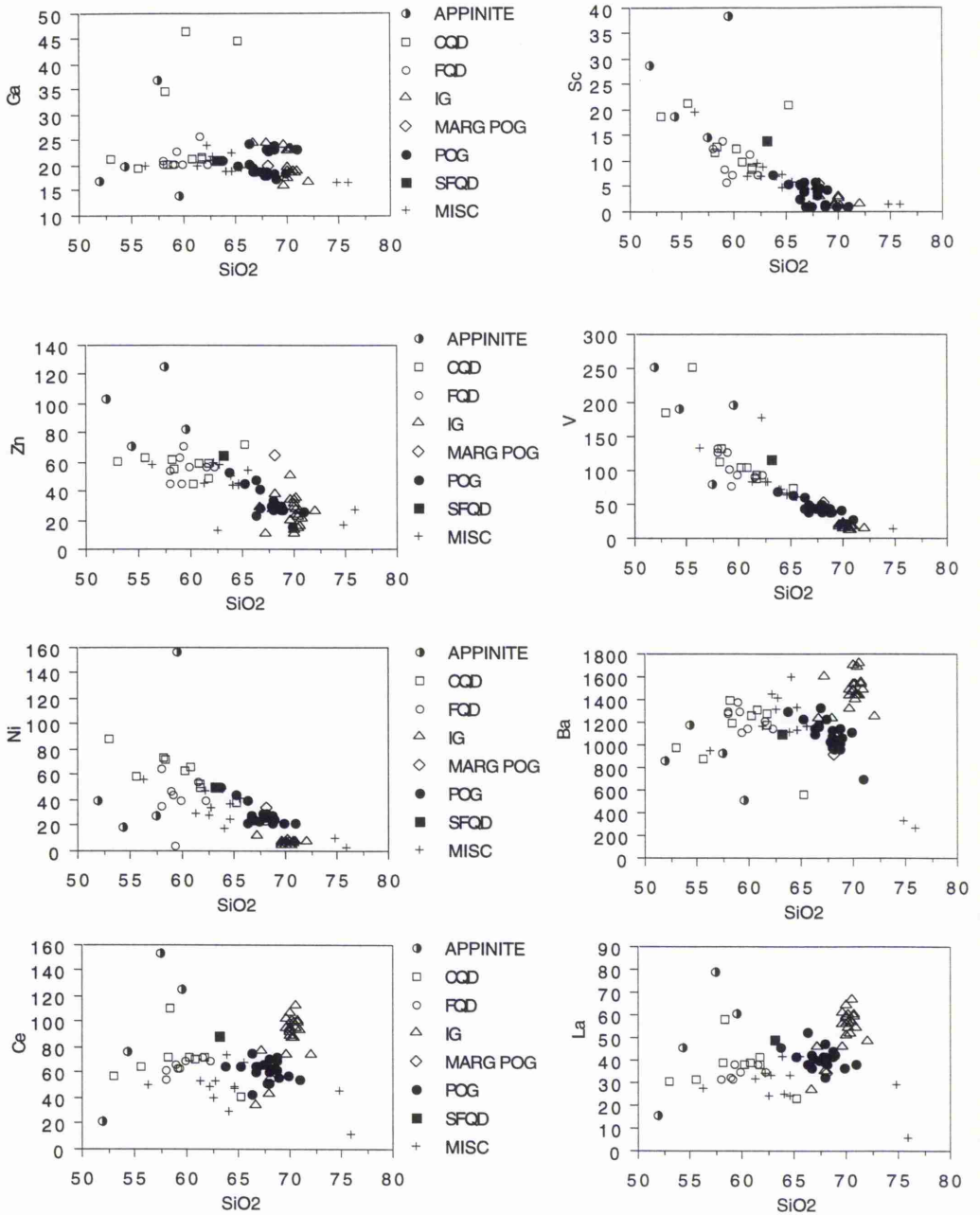


Fig. 6.2(continued) Harker diagrams for Ga, Zn, Ni, Ce, Sc, V, Ba and La.



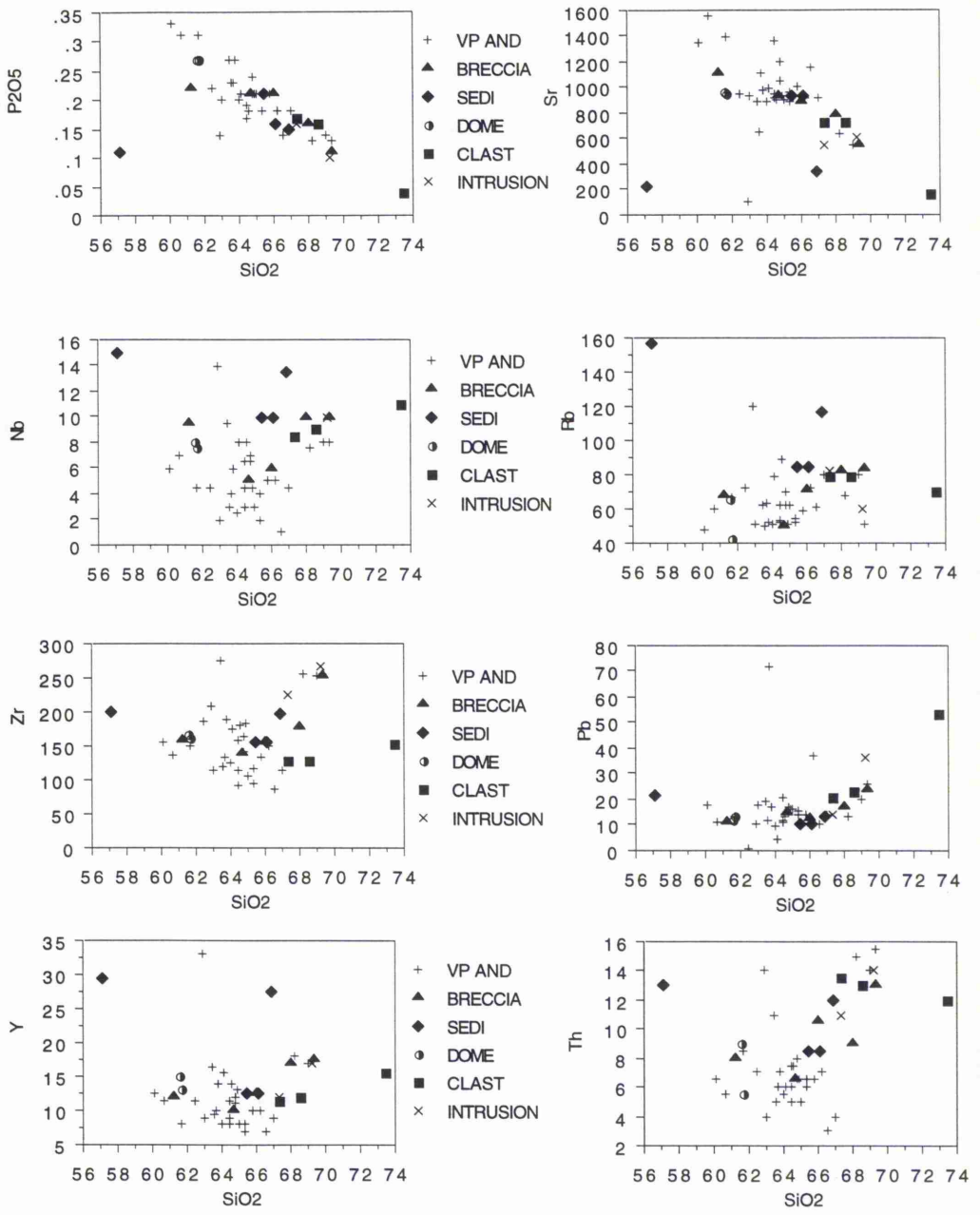


Fig. 6.3(continued) Harker diagrams for P<sub>2</sub>O<sub>5</sub>, Nb, Zr, Y, Sr, Rb, Pb and Th.

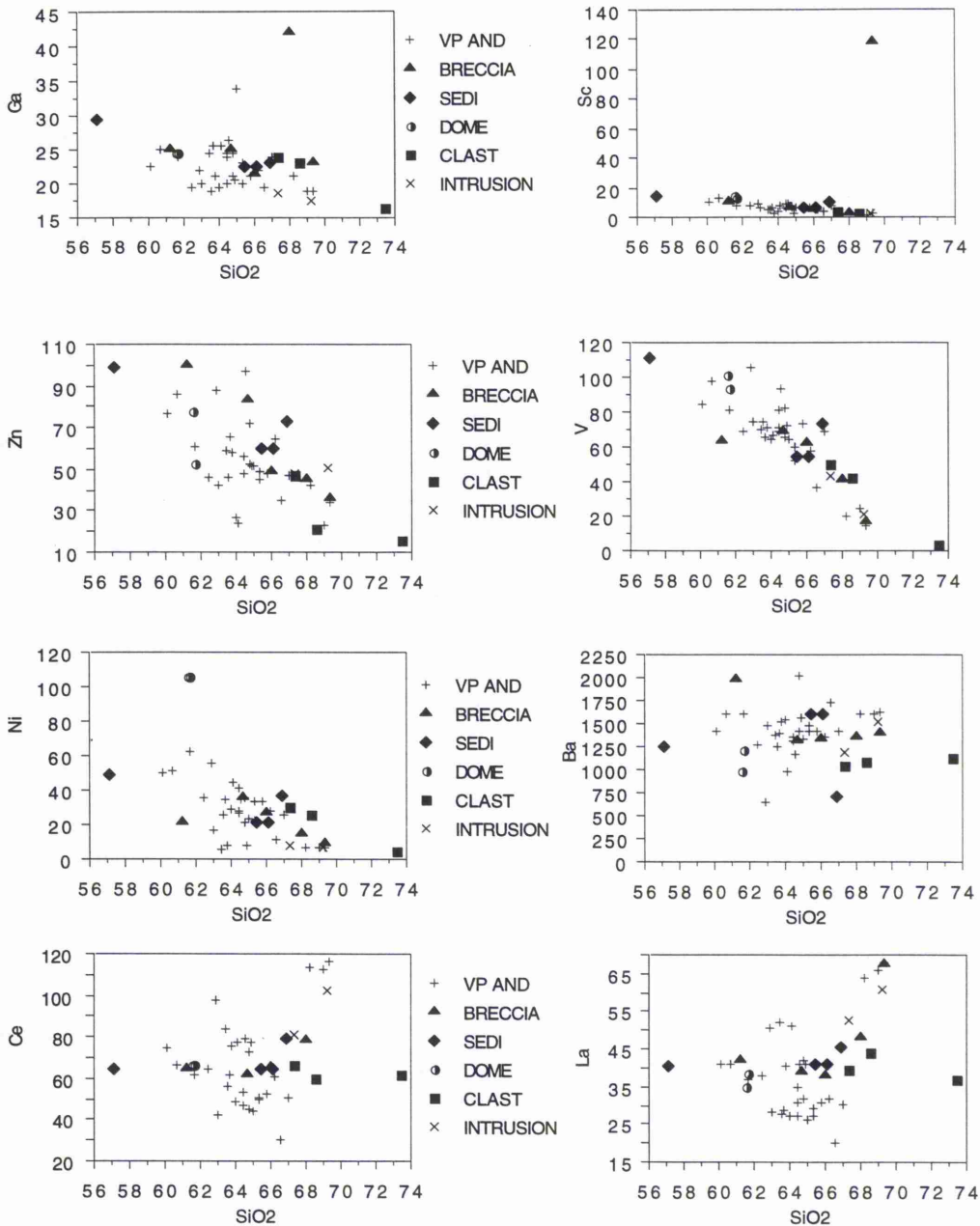


Fig. 6.3(continued) Harker diagrams for Ga, Zn, Ni, Ce, Sc, V, Ba and La.

### 6.2.3 Classification of the Ben Nevis Plutonic rocks

A variety of techniques using weight % oxide, normative composition (norms) and published modal analyses (modes) are applied to the Ben Nevis Complex. The results are discussed below.

#### 6.2.3.i AFM (Igneous) diagram

Samples from the Ben Nevis Complex were plotted on the AFM (igneous) diagram with Fe as FeO\* i.e. the total Fe content of a sample is expressed as FeO in accordance with the standard procedure of Rickwood (1989). No component of the Ben Nevis Complex shows iron enrichment, and the complex as a whole defines a typical calc-alkaline trend (Fig. 6.4). Overlap between volcanic and plutonic samples is almost total, suggesting a similar petrogenetic origin.

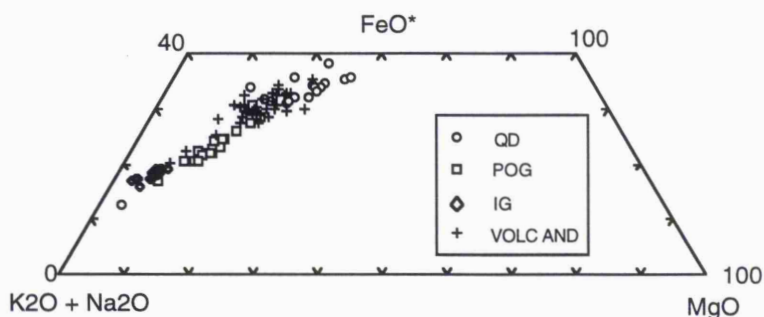


Fig 6.4 The AFM diagram for the Ben Nevis Complex which define a typical Calc-alkaline trend with no iron enrichment.

#### 6.2.3.ii R1-R2 multication diagram

Use of weight % oxide data and discriminant diagrams based on a subset of the major element or norm/mode data, has been criticised on the grounds that they do not represent the cation distribution of the magma or whole rock composition of the sample being analysed (Pearce 1969 and Wright 1974). For example, a rock of dacitic composition plots on the AFM (igneous) diagram using <15% of its whole rock chemistry. In order to surmount these problems, De la Roche et al. (1980) devised the R1-R2 multication classification diagram. This utilises all the major element data (expressed as millication proportions) and can be applied to the majority of igneous rock types. Formulae for the calculation of the two parameters are:

$$R1 = 4Si - 11(Na + K) - 2(Fe + Ti)$$
$$R2 = 6Ca + 2Mg + Al$$

The main drawbacks to use of this scheme are twofold; firstly, the two parameters have no immediate petrogenetic meaning, making the diagram and the results obtained difficult to comprehend, and secondly, field boundaries are curvilinear and therefore difficult to reproduce, particularly as De la Roche et al. (1980) neglected to publish the coordinates for the intersections between different fields.

Two trends are visible in Fig. 6.5; the first, expressed by the Outer Granite samples shows decreasing R2 with increasing R1 and the second, defined by the Inner Granite, shows approximately constant R2 with increasing R1. The range of R1 values is comparable to that of the Outer Granite.

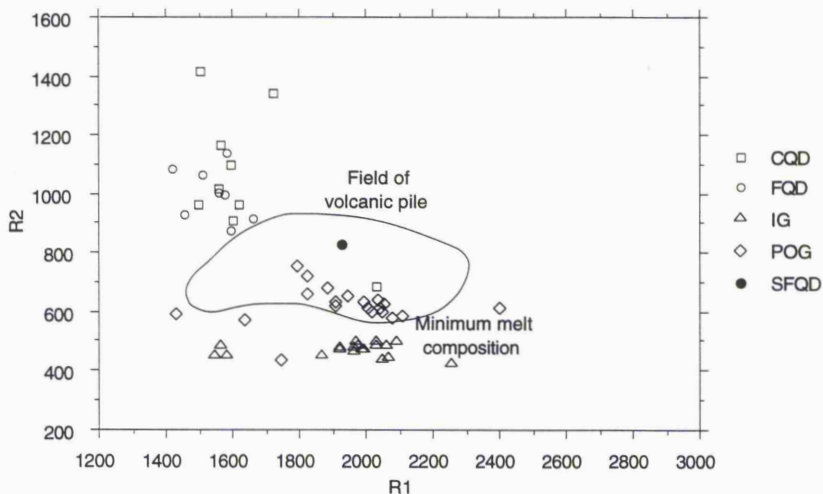


Fig. 6.5a R1-R2 multication diagram for the plutonic rocks.

The data presented here are comparable to that calculated from the analyses of Haslam (1968) by Batchelor & Bowden (1985). From this data, Batchelor & Bowden (1985) were able to show that the Inner Quartz Diorite (nomenclature of Haslam 1968) has lower R2 contents for a given R1 value than the Outer Quartz Diorite. Data from a larger number of quartz diorite samples presented in this study, obscures this relationship; in fact in general the Coarse Quartz Diorite has higher R2 values than the Fine Quartz Diorite and shows a large degree of scatter which is absent in the later Porphyritic Outer Granite and Inner Granite units. The more 'primitive' composition of the Coarse Quartz Diorite can be explained by mingling between the appinite and Coarse Quartz Diorite magmas, as the two samples (SURGE & BN174) with the highest R2 values are obtained from the zone of appinite/Coarse Quartz Diorite interaction in the vicinity of the surge chamber (chapter 4). Scatter is attributed to variations in R1 and R2 between separate pulses of the Fine Quartz Diorite and Coarse Quartz Diorite.

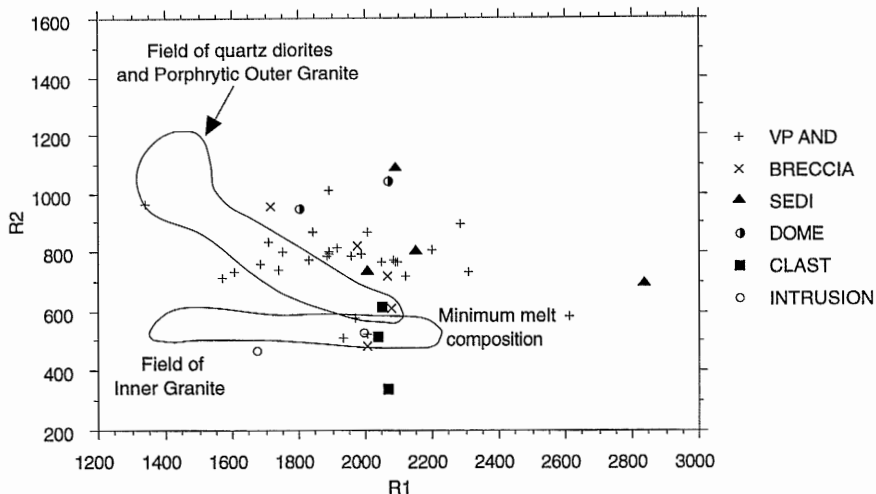


Fig. 6.5b R1-R2 multication diagram for the volcanic rocks.

Batchelor & Bowden (1985) examined the R1-R2 diagram in order to determine whether variations in these two parameters could be linked to petrogenetic models (such as fractional crystallisation, assimilation-fractional crystallisation, magma mixing/mingling, partial melting and crustal contamination). From plutons with a number of sequential 'intrusions', two trends were identified, a source trend producing decreasing R2 in successive intrusions, and a series trend developing shifts in both R1 (increasing) and R2 (decreasing). After discussing the various petrogenetic processes, Batchelor & Bowden (1985) concluded that the source trend resulted from the progressive addition of crustal partial melts to a high alumina basaltic source magma. Crystal fractionation was believed to be the process behind development of the series trend.

On the R1 and R2 diagram, the Fine Quartz Diorite and Coarse Quartz Diorite range between monzodiorite through tonalite to granodiorite whereas the Porphyritic Outer Granite falls in the tonalite and granodiorite fields. The Inner Granite ranges between quartz monzonite and monzogranite. Both granites trend toward the minimum melt composition of Tuttle & Bowen (1958).

### 6.2.3.iii I- and S-type classification

In normative mineral calculations, the presence of alumina in excess of that required to combine with  $\text{Na}_2\text{O}$ ,  $\text{K}_2\text{O}$  and  $\text{CaO}$  to form feldspar is assigned to corundum. If  $\text{CaO}$  is in excess of that required to bind with alumina to form feldspar, it is assigned to diopside. Diopside normative rocks cannot, therefore, also have corundum in the norm and vice versa. Plotting diopside and corundum against  $\text{SiO}_2$  (Fig. 6.6) illustrates the degree of alumina saturation in the Ben Nevis Complex. This diagram is the equivalent of the A/CNK

$(Al_2O_3/[CaO + Na_2O + K_2O])$  value where  $A/CNK > 1$  demonstrates excess alumina. Fractional crystallisation leads to relative increases in  $Na_2O$  and  $K_2O$ ; hence, the Ben Nevis Complex magmas trend from diopside normative to corundum normative compositions.

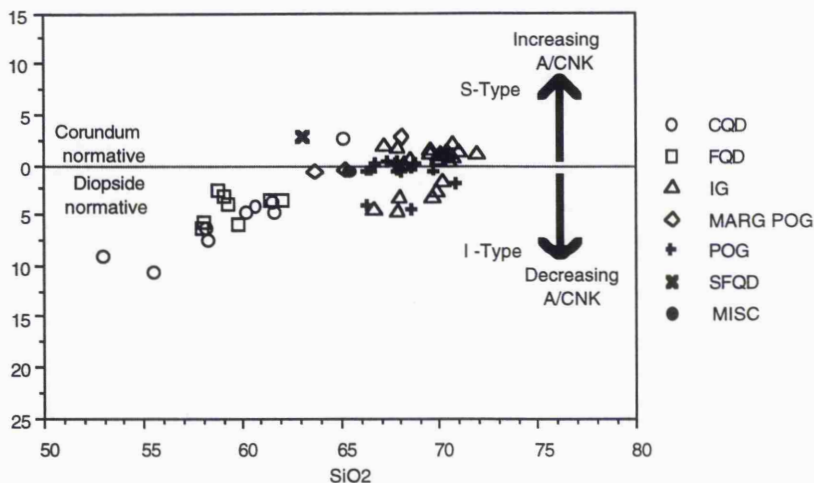


Fig 6.6 Corundum and Diopside normative compositions for the plutonic rocks of the Ben Nevis Complex.

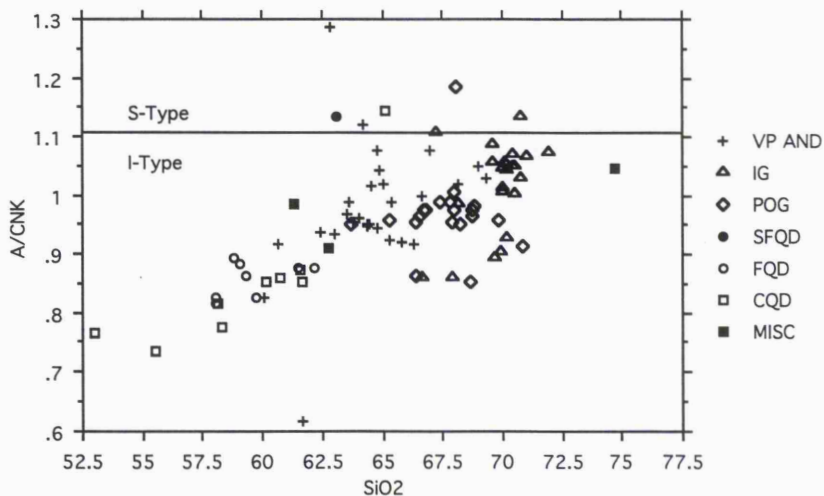


Fig. 6.7  $A/CNK$  for the Ben Nevis Complex. An  $A/CNK$  value of 1.1 approximates to a corundum normative value of 1%.

Normative corundum values  $>1\%$  characterise granite as S-type (Chappell & White 1974), (the equivalent A/NCK value is 1.1, see Fig. 6.7) The majority of the Ben Nevis Complex samples have corundum  $<2\%$  and are therefore not strongly peraluminous or strongly S-type in character (Chappell & White 1974). The trend from I-type to weakly S-type is common throughout the Newer Granites of Northern Britain and there are relatively few examples of strongly S-type granites (Stephens & Halliday 1984).

Two further geochemical plots confirm an I-type classification for the Ben Nevis Complex. On a  $\text{Na}_2\text{O}$ - $\text{K}_2\text{O}$  plot (Fig. 6.8), the Ben Nevis data fall entirely within the I-type granite field of Chappell & White (1984). From Fig. 6.9 it is evident that the Ben Nevis magmas are metaluminous I-type granites.

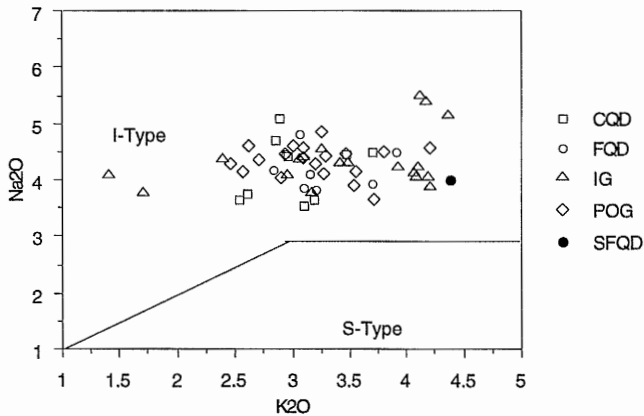


Fig. 6.8  $\text{K}_2\text{O}$  v  $\text{Na}_2\text{O}$  for the plutonic rocks. Fields for I-Type and S-Type compositions from Norman et al. (1992).

A subset of samples in Fig. 6.9 from the Porphyritic Outer Granite (BN321, BN323POG & BN327) and Inner Granite (OBN36, BN315, BN316 & BN326) plot with low A/CNK and low A/NK. This is reflected in major element chemistry by abnormally high  $\text{Na}_2\text{O}$  contents ( $>5\%$  as compared to  $<4.5\%$ ). The same samples have elevated Ga contents and both the Porphyritic Outer Granite and Inner Granite samples cluster in the same area of Ga and  $\text{Na}_2\text{O}$  Harker diagrams. Fig. 6.10 is a plot of Ga against  $\text{Al}_2\text{O}_3$ , a distinct split in the data is visible between high Ga and low Ga samples; arguably, the high Ga samples have slightly lower  $\text{Al}_2\text{O}_3$  contents. In most geochemical processes, Ga closely follows Al (Gottardi et al. 1972), although the difference in atomic radii results in stronger Al bond formation and consequently, Ga tends to accumulate into later magmatic products and residual minerals. However, in the Ben Nevis Complex, the high Ga samples have similar  $\text{SiO}_2$  contents to the low Ga samples and consequently, magma fractionation cannot be the cause of Ga enrichment in this case. Wager & Mitchell (1951) showed that Ga increased dramatically in the latest plagioclase of the Skaergaard intrusion, and Walenczak (1959) demonstrated that the Ga/Al ratio of plagioclase was at least double that of the same ratio in K-feldspar. Ga and  $\text{Na}_2\text{O}$  enrichment can therefore be explained by late stage albitisation of plagioclase in the Porphyritic Outer Granite and Inner Granite. In thin section, high Ga samples have higher

plagioclase contents and lower K-feldspar. An albite rich rim is often developed throughout the plutonic rocks (chapter 5) and it is suggested that development of an albite rich rim is more extensive in the high Ga samples than in the low Ga samples. There is no geographical pattern to the distribution of high Ga and Na<sub>2</sub>O samples and localised variations in the abundance of Cl, F and B may have contributed to locally increased Ga contents in the circulating fluids (Goldschmidt 1954).

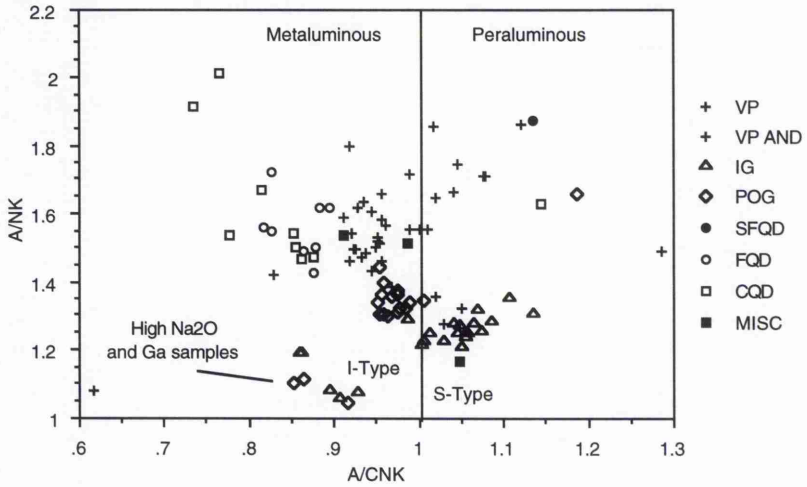


Fig 6.9 Shand's Index. The peralkaline field fall below A/NK = 1. The Ben Nevis Complex is mildly S-type and the Inner Granite is peraluminous.

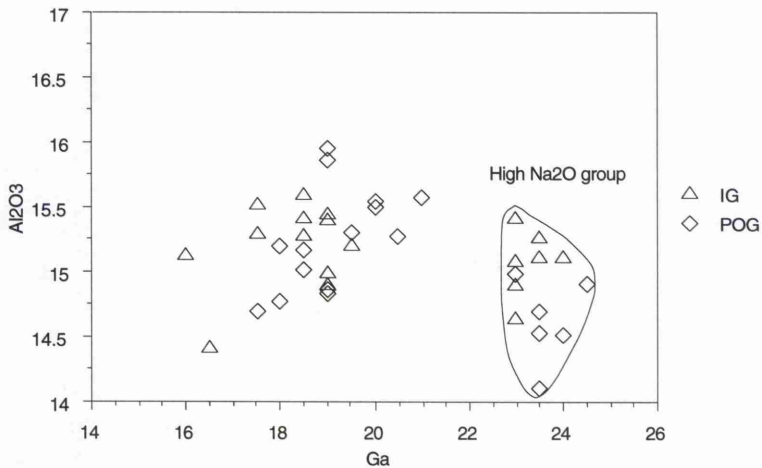


Fig. 6.10 High Ga abundance is illustrated for those samples of the Porphyritic Outer Granite and Inner Granite with anomalously high Na<sub>2</sub>O.

High Ga/Al ratios are typical of A-type granites (Whalen et al. 1987); however the Ben Nevis samples with high Ga do not have A-type characteristics e.g.  $(\text{Ga}/\text{Al} \times 10000) < 3$  whereas A-type granites have  $(\text{Ga}/\text{Al} \times 10000) > 3$ . (Whalen et al. 1987).

#### 6.2.3.iv Norm calculations

CIPW Norm calculations often do not match the observed mineralogy. Norms are calculated on the assumptions that the magma was anhydrous, and minerals such as amphibole and biotite are not permitted, that the  $\text{Fe}/(\text{Fe}+\text{Mg})$  ratio of all mafic minerals is the same, and no provision is made for minor solid solution between Al and Ti in mafic minerals. K in biotite is assigned to orthoclase, artificially increasing the proportion of this mineral relative to the mode. These are all causes of variation between the observed mode and the calculated norm.

The closest agreement between modal and normative feldspar composition is found by assuming that all albite in the norm is found as plagioclase in the mode. Norm calculations for the Inner Granite achieve the closest comparison with the mode due to the fact that it has the lowest proportion (<10%) of the hydrous minerals biotite and hornblende (biotite only in this case).

Both of the lamprophyre samples (BN391 and BN400) are nepheline normative. Calcic-amphibole is also nepheline normative, and it is believed that the large proportion of amphibole in these samples is the cause of nepheline normative compositions.

#### 6.2.3.v QAPF

When plotted on the QAPF tetrahedron (Fig. 6.11) of Le Bas & Streckeisen (1991), the plutonic rocks range from monzodiorite through granodiorite/quartz monzodiorite to granite (monzogranite). Modal data of Haslam (1968) range from tonalite/quartz diorite/gabbro through quartz monzodiorite to quartz monzonite (Fig. 6.11). Comparison between the two data sets highlights the increase in normative orthoclase due to the assignment of K from biotite to normative orthoclase. This is particularly noticeable in the Fine Quartz Diorite, Coarse Quartz Diorite and Sgurr Finnisg-aig Quartz Diorite.

#### 6.2.3.vi An-Ab-Or

An An-Ab-Or classification diagram based on Barth-Niggli molecular norms was developed by O'Connor (1965) for felsic rocks with >10% normative quartz. The diagram is based entirely on normative feldspar compositions recast to 100%, and represents projection of the data from the quartz apex onto the feldspar face of the Q-Ab-An-Or granite tetrahedron. Although, the Ben Nevis Complex data are plotted using CIPW norms, the deviation between Barth-Niggli and CIPW norms on the An-Ab-Or projection is less than 2% (Rollinson 1993). Barker (1979) modified the field boundaries of O'Connor (1965) and it is onto this modified version that the samples from Ben Nevis Complex are plotted (Fig. 6.12). This diagram represents a more accurate method of estimating feldspar

composition than a modal classification (Rollinson 1993) as it reflects any solid solution between the two feldspar types.

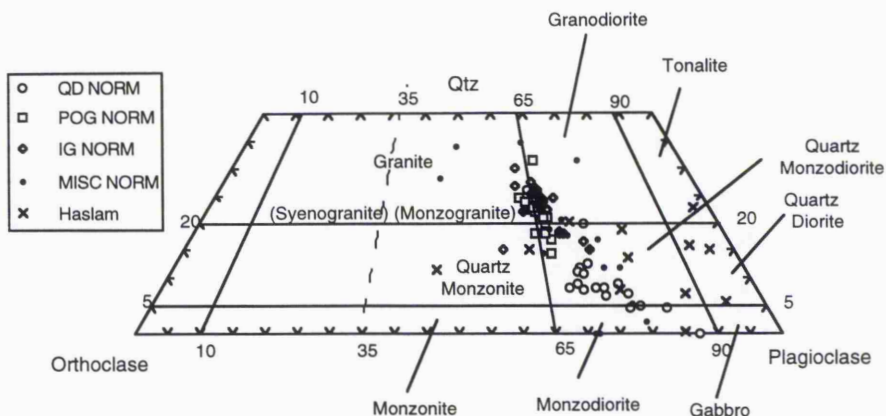


Fig 6.11 Normative compositions for the intrusive members of the Ben Nevis Complex are plotted on the QAPF classification scheme of Le Bas & Streckeisen (1991). The modal analyses of Haslam (1968) are plotted for comparison.

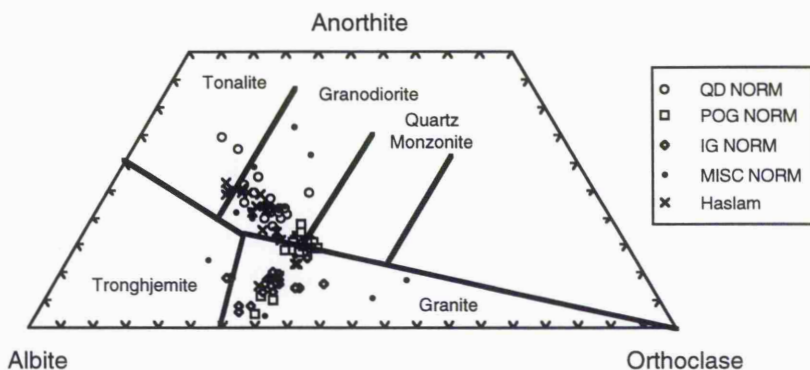


Fig 6.12 Classification of the Ben Nevis intrusive rocks on Barker's (1979) modification of O'Connor (1965). CIPW norms are also plotted for the samples of Haslam (1968).

The majority of Ben Nevis Complex plutonic rocks have normative quartz > 10%; the exceptions to this rule are a number of dyke samples, the Fine Quartz Diorite and the Coarse Quartz Diorite. BN68b, identified as crustally contaminated (chapter 5), is the only sample of Coarse Quartz Diorite with normative quartz > 10%; the Sgurr Finnisg-aig Quartz Diorite also has normative quartz > 10%, highlighting the difference between the Sgurr Finnisg-aig Quartz Diorite and the Fine Quartz Diorite and Coarse Quartz Diorite units.

The Ben Nevis Complex data trend from granite through granodiorite to tonalite (Fig. 6.12). A distinct elbow in the data is located at the quartz monzonite-granodiorite-granite join and effectively separates the Outer Granite from the Inner Granite. For samples other than the Fine Quartz Diorite and Coarse Quartz Diorite classification of the Ben Nevis data, using the modified O'Connor (1965) scheme, yields similar results to the QAPF classification scheme when applied to the data of Haslam (1965) (Fig. 6.11).

#### 6.2.3.vii Classification of the Plutonic Rocks

Using a combination of the modified O'Connor (1965) An-Ab-Or discrimination diagram (Fig. 6.12), the Le Bas & Streckeisen (1991) QAPF diagram (Fig. 6.11) and the De la Roche et al. (1980) R1-R2 multication diagram (Fig. 6.5), the plutonic rocks of the Ben Nevis Complex can be classified as:

- 1) Fine Quartz Diorite and Coarse Quartz Diorite are identified as quartz diorites and quartz monzodiorites with rare tonalite and granodiorite.
- 2) Samples from the Sgurr Finnisg-aig Quartz Diorite and Porphyritic Outer Granite are defined as tonalites and granodiorites.
- 3) The Inner Granite ranges between quartz monzonite and monzogranite.

#### 6.2.4 Tectonic discrimination from granitoid chemistry

Relatively few tectonic discrimination diagrams have been published for granitic rocks. Two reasons for this apparent lack of attention are; firstly, by the time granite is exposed at the surface unambiguous evidence of the tectonic environment into which it was intruded has been removed by erosion. Secondly, the petrogenetic history of granite is complex; crystal accumulation, crustal contamination, magma mingling, volatile fluxing, late stage fluids, etc all contribute to complicate the tectonomagmatic interpretation of granite.

Pearce et al. (1984) presented a scheme based on the elements Rb, Y, Nb, Yb and Ta. New chemical analyses from the Ben Nevis Complex include a subset of these elements, namely Rb, Y and Nb. The discriminant diagrams of Pearce et al. (1984), although based on empirical observations, were shown by geochemical modelling to have a theoretical basis in the different petrogenetic pathways traced by granites from different tectonic settings. No field was presented for post-orogenic granites.

Data from the Ben Nevis granites lie within the volcanic arc field in Rb-(Y+Nb) space (Fig. 6.13a) and also in Y-Nb space (Fig. 6.13b). In Fig. 6.13a, the Ben Nevis samples lie close to the volcanic arc-within plate-syn-collision join.

A discrimination scheme for igneous rocks with >60% SiO<sub>2</sub> was published by Maniar & Piccolo (1989). Several bivariate chemical plots are utilised until, by a process of elimination, a single tectonic setting is reached. In this scheme, the Ben Nevis data

consistently plot within the island arc - volcanic arc - continental collision fields (e.g. Fig. 6.14a and 6.14b).

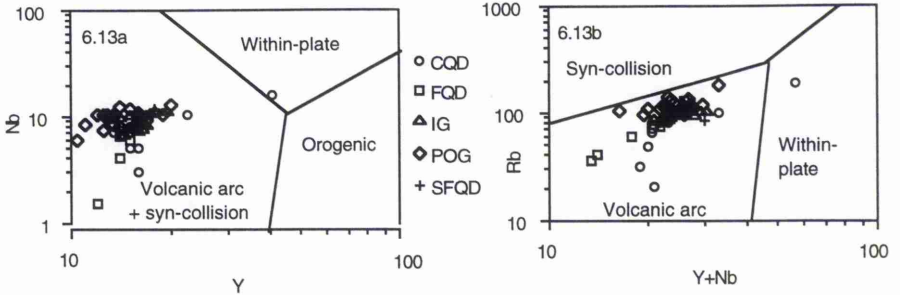


Fig. 6.13a and 6.13b. Tectonic discrimination of the Ben Nevis plutonic rocks according to the discrimination diagrams of Pearce et al. (1984).

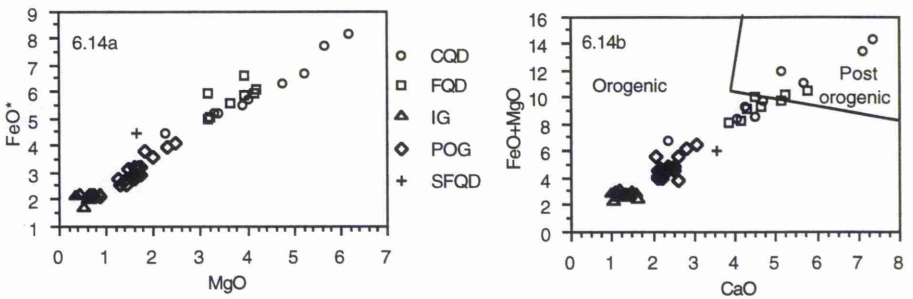


Fig. 6.14a and 6.14b. Tectonic discrimination of the Ben Nevis plutonic rocks according to the discrimination diagrams of Maniar & Piccoli (1989). In 6.14a, the plutonic rocks have  $FeO^* < 10\%$  and therefore fall within the orogenic field with no overlap into other tectonic fields. In 6.14b, the plutonic rocks overlap slightly with the post-orogenic field.

These two discrimination schemes suffer from the inability to discriminate post collision granites from those from other tectonic settings. Independent geological evidence (Watson 1984) reveals that the Newer Granite plutons of Northern Britain were intruded after subduction along the lapetus suture had ceased. Maniar & Piccoli (1989) suggested that post orogenic granites can be distinguished from other granites by virtue of the fact that they trend across field boundaries; Pearce et al. (1984) stated that post orogenic granites lie near the top of the volcanic arc field (in  $Rb-[Y+Nb]$ ) or span field boundaries. Difficulties in defining a scheme which discriminates between post-collision and granites from other settings, stems from the fact that they are very often mixtures of mantle and crustal partial melts.

Batchelor & Bowden (1985) subdivided the R1-R2 multication diagram into a number of fields representing separate tectonomagmatic environments. Data from the Outer Granite fall within the post-tectonic field (group 3), and that from the Inner Granite falls within the late orogenic field (group 4). A comparison with the Etive complex reveals a

similar pattern (Batchelor & Bowden 1985) with the Outer Granite of the Ben Nevis Complex comparable to the Cruachan granite and the Inner Granite to the Starav granite.

Tectonic discrimination of the Ben Nevis Complex granites on the basis of their geochemistry is equivocal. Although the data plot within the fields of arc-related granites in the schemes of Pearce et al. (1984) and Maniar & Piccoli (1989), so do post orogenic granites. The Ben Nevis data do not fall into the field of post orogenic granite described by Maniar & Piccoli (1989), but this field is derived from a limited data set that does not include samples from the Caledonian orogeny. The R1-R2 scheme of Batchelor & Bowden (1985) appears to fit the geological interpretation of Watson (1984) for intrusion of the Newer Granites after subduction had ceased. This may however, merely reflect the fact that the fields were drawn from data obtained largely from Caledonian granites.

There is an inherent danger in designing tectonomagmatic discrimination diagrams for granitic rocks given the variety of different petrogenetic pathways available to these rocks. Diagrams based on a globally limited (though regionally extensive) data set may not encompass all the possible granite compositions particular to a specific tectonic environment. The Ben Nevis Complex data proves this for the Maniar & Piccoli (1989) scheme where these post orogenic granites plot outside the post-orogenic field of these authors.

## 6.2.5 Classification of the Ben Nevis volcanic rocks

### 6.2.5.i The IUGS TAS classification

Classification of the volcanic rocks is based on the chemical composition of fresh specimens using the TAS (total alkalis vs silica) classification diagram published by Le Maitre et al. (1989) on behalf of the IUGS.

The volcanic rocks have variously been described as andesite (Teall 1888 and Maufe 1910) and rhyodacite (Haslam 1968). However, the range of compositions is in fact greater than previously believed and the larger data set presented in this study (Fig. 6.15) range from trachyandesite/andesite to trachyte/dacite.

### 6.2.5.ii Discrimination according to trace element variations

Discrimination diagrams for volcanic rocks, based on the abundances of Ti, Zr, Y, Nb, Ce, Ga and Sc, have been presented by Winchester & Floyd (1977). Unlike  $K_2O$  and  $Na_2O$ , these elements are generally considered to remain immobile during secondary alteration processes unless circulating fluids contain high activities of complexing agents such as F (Pearce & Norry 1979).

A selection of diagrams based on Winchester & Floyd (1979) is presented in Fig 6.16. The Ben Nevis data consistently trend from andesite to dacite-rhyodacite and do not cross into the alkaline fields. On the TAS diagram of Le Maitre et al. (1989) the Ben Nevis

volcanic data are shown to be mildly alkaline, and span the divide between the calc-alkaline and alkaline series (Fig. 6.15). One reason for the discrepancy between these two classification schemes is that the field boundaries for volcanic rocks in the diagrams of Winchester & Floyd (1977) are not compatible with those of the TAS diagram. For instance, rhyolite in the diagrams of Winchester & Floyd (1977) has  $\text{SiO}_2 > 72\%$  whilst in the TAS diagram the lower limit is 69%.

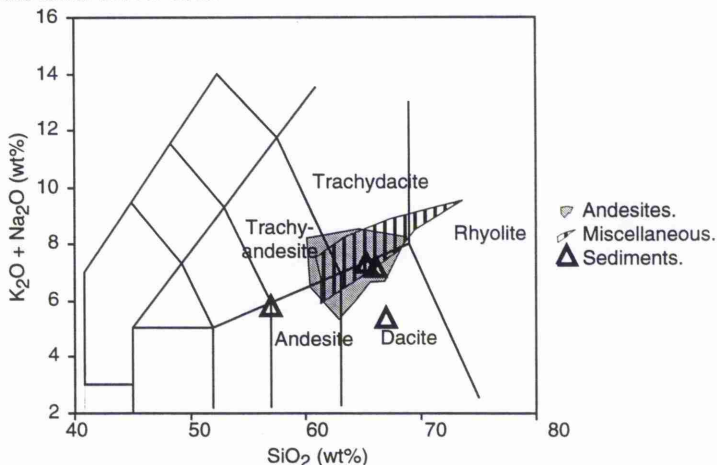


Fig 6.15 Total alkali vs  $\text{SiO}_2$  classification diagram for the volcanic rocks of the Ben Nevis Complex. Field boundaries are from Le Maitre et al. (1989).

### 6.2.5.iii R1-R2 multication diagram

On the R1-R2 multication diagram (Fig. 6.5b) of De la Roche et al. (1980), the samples from the volcanic pile plot midway between the Outer Granite and Inner Granite trends with approximately constant R2 and increasing R1. This would suggest that, if the progression of Batchelor & Bowden (1985) is accepted (decreasing R2 with time), the volcanic pile was extruded after intrusion of the Outer Granite but prior that of the Inner Granite. Field evidence, however, suggests that the volcanic pile was extruded either shortly before intrusion of the Outer Granite or early in its formation (chapter 3).

The source trend of Batchelor & Bowden (1985) is based on contamination of an alumina rich basaltic parent magma by an increasing proportion of crustal melts. This model cannot work for the Ben Nevis Complex, where the earliest magmas (near source andesites) have compositions midway between the intermediate (Outer Granite) and final magmatic (Inner Granite) events in R1-R2 space. If high R2 values are indicative of a high mantle contribution, then samples obtained from the intrusive dome (chapter 3), with the highest Ni and MgO contents of the volcanic pile, should have more mantle-like isotopic signatures than the more evolved clast (CL) with low R2. Additionally, the quartz diorites should also have more mantle-like signatures than the Inner Granite. Neither of these statements is correct and the R1-R2 diagram should not be used to model magmas without isotopic evidence to support any conclusions.

In Fig. 6.5, it is evident that the intrusions (BN259 & INT) have similar R1 & R2 to the Inner Granite. This is not surprising given the fact that these intrusions are injections of the Fault facies tuffisite within the volcanic pile and that the Fault Facies is a slightly more basic version of the Inner Granite.

The sediments have a similar geochemistry to the andesites, indicating that these rocks contain a substantial proportion of volcanic ash most likely from the same volcanic centre as the andesites. Also plotting with similar values to the andesites are the samples obtained from the volcanic breccias. Individual clasts from these breccias plot with lower R2 values than the main andesite trend. Two of these samples (BN288a and BN288b) are derived from a distinctive feldspar porphyry bearing volcanic breccia. The clasts are similar in geochemistry, and it is suggested that these were derived from a volcanic dome near or within (i.e. blocking) the source vent of the host volcanic breccia. The fact that all the clasts obtained from the volcanic breccias (BN288a, BN288b and CL) plot with low R2 may indicate that the volcanic source produced high silica magma domes which partially blocked the vent before being excavated by subsequent explosive nuées ardentes style eruptions.

The two samples from the intrusive dome have slightly higher R2 values corresponding to higher MgO, CaO and Ni abundances, indicating a relatively primitive origin. A number of andesite samples have slightly lower R2 than the main andesite trend (83BN1, 83BN2, BN247 and BN206). These are found at both the top and the base of the volcanic pile and once again illustrate the absence of spatial or temporal chemical trends in the volcanic pile. The Ben Nevis volcanics are near source lavas flows and lava domes. If they were all extruded from the same vent, then the magma chamber source to this vent underwent continuous fractionation, extrusion and replenishment.

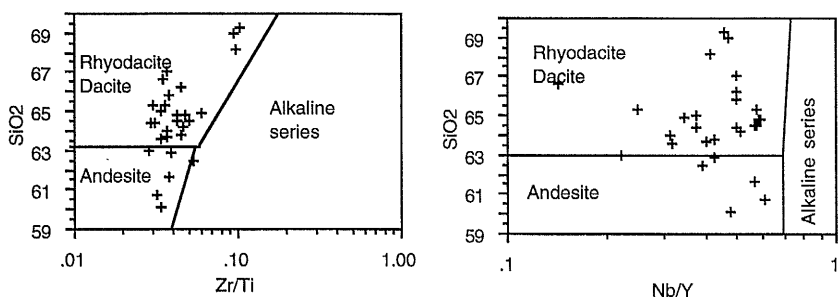


Fig. 6.16 Two of the classification diagrams of Winchester & Floyd (1977) and applied to the volcanic rocks of the Ben Nevis Complex.

Diopside-corundum vs silica (Fig. 6.17) reveals a similar pattern to the granites and a similar interpretation is inferred. BN247 has a large corundum content relative to the rest of the andesite samples; it is not clear why, though increased crustal contamination is

suspected. BN245 reveals relatively high normative diopside; this is explained by high CaO, MgO and Ni contents and suggests that this sample is relatively primitive.

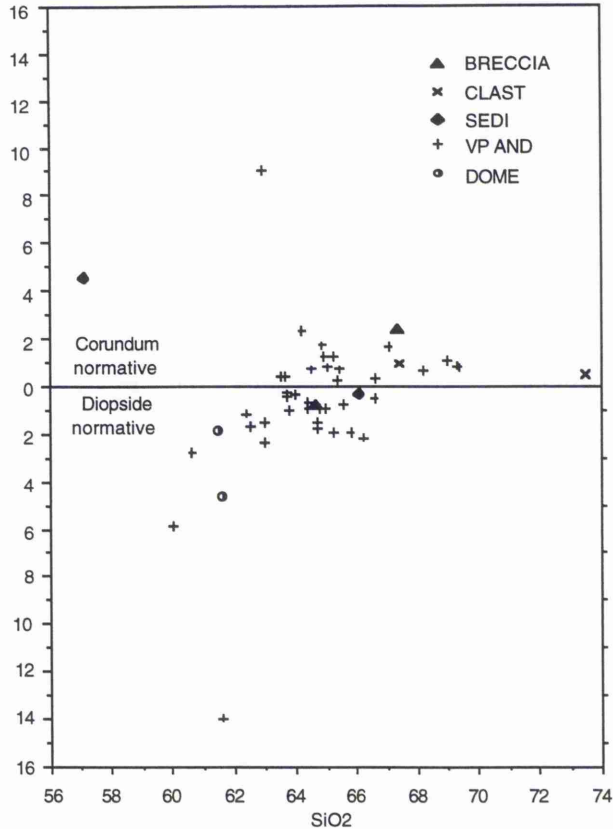


Fig. 6.17 Diopside and corundum normative compositions of the volcanic pile. Compare with the same diagram for the plutonic rocks (Fig 6.8).

### 6.3 Comparison with experimental studies on Granite systems

In pure Ab-Or-Q-H<sub>2</sub>O experiments, increasing pressure causes the quartz-feldspar boundary to migrate from the quartz apex towards the albite apex on the anhydrous base in the Ab-Or-Q-H<sub>2</sub>O tetrahedron. Although these experiments are based on pure end-member compositions (i.e. no anorthite, or mafic minerals and water saturated), Tuttle & Bowen (1958) showed that natural rock systems with more than 80% normative quartz + albite + orthoclase closely followed the experimental results. The Ben Nevis samples with >80 wt% normative quartz + albite + orthoclase include most of the Porphyritic Outer Granite, all the Inner Granite and a few samples from the andesites of the volcanic pile. All the Ben Nevis data are plotted on Fig. 6.18 and whilst the more mafic samples fall below the 80% cut-off, a trend in the data is visible at roughly the same location as the 'thermal trough' of Tuttle & Bowen (1958). The data trend towards the experimentally determined 1kbar minimum and

demonstrates the high level of the Ben Nevis magma chamber. The trend lines on Fig. 6.18 are not fractionation trends and are merely presented in order to illustrate the overall sense of convergence toward the 1kbar minimum.

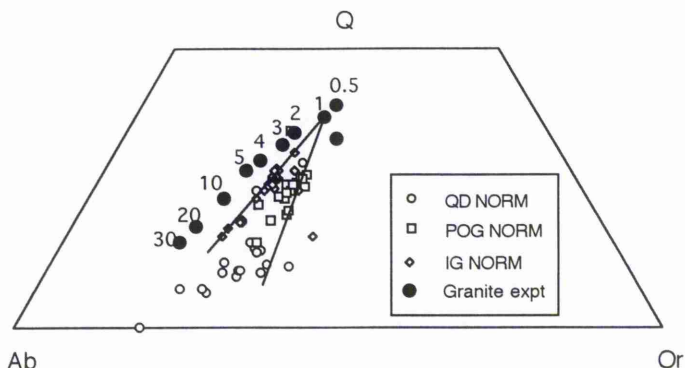


Fig. 6.18 The Ben Nevis plutonic rocks trend toward the 1Kbar minimum composition. Experimental data from Schairer & Bowen (1935), Tuttle & Bowen (1958), Steiner et al. (1975), Luth et al. (1964) and Huang & Wyllie (1975).

#### 6.4 Spidergrams

Normalised multi-element variation diagrams or spidergrams, are based on a grouping of a number of incompatible (bulk distribution coefficient  $<1$ ) elements normalised to estimates of their abundances in primordial mantle (e.g. Wood et al. 1979), chondrite (e.g. Sun 1980) and MORB (e.g. Pearce 1983). Arc related magmas are believed, at least in part, to have been derived from depleted MORB-like mantle, therefore the Pearce (1983) MORB-normalised spidergram is the one onto which the data from Ben Nevis are plotted (Figs. 6.19a and 6.19b). In this diagram, the elements are subdivided into two groups and arranged such that the incompatibility of both groups increases from the margin toward the centre. Elements with large ionic potentials are plotted on the left hand side of the diagram (Sr - Ba). Ionic potential is a measure of an elements mobility in the presence of aqueous fluids. The second group, on the right hand side of the diagram (Th - Ni), are immobile in aqueous fluids and the bulk distribution coefficient between garnet lherzolite and small degree partial melts is used to determine the incompatibility of an element and its order on the spidergram.

Spidergrams for the Ben Nevis Complex are presented in Fig. 6.19a-h; the average composition of each component to the Ben Nevis Complex is presented in Fig. 6.19i. Apart from scatter in the Sc and Ni positions, the patterns for the Ben Nevis Complex are extremely uniform. Notably, the sediments of the volcanic pile are indistinguishable from the igneous rocks; obviously these fine grained muds must contain a large component of volcanic ash.

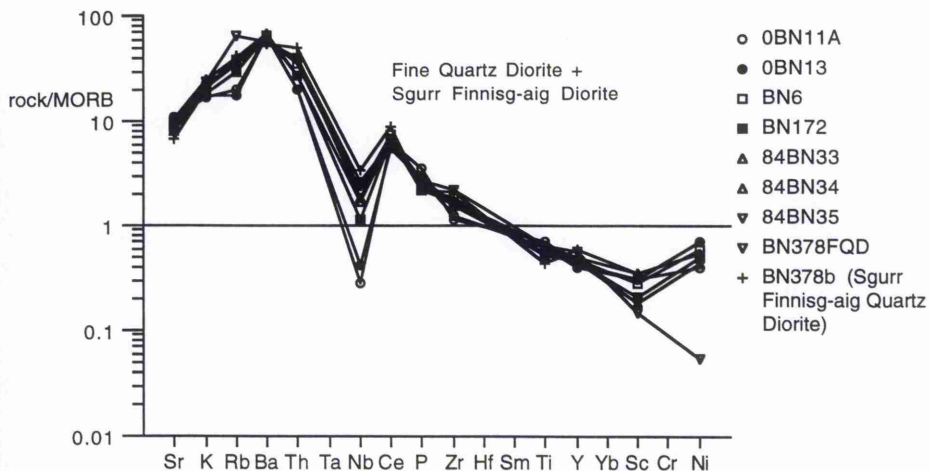


Fig 6.19a Spidergrams for the Fine Quartz Diorite and Sgurr Finnisg-aig Diorite of the Ben Nevis Complex, normalised against the MORB composition of Pearce (1983).

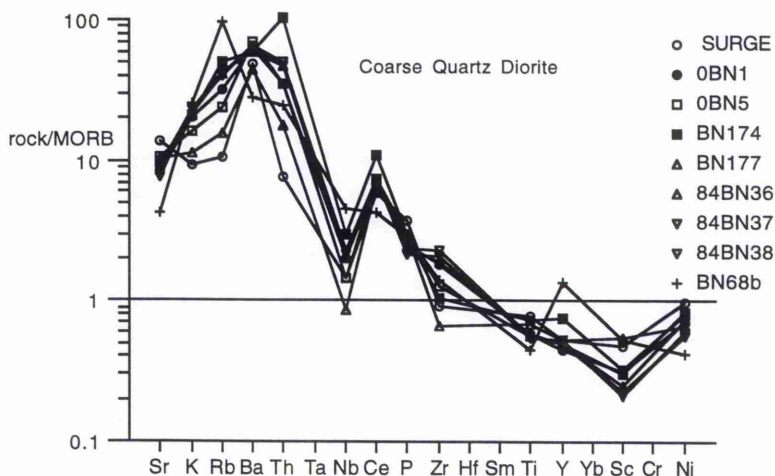


Fig. 6.19b Spidergrams for the Coarse Quartz Diorite of the Ben Nevis Complex normalised against MORB composition of Pearce (1983).

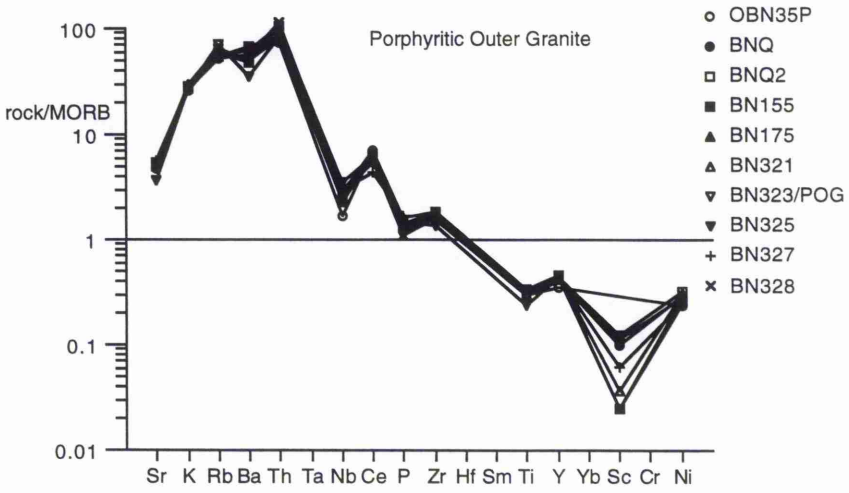
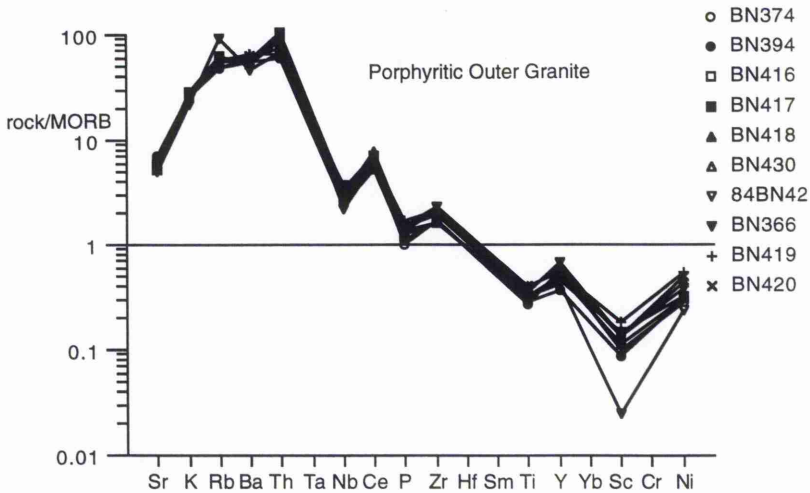


Fig. 6.19c Spidergrams for the Porphyritic Outer Granite of the Ben Nevis Complex, normalised against the MORB composition of Pearce (1983).

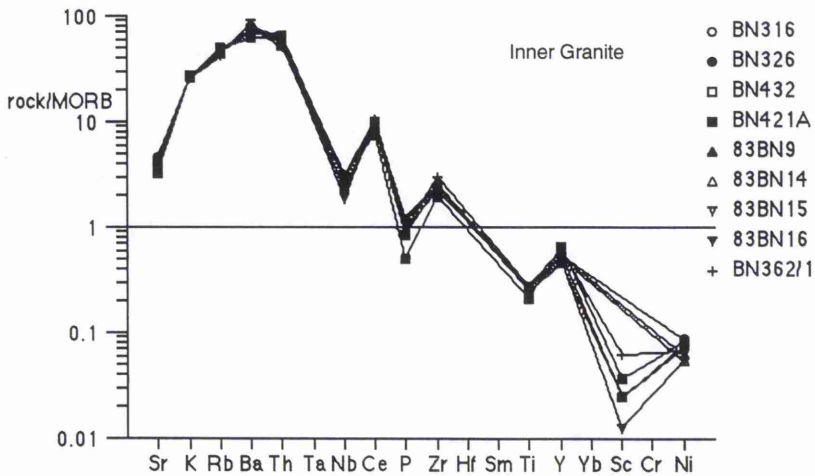
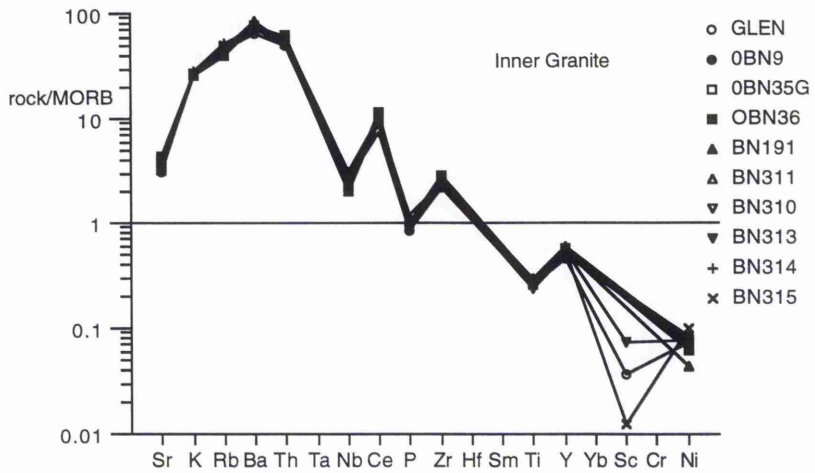


Fig 6.19d Spidergrams for the Inner Granite of the Ben Nevis Complex, normalised against the MORB composition of Pearce (1983).

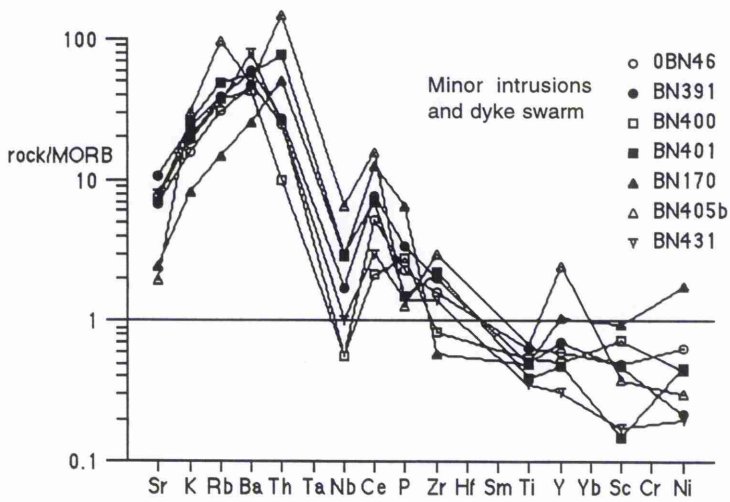
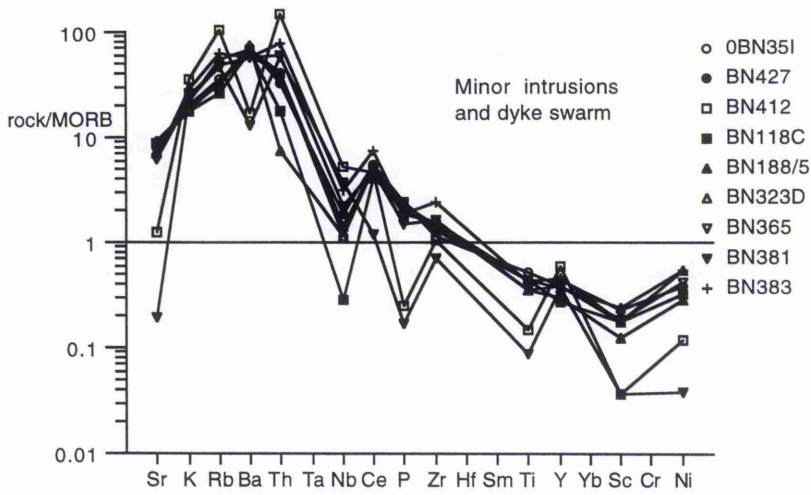


Fig. 6.19e Spidergrams for the minor intrusions of the Ben Nevis Complex and for members of the Ben Nevis Dyke swarm, normalised against MORB composition of Pearce (1983).

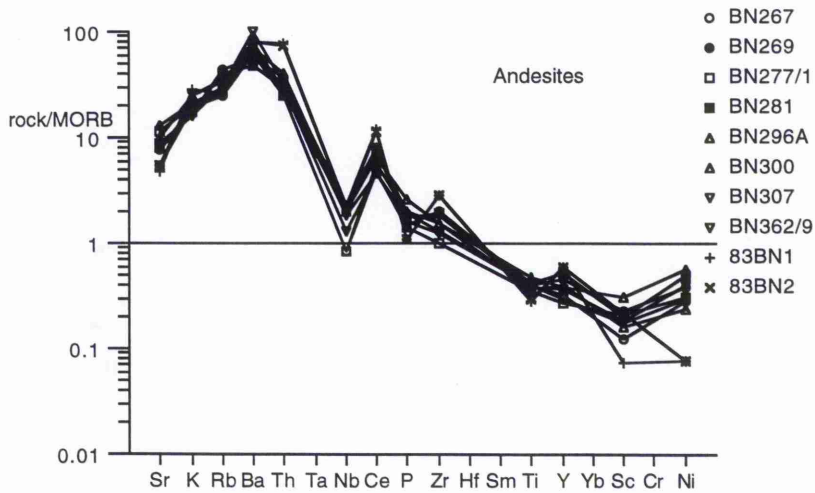
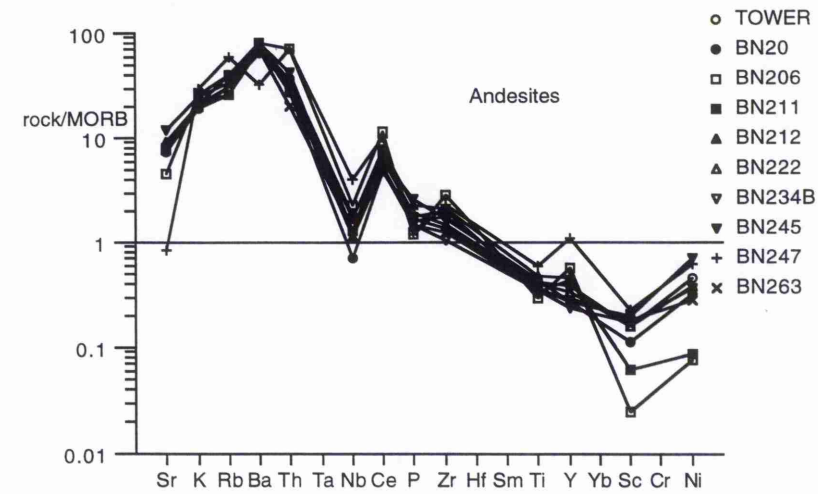


Fig 6.19f Spidergrams for the andesites of the Ben Nevis Complex, normalised against the MORB composition of Pearce (1983).

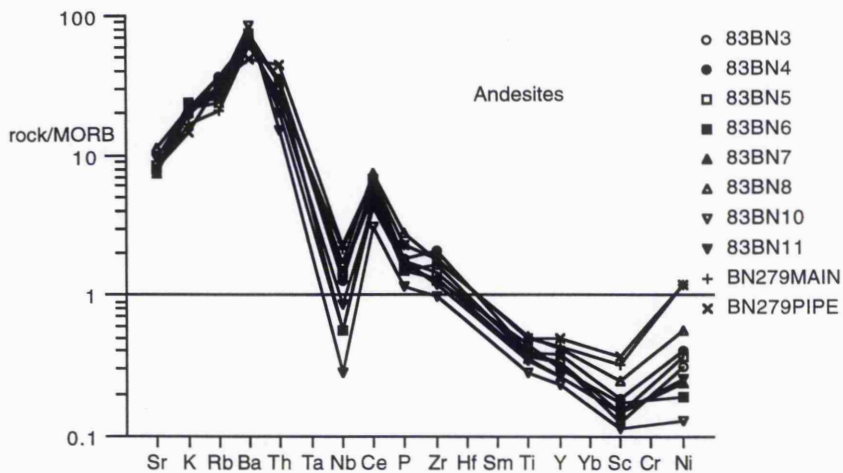


Fig 6.19f Spidergrams for the andesites of the Ben Nevis Complex, normalised against the MORB composition of Pearce (1983).

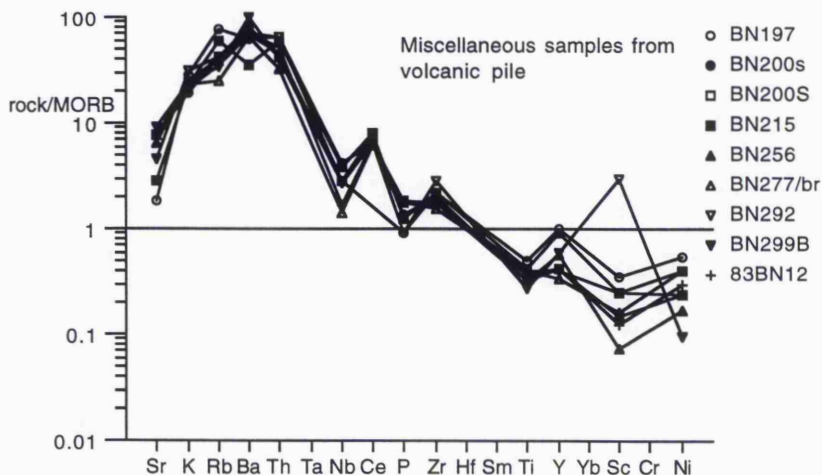


Fig 6.19g Spidergrams for the miscellaneous samples from the volcanic pile of the Ben Nevis Complex, normalised against the MORB composition of Pearce (1983).

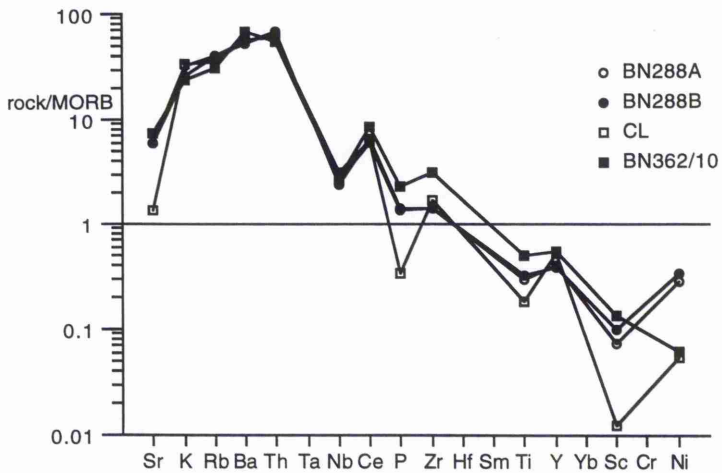


Fig 6.19g Spidergrams for the miscellaneous members of the volcanic pile of the Ben Nevis Complex, normalised against the MORB composition of Pearce (1983).

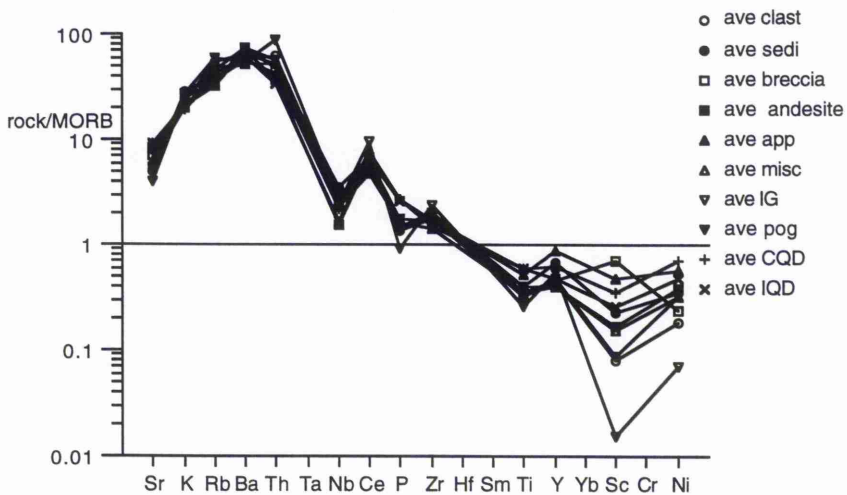


Fig 6.19h Averaged spidergrams for the Ben Nevis Complex, normalised against the MORB composition of Pearce (1983).

The Ben Nevis Complex is LILE enriched, HFSE depleted and has a Nb anomaly; together these features produce a spiky MORB normalised spidergram typical of subduction zones (Pearce 1982). HFSE depletion has variously been attributed to high degrees of partial melting (Pearce & Norry 1979), stability of minor residual phases (Saunders et al. 1980), magma-magma interactions (Kelemen et al. 1990) and remelting of depleted mantle (Green 1973). Nb anomalies have been ascribed to similar processes (Pearce 1983) and also to early removal of Nb from the mantle wedge by slab derived fluids, prior to melting of the wedge (Ayers & Watson 1991).

Enrichment of the LILE is conventionally attributed to a combination of high rock-melt incompatibility and high mobility in the presence of aqueous fluids derived from the dehydrating slab. Recent isotopic modelling has limited the involvement of slab derived LILE (<15% for Sr and Th) and suggests that the most important component added to the mantle wedge by the slab is water (Ellam et al. 1990, Hawkesworth et al. 1991, McCulloch & Gamble 1991). Addition of water from the slab to the wedge lowers the solidus and promotes melting. During normal subduction volatile components are transferred from the slab into the mantle wedge. Transfer slows as younger and drier slab material is subducted. Once the ridge enters the subduction zone, subduction ceases. Thermal rebound of the chilled wedge promotes melting of the wedge and possibly the slab. Saunders et al. (1987) believed that the Lorne Plateau lavas, and therefore the parent melts to the south-west Highland granites (Thirlwall 1988 and ref therein), were generated by subduction of a ridge.

Spiky spidergrams and apparent subduction related geochemistry do not give an unambiguous indication of active subduction during magma generation, merely that the mantle had recently been modified by subduction zone processes. Subduction zone processes metasomatise the mantle wedge (Peccerillo 1985), hence any melt product from this zone will have a subduction signature even after active subduction has ceased. This signature may persist in the mantle for as long as 30Ma (Rogers et al. 1985)

In section 6.2.2.i it was recognised that the Ben Nevis magmas represent a high-K suite; lavas from the Lorne Plateau are also high-K and a number of granite plutons north and south of the Ben Nevis are mildly shoshonitic (e.g. Kilmelford - Zhou 1987, Ach'uaire hybrids - Thompson & Fowler 1986). Such magmas are generally produced during transition from active subduction to other tectonic regimes (Barberi et al. 1974, Gill et al. 1984 and Wilkin & Bornhurst 1993). The final ORS volcanic episode in Scotland, the Hoy lavas of Orkney, includes alkali olivine-basalts and hawaiites heralding the onset of Carboniferous extensional volcanism (Thirlwall 1979). However, the mechanism by which mantle melts are generated after subduction is not clear (chapter 8); thermal recovery after subduction of a spreading centre is one possibility. In Baja California, magma eruptions continued 15-20Myrs after subduction had ceased (Rogers & Saunders 1989).

## 6.5 Fractional crystallisation and differentiation of the Ben Nevis Complex

### 6.5.1.i Introduction

Modelling is based on mass balance calculations for the major elements. Further constraints on fractionation models are imposed by crystal-liquid partition coefficients and qualitative analyses of fractionation vectors.

Problems with fractional crystallisation modelling stem from:

i) Magmas are viscous systems and often represent a mix of cumulate + liquid; most granites are believed to be emplaced as crystal-liquid mushes. Exceptionally, A-type granite with high activities of the complexing elements such as F, Cl and B are believed to represent liquid compositions (Pitcher 1993).

ii) In the plutonic environment, the type of fractional crystallisation varies between perfect equilibrium, where all of the crystal is in equilibrium with the melt, and Rayleigh fractionation, where just the surface of the crystal is in equilibrium. The importance of each end-member process can vary between different elements and different mineral phases within the same magma (McCarthy & Hasty 1976).

iii) Bulk distribution coefficients ( $K_d$ ) vary continuously as melt composition,  $f_{H_2O}$ , pressure and temperature vary (Rollinson 1993).

iv) Accessory minerals may strongly control some trace elements, e.g. Zr in zircon, apatite etc. These are difficult to incorporate into fractionation models due their low abundance and poorly defined distribution coefficients, for instance, U in ilmenite has reported bulk distribution coefficients of 0.517 and 3.2 (Nash & Crecraft 1985) and is therefore compatible or incompatible with respect to ilmenite, depending on the  $K_d$  chosen.

v) Late stage fluids and alteration may remove or add mobile elements.

vi) Fractionation requires the removal of either the liquid or the cumulus phases; the efficiency of such processes varies.

The data from volcanic pile and the miscellaneous members of the Ben Nevis Complex are not discussed here due to the large degree of scatter in these groups. Chemical evolution of both of these groups, on the basis of identical spidergrams to the plutonic rocks (Fig. 6.19b), follows similar pathways to the plutonic rocks.

### 6.5.1.ii Mass Balance Modelling

The unit of the Ben Nevis Complex most likely to yield reasonable results in mass balance modelling is the Porphyritic Outer Granite. The Fine Quartz Diorite, Coarse Quartz

Diorite, Inner Granite and volcanic pile all show varying degrees of scatter around a general trend; consequently mass balance modelling was applied only to the Porphyritic Outer Granite.

Mass balance modelling is based on a numerical expression of the Lever Rule. In the case of fractional crystallisation, a linear mixing calculation requires that compositions of the extraction assemblage, the parent magma and daughter magma must be linearly related (Ragland 1989). The basic equation is;

$$Z = FX + (1 - F)Y$$

Where Z = parent magma, Y = residual liquid, X = extract assemblage  
and F = fraction of liquid extracted

The mass balance calculations used were those of Geist et al. (1989) and are based on the work of Stormer & Nicholls (1978). A daughter composition is calculated from a parent magma using major element data for the main crystal phases and is then compared with the analysed composition. The crystals extracted from the parent are represented by the % cumulate. The statistical significance of the calculation is determined by the sum of the weighted residual squared ( $R^2$ ). Values below about 0.1 are normally regarded as acceptable. Not surprisingly, given the small variation between the parent and daughter compositions,  $R^2$  is small in a number of the calculations. Solutions can be translated such 100% Parent = X% daughter + X% of Mineral A + X% of mineral B + X% of mineral C etc.

#### 6.5.1.iii Trace element vector modelling

The effect of mineral extraction is determined by the relationship between the theoretical distribution coefficient and the element content of the rock according to;

$$\text{Conc. in mineral/Conc. in liquid} = K_d$$

Where  $K_d$  is the distribution coefficient

This method is quantitative and based on the superimposition of vectors representing the trend taken by the magma, if a particular mineral was the fractionating phase, on trace element variation diagrams. A number of crystal phases show zoning in thin section (chapter 5); consequently, the assumption of Rayleigh fractionation is not unreasonable.

Elements with similar behaviour are grouped together as:

- i) Large ion lithophile elements - LILE (K, Rb, Sr Ba)
- ii) High field strength elements - HFSE (Zr, Nb, Ti)
- iii) Rare Earth or Rare Earth like elements - REE (La, Ce, Y)
- iv) Compatible elements (Ni, V)

### 6.5.2 Mass Balance

Mass balance modelling for the Porphyritic Outer Granite is based on the minerals amphibole, biotite, clinopyroxene (cpx), orthopyroxene (opx), plagioclase and magnetite. Although small amounts of idiomorphic amphibole are identified in a number of specimens, the majority of amphibole is formed by the replacement of pyroxene. Those amphiboles with only vestigial traces of pyroxene are zoned from tremolitic/actinolitic cores to actinolitic hornblende rims. Two processes act to form such zonation, these being melt/fluid interaction with the rim, and replacement of pyroxene in the core. For mass balance modelling purposes, an analyses from a position midway between the rim and core of a large amphibole crystal was selected.

No primary pyroxene was identified during probe analyses of the Porphyritic Outer Granite; pyroxene is present only as vestigial traces in most of the Porphyritic Outer Granite, consequently a representative pyroxene analysis was taken from OBN18e, a sample of the Fine Quartz Diorite. End-member compositions for plagioclase were obtained from Deer et al. (1992).

Biotite was shown in chapter 5 to have undergone a large number of complex substitutions in the magmatic and subsolidus regimes; consequently a biotite analysis of Haslam (1968), obtained from a mineral separate, was taken to represent the average biotite composition for the Porphyritic Outer Granite.

The mass balance equations are unweighted, Wright (1974) notes that for solutions with low residuals, weighting makes little difference to the final result. Gill (1981) recognised that the assemblage cpx + opx + magnetite has the same effect as hornblende on mass balance calculations.

Compositions for the parent (BN419), daughter (BN175) and mineral phases are displayed in Table 6.2; the results are portrayed in Table 6.3. The best results are obtained when the mineral assemblage includes;

[1]	Ab + An + Biotite + Amphibole + Magnetite	R2=0.073
[2]	Ab + An + Biotite + Cpx + Magnetite	R2=0.011
[3]	Ab + An + Biotite + Cpx + Opx + Magnetite	R2=0.002
[4]	Ab + An + Biotite + Amphibole + Cpx + Magnetite	R2=0.003

BN419 is a sample from the marginal Porphyritic Outer Granite variant and contains no large salmon pink alkali feldspar phenocrysts which characterise the normal Porphyritic Outer Granite. Therefore, the above equations were re-calculated with a sample of normal Porphyritic Outer Granite (BN418) as the parent. Similar results were obtained (Table 6.3).

Table 6.2 Major element composition of the parent magma, daughter magma and mineral phases used in mass balance modelling.

Element	BN419		BN418		BN175		AB	AN	BIOT	AMPH
MAG	OPX	CPX								
SiO <sub>2</sub>	63.73	66.38	67.38	67.84	43.88	36.56	52.27	0.61	52.96	52.66
TiO <sub>2</sub>	0.60	0.56	0.49	0.00	0.00	3.91	0.23	0.12	0.26	0.35
Al <sub>2</sub> O <sub>3</sub>	15.57	15.27	14.84	19.65	36.08	14.45	2.41	0.13	2.12	1.26
FeO*	4.08	3.61	2.94	0.03	0.00	16.46	9.21	98.78	18.49	6.911
MnO	0.07	0.06	0.04	0.02	0.00	0.28	0.57	0.07	0.34	0.24
MgO	2.45	1.99	1.73	0.04	0.00	14.63	17.64	0.00	23.74	14.69
C <sub>2</sub> O	3.07	2.63	2.18	0.00	19.37	0.24	12.31	0.00	1.49	22.67
Na <sub>2</sub> O	3.99	4.06	4.02	11.07	0.22	0.37	0.51	0.00	0.16	0.61
K <sub>2</sub> O	3.87	4.18	4.09	0.29	0.00	8.9	0.25	0.00	0.03	0.01

Assemblage [3] yields large negative values for opx (-3% for BN419 and -24% for BN418) in the extracted cumulate, and assemblage [4] contains large negative values for amphibole in the cumulate (-6% for BN419 and -55% for BN418); this requires the incorporation of additional material into the magma during crystallisation. This is thought unlikely. Assemblage [1], with BN418 as the parent and BN175 as the daughter, results in  $R^2=0.104$  and is outside of the range of values for which mass balance equations are believed to be significant.

The difference between assemblages [1] and [2] is the presence or absence of amphibole or cpx. Opx is not required to balance the major element composition of the Porphyritic Outer Granite; this fits with the observation made in chapter 5, that opx often forms corroded cores to cpx in the quartz diorites and it is suggested that opx crystallisation had ceased or was not important during the evolution of the Porphyritic Outer Granite.

### 6.5.3 Qualitative vector modelling

Superimposition of mineral fractionation vectors onto trace element variation diagrams provides additional evidence on the main fractionating phases within the Porphyritic Outer Granite and the plutonic rocks of the Ben Nevis Complex in general.

Plots of the feldspar components reveal that plagioclase fractionation played an important role in the evolution of all the plutonic units to the Ben Nevis Complex (Fig. 6.20). The Inner Granite exhibits lower CaO contents but higher Na<sub>2</sub>O indicating the greater importance of the albite molecule in this unit. Comparison of the Fine Quartz Diorite and Coarse Quartz Diorite with the Porphyritic Outer Granite reveals decreasing anorthite in the quartz diorites but only a slight decrease in the Porphyritic Outer Granite.

Table 6.3 Results of mass balance modelling for the Porphyritic Outer Granite.

PARENT	DAUGHTER	%Extracted	Cumulate		R <sup>2</sup>	Assemblage No. if in text.
			(Composition)			
BN419	BN175	19	Ab	30.42	0.68	Not valid
			An	28.79		
			Biot	36.92		
			MAG	3.88		
BN419	BN175	18	Ab	27.86	0.41	Not valid
			An	22.88		
			Biot	39.03		
			CPX	10.23		
BN419	BN175	17	Ab	23.87	0.51	Not valid
			An	26.92		
			Biot	37.92		
			Amph	11.29		
BN419	BN175	17	Ab	29.53	0.07	[1]
			An	28.07		
			Biot	24.92		
			Amph	13.12		
BN419	BN175	18	MAG	4.36	0.01	[2]
			Ab	32.40		
			An	24.25		
			Biot	28.61		
BN419	BN175	18	CPX	10.81	0.00	[3]
			MAG	3.93		
			Ab	33.45		
			An	22.48		
BN419	BN175	18	Biot	30.72	0.00	[4]
			CPX	12.50		
			OPX	-3.04		
			MAG	3.90		
BN418	BN175	6	Ab	33.48	1.04	[1]
			An	22.68		
			Biot	30.74		
			Amph	-6.55		
BN418	BN175	7	CPX	15.90	0.07	[2]
			MAG	3.75		
			Ab	17.78		
			An	34.79		
BN418	BN175	7	Biot	31.02	0.00	[3]
			Amph	8.78		
			MAG	7.64		
			Ab	22.56		
BN418	BN175	7	An	29.76	0.00	[3]
			Biot	31.50		
			CPX	9.33		
			MAG	6.85		
BN418	BN175	7	Ab	32.66	0.00	[3]
			An	14.55		
			Biot	48.04		
			CPX	23.09		
BN418	BN175	7	OPX	-24.53	0.01	[4]
			MAG	6.19		
			Ab	33.07		
			An	15.65		
			Biot	49.22		
			Amph	55.73		
			CPX	52.78		
			MAG	5.01		

## Rb-Sr

Both plagioclase and K-feldspar have  $K_d > 1$  for Sr in acidic melts; in contrast  $K_d$  for Rb in plagioclase is  $< 1$  and in alkali feldspar is  $> 1$  (Nash & Crecraft 1985). Both pyroxene and amphibole have  $K_d$  for Rb and Sr  $< 1$  (Hanson 1978). Biotite has  $K_d$  for Sr  $< 1$  whereas that for Rb is  $> 1$ .

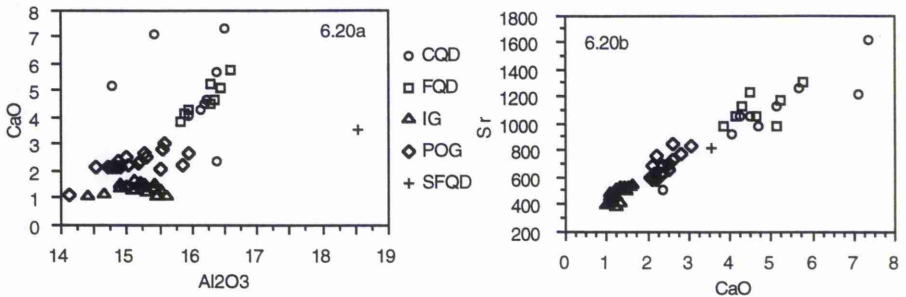


Fig. 6.20a and 6.20b indicate that feldspar fractionation was continuous during the evolution of the Ben Nevis Complex. 6.20a illustrates the high Albite content of the plagioclase in the Inner Granite.

The trend of the quartz diorites (Fig. 6.21) can be explained by plagioclase and pyroxene fractionation. Crystallisation of the Porphyritic Outer Granite followed a different path and the gradient of this line can be explained by plagioclase and K-feldspar fractionation. The relatively flat to slightly decreasing Rb with decreasing Sr trend of the Inner Granite appears to reflect a further increase in the proportion of K-feldspar, but Haslam (1968) reports that the modal value for K-feldspar is lower in the Inner Granite than the Porphyritic Outer Granite, and it is suggested that the horizontal trend reflects the importance of biotite as a fractionating phase in the Inner Granite.

## K-Rb

K and Rb tend to follow each other in geochemical processes and Rb is concentrated into K-rich phases during fractionation. The bonding energy of Rb is, however, lower than that of K because of its larger ionic radius, therefore K is slightly enriched in the mineral phases and Rb is slightly enriched in the melt phase. Progressive lowering of the K/Rb ratio of the melt results. If an aqueous phase is present during the later stages of crystallisation, it will also have a low K/Rb ratio and become progressively more Rb enriched with fractionation; this evolutionary trend has been termed the pegmatite-hydrothermal trend (Shaw 1968). In contrast, crystallisation in a water deficient system will lead to increasing K and Rb in the melt and approximately constant K/Rb ratios. Shaw (1968) refers to this trend as the Main or Magmatic trend. Two clear trends are defined in Fig. 6.22. The quartz diorites show enrichment in K and Rb with evolution parallel to the magmatic trend of Shaw (1968). This reflects partitioning into K-rich minerals, particularly biotite. K/Rb ratios for the quartz diorite show considerable scatter around a steadily decreasing trend

demonstrating progressive enrichment in Rb with fractionation. The Porphyritic Outer Granite on this diagram (increasing Rb at  $\approx$  constant  $K_2O$ ) is parallel to the pegmatite-hydrothermal trend of Shaw (1968) and interpreted as the result of the partitioning of Rb into an ever increasing fluid phase. K/Rb ratios during fluid phase movement remain relatively constant with increasing fractionation. This is in

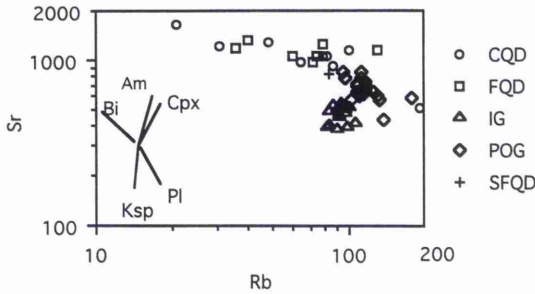


Fig 6.21 Variation in Sr and Rb within the plutonic rocks of the Ben Nevis Complex. Mineral vectors superimposed. Bi = Biotite, Am = Amphibole, Ksp = K-feldspar, Pl = plagioclase and Cpx = clinopyroxene.

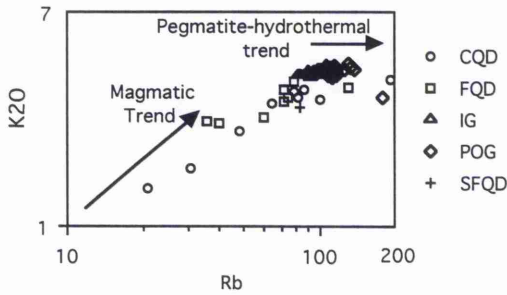


Fig 6.22 The relationship between  $K_2O$  and Rb in the plutonic rocks, and illustrating the magmatic and pegmatite-hydrothermal trends of Shaw (1968).

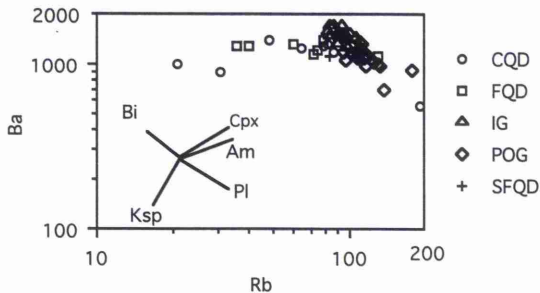


Fig 6.23 Variation in Ba and Rb within the plutonic rocks of the Ben Nevis Complex. Mineral vectors superimposed. See Fig 6.21 for key to mineral symbols.

agreement with the large degree of late stage K-feldspar crystallisation within the Porphyritic Outer Granite. The abrupt change between the magmatic trend and the pegmatite trend reveals that there was no gradual build-up of fluids during formation of the Outer Granite and that the Porphyritic Outer Granite was intruded with a relatively high water content and should therefore be considered as a separate magma body to the quartz diorites. In chapter 5, it was shown that the degree to which pyroxene was converted to amphibole depended on the initial crystallising assemblage of the magma and on the amount of late stage fluid movement through the rock after crystallisation. Pyroxene to amphibole conversion is largely complete in the Porphyritic Outer Granite and may be linked to late stage fluid movements in the Porphyritic Outer Granite.

#### Ba-Rb

Ba has  $K_d > 1$  for the minerals cpx, amphibole and plagioclase, and  $K_d < 1$  for K-feldspar and biotite. Fig. 6.23 shows that fractionation of the quartz diorites can be modelled in terms of plagioclase plus either cpx or amphibole. The Porphyritic Outer Granite is dominated by plagioclase, K-feldspar and possibly biotite. The Inner Granite shows no obvious trend, consistent with varying quantities of biotite, K-feldspar and plagioclase and imperfect separation of fluid and mineral phases (McCarthy and Hasty 1976).

#### CaO-Y

Three trends are visible in Fig. 6.24; the Fine Quartz Diorite and Coarse Quartz Diorite show decreasing CaO with increasing Y. A mix of plagioclase, clinopyroxene and magnetite or plagioclase, amphibole and magnetite can explain this trend. Minerals such as hornblende and the accessory minerals zircon, apatite and titanite account for the rapid decrease in Y visible in the Porphyritic Outer Granite, whereas the influence of plagioclase causes CaO to decrease. Decreasing CaO with increasing Y in the Inner Granite can be explained by plagioclase fractionation.

#### Ce-Y

Ce is a light Rare Earth Element (LREE) whereas the behaviour of Y is comparable to a heavy Rare Earth (HREE). Both the Outer Granite and Inner Granite show relatively steep trends (Fig. 6.25); the Inner Granite, however, shows rapidly increasing Y at approximately constant Ce, whereas the Outer Granite shows rapidly decreasing Y with a slight decrease in Ce. One explanation for the trend of the Inner Granite is that it is caused by the progressive breakdown of Y-enriched phases in the source region (e.g. amphibole, zircon or garnet), whereas that of the Outer Granite is consistent with removal of REE. In this diagram, the Porphyritic Outer Granite has similar REE abundances to the quartz diorites and it is not possible to differentiate between the two units. This suggests that the Porphyritic Outer Granite cannot be derived by fractional crystallisation of the same parent magma as that of the quartz diorites of the Ben Nevis Complex.

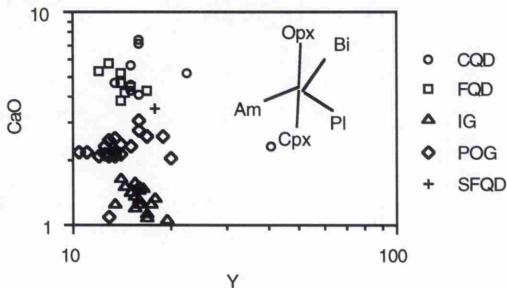


Fig 6.24 Variation in CaO and Y within the plutonic rocks of the Ben Nevis Complex. Mineral vectors superimposed. See Fig 6.21 for key to mineral symbols.

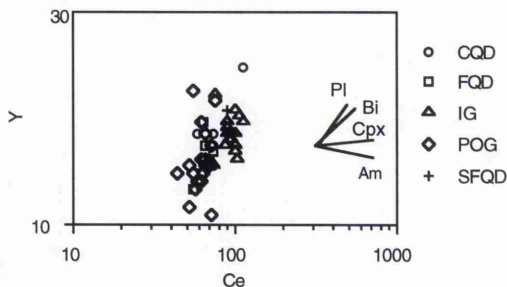


Fig 6.25 Variation in Ce and Y within the plutonic rocks of the Ben Nevis Complex. Mineral vectors superimposed. See Fig 6.21 for key to mineral symbols.

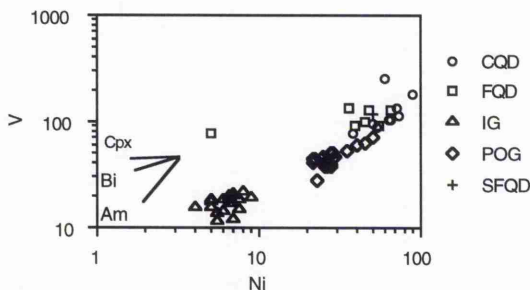


Fig 6.26 Variation in V and Ni within the plutonic rocks of the Ben Nevis Complex. Note the compositional overlap between the POG and the FQD + CQD units. Mineral vectors superimposed. See Fig 6.21 for key to mineral symbols.

#### V-Ni

Fractionation trends in the quartz diorites and Porphyritic Outer Granite (Fig. 6.26) are strongly controlled by the extraction of biotite and amphibole, but amphibole is not a

major primary magmatic phase in the Outer Granite and its place is taken by pyroxene which cannot cause the variations observed in this diagram. This suggests that amphibole fractionation occurred at depth. Considerable scatter is evident in the Inner Granite and the overall trend of this unit is controlled by the extraction of biotite.

#### TiO<sub>2</sub>-Zr

None of the major mineral phases can account for the depletion of Zr and zircon fractionation plus magnetite, and possibly biotite and amphibole, controls the trend of the Porphyritic Outer Granite (Fig. 6.27). Fractionation of the quartz diorites is best explained in terms of plagioclase, magnetite and clinopyroxene or amphibole. The Inner Granite shows increasing TiO<sub>2</sub> with increasing SiO<sub>2</sub> and can be explained by plagioclase dominating the fractionating assemblage.

#### Y-Zr

These elements, like Ti, are believed to be immobile unless fluids with high activities of F and Cl are present. All the units in the Ben Nevis Complex show steep gradients (Fig. 6.28) and overlap to a large degree. However, the fractionation vector of the different units is one of increasing Y with increasing Zr in the quartz diorites and Inner Granite but of decreasing Y and Zr in the Porphyritic Outer Granite. The Porphyritic Outer Granite can be explained in terms of zircon and amphibole fractionation, whereas the trend of the quartz diorites denotes plagioclase and clinopyroxene fractionation. A similar interpretation can be placed on the Inner Granite trend; alternatively, the breakdown of amphibole in the source region may be invoked.

#### V-TiO<sub>2</sub>

Vanadium is a compatible element and partitioned into mineral phases such as biotite, amphibole and pyroxene. The Inner Granite lies directly below the Porphyritic Outer Granite in Fig. 6.29; if the Inner Granite were generated by fractional crystallisation from the Porphyritic Outer Granite, then to achieve these low TiO<sub>2</sub> contents, but retain similar V abundances as the Porphyritic Outer Granite, cpx must dominate the mineral assemblage. The only mafic mineral observed in normal Inner Granite is biotite; therefore, the Inner Granite is believed to have been derived from a separate source to the Porphyritic Outer Granite/quartz diorite. The trend of the quartz diorites and Porphyritic Outer Granite can be interpreted in terms of magnetite, biotite and possibly amphibole or cpx.

#### 6.5.4 Conclusion

Mass balance calculations for the Porphyritic Outer Granite yield acceptable results ( $R_2 < 0.1$ ) for the assemblage; plagioclase, biotite, magnetite and clinopyroxene, and also for the assemblage; plagioclase, biotite, magnetite and amphibole although  $R_2$  is larger than in the former case. Vector modelling is consistent with the mass balance calculations with

the addition of accessory phases in order to explain depletions in the HFSE such as Zr, Nb and Y.

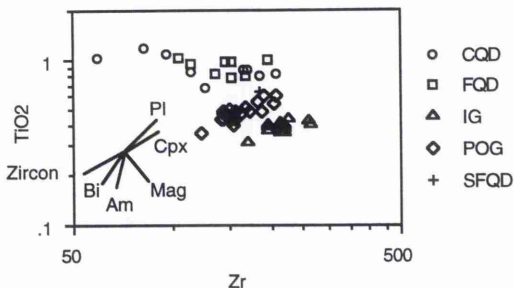


Fig 6.27 Variation in TiO<sub>2</sub> and Zr within the plutonic rocks of the Ben Nevis Complex. Mineral vectors superimposed. See Fig 6.21 for key to mineral symbols.

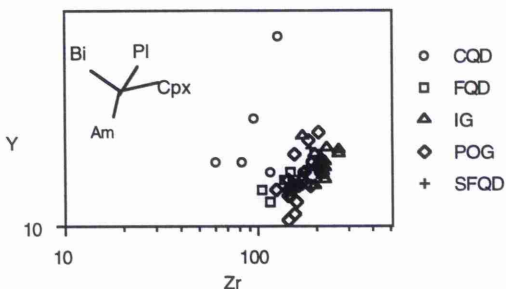


Fig 6.28 Variation in Y and Zr within the plutonic rocks of the Ben Nevis Complex. Mineral vectors superimposed. See Fig 6.21 for key to mineral symbols.

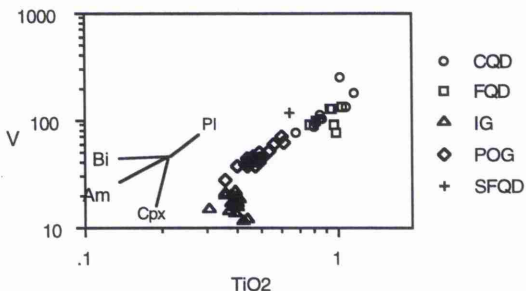


Fig 6.29 Variation in V and TiO<sub>2</sub> within the plutonic rocks of the Ben Nevis Complex. Mineral vectors superimposed. See Fig 6.21 for key to mineral symbols.

There is a certain amount of evidence that, although the Porphyritic Outer Granite and quartz diorites fall along a common trend in Harker diagrams albeit with an inflexion at 63% SiO<sub>2</sub>, the two units are in fact members of separate magma bodies with different

geochemistries and physical conditions. Thus the inflexion at 63% SiO<sub>2</sub>, which would require a sudden change in the fractionating assemblage, therefore reflects a change in the chemistry of the parent magma. The term Outer Granite should be abandoned as the Porphyritic Outer Granite cannot be related by simple fractional crystallisation to the quartz diorites.

The chemical evolution of the Ben Nevis Complex was dominated by the fractionation of plagioclase. Comparisons with distribution coefficient vectors reveal that the quartz diorites can be modelled by removing plagioclase, magnetite, biotite and either cpx or amphibole. HFSE ratios require the removal of amphibole (Figs. 6.25 and 6.26) and yet amphibole is largely a replacement mineral rather than a primary magmatic phase in the Ben Nevis granites (chapter 5). Experimental studies (Yoder & Tilley 1962) indicate that hydrous silicate melts crystallising under high pressures favour the formation of hornblende, whereas those at lower pressures favour the formation of pyroxene. At deeper crustal levels and therefore higher pressures, amphibole is stable and is preferred over pyroxene. As the residual liquid was tapped during fractionation in this deeper magma chamber, and emplaced into higher crustal levels, pyroxene replaced amphibole fractionation. Consequently the trace element chemistry of the Ben Nevis Complex reflects amphibole fractionation for some elements and a combination of pyroxene and amphibole in others.

This model can be tested with the lavas from the volcanic pile where there is unambiguous evidence of amphibole as a major primary magmatic phase (chapters 3 and 5 and Haslam 1968). If trace element variations in these lavas parallel that of the quartz diorites and Porphyritic Outer Granite, then amphibole is likely to have played a major role in the evolution of the quartz diorites and Porphyritic Outer Granite. Figs. 6.30a and 6.30b indicate that the trace element ratios of the andesites closely follow those of the quartz diorites and Porphyritic Outer Granite, confirming the belief that amphibole played a major role in the chemical evolution of these magmas despite its absence as a major magmatic phase.

The most noticeable feature of the Porphyritic Outer Granite is the decline in Zr, Y and Nb with fractionation, which reflects removal of accessory minerals, in particular zircon. The effects of late stage fluid migration are also evident from the geochemical variation in the Porphyritic Outer Granite.

Plagioclase, and to a lesser extent biotite and K-feldspar, dominate the fractionating assemblage in the Inner Granite. The plagioclase is enriched in the albite molecule compared to plagioclase of the quartz diorites and Porphyritic Outer Granite. Extremely steep trends of increasing REE and HFSE with SiO<sub>2</sub> are identified.

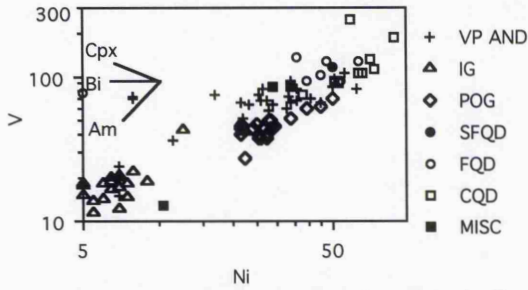


Fig 6.30a Variation in V and Ni within the plutonic and volcanic rocks of the Ben Nevis Complex. Mineral vectors superimposed. For key to mineral symbols see Fig 6.21.

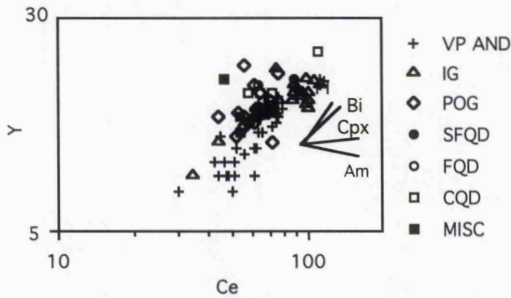


Fig 6.30b Variation in Ce and Y within the plutonic and volcanic rocks of the Ben Nevis Complex. Mineral vectors superimposed. See Fig 6.21 for key to mineral symbols.

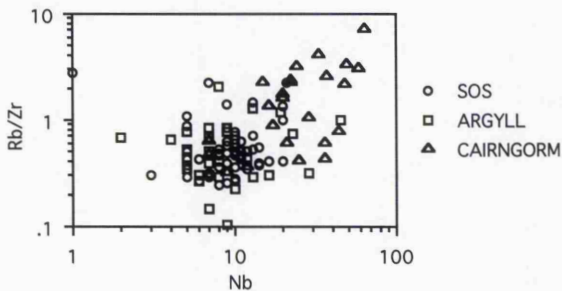


Fig 6.31 Variation in Rb/Zr and Nb in the Cairngorm, South of Scotland and Argyll Suites. Published data from Halliday & Stephens (1984).

## 6.6 Relationship of the Ben Nevis Complex to subduction

Brown et al. (1984) used LILE/HFSE ratios to distinguish primitive calcic arc granitoids (low LILE and HFSE abundances), normal calc-alkaline continental arc granitoids (enhanced LILE abundances and low LILE/HFSE ratios), mature alkali-calcic arc granitoids (high LILE & HFSE abundances and higher LILE/HFSE ratios) and back-arc/anorogenic alkaline granitoids (highest HFSE abundances).

Two processes control the composition of granitoid magmas with relation to arc maturity in space and time. Firstly, subduction zone enrichment of the lithospheric mantle, locally coupled with crustal assimilation and fractional crystallisation in zones of thickened crust, leading to enhanced granitoid LILE and LREE abundances. Secondly, increasing contributions of within-plate sub-continental lithosphere, with increasing distance from the trench, produce high HFSE abundances. HFSE/LILE ratios are not significantly affected by fractional crystallisation, although removal of Zr and Y during crystallisation of the Porphyritic Outer Granite is evident from the higher Rb/Zr and lower Zr and Y contents of this unit (Fig. 6.31). Where Rb/Zr is plotted against Nb or Y, increasing arc maturity is reflected in increasing Rb/Zr and HFSE abundances (Fig. 6 of Brown et al. 1984).

A clear distinction between the S. Uplands and Cairngorm plutons is illustrated by Brown et al. (1984) and also in Fig. 6.31, with the S. Uplands examples having lower HFSE contents for a given Rb/Zr ratio. Brown et al. (1984) believed that this feature was related to the composition of the underlying mantle, the S. Uplands plutons being influenced by subduction zone enrichment processes and the Cairngorm plutons reflecting within plate enrichment processes.

Data from Ben Nevis and other members of the Argyll suite (Halliday & Stephens 1984); plot with lower Rb/Zr ratios and HFSE contents (Fig. 6.31) than either the S. Uplands or the Cairngorm areas. The upper crustal rocks in the area of both the Ben Nevis and the Cairngorm plutons are comprised of Dalradian metasediments. Upper crustal contamination cannot therefore explain differences between Ben Nevis and Cairngorm. The best estimates of mantle composition beneath Northern Britain are derived from xenoliths excavated from the lithospheric mantle (Hunter et al. 1984 and Menzies & Halliday 1988) or from primitive Old Red Sandstone (ORS) lavas (Thirlwall 1988 and refs. therein). There is insufficient whole-rock geochemistry from xenoliths for comparisons to be made with the granitoid data. No significant variation is observed in Rb/Zr-Nb (Fig. 6.32) for primitive ORS lavas across Northern Britain. The ORS lavas are contemporaneous and cogenetic with the Newer Granites (Frost & O'Nions 1985, Thirlwall 1982 & 1986 and Halliday et al. 1984a); if the mantle is zoned in Rb/Zr-Nb space across Northern Britain, then the ORS lavas should mirror any such zonation. This is not the case, and the variation in HFSE and LILE abundances cannot be related to the mantle. The ORS lavas are believed to be primary mantle melts which have suffered only small degrees of crystal fractionation and crustal contamination (Thirlwall 1988 and refs. therein). In contrast, isotopic evidence for the granites indicate that these magmas are mixtures of crustal and mantle compositions (e.g. Frost & O'Nions 1985, Halliday et al. 1984a and chapter 7). Contamination of the granites is believed to have occurred in the lower crust. If neither the upper crustal rocks or the mantle are zoned (in Rb/Zr-Nb space) across Northern Britain, any geochemical variation must therefore be attributed to variations in the chemistry of the lower crust and the model of Brown et al. (1984) needs revision.

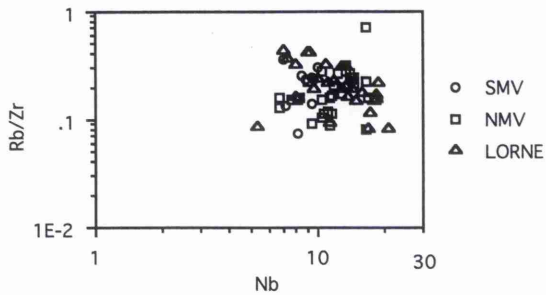


Fig 6.32 Variations in Rb/Zr and Nb for the ORS lavas of Scotland. Data from Thirlwall (1983).

## 6.7 Conclusion

The Ben Nevis Complex represents a typical Argyll suite (Halliday & Stephens 1984) calc-alkaline pluton. Members of the plutonic rocks range from quartz diorite to monzogranite, whereas the volcanic rocks are andesitic to dacitic and rarely rhyolitic. The complex as a whole is mildly alkaline and a number of the volcanic samples cross into the alkaline series (Le Maitre et al. 1989) and are therefore classified as trachyandesites and trachytes.

The plutonic rocks were intruded to a high level in the crust.

Mass balance and trace element modelling of the compositions of the plutonic rocks reveals that plagioclase dominated the fractionating mineral assemblage throughout the formation of the Ben Nevis Complex. If the quartz diorites are taken as one unit, then four parental magmas are required in order to generate each of the four main units making up the Ben Nevis Complex, i.e. quartz diorites, Porphyritic Outer Granite, Inner Granite and volcanic pile. However, the validity of grouping the quartz diorites into a single fractionating system is questioned on the grounds that later pulses have more primitive compositions than earlier pulses. The same conclusion is reached for the andesites of the volcanic pile; this variation in magma chemistry over time will be addressed in chapter 7.

Increasing HFSE and REE abundances with fractionation in the Inner Granite; can be attributed to the breakdown of accessory phases and amphibole in the source region.

Potassium contents characterise the Ben Nevis Complex as a high-K calc-alkaline pluton. Spiky spidergrams indicate the influence of subduction in the source region, but there is no simple zonation in geochemistry of the Newer Granite suite with distance from the trench/suture. Geochemical trends in LILE and HFSE ratios are not related to upper crustal composition or distance from the suture and it is suggested that variations in the composition of the lower crust can explain geochemical trends across Northern Britain. This view is examined further in the following chapter.

***EVERYONE SHOULD  
BELIEVE IN SOMETHING;***



***I BELIEVE  
I'LL HAVE ANOTHER BEER.***

# CHAPTER 7

## ISOTOPE GEOLOGY

### 7.1 Introduction

#### 7.1.1 General statement

The data presented in this chapter represent the first detailed isotopic study of the Ben Nevis Complex. A summary of the literature concerning isotopic techniques applied to the British Caledonides is used to set the scene, before describing the isotope geology of Ben Nevis. The composition of possible source regions is reviewed before discussing the origin and evolution of the Ben Nevis Complex.

In addition to their use in absolute dating, radiogenic isotopic ratios are powerful tools for tracing the source characteristics and evolution of magmas. Relationships within and between individual plutons have been used to identify systematic local and regional variations in the type or types of source material involved in production of granite magmas and the spatial and temporal variations in the nature of these sources.

#### 7.1.2.i Commonly used acronyms in diagrams

LPL = Lorne Plateau Lavas

ORS = Old Red Sandstone

SWH = South West Highland Mantle in the sense of Thirlwall (1986 and refs. therein)

MME = Mafic Microgranular Enclaves

EVP = Etive volcanic-plutonic complex

The following shorthand notation is used for different components of the Ben Nevis Complex

FQD = Fine Quartz Diorite

POG = Porphyritic Outer Granite

CQD = Coarse Quartz Diorite

MARG POG - Marginal variant of POG

SFQD = Sgurr Finnisg-aig Quartz Diorite

IG = Inner Granite

CISTE = Base of volcanic pile

SUMMIT = Top of volcanic pile

V. MISC = Rhyolite clast and dome sample

MISC = Dykes and Appinites

#### 7.1.2.ii Notation of Results

Initial Nd isotope ratios are expressed in  $\epsilon\text{Nd}$  units.  $\epsilon\text{Nd}_t$  will refer to  $\epsilon\text{Nd}$  at the time of emplacement (425Ma, see section 7.4.3) as will  $\epsilon\text{Sr}_t$ . Bulk Earth values for Nd at the present day are from Jacobsen & Wasserburg (1980) and values for Sr at the present day are from Faure (1986); these are listed below:

$$(^{143}\text{Nd}/^{144}\text{Nd})_{\text{CHUR}} = 0.51264$$

$$(^{87}\text{Sr}/^{86}\text{Sr})_{\text{UR}} = 0.0816$$

$$(^{147}\text{Sm}/^{144}\text{Nd})_{\text{CHUR}} = 0.1966$$

$$(^{87}\text{Rb}/^{86}\text{Sr})_{\text{UR}} = 0.7045$$

The derivation of mathematical equations and the theories behind the use of isotopes as a geological tool can be found in Faure (1986) and, unless an equation warrants special attention, the reader is referred to the relevant chapters therein.

In all diagrams where individual data points represent samples from Ben Nevis, analytical error is less than the size of the symbol representing the data point.

## 7.2 Isotope Geochemistry

### 7.2.1 Rubidium - Strontium $^{87}\text{Rb}$ decays to $^{87}\text{Sr}$ $T_{1/2} = 48.8 \times 10^9$ a

Rb typically substitutes for K and is found in the common rock forming minerals, notably mica and K-feldspar. Sr substitutes for Ca and is also found in the common rock forming minerals, especially plagioclase and apatite. During fractional crystallisation Sr behaves as a compatible element as soon as plagioclase begins to form, whereas Rb is strongly incompatible until biotite or K-feldspar are stable, becoming concentrated into late stage melts and fluids. Consequently the Rb/Sr ratio of a closed-system fractionating magma will increase, whereas the  $^{87}\text{Sr}/^{86}\text{Sr}$  ratio remains constant and a plot of  $^{87}\text{Rb}/^{86}\text{Sr}$  against  $^{87}\text{Sr}/^{86}\text{Sr}$  will generate a horizontal line. The gradient of this line will increase with time because  $^{87}\text{Rb}$  will decay to  $^{87}\text{Sr}$ ; the gradient of this line is directly related to the age of the rock.

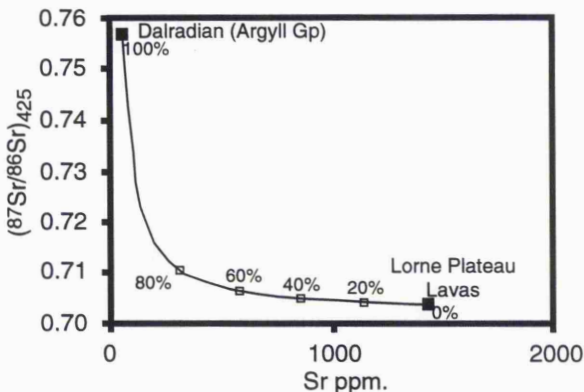


Fig. 7.1 Contamination of high Sr content Lorne Plateau Lava (L-56 Thirlwall 1982) by low Sr content Dalradian Schist (A561 Dempster 1985). Initial ratios remain low  $<0.71$  until  $>80\%$  assimilation of Dalradian Schist. Mixing Equation from Faure (1986) = Equation 9.21.

Because Rb is concentrated in silica-rich melts, the continental crust has a high concentration of Rb, and with time, consequently develops a high  $^{87}\text{Sr}/^{86}\text{Sr}$  ratio relative to the mantle. Whereas high initial  $^{87}\text{Sr}/^{86}\text{Sr}$  ratios imply a large crustal component, low  $^{87}\text{Sr}/^{86}\text{Sr}$  ratios do not necessarily preclude a significant crustal component to the magma. Mantle melts tend to have high concentrations of Sr relative to typical crustal values ( $10^2$  vs  $10^1$  ppm respectively). Moreover, plagioclase, the main reservoir of Sr, readily enters the melt phase during mantle melting. In contrast, under typical crustal conditions, plagioclase is relatively stable and may remain as a residual phase during partial melting (Faure 1986). Fig. 7.1 demonstrates the effect of progressively contaminating a high Sr content, low  $^{87}\text{Sr}/^{86}\text{Sr}$  melt with a low Sr abundance, high  $^{87}\text{Sr}/^{86}\text{Sr}$  melt. The low initial

$^{87}\text{Sr}/^{86}\text{Sr}$  ratio of L-56 persists until a large degree (>80%) of contamination has been achieved. This 'buffering' toward mantle compositions is further compounded if the contaminant is relatively young because radioactive decay will have had insufficient time to add  $^{87}\text{Sr}$  to the crustal component.

7.2.2 Samarium - Neodymium  $^{147}\text{Sm}$  decays to  $^{144}\text{Nd}$   $T_{1/2} = 1.06 \times 10^{11} \text{a}$

Sm and Nd are both Light Rare Earth Elements (LREE) and occur in many of the common rock forming minerals, but are especially concentrated in accessory minerals such as zircon, apatite, allanite and titanite. Sm and Nd have very similar chemical properties which inhibits fractionation between the two elements on the same scale the Rb-Sr system (0.1-0.5 vs 0.1-10,000 respectively). Consequently the Sm/Nd ratio varies only slightly between different rock and mineral types. In a closed-system fractionating magma, the concentrations of Nd and Sm increase slightly whereas Sm/Nd decreases.

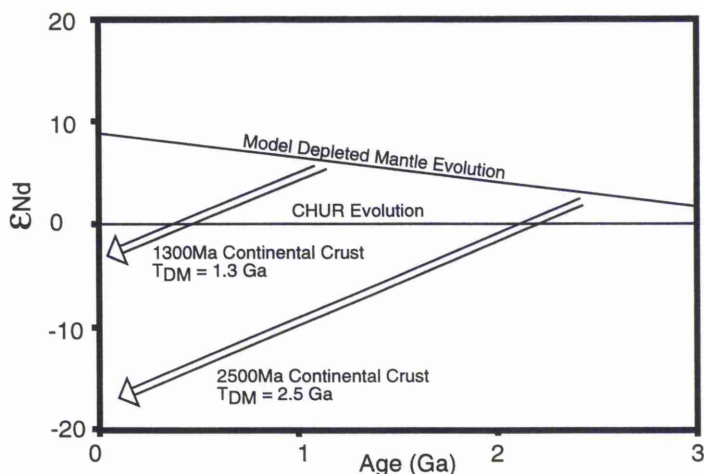


Fig. 7.2 Evolution of  $^{143}\text{Nd}/^{144}\text{Nd}$  (expressed in  $\epsilon_{\text{Nd}}$  units) with time for several model reservoirs. Model ages calculated relative to depleted mantle ( $T_{\text{DM}}$ ) for the Lorne Plateau Lavas are identical to  $\approx 1.3\text{Ga}$  continental crust. If the Lorne Plateau Lavas are derived from LREE-enriched mantle then  $T_{\text{DM}}$  ages for these magmas are meaningless. CHUR values from Jacobsen & Wasserburg (1980) and DM from Liew & Hofmann (1988).

A common technique applied to Sm-Nd results is to express the data in terms of model age calculations. A model age is believed to reflect the period of time elapsed since fractionation of the REE and separation of the melt from a reservoir of chosen composition. This technique is only valid if the rock is not a mixture of sources and if the chosen reservoir composition is the correct one. Fig. 7.2 graphically describes the evolution of several reservoirs these being: depleted mantle, a uniform mantle reservoir represented by the chondritic uniform reservoir (CHUR) model composition, and two crustal reservoirs of different ages but with the same Sm/Nd ratio. Intersection of the crustal evolution curve with those of the two mantle reservoirs provides model age estimates. Liew & McCulloch (1985) give reasons for the use of  $T_{\text{DM}}$  or depleted mantle extraction ages rather than

TCHUR or extraction from CHUR. It should be noted that model age calculations are sensitive to the assumptions made concerning the nature of the mantle and the crustal protolith (see section 7.6).

### 7.2.3 Uranium - Lead Complex decay chains

$$^{235}\text{U to } ^{207}\text{Pb } T_{1/2} = 0.7038 \times 10^9 \text{a}$$

$$^{238}\text{U to } ^{206}\text{Pb } T_{1/2} = 4.4680 \times 10^9 \text{a}$$

Uranium has a very low Bulk Earth Abundance (Chondritic value  $\approx 1 \times 10^{-2}$  ppm) (Faure 1986). Partial melting and fractional crystallisation cause U to concentrate into the melt phase and so into rocks of increasingly silicic composition. Consequently, U and the radiogenic isotopes of Pb are concentrated within the continental crust relative to the mantle. The abundance of Pb, whilst higher overall, closely follows that of U with the exception of alkali feldspar, into which Pb readily enters but not U. Concentrations of U in the common rock forming minerals are uniformly low; certain accessory minerals, however contain U either as a major constituent or as a substitute for other elements; these minerals include uraninite, zircon, allanite, monazite, apatite and titanite.

### 7.2.4 Oxygen. Stable Isotope, ratio of $^{18}\text{O}$ to $^{16}\text{O}$

Oxygen isotope results are expressed as  $\delta^{18}\text{O}$  values and represent the deviations in parts per thousand (‰, per mil) of the sample from an internationally agreed standard, usually Standard Mean Ocean Water (SMOW).

Crustal processes such as weathering, hydrothermal alteration and metamorphism can cause major changes in  $\delta^{18}\text{O}$ . A rock which has gone through an orogenic cycle is enriched in  $^{18}\text{O}$  relative to magma arriving at the Earth's surface directly from the mantle, ( $\delta^{18}\text{O} > 7$  vs  $\delta^{18}\text{O} \approx 6$  respectively). Increasing temperatures during prograde metamorphism lead to lower  $\delta^{18}\text{O}$  such that upper crustal partial melts are less enriched in  $\delta^{18}\text{O}$  than the metasediments from which they were derived (Harmon 1984). Interaction between magma and meteoric water can lower  $\delta^{18}\text{O}$  dramatically.

## 7.3 Summary of the literature

The following section summarises the isotopic literature from the British Caledonides and the state of knowledge reached prior to this study on the Ben Nevis Complex. Data from the Newer Granites are reviewed first, followed by the lower crust and finally the Old Red Sandstone (ORS) lavas.

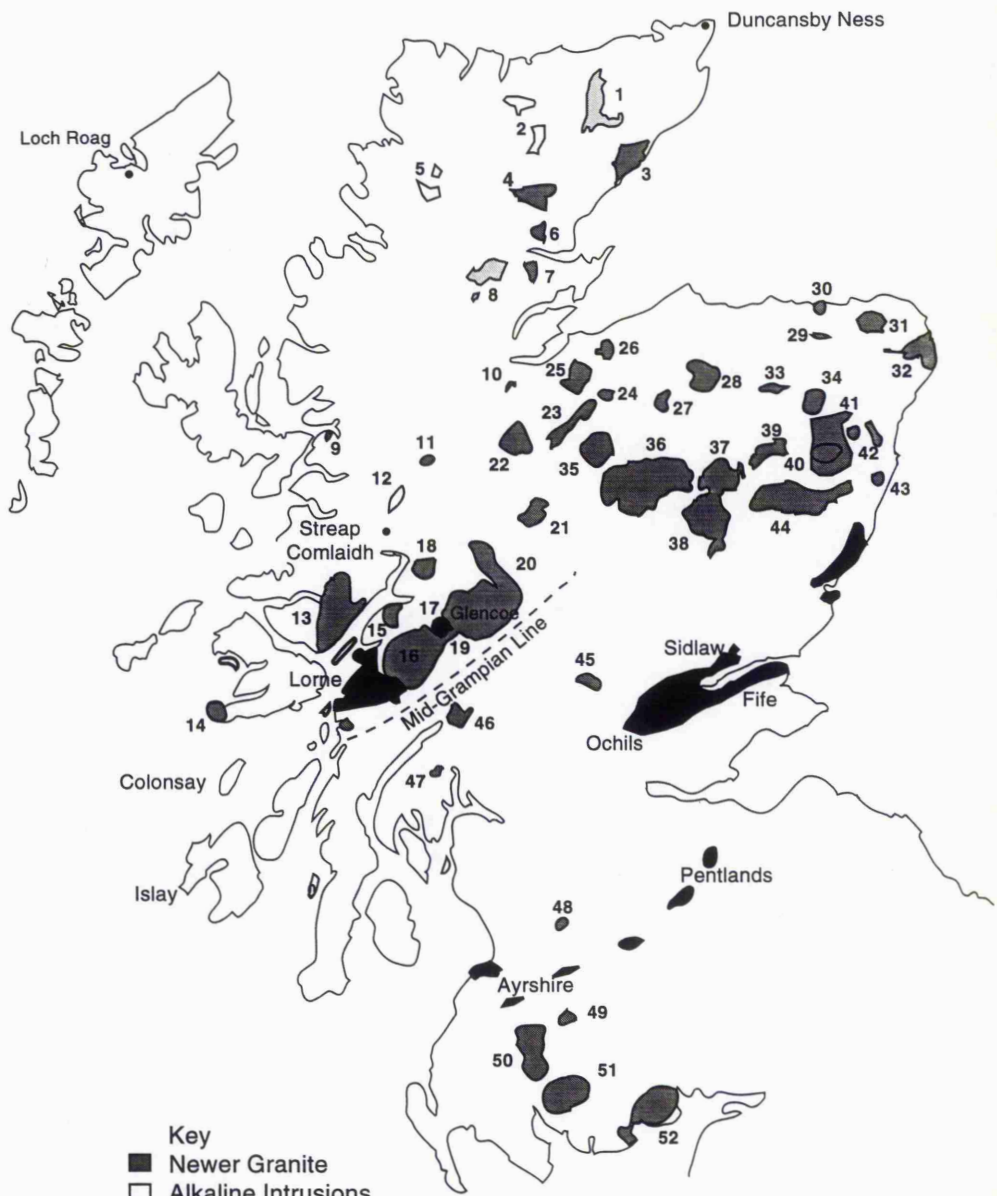
### 7.3.1 Newer Granites

The distribution of the Newer Granites is shown in Fig. 7.3.

### Key to locations in Fig. 7.3

- |                     |                               |
|---------------------|-------------------------------|
| 1. Strath Halladale | 27. Grantown                  |
| 2. Ben Loyal        | 28. Ben Rinnes                |
| 3. Helmsdale        | 29. Aberchirder               |
| 4. Lairg-Rogart     | 30. Longmanhill               |
| 5. Borralan         | 31. Strichen                  |
| 6. Migdale          | 32. Peterhead                 |
| 7. Fearn            | 33. Kennethmont               |
| 8. Carn Chuinneag   | 34. Bennachie                 |
| 9. Ratagain         | 35. Monadhliath               |
| 10. Abriachan       | 36. Cairngorm                 |
| 11. Cluanie         | 37. Glen Cairn                |
| 12. Glen Dessary    | 38. Lochnagar                 |
| 13. Strontian       | 39. Ballater                  |
| 14. Ross of Mull    | 40. Hill of Fare              |
| 15. Ballachulish    | 41. Skene complex             |
| 16. Etive           | 42. Aberdeen                  |
| 17. Glencoe         | 43. Auchlee                   |
| 18. Ben Nevis       | 44. Kincardine (Mt Battock)   |
| 19. Rannoch Moor    | 45. Comrie                    |
| 20. Strath Ossian   | 46. Garabal Hill              |
| 21. Strathspey      | 47. Arrochar                  |
| 22. Foyers          | 48. Distinkhorn               |
| 23. Glen Kyllachy   | 49. Cairnmore of Cairnsphairn |
| 24. Findhorn        | 50. Loch Doon                 |
| 25. Moy             | 51. Cairnmore of Fleet        |
| 26. Ardclach        | 52. Criffell-Dalbeattie       |

Fig. 7.3 Locations of the main granitoid intrusions, Old Red Sandstone Lavas, Mid-Grampian Line and key xenolith localities in Scotland.



- Key**
- Newer Granite
  - Alkaline Intrusions
  - Old Red Sandstone Lavas
  - ▒ Other Intrusions
  - Xenolith Localities

For key to the Location of main Newer Granite intrusions, see opposite.

### 7.3.1.i Zircon studies

Pidgeon and Aftalion (1978) presented the first regional application of an isotopic system as a petrogenetic tracer within the British Caledonian Granites (BCG). Granites to the north of the Highland Boundary Fault were shown to contain a substantial volume of old xenocrystic zircon producing strongly discordant U-Pb arrays with upper intercepts of  $\approx 1600\text{Ma}$ . Ancient inherited zircon was not present in granites outcropping south of the Highland Boundary Fault and, consequently, the Highland Boundary Fault was believed to mark a major change in the basement of Northern Britain, separating old Proterozoic basement to the north from younger Palaeozoic basement in the south.

In a study of zircon obtained from upper crustal rocks exposed north and south of the Highland Boundary Fault, Halliday et al. (1979) proposed an alternative model to that of Pidgeon & Aftalion (1978). Upper crustal rocks north of the Highland Boundary Fault (Lewisian gneisses, Moinian and Dalradian metasediments), like the granites, contain old zircon. Although those upper crustal rocks exposed south of the Highland Boundary Fault (Southern Uplands Lower Palaeozoic Sediments) also have upper intercepts of  $\approx 1600\text{Ma}$ , individual data points cluster towards the lower intercept, and Halliday et al. (1979) suggested that the proportion of old zircon was so low that it would be swamped by fresh magmatic zircon.

Evidence of an inherited zircon population was found in all the phases of the Strontian pluton (Halliday et al. 1979 and Rogers & Dunning 1991), although of minor importance in the Loch Sunart Granodiorite (tonalite of Sabine 1968). Similarly, the pyroxene mica diorite facies of the Ratagain pluton, previously thought to be the facies least likely to have interacted with continental crust (Nockolds 1941), was also found to contain zircon crystals at least as old as  $1835\text{Ma}$ . These upper intercept ages cannot be considered as the age of the protolith, merely the average upper intercept age of the zircon population analysed. Not only could the magma interact with a large number of crustal sources of varying ages (no single upper intercept age), but also some of those sources, such as Moine metasediments, are likely to include zircon crystals from a number of different crust-building events (Rogers & Dunning 1991).

Conventional U-Pb isotopic analysis of zircons from the Glen Kyllachy granodiorite indicate significant inheritance. On a concordia diagram, the data points scatter about a 'reference' reverse discordia which intersects with concordia at  $300\text{-}350\text{Ma}$  and  $1500\text{-}1600\text{Ma}$ . Scatter of the data about this reference discordia suggests that the inherited zircon population is composed of a number of zircons of significantly different ages (Pidgeon & Aftalion 1978). The SHRIMP ion microprobe enabled Pidgeon & Compston (1992) to identify three inherited zircon populations with different ages in the Glen Kyllachy granodiorite. The oldest age is obtained from two discordant points from a single zircon crystal which yields a late Archaean intersection with concordia. The validity of a discordia array constructed through such a limited data set is open to question. A second grouping of

data points cluster close to concordia between 1700Ma and 1850Ma. The third group cluster near concordia at  $\approx 1100$ Ma; again this third group is obtained from a single zircon crystal. The significance of the data is unclear. Although the data indicate the presence of three zircon populations within the Glen Kyllachy granite it is not apparent whether the data represent zircon crystals obtained from rocks generated in three crust-building episodes which are present beneath the pluton, or from a sediment that contains all three zircon populations and was incorporated into the Glen Kyllachy magma either during partial melting or wall rock assimilation.

### 7.3.1.ii Pb isotopes

Because Pb is considerably more abundant in K-feldspar than U (up to several hundred ppm vs  $< 1$  ppm), K-feldspar effectively preserves the original Pb isotopic composition of the magma from which it crystallised with negligible addition of radiogenic Pb derived from the decay of U. Blaxland et al. (1979) showed that the Pb isotopic composition of feldspars from Newer Granites increased in radiogenic Pb southwards. A best-fit regression line constructed through the Newer Granite data intersects the conventional growth curve of Stacey & Kramers (1977) at  $\approx 2700$ Ma (Fig. 7.4). Blaxland et al. (1979) believed that this indicated the involvement of ancient U-depleted granulite facies basement, the importance of which decreased southwards. A change in basement across the Midland Valley of Scotland was proposed in broad agreement with Pidgeon & Aftalion (1978).

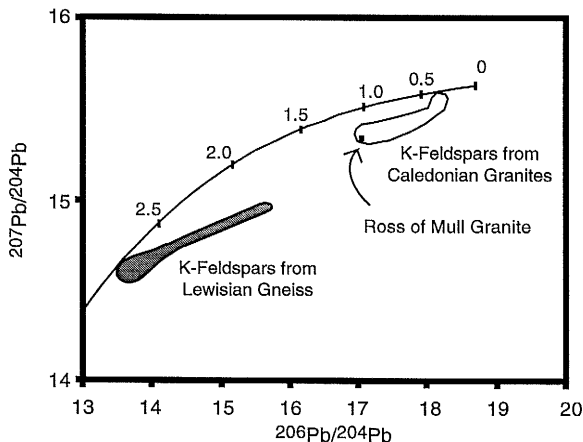


Fig. 7.4 Pb isotope data for K-Feldspars from Newer Granites. (Data from Blaxland et al. 1978 and van Breemen et al. 1979) and for Lewisian Samples (Data from Chapman & Moorbath 1977) plotted relative to two-stage Earth Evolution Curve (Stacey & Kramers 1975). Alkali feldspar from the Newer Granite is more radiogenic than alkali feldspar from the Lewisian, but tends to become more Lewisian-like closer to the area of Lewisian outcrop, e.g. Mull.

Halliday (1981) argued that Pb isotopic compositions for K-feldspars obtained from those granites closest to the region of Lewisian outcrop were more radiogenic than available

Lewisian values, thus precluding substantial Lewisian involvement (Fig. 7.4). He suggested that partial melts from Grenvillian, Moinian or Caledonian metamorphic reservoirs were more important than from the Lewisian. Further, the U content of zircon was shown to correlate with the Pb content of K-feldspar in the British Caledonian Granites. Because zircon is known to be crustally derived, the Pb isotope composition of K-feldspar must reflect the composition of the crustal source (Halliday 1981).

### 7.3.1.iii Oxygen studies

$\delta^{18}\text{O}$  tends to increase with increasing A/CNK (i.e. molar  $\text{Al}_2\text{O}_3/\text{CaO}+\text{Na}_2\text{O}+\text{K}_2\text{O}$ ), an index of alumina saturation, within individual plutons. Harmon (1984) believed this to be due in part to fractional crystallisation and in part to increasing contamination with  $^{18}\text{O}$ -rich crustal rocks.

A statistically significant correlation is observed between  $\delta^{18}\text{O}$  and initial  $^{87}\text{Sr}/^{86}\text{Sr}$  indicating increasing crustal contamination. The Cheviot and Ben Cruachan plutons both have very low  $\delta^{18}\text{O}$  (<5‰), attributed by Harmon & Halliday (1980) to interaction between the magma and  $^{18}\text{O}$ -depleted ground water.

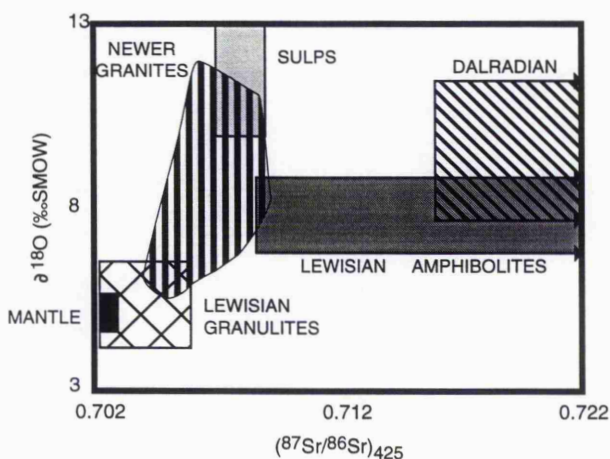


Fig. 7.5  $\delta^{18}\text{O}$  vs  $(^{87}\text{Sr}/^{86}\text{Sr})_{425}$  for the Newer Granites with fields for upper crustal rocks at 425Ma. SULPS = Southern Uplands Lower Palaeozoic Sediment. Adapted from Harmon (1984).

### 7.3.1.iv Sr isotopes

Initial  $^{87}\text{Sr}/^{86}\text{Sr}$  ratios for the Newer Granites range from near contemporary mantle values to much higher crustal values (0.703-0.7184) in a similar manner to  $\delta^{18}\text{O}$  (6‰-12‰) (Fig. 7.5). Newer Granites exposed north and south of the Highland Boundary Fault do not lie on simple mixing lines (Harmon & Halliday 1980) between contemporary mantle and any of the exposed upper crustal compositions, with the exception of Southern Uplands Lower Palaeozoic Sediment (SULPS); however SULPS is not found north of the

Southern Uplands. In addition, those granites north of the Highland Boundary Fault require a source with abundant ancient zircons; SULPS, Harmon & Halliday (1980) argued, could not supply sufficient ancient zircons to significantly affect the U-Pb zircon systematics of a magma and was therefore discounted as a magma source north of the Highland Boundary Fault. South of the Highland Boundary Fault, SULPS is a suitable end-member for the Newer Granites where a source for abundant ancient zircons is not required. Additionally, SULPS is not found north of the Southern Uplands Fault.

Harmon & Halliday (1980) suggested that the crustal contaminant for the northernmost granites is derived at least in part from an old, U-depleted crustal source such as the Lewisian granulites, which are Rb-depleted, have low  $^{87}\text{Sr}/^{86}\text{Sr}$  ratios ( $<0.705$  at 425Ma) and relatively low  $\delta^{18}\text{O}$  ( $<7\text{‰}$ ). The Pb isotope data, however, limit the involvement of Lewisian granulite (Halliday 1981 and Clayburn 1981).

### 7.3.1.v Neodymium studies

$\epsilon\text{Nd}_t$  values for the Newer Granites range from +1.3 to -13.3. The most negative (lowest) values are restricted to the Scottish Highlands ( $<-6$ ). Geographical variations in  $\epsilon\text{Nd}_t$  can be explained in two ways. Firstly, low values could reflect contamination by a greater volume of crustal material. Secondly, low  $\epsilon\text{Nd}_t$  can be generated by contamination with a different (older ?) crustal material to that in high  $\epsilon\text{Nd}_t$  granites. Fig. 7.6 discriminates between the two possibilities. If the degree of crustal contamination was the cause of  $\epsilon\text{Nd}_t$  variation, then decreasing  $\epsilon\text{Nd}_t$  should correlate with increasing  $\delta^{18}\text{O}$ . Fig. 7.6 shows that both high and low  $\epsilon\text{Nd}_t$  granites have similar  $\delta^{18}\text{O}$ . The contaminant in those magmas with low  $\epsilon\text{Nd}_t$  and inherited zircon is different from that in granites with high  $\epsilon\text{Nd}_t$  and no inherited zircon (Halliday 1984).

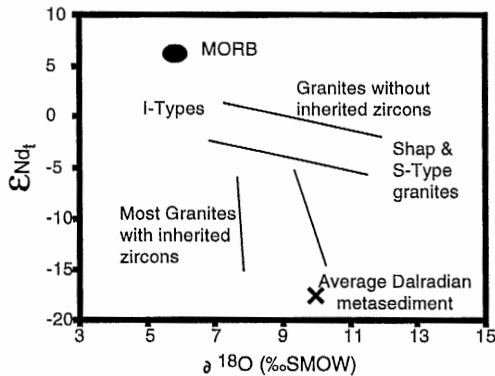


Fig. 7.6  $\epsilon\text{Nd}_t$  vs  $\delta^{18}\text{O}$  for the Newer Granites. Similar  $\delta^{18}\text{O}$  but different  $\epsilon\text{Nd}_t$  reveals the presence of two separate contaminants, one of which contains ancient zircons, the other does not. Adapted from Halliday (1984).

Low  $\epsilon\text{Nd}_t$  corresponds to high Nd model ages. Model age calculations ( $T_{\text{CHUR}}$ ) for the Newer Granites range from 590Ma (e.g. Shap), implying little incorporation of ancient

continental crust, to 1500Ma (e.g. Strichen), suggesting a large proportion of ancient continental crust was involved in the formation of the granite (Hamilton et al. 1980). TCHUR values for granites with no inherited zircon, low initial  $^{87}\text{Sr}/^{86}\text{Sr}$  and low  $\delta^{18}\text{O}$  ratios (all features previously taken as indicating a dominantly mantle origin) are around 1000Ma implying a major crustal input (but see section 7.6).

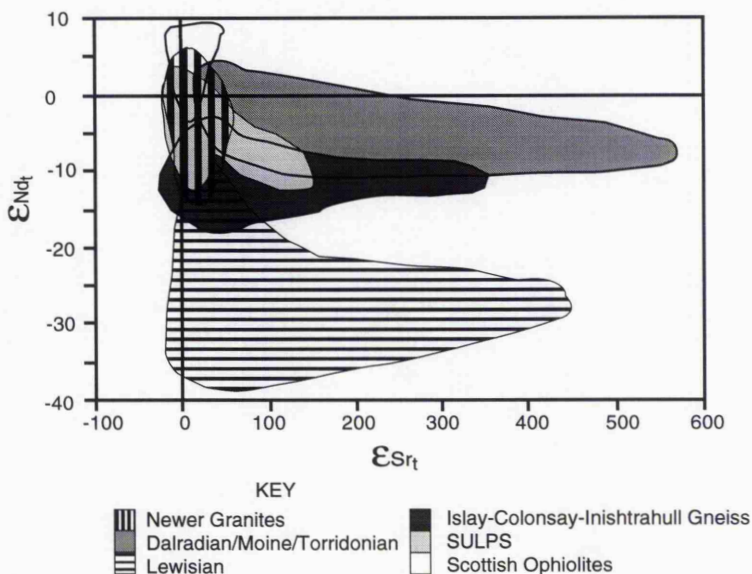


Fig. 7.7  $\epsilon\text{Sr}_t$  vs  $\epsilon\text{Nd}_t$  for Newer Granites at time of emplacement and crustal fields calculated at 425Ma. No simple two component mix can explain the distribution of the Newer Granite data set. Data from Frost & O'Nions (1985), Thirlwall (1982, 1983, 1986 & 1988), Tindle (1982), Thirlwall & Bluck (1984), Taylor et al. (1984), Waters et al. (1990), Whitehouse (1990, 1989, 1988), Marcantonio et al. (1988), Morton & Taylor (1991), Thirlwall & Burnard (1990), Fowler (1992) Dempster & Bluck (1991), Halliday (1984), Holden et al. (1987) & Clayburn (1988).

A combined Sm-Nd and Rb-Sr study identified no correlation between initial Nd and Sr isotopic ratios, although those samples with the lowest initial  $^{87}\text{Sr}/^{86}\text{Sr}$  values tended to have the highest initial  $^{143}\text{Nd}/^{144}\text{Nd}$  (Hamilton et al. 1980). Fig. 7.7 is a graph of  $\epsilon\text{Sr}_t$  against  $\epsilon\text{Nd}_t$  for the Newer Granites, along with fields for the upper crustal rocks of Northern Britain. The diagram reveals that no individual source can be a major component to the Newer Granite magmas and that no single two-component mixing model can explain all the Newer Granite data.

#### 7.3.1.vi The Mid-Grampian Line

Pidgeon & Aftalion (1978) presented evidence, obtained from U-Pb zircon studies of the British Caledonian Granites, for a major change in the basement of Northern Britain across the Highland Boundary Fault. Removal of the Ben Vuirich Older Granite from the data set translates the zircon inheritance boundary northwards, to a point midway between the

Great Glen Fault and the Highland Boundary Fault. This location coincides with that of the Mid-Grampian Line, located in Fig. 7.3 and defined by Halliday (1984) as the boundary separating Newer Granite magmas with  $\epsilon\text{Nd}_t$  values  $<-6$  to the north from those  $>-6$  to the south. Newer Granites south of the Mid-Grampian Line but intruding Dalradian metasediments, such as Lochnagar, Hill of Fare and Garabal Hill, have high  $\epsilon\text{Nd}_t$  values ( $>-6$ ), limited ancient zircon inheritance and  $\delta^{18}\text{O}$  values of  $\approx 10\%$  (Halliday 1984). Contamination of a typical metaluminous magma by Dalradian metasediment would produce a granitic magma with low  $\epsilon\text{Nd}_t$  and an inherited zircon population. The observed contrast in isotopic behaviour across the Mid-Grampian Line cannot therefore be explained by contamination with different types of upper crustal rock as the exposed rocks do not reveal a pattern comparable to that of the Newer Granites. One interpretation of the Mid-Grampian Line therefore, is that it reflects a fundamental change in the basement architecture of Northern Britain with young continental crust occurring south of the Mid-Grampian Line and older crust to the north, and that it may represent the surface expression of the rifted margin to the Dalradian sedimentary basin (Halliday 1984).

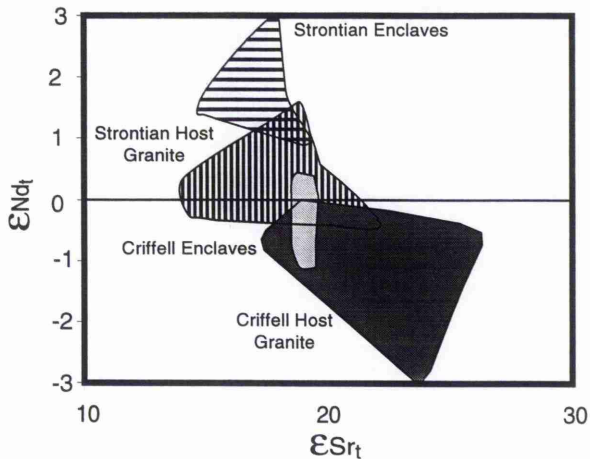


Fig. 7.8  $\epsilon\text{Nd}_t$  vs  $\epsilon\text{Sr}_t$  for enclaves and granites from Strontian and Criffell.  $\epsilon\text{Nd}_t$  for enclaves displaced to higher (more primitive) values. Data from Holden et al. (1987).

### 7.3.1.vi Mantle melting

There is direct evidence for partial melting of the mantle contemporaneously with the intrusion of the Newer Granites (Rogers & Dunning 1991 and Thirlwall 1988). This evidence includes the presence of high MgO and Ni basalts, andesites and diorites and the widespread occurrence of lamprophyre dykes and appinitic bodies. In addition, Holden et al. (1987) documented the isotope geochemistry of mafic microgranular enclaves (MME) and host rock pairs for the Strontian and Criffell plutons; their results are displayed in Fig. 7.8. In both cases, relatively high enclave  $\epsilon\text{Nd}_t$  values could be explained if the enclaves represent syn-plutonic injections of mafic magma into the host granitoid. Enclaves may therefore represent the remains of mantle derived heat and/or mass transfer processes

operating during the formation of the Newer Granite magmas. Alternatively, the MME may be the remains of dykes emplaced during intrusion of the Strontian and Criffell plutons (Holden et al. 1987) and therefore, genetically unconnected with the granites.

#### 7.3.1.vii The Etive Complex

Frost & O'Nions (1985), in a study of the Etive Complex, limited the involvement of Dalradian metasediments to <25%. They believed that the mantle contribution to the Etive granites was negligible, although passage of mantle derived magmas through the crust during the eruption of the Lorne and Glencoe lavas prior to the intrusion of the granites, may have facilitated their intrusion by heating the surrounding rock. As contamination by Dalradian metasediments would push initial Sr and Nd isotopic ratios to higher  $\epsilon\text{Sr}_t$  and lower  $\epsilon\text{Nd}_t$ , a large proportion of the Etive granite magma must be derived from lower crust with relatively unradiogenic Sr, Pb and radiogenic Nd compositions. The nature of this component is now described.

#### 7.3.2 The Lower Crust

The nature of the lower crust across Northern Britain has been a matter for considerable debate. Most authors agree that the lower crust played a role in the formation of the Newer Granites (e.g. Frost & O'Nions 1985) however, no correlative with the required isotopic composition is exposed at the surface with the possible exception of SULPS. High Rb and U concentrations, Pb-Pb and Sm-Nd isotopic data rule out Lewisian granulites as sources to the Etive granites. Low initial  $^{87}\text{Sr}/^{86}\text{Sr}$  ratios rule out the Dalradian and Moian metasediments, and although SULPS has the required isotopic geochemistry, it is unable to supply old inherited zircon, as well as not being exposed north of the Highland Boundary Fault.

##### 7.3.2.i Seismic evidence

Deep crustal seismic experiments (e.g. LISPB profile of Bamford 1979) across Northern Britain indicate that rock with similar geophysical properties to the Lewisian exists below the surface as far south as the Southern Uplands Fault (SUF) (Fig. 7.9). It should be noted that seismic methods are unable to resolve between different tectonic units formed from similar rock types but of different ages e.g. Islay-Colonsay gneiss vs Lewisian Gneiss.

A major problem with invoking Lewisian granulite as a major source for the Newer Granites is its refractory nature. Watson & Dunning (1979) surmounted this problem by suggesting that the basement below the Moine and Dalradian Supergroups had been intruded by a greater volume of felsic magma than the Lewisian exposed at the surface in the Hebridean Craton and was therefore more fusible. Orogenic events which may have intruded felsic magmas into this basement include the Laxfordian (1800Ma), the Grenvillian (1000Ma), the Morarian (750Ma) and early Caledonian (>450Ma).

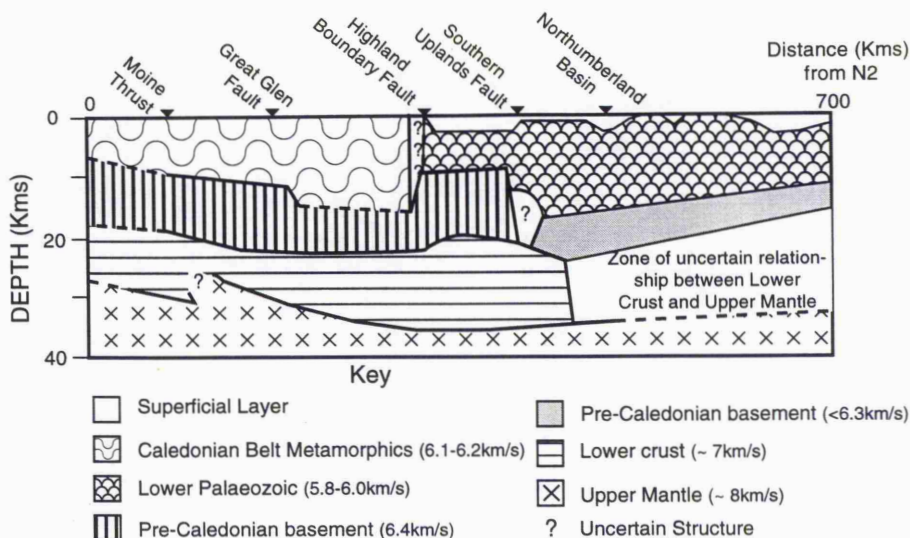


Fig. 7.9 LISPB profile across Northern Britain (Bamford 1979).

### 7.3.2.ii Xenoliths

Evidence for the composition of the lower crust and upper mantle can be obtained from xenoliths believed to have been excavated from these regions. Systematic changes occur in granitoid chemistry, especially in Ba, Sr, Na, Zr and REE abundances, from north to south across Scotland (Stephens & Halliday 1984). Any xenolith population mirroring such a pattern identifies a likely source region for the granite magmas. Analysis of lower crustal granulite facies xenoliths reveals no comparable regional variation (Halliday et al. 1985), whereas xenoliths from the lithospheric mantle do show similar regional chemical variations. The Newer Granites appear, therefore, to have been generated in part from the lithospheric mantle which is chemically zoned across northern Britain (Menzie et al. 1987). But lithospheric mantle cannot be the only source as the mantle cannot supply ancient zircons (Halliday 1981), and the isotopic systematics of Rb-Sr, U-Pb, Sm-Nd and  $^{18}\text{O}$  are all displaced towards compositions more akin to those of the continental crust (Frost & O'Nions 1985).

Lower crustal xenoliths from the Northern Highlands have younger  $T_{Dm}^{Nd}$  model ages than Lewisian granulite-facies gneisses. From this evidence, Menzie & Halliday (1988) concluded that the lower crust in this area was younger than most Lewisian granulite-facies gneiss. Sm-Nd model ages give no impression of a distinct crustal growth event and there is a considerable amount of geophysical evidence (Hall et al. 1984) and geological evidence (Shackleton 1979 and Bluck 1984) for a complex history of lower crustal accretion and thrusting in this area.

### 7.3.2.iii Evidence for Grenvillian lower crust

Clayburn et al. (1983), Davies et al. (1984) and Holden (1987) favour a Grenvillian (1000Ma) age for the lower crust based on similar  $T_{\text{CHUR}}$  and zircon U-Pb upper concordia intercept ages of  $\approx 1000\text{Ma}$  for the Newer Granites. Evidence for a Grenvillian primary crustal building event in Scotland is equivocal. Areas adjacent to Scotland during the Grenvillian Orogeny in Canada and Scandinavia, are characterised by crustal recycling and not crustal formation (McCulloch & Wasserburg 1978 and Field & Råheim 1981). It is therefore, not unreasonable to expect that if Grenvillian events do occur in Scotland then they should relict similar recycling processes; consequently, the apparently favourable  $T_{\text{CHUR}}$  and U-Pb zircon upper intercept ages are coincidental (Frost & O'Nions 1985).

A granulite-facies metasedimentary xenolith from Partan Craig (Midland Valley) has yielded a  $T_{\text{CHUR}}$  model age of  $1180 \pm 55\text{Ma}$  and van Breemen & Hawkesworth (1980) interpret this as the age of granulite-facies metamorphism. However, it is unlikely that the model age corresponds directly with any rock forming event (Frost & O'Nions 1985) and the Nd of this sample could have come from a number of different sources.

It should be noted that upper intercept ages derived from zircon *populations* represent *averages* of the crust through which the magma has passed, and model age calculations will only be correct if the assumptions on which the model is based (e.g. mantle composition) are correct.

It is unlikely that the lower crust beneath Northern Britain was formed during a single event. There is stratigraphic, tectonic and geochemical evidence to support this :

- i) The Pb isotope composition of K-feldspars obtained from the Newer Granites are increasingly radiogenic southwards from the area of Lewisian outcrop (Blaxland et al. 1979).
- ii) Postulated existence of the Mid-Grampian Line (Halliday & Stephens 1984).
- iii) Absence of inherited zircons south of the Highland Boundary Fault (or Mid-Grampian Line) (Pidgeon & Aftalion 1978).
- iv) Sm-Nd model ages for xenoliths excavated from the lower crust decrease to the south and may indicate decreasing age of lithospheric mantle from north to south (Menzies & Halliday 1988).
- v) If SULPS is interpreted as an accretionary prism then the crust beneath the prism must be, in part, oceanic and therefore younger than that to the North (Legget et al. 1979).
- vi) There is a tendency for the Newer Granites to become more Lewisian-like (isotopically and chemically) towards the area of Lewisian outcrop, either because of assimilation of Lewisian at depth, or derivation from the lithospheric mantle formed at the same time and subsequently suffering the same enrichment and depletion events as the Lewisian (Halliday et al. 1985).
- vii) There is much evidence that the ages of mantle and crustal lithosphere are linked

(Cohen et al. 1984 and Richardson et al. 1984). If the age of the crustal lithosphere increases to the north (point iv), then the mantle lithosphere should mirror this pattern and the preliminary work of Menzies et al. (1987) suggests that this is the case.

The upper crustal rocks of Northern Britain show striking variations from north to south and it is not unreasonable to assume that the lower crust varies in a similar manner. Given the number of proposed events affecting northern Britain (e.g. Watson & Dunning 1979) prior to the Caledonian, it is not surprising that the lower crust is heterogeneous, as suggested above.

### 7.3.3 Old Red Sandstone Volcanics

The location of volcanic rocks of comparable age to the Newer Granites is shown in Fig. 7.3. Together, these outcrops form an extensive calc-alkaline suite of basalts, andesites, dacites, rhyolites and pyroclastics, parts of which have close spatial and temporal relationships with high-level permitted Newer Granite intrusions such as Ben Nevis and Glencoe. Locally shoshonitic magmas occur and the youngest lavas (Hoy lavas of Orkney) are broadly alkaline (Fitton et al. 1982). Rocks rich in Ni and Cr are unusually abundant and have compatible element concentrations little different from primitive magmas (Thirlwall 1981). Any variation observed in these primitive magmas must therefore be source-related.

Temporal and spatial chemical variations in the Old Red Sandstone (ORS) volcanics outcropping north of the Southern Uplands have been cited as evidence for the existence of a subduction zone (Thirlwall 1981), active during much of the Silurian. The strike of this subduction zone changed across Northern Britain, from ENE-WSW in Ireland and Southern Scotland to N-S in the North Sea (Thirlwall 1981). Spatial chemical variations have been observed in modern arcs unconnected with the geometry of the subducting plate (e.g. Gamble et al. 1992) and so geochemical data do not provide unequivocal evidence of subduction.

In modern subduction zones the arc-trench gap is normally greater than 90km and often more than 150km (Yardley et al. 1982). Those magmas outcropping south of the Highland Boundary Fault cannot therefore be generated by subduction related magmatic processes centred on the Iapetus suture/Solway Line. Thirlwall (1981 & 1988) also believes that the Southern Uplands magmas are younger than those further north. However, recent U-Pb work (Rogers and Paterson pers. comm.) has shown that Criffell is older than previously thought and comparable in age (414Ma) to certain rocks further north, and any model based on the younger Rb-Sr isochrons for those plutons in the Southern Uplands must be re-examined.

Whilst tectonic models based on geochemical variations alone are open to question, the ORS lavas provide useful data on the chemistry of the upper mantle. Sr and Nd isotope analyses of primary ORS lavas (Ni > 100ppm, Cr > 150ppm) within the Midland Valley and the South West Highlands (Lorne and Glencoe) reveal the existence of two mantle sources

(Thirlwall 1982). Lavas in the South West Highlands have relatively unradiogenic compositions, some of which fall below the mantle array in  $\epsilon Nd_t$  and  $\epsilon Sr_t$  space (Fig. 7.10). Midland Valley lavas parallel the trend of the mantle array, but are displaced to higher  $\epsilon Sr_t$  compositions. Both South West Highland and Midland Valley ORS lavas have a similar range of  $\epsilon Sr_t$  values but different  $\epsilon Nd_t$ . Similar isotopic ratios to the Lorne lavas have been observed within the Skye Plateau Basalts (Carter et al. 1978 and Thirlwall & Jones 1983); and these authors interpret  $\epsilon Nd_t$  values below the mantle array as being due to the effects of contamination with granulite facies Lewisian basement. However, Pb isotope, trace element and REE data from the Lorne lavas are inconsistent with large amounts of contamination by Lewisian crust, and Thirlwall (1982) attributes the observed pattern to the presence of LREE-enriched mantle beneath the Southwest Highlands. Displacement of the Midland Valley data to more radiogenic values than the mantle array illustrates the incorporation of subducted SULPS-like sediment into a depleted mantle source prior to extrusion (Thirlwall 1986).

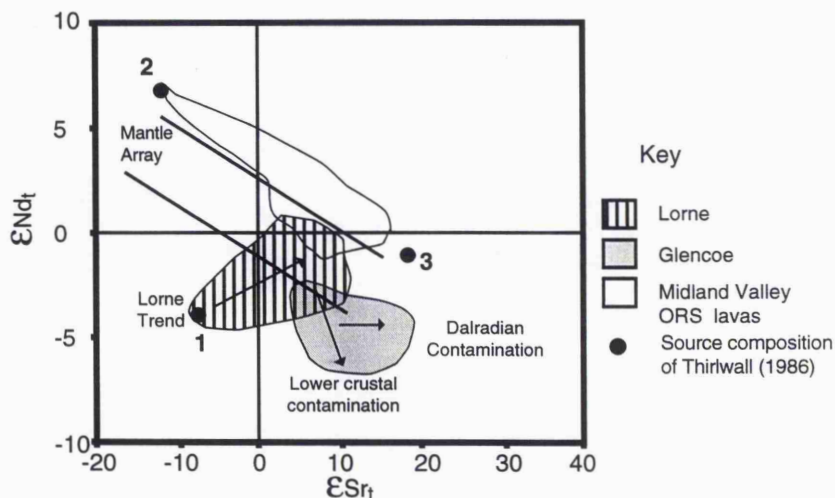
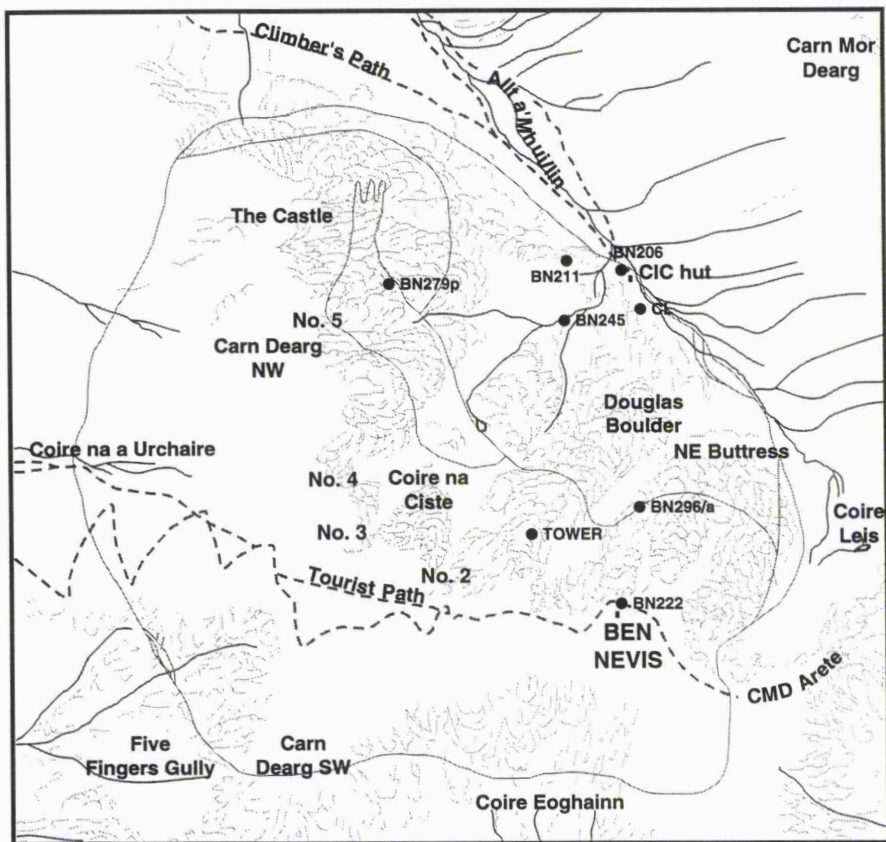


Fig. 7.10  $\epsilon Nd_t$  vs  $\epsilon Sr_t$  for Old Red Sandstone (ORS) lavas and the Mantle array. Numbers 1-3 refer to Thirlwall's (1982) three source compositions, 1=Southwest Highland mantle, 2=Depleted mantle and 3=Subducted slab. Data from Frost & O'Nions (1985) and Thirlwall (1982, 1983 & 1986).

Pb isotope data for the South West Highland lavas (Thirlwall 1986) restrict the involvement of any continental crust during their formation to  $\approx 1750$ Ma Rb-depleted granulite facies rocks. Thirlwall (1986) believed such crust to be absent within Northern Britain and a mantle source for the ORS lavas with low  $\mu$ , Rb/Sr and Sm/Nd was proposed. Located deep in the lithospheric mantle and unlike enriched lithosphere below the Lewisian (Menzies et al. 1987), this source is believed to have contributed melts to some of the Newer Granites. Recent studies of the basement of Islay-Colonsay, Inishtrahull and (possibly) the Rockall Plateau (Morton & Taylor 1991) document the existence of  $\approx 1800$ Ma crust (Dickin & Bowes 1991 Dickin 1992 and Muir et al. 1992) and in this

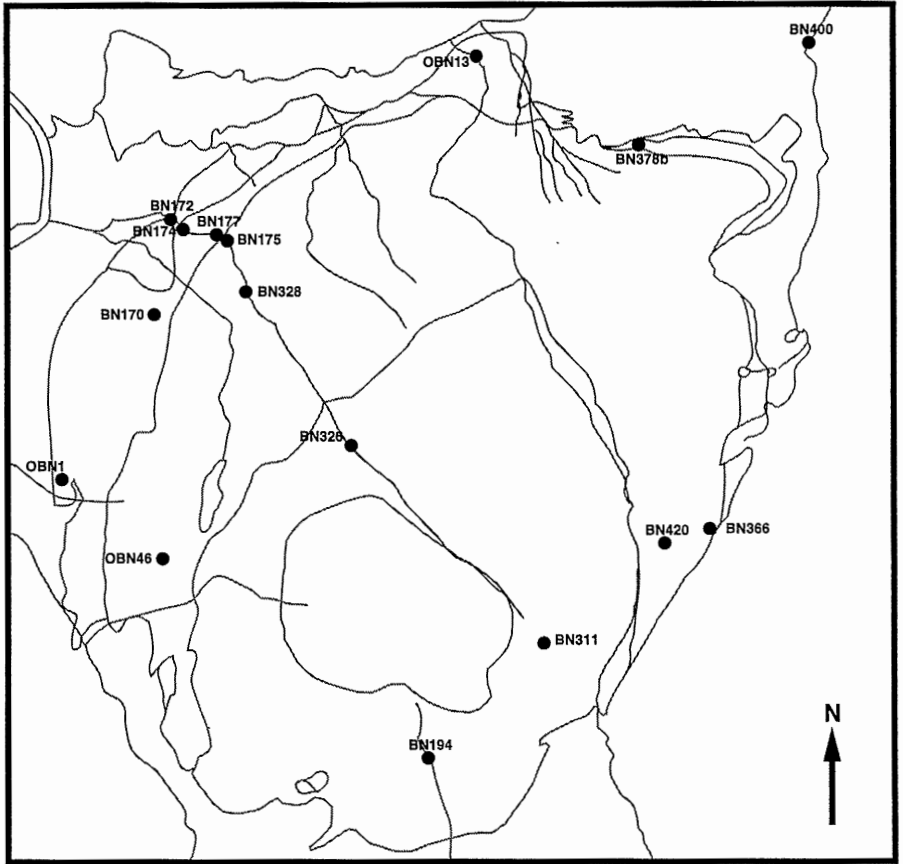


Key

● BN206 Location of sample.

0.5 km

Fig. 7.11b The location of volcanic samples analysed for Nd and Sr isotopes.



**KEY**

● BN174 Location of exposure

Fig. 7.11a The location of intrusive samples analysed for Nd and Sr isotopes.

thesis the possibility that the Islay-Colonsay basement may be a possible source for Ben Nevis will be examined.

## 7.4 Isotope Geology of the Ben Nevis Complex

### 7.4.1 Introduction

Isotopic analysis was carried out using the facilities of the Isotope Geosciences Unit at the Scottish Universities Research and Reactor Centre. Details of methods and instrumentation are given in Appendix IV and the results are presented in this chapter. New Rb-Sr isotope results will be presented first followed by the new Sm-Nd data.

In accordance with the geochemistry chapter (chapter 6), the SiO<sub>2</sub> content is used as an index of magmatic evolution. The geographical location of intrusive and volcanic samples analysed in this study is illustrated in Figs. 7.11a and 7.11b respectively and listed in Appendix I.

In the literature review above, two papers present isotopic data for the Ben Nevis Complex (Hamilton et al. 1980 and Harmon & Halliday 1980). Only general comparisons can be made with results presented here, because the sample locations and lithologies in the published results are unknown. Both papers term the samples studied 'granite', but historically the entire Complex has been referred to as granite (e.g. Maufe 1910 Outer Granite and Inner Granite). Hamilton et al. (1980) published a grid reference for their sample; however this reference (NM115716) does not fall within the outcrop of the Ben Nevis Complex. The published data are within the fields of Porphyritic Outer Granite and Inner Granite (Fig. 7.12b) as defined in this study and are therefore ignored.

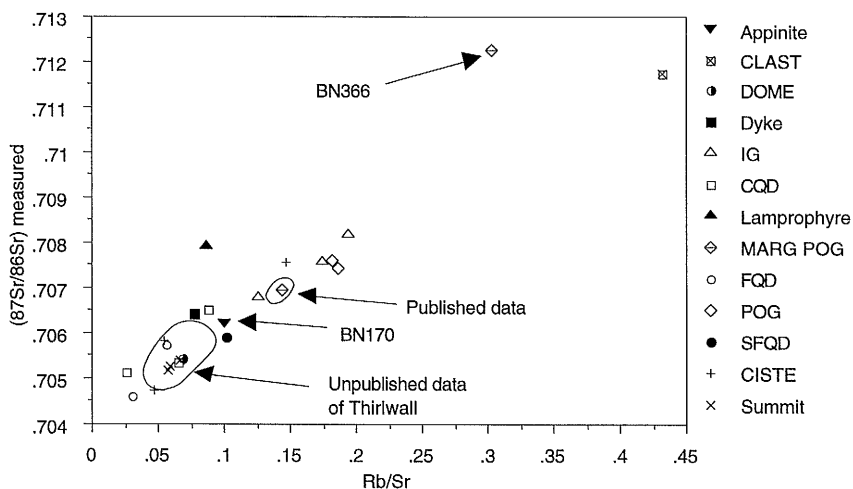


Fig. 7.12a ( $^{87}\text{Sr}/^{86}\text{Sr}$ ) measured vs Rb/Sr for Ben Nevis Complex. Note position of BN170 (appinite) relative to rest of data. Field of Thirlwall unpublished data. Published results from Hamilton et al. (1980) and Harmon & Halliday (1980).

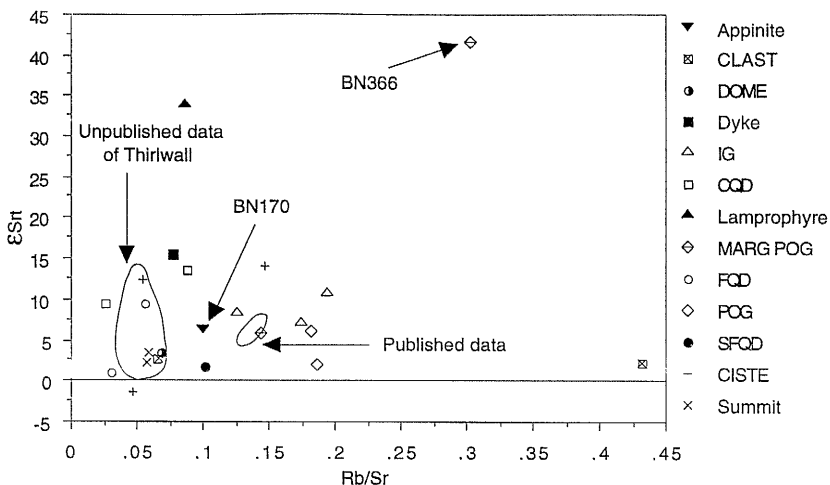


Fig. 7.12b  $\epsilon Sr_t$  vs Rb/Sr for Ben Nevis Complex. Field of Thirlwall unpublished data. Published results from Hamilton et al. (1980) and Harmon & Halliday (1980).

In addition to my own samples, Dr M. F. Thirlwall (Royal Holloway and Bedford New College, University of London) was kind enough to send me his unpublished geochemical and Rb-Sr data for the Ben Nevis Volcanics. Rb-Sr analyses were available for five of the twelve samples. In Figs. 7.12a and 7.12b Thirlwall's data are presented in the form of a field rather than individual data points. Direct comparisons with data presented here are not possible because a number of his samples were not collected from outcrop but from scree. Presenting Thirlwall's data as a field is a valid method because the data cluster together (Figs. 7.12a & 7.12b). This is perhaps not surprising given that the range in silica content of these samples is small, falling between 63% and 63.5%, with one exception BN5024 ( $SiO_2 = 65\%$ ). Initial Sr isotope ratios for this sample are slightly higher than for the main group but no further interpretation can be made from this sample as it was retrieved from scree. Obtaining samples from scree suffers from a major problem, namely that individual clasts within volcanic breccias include eutaxitic ignimbrite clasts and rhyolite neither of which is found *in situ* on Ben Nevis and may therefore be derived from a source several tens of kilometres distant (chapter 3). Sampling of scree cannot differentiate between clasts obtained from breccias, flows or sills/domes and cannot aid in the identification of temporal variations in the development of the underlying magma chamber.

#### 7.4.2 Selection of samples

##### 7.4.2.i Intrusive members of the Ben Nevis Complex

Samples from the plutonic rocks were selected on the basis of whole rock major and trace element chemistry and petrological criteria, and represent the range of compositions

found within individual units and the Ben Nevis Complex as a whole. In addition, a sample of appinite from the surge chamber locality, along with a sample from a lamprophyre dyke were analysed. Appinites are believed to represent the plutonic equivalents of lamprophyres and both are sometimes interpreted as representative of the parent magmas to the Newer Granites (Pitcher 1993 and refs. therein). A basic example of the Ben Nevis dyke swarm was also analysed.

#### 7.4.2.ii The Volcanic Pile

In chapter 3, the volcanic pile is subdivided into five units, two of which, the Coire na Ciste fm. and the Summit andesite fm., are comprised of andesite to a greater or lesser degree. Three samples were selected from the Coire na Ciste fm. and represent the base of the volcanic sequence, and three samples were analysed from the Summit andesite fm. representing the top of the volcanic pile. The three specimens as far as possible represent the most basic and the most siliceous samples. The two groups of andesite are referred to as the Ciste andesites and the Summit andesites respectively.

Two additional samples from the volcanic pile were analysed. The most acidic rock types found anywhere in the volcanic pile are fine grained rhyolite clasts within a number of the volcanic breccias. One of these clasts, from a volcanic breccia near the CIC hut and therefore towards the base of the volcanic pile, was selected for isotope analysis. It should be noted that no rhyolite was found at outcrop within the volcanic pile and the rhyolite clasts may be unrelated to the Ben Nevis Complex, although it is geochemically similar (chapter 6). In terms of Ni and MgO contents, the most primitive rock analysed from the volcanic pile is represented by a small intrusive dome exposed above the amphitheatre on Ledge Route (chapter 3) and a sample of this intrusion was selected for analysis.

#### 7.4.3 The age of the Ben Nevis Complex

Whole-rock Rb-Sr isochrons can be calculated for the Ben Nevis Complex or for individual units from the data presented in Table 7.1. Typical Newer Granite ages are obtained (430Ma-400Ma); however, the spread of ages, analytical error and mean weighted square deviation (MSWD) render discussion of these ages as meaningless. Two factors contribute to the spread of ages and large errors; these are:

i) Rb/Sr ratios are uniformly low (<0.5), reducing the precision of the Rb-Sr whole-rock method of dating.

ii) The samples analysed are not related by simple fractional crystallisation processes (chapter 6) and their initial Sr ratios differ slightly from each other as a consequence.

Radiometric ages obtained from the Ben Nevis Complex during regional surveys are listed below (Table 7.1) and range between  $390 \pm 5$ Ma and  $449 \pm 20$ Ma. Additionally, two fission track ages were published by Hurford (1977) and gave anomalously young ages of

354±38 (titanite) and 237±24 (apatite). Hurford (1977) believed these young ages to reflect post-intrusion events and alteration. Bailey & Maufe (1916 & 1960) believed that the Ben Nevis Complex was formed at the same time as the Etive-Glencoe complex. Fossils collected within the Glencoe cauldron are late Silurian to Devonian.

Modern U-Pb dating of Highland Caledonian plutons has produced a cluster of ages around 425Ma (Rogers & Dunning 1991), the only exception being the Glen Sanda Granodiorite (Strontian) with 418Ma (Paterson et al. 1993). For this reason an age of 425Ma is a reasonable assumption for the age of the Ben Nevis Complex. However, because the rocks of the Ben Nevis Complex have low Rb/Sr ratios (<0.5), changing this age by as much as 25Ma has little effect on the initial isotope ratios calculated. Similar Sm/Nd ratios for samples from the Ben Nevis Complex mean that everything is translated to the same degree such that their relative positions do not change. This also holds for Rb-Sr isotopes.

Table 7.1 Radiometric Ages for the Ben Nevis Complex in the literature.

Miller & Brown (1965)	449±10Ma K-Ar Biotite	456±20Ma (recalculated)
Outer Granite {	394±18Ma K-Ar Biotite	
	421±19Ma K-Ar Biotite	
Inner Granite	405±15Ma K-Ar Biotite	407±18Ma (recalculated)
Harper (1967) Ben Nevis	411±6Ma K-Ar Biotite	
Brown (1972)	411±6Ma K-Ar Whole-rock	
Andesites{	416±5Ma K-Ar Whole-rock	
	390±5Ma K-Ar Whole-rock	
Andesite	413±5Ma Rb-Sr Whole-rock	
Plutonics	410±6Ma Rb-Sr Whole-rock	
Recalculated ages use the decay constants of Steiger & Jäger (1977)		

#### 7.4.4 Strontium isotope results

Strontium isotope data for the Ben Nevis Complex are presented in Table 7.2.

##### 7.4.4.i Volcanic Pile

Samples from the base of the volcanic pile have initial Sr isotope ratios of between 0.70391 ( $\epsilon\text{Sr}_t = -1.3$ ) and 0.70500 ( $\epsilon\text{Sr}_t = 14.1$ ), whereas those from the top of the volcanic pile have a more restricted range of between 0.70416 ( $\epsilon\text{Sr}_t = 2.2$ ) and 0.70425 ( $\epsilon\text{Sr}_t = 3.5$ ). The rhyolitic clast has an initial Sr isotope ratio of 0.70416 ( $\epsilon\text{Sr}_t = 2.2$ ) and that from the intrusive dome is 0.70425 ( $\epsilon\text{Sr}_t = 3.5$ ).

Table 7.2 Sr and Nd Isotope Results for the Ben Nevis Complex.

Sample	Type	Rb	Sr	Rb/Sr	$^{87}\text{Rb}/^{86}\text{Sr}$	$^{87}\text{Sr}/^{86}\text{Sr}$	$\epsilon\text{Sr}_t$	Sm	Nd	Sm/Nd	$^{147}\text{Sm}/^{144}\text{Nd}$	$^{143}\text{Nd}/^{144}\text{Nd}$	$\epsilon\text{Nd}_t$
BN206	Ciste	80	545	0.1468	0.4247	0.70757 ± 3	14.1	5.507	36.25	0.1520	0.0919	0.512003 ± 6	-6.71
BN211	Ciste	51	932	0.0548	0.1584	0.70583 ± 2	12.3	3.321	19.13	0.1736	0.1049	0.512010 ± 6	-7.28
BN245	Ciste	66.5	1399	0.0472	0.1365	0.70474 ± 5	-1.3	4.626	28.58	0.1618	0.0978	0.512037 ± 6	-6.37
BN222	Summit	63	1106	0.0570	0.1648	0.70516 ± 4	2.2	3.655	20.27	0.1803	0.1090	0.511972 ± 14	-8.25
BN296A	Summit	70	1194	0.0586	0.1695	0.70528 ± 2	3.5	5.487	28.37	0.1934	0.1169	0.512043 ± 6	-7.29
TOWER	Summit	63	924	0.0671	0.1941	0.70537 ± 2	2.7	4.045	41.11	0.0984	0.0595	0.511978 ± 7	-5.44
BN279P	Dome	66	970	0.0676	0.1967	0.70544 ± 3	3.5	5.604	32.96	0.1700	0.1028	0.512048 ± 6	-6.42
CL	CLAST	71	163	0.4321	1.2507	0.71173 ± 4	2.2	3.753	22.48	0.1669	0.1009	0.512027 ± 6	-6.73
OBN13	FQD	36	1179	0.0301	0.0871	0.70461 ± 2	1.1	4.922	30.04	0.1466	0.0886	0.512060 ± 5	-5.42
BN172	FQD	61	1066	0.0568	0.1642	0.70573 ± 4	9.5	4.205	23.44	0.1795	0.1085	0.512013 ± 6	-7.41
BN378b	SFQD	84	827	0.1016	0.2938	0.70591 ± 3	1.8	6.247	38.08	0.1640	0.0992	0.512073 ± 6	-5.76
OBN1	CQD	65	985	0.0655	0.1894	0.70535 ± 2	2.8						
BN177	CQD	31	1225	0.0253	0.0732	0.70511 ± 3	9.4	5.944	32.43	0.1833	0.1108	0.512046 ± 5	-6.91
BN174	CQD	101	1135	0.0886	0.2562	0.70651 ± 5	13.5	6.895	49.06	0.1405	0.0850	0.512062 ± 6	-5.18
BN366	MARG POG180	594	0.3030	0.8771	0.71225 ± 2	41.7	5.594	29.27	0.1911	0.1155	0.512071 ± 7	-6.66	
BN420	MARG POG113	776	0.1443	0.4176	0.70694 ± 3	5.8	4.922	30.04	0.1638	0.0990	0.512081 ± 7	-5.57	
BN175	POG	111	608	0.1819	0.5263	0.70762 ± 4	6.1						
BN328	POG	116	620	0.1871	0.5413	0.70742 ± 2	2.0	3.666	23.86	0.1536	0.0929	0.512049 ± 7	-5.86
BN194	IG	85	671	0.1259	0.3643	0.70679 ± 4	8.2	5.259	33.08	0.1590	0.0961	0.512030 ± 7	-6.41
BN311	IG	101	520	0.1942	0.5620	0.70816 ± 2	10.7	5.375	36.20	0.1485	0.0898	0.512000 ± 7	-6.65
BN326	IG	94	541	0.1741	0.5036	0.70755 ± 3	7.0	4.998	35.33	0.1415	0.0855	0.511995 ± 7	-6.52
OBN46	DYKE	63	810	0.0772	0.2232	0.70645 ± 3	15.5	4.934	26.47	0.1864	0.1127	0.512104 ± 6	-5.88
BN400	LAMP	76	876	0.0868	0.2510	0.70791 ± 2	33.9	4.657	27.22	0.1711	0.1034	0.512013 ± 7	-7.15
BN170	Appinite	30	293	0.1005	0.2908	0.70619 ± 2	6.0	9.900	53.39	0.1854	0.1121	0.512024 ± 6	-7.40

#### 7.4.4.ii Plutonic members of the Ben Nevis Complex

Initial Sr isotope ratios for the Fine Quartz Diorite are 0.70408 ( $\epsilon\text{Sr}_t = 1.1$ ) and 0.70468 ( $\epsilon\text{Sr}_t = 9.7$ ), and that from the Sgurr Finnisg-aig Quartz Diorite is 0.70413 ( $\epsilon\text{Sr}_t = 1.8$ ). Values from the Coarse Quartz Diorite range between 0.70420 ( $\epsilon\text{Sr}_t = 2.8$ ) and 0.70496 ( $\epsilon\text{Sr}_t = 13.5$ ). The Porphyritic Outer Granite has initial Sr isotope ratios of between 0.70414 ( $\epsilon\text{Sr}_t = 2.0$ ) and 0.70694 ( $\epsilon\text{Sr}_t = 41.7$ ); however, the majority fall between 0.70450 and 0.70476 with only one sample (BN366) having an initial Sr ratio greater than 0.70476. Samples from the Inner Granite have initial Sr ratios of between 0.70450 ( $\epsilon\text{Sr}_t = 7.0$ ) and 0.70476 ( $\epsilon\text{Sr}_t = 10.7$ ).

#### 7.4.4.iii Miscellaneous intrusions

Initial Sr isotope ratios of 0.70510 ( $\epsilon\text{Sr}_t = 15.5$ ), 0.70639 ( $\epsilon\text{Sr}_t = 33.9$ ) and 0.70443 ( $\epsilon\text{Sr}_t = 6.0$ ) were recorded for the basic dyke, the lamprophyre dyke and the appinite respectively.

#### 7.4.5. Neodymium Isotope Results

Neodymium isotope data from the Ben Nevis Complex are presented in Table 7.2.

##### 7.4.5.i Volcanic Pile

Initial  $^{143}\text{Nd}/^{144}\text{Nd}$  results for the base of the volcanic pile range from 0.511718 ( $\epsilon\text{Nd}_t = -7.28$ ) to 0.511765 ( $\epsilon\text{Nd}_t = -6.37$ ), and from 0.511669 ( $\epsilon\text{Nd}_t = -8.25$ ) to 0.511812 ( $\epsilon\text{Nd}_t = -5.44$ ) in samples from the top of the volcanic pile. The sample from the rhyolitic clast has an initial Nd ratio of 0.511746 ( $\epsilon\text{Nd}_t = -6.73$ ), whereas that from the intrusive dome is 0.511762 ( $\epsilon\text{Nd}_t = -6.43$ ).

##### 7.4.5.ii Plutonic members of the Ben Nevis Complex

Samples from the Fine Quartz Diorite have initial Nd isotope ratios in the range from 0.511711 ( $\epsilon\text{Nd}_t = -7.42$ ) to 0.511813 ( $\epsilon\text{Nd}_t = -5.42$ ), those from the Coarse Quartz Diorite are between 0.511738 ( $\epsilon\text{Nd}_t = -6.90$ ) and 0.511825 ( $\epsilon\text{Nd}_t = -5.19$ ), the Sgurr Finnisg-aig Quartz Diorite has an initial Nd isotope ratio of 0.511791 ( $\epsilon\text{Nd}_t = -5.74$ ). Samples from the Porphyritic Outer Granite have initial isotope ratios of between 0.511737 ( $\epsilon\text{Nd}_t = -6.91$ ) and 0.511805 ( $\epsilon\text{Nd}_t = -5.58$ ), and those from the Inner Granite range between 0.511750 ( $\epsilon\text{Nd}_t = -6.66$ ) and 0.511763 ( $\epsilon\text{Nd}_t = -6.41$ ).

##### 7.4.5.iii Miscellaneous intrusions

Initial Nd isotope ratios of 0.511790 ( $\epsilon\text{Nd}_t = -5.88$ ), 0.511725 ( $\epsilon\text{Nd}_t = -7.15$ ) and 0.511712 ( $\epsilon\text{Nd}_t = -7.40$ ) were determined for the basic dyke, the lamprophyre dyke and the appinite respectively.

## 7.4.6 Discussion of the Sr isotope results

### 7.4.6.i Discussion of Sr isotope results for the volcanic pile

The most variable initial Sr isotope ratios in the volcanic pile are found in the Ciste andesites; those samples with the highest initial Sr isotope ratio also have the highest SiO<sub>2</sub> content, but correlation between the two parameters is poor (Fig. 7.13). The analyses from the summit andesites form a tight group, with a limited range of both SiO<sub>2</sub> (63.65-64.79%) and  $\epsilon Sr_t$ . All of Thirlwall's unpublished data have similar initial Sr isotope ratios to the Summit andesites with the exception of BN5024 which has a slightly higher value.

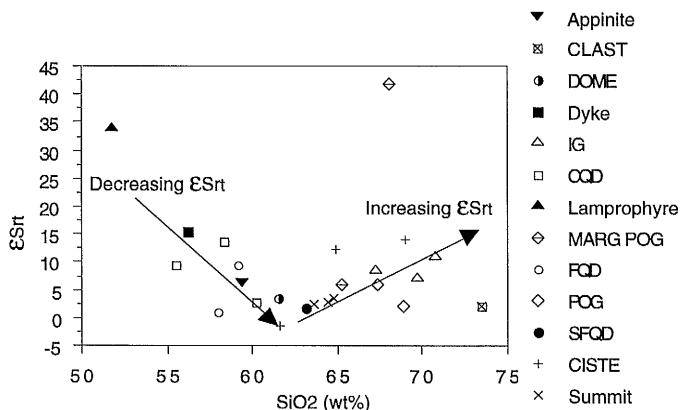


Fig. 7.13 SiO<sub>2</sub> vs  $\epsilon Sr_t$ . Initially variable but generally decreasing  $\epsilon Sr_t$  with fractionation followed by increasing  $\epsilon Sr_t$  with fractionation.

The rhyolite clast does not have the highest initial Sr isotope ratio; despite the fact that it has the highest SiO<sub>2</sub>, in fact it has one of the lowest values obtained from the Ben Nevis Complex. The high Ni and MgO intrusive dome does not have the lowest initial ratio and is comparable to the summit andesites. This is in accordance with the intrusion being one of the last magmatic events recorded in the volcanic pile (i.e. of similar age to the volcanic pile).

In chapter 6 it was noted that the andesites plotted with considerable scatter on Harker diagrams, albeit along an overall trend, and simple closed system fractionation could not have caused the observed chemical variation. The volcanic pile does not become more evolved with time, rather chemical differences between vertically adjacent lava flows follow a non-linear pattern. It was concluded that the magma chamber source to the Ben Nevis Volcanic Pile was small and underwent continuous fractionation, extrusion and replenishment. The isotope data presented here support such a hypothesis. Simple AFC processes cannot explain the isotopic variation and neither can increasing contamination with time or closed system fractionation. If AFC processes dominated the isotopic evolution of the Ben Nevis Complex, then the clast should have the highest initial Sr isotope ratios as

the local Dalradian contaminants had much higher  $(^{87}\text{Sr}/^{86}\text{Sr})_{425}$  than the Ben Nevis magmas; this is not so. In such a model the Ciste andesites should have the lowest initial Sr isotope ratios whereas they have the highest ratios of the volcanic pile (BN206 & BN211).

#### 7.4.6.ii Granites

Geochemical variation in the plutonic members of the Ben Nevis Complex; requires the existence of at least four separate parent magmas (chapter 6) and this number is increased dramatically if individual pulses in the Fine Quartz Diorite, Sgurr Finnisg-aig Quartz Diorite and Coarse Quartz Diorite units are taken as separate magmas with slightly different parental magma compositions for each pulse. The Sr isotope data support such a model, as each of the five units of the Ben Nevis Complex fall into separate areas of Fig. 7.12b. There is no relationship between  $\epsilon\text{Sr}_t$  and  $\text{SiO}_2$  within individual pulses (Fig. 7.13). Results from the plutonic units as a whole show an initial decrease in  $\epsilon\text{Sr}_t$  with fractionation (to  $\approx 63\%$   $\text{SiO}_2$ ), followed by a general increase in  $\epsilon\text{Sr}_t$  with fractionation. This is believed to be significant and is discussed further later in this chapter.

BN366 exhibits anomalously high  $\epsilon\text{Sr}_t$  relative to other samples from the Porphyritic Outer Granite. BN366 was obtained from the marginal variant of the Porphyritic Outer Granite close to the Dalradian contact (Fig. 7.11a). The Dalradian schist (Leven Schist fm.) in this location is strongly veined by the marginal Porphyritic Outer Granite and is highly brecciated (chapter 4). It is therefore likely that BN366 is contaminated to a greater degree by Dalradian metasediments than the main Porphyritic Outer Granite outcrop. BN420, another sample of the marginal variant, has a similar initial Sr isotope ratio to the normal K-feldspar phenocryst-bearing Porphyritic Outer Granite.

Published chemical analyses (Lambert et al. 1982 and Hickman & Wright 1983) from Dalradian schists are presented along with data from the Ben Nevis Complex in Figs. 7.14a and 7.14b. Compared to the majority of Porphyritic Outer Granite samples, BN366 has a higher Rb content (Fig. 7.14a), similar to that of the Dalradian schists, suggesting that contamination by Dalradian schist has added Rb to BN366. The Dalradian has a lower Sr content than the majority of Ben Nevis Complex samples (Fig. 7.14b); consequently large scale bulk contamination of Porphyritic Outer Granite by Dalradian schist would lower the Sr concentration of the resultant magma. Although BN366 has one of the lowest Sr concentrations in the Porphyritic Outer Granite, it is not significantly different. One explanation for this feature is that whereas only a small amount of contamination has occurred, which has lowered the Sr content only slightly, the contaminant had a high  $(^{87}\text{Sr}/^{86}\text{Sr})_{425}$  ratio. A plot of  $\epsilon\text{Sr}_t$  vs Rb/Sr for the Dalradian and the Ben Nevis Complex (Fig. 7.15) reveals that the Dalradian has much higher  $\epsilon\text{Sr}_t$  than the Ben Nevis Complex and, consequently, even limited contamination could alter  $\epsilon\text{Sr}_t$  significantly.

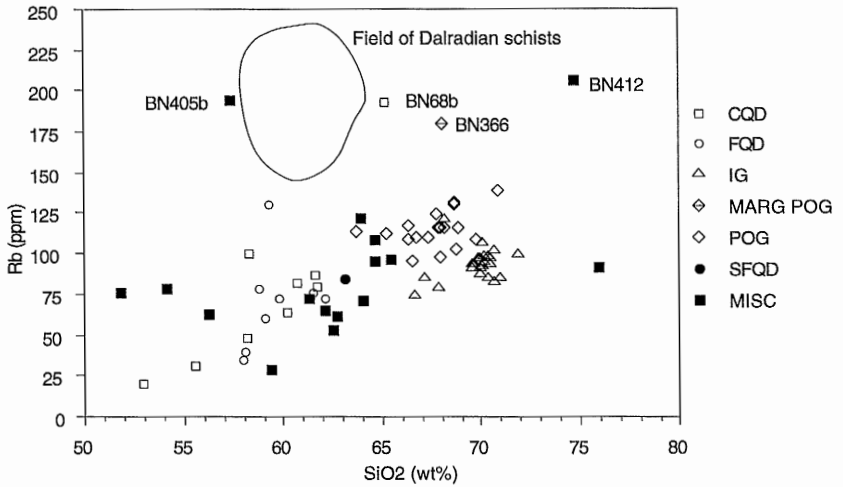


Fig. 7.14a Rb vs SiO<sub>2</sub> for the Ben Nevis intrusive lithologies along with the field for Dalradian Schists. Data for Dalradian from Lambert et al. (1982) and Hickman & Wright (1983). Miscellaneous group incorporates the minor intrusions of the Ben Nevis Complex.

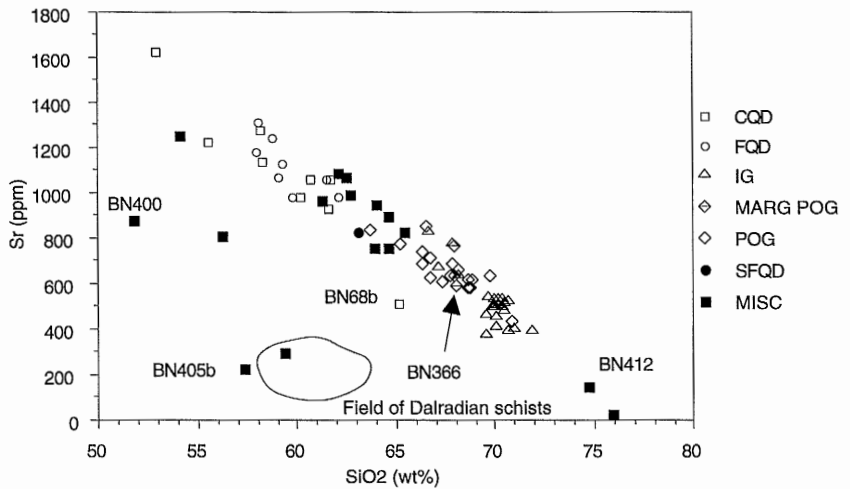


Fig. 7.14b Sr vs SiO<sub>2</sub> for the Ben Nevis intrusive lithologies along with the field for Dalradian Schists. Data for Dalradian from Lambert et al. (1982) and Hickman & Wright (1983). Miscellaneous group incorporates the minor intrusions of the Ben Nevis Complex.

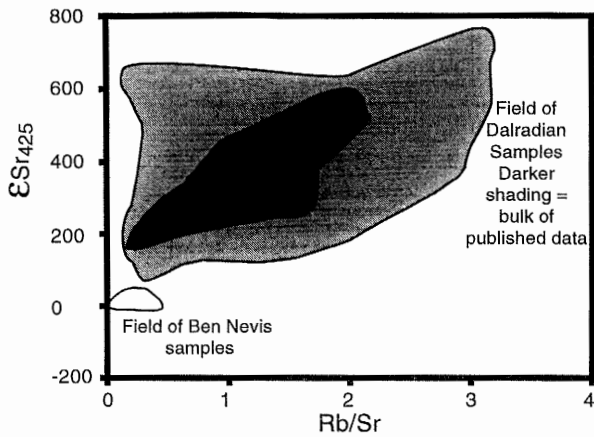


Fig. 7.15  $\epsilon Sr_{425}$  vs Rb/Sr for Ben Nevis magmas and Dalradian Schists. Dalradian samples have significantly higher  $\epsilon Sr_t$  than Ben Nevis. Minor contamination may therefore have a noticeable effect on the Sr isotope ratios of the BNC. Dalradian data from Dempster (1985), Lambert et al. (1982), O'Nions et al. (1983) & Frost & O'Nions (1985).

Three other samples from the Ben Nevis Complex have similar Rb contents to BN366 and the field of Dalradian schists (Fig. 7.14a); these being BN405b, BN68b and BN412. BN405b is from an appinite exposed on the flanks of Aonach Nid. BN68b is a sample from the Coarse Quartz Diorite, and on the basis of mineral chemistry was shown to be contaminated by local Dalradian metasediments (chapter 5); and BN412 is the granite sill formerly identified by Anderson (1935) and Haslam (1968) as part of the Fine Quartz Diorite and now recognised as a post-Porphyritic Outer Granite intrusion (chapter 4). All these localities with elevated Rb contents are found along the margin of the Ben Nevis Complex, close to the contact with the Dalradian. Both BN68b and BN405b have low Sr contents relative to the majority of Ben Nevis Complex analyses (Fig. 7.14b) and bulk contamination by Dalradian metasediment is the most likely explanation for these and for BN366.

#### 7.4.6.iii Miscellaneous intrusions

BN400 is a sample taken from a lamprophyre dyke and therefore was predicted to have a low  $\epsilon Sr_t$ , consistent with lamprophyres representing the parental magmas of the Newer Granites (Rock et al. 1988). However, this sample has one of the highest  $\epsilon Sr_t$  values (33.9). The dyke from which the sample was obtained is cross-cut by a small (<5m movement) sinistral fault and, whereas the sample was collected away from signs of obvious alteration, it is believed that the high  $\epsilon Sr_t$  of this sample can be attributed to the passage of high  $^{87}Sr/^{86}Sr$  rich fluids along this fault. Alternatively, it is possible that the lamprophyre-parent-magma model is wrong, but it is difficult to envisage a mechanism by which high Ni, Cr and Mg# magmas can be generated in the lower crust.

The appinites of the Ben Nevis Complex are, according to Haslam (1968), reaction

products between Ballachulish limestone and the outer margins of the Ben Nevis Complex. Although this model is certainly applicable to the thin (<2cm wide) band of hornblende rich Porphyritic Outer Granite in contact with the Ballachulish limestone in the Red Burn (Chapters 4 & 5), it is unlikely to be the case for the much more extensive surge chamber (BN170) and Aonach Nid (BN405b) appinites (Yarr 1992, and also chapters 4, 5 & 6). The appinite does not have high  $\epsilon Sr_t$ , which the model of Haslam (1968) predicts, and is little different ( $\epsilon Sr_t=6.0$ ) from other values obtained from the Ben Nevis Complex; in fact BN170 intrudes the Coarse Quartz Diorite and has a lower  $\epsilon Sr_t$  than either BN177 ( $\epsilon Sr_t=9.4$ ) or BN174 ( $\epsilon Sr_t=13.5$ ).

#### 7.4.7 Discussion of Nd isotope ratios for the Ben Nevis Complex

Because of the highly variable nature of  $\epsilon Nd_t$  for the Ben Nevis Complex and the large degree of overlap in Nd isotopes between the volcanics, the granites and the miscellaneous intrusions, all the components of the Ben Nevis Complex will be discussed in a single section.

The relationship between Sm or Nd and  $SiO_2$  is complex (Figs. 7.16a-d). In the Coarse Quartz Diorite, both Nd and Sm increase with increasing  $SiO_2$  (Figs. 7.16a & 7.16b), whereas in the Porphyritic Outer Granite both elements decrease with increasing  $SiO_2$ . In the Fine Quartz Diorite, Nd decreases whereas Sm increases with increasing  $SiO_2$ . The Inner Granite and the samples from the Ciste and Summit andesites reveal no overall correlation between  $SiO_2$  and Sm or Nd. With regard to the Ben Nevis Complex as a whole, there is a general decrease in both Sm and Nd with  $SiO_2$ , but considerable variation is observed about this general trend. Sm/Nd ratios decrease with increasing  $SiO_2$  (Fig. 7.16c).

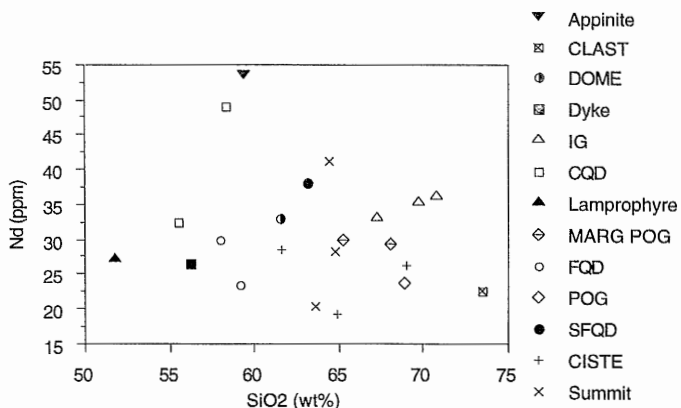


Fig. 7.16a A plot of Nd vs  $SiO_2$  for the Ben Nevis Complex and showing no correlation.

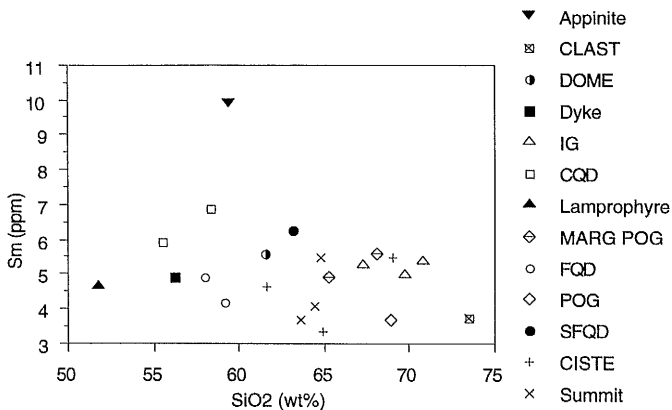


Fig. 7.16b A plot of Sm vs SiO<sub>2</sub> for the Ben Nevis Complex and showing no correlation.

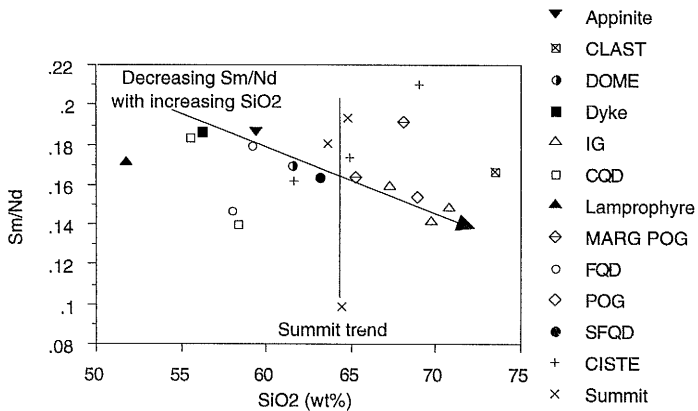


Fig. 7.16c A plot of Sm/Nd vs SiO<sub>2</sub> for the Ben Nevis Complex and showing moderate correlation between the two parameters. Note the highly variable Sm/Nd ratio exhibited by the summit andesites at  $\approx$  constant SiO<sub>2</sub>.

Andesites from the volcanic pile, including the Summit andesites, show the greatest degree of variability in  $\epsilon Nd_t$ , which is in marked contrast to the uniform  $\epsilon Sr_t$  values for the Summit andesites. Results from the Inner Granite remain in a tight cluster and BN366 (contaminated marginal Porphyritic Outer Granite) has slightly lower  $\epsilon Nd_t$  than the Porphyritic Outer Granite. The sample from the intrusive dome and the rhyolite clast have similar  $\epsilon Nd_t$  values. The clast represents the earliest and most evolved composition within the volcanic pile, whereas intrusion of the dome is one of the last magmatic events in the volcanic pile and it has one of the least evolved compositions. It can therefore be stated that the volcanic pile does not show a regular variation in  $\epsilon Nd_t$  with time or with composition.

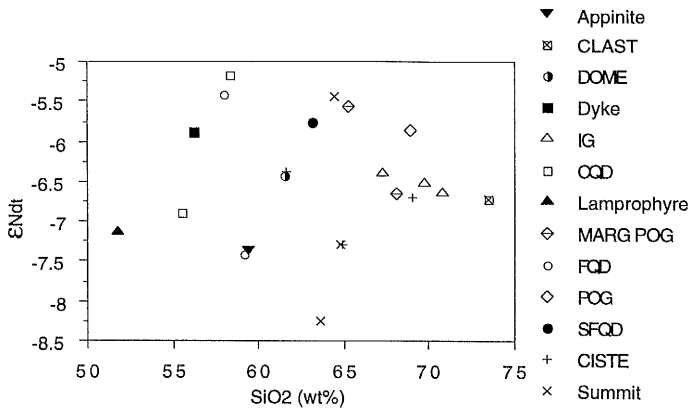


Fig. 7.16d A plot of  $\epsilon Nd_t$  vs  $SiO_2$  for the Ben Nevis Complex and showing no correlation.

If the parental magmas to the Ben Nevis Complex were derived ultimately from either Depleted Mantle (Frost & O'Nions 1985) or from LREE-enriched SWH mantle (Thirlwall 1981), then they have been affected by a large degree of contamination. Variation in isotopes between and within different units of the Ben Nevis Complex reveals that simple fractional crystallisation from a single parent magma cannot be a viable model. Assimilation fractional crystallisation is also an unworkable model. If such a process were operating during the evolution of the Ben Nevis Complex, then the latest magmas should reveal more contaminated isotopic signatures than the earlier intrusions. In fact the most contaminated samples are found within the Summit andesites and the Fine Quartz Diorite, which are amongst the earliest magmas of the Ben Nevis Complex (chapters 3 and 4).

#### 7.4.8 Combined Sr and Nd Isotope Results

A combined  $\epsilon Nd_t$  and  $\epsilon Sr_t$  diagram for the Ben Nevis Complex is presented in Fig. 7.17. The volcanic data have apparently the simplest isotopic variation and are discussed first, followed by the intrusive members of the Ben Nevis Complex.

##### 7.4.8.i Volcanics

The Summit andesites, with the addition of the rhyolite clast and the sample from the dome, define a vertical trend (Fig. 7.17) with decreasing  $\epsilon Nd_t$  at constant  $\epsilon Sr_t$ . Samples from the Ciste andesites at the base of the volcanic pile plot on Fig. 7.17 with higher  $\epsilon Sr_t$  relative to the Summit andesites with the exception of BN245 which has the lowest  $\epsilon Sr_t$  of the Ben Nevis Complex (-1.3). This sample also has high MgO, CaO and Ni contents relative to the rest of the andesites and in terms of these elements is apparently the least fractionated andesite flow exposed on Ben Nevis.

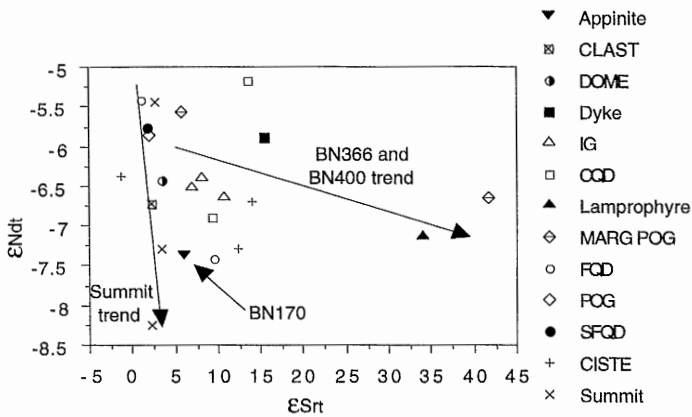


Fig. 7.17  $\epsilon Nd_t$  vs  $\epsilon Sr_t$  shows no simple overall correlation between the two isotopic systems. Secondary contamination, although represented by a single arrow is likely to occur at any point along the Summit trend depending on the isotopic composition of the sample on entering the upper crust. Note the position of BN170.

The fact that the Summit andesites form such a strong vertical trend in Fig. 7.17, suggests that only one contaminant was incorporated into the primary magma(s) of the Summit andesites, whereas the samples from the Ciste andesites which scatter off the vertical trend to higher  $\epsilon Sr_t$  (Fig. 7.17), provide evidence for a second component.

It is possible that the contaminant is the same for both the Ciste and Summit andesites, and that the isotopic variation displayed by these units is the result of different parental magma compositions. If this is the case, then the source of the Summit andesites is required to have a similar isotopic composition to the source of the Ciste andesites, but with a higher Sr/Nd ratio. A plot of  $\epsilon Nd_t$  vs Sr/Nd (Fig. 7.18) reveals that the Summit and Ciste andesites have similar Sr/Nd ratios. The cause of decreasing  $\epsilon Nd_t$  at constant  $\epsilon Sr_t$  in the Summit andesites must therefore be attributed to contamination of a high Sr/Nd-high  $\epsilon Nd_t$  magma. Dispersal of the Ciste andesites off this trend can be explained either by contamination with a different composition or by additional contaminants in the basal samples. Given that the Summit trend in Fig 7.17 is vertical, the contaminant is likely have high Sr/Nd, low  $\epsilon Nd_t$  and similar  $\epsilon Sr_t$  to the parent magma of the Summit andesites.

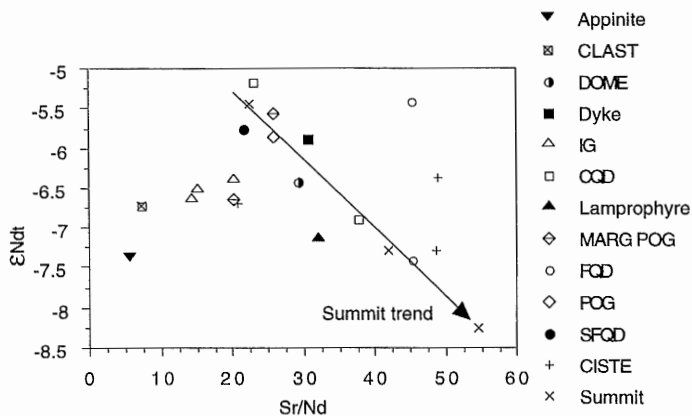


Fig. 7.18  $\epsilon Nd_t$  vs Sr/Nd. The summit trend is defined by decreasing  $\epsilon Nd_t$  and increasing Sr/Nd ratios. A combination of plagioclase fractionation and crustal contamination disperses the other samples off the summit trend.

In Fig. 7.17, the rhyolitic clast falls on the trend of the Summit andesites but in Fig. 7.18, this sample lies well off the trend defined by the Summit andesites. Crystal fractionation is unable to alter initial isotope ratios, but can have significant effects on the elemental abundances. In chapter 6 plagioclase fractionation was shown to have occurred throughout the evolution of the Ben Nevis Complex. Removal of plagioclase from the melt would lower Sr contents, whereas Nd would remain approximately constant or increase. Plagioclase fractionation is believed to be the cause for the migration of the evolved rhyolite sample off the Summit andesite trend in Fig. 7.18 i.e. to a lower Sr/Nd ratio. However, the trend of increasing Sr/Nd with decreasing  $\epsilon Nd_t$  in the Summit andesites cannot be attributed to crystal fractionation because crystal fractionation cannot alter isotopic ratios. The Summit andesites differ chemically by only small amounts (e.g. they have similar  $SiO_2$  contents 63.65 - 64.79%). If simple AFC processes were the cause of this limited variation then the least evolved sample, BN222, should have the highest  $\epsilon Nd_t$ , whereas in fact it has the lowest  $\epsilon Nd_t$ . There is no simple correlation between fractionation and Sr/Nd ratio (Fig. 7.19). The Summit andesites have a vertical trend in Fig. 7.19, revealing that contamination was apparently the dominant control on Sr/Nd ratios in this groups of rocks.

#### 7.4.8.ii Intrusives

Those samples from the granitic rocks which fall close to or on the Summit andesite trend in Fig. 7.17 also fall on or close to the same trend defined by the Summit andesites in Fig. 7.18. It is likely, therefore, that they have been contaminated by the same material.

BN366 and BN400 have high  $\epsilon Sr_t$  and lie well off the trend defined by the Summit andesites (Fig. 7.17); and the reason for this has been discussed above. The Inner Granite clusters towards slightly higher  $\epsilon Sr_t$  values and the Porphyritic Outer Granite and marginal Porphyritic Outer Granite lie close to the Summit trend. The appinite (BN170) has one of

the lowest  $\epsilon\text{Nd}_t$  values as does the lamprophyre and yet both are sometimes interpreted as representative of the parent magmas to the Newer Granites (Pitcher 1993 and refs. therein). Halliday et al. (1984c) noted that the appinites from the Ratagain complex, although mantle derived had low  $\epsilon\text{Nd}_t$  (-7) and they attributed this to vapour phase transport in the lower crust. The high temperature and high volatile contents of these magmas would also aid interaction between the magma and the crust (see section 7.6.3). The lamprophyre and the appinite from Ben Nevis may therefore represent extensions of the Summit trend. In addition to contamination with the Summit trend contaminant, BN400 has also suffered contamination by a high  $^{87}\text{Sr}/^{86}\text{Sr}$  component.

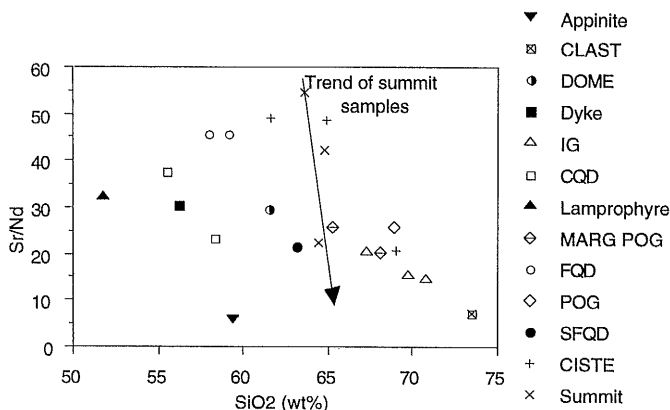


Fig. 7.19 Sr/Nd vs SiO<sub>2</sub>. Vertical trend of the Summit samples is not the result of fractional crystallisation.

#### 7.4.8.iii Discussion

The Ben Nevis Complex can be modelled isotopically in terms of three components; a parental magma, a high Sr/Nd + low  $\epsilon\text{Nd}_t$  contaminant, and a high  $\epsilon\text{Sr}_t$  contaminant.

Contacts within the quartz diorites and between the Fine Quartz Diorite, Coarse Quartz Diorite, Porphyritic Outer Granite and Inner Granite, all indicate that fractionation of the plutonics occurred below the current level of exposure. The geochemistry reveals separate parent magmas for the Porphyritic Outer Granite and Inner Granite. Additionally both the volcanic pile and the quartz diorites show no trend of increasing fractionation with time and are believed to have been intruded/extruded as a large number of small volume magmas with slightly different compositions (chapter 6).

The fact that a number of the intrusive samples fall along the trend defined by the Summit andesites (Fig. 7.17) indicates that the intrusive and extrusive rocks have, at least in isotopic terms, the same parental magma. The least contaminated samples of the volcanic pile and the intrusive rocks (TOWER and OBN13 respectively) lie adjacent to each other in Fig. 7.17. Displacement of BN366 and BN400 off the trend defined by the Summit andesites

to higher  $\epsilon\text{Sr}_t$  is attributed to Dalradian contamination ( $\epsilon\text{Nd}_{425} < 7.36$   $\epsilon\text{Sr}_{425} > 100$ , Frost & O'Nions 1985). It is therefore suggested that dispersal of the other Ben Nevis samples away from the Summit andesite trend to higher  $\epsilon\text{Sr}_t$  is also due to Dalradian contamination. This requires the trend defined by the Summit andesites to have formed below the level of Dalradian metasediments (i.e. contamination of the parent magmas occurred in the lower crust). This lower crustal contaminant is required to have high Sr/Nd, low Rb, low  $\epsilon\text{Sr}_t$  and low  $\epsilon\text{Nd}_t$ . There is no simple correlation between Sr/Nd ratios and either  $\epsilon\text{Nd}_t$  (Fig. 7.18) or  $\text{SiO}_2$  (Fig. 7.19) for samples that fall off the Summit trend in Fig. 7.17. This results from the combined and variable effects of crustal contamination and plagioclase fractionation.

From the geochemistry (chapter 6) it was suggested that the andesites were erupted from a small volume magma chamber which underwent continuous fractionation, extrusion and replenishment. It is suggested here that this chamber was situated in the lower crust and the magmas that replenished the system primarily affected  $\epsilon\text{Nd}_t$  with no noticeable variation in  $\epsilon\text{Sr}_t$ . The andesites spent only a limited period of time in the upper crust prior to eruption; this would account for preservation of primary magmatic amphibole in the andesitic lavas (chapters 3 & 6). The earliest andesite lava flows show signs of limited contamination with the Dalradian, whereas the later eruptions do not. Either the Ciste andesites spent a longer period in the upper crust prior to eruption or some other process was operating, such as wall-rock assimilation in the conduit. The fact that both the early volcanics ( $\epsilon\text{Sr}_t$ ) and the early plutonics ( $\epsilon\text{Nd}_t$  and  $\epsilon\text{Sr}_t$ ) show a greater degree of variability than the later magmas is believed to be significant and is discussed below.

## 7.5 Source compositions

Over the last 25 years a great wealth of isotopic data from the sedimentary, metamorphic and igneous rocks of Northern Britain has been published. Despite intensive study of the Newer Granites, related Old Red Sandstone volcanics, xenoliths and upper crustal lithologies, the composition of the lower crust and upper mantle beneath Northern Britain still attracts considerable debate. In the following discussion of the upper mantle and the lower crust, data from across Northern Britain will be examined. It should however, be remembered that the crust of Northern Britain is comprised of a number of fault-bounded blocks or terranes (Curry et al. 1982). The exact relationships between these terranes are poorly understood, and have been the subject of much discussion (Thirlwall 1988 and Bluck & Dempster 1991). It is possible that movement along deep-seated faults, such as the Great Glen fault, may have juxtaposed lower crustal metamorphics and lithospheric mantle of different compositions and ages on either side of the fault.

### 7.5.1 Mantle Source Compositions

Evidence for the composition of parental mantle derived melts generated during the late Caledonian orogeny may be found from the study of appinites and lamprophyres (Pitcher 1993), mafic microgranular enclaves (MME) (Holden et al. 1987) and of contemporaneous

ORS lavas (Thirlwall 1988). In addition Permo-Carboniferous and Tertiary dykes contain xenoliths believed to have been excavated from the lithospheric mantle (Halliday et al. 1993, Menzies et al. 1987 and Menzies & Halliday 1988). Because of the volume of data available on the possible mantle sources, this section will be split into smaller units dealing with individual topics, before attempting to bring all the data together in a single model.

#### 7.5.1.i Xenoliths

Mafic and ultramafic xenoliths found within Carboniferous and Tertiary volcanics and hypabyssal intrusions from across Northern Britain are believed to have been excavated from the lithospheric mantle (Halliday et al. 1985). This group of xenoliths provides chemical evidence for a major change in the composition of the lithospheric mantle across Northern Britain (Menzies et al. 1987). Halliday et al. (1985) demonstrated that the variation in Sr and REE abundance observed in lithospheric mantle xenoliths could be matched with similar variations in granitoid chemistry across Northern Britain. These authors concluded that the variations in granitoid chemistry 'are fundamentally the result of melting lithospheric mantle which is chemically zoned across Northern Britain'. Such a model, however cannot account for the presence of inherited zircons in those granites north of the Mid-Grampian Line.

Menzies (1991) believed that variations in the chemistry of the lithospheric mantle are related to the age of the overlying crust. Archaean lithospheric mantle differs chemically and physically from younger lithospheric mantle because of its greater interaction with the asthenosphere and because plate tectonic processes acting during the Archaean were different from those acting today. If magmas are generated in the lithospheric mantle, then variations in the age and chemistry of this source region will be mirrored in the chemistry of the erupted/intruded magmas.

The xenolith locations for which data are available can be found in the Northern Highlands (Fig.3) and in the Midland Valley; no xenolith locality has been examined in the Grampian terrane or in the Southern Uplands. The upper crust to the north of the Grampian terrane is believed to be underlain by Lewisian-like (i.e. Archaean in age) lower crust whereas that to the south is much younger (Permo-Carboniferous according to Halliday et al. (1993), but other estimates include Ketilidian (Houghton 1988) and Grenvillian (Davies et al. 1984)). If chemical variations in the lithospheric mantle are related to the age of the lower crust (Menzies 1991), then it is hardly surprising, given the disparity in ages of the lower crust between the Northern Highlands and the Midland Valley, that variations in the chemistry of the lithospheric mantle could be observed from lithospheric mantle xenoliths. Menzies et al. (1987) and Menzies & Halliday (1988) attribute zonation of the lithospheric mantle to the presence of ancient LREE-enriched lithospheric mantle beneath the Hebridean craton and younger lithospheric mantle beneath the Midland Valley with depleted isotopic characteristics, comparable to Ocean Island Basalt source mantle (Menzies & Halliday 1984).

Xenoliths from Streat Comlaidh are noticeably different from the Hebridean localities (Fig. 7.20) in that they do not show evidence of time-integrated LREE-enrichment and have high  $\epsilon_{\text{Sr}_t}$ . Menzies & Halliday (1988) suggested that the onset of subduction during the Caledonian Orogeny contributed localised enrichments in LILE to the mantle lithosphere below Streat Comlaidh.

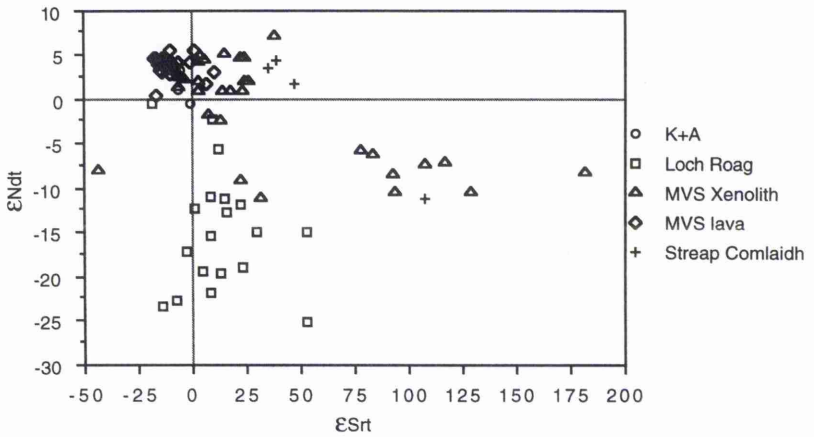


Fig. 7.20  $\epsilon_{\text{Nd}_t}$  vs  $\epsilon_{\text{Sr}_t}$  for the Permo-Carboniferous lavas of Scotland (Smedley 1986, 1988a & b), and  $\epsilon_{\text{Nd}_{300}}$  vs  $\epsilon_{\text{Sr}_{300}}$  data for Scottish mantle xenoliths (Menzies & Halliday 1988, Menzies et al. 1987 and Halliday et al. 1993). The data indicate the presence of extreme LREE-enriched mantle in the NW of Scotland, whereas further south in the Midland Valley, the data for mantle xenoliths are comparable to depleted mantle or Ocean Island Basalt source mantle and overlap strongly with the Scottish Permo-Carboniferous lavas. K+A = Permo-Carboniferous from Kintyre and Arran. MVS = Midland Valley. Data points labelled Loch Roag also include those from Duncansby Ness.

It should be noted that host magma is unlikely to have excavated xenoliths from the entire lithospheric sequence. This would be particularly important if the lithospheric mantle is vertically stratified as proposed by Thirlwall (1988 and refs. therein). Vertical stratification of the lithosphere (crustal and/or mantle) could explain the presence of the Mid-Grampian Line (Halliday & Stephens 1984) in that melting at different levels in the lithosphere would produce magmas of differing composition rather than the presence of older continental crust north of the Mid-Grampian Line and its absence to the south as advocated by Pidgeon & Aftalion (1978) and Halliday & Stephens (1984).

Halliday et al. (1993) refined Menzies' (1991) global model with regard to the Scottish lithospheric mantle. In the revised model, basaltic magmas are intruded into the base of the lithosphere forming a basaltic underplate. Assimilation and fractional crystallisation (AFC) processes (De Paolo 1981) between the underplated magmas and the lower crust result in the formation of a mafic underplate with bulk geochemical and isotopic characteristics of the lower crust into which it was emplaced. The underplate was believed to have been formed by subduction towards the end of the Caledonian Orogeny, and could therefore have been a major source of heat and/or material during the generation of the

Newer Granite and Old Red Sandstone lavas. Nb depletions in the xenoliths from Loch Roag, Duncansby Ness and Streap Comlaidh and in the Newer Granites led Halliday et al. (1993) to propose a direct genetic link between the formation of the Newer Granites and the basaltic underplate.

Mass balance models indicate an average ratio of Lewisian-derived Nd to underplated parent magma Nd in the lithospheric mantle xenoliths of Loch Roag and Duncansby Ness of about 2 (Halliday et al. 1993). Given such large degrees of lower crustal contamination in the underplated magmas at least some correlation between the lower crustal xenoliths and the chemistry of the Newer Granites might be expected. An explanation for this problem can be found in Halliday et al. (1993). The authors suggested that the lithospheric mantle underlying the Hebridean craton, although related to the overlying Lewisian, has not suffered the same extreme depletions in Rb and U. If contamination of subduction-related basaltic magma occurred in the sub-Lewisian lithospheric mantle, then the volume of contamination required in the mass balance models would be significantly reduced; however the presence of inherited zircons in Newer Granites north of the Mid Grampian Line indicates that at least some contamination by the lower crust has occurred (Halliday & Stephens 1985).

The lithospheric mantle beneath the Midland Valley is likely to be more complex than suggested by Halliday et al. (1993). If Nb anomalies are taken as evidence of a genetic link between xenolith, granites and the subduction, then a number of Midland Valley xenoliths are also subduction related (Fig. 7.21) as they have similar MORB-normalised spidergrams comparable to the Hebridean xenoliths.

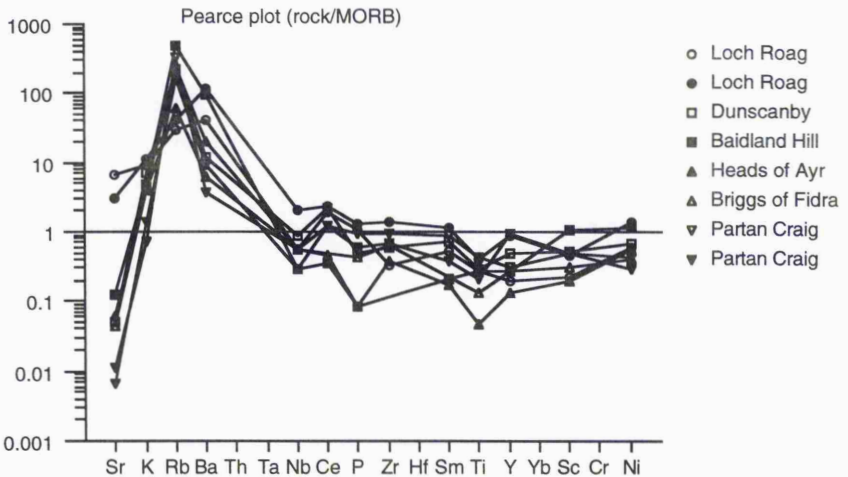


Fig. 7.21 MORB normalised spidergrams for mantle xenoliths from the Midland Valley and Loch Roag + Duncansby Ness. The samples from the Midland Valley also show Nb depletion and are comparable to Duncansby Ness. The data are from Halliday et al. (1993) and are presented by these authors as 'representative xenolith compositions' from these localities.

Regardless of the mechanism of variation in the lithospheric mantle beneath Northern Britain, the correlation between Newer Granite chemistry and xenoliths excavated from the lithospheric mantle reveals that the lithospheric mantle played an important role in the genesis of the Newer Granites. No direct evidence for the composition of the lithospheric mantle beneath the Ben Nevis Complex can be obtained, and although Streap Comlaidh is geographically the closest xenolith locality (the mountain of Streap Comlaidh can be easily seen, on sunny days!, from the summit of Ben Nevis some 30km distant) for which data are available, it lies on the opposite side of the Great Glen Fault, the significance of which remains unclear (e.g. Bluck & Dempster 1991). A similar problem occurs with any of the xenolith localities further south, in that they lie within the Midland Valley, on the other side of the Highland Boundary Fault. In addition Halliday et al. (1993) believe that the Midland Valley mantle xenoliths are the same age as their Permo-Carboniferous hosts and do not therefore represent samples of the lithospheric mantle present beneath the Midland Valley during Old Red Sandstone times.

7.5.1.ii Old Red Sandstone and Permo-Carboniferous Lavas

The distribution of Old Red Sandstone lavas in Scotland is depicted in Fig. 7.3.

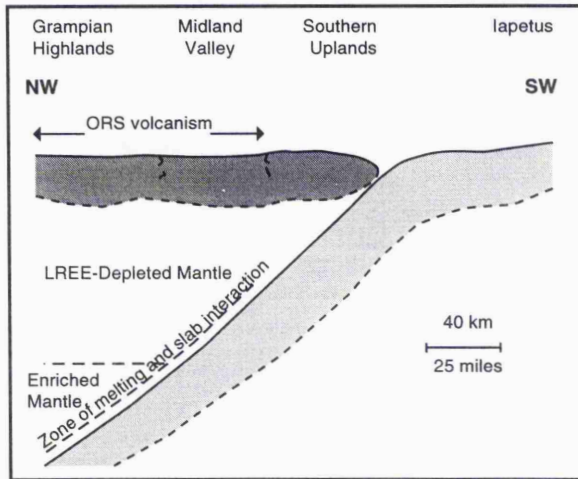


Fig. 7.22 Vertical stratification of the upper mantle across Northern Britain at 410Ma. Diagram from Thirlwall (1982).

Evidence for distinct chemical and isotopic provinces within lavas of Old Red Sandstone age across Northern Britain was presented in a series of papers by Thirlwall (1981, 1982, 1983, 1986 & 1988). Samples analysed by Thirlwall (1988 and refs. therein) have  $Ni > 100\text{ppm}$  and  $Cr > 150\text{ppm}$ ; they are therefore believed to have suffered minimal contamination or fractional crystallisation during passage through the crust and are thus close to being primitive melts. Lavas from the Midland Valley have isotopic and chemical characteristics typical of arc lavas, and can be modelled in terms of a depleted mantle source plus a variable slab-derived component (Thirlwall 1982 & 1986). Samples from the Lorne Plateau Lavas and Glencoe have negative  $\epsilon Nd_t$  and some have negative  $\epsilon Sr_t$

(Fig. 7.10). Contamination of depleted mantle by crustal or lithospheric mantle melts was discounted and a LREE-enriched mantle source was proposed, and is referred to as the Southwest Highland (SWH) mantle (Thirlwall 1988 and refs. therein). As no such mantle composition is sampled by the British Tertiary magmas, Thirlwall (1982) favoured a vertically stratified mantle beneath Scotland (Fig. 7.22) with depleted mantle sandwiched between LREE-enriched mantle and the lower crust.

Slight overlap between the fields of the Lorne Plateau Lavas and the Midland Valley ORS lavas (Fig. 7.10) led Thirlwall (1986) to suggest that small quantities of SWH mantle were involved in the generation of the northernmost ORS lavas within the Midland Valley. A three component model was proposed to explain the geochemical variation in Old Red Sandstone lavas (Thirlwall 1986 and refs. therein). This interpretation is displayed in Fig. 7.10 and Fig. 7.24. These three sources are:

- 1) South West Highland Mantle with  $^{206}\text{Pb}/^{204}\text{Pb}$  of  $\approx 17.0$ ,  $^{87}\text{Sr}/^{86}\text{Sr}$  of  $\approx 0.7030$  ( $\epsilon\text{Sr}_{410} \approx -10$ ) and  $\epsilon\text{Nd}_t \approx -2$ .
- 2) Depleted mantle with  $^{206}\text{Pb}/^{204}\text{Pb}$  of  $\approx 18.1$ ,  $^{87}\text{Sr}/^{86}\text{Sr}$  of  $< 0.7035$  ( $\epsilon\text{Sr}_{410} < -10$ ) and  $\epsilon\text{Nd}_t > +6$ .
- 3) A source common to both Lorne Plateau lavas and Midland Valley lavas and considered to be subducted sediment with  $^{206}\text{Pb}/^{204}\text{Pb}$  of  $\approx 18.1$ ,  $^{87}\text{Sr}/^{86}\text{Sr}$  of  $> 0.705$  ( $\epsilon\text{Sr}_{410} > 16$ ) and  $\epsilon\text{Nd}_t < -2$ .

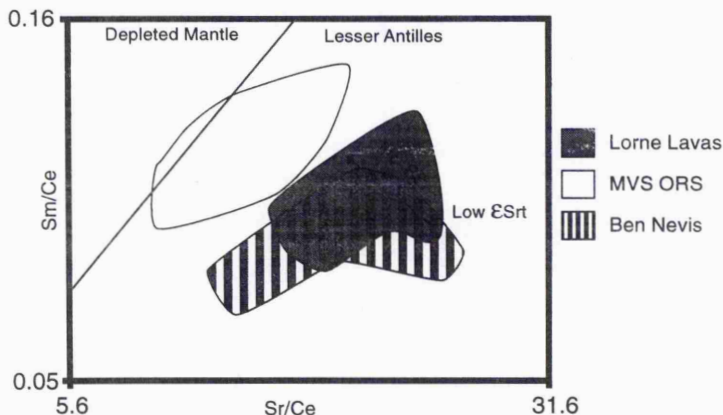


Fig. 7.23 Log Sm/Ce vs log Sr/Ce for samples from the ORS lavas of the Midland Valley (MVS) and the Lorne Plateau. Increasing Sr/Ce is believed by Hawkesworth & Powell (1980) to be the trace element analogue of increasing  $\epsilon\text{Sr}$ . This is not the case in for the Lorne samples where high Sr/Ce correlates with low  $\epsilon\text{Sr}$  and the high Sr/Ce of the LPL is a feature of the source region. Also included are the high Ni (>60ppm) samples from the Ben Nevis Complex. Fractional crystallisation drives the data to lower Sr/Ce at approximately constant Sm/Ce. The BNC data lie within the field for the Lorne Plateau suggesting that any involvement of DM (Frost & O'Nions 1985) was minimal. Data from Thirlwall (1986, 1983 & 1982).

Some 50Ma after the cessation of Late Caledonide magmatism, central Scotland

underwent a further period of volcanism linked to extension of the Midland Valley graben. Smedley (1986, 1988a & 1988b) believed that Permo-Carboniferous lavas of the Midland Valley were chemically comparable to the Old Red Sandstone lavas once the effects of subduction had been accounted for.  $\epsilon\text{Nd}_t$  and  $\epsilon\text{Sr}_t$  for the Permo-Carboniferous lavas lie within the field of xenoliths excavated from the lithospheric mantle below the Midland Valley (Smedley 1988b).

Exposures of Permo-Carboniferous lava can also be found on Kintyre and Arran, both areas which are supposedly underlain by SWH mantle (Thirlwall 1983 & 1986). Smedley (1988b) presented evidence for variations between Permo-Carboniferous lavas from the Midland Valley and Kintyre & Arran comparable to those observed by Thirlwall (1988 and refs. therein) in the Old Red Sandstone lavas of these two regions. Smedley (1988b) recognised that  $\epsilon\text{Nd}_t$  values in the range +1 to +2 for the Kintyre & Arran Permo-Carboniferous lavas are considerably more radiogenic than the value of -2 adopted by Thirlwall (1986) for the SWH mantle. Either the Kintyre & Arran lavas represent a mix of depleted mantle (i.e. Midland Valley mantle) and SWH mantle, or the SWH mantle source is more radiogenic than that suggested by Thirlwall (1986). Smedley (1988b) opted for the latter on the basis that there is no independent evidence from granitoid chemistry or lithospheric mantle xenoliths for Midland Valley type depleted mantle beneath the South-west Highlands. This however assumes that the granitoids or xenoliths would have sampled such a source region. There are also no mantle xenolith data from the South-west Highlands. The ORS data from Lorne (Thirlwall 1986) point to more radiogenic Nd compositions than  $\epsilon\text{Nd}_t$  -2 (Fig. 7.10), which Thirlwall (1986) attributed to increasing proportions of subducted SULPS-like sediment. Smedley (1988b), however, suggested that the more radiogenic Nd compositions supported her belief that the SWH mantle is less LREE-enriched than believed by Thirlwall (1986) with an  $\epsilon\text{Nd}_t$  of between +1 and +2.

Smedley's conclusion are here criticised on the following grounds:

- 1) Subduction related magmas are enriched in LILE (Pearce 1983) (e.g. K, Ba, Rb and Sr) relative to REE and high field strength elements (HFSE). Thirlwall plotted Sm/Ce against Sr/Ce for the ORS lavas (Fig. 7.23). From this diagram, it is evident that the Lorne Plateau lavas have, on average, higher Sr/Ce ratios than the Midland Valley ORS lavas. Both magmas lie in the high Sr/Ce arc volcanic field represented by the Lesser Antilles. In the Lesser Antilles, increasing Sr/Ce correlates with increasing  $\epsilon\text{Sr}_t$  which is explained by the increasing contribution of subducted sediment derived material to the mantle source region (Hawkesworth and Powell 1980). However, those samples from the Lorne plateau with the highest Sr/Ce ratios have the lowest  $\epsilon\text{Sr}_t$  (<0) and the lowest  $\epsilon\text{Nd}_t$  ( $\approx$ -2). Thirlwall (1986) discounted fractionation of minor phases as a mechanism for producing the high Sr/Ce ratios of the Lorne lavas because no suitable accessory phases could be identified in the phenocryst assemblage of these magmas. Neither can plagioclase fractionation have lowered the Sr/Ce ratios of the Midland Valley ORS lavas as these magmas are believed to have undergone very little fractionation because of their high Ni, Cr and MgO contents. This

suggests that high Sr/Ce ratios are a feature of the SWH mantle which has  $\epsilon\text{Nd}_t = -2$ , as suggested by Thirlwall (1986).

2) Pb isotope ratios from the Lorne Plateau lavas are significantly lower than the majority of the Midland Valley ORS lavas (Thirlwall 1986). The only variation in Pb isotope ratios documented by Smedley (1988b) between the Midland Valley and Kintyre & Arran Permo-Carboniferous lavas is a relatively small shift (of 0.05) to lower  $^{207}\text{Pb}/^{204}\text{Pb}$ . The remaining Pb isotope ratios for the Kintyre & Arran lavas plot within the field defined by the Midland Valley Permo-Carboniferous lavas. This suggests that the Kintyre & Arran Permo-Carboniferous lavas are sampling a different mantle composition(s) to the Lorne lavas and that it is chemically and isotopically more closely related to the Midland Valley mantle than the SWH of Thirlwall (1986). This would account for the higher  $\epsilon\text{Nd}_t$  values of the Kintyre & Arran Permo-Carboniferous lavas when compared to the Lorne lavas.

Thirlwall (1986 & 1982) speculated on the reason for a slight overlap between Lorne lavas and northern examples of the Midland Valley lavas (Figs. 7.10 & 7.24). The Midland Valley examples which fall within the field of Lorne Lavas are characterised by slightly lower  $\epsilon\text{Nd}_t$  and low  $(^{206}\text{Pb}/^{204}\text{Pb})_{410}$ . It was suggested that small quantities of SWH mantle were involved in the generation of lavas in the north of the Midland Valley. If this is the case then it is possible that small amounts of SWH mantle are also involved in the generation of the northernmost examples of Permo-Carboniferous lavas which outcrop on Kintyre and Arran.

#### 7.5.1.iii The extent of South West Highland LREE enriched mantle

Parental magmas for the Loch Borrallan and Loch Ailsh syenites, along with other alkaline magmas of the NW Highlands, were believed by Halliday et al. (1987) to have been generated by low degree partial melting of cold, ancient lithospheric mantle analogous to that identified from xenoliths below Loch Roag. Thompson & Fowler (1986), Fowler (1988 & 1992) and Thirlwall & Burnard (1990) disagreed with such a model and suggested that contamination of a parent magma derived from the asthenosphere with Lewisian or Moine partial melts was a more suitable model.

Compositional continuity between NW Highland syenites has been demonstrated by Thompson & Fowler (1986); therefore any model developed for one syenite intrusion must also be applicable to the remainder.  $\epsilon\text{Nd}_t$  values for Glen Dessary (Fig. 7.25) range between +3.2 and -1.3 (exceptionally -11.1). No overlap with Loch Borrallan occurs except where there is good evidence for crustal contamination. This suggests that, if the two plutons have a common mantle source, the Glen Dessary magmas represent a more primitive, less contaminated sample, in terms of Nd isotopes, than Loch Borrallan. The mantle source for the syenitic magmas has higher  $\epsilon\text{Nd}_t$  than is estimated for the SWH mantle (+3.2 vs -2 respectively). Furthermore, whereas the Lorne Lavas show a weak positive correlation between  $\epsilon\text{Nd}_t$  and  $\epsilon\text{Sr}_t$ , the Glen Dessary and Loch Borrallan intrusions both reveal negative

correlation between  $\epsilon\text{Nd}_t$  and  $\epsilon\text{Sr}_t$ , the Glen Dessary and Loch Borrallan intrusions both reveal negative correlations between  $\epsilon\text{Nd}_t$  and  $\epsilon\text{Sr}_t$  (Fig. 7.25). Fowler (1992) believed that depleted mantle was a more suitable source for the syenites, and consequently the northern limit of SWH mantle must lie to the south of Glen Dessary.

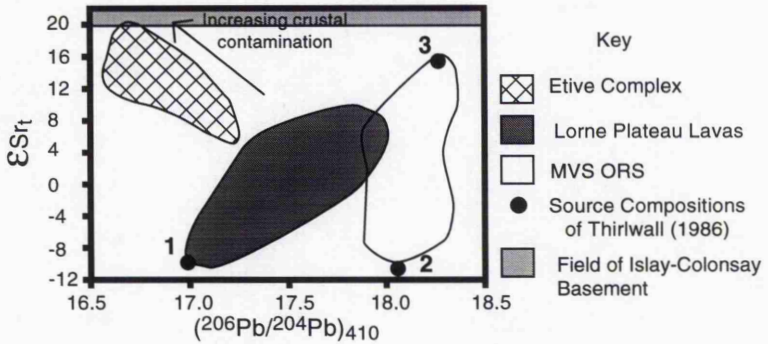


Fig. 7.24  $\epsilon\text{Sr}_t$  vs  $^{206}\text{Pb}/^{204}\text{Pb}$ . Data from Thirlwall (1986) and Frost & O'Nions (1985). Lorne trend to increasing  $\epsilon\text{Sr}$  is not caused by the same contaminant which is affecting the Etive Pluton.

#### 7.5.1.iv Lamprophyres

Lamprophyres are often considered as representative of source mantle compositions for both lavas and Newer Granites throughout the British Caledonides (Rock et al. 1988 and refs. therein). Many granite plutons, including Ben Nevis, are intimately related with lamprophyres. Field and chemical evidence throughout the Caledonides, indicate that the relationship is genetic (Fowler 1988, Rock & Hunter 1987, Thompson & Fowler 1986, and Macdonald et al. 1986). Appinites are considered as the plutonic equivalents of the lamprophyre suite (Rock 1984) and have been shown to be closely related to the early mafic magmas in many granite plutons (e.g. Pitcher & Berger 1972, see also chapter 5 & 6). In the Ben Nevis Complex, the appinites are intimately related to the Coarse Quartz Diorite and the lamprophyre dykes are found cross-cut by and cross-cutting the Fine Quartz Diorite, Coarse Quartz Diorite and Porphyritic Outer Granite. The implication therefore, is that lamprophyres have a similar relationship with Ben Nevis and other Newer Granite plutons as appinites.

Thompson & Fowler (1986) and Fowler (1988) believed that minette lamprophyres are representative of the mantle source to the Newer Granites. Detailed studies of relationships between lamprophyre and granite magmas within composite dykes have documented a close genetic relationship between the two magmas (Rock & Hunter 1987 and Macdonald et al. 1986). On Mull, geochemical modelling using lamprophyre magma and phenocryst assemblages from lamprophyres has shown that it is possible to generate granite from lamprophyre by fractional crystallisation and/or crustal contamination (Rock & Hunter 1987). A similar model was proposed for granite and lamprophyre magmas within

ratios for lamprophyres are identical to those from the adjacent granitoid plutons, Ross of Mull and Criffell respectively. Unfortunately no combined isotope data have been published and conclusions based on a single isotope system are not necessarily definitive. For instance, both Lewisian granulite and depleted mantle have similar  $\epsilon\text{Sr}$  at 425Ma.

The Newer Granites in the Southwest Highlands are characteristically rich in K, Ba and Sr, and a variety of evidence supports models based on contamination of mantle derived melts by continental crust (e.g. Thirlwall & Burnard 1990, Harmon et al. 1984 and Holden et al. 1987). Rock & Hunter (1987) criticised the suggestion of Harmon et al. (1984) that high Ni and MgO lavas from the Lorne plateau are direct derivatives of the mantle source region, on the basis that they lack the requisite high K, Ba and Sr values required and are regionally restricted. It is not clear where Rock & Hunter (1987) obtained their data for the Lorne Plateau lavas from, as the analyses published by Thirlwall (1981) reveal that these lavas are mildly shoshonitic (i.e. high  $\text{K}_2\text{O}$ ), with Sr contents >800ppm (often >1000ppm) and Ba contents >700ppm (often >1000ppm), and definitely comparable to the Newer Granites as suggested by Harmon et al. (1984). Rock & Hunter (1987) went on to propose that lamprophyres are more likely to include representative mantle source compositions. Such a hypothesis is based on the high Sr, Ba and K contents of lamprophyres, their widespread distribution and the lack of any other form of primitive magma around many granite plutons e.g. Mull. Rock et al. (1988) also showed that regional variations in lamprophyre compositions match those observed in Old Red Sandstone lavas (Thirlwall 1981) and in the Newer Granites (Stephens & Halliday 1984). The chemical trends of Rock et al. (1988) increase or decrease to the north and to the south of a line centred in the Grampian Highlands and the authors developed the following model to account for the observed geochemical variation in lamprophyre chemistry.

1) Ti & Yb derived from DMM most likely to have been located above the subducting plate.

2) Sr, K, Rb, Ba, Th, LREE and P transported by aqueous fluids emanating from the subducting plate and enriching the overlying mantle wedge.

3) Zr, Hf, Nb & Ta transported by  $\text{CO}_2$  rich fluids derived from degassing of a sub-lithospheric source.

In this model regional chemical zonation displayed by Late Caledonian magmas is attributed to subduction along a line south of the English Lake District, and is coupled with increasing metasomatic enrichment of the mantle from Central Scotland northwards (Rock et al. 1988 and Macdonald et al. 1985). Interestingly, recent discussion on the closure of Iapetus has also centred on the occurrence of a subduction zone to the south of the English Lake District which was active after subduction had ceased along the Solway Line (Soper 1986, Soper & Woodcock 1990 and Soper et al. 1992, see also chapter 8).

#### 7.5.1.v Conclusion

From the above discussion it can be seen that the nature of the upper mantle below Northern Britain is extremely complex. Problems with the published literature are that it represents an incomplete study of lamprophyre/apprinite intrusions, a lack of combined isotopic studies from these rocks and a limited number of detailed geochemical and isotopic studies from individual plutons and associated intrusions. There is also a pressing need for data on mantle derived xenoliths from a site in the Grampian Highlands. Nevertheless, the following conclusions can be drawn from the above discussion.

- i) Extreme LREE-enriched lithospheric mantle underlies the Hebridean craton.
- ii) Depleted mantle underlies the Midland Valley and Southern Uplands.
- iii) Depleted mantle forms the mantle component to alkaline magmatism in the Northern Highlands.
- iv) LREE-enriched mantle underlies the South West Highlands and is the dominant mantle component within lavas and granites in this region. This source is not recognised in mantle xenoliths from the Hebridean craton or the Midland Valley, and Permo-Carboniferous lavas do not represent simple derivatives of this source, if at all.

#### 7.5.2 The Lower Crust

In addition to the mantle and local upper crustal sources, there is evidence for contamination in the lower crust (e.g. Frost & O'Nions (1985)). The nature of this source is the subject of much debate because of the supposed absence of any upper crustal correlative. Recently, Dickin & Bowes (1991) presented evidence for the Islay-Colonsay-Inishtrahull basement gneisses as the surface expression of the lower crust at least within part of the Grampian terrane. This will be discussed further.

From indirect methods (granitoid, lava and lamprophyre chemistry and geophysical experiments), it is known that the lower crust has the following characteristics.

- i) It contains zircon crystals older than  $\approx 1000\text{Ma}$  and possibly with an average Middle Proterozoic age (Pidgeon & Aftalion 1978). Clayburn (1988) favoured a mix of Grenvillian and Lewisian crust, but there is no evidence that the Grenvillian orogeny was a crustal building event either in Scotland or in adjacent regions on palaeo-tectonic reconstructions (Frost & O'Nions 1985). Pidgeon & Compston (1992) documented the occurrence of a  $\approx 1800\text{Ma}$  zircon xenocryst component in all of the granites studied north of the Highland Boundary Fault; however the relevance of the small number of granites studied (4), and the small number of data points presented from each granite, to the Caledonides as a whole is unclear.

- ii)  $\delta^{18}\text{O}$  and initial  $^{87}\text{Sr}/^{86}\text{Sr}$  ratios from the Newer Granites exposed in the Grampian Highlands reveal that the lower crust has not undergone a period of upper crustal residence or interacted with meteoric fluids (Halliday & Stephens 1984 and Harmon 1980)

and has the following isotopic characteristics,  $\delta^{18}\text{O} < 10\%$ ,  $^{87}\text{Sr}/^{86}\text{Sr} = 0.705\text{-}0.707$ ,  $^{206}\text{Pb}/^{204}\text{Pb} = 16.5\text{-}17$  and negative  $\epsilon\text{Nd}_t$  (Harmon et al. 1984 and Halliday et al. 1985).

iii) It is geophysically comparable to Lewisian granulite-facies gneiss (Bamford 1979 and Shackleton 1979).

iv) Low Rb/Ba and Rb/Sr ratios of many granites indicate a granulite source (Thirlwall 1983).

v) The lack of a significant Eu anomaly limits the involvement of feldspar as a fractionating phase or as a restitic phase to a negligible amount (unless  $f\text{O}_2$  is high).

vi) The lower crust probably ages northwards. This need not reflect an increase in the time lapsed since separation from the mantle, merely that the average age of the components making up the lower crust increases, as would be expected if the lower crust were made of sediments increasingly rich in Lewisian detritus as the North-West Foreland is approached.

vii) It has a significant volume both laterally and vertically to influence the geochemistry of magmas passing through and/or temporarily ponded within the lower crust.

viii) It is mafic to intermediate in composition (Harmon et al. 1984).

ix) From chemical variations in lamprophyres, Rock et al. (1988) proposed that this lower crust was the source of Zr, Nb, Ta and Hf to these magmas.

Recent work on the Islay-Colonsay amphibolite gneiss has revealed that it is considerably younger than the Lewisian (Marcantonio et al. 1988), of which it was previously believed to be a southerly extension. Daly et al. (1991) extended the area of outcrop of this younger gneiss below Northern Ireland to Inishtrahull and Dickin & Bowes (1991) suggested that the Rockall Plateau is also part of this crustal block. A U-Pb zircon age for the Islay-Colonsay gneiss cluster gives  $1782 \pm 5\text{Ma}$  (Marcantonio et al. 1988) and Sm-Nd model ages average 1.95Ga, suggesting the involvement of older crust was minimal. Although only limited isotopic data have been published for the Islay-Colonsay basement, those which are available are remarkably similar to the required composition of the lower crust. Harmon et al. (1984) believed that the lower crustal component to the Etive pluton had the following isotopic characteristics;  $\delta^{18}\text{O} \approx 8\text{-}10\%$ , initial  $^{87}\text{Sr}/^{86}\text{Sr} = 0.705\text{-}0.707$ ,  $^{206}\text{Pb}/^{204}\text{Pb} = 16.5\text{-}17$  and  $\epsilon\text{Nd}_t \approx -10$  (from their Fig 8); whereas the Islay-Colonsay gneiss has  $(^{87}\text{Sr}/^{86}\text{Sr})_{425} = 0.706\text{-}0.710$ ,  $^{207}\text{Pb}/^{204}\text{Pb} = 16.5\text{-}18.9$  and  $\epsilon\text{Nd}_{425}$  in the range  $-12$  to  $-16$  (Marcantonio et al. 1988 and Dickin 1992).

Dempster & Bluck (1989) and Rogers et al. (1989) both suggested that the Islay-Colonsay block is an exotic terrane and may therefore underlie the Dalradian metasediments as a structurally emplaced wedge; however, geomagnetic evidence indicates that the Islay-Colonsay basement is continuous with the basement of the Dalradian (Westbrook & Borradaile 1978). Furthermore, clasts within the Port Askaig Tillite have been tentatively matched with the gneisses of Colonsay (Fitches et al. 1990). Geographically the Islay-Colonsay basement is the closest exposure of basement to Ben Nevis.

## 7.6 Discussion

A summary of possible source compositions is presented in Table 7.3.

Table 7.3 Characteristics of possible source rock compositions for the Ben Nevis Complex.

(εSr and εNd parameters at 425Ma.)				
Source region	εNd	εSr	δ <sup>18</sup> O	<sup>206</sup> Pb/ <sup>204</sup> Pb
1) Depleted mantle	7.3	-7.0	5.7	17.6
2) South West Highland Mantle	-2.0	-3.5		17.0
3) Subducted Slab	<-2.0	>4.0		18.1
4) SULPS	-6.1	-47.4	12.5	17.6
5) Dalradian	-15.6	>10.0	10.8	18.4
6) Lewisian Amphibolite	-24.7	>10.0	10.0	14.4
7) Lewisian Granulite	-19.0	<0.0	5.0	14.8
8) Lower Crust	<0.0	<80.0	<10.0	16.5
9) Islay-Colonsay Basement	-14.3	62.0		17.0

Data from Harmon et al. (1984), Halliday et al. (1985), Morton & Taylor (1991), Thirlwall (1986), Smedley (1986, 1988a & 1988b), Holden et al. (1987), Marcantonio et al. (1988), Dickin & Bowes (1991) and Frost & O'Nions (1985).

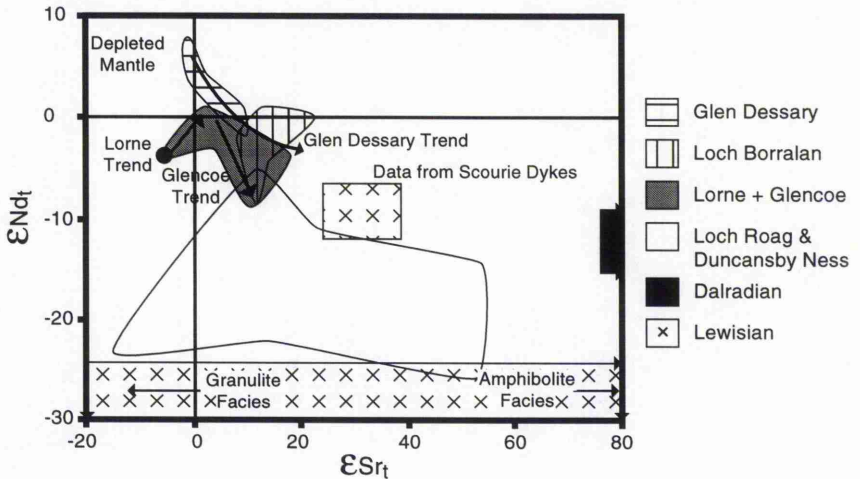


Fig. 7.25  $\epsilon Nd_t$  vs  $\epsilon Sr_t$  data for Loch Borralan and Glen Dessary (Thirlwall & Burnard 1990 and Fowler (1992) and xenolith data (see Fig. 7.20 for references). Enriched Hebridean type mantle cannot be the source for the alkaline intrusions.

The presence of lamprophyre dykes and appinitic bodies in the Ben Nevis Complex testify to the mantle being one source of magma, as well as a source of heat during melting in

the lower crust. When compared to the Lorne Plateau and Midland Valley ORS lavas (Fig. 7.26), the Ben Nevis Complex has a similar range in  $\epsilon\text{Sr}_t$  (if BN366 and BN400 are discounted because of Dalradian contamination in these magmas), but is displaced to lower  $\epsilon\text{Nd}_t$ . This trend is most strongly defined by the Summit andesites which have decreasing  $\epsilon\text{Nd}_t$  at constant  $\epsilon\text{Sr}_t$ . Trace element variations in the andesites of Ben Nevis reveal amphibole fractionation at depth, possibly in the lower crust, and limited upper crustal residence prior to extrusion (chapter 6), which leads to the suggestion that contamination of low Sr/Nd-high  $\epsilon\text{Nd}_t$  parental magmas occurred in the lower crust. Debate on the composition of the lower crust has been enlivened with the recognition of  $\approx 1.8\text{Ga}$  basement gneiss on Islay and Colonsay, and this is the first isotopic study to consider both the Islay-Colonsay Basement and SWH mantle as possible sources for a Newer Granite pluton.

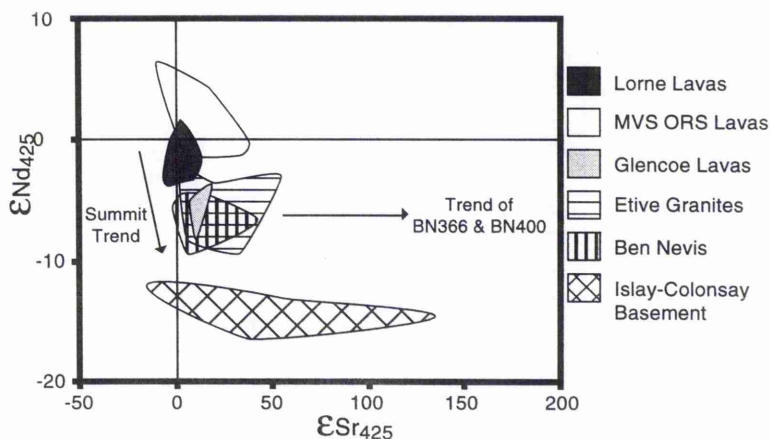


Fig. 7.26 The Summit trend of the Ben Nevis Complex could be explained by contaminating SWH mantle melts with Islay-Colonsay Basement crustal material. The overlap in isotopic composition between the Ben Nevis Complex and the Etive Complex is demonstrated in this diagram. Data from Marcantonio et al. (1988), Frost & O'Nions (1985) and the references for the Lorne samples can be found in Fig. 7.25.

#### 7.6.1 Composition of the Mantle Source

The SWH mantle is the most obvious mantle source for the Ben Nevis Complex on the grounds of proximity, but there is no overlap with the Lorne Plateau Lavas in  $\epsilon\text{Sr}_t$ - $\epsilon\text{Nd}_t$  space (Fig. 7.26), and the Ben Nevis Complex data could be explained by contamination in the lower crust of a depleted mantle component. Indeed, Frost & O'Nions (1985) suggested that the Lorne lavas themselves may, at least in part, represent depleted mantle contaminated by a lower crustal component. Their evidence was based on  $\delta^{18}\text{O}$  values for the Lorne lavas of  $>7.5\text{‰}$  which is higher than the  $\delta^{18}\text{O}$  value of the depleted mantle ( $5.7 \pm 0.3\text{‰}$ ; Taylor 1980). The Lorne Lavas analysed for  $\delta^{18}\text{O}$  by Frost & O'Nions (1985) do not, however, represent the Lorne Plateau compositions with the highest Sr/Ce ratios, lowest  $\epsilon\text{Sr}_t$  and lowest  $\epsilon\text{Nd}_t$ , which are believed to be the lava compositions most similar to the SWH mantle source (i.e. the highest  $\epsilon\text{Nd}_{400}$  and lowest  $\epsilon\text{Sr}_{400}$  values obtained by Frost &

O'Nions (1985) from the Lorne Plateau lavas are 3.3 and 0.0 respectively; Thirlwall (1988) believed that the SWH mantle has values of -2.0 and -3.5 respectively.

Fig. 7.24 is a plot of  $\epsilon\text{Sr}_{410}$  against  $(^{206}\text{Pb}/^{204}\text{Pb})_{410}$  for the Etive Complex, the Lorne Plateau and Midland Valley ORS lavas. The Ben Nevis Complex has very nearly a 100% overlap with the Etive Complex in  $\epsilon\text{Sr}_t$ - $\epsilon\text{Nd}_t$  space (Fig. 7.26) and is also chemically very similar (chapter 6). In Fig. 7.24, the Midland Valley ORS lavas define a vertical trend with increasing  $\epsilon\text{Sr}_t$  (-9 to 16) at constant  $(^{206}\text{Pb}/^{204}\text{Pb})_{410}$  (18.0), whereas the Lorne Plateau lavas show a positively correlated trend of increasing  $\epsilon\text{Sr}_{410}$  (-9 to 10) and increasing  $(^{206}\text{Pb}/^{204}\text{Pb})_{410}$  (17.0-18.0). In contrast, the Etive Complex is negatively correlated with increasing  $\epsilon\text{Sr}_{410}$  (4 to 20) and decreasing  $(^{206}\text{Pb}/^{204}\text{Pb})_{410}$  (17.2-16.5). Thirlwall (1986) used the isotopic relationships displayed in this graph to demonstrate that the low  $(^{206}\text{Pb}/^{204}\text{Pb})_{410}$  component to the Lorne Plateau lavas is not crustally derived but a feature of the mantle source. Speculation on the nature of a possible lower crustal component for the Lorne Plateau lavas led Thirlwall (1986) to identify a hypothetical lower crustal crust with low  $\epsilon\text{Sr}_{410}$  (<-9), low  $(^{206}\text{Pb}/^{204}\text{Pb})_{410}$  (<15.0) and an  $\epsilon\text{Nd}_t$  value of -2.  $^{207}\text{Pb}/^{204}\text{Pb}$  and  $^{206}\text{Pb}/^{204}\text{Pb}$  isotope ratios for the Lorne Plateau lavas yield an apparent age of  $1748 \pm 180\text{Ma}$ . Extraction of the hypothetical crust from the mantle at  $\approx 1900\text{Ma}$  and subsequent granulite facies metamorphism at  $\approx 1750\text{Ma}$ , which led to extreme U-depletion and mild Rb depletion could explain the distribution of Lorne lavas in Fig. 7.24. This crustal composition could only explain the isotopic composition of the Lorne Plateau if the lavas were comprised of largely crustally derived Sr and mantle derived Pb. Such a suggestion is excluded by the linear Sr-Pb isotope correlation in the Lorne Plateau lavas (Fig. 7.24) and by high Sr/Pb ratios in the lavas (Thirlwall (1986). Thirlwall (1986) believed that crust of this age was absent in Northern Britain; however recent work on the basement of Islay-Colonsay has led to the recognition of a  $\approx 1800\text{Ma}$  crust which may extend beneath the Grampian Highlands (Marcantonio et al. 1988), but the isotopic composition of this crust is not comparable to that required by Thirlwall (1986) i.e.  $(^{206}\text{Pb}/^{204}\text{Pb})_{410} = 17.0$ ,  $\epsilon\text{Sr}_{410} > 4$  and  $\epsilon\text{Nd}_{410} < -7$  (data from Marcantonio et al. 1988 and Dickin & Bowes 1991).

Extrapolation of the Etive Complex trend in Fig. 7.24 intersects with the Lorne Plateau trend at  $(^{206}\text{Pb}/^{204}\text{Pb})_{410} \approx 17.2$  and  $\epsilon\text{Sr}_{410} \approx 0$  or with the depleted mantle end-member of the Midland Valley ORS lavas. Geochemical trends across Northern Britain for Ba, Sr, K, P and LREE/HREE ratios have been described in primitive ORS lavas (Thirlwall 1981) and lamprophyres (Rock et al. 1987), both of which are believed to be mantle derived (Thirlwall 1981 & Rock 1991). Similar trends across Northern Britain are observed in the Newer Granites and are again related to chemical variation in the mantle (Stephens & Halliday 1984 and Halliday et al. 1985). On the basis of this evidence, the mantle source for the Ben Nevis Complex is believed to be the SWH mantle as defined by Thirlwall (1986).

## 7.6.2 The Summit Andesite Trend

Isotope data for the Ben Nevis Complex are displaced from the field defined by the Lorne Plateau lavas to lower  $\epsilon\text{Nd}_t$ , whereas  $\epsilon\text{Sr}_t$  values are similar. The samples from the Summit andesites display a vertical trend in Fig. 7.17 with decreasing  $\epsilon\text{Nd}_t$  at approximately constant  $\epsilon\text{Sr}_t$ ; this trend is believed to have been generated in the lower crust. Fig. 7.18 reveals that this trend is matched by increasing Sr/Nd ratios. This cannot be attributed to simple fractional crystallisation as the  $\text{SiO}_2$  contents of these samples vary by less than 2%, and it is therefore believed that the Summit trend is the result of contamination by a low  $\epsilon\text{Nd}_t$ , low  $\epsilon\text{Sr}_t$  and high Sr/Nd ratio lithology assuming simple bulk contamination or the addition of partial melts from a crustal lithology providing plagioclase feldspar was not a residual phase.

Harmon et al. (1984) provided the following estimate of lower crustal composition  $\delta^{18}\text{O} \approx 8\text{-}10\%$ ,  $^{87}\text{Sr}/^{86}\text{Sr} = 0.705\text{-}0.707$  ( $\epsilon\text{Sr}$  15 to 40),  $^{206}\text{Pb}/^{204}\text{Pb} = 16.5\text{-}17$  and  $\epsilon\text{Nd}_t \approx -10$  (from their Fig 8). These authors believed that no upper crustal correlative existed in Northern Britain (section 7.3.1.iv) and suggested that the lower crust beneath the Grampian Terrane is Grenvillian in age. This age was obtained from the coincidence of  $T_{\text{CHUR}}$  model ages and Pb isotope upper intercepts with concordia. Both, however, represent averages of the isotopic components incorporated within a magma.

$\epsilon\text{Nd}_{425}$  and  $\epsilon\text{Sr}_{425}$  data for the Islay-Colonsay basement are presented in Fig. 7.26. From this diagram it is evident that the Islay-Colonsay basement is a feasible source for the Ben Nevis magmas. In Fig. 7.24, the Islay Colonsay basement falls on the end of the trend defined by the Etive complex and again provides evidence for the involvement of basement with a similar isotopic composition to the Islay-Colonsay gneiss during the formation of the Ben Nevis Complex.

In Fig. 7.18, however, the trend defined by the Summit andesites ends with higher Sr/Nd ratios ( $>30.0$ ) than the Islay-Colonsay Basement ( $<30.0$ ). There are three possible reasons for this discrepancy:

- 1) The Islay-Colonsay basement is not a source to the Ben Nevis Complex.
- 2) The available analyses for the Islay-Colonsay basement do not fully represent the lower crust beneath the Grampian Highlands and this may have higher Sr/Nd ratios.
- 3) Fractionation of a HREE-enriched phase during contamination could drive the Summit trend towards higher Sr/Nd ratios.
- 4) Partial melting of the lower crust involved plagioclase, therefore yielding partial melts with Sr/Nd ratios greater than the starting material.

Amphibole fractionation has already been invoked to explain the trace element characteristics of the plutonic and volcanic rocks. Removal of these phase during fractional crystallisation is capable of driving Sr/Nd to higher ratios (Nd has a bulk distribution

coefficient of 3.0 for amphibole according to Henderson 1984). This may be a possible explanation. Also, if plagioclase is not a residual phase during partial melting of the lower crust, then the Sr/Nd ratio of the partial melt is likely to be higher than that of the crust from which it was derived.

Dickin (1992) noted that the Pb isotope composition of the Islay-Colonsay basement was in the same range as the Pb isotope composition of K-feldspar from the Newer Granites not affected by Dalradian contamination.

### 7.6.3 The trend of BN366

Scatter in the data off the Summit trend could be explained by slight variations in the composition of the lower crustal contaminant. However, BN366 has much higher  $\epsilon\text{Sr}_t$  than the remaining Ben Nevis Complex samples (excluding BN400) and it was suggested in section 7.4.6.iii that the increase in  $\epsilon\text{Sr}_t$  resulted from localised contamination with Dalradian upper crustal compositions. Unlike the Sm and Nd concentration data (Figs. 7.16a-d) and Nd isotopes, the Rb and Sr contents and Sr isotopic composition of the Ben Nevis Complex can be related to fractional crystallisation (Figs. 7.13, 7.14a & 7.14b), although the relationship is not simple one. On Fig. 7.13, the earliest components of the volcanic pile, the Ciste andesites, and the earliest and most basic members of the plutonic rocks, show variable but decreasing  $\epsilon\text{Sr}_t$ . In contrast, the later magmas in the volcanic pile show uniform Sr isotopes and the more siliceous and later members of the plutonic rocks show increasing  $\epsilon\text{Sr}_t$  with increasing  $\text{SiO}_2$ . Variations in isotopic ratios cannot be caused by fractional crystallisation alone. This leads to the suggestion that, in terms of Sr isotopes, the low  $\text{SiO}_2$  magmas were contaminated early in the development of the upper crustal magmatic plumbing system when the potential for contamination with Dalradian country rocks adjacent to the magma conduit was greatest. As the plumbing system evolved, the opportunities for interaction with the Dalradian country rocks in the magma conduits declined and consequently the variation in  $\epsilon\text{Sr}_t$  also declined. This could be due to a variety of reasons.

- 1) Removal of the least stable (i.e. most easily melted) mineral phases in the country rock during passage of the early magmas.
- 2) Later magmas are higher in  $\text{SiO}_2$  and therefore represent lower  $T^\circ$  melts with less ability to interact with the country rock.
- 3) Establishment of a protective crystalline 'sleeve' around the magma conduit preventing access to the country rocks for the later magmas (Fig. 7.27).

A similar model has been developed for the Skye Plateau basalts (Thirlwall & Jones 1983). The trend of increasing  $\epsilon\text{Sr}_t$  and increasing  $\text{SiO}_2$  can be explained by temporary ponding in a crustal magma chamber below the Ben Nevis chamber during which assimilation of local Dalradian metasediments accompanied fractional crystallisation. Ponding an upper crustal magma chamber is also required to explain the presence of pyroxene in the plutonic rocks. The andesites have primary magmatic amphibole and are

therefore believed to have spent only a relatively short period in the upper crust. The crystallisation of pyroxene and contamination with a high  $^{87}\text{Sr}/^{86}\text{Sr}$  component is unlikely to have occurred in the Ben Nevis chamber as the Fine Quartz Diorite shows evidence of chilling against the Dalradian and bears pyroxene both as a phenocryst phase and a groundmass phase. Sharp contacts again indicate that fractional crystallisation cannot have occurred at the current level of exposure. This all points to the presence of a magma chamber below the Ben Nevis chamber but still in the upper crust.

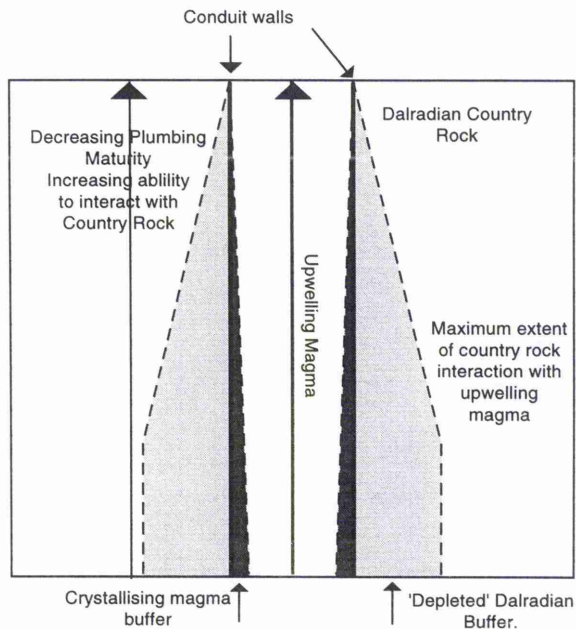


Fig. 7.27 Model for the evolution of the Ben Nevis Complex plumbing system with time. Increasing maturity of the system reduces the potential for wall-rock contamination during passage of the magmas through the crust. Later increases in  $\epsilon\text{Sr}_t$  with  $\text{SiO}_2$  reflect moderate AFC processes in the upper crustal magma chamber (Fig. 7.29).

Further evidence for the origin of the Ben Nevis Complex can be gleaned from Nd model age calculations. A Nd model age may represent a crustal residence age for Nd (O'Nions et al. 1983) i.e. the period of time elapsed since separation from the mantle. Typical model ages are calculated with respect either to a chondritic model composition of Bulk Earth ( $T_{\text{CHUR}}$ ) or relative to depleted mantle ( $T_{\text{DM}}$ ). If a magma is extracted from depleted mantle and does not undergo contamination from another source of Nd, then  $T_{\text{DM}}$  = emplacement age. If the magma represents a crustal melt, and the crust involved was formed several tens of millions of years prior to partial melting, then  $T_{\text{DM}}$  will represent the time at which the crust separated from the mantle, assuming that this mantle was depleted mantle.  $T_{\text{DM}}$  provides an estimate for the minimum age of the crustal component when a magma is a mix of a single crustal and a single depleted mantle source. The incorporation of additional sources of Nd further compounds problems with model age interpretations and  $T_{\text{DM}}$  then

yields an estimate for the minimum age of the average crustal component. The Ben Nevis Complex is believed to be multi-component multi-source magmas with SWH mantle  $\pm$  subducted slab, Islay-Colonsay basement and Dalradian metasediments. As a consequence, model age calculations for Ben Nevis should be treated with caution unless this complex origin is considered.

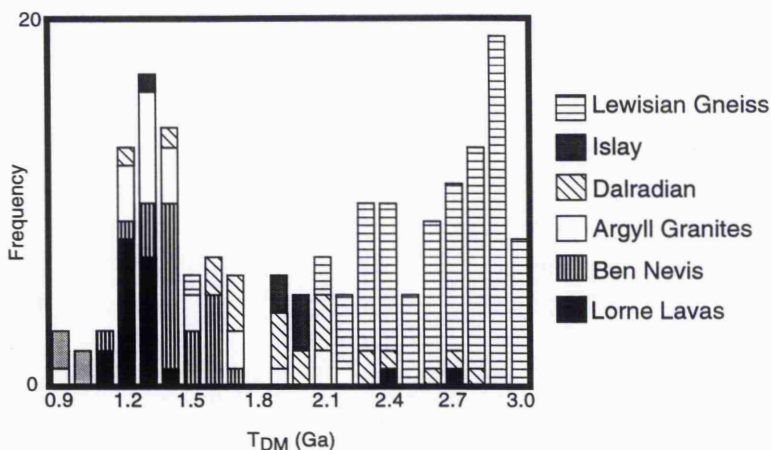


Fig. 7.28 Model age ( $T_{DM}$ ) data for Caledonide magmas. The LPL, although believed to be largely primitive mantle melts have  $T_{DM} > 1300\text{Ma}$ . Magmas derived wholly of partially from SWH mantle parent melts will also have high  $T_{DM}$ . It may be significant that the BNC and Argyll suite (Stephens & Halliday 1984) granite data plot between the LPL and ICB data sets. South of Scotland suite granites plot with  $T_{DM} = 1000\text{Ma}$  consistent with a Depleted mantle + SULPS origin for these magmas (Halliday et al. (1980).

The samples of the Lorne Plateau lavas analysed by Thirlwall (1983) are, on the basis of whole rock geochemistry, believed to represent mantle compositions that have undergone insignificant fractional crystallisation and crustal contamination. Yet  $T_{DM}$  for high Sr/Ce, low  $\epsilon\text{Sr}_t$  and low  $\epsilon\text{Nd}_t$  samples of the Lorne Plateau cluster around 1.3Ga, a figure which if obtained from a Caledonian granite would lead to the almost inevitable conclusion that the magma had either assimilated a large volume of old crustal material or were crustal melts (e.g. Hamilton et al. 1980). The reason for  $T_{DM}$  of 1.3Ga in the least-contaminated Lorne lavas is due to the LREE enriched nature of the SWH mantle, resulting in negative  $\epsilon\text{Nd}_t$  over time (Fig. 7.2). Halliday (1984) used model age calculations to imply that the Newer Granites contained substantial volumes of old crustal material, but the granite could contain a large volume of SWH mantle and have an 'old' model age. Fig. 7.28 is a frequency diagram of  $T_{DM}$  for members of the Argyll suite, Lorne Plateau Lavas, Ben Nevis, Islay-Colonsay Basement, Lewisian gneisses and Dalradian metasediments. The Argyll suite of which Ben Nevis is a member, strongly overlaps with the Lorne Plateau field although biased to slightly higher ages consistent with contamination by  $\approx 1,800$  Myr lower crust. Although this evidence should be treated with caution, it is perhaps significant that the Nd model ages for the Argyll suite do not cluster to lower values than the Lorne Plateau lavas which would imply that different reservoirs other than those proposed may have been

important in the formation of this suite.

## 7.7 Summary and Model for the evolution of the Ben Nevis Complex

The Ben Nevis Complex has a complex multi-component origin. Either fluids enriched in hydrophile elements emanating from a subducted slab initiated melting within time integrated LREE enriched mantle or thermal rebound of the mantle after subduction of a ridge initiated melting (Rogers & Saunders 1989). Ponding of melts in the lower crust resulted in assimilation of lower crustal rocks comparable in composition to the Islay-Colonsay gneiss. Simultaneous fractional crystallisation and assimilation would generate dacite volcanic and granodiorite/tonalite plutons i.e. melts of broadly granitic composition (Huppert & Sparks 1988), precisely the dominant rock types in the Ben Nevis Complex. The first magmas to migrate into the upper crust (Ciste andesites and the quartz diorites) interacted slightly with Dalradian metasediments in the magma conduit. The extent of this interaction declined rapidly such that later volcanics show no signs of Dalradian contamination. The development and growth of an upper crustal magma chamber led to renewed interaction with the Dalradian and increasing contamination accompanied increasing fractionation prior to final ascent and emplacement as a series of pulses, into the Ben Nevis magma chamber. This model is summarised in Fig. 7.29 (overleaf).

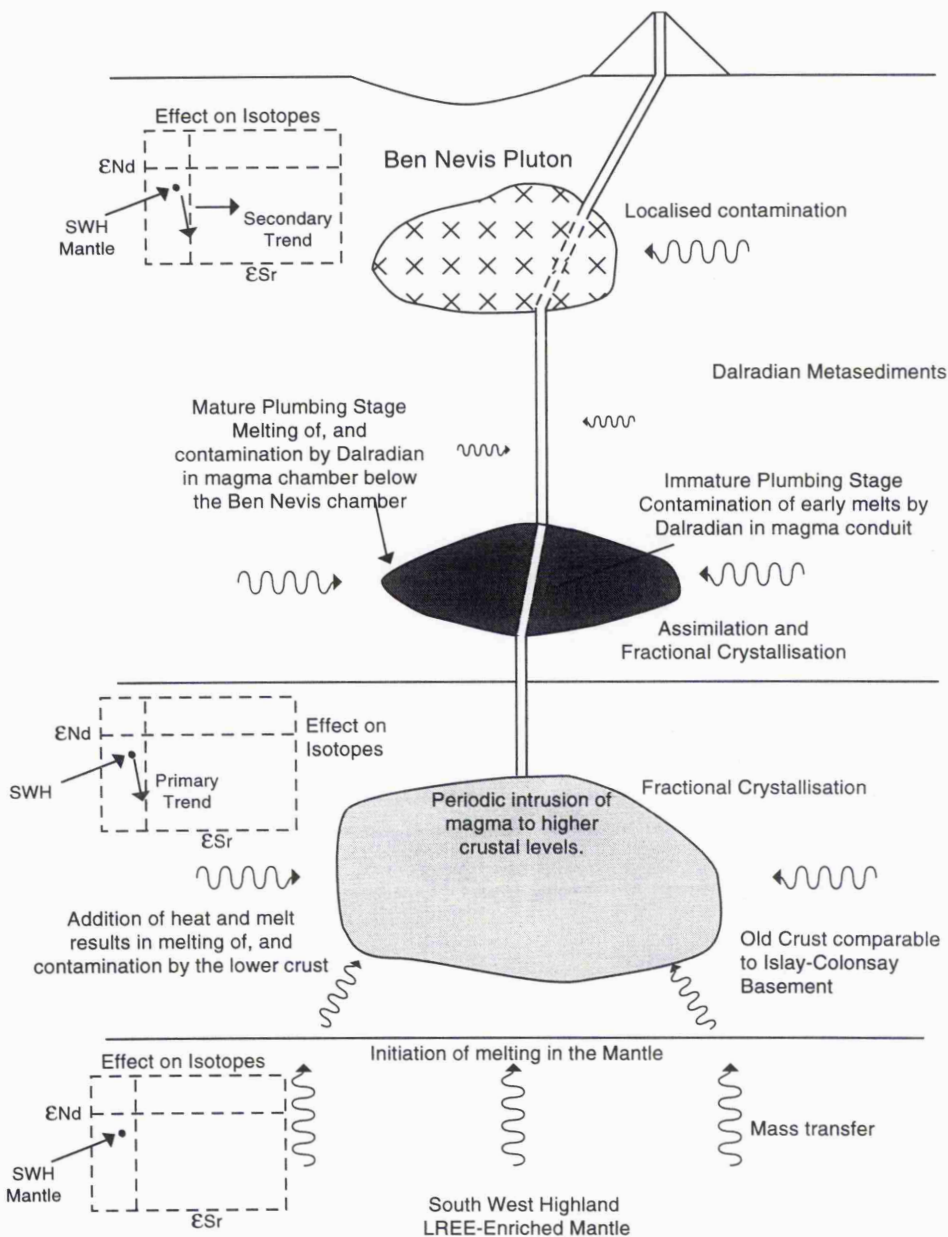


Fig. 7.29 Model for the evolution of the Ben Nevis magma system. Melting is initiated in LREE enriched mantle. Magma ponds in the crust and is periodically intruded to higher crustal levels. Early magmas suffer contamination in the magma conduit. Later plutonic magmas are contaminated in a mid-crustal magma chamber by AFC-type processes prior to final intrusion in the Ben Nevis chamber.



THE LAST GREAT ACT OF  
DEFIANCE

# CHAPTER 8

## CONCLUSIONS

### 8.1 Introduction

#### 8.1.1 General Statement

This study has primarily been concerned with the volcanology and petrogenesis of the Ben Nevis Complex. The following discussion mirrors the above split in that the volcanic pile is discussed in the wider context of Grampian geology, before a summarising the petrogenetic evolution of the Ben Nevis Complex. The relationship of the Ben Nevis Complex, the Newer Granites and contemporaneous volcanic activity is explored with respect to the tectonic regime prevalent towards the end of the Caledonian Orogeny.

The term Siluro-Devonian magmatism will refer to the Newer Granites, Old Red Sandstone (ORS) lavas and contemporaneous minor intrusions of mid-Silurian and early Devonian age.

### 8.2 The evolution of the Volcanic Pile - a tale of many breccias

In chapter 3, the volcanic pile was shown to have formed in a low-lying region that was probably underwater for much, if not all, of the period represented by the volcanic pile preserved today. It was also demonstrated that local relief was in excess of 300m and had a profound influence on the distribution of the various formations within the volcanic pile. Taubeneck (1967) showed that local relief in the Glencoe caldera exceeded 650m (2,000ft). If, as widely believed, uplift and erosion of the Caledonian mountain belt had largely been completed prior to the Siluro-Devonian magmatic event (Watson 1984, Dempster 1985 and Soper 1986), then regional relief could have exceeded 2,000m. Lava and pyroclastic material were erupted onto this dissected landscape (Watson 1984 and Soper 1986). The area forming Ben Nevis today was occupied by a freshwater lake fed by debris flows comprising local Dalradian metasediments and clasts derived from contemporaneous sediments; periodic collapse of sediment accumulations along the margins of the lake generated low-volume clastic turbidites. Geochemically, these fine grained mudstones are very similar to the igneous members of the Ben Nevis Complex and are composed of a large proportion of volcanic ash.

Harris (1992) describes the evolution of Scotland during the Devonian (in fact the Lower Old Red Sandstone is now believed to extend into the late Silurian from radiometric (Thirlwall 1988) and palynological evidence (Marshall 1991)) as one dominated wholly by terrestrial conditions. Active faulting, including movement along the Great Glen Fault, accompanied intrusion of the Newer Granites (Hutton 1988a). Tectonic controls on the distribution and facies of Highland Border and Great Glen ORS basins have been demonstrated by Mykura & Owens (1983) and Bluck (1983 & 1984). The overall sense of fault

movement is unclear; Hutton (1988a) demonstrated dextral movements along the Great Glen during intrusion of the Strontian granite whereas evidence from Ratagain reveals sinistral movements (Hutton & McErlean 1991). Both the Loch Sunart Granodiorite of the Strontian pluton and the Ratagain pluton were intruded at 425Ma (Rogers & Dunning 1991).

The deposits and faunas of the Lower Old Red sandstone indicate a warm arid climate, agreeing with palaeomagnetic data which show that Britain was situated less than 30° south of the equator. Such arid upland terrains are characterised by flash-floods and the movement of large volumes of sediment, whereas the occurrence of fine grained mudstones on Ben Nevis suggests a low energy environment locally. The local basement of the volcanic pile is comprised of garnet grade Leven Schists that were buried to a depth equivalent to 5kbars (Harte 1988) during the Caledonian Orogeny. Prior to deposition of the Allt a' Mhuillinn Formation, a substantial volume of material must have been stripped off. Extrusion and rapid burial by the volcanic rocks acted as an 'armour' plate preserving the underlying and more easily eroded Allt a' Mhuillinn Formation. Active erosion has been demonstrated in the volcanic pile, and is indicative of periodic emergence and/or drier episodes during the evolution of the volcanic pile.

The western Highlands formed the highest terrain in the Scottish ORS landscape, with erosion and transport of sediments southwards into the Highland border (Bluck 1983 & 1984 and Friend & Macdonald 1968). Large rivers also flowed to the northwest, emptying into the Orcadian basin (Mykura 1992). Paradoxically, the Ben Nevis sediments are the highest exposures of ORS sediments in Scotland, but are comprised of sediments deposited in a low-lying area. ORS sediments on both the eastern and western flanks of the Great Glen in the vicinity of Loch Ness have been shown to have been deposited in relatively small fault-bounded basins (Mykura 1983 and Mykura & Owens 1983). The Lower Old Red Sandstone sediments on the western shores of Loch Ness were believed to have been deposited in alluvial fans that bounded a narrow NNE-trending basin with active fault scarps on its northwestern and southeastern margins (Mykura & Owens 1983). Fine grained mudstones were deposited in playa lakes beyond the toes of the alluvial fans. A similar interpretation is placed on the Middle Old Red Sandstone deposits outcropping on the eastern shores of Loch Ness (Mykura 1983). Active faulting during deposition of both sequences led to oversteepening of the basin flanks and failure of the alluvial cone slopes leading to landsliding. Landsliding is one mechanism by which debris flows can be generated (Leeder 1982). This early Old Red Sandstone episode of faulting along the Great Glen is believed to have been dominated by essentially vertical movements (Smith 1977, Parsons 1979 and Mykura 1983). Fault planes with vertical displacements (downthrown to the north-east) are cross-cut by later dextral strike-slip fault planes. Estimates on the direction and distance of post Lower Old Red Sandstone movements along the Great Glen Fault vary from 133km of sinistral movement (Holgate 1969) to 50km of dextral movement (Flinn 1977); see review by Rogers et al. (1989). No geological evidence has been found to support palaeomagnetic studies that indicate post-Devonian sinistral movements of 2,000km (Storetvedt 1975). The southern margin of the Loch Ness ORS basin was located just south

of Foyers (Mykura 1983 and Mykura & Owens 1983); therefore the Ben Nevis sediments are not considered to be a southerly outlier of this basin. Stoker (1982) suggested that the ORS deposits of Rubha na h-Earba, some 15km south of Ft. William, are Lower Old Red Sandstone in age and not, as believed by Peach (in Bailey & Maufe 1916), Middle Old Red Sandstone. However, this latter age is equivocal (Mykura 1992).

It should be noted that the Great Glen sediments are terrestrial in origin, and fine grained mudstones are interpreted as playa lake deposits (Mykura 1983 and Mykura & Owens 1983), therefore supporting a similar interpretation for the Allt a' Mhuillin Formation. Although these ORS outcrops are today restricted to narrow slivers along the Great Glen, the size of the depositional basin is believed to have been larger. Smith (1977), Mykura (1983) and Mykura & Owens (1983) all present evidence for substantial compression after deposition of the Lower and Middle Old Red Sandstones. The fine grained sediments in the volcanic pile on Ben Nevis may therefore represent the playa lake deposits from a fault bounded basin to the west of the Great Glen Fault and extending eastwards for some unknown distance; the Old Red Sandstone deposits in the Glencoe calder may represent a second outcrop of the same basin. Oversteepening of the basin margins during extensional movements led to the generation of landslides which passed into debris flows on entering the playa lake.

The first macroscopic evidence of volcanic activity is found in the form of volcanoclastic breccias (i.e. the intervening breccia at the base of the Coire na Ciste Formation) that are thought to have been deposited by one or more lahars. The source vent for these early andesitic clasts may have been several tens of kilometres distant, although more local sources, such as Coille Lèanachain or a vent above the developing Ben Nevis magma system, are equally possible. Pyroclastic and volcanoclastic depositional products are interspersed with episodes of relative tranquillity and the localised deposition of fine grained mudstone. Rare sedimentary debris flow deposits, comparable to those of the Allt a' Mhuillin Formation, demonstrate the persistence of a metasedimentary source region poking through the volcanoclastic deposits. Roberts (1966) reported that part of the Dalradian basement to the Glencoe caldera, remained above the level of volcanic cover until the eruption of the caldera forming Group 2 ignimbrites.

The proximity of the Ben Nevis basin to caldera forming eruptions is demonstrated by the presence of clasts of ignimbrite within a number of the volcanic breccias. These clasts are found in the most heterogeneous examples of the Coire na Ciste Formation and it is assumed that the more homogeneous breccias, predominantly comprised of a single clast type, were generated by block and ash flows initiated from the collapse of lava domes or lava flows. Clasts of rhyolite are also found in a number of the volcanic breccias and, like the ignimbrites, are not found *in situ* on Ben Nevis. Variability in the distribution of ignimbrite and rhyolite clasts suggests that either the source region suffered periodic burial and excavation of different components or, more likely, a number of different source regions contributed material to the Ben Nevis basin.

A period of quiescence is noted between the deposition of the Coire na Ciste Formation and the eruption of air fall deposits of the Ledge route Formation. This is preserved in the form of a relatively thick (20m+) band of fine grained mudstone, the Trident Member. Syn-depositional faulting is much in evidence during deposition of this unit, and a steep fault scarp was generated within the Trident basin from which blocks fell. Gradual dominance of the Ledge route Formation by coarse air fall deposits of the Ledge route Member led to the rapid build up of the Ledge route Formation and the generation of steep slopes prone to failure. An unusual feature of this airfall deposit is the absence of a fine grained component and the uniformity of clast size. This is surprising given the presence of sedimentary bands within the Ledge route Member, which implies periods of dormant activity in the volcanic vent. The lateral extent of the Ledge route Member varies markedly; it is thickest on Ledge route below Carn Dearg (NW) and thins rapidly towards Castle Ridge where it is interbedded with andesite. The Ledge route Member also thins rapidly towards the northern rim of Coire na Ciste where it is found in association with fine grained mudstones. It is possible that similar deposits in the Orion Face above the 'bowl' are contiguous with the Ledge route Member; however, there are no linking exposures on Observatory Ridge, or on Tower Ridge, or along the southern rim of Coire na Ciste. It is thought, therefore, that the Orion Face exposures form a separate air fall deposit from the Ledge route Member, though again the uniformity of grain size is unusual. Lateral variation in the volcanic pile is well demonstrated by the Ledge route formation and points to a source, at least for this horizon, north of Castle Ridge, in the area now occupied by the Ben Nevis granites.

Localised eruptions of lava during the deposition of the Coire na Ciste Formation point to the subterranean development of the Ben Nevis magmatic plumbing system. The low gas content (no vesicles) and high silica contents of these andesites (>60% for most samples) indicate that the lavas had a high viscosity and were therefore unable to travel for large distances (Walker 1973b); consequently a local source is inferred. The eruption of the Ben Nevis andesites under water could be one explanation for the absence of vesicles; this would also have the effect of increasing the mobility of the lava, however, the depths of water required are unreasonable for a terrestrial situation (>1km according to McBirney 1963). Eruptions under a few metres or a few tens of metres of water can explain a number of features of the Ben Nevis andesites.

The hiatus between the Coire na Ciste and subsequent formations is not everywhere developed; in Gardyloo Gully the transition between Coire na Ciste and Summit Formations is gradual whereas on Castle Ridge, andesites first dominate the sequence below the Ledge route Formation. Such variation may be due to the construction of these formations on lithostratigraphic grounds, and consequently formation boundaries are diachronous. Regardless of the positioning of the boundary between the Coire na Ciste and Summit Formations, it is clear that the base of the volcanic pile is dominated by volcanic breccias, whereas the top of the pile is comprised mainly of andesite. A major shift in the local volcanic environment is demonstrated by this change.

The recognition of a felsite dyke within the Summit andesite Formation of Five Fingers Gully is crucial to understanding the relative timing of the plutonic and volcanic members of the Ben Nevis Complex. Felsite dykes are found in the Nameless Burn and in Allt an t-Sneachda where they are cross-cut by and intrude early pulses of the Fine Quartz Diorite. The fact that the felsite intrudes the Summit Formation reveals that the Coire na Ciste Formation predates the plutonic rocks. This is perhaps not surprising given that the volcanic breccias may be sourced from several kilometers or even several tens of kilometres distant and may therefore be unrelated to the Ben Nevis magma system. Sporadic outcrops of lava within the Coire na Ciste Formation testify to localised volcanic activity. It is possible that the felsite was intruded before extrusion of the Summit Formation had ceased and therefore the andesites are directly comparable to the quartz diorites; however, it is believed that the andesites were erupted prior to significant development of the Ben Nevis magma chamber. Eruptions of andesite, subsequently removed by erosion, may have had a progressively closer relationship with the quartz diorites as the magma system changed from extrusive to intrusive; this, however, is speculative.

New work on the Glencoe caldera (Moore & Kokelaar 1994, abstract in press) has shown that tectonic movements, burial of high relief, persistent deposition of sediments during periods of volcanic quiescence, canyon incision and a location within a small fault-controlled depositional basin are all features of the Glencoe caldera. The similarity with the sedimentary and palaeogeographic interpretations of the Ben Nevis volcanic pile is striking.

### 8.3 Granite Intrusion

The plutonic members of the Ben Nevis Complex were intruded to a high level in the crust and possibly crystallised under pressures as low as 1kbar or less.

The Fine Quartz Diorite is clearly composed of a number of smaller pulses and does not represent a closed fractionating system, but a collection of pulses that define a trend on chemical variation diagrams. This indicates the operation of similar open-system processes rather than direct evolution from a single parent magma.

The mechanism of intrusion changed between the emplacement of the Porphyritic Outer Granite and of the Inner Granite. The Fine Quartz Diorite, Sgurr Finnisg-aig Quartz Diorite, Coarse Quartz Diorite and Porphyritic Outer Granite have a number of features consistent with a forceful ballooning style of intrusion whereas the Inner Granite fits a passive subterranean intrusion mechanism.

Localised concentrations of volatiles, at the margins of the Coarse Quartz Diorite and the Porphyritic Outer Granite, led to explosive pressure reduction and the development of intrusion breccias along the eastern margin and at the contact between the Coarse Quartz Diorite and Fine Quartz Diorite in Allt Coire Duibh.

Formation of intrusion breccias below the surface does not necessarily lead to the eruption of magmatic material at the surface. The presence of abundant Dalradian xenoliths in the breccia zone that have moved less than 5m, illustrates the limited amount of particle movement. Venting at the surface was probably restricted to the emission of volatiles. Surficial expression of these intrusion breccias may have been limited to the development of fumarolic vents such as those that outcrop on Raasay (Selley 1965) and in the ORS of Kintyre (Friend & Macdonald 1968).

Steep outwardly dipping contacts with sharp junctions against the adjacent lithologies and relatively uniform textures and compositions indicate that the Inner Granite was intruded during subterranean cauldron collapse, as advocated by Bailey & Maufe (1916). Sometime after intrusion of the Inner Granite the roof of the magma chamber failed catastrophically, resulting in the venting of part of the Inner Granite onto the surface and formation of a caldera. The only remnant of this ejected magma within the Ben Nevis Complex is a thin discontinuous ring-dyke (the Fault facies) exposed along the contact between the volcanic pile and the Inner Granite. Localised injections of the Fault facies can be found within the volcanic pile, but not within the Inner Granite; the reason for this is unclear. In Glencoe, injections from the Fault Intrusion are predominantly found outside the ring fault (Clough et al. 1909). It is possible that the Inner Granite had not fully achieved its final position and subsequent upward movement (resurgence ?) has removed injections of the Fault facies; alternatively, the Fault facies exploited fractures in the volcanic pile which developed during collapse. At least 2.3km<sup>3</sup> of the Inner Granite magma is believed to have been ejected onto the land surface during caldera formation.

Dyke offsets and bends indicate a dextral stress regime in contrast to the sinistral regime invoked for the Southwest Highlands, Strath Ossian and the Etive Complex (Jacques & Reavy in press, Key et al.1993 and Morris & Hutton 1993). However, support for a dextral regime comes from Strontian (Hutton 1988a), anticlockwise rotation of members of the Etive dyke swarm (chapter 4) and from movements along faults within the Dalradian (Treagus 1991). Treagus (1991) considers movements along faults within the Dalradian to have finished prior to extrusion of the Lorne lavas: movements along NE-SW faults within the Ben Nevis complex were, however, contemporaneous with NE-SW striking members of the Ben Nevis Dyke swarm. Clearly the structural evolution of the Grampian area towards the end of the Caledonian Orogeny is complex.

The Ben Nevis Complex was probably active over several million years. Branney (1988) argued for the evolution of the Borrowdale Volcanic Group over a period of between 15 and 36Ma depending on the timescale used and correlations with formations outwith the Borrowdale Group. The Valles Caldera (New Mexico) was active for 10Ma prior to caldera collapse (Smith et al. 1970) and the San Juan volcanic field evolved over a 25Ma period of which 5Ma was pre-caldera activity (Lipman 1984). It is therefore feasible that the Inner Granite of the Ben Nevis Complex post-dates the earlier volcanic pile and Fine Quartz

Diorite - Porphyritic Outer Granite magmatism by several million years. During this intervening period, most of the Ben Nevis dyke swarm was injected.

#### 8.4 Petrogenesis

The early magmatic history of the Ben Nevis Complex is one of variable mineralogy and chemistry, but with time the magma system generated increasingly more uniform products culminating in homogenous monzonite (Inner Granite). Field, petrographic, mineralogical, chemical and isotopic evidence all support this general feature of the Ben Nevis Complex.

Haslam (1965) believed that the Ben Nevis Complex followed a simple liquid line of descent which he attributed to crystal fractionation from a single parent magma similar in composition to the pyroxene mica diorite of the Ratagain intrusion (Nicholls & Mitchell 1947). This simple model is shown to be more complex, and no single parental magma can generate all the geochemical variations exhibited by units of the Ben Nevis Complex. A separate parent magma is required for each of the units forming the Ben Nevis Complex (i.e. Fine Quartz Diorite, Sgurr Finnisg-aig Quartz Diorite, Coarse Quartz Diorite, Porphyritic Outer Granite, Inner Granite and volcanic pile). It is also likely that different pulses within the quartz diorites and different extrusions of the volcanic pile were generated from separate batches of magma with slightly different proportions of crustal and mantle melt, and having undergone variable degrees of crystal fractionation. Mixing and crystal fractionation is believed to have occurred initially in a small-volume, deep crustal magma chamber that underwent continuous fractionation, extraction and replenishment. Magmas migrated toward the surface at irregular intervals. The addition of fresh material into this small chamber, either from the mantle or from the lower crust, would have had a marked effect on the chemical and isotopic composition of the resultant magma. This accounts for the initial variability of both the intrusive and extrusive rocks.

The andesites were erupted onto the land surface after having spent relatively little time in the upper crust. These early magmas show the greatest variation in  $\epsilon\text{Nd}_t$ , but with growth of the lower crustal chamber, the magma system became buffered from the wilder fluctuations in isotopic ratios, culminating in the tight grouping of samples from the Inner Granite. Andesites found within the volcanic pile can be subdivided into two groups; firstly, those with variable Nd and Sr isotopes, and secondly, those with variable Nd isotopes only. The former group is found only at the base of the volcanic pile and these early andesites were contaminated in the magma conduit. The contamination process can be thought of as analogous to a pipe cleaner (the magma) removing grains of dirt (minimum melt phases) from the inside of a pipe (the conduit); the first section of the pipe cleaner shows the greatest contamination, the degree of which progressively decreases. In the magma conduit two complementary processes acted to remove the local country rock as a source of contamination; firstly, removal of the minimum melt phases and secondly, accretion of solidified/congealed magma onto the conduit wall.

Further indications of a limited residence time for the andesites in the upper crust can be gleaned from mineralogical evidence. Unlike the plutonic rocks, the andesites show preserved amphibole phenocrysts; if they had spent time in an upper crustal chamber pyroxene would be expected to dominate the phenocryst assemblage as it does in the quartz diorites; this is not the case and the andesites preserve intact the crystallising assemblage of the lower crustal magma chamber.

During the evolution of the Ben Nevis Complex, the rate of cooling decreased, resulting in the progressive increase in grain size and allowing successive pulses to mingle. The boundaries between individual pulses became increasingly blurred, such that pulses in the Coarse Quartz Diorite are only observed by variation in mineralogy and chemistry (i.e. cryptic pulses). This culminated with intrusion of the relatively homogenous Porphyritic Outer Granite and Inner Granite.

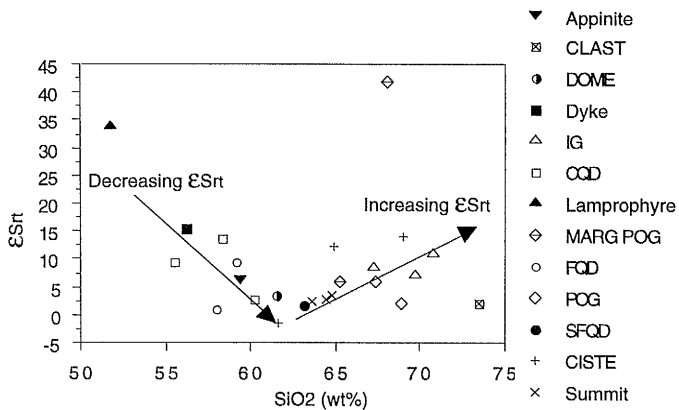


Fig. 8.1  $SiO_2$  vs  $\epsilon Sr_t$ . Initially variable but generally decreasing  $\epsilon Sr_t$  with fractionation followed by increasing  $\epsilon Sr_t$  with fractionation.

Crystallisation in an upper crustal magma chamber, prior to final intrusion into the Ben Nevis chamber, is required in order to explain the increased  $\epsilon Sr_t$  values for the Porphyritic Outer Granite and Inner Granites and the abundance of pyroxene instead of amphibole. Sr isotope data from the Ben Nevis Complex show two trends, these being variable but generally decreasing  $\epsilon Sr_t$  with increasing  $SiO_2$ , and secondly, increasing  $\epsilon Sr_t$  with increasing  $SiO_2$  (Fig. 8.1). The first trend can be explained by the higher temperatures of the earlier pulses (1059°C versus 900°C), and by the presence of 'virgin' Dalradian metasediment which had not yet suffered partial melting. As the magma system evolved, the volume of metastable phases in the metasediments decreased, as did the ability of the magmas to melt the adjacent rock; consequently  $\epsilon Sr_t$  decreases with increasing  $SiO_2$ . Contamination of the early mafic magmas is also recognised in the Skye plateau basalts (Thirlwall & Jones 1983) and in the Aeolian arc (Peccerillo & Wu 1992). With growth of the upper crustal magma chamber AFC processes contributed increasing  $^{87}Sr$  to the Ben

Nevis magmas, hence increasing in  $\epsilon\text{Sr}_t$  with  $\text{SiO}_2$ . On emplacement within the Ben Nevis magma chamber, interaction with the Dalradian ceased, with the exception of those magmas right against the contact (e.g. BN366).

The geochemistry of the Ben Nevis Complex is strongly controlled by the fractionation of plagioclase, biotite, magnetite and amphibole  $\pm$  alkali feldspar. On reaching the upper crustal chamber, pyroxene replaced amphibole as the major crystallising mafic phase; however, this change only partly overprinted the earlier effects of amphibole fractionation. The formation of pyroxene phenocrysts cannot have occurred in the Ben Nevis chamber itself as the Fine Quartz Diorite has pyroxene both as a phenocryst phase and as a groundmass phase; furthermore, sharp contacts between separate pulses of differing compositions are inconsistent with *in situ* fractionation.

The separation of a late stage fluid progressively lowered the K/Rb ratios of the Porphyritic Outer Granite. Movement of late stage fluids led to the conversion of magmatic pyroxene to calcic amphibole in the subsolidus. In a number of localities within the Porphyritic Outer Granite and Inner Granite, the activity of halogens within aqueous fluids; may have been sufficient to locally mobilise gallium, and this element was incorporated in to the albite rich rims of plagioclase. The quartz diorites retain a magmatic K/Rb ratio, and the reduced movement of fluids in these rocks is demonstrated by the increased degree of preservation of pyroxene. The efficiency of pyroxene replacement in the quartz diorites appears to be related to the early fractionating phases; if biotite was an early phase then pyroxene is almost always largely replaced by amphibole. If biotite crystallisation was suppressed, then the degree of pyroxene preservation is generally good. Presumably, the initial crystallising assemblage is controlled by variations in  $P$ ,  $\text{H}_2\text{O}$ ,  $f\text{O}_2$  and temperature, and the mineral assemblage is merely reflecting variations in these parameters which also control the extent of pyroxene replacement. The composition of quartz diorites with little replacement of pyroxene by amphibole overlaps with those quartz diorites with abundant amphibole.

The Inner Granite cannot be related to the earlier intrusions by simple AFC or fractional crystallisation processes. Steep increases in REE and HFSE abundances with increasing  $\text{SiO}_2$  probably reflect the increasing incorporation of amphibole and minor accessory phases into the partial melts of the source region.

Appinite intrusion is intimately related to formation of the Ben Nevis Complex; in particular, the Coarse Quartz Diorite reveals appinite emplacement before (xenoliths), during (mixing) and after (intrusive contacts) intrusion of this unit. Appinitic xenoliths (Haslam 1970) illustrate pre-intrusion activity whereas intrusive contacts between appinite pipes and the Coarse Quartz Diorite demonstrate post-intrusion relationships. Syn-Coarse Quartz Diorite intrusion is revealed in those Coarse Quartz Diorite pulses exposed in the vicinity of the Surge chamber which have the most basic chemistry within the Coarse Quartz Diorite unit. This is attributed to mingling between appinite and quartz

diorite. Volatile fluxing during crystallisation of the Coarse Quartz Diorite is believed to have locally increased the  $fO_2$  and resulted in the formation of foxy-brown biotites; additionally volatiles aided conversion of pyroxene to amphibole. Mixing between the appinite and the Coarse Quartz Diorite was aided by the high volatile contents of the appinite. Castro et al. (1990) noted that mixing in the sub-volcanic environment requires high energy flows, in contrast to mixing in large magma chambers where thermal and buoyancy driven convection operates. The model of Haslam (1970), whereby the appinites represent the reaction products between granitic magma and the Ballachulish limestone, cannot explain the typical Ben Nevis Complex chemistry of the surge chamber appinite or the lack of enrichment in  $^{87}\text{Sr}$ .

## 8.5 The Siluro-Devonian magmatic event

### 8.5.1 I and S-type granite formation

I- and S-type magmas in the type area of the Lachlan Fold Belt are believed to represent partial melts of different types of lower continental crust that were intruded as mixes of partial melt plus refractory residuum (i.e. restite of White & Chappell 1977) into the upper crust. According to the model of White & Chappell (1977), progressive separation of restite from the melt would ultimately lead towards a low temperature near minimum melt, and generate a chemical trend similar to that observed for the Ben Nevis Complex. Whereas this model generally holds for S-type granitoids, a consensus of opinion for the origin of I-types is yet to be achieved. Cameron & Cameron (1985) have shown that the I-type magmas of Baja, California, have isotopic compositions similar to the local mantle and consequently, the contribution of continental crust is believed to be minimal. It could be argued that the crust in this area is relatively young, and therefore decay of Rb and Sm will have had little time in which to build a crustal signature. But the volume of basic material in this area forms  $\approx 15\%$  of the total, indicating substantial involvement of the mantle during granite formation (Pitcher 1979b). In the Lachlan Fold Belt, basic rocks form  $<1\%$  of the exposed area.

The widespread occurrence of lamprophyre and appinite reveals that mantle melting was a feature of the late Caledonian magmatic episode in Northern Britain. Moreover, the recognition of mafic microgranular enclaves (MME) with a more mantle-like isotopic signature than the host granitoid (e.g. Holden et al. 1987) negates the possibility that MME represent restitic inclusions. Eichelberger (1980) favours a two stage model for I-type granites, where intrusion of basic material into the base of the crust is followed by melting of the crust and mixing of the two melts.

### 8.5.2 Lamprophyres and Appinites

A close genetic link between the Newer Granite plutons and lamprophyre dykes/appinite intrusions has been demonstrated by Macdonald et al. (1986), Rock & Hunter (1987) and Holden (1987). Notably, S-type granites from the same period are

associated with relatively few lamprophyre dykes, e.g. Cairnsmore of Fleet (Rock et al. 1986).

It is generally accepted that lamprophyres with high Mg# (65-80%), Ni (90-700ppm), Cr (200-500ppm) and Sc (15-30ppm), represent near-primary mantle melts (Rock 1991) after 1-20% melting of a mantle lherzolite source (Frey et al. 1978 and Rhodes 1981). Therefore lamprophyres may represent the mantle component in the Newer Granites.

Calc-alkaline lamprophyres have their origins in the mantle wedge, are enriched in LILE and LREE, and post-date regional metamorphism and most deformation (Wyman & Kerrich 1993). They are intruded after subduction has ceased and strike slip and/or extensional tectonics dominate (Barnes et al. 1986). Partial melting of the mantle wedge may be triggered by collision, uplift and decompression. The majority of modern multi-element and radiometric studies agree that calc-alkaline lamprophyres are derived from mantle which has been metasomatised by fluids emanating from a subducting/subducted slab (e.g. Rock 1991, Wyman & Kerrich 1993 and Greenough et al. 1993).

Published multi-isotope studies of the Caledonian lamprophyres are conspicuously lacking. From the compilation of data presented by Rock (1991, Fig. 5.12a), the majority of Caledonian and Hercynian calc-alkaline lamprophyres have  $\epsilon\text{Nd}_t$  and  $\epsilon\text{Sr}_t$  that fall within the mantle array ranging from +5 to -5 and +5 to -50 respectively. However, all the data presented in this diagram are obtained from Caledonian lamprophyres outcropping south of the Southern Uplands Fault, or from Hercynian examples. A single analysis from Argyll has  $\epsilon\text{Nd}_t$  -3 and  $\epsilon\text{Sr}_t$  +20. The similarity between this sample and the Southwest Highland mantle (SWH) of Thirlwall (1986) is striking.

Lamprophyres (and appinites) were described by Rock et al. (1988) as the only regionally extensive basic magma within Northern Britain of Caledonian age and, therefore, representative of the underlying mantle source for the Newer Granites. ORS lavas, such as those from Lorne and the Midland Valley, were discounted because they lacked the requisite chemistry (although this is not correct, see chapter 7), and are lacking around many of the Newer Granite plutons. However, this lack of exposure is hardly surprising given the fact that granites are intrusive and lavas extrusive. If granite is exposed at the surface today, then the lavas exposed at the surface during intrusion of the granites will have long since been removed by erosion, unless caldera collapse occurred, such as at Ben Nevis and Glencoe. The exposures of ORS lavas in the Midland Valley and in the Southwest Highlands are associated with Lower Old Red Sandstone sediments (Fitton et al. 1982 and chapter 3). These sediments are not found around many of the Newer Granite plutons again illustrating that erosion has removed the lavas and sediments found on the ancient land surface at the time of Newer Granite intrusion.

Lamprophyres exposed on Lismore, with widths >12m, have been proposed as possible feeder dykes for the nearby Lorne Plateau lavas (Morrison et al. 1987).

Lamprophyres with widths >10m are unlikely to have been chilled significantly by passage through the crust and are therefore thought to have erupted onto the surface (Delaney & Pollard 1982). There are, however, chemical differences between the two groups, notably the LPL are enriched in Sr, Ba, Nb, Ce, P, Zr and Ti relative to the Lismore lamprophyres (Fig. 8.2). Variations in the HFSE abundances of Caledonian lamprophyres from Lismore were ascribed to the fractionation of accessory mineral phases, whereas variations in Rb were related to variable LREE enrichments that were caused by changes in the relative contribution of the subducted slab (Morrison et al. 1987). Presumably, these authors would suggest that similar mechanisms may have caused the variations between the Lorne Plateau lavas and the Lismore lamprophyres. Pitcher (1993) has also suggested that the high-K lavas of the Lorne Plateau were fed by lamprophyre/appinitic feeders and a similar proposal was put forward by Fowler (1988), from work on the Ach'uaire hybrids. That lamprophyres and Lorne Plateau lavas represent near-mantle melts (Rock 1991 and Thirlwall 1981) is undisputed; however the exact relationship between the two groups is unclear.

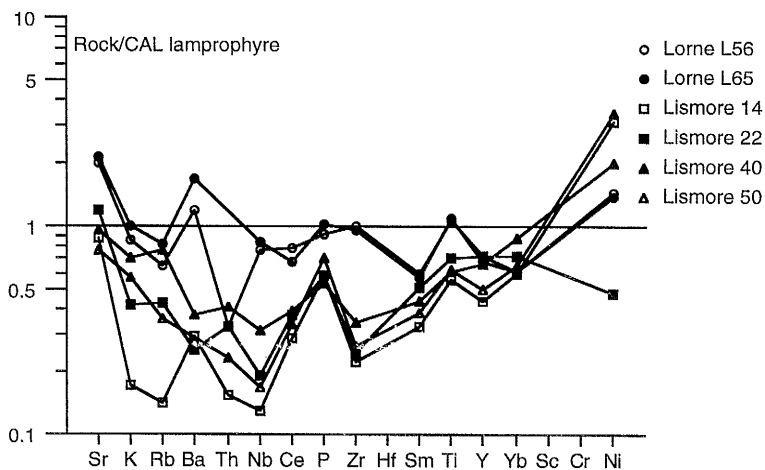


Fig. 8.2 Comparison of data from the Lorne Plateau lavas (Thirlwall 1986, 1983 & 1982) with the lamprophyres of Caledonian age from Lismore, Ardgour. Normalised against average Calc-alkaline lamprophyre (Rock 1991).

There are a number of problems with invoking active subduction along the lapetus suture as the source for Caledonian age lamprophyres in Northern Britain. These problems are discussed below and similarly affect the Newer Granites and ORS lavas.

### 8.5.3 Subduction

The relationship of the Newer Granites to subduction is uncertain; the most popular two-plate models lead to closure of lapetus during the Ordovician to mid-Silurian (Brown 1992), and cannot therefore be directly related to Newer Granite magmatism (425-400Ma). Adiabatic decompression is an alternative mechanism (Simpson et al. 1979 and Pitcher 1982), but it is apparent from K-Ar mica cooling ages of 440-420Ma that the

Highland terrain was already deeply eroded before generation and emplacement of the Newer Granites. In addition, the thickness of the slate belts was never sufficient to induce the rapid uplift and decompression required to produce widespread melting in the lower crust (Soper 1986). Modern arc-trench gaps are at least 90km and very often 150km+ (Yardley et al. 1982); northward subduction along the line of the inferred Iapetus suture cannot therefore account for granite and volcanic exposures in the Southern Uplands.

The problems with two-plate models led Soper & Hutton (1984) to develop a three plate-model, the most recent version of which (Fig. 8.3) is presented in Soper et al. (1992). In this version, closure of Iapetus is achieved by  $\approx 420$ Ma and subduction of Iapetus beneath the Highlands resulted in the production of voluminous granite intrusions and lava eruptions. South of the Highland Boundary Fault (HBF) early Devonian docking of a number of allochthonous terranes, that were separated from each other by small ocean basins, generated subduction-related magmatism in this region. The terranes are believed to have rifted from Gondwana in the early Palaeozoic (Soper 1986).

MORB-normalised spidergrams (Pearce 1983) for the Silurian-Devonian igneous rocks of Northern Britain yield typical subduction-related patterns (i.e. LILE enriched, Ta and Nb anomalies, and to a lesser extent HFSE depletion). This pattern is attributed to the influence of the subducted slab (Pearce 1983). It is not, however, clear if the slab itself melts or is merely a catalyst promoting melting in the overlying mantle wedge due to the expulsion of fluids from altered oceanic crust and subducted sediment. Defant & Drummond (1990) found that the slab only melted when it was relatively young ( $<25$ Ma), and therefore relatively hot. Despite recognition of the short-lived (1.5Ma) isotope of  $^{10}\text{Be}$  in island arc magmas (Brown et al. 1982), Hawkesworth et al. (1991) limit the contribution of the slab in island arcs to  $<15\%$ . Modelling of Be and B lends itself to the conclusion that the contribution of the slab to the overlying wedge was dominated by relatively homogeneous fluids/hydrous melts (Morris et al. 1990); and a number of authors have shown that the most important contribution of the slab during subduction-related magmatism is water which promotes melting in the wedge by lowering the solidus (McCulloch & Gamble 1991).

A number of features of the Lorne Plateau lavas are inconsistent with normal arc magmatism (i.e. where fluids dominate the slab-wedge interaction), in particular: highly fractionated REE abundances (La/Yb ratios of between 7 and 32), high K/Rb ratios (400+) and low Rb/Sr ratios ( $<0.5$ ). On MORB-normalised spidergrams (Pearce 1983), the Lorne lavas are comparable to those from Baja, (California, Rogers et al. 1985), the Antarctic Peninsula (Hole 1988), Adak Island, (the Aleutian Islands, Kay 1978 and Defant & Drummond 1990) and the La Yeguada Complex (Panama, Defant et al. 1991) shown in Fig. 8.4. In these locations slab melting and subduction of a Mid-Ocean Ridge is believed to have occurred. Rogers & Saunders (1989) suggested that the Lorne lavas were generated after subduction of a mid-ocean ridge, but ridge subduction cannot account for the time-integrated LREE enrichment of the Lorne lavas (Thirlwall 1986).

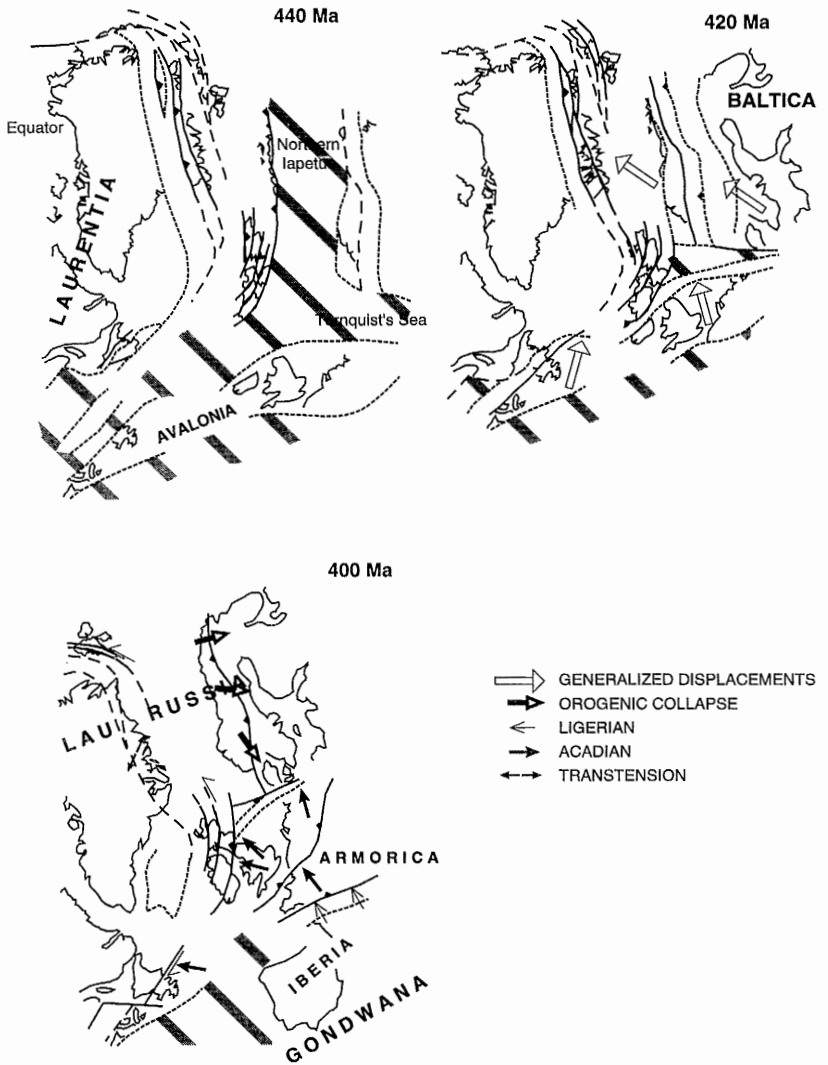


Fig. 8.3 Cartoon reconstructions to illustrate the Silurian closure of Iapetus, and the presence of micro-plates and multiple subduction zones, adapted from Soper et al. (1992).

It is unlikely that the SWH mantle of Thirlwall (1986) is located in the asthenosphere as this is generally believed to be well mixed. Additionally, the Permo-Carboniferous lavas of Kintyre and Arran have more radiogenic Nd isotopes than those from the Midland Valley and are indicative of mixing between a depleted mantle source and the SWH mantle (Smedley 1988b and chapter 7). From the Devonian period to the Permian period, Scotland 'drifted' from 30°S to 12°N (Harris 1992); therefore the SWH mantle is required to be located within the attached lithospheric mantle of Scotland. Moreover, for a segment of the mantle to build up a distinctive isotopic character, it must have been separated from convective flow in the asthenosphere for a substantial period of time (1Ga, Thirlwall 1986). The time-integrated LREE enrichment of the SWH mantle is therefore unlikely to have been preserved in a convecting asthenosphere for a sufficient length of time. Thirlwall (1986) believed that the SWH mantle source is sub-lithospheric and underlying depleted mantle; however Frost & O'Nions (1985) suggested that a lithospheric mantle position was more likely.

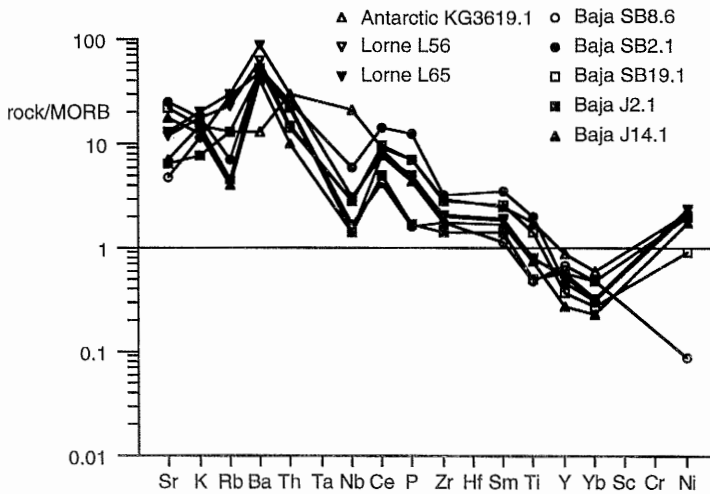


Fig. 8.4 Comparison of the Lorne Plateau lavas (Thirlwall 1986, 1983 & 1982) with high Mg# basalts from Baja California (Rogers & Saunders 1989) and from the Antarctic Peninsula (Hole 1988). MORB values from Pearce (1983).

In the Aeolian arc, a change from 'normal' calc-alkaline magmatism to the eruption of high Mg# andesites (bajaites of Rogers et al. 1985 and adakites of Defant & Drummond 1990) is reflected in a change in the mineral assemblage from olivine + clinopyroxene + orthopyroxene + plagioclase + magnetite to plagioclase + magnetite + amphibole + biotite and no pyroxene. This was attributed to the breakdown of amphibole in the mantle wedge on the cessation of fluid migration from the slab into the overlying mantle wedge. Early amphibole crystallisation is a feature of the Ben Nevis complex and may be related to the earlier subduction of a ridge. Interestingly, Romick et al. (1992) infer early amphibole fractionation, despite its absence as a phenocryst phase, in lavas from Adak Island in the Aleutians. This location is, for Defant & Drummond (1990), the type area for slab-

melting/ridge subduction. A feature of the ridge-subduction generated dacites of the La Yeguada Complex is high Na<sub>2</sub>O contents (>3.5%); this is also a characteristic feature of the Argyll suite (Stephens & Halliday 1984) and may therefore, also be the result of ridge subduction.

#### 8.5.4 Conclusions

Rogers et al. (1985) noted that a subduction zone signature can persist in the lithospheric mantle for 30Ma after the cessation of active subduction; consequently active subduction is no longer required in the generation of Lorne lavas and Newer Granites north of the HBF. Geothermal rebound after subduction of a mid-ocean ridge promotes melting in the mantle wedge. The enhanced geothermal gradient will also aid partial melting in the lower crust. Siluro-Devonian magmas of the Southwest Highlands represent variable proportions of the slab, time integrated LREE enriched lithospheric mantle, the lower crust and the upper crust. Siluro-Devonian magmas south of the HBF do not have the same chemical characteristics as bajaites (Fig. 8.5) and active subduction south of the English Lake District is invoked.

#### 8.6 Further Research

A precise U-Pb radiometric date is required for the different components of the Ben Nevis Complex in order to constrain the temporal location of the Ben Nevis Complex in the Scottish Caledonian.

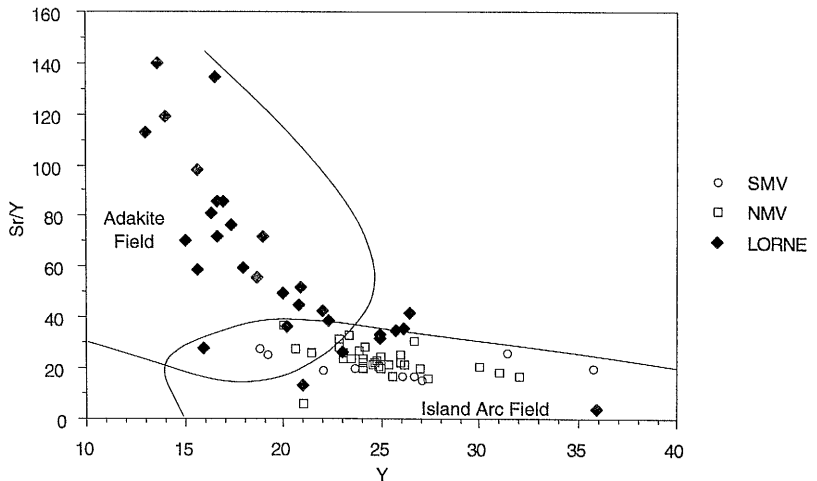


Fig. 8.5 Sr/Y vs Y. Data from the Lorne Plateau fall within the field of adakites (bajaites) and those from south of the Highland Boundary Fault fall within the 'normal' arc basalt field. Field boundaries from Defant et al. 1991. Lorne data from Thirlwall (1986, 1983 & 1982).

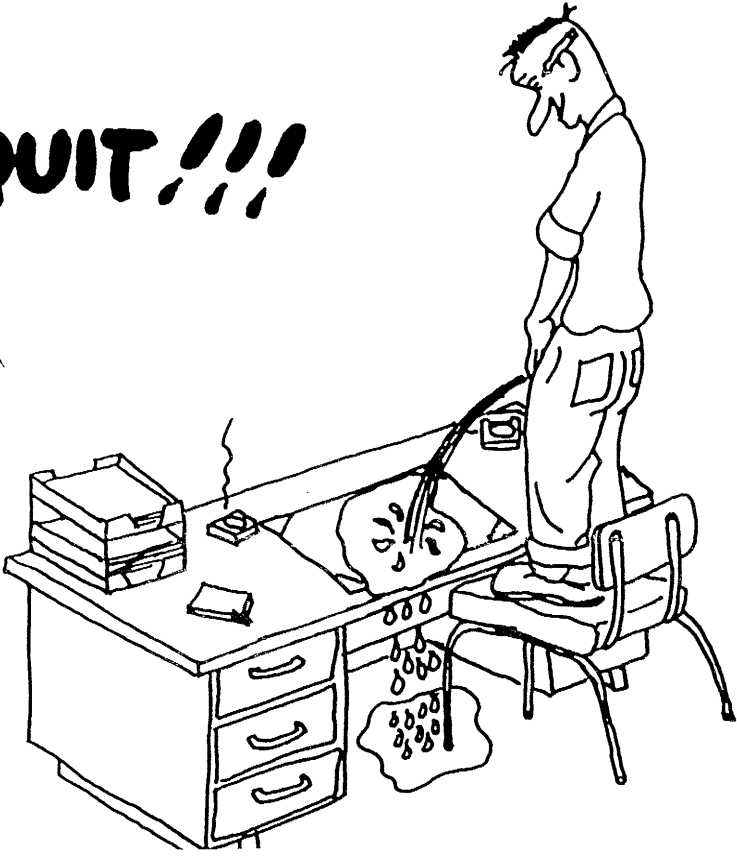
A study of the lamprophyres of the Southwest Highlands would improve our understanding of the mantle in this area. The presentation of chemical data from regional groupings of lamprophyre dykes as averages is less than helpful and the absence of multi-isotope studies does little to aid petrogenetic modelling. The recognition of the summit trend on Ben Nevis (i.e. decreasing  $\epsilon\text{Nd}_t$  at constant  $\epsilon\text{Sr}_t$ ) highlights the dangers of forming petrogenetic models from data derived from a single isotope system.

The spatial and temporal relationship between lamprophyre and granite needs to be explored, again multi-isotope studies are needed. The Ben Nevis Complex is one possible location in which to carry out such a project as lamprophyres are known to pre- and post-date intrusion of the Fine Quartz Diorite-Porphyritic Outer Granite units. This study should be tied in with similar work on mafic inclusions.

No xenolith data are available for the composition of the lower crust/lithospheric mantle beneath the Southwest Highlands. This is important as the Southwest Highlands lie between the stable cratonic Northern Highlands and the possible allochthonous terranes of the Midland Valley and Southern Uplands (Bluck 1984). The Southwest Highlands, therefore, occupy a crucial location in terms of the development and age of the lithospheric mantle across Scotland and correlations with xenolith localities across the Great Glen Fault and Highland Boundary Fault may not be valid. A survey of mantle nodules may facilitate the identification of discrete zones of enrichment/depletion within the lithospheric mantle

Tectonic models for the later part of the Caledonian Orogen need to be revised to account for the dextral sense of movements along the Great Glen Fault and within the Dalradian.

**I QUIT!!!**



## References

- Anonymous, 1983, Ben Nevis and its Observatory. Famedram Publishers Gartocharn.
- Anderson, E. M., 1936, The dynamics of the formation of cone sheets, ring dykes and cauldron subsidences. *Proc. R. Soc. Edinburgh*. **56**. 128-157.
- Anderson, J. G. C., 1935. The Marginal intrusions of Ben Nevis; Coille Lèanachain Complex; and the Ben Nevis Dyke swarm. *Trans. Geol. Soc. Glas.* **19**. 225-269.
- Anderson, T. & Flett, J. S., 1903, Report on the eruption of the Soufrière in St. Vincent in 1902 and on a visit to Montagne Pelée in Martinique. *Phil. Trans. Roy. Soc. London*, **200**. 353-553.
- Anderton, R., Bridges, P. H., Leeder, M. R. & Sellwood, B. W., 1979, A dynamic stratigraphy of the British Isles. Allen & Unwin.
- Aramaki, S. & Yamasaki, M., 1963, Pyroclastic Flows in Japan. *Bull. Volcanol.* **26**. 89-99.
- Arculus, R. J. & Johnson, R. W., 1978, Criticism of generalised models for the magmatic evolution of arc-trench systems. *Earth Planet. Sci. Lett.* **39**. 118-126.
- Ayers, J. C. & Watson, E. B., 1991, Solubility of apatite, monazite, zircon and rutile in supercritical aqueous fluids with implications for subduction zone geochemistry. *Phil. Trans. Roy. Soc. London* **335**. 365-395.
- Bailey, E. B., 1910, Recumbent Folds in the Schists of the Scottish Highlands. *Quart. J. Geol. Soc.* **66**. 586-620.
- Bailey, E. B. & Maufe, H. B., 1916, The geology of Ben Nevis and Glencoe and the surrounding country. *Memoirs Geol. Surv. Gt. Britain*. **53**. 1st edition.
- Bailey, E. B. & Maufe, H. B., 1960, The geology of Ben Nevis and Glencoe and the surrounding country. *Memoirs Geol. Surv. Gt. Britain*. **53**. 2nd edition.
- Bamford, D., 1979, Seismic constraints on the deep geology of the Caledonides of northern Britain. In: Harris, A. L., Holland, C. H. & Leake, B. E. (eds.), *The Caledonides of the British Isles Reviewed*. *Spec. Pub. Geol. Soc. London*, **NO. 8**. 93-96.
- Barberi, F., Innocenti, F., Ferrara, G., Keller, J. & Villari, L., 1974, Evolution of Eolian arc volcanism (southern Tyrrhenian Sea). *Earth Planet. Sci. Lett.* **21**. 269-276.
- Barker, F., 1979, Trondhjemites: Definition, environment and hypothesis of origin. In: Barker, F., (ed.) *Trondhjemites, Dacites and related rocks*. Elsevier, Amsterdam.
- Barnes, R. P., Rock, N. M. S. & Gaskarth, J. W., 1986, Late Caledonian dyke-swarms in southern Scotland: new field, petrological and geochemical data from Wigtown Peninsula, Galloway. *Geol. J.* **21**. 101-125
- Barrière, M., 1977, Deformation associated with the Ploumanac'h intrusive complex, Brittany. *J. Geol. Soc. Lond.* **134**. 311-324.
- Barrow, G., 1893, On an intrusion of muscovite biotite gneiss in the southeast Highlands of Scotland and its accompanying metamorphism. *Quart. J. Geol. Soc.* **49**. 330-358.
- Barrow, G., 1912, On the geology of Lower Deeside and the southern Highland Border. *Proc. Geol. Assoc. Lond.* **23**. 268-273.
- Barth, A. P. 1990, Mid-crustal emplacement of Mesozoic plutons, San Gabriel mountains, California, and implications for the geologic history of the San Gabriel terrane. In: Anderson

- J. L. (ed.) The nature and origin of Cordilleran Magmatism. *Gaol. Soc. Am. Memoir* **174**. 33-45.
- Batchelor, R. A., & Bowden, P., 1985, Petrogenetic interpretation of granitoid rock series using multicationic parameters. *Chem. Geol.* **48**. 43-55.
- Blaxland, A. B., Aftalion, M. and van Breemen, O., 1979, Pb isotopic composition of feldspars from Scottish Caledonian Granites, and the nature of the underlying crust. *Scott. J. Geol.* **15**. 139-151.
- Bluck, B. J., 1984, Pre-carboniferous history of the Midland Valley of Scotland. *Trans. Roy. Soc. Edin. Earth Sci.* **75**. 275-295.
- Bluck, B. J., 1983, Role of the Midland Valley of Scotland in the Caledonian Orogeny. *Trans. Roy. Soc. Edin. Earth Sci.* **73**. 119-136.
- Bluck, B. J. & Dempster, T. J., 1991, Exotic metamorphic terranes in the Caledonides: Tectonic history of the Dalradian Block, Scotland. *Geology* **19**. 1133-1136.
- Blundy, J. D. & Holland, T. J. B., 1990, Calcic amphibole equilibria and a new amphibole plagioclase geothermometer. *Contrib. Mineral. Petrol.* **104**. 208-224.
- Branney, M. J., 1988, Sub-aerial explosive volcanism, sedimentation, intrusion and subsidence in the Barrowdale Volcanic Group of SW langdale, English Lake District. Unpublished thesis University of Sheffield.
- Brown, G. C., 1979, Geochemical and geophysical constraints on the origin and evolution of Caledonian granites. In: Harris, A. L., Holland, C. H. & Leake, B. E. (eds.), *The Caledonides of the British Isles Reviewed*. *Spec. Pub. Geol. Soc. London*, NO. **8**. 645-651.
- Brown, G. C. & Locke, C. A., 1979, Space-time Variations in British Caledonian Granites: some geophysical correlations. *Earth Planet. Sci. Lett.* **45**. 69-79.
- Brown, G. C., Thorpe, R. S. & Webb, P. C., 1984, The geochemical characteristics of granitoids in contrasting arcs and comments on magma sources. *J. Geol. Soc. Lond.* **141**. 413-426.
- Brown, J. F., 1972, Rb-Sr studies and related geochemistry on the Caledonian calc-alkaline igneous rocks of North-west Argyllshire. Unpublished thesis. Uni. College, Oxford.
- Brown, L., Klein, J., Sacks, I. S. & Tera, F., 1982,  $^{10}\text{Be}$  in island-arc volcanoes and implications for subduction. *Nature* **299**. 718-720.
- Brown, P. E., 1992, Caledonian and earlier magmatism. In: *The Geology of Scotland* 3rd edition, (ed.) G. Y. Craig. 229-295.
- Brown, P. E., Tocher, F. E. & Chambers, A. B., 1982, Amphiboles in the Lilloise intrusion, East Greenland. *Min. Mag* **45**. 47-54.
- Bryce, J., 1864, On the Geological structure of Ben Nevis. *Proc. Phil. Soc Glasgow* **5**. 104-105.
- Busby-Spera, C. J., 1986, Depositional features of rhyolitic and andesitic volcanoclastic rocks of the Mineral Lang submarine caldera complex, Sierra Nevada, California. *J. Volcanol. Geotherm. Res.* **27**. 43-76.
- Cameron, K. L. & Cameron, M., 1985, Rare Earth Element,  $^{87}\text{Sr}/^{86}\text{Sr}$  and  $^{143}\text{Nd}/^{144}\text{Nd}$  compositions of Cainozoic orogenic dacites from Baja California, northwestern Mexico and

- adjacent west Texas: evidence for the predominance of a subcrustal component. *Contrib. Mineral. Petrol.* **91**. 1-11.
- Carter, S. R., Evensen, N. M., Hamilton, P. J. & O'Nions, R. K., 1978, Neodymium and Strontium isotope evidence for crustal contamination of continental volcanics. *Science* **202**. 743-747.
- Cas, R. A. F., 1978, Silicic lavas in Palaeozoic flysch-like deposits in New South Wales, Australia: behaviour of deep subaqueous silicic flows. *Geol. Soc. Am. Bull.* **89**. 1708-1714.
- Cas, R. A. F. & Wright, J. V., 1991, Subaqueous pyroclastic flows and ignimbrites. *Bull. Volcanol.* **53**. 537-580.
- Cas, R. A. F. & Wright, J. V., 1988, Volcanic successions: modern and ancient. Unwin & Hyman.
- Cas, R. A. F., Powell, C. McA., Fergusson, C. L., Jones, J. G., Roots, W. D. & Fergusson, J., 1981, The Lower Devonian Kowmung Volcaniclastics: a deep-water succession of mass-flow origin, northeastern Lachlan Fold Belt, N. S. W. J. *Geol. Soc. Aust.* **28**. 19-31.
- Castro, A., 1987, On granitoid emplacement and related structures. *Geol. Rund.* **76**. 101-124.
- Castro, A. & Stephens, W. E., 1992, Amphibole-rich polycrystalline clots in calc-alkaline granitic rocks and their enclaves. *Canad. Miner.* **30**. 1093-1112.
- Castro, A., De la Rosa, J. D. & Stephens, W. E., 1990, Magma mixing in the subvolcanic environment: petrology of the Gerena interaction zone near Seville, Spain. *Contrib. Mineral. Petrol.* **105**. 9-26.
- Chapman, H. J. & Moorbath, S., 1977, Lead isotope measurements from the oldest recognised Lewisian Gneisses of north-west Scotland. *Nature* **268**. 41-42.
- Chappell, B. W. & Stephens, W. E. 1988, Origin of infracrustal (I-Type) granite magmas. *Trans. Roy. Soc. Edinburgh.* **79**. 71-86.
- Chappell, B. W. & White, A. J. R., 1992, I- and S-type granites in the Lachlan Fold Belt. *Trans. Roy. Soc. Edinburgh.* **83**. 1-26.
- Chappell, B. W. & White, A. J. R., 1974, Two contrasting granite types. *Pacific Geology.* **8**. 173-174.
- Clarke, D. B., 1992, Granitoid rocks. Chapman & Hall, London.
- Clayburn, J. A. P., 1988, The crustal evolution of central Scotland and the nature of the lower crust: Pb, Nd and Sr isotopic evidence from Caledonian granites. *Earth Planet. Sci. Lett.* **90**. 41-51.
- Clayburn, J. A. P., Harmon, R. J., Pankhurst, R. J. & Brown, J. F., 1983, Sr, O and Pb isotope data for the origin and evolution of the Etive Complex, Scotland. *Nature.* **303**. 492-497.
- Clough, C. T., Maufe, H. B. & Bailey, E. B., 1909, The cauldron-subsidence of Glencoe and associated igneous phenomena. *Q. J. Geol. Soc.* **65**. 611-678.
- Cocks, L. R. M. & Fortey, R. A., 1990, Biogeography of Ordovician and Silurian faunas. In: McKerrow, R. S. & Scotese, C. R. (eds.). *Palaeozoic Palaeogeography and Biogeography*. *Geol. Soc. Lond. Memoir* **12**. 97-104.

- Cohen, R. S., O'Nions, R. K. and Dawson, J. B., 1984, Isotope geochemistry of xenoliths from East Africa: implications for development of mantle reservoirs and their interaction. *Earth Planet. Sci. Lett.* **68**. 209-220.
- Crandell, D. R., 1971, Post-glacial lahars from Mount Rainier volcano, Washington. *US. Geol. Surv. Prof. Pap.* **677**. 1-84.
- Curry, G. B., Ingham, B. J., Bluck and Williams, A, 1982, The significance of a reliable Ordovician age for some Highland Border rocks in Central Scotland. *J. Geol. Soc. Lond.* **139**. 451-454.
- Daly, R. A., 1933, *Igneous Rocks and The Depths of the Earth*. Hafner, New York.
- Davies, G. R., Upton, G. J. & Strogon, P., 1984, Strontium and neodymium isotope evidence for age and origin of crustal xenoliths from the Midland Valley of Scotland and Central Ireland. *Trans. Roy. Soc. Edin. Earth Sci.* **75**. 297.
- Deer, W. A., Howie, R. A. & Zussman, J., 1992, *An introduction to the Rock Forming Minerals*. 2nd Ed. Longman Scientific & Technical.
- Defant, M. J. & Drummond, M. S., 1990, Subducted lithosphere-derived andesitic and dacitic rocks in young volcanic arc setting. *Nature* **347**. 662-665.
- Defant, M. J., Richerson, P. M., De Boer, J. Z., Stewart, R. H., Maury, R. C., Bellon, H., Drummond, M. S., Feigenson, M. D. & Jackson, T. E., and their aunties 1991, Dacite Genesis via both Slab Melting and Differentiation: Petrogenesis of La Yeguada Volcanic Complex, Panama. *J. Petrol.* **32**. 1101-1142.
- Delaney, P. T. & Pollard, D. D., 1981, Deformation of host rocks and flow of magma during growth of minette dykes and breccia bearing intrusions near Ship Rock, New Mexico. *U.S.G.S., Prof. Pap.* **1202**.
- De la Roche, H., Leterrier, J., Grande Claude, P. & Marchal, M., 1980, A classification of volcanic rocks using R1-R2 diagrams and major element analyses - its relationship with current nomenclature. *Chem. Geol.* **29**. 180-210.
- Dempster, T. J., 1985, Uplift patterns and orogenic evolution in the Scottish Dalradian. *J. Geol. Soc. Lond.* **142**. 111-128.
- Dempster, T. J. & Bluck, B. J., 1991, Xenoliths in the lamprophyre dykes of Lomondside: constraints on the nature of the crust beneath the southern Dalradian. *Scott. J. Geol.* **27**. 157-165.
- Dempster, T. J. & Bluck, B. J., 1989, The age and origin of boulders in the Highland Border Complex: Constraints on terrane movement. *J. Geol. Soc. Lond.* **146**. 377-379.
- DePaolo, D. J., 1981, A neodymium and strontium isotope study of the Mesozoic calc-alkaline granitic batholiths of the Sierra Nevada and Peninsular Ranges, California. *J. Geophys. Res.* **86**. 10470-10488.
- Dewey, J. F., 1969, Evolution of the Appalachian-Caledonian orogen. *Nature* **222**. 124-129.
- Dickin, A. P. 1992, Evidence for an early Proterozoic crustal province in the North Atlantic Region. *J. Geol. Soc. Lond.* **149**. 483-486
- Dickin, A. P. & Bowes, D. R., 1991, Isotopic evidence for the extent of early Proterozoic basement in Scotland and northwestern Ireland. *Geol. Mag.* **128**. 385-388.

- Downie, C., Lister, T. R., Harris, A. L. & Fettes, D. J., 1971, A palynological investigation of the Dalradian rocks of Scotland. *Rep. Inst. Geol. Sci.* **No. 71/9**.
- Droop, G. T. R., 1987, A general equation for estimating  $Fe^{3+}$  concentrations in ferromagnesian silicates and oxides from microprobe analyses, using stoichiometric criteria. *Min. Mag.* **51**. 431-435.
- Droop, G. T. R. & Treloar, P. J., 1981, Pressure of metamorphism in the aureole of the Etive Granite Complex. *Scott. J. Geol.* **17**. 87-102.
- Droop, G. T. R. & Charnley, N. R., 1985, Comparative geobarometry of pelitic hornfelses associated with the Newer Gabbros: a preliminary study. *J. Geol. Soc. Lond.* **142**. 53-62.
- Druitt, T. H. & Sparks, R. S. J., 1982, A proximal ignimbrite facies on Santorini, Greece. *J. Volcanol. Geotherm. Res.* **13**. 147-171.
- Eichelberger, J. C., 1980, Vesiculation of mafic magma during replenishment of silicic magma reservoirs. *Nature* **288**. 446-458.
- Ellam, R. M., Hawkesworth, C. J. & McDermott, F., 1990, Pb isotope data from the Proterozoic subduction-related rocks: Implications for crust-mantle evolution. *Chem. Geol.* **83**. 165-181.
- England, P. C. & Richardson, S. W., 1977, The influence of erosion on the mineral facies of rocks from different metamorphic environments. *J. Geol. Soc. Lond.* **134**. 201-213.
- Enos, P., 1977, Flow regimes in debris flows. *Sedimentology* **24**. 133-142.
- Faure, G., 1986, *Principles of Isotope Geology*. John Wiley & Sons., New York.
- Fenn, P. M., 1986, On the origin of Graphic Granite. *Am. Mineral.* **71**. 325-330.
- Fettes, D. J., 1970, The structural and metamorphic state of the Dalradian rocks and their bearing on the age of emplacement of the basic sheet. *Scott. J. Geol.* **6**. 108-118.
- Fettes, D. J., Graham, C. M., Harte, B. & Plant, J. A., 1986, Lineaments and basement domains: an alternative view of Dalradian evolution. *J. Geol. Soc. Lond.* **143**. 453-464.
- Field, D. & Råheim, A., 1981, Age relationships in the Proterozoic high grade gneiss regions of southern Norway. *Precamb. Res.* **14**. 261-275.
- Fink, J., 1991, Volcanoes' volatile behaviour. *Nature* **352**. 188.
- Fisher, R. V., 1971, Features of coarse-grained, high concentration fluids and their deposits. *J. Sed. Petrol.* **41**. 916-927.
- Fisher, R. V., 1966, Rocks composed of volcanic fragments and their classification. *Earth Sci. Rev.* **1**. 287-298.
- Fisher, R. V., 1961, Proposed classification of volcanoclastic sediments and rocks. *Geol. Soc. Am. Bull.* **72**. 1409-1414.
- Fisher, R. V. & Heiken, G., 1982, Mount Pelée, Martinique: May 8<sup>th</sup> and May 20<sup>th</sup>, 1902, pyroclastic flows and surges. *J. Volcanol. Geotherm. Res.* **13**. 339-371.
- Fitches, W. R., Muir, R. J., Maltman, A. J. & Bentley, M. R., 1990, Is the Colonsay-west Islay block of SW Scotland an allochthonous terrane? Evidence from Dalradian Tillite clasts. *J. Geol. Soc. Lond.* **147**. 417-420.
- Fitton, J. G., Thirlwall, M. F. & Hughes, D. J., 1982, Volcanism in the British Isles. In: Thorpe, R. S. (ed.), *Andesites*. 611-636.

- Flinn, D., 1977, Transcurrent faults and associated cataclasis in Shetland. *J. Geol. Soc. Lond.* **133**. 231-248.
- Fowler, M. B., 1992, Elemental and O-Sr-Nd isotope geochemistry of the Glen Dessary syenite, NW Scotland. *J. Geol. Soc. Lond.* **149**. 209-220.
- Fowler, M. B., 1988, Ach'uaine Hybrid Appinite Pipes: evidence for mantle-derived shoshonitic parent magmas in Caledonian magma genesis. *Geology* **16**. 1026-1030.
- Frey, F. A., Green, D. H. & Roy, S. D., 1978, Intergrated models of basalt petrogenesis: a study of quartz tholeiites to olivine melilitites from south eastern Australia utilising geochemical and experimental petrological data. *J. Petrol.* **19**. 463-513.
- Friend, P. F. & Macdonald, R., 1968, Volcanic sediments, stratigraphy and tectonic background of the Old Red Sandstone of Kintyre, W. Scotland. *Scott. J. Geol.* **4**. 265-282.
- Frost, C. D. & O'Nions, R. K., 1985, Caledonian magma genesis and crustal recycling. *J. Petrol.* **26**. 515-544.
- Furnes, H., Friedliefsson, I. B. and Atkins, F. B., 1980, Subglacial volcanics - on the formation of acid hyaloclastites. *J. Volcanol. Geotherm. Res.* **8**. 95-110.
- Gallagher, M. J., Michie, U. McLaren., Smith, R. T. & Haynes, L. 1971, New evidence of uranium and other mineralisation in Scotland. *Trans. Instn. Min. Metall.* **80**. B150-173.
- Gamble, J. A., Wright, I. C. & McCulloch, M. T., 1992, Basalt petrology and petrogenesis in an oceanic to continental volcanic arc-back-arc basin setting. Abstract for paper presented at Special Meeting Volcanic Studies Group 9-10 May 1992. Volcanism associated with extension at consuming plate margins. p10-11.
- Geikie, A., 1897, *Ancient Volcanoes of Great Britain*. 2vols. London.
- Geist, D. J., McBirney, A. R. & Barker, B. H., 1989, MacGPP: A program for creating and using geochemical data files. Unpublished report, University of Oregon.
- Gill, J. B., 1981, *Orogenic andesites and plate tectonics*. Springer Berlin.
- Gill, J. B., Stock, A. L. & Whelan, P. M., 1984, Volcanism accompanying back-arc basin development in the southwest Pacific. *Tectonophys.* **102**. 207-224.
- Glover, B. W., 1993, The sedimentology of the Neoproterozoic Grampian Group and the significance of the Fort William Slide between Spean Bridge and Rubha Cuil-cheanna, Inverness-shire. *Scott. J. Geol.* **27**. 24-44.
- Glover, B. W. & Winchester, J. A., 1989, The Grampian Group: A major Late Proterozoic clastic sequence in the Central Highlands of Scotland. *J. Geol. Soc. Lond.* **146**. 85-96.
- Goldschmidt, V. M., 1954, *Geochemistry*. Clarendon Press, Oxford.
- Gottardi, G., Burton, J. D. & Culkin, F., 1972, Gallium. In: Wedepohl (ed.) *Handbook of geochemistry*. **11-3** Springer-Verlag, Berlin.
- Graham, C. M. & Bradbury, H. J., 1981, Cambrian and Late Cambrian basaltic activity in the Scottish Dalradian: a review. *Geol. Mag.* **118**. 27-39.
- Green, D. H., 1973, Conditions of melting of basanite magma from garnet-peridotite. *Earth Planet. Sci. Lett.* **17**. 456-465.
- Greenough, J. D. Owen, J. V. & Ruffman, A., 1993, Noble Metal Concentrations in Shoshonitic Lamprophyres: Analysis of the Weekend Dykes, Eastern Shore, Nova Scotia, Canada. *J. Petrol.* **34**. 1247-1270.

- Groome, D. R. & Hall, A., 1974, The geochemistry of the Devonian lavas of the Lorne Plateau, Scotland. *Min. Mag.* **39**. 621-640.
- Hall, J., Brewer, J. A., Matthews, D. H. & Warner, M. R., 1984, Crustal structure across the Caledonides from the WINCH seismic reflection profile. *Trans. Roy. Soc. Edin. Earth Sci.* **75**. 97-109.
- Halliday, A. N., 1984, Coupled Sm-Nd and U-Pb systematics in Late Caledonian Granites and the basement under Northern Britain. *Nature*. **307**. 229-233.
- Halliday, A. N., 1981, On the sources of Uranium in some Scottish Caledonian Granites. *Min. Mag.* **44**. 437-442.
- Halliday, A. N., Dickin, A. P., Hunter, R. N., Davies, G. R., Dempster, T. J., Hamilton, P. J., & Upton, B. G. J., 1993, Formation and composition of the Lower Continental Crust: Evidence from Scottish Xenolith Suites. *J. Geophys. Res.* **98**. 581-607.
- Halliday, A. N., Graham, C. M., Aftalion, M. & Dymoke, P., 1989, The depositional age of the Dalradian Supergroup: U-Pb and Sm-Nd isotopic studies of the Tayvallich volcanics, Scotland. *J. Geol. Soc. Lond.* **146**. 3-6.
- Halliday, A. N., Aftalion, M., Parsons, I., Dickin, A. P., & Johnson, M. R. W., 1987, Syn-orogenic alkaline magmatism and its relationship to the Moine Thrust Zone and the thermal state of the Lithosphere in North West Scotland. *J. Geol. Soc. Lond.* **144**. 611-617.
- Halliday, A. N., Stephens, W. E., Hunter, R. H., Menzies, M. A., Dickin, A. P. & Hamilton, P. J., 1985, Isotopic and chemical constraints on the building of the deep Scottish Lithosphere. *Scott. J. Geol.* **21**. 464-491.
- Halliday, A. N., Harmon, R. S. & Stephens, W. E., 1984a, Radiogenic and stable isotope evidence for the origin of the British Caledonian Granites and the nature of the basement in northern England and Scotland. In: *Proceedings of Conference on Open Magmatic systems*. ISFM SMU 66-68.
- Halliday, A. N., Aftalion, M., Upton, B. G. J., Aspen, P. & Jocelyn, J., 1984b, U-Pb isotopic ages from a granulite facies xenolith from Partan Craig in the Midland Valley of Scotland. *Trans. Roy. Soc. Edin. Earth Sci.* **75**. 71-74.
- Halliday, A. N., Dickin, A. P., Fallick, A. E., Stephens, W. E., Hutton, D. H. W., Yardley, B. W. D. & Harmon, R. S., 1984c, Open mantle and crust systems during ascent and emplacement of late Caledonian alkali-rich magmas: a detailed multidisciplinary study of the Ratagain complex, N. W. Scotland. In: *Proceedings of Conference on Open Magmatic systems*. ISEM SMU 175-176.
- Halliday, A. N., Stephens, W. E. & Harmon, R. S., 1980, Rb, Sr & O isotope relationships in 3 zoned Caledonian granitic plutons, Southern Uplands, Scotland: Evidence for varied sources and hybridisation of magmas. *J. Geol. Soc. Lond.* **137**. 329-348.
- Halliday, A. N., Aftalion, M., van Breemen, O. & Jocelyn, J., 1979, Petrogenetic significance of Rb-Sr and U-Pb isotopic systems in the 400 Ma old British Isles granitoids and their hosts. In: Harris, A. L., Holland, C. H. & Leake, B. E. (eds.), *The Caledonides of the British Isles Reviewed*. *Spec. Pub. Geol. Soc. London*, **NO. 8**. 139-144.
- Halliday, A. N. & Stephens, W. E., 1984, Crustal controls on the genesis of the 400 Ma Caledonian granites. *Phys. Earth. Planet. Inter.* **35**. 89-104.

- Hamidullah, S., & Bowes, D. R., 1987, Petrogenesis of the appinite suite, Appin district, W. Scotland. *Acta Universitatis Carolinae-Geologica* **4**. 295-396.
- Hamilton, P. J., O'Nions, R. K. & Pankhurst R. J., 1980, Isotopic evidence for the provenance of some Caledonian granites. *Nature* **287**. 279-284.
- Hammarstrom, J. M. & Zen, E., 1992, Discussion of Blundy & Holland's (1990) Calcic amphibole equilibria and a new amphibole-plagioclase geothermometer. *Contrib. Mineral. Petrol.* **111**. 264-268.
- Hammarstrom, J. M. & Zen, E., 1986, Aluminium in Hornblende: an empirical Igneous Geobarometer. *Am. Mineral.* **71**. 1297-1318.
- Hampton, M. A., 1972, The role of subaqueous debris flow in generating turbidity currents. *J. Sed. Petrol.* **42**. 775-793.
- Hanson, G. N., 1978, The application of trace elements to the petrogenesis of igneous rocks of granitic composition. *Earth Planet. Sci. Lett.* **38**. 26-43.
- Harker, A., 1909, *The Natural History of Igneous Rocks*. Methuen London.
- Harker, A., 1908, *The Geology of the Small Isles of Inverness-shire*. Mem. geol. Surv. G.B., Scotland, H.M.S.O., Edinburgh.
- Harmon, R. S., 1984, Stable isotope geochemistry of Caledonian granites from the British Isles and E. Greenland. *Phys. Ea. & Planet. Interiors.* **35**. 105-120.
- Harmon, R. S. & Halliday, A. N., 1980, Oxygen and strontium isotope relationships in the British Late Caledonian Granites. *Nature* **283**. 21-25.
- Harmon, R. S., Halliday, A. N., Clayburn, J. A. P. & Stephens, W. E., 1984, Chemical and isotopic systematics of the Caledonian intrusions of Scotland and Northern England: a guide to magma source region and magma-crust interaction. *Phil. Trans. R. Soc. London* **A310**. 709-742.
- Harper, C. T., 1967, The geological interpretation of potassium-argon ages of metamorphic rocks from the Scottish Caledonides. *Scott. J. Geol.* **3**. 46-66.
- Harris, A. L., 1992, The growth and structure of Scotland. In: G. Y. Craig (ed.). *The Geology of Scotland*. 3rd edition. The geological Society. 1-24.
- Harris, A. L., 1989, Discussion of Rogers et al. (1989). *J. Geol. Soc. Lond.* **146**. 789-798.
- Harris, A. L. & Pitcher, W. S., 1975, The Dalradian Supergroup. In: Harris, A. L., Shackleton, R. M., Watson, J., Downie, C., Harland, W. B. & Moor bath, S. (eds.), *A correlation of Precambrian rocks in the British Isles*. *Spec. Rep. Geol. Soc. Lond.* **6**. 52-75.
- Harris, A. L. & Johnson, M. R. W., 1992, Moine. In: G. Y. Craig (ed.). *The Geology of Scotland*. 3rd edition. The geological Society. 87-123
- Harrison, T. N., 1987, *The evolution of the Eastern Grampians Granites*. Unpub. Thesis Aberdeen University.
- Harry, W. T. & Richey, J. E., 1963, Magmatic pulses in the emplacement of plutons. *Lpool & Manchr Geol. J.* **3**. 254-268.
- Harte, B. N. 1988, Lower Palaeozoic metamorphism in the Moine-Dalradian belt of the British Isles. In: Harris, A. L. & Fettes, D. J. (eds.), 1988, *The Caledonian-Appalachian Orogen*. *Geol. Soc. London, Spec. Pub. No. 38*. 123-134.

- Haslam, H. W., 1986, Mineral investigations in the Ben Nevis and Ballachulish areas of the Scottish Highlands. Mineral Reconnaissance Programme Rep. Br. Geol. Surv., **No. 80**.
- Haslam, H. W., 1971, Andalusite in the Mullach nan Coirean granite, Inverness-shire. *Geol. Mag.* **108**. 97-102.
- Haslam, H. W., 1970, Appinite xenoliths and associated rocks from the Ben Nevis igneous complex. *Geol. Mag.* **10**. 341-356
- Haslam, H. W., 1968, The crystallisation of intermediate and acid magmas at Ben Nevis, Scotland. *J. Petrol.* **9**. 84-104.
- Haslam, H. W., 1965, The Ben Nevis Igneous Complex. Unpub. Thesis Trinity College Cambridge.
- Houghton, P. D. W., 1988, A cryptic flysch terrane in Scotland. *J. Geol. Soc. Lond.* **145**. 685-703.
- Hawkesworth, C. J. & Powell, M., 1982, Magma genesis in the Lesser Antilles island arc. *Earth Planet. Sci. Lett.* **46**. 344-360.
- Hawkesworth, C. J., Hergt, J. M., McDermott, F. & Ellam, R. M., 1991, Destructive margin magmatism and the contributions from the mantle wedge and subducted crust. *Australian J. Earth Sci.* **38**. 577-584.
- Henderson, P., 1984, Rare earth element geochemistry. Elsevier, Amsterdam.
- Hewitt, D. A. & Wones, D. R., 1975, Physical properties of some synthetic Fe-Mg-Al trioctahedral micas. *Am. Mineral.* **60**. 854-862.
- Hickman, A. H., 1975, The stratigraphy of late Precambrian metasediments between Glen Roy and Lismore. *Scott. J. Geol.* **11**. 117-142.
- Hildreth, W., 1981, Gradients in silicic magma chambers: implications for lithospheric magmatism. *J. Geophys. Res.* **86**. 10153-10192.
- Holden, P., Source and Equilibration studies of xenoliths from the Caledonian of Scotland. Unpublished thesis University of St Andrews.
- Holden, P., Halliday, A. N., Stephens, W. E. & Henney, P. J., 1991, Chemical and isotopic evidence for major mass transfer between mafic enclaves and felsic magma. *Chem. Geol.* **92**. 135-152.
- Holden, P., Halliday, A. N. & Stephens, W. E., 1987, Neodymium and Strontium isotope content of microdiorite enclaves points to mantle input to granitoid production. *Nature* **330**. 53-56.
- Howett, K., 1990, Rock Climbing in Scotland. Constable & Company Ltd.
- Hickman A. H. & Wright, A. E., 1983, Geochemistry and chemostratigraphical correlation of slates, marbles and quartzites of the Appin Group, Argyll, Scotland. *Trans. R. Soc. Edinburgh Earth Sci.* **73**. 251-278.
- Highton, A. J. 1992, The tectonostratigraphic significance of pre-750Ma metagabbros within the northern Central Highlands, Inverness-shire. *Scott. J. Geol.* **28**. 71-76.
- Hole, M. J., 1988, Post-subduction alkaline volcanism along the Antarctic Peninsula. *J. Geol. Soc. London.* **145**. 985-998.
- Holgate, N., 1969, Palaeozoic and Tertiary transcurrent movements on the Great Glen Fault. *Scott. J. Geol.* **5**. 97-139.

- Hollister, L. S., Grissom, G. C., Peters, E. K., Stowell, H. H. & Sisson, V. B., 1987, Confirmation of the empirical correlation of Al in hornblende with pressure of solidification of calc-alkaline plutons. *Am. Mineral.* **72**. 231-239.
- Hsü, L. C., 1968, Selected phase relations in the system Al-Mn-Fe-Si-O-H: a model for garnet equilibria. *J. Petrol.* **9**. 40-83.
- Huang, W-L. & Wyllie, P. J., 1975, Melting relations in the system NaAlSi<sub>3</sub>O<sub>8</sub> - KAlSi<sub>3</sub>O<sub>8</sub> - SiO<sub>2</sub> to 35 kilobars, Dry and excess water. *J. Geol.* **83**. 737-748.
- Hunter, R. H., Upton, B. G. J. & Aspen, P., 1984, Meta-igneous granulite and ultramafic xenoliths from basalts of the Midland Valley of Scotland: petrology and mineralogy of the lower crust and upper mantle. *Trans. Roy. Soc. Edin. Earth Sci.* **75**. 75-84.
- Huppert, H. E. & Sparks, R. S. J., 1988, The generation of granitic magmas by intrusion of basalt into Continental crust. *J. Petrol.* **29**. 599-624.
- Hurford, A. J., 1977, A preliminary fission track dating survey of the Caledonian 'newer and last granites' from the Highlands of Scotland. *Scott. J. Geol.* **13**. 271-284.
- Hutchinson, C. S., 1983, Economic deposits and their tectonic setting. The MacMillan Press Ltd.
- Hutton, D. H. W., 1988a, Igneous emplacement in a shear zone termination: the biotite granite at Strontian, Scotland. *Geol. Soc. Am. Bull.* **100**. 1392-1399.
- Hutton, D. H. W., 1988b, Granite emplacement mechanisms and tectonic controls: inferences from deformation studies. *Trans. Roy. Soc. Edin. Earth Sci.* **79**. 245-255.
- Hutton, D. H. W. & McErlean, M., 1991, Silurian and early Devonian sinistral deformation of the Ratagain Granite, Scotland: Constraints on the age of Caledonian movements on the Great Glen Fault system. *J. Geol. Soc. Lond.* **148**. 1-4.
- Hutton, D. H. W., Stephens, W. E., Yardley, B. W. D., McErlean, M. & Halliday, A. N., 1991. The Ratagain plutonic complex. In: May, S. (ed.) *The geology of the Kintail District. Memoir of the B. G. S.* (in press).
- Irvine, T. N. & Barager, W. R. A., 1971, A guide to the chemical classification of the volcanic rocks. *Can. J. Earth Sci.*, **8**. 523-548.
- Jacobsen, S. B. & Wasserburg, G. J., 1980. Sm-Nd isotopic evolution of Chondrites. *Earth Planet. Sci. Lett.* **50**. 139-155.
- Jacques, J. M. & Reavy, R. J., in press, Lineamental control on the siting of Caledonian plutonism in the SW Scottish Highlands. *J. Geol. Soc. Lond.*
- Jagger, M. D., Max, M. D., Aftalion, M. & Leake, B. E., 1988, U-Pb zircon age of basic rocks and gneisses intruded into the Dalradian rocks of Cashel, Connemara, Western Ireland. *J. Geol. Soc. Lond.* **145**. 645-648.
- Johnson, M. C. & Rutherford, M. J., 1989, Experimental calibration of the aluminium-in-hornblende geobarometer with application to Long Valley caldera (California) volcanic rocks. *Geology*, **17**. 837-841.
- Johnson, M. R. W., 1992, Dalradian In: G. Y. Craig (ed.). *The Geology of Scotland*. 3rd edition. The geological Society. 125-160.
- Johnson, M. R. W., 1963, Some time relations of movements and metamorphism in the Scottish Highlands. *Geologie Mijnb.* **42**. 287-294.

- Johnstone, G. S., The Moine succession. In: Harris, A. L., Shackleton, R. M., Watson, J., Downie, C., Harland, W. B. & Moorbath, S. (eds.), A correlation of Precambrian rocks in the British Isles. Spec. Rep. Geol. Soc. Lond. **6**. 30-42.
- Johnstone, G. S., Smith, D. I. & Harris, A. L., 1969. The Moinian Assemblage of Scotland. In: Kay, M. (ed.). North Atlantic geology and continental drift. Am. Assoc. Petrol. Geol. **12**. 159-180.
- Judd, J. W., 1874, On the secondary rocks of Scotland, second paper on the ancient volcanoes of the Highlands and the relations of their products to the Mesozoic strata. Q. J. Geol. Soc. Lond. **119**. 291-294.
- Kay, R. W., 1978, Aleutian magnesian andesites: melts subducted Pacific ocean crust. J. Volcanol. Geotherm. Res. **4**. 117-132.
- Kelemen, P. B., Johnson, K. T. M., Kinzler, R. J. & Irving, A. J., 1990, High-field-strength element depletions in arc basalts due to magma-magma interaction. Nature **345**. 521-524.
- Key, R. M., Phillips, E. R. & Chacklesfield, B. C., 1993, Emplacement and thermal metamorphism associated with the post-orogenic Strath Ossian Pluton, Grampian Highlands, Scotland. Geol Mag. **130**. 379-390.
- Kilburn, C. R. J. & Luongo, G., 1993, Active lavas: monitoring and modelling. U. C. L. P. London.
- Klemperer, S. L., Ryan, P. D. & Snyder, D. B., 1991, A deep seismic reflection traverse across the Irish Caledonides. J. Geol. Soc. Lond. **148**. 149-164.
- Krauskopf, K. B., 1948, Lava movement at the Paracutin volcano, Mexico. Geol. Soc. Am. Bull. **59**. 1267-1284.
- Kretz, R., 1982, Transfer and exchange equilibria in a portion of the pyroxene quadrilateral as deduced from experimental data. Geochim. Cosmochim. Acta. **46**. 411-421.
- Krogh, T. E., 1982, Improved accuracy of U-Pb zircon ages by the creation of more concordant systems using an air abrasion technique. Geochim. Cosmochim. Acta. **46**. 631-635.
- Kynaston, H., 1903, Note on the Volcanic Rocks of Glen Coe and their relation to the granite of Ben Cruachan. Rep. Brit. Assoc., Belfast Meeting, 1902, Transactions of Sections. 602-603.
- Lacroix, A., 1904, La Montagne Pelée et ses Éruptions. Masson et Cie, Paris.
- Lambert, R. St. J., 1969, Isotopic studies relating to the Pre-Cambrian history of the Moinian of Scotland. Proc. Geol. Soc. Lond. **1652**. 24-245
- Lambert, R. St. J. & McKerrow, W. S., 1976, The Grampian Orogeny. Scott. J. Geol. **12**. 271-292.
- Lambert, R. St. J., Holland, J. G. & Winchester, J. A., 1982, A geochemical comparison of the Dalradian Leven Schists and the Grampian Division Monadhliath Schists of Scotland. J. Geol. Soc. Lond. **139**. 71-84.
- Lapidus, D. F., 1987, Collins dictionary of geology. Collins, Glasgow.
- Le Bas, M. J. & Streckeisen, A., 1991, The IUGS systematics of igneous rocks. J. Geol. Soc. Lond. **148**. 825-834.

- Le Maitre, R. W., Bateman, P., Dudek, A., Keller, J., Lameyre, Le Bas, M. J., Sabine, P. A., Schmid, R., Sorensen, H., Streckeisen, A., Wooley, A. R. & Zanettin, B., 1989, A classification of igneous rocks and glossary of terms. Blackwell, Oxford.
- Leake, B. E., 1990, Granite magmas. Their sources, initiation and consequences of emplacement. *J. Geol. Soc. Lond.* **147**. 579-589.
- Leake, B. E., 1978, Nomenclature of amphiboles. *Am. Mineral.* **63**. 1025-1052.
- Leake, B. E., 1971, On aluminous and edenitic amphiboles. *Min. Mag.* **38**. 389-407.
- Leeder, M. R., 1982, *Sedimentology: Process and Product*. Chapman & Hall.
- Leggett, J. K., McKerrow, W. S. & Eales, M. H., 1979, The Southern Uplands: A Lower Palaeozoic accretionary prism. *J. Geol. Soc. Lond.* **136**. 755-770.
- Liew, T. C. & Hofmann, A. W., 1988, Precambrian crustal components, plutonic associations, plate environment of the Hercynian Fold Belt of central Europe: Indications from a Nd and Sr isotopic study. *Contrib. Mineral. Petrol.* **98**. 129-138.
- Liew, T. C. & McCulloch, M. T., 1985, Genesis of granitoid batholiths of Peninsular Malaysia from a Nd-Sr isotopic and U-Pb zircon study. *Geochim. Cosmochim. Acta.* **49**. 587-600.
- Lindsay, M. G., Haselock, P. J. & Harris, A. L., 1989, The extent of Grampian orogenic activity in the Scottish Caledonides. *J. Geol. Soc. Lond.* **146**. 733-735.
- Lipman, P. W., 1984, The roots of ash flow calderas in western North America: windows into the tops of granitic batholiths. *J. Geophys. Res.* **89**. 8801-8841.
- Luth, W. C., Jahns, R. H. & Tuttle, O. F., 1964, The granite system at pressures of 4-10kbar. *J. Geophys. Res.* **69**. 759-773.
- Macculloch, J., 1817, Observations on the mountain Cruachan in Argyllshire, with some remarks on the surrounding country. *Trans. Geol. Soc.* **4**. 117-138.
- Macdonald, R., Rock, N. M. S., Rundle, C. C. & Russell, O. J., 1986, Relationships between Caledonian lamprophyric and acidic magmas in a differentiated dyke, SW Scotland. *Mineral Mag.* **50**. 547-557.
- Macdonald, R., Thorpe, R. S., Gaskarth, J. W. & Grindrod, A. R., 1985, Multi-source origin for Caledonian lamprophyres of Northern Britain. *Mineral Mag.* **49**. 485-494.
- Mackie, W., 1907, The occurrence of volcanic tuffs on Ben Nevis. *Trans. Edin. Geol. Soc.* **9**. 69-72.
- Macknight, T., 1821, Mineralogical Notices and Observations. *Mem. Wernerian Nat. Hist. Soc.* **3**. 104-122.
- Macknight, T., 1811, On the mineralogy and Local Scenery of certain Districts in the Highlands of Scotland. *Mem. Wernerian Nat. Hist. Soc.* **1**. 274-357.
- Maniar, P. D. & Piccoli, P. M., 1989, Tectonic discrimination of Granitoids. *Geol. Soc. Am. Bull.* **101**. 635-643.
- Marcantonio, F., Dickin, A. P., McNutt, R. H. & Heaman, L. M., 1988, A 1,800-million-year-old- gneiss terrane in Islay with implications for the crustal structure and evolution of Britain. *Nature* **335**. 62-64.
- Marsh, B. D., 1982, On the mechanics of the igneous diapirism, stoping and zone melting. *Am. J. Sci.* **282**. 808-855.

- Marshall, J. E. A., 1991, Palynology of the Stonehaven Group; Scotland: Evidence for a Mid-Silurian age and its geological implications. *Geol. Mag.* **128**. 283-286.
- Mathez, E. A., 1973, A Refinement of the Kudo-Weill plagioclase thermometer, and its application to basaltic rock. *Contrib. Mineral. Petrol.* **41**. 61-72.
- Maufe, H. B., 1910, The geological structure of Ben Nevis: *Mem. Geol. Surv. U. K., Summ. Prog.* (for 1910), 80-89.
- McBirney, A. R., 1963, Factors governing the nature of submarine volcanism. *Bull. Vol.* **26**. 455-469.
- McCarthy, T. S. & Hasty, R. A., 1976, Trace element distribution patterns and their relationship to the crystallisation of granitic melts. *Geochim. Cosmochim. Acta* **40**. 1351-1358.
- McCulloch, M. T. & Gamble, J. A., 1991, Geochemical and geodynamical constraints on subduction zone magmatism. *Earth Planet. Sci. Lett.* **102**. 358-374.
- McCulloch, M. T. & Wasserburg, G. J., 1978, Barium and Neodymium isotopic anomalies in the Allende meteorite. *Astrophys. J.* **222**. L15-L19.
- Menzies, M. A., 1991, Archaean, Proterozoic and Phanerozoic lithospheres. In: Menzies, M. A. (ed.), *Continental Mantle*. Oxford Monographs on Geology and Geophysics **No. 16**. 67-86. Oxford University Press.
- Menzies, M. A. & Halliday, A. N., 1988, Lithospheric mantle domains beneath the Archaean and Proterozoic crust of Scotland. In: Menzies, M. A. & Cox, K. G. (eds.) *Oceanic and continental lithosphere: similarities and differences*. *J. Petrol. Special Lithosphere Issue* 275-302
- Menzies, M. A. & Halliday, A. N., 1984, Isotopic evidence for mantle heterogeneity beneath the Midland Valley and adjacent regions from studies of inclusion suites. *Trans. Roy. Soc. Edin. Earth Sci.* **75**. 298.
- Menzies, M. A., Halliday, A. N., Zenon Palacz, Hunter, R. H., Upton, B. G. J., Aspen. P. & Hawkesworth, C. J., 1987, Evidence from mantle xenoliths for an enriched lithospheric keel under the Outer Hebrides. *Nature* **325**. 44-47.
- Mercy, E. L. P., 1963, The geochemistry of some Caledonian granitic and metasedimentary rocks. In: Johnson, M. R. W. and Stewart, F. M. (eds.), *The British Caledonides*. Oliver and Boyd, Edinburgh 189-215.
- Miller, C. F. & Stoddard, E. F., 1981, The role of manganese in the paragenesis of magmatic garnet: an example from the Old-Woman-Puite Range, California. *J. Geol.* **89**. 233-246.
- Miller, J. A. & Brown, P. E., 1965, Potassium-Argon age studies in Scotland. *Geol. Mag.* **102**. 106-134.
- Morimoto, N., 1988, Nomenclature of pyroxenes. *Am. Mineral.* **73**. 1123-1133.
- Morris, G. A. & Hutton, D. H. W., 1993, Evidence for sinistral shear associated with the emplacement of the early Devonian Etive dyke swarm. *Scott. J. Geol.* **29**. 69-72.
- Morris, J. D., Leeman, W. P. & Tera, F., 1990, The subducted component in island arc lavas: Constraints from Be isotopes and B-Be systematics. *Nature* **344**. 31-36.

- Morrison, M. A., Hendry, G. L. & Leat, P. L., 1987, Regional and tectonic implications of parallel Caledonian and Permo-Carboniferous lamprophyre dykes swarms from Lismore, Ardour. *Trans. Roy. Soc. Edin. Earth Sci.* **77**. 279-288.
- Morton, A. G. & Taylor, P. N., 1991, Geochemical and isotope constraints on the nature and age of basement rock from Rockall Bank, NE Atlantic. *J. Geol. Soc. Lond.* **148**. 631-634.
- Muir, R. J., Fitches, W. R. F. & Maltman, A. J., 1992, The contribution of Early Proterozoic basement to Caledonian magma genesis in NW Britain and Ireland. *Trans. Roy. Soc. Edinburgh.* **83**. 495.
- Mullineaux, D. R & Crandell, D. R., 1962, Recent lahars from Mount St. Helens, Washington, *Geol. Soc. Am. Bull.* **73**. 855-870.
- Myers, J. S., 1975, Cauldron subsidence and fluidisation: Mechanisms of intrusion of the Coastal Batholith of Peru into its own Volcanic ejecta. *Geol. Soc. Am. Bull.* **86**. 1209-1220.
- Mykura, W., 1992, Old Red Sandstone. In: *The Geology of Scotland 3rd edition*, (ed.) G. Y. Craig. 297-346.
- Mykura, W., 1983, Old Red Sandstone east of Loch Ness, Inverness-shire. *Report. Inst. Geol. Sci.* 82/7.
- Mykura, W., 1976, *British Regional Geology: Orkney & Shetland*. H. M. S. O.
- Mykura, W. & Owens, B., 1983, The Old Red Sandstone of the Mealfuorvonie outlier, west of Loch Ness, Inverness-shire. *Report. Inst. Geol. Sci.* 83/7.
- Nash, W. P. & Crecraft., H. R., 1985, Partition coefficients for trace elements in silicic magmas. *Geochim. Cosmochim. Acta.* **49**. 2309-2322.
- Nicholls, G. D., 1951, An unusual pyroxene-rich xenolith in the diorite of the Glenelg-Ratagain complex. *Geol. Mag.* **88**. 284-314.
- Nickel, E., Kock, H. & Nungässer, W., 1967, Modellversuche zur Fließregelung in Graniten (Beiträge zur Tektonik von Fließgefügen III) *Schw. Min. Petrol. Mitt.* **47**. 399-497.
- Nockolds, S. R. & Allen, R., 1953, The geochemistry of some Igneous Rock Series. *Geochim. Cosmochim. Acta* **4**. 105-142.
- Nockolds, S. R. & Mitchell, R. L., 1947, The geochemistry of some Caledonian plutonic rocks: a study in the relationship between the major and trace elements of igneous rocks and their minerals. *Trans. Roy. Soc. Edinburgh.* **61**. 533-575.
- Norman, M. D., Leeman, W. P. & Mertzman, S. A., 1992, Granites and rhyolites from the Northwestern U.S.A.: temporal variation in magmatic processes and relations to tectonic setting. *Trans. Roy. Soc. Edinburgh.* **83**. 71-82.
- Norrish, K. & Hutton, J. T., 1969, An accurate X-ray spectrographic method for the analysis of a wide range of geological samples. *Geochim. Cosmochim. Acta.* **33**. 431-453.
- O'Connor, J. T., 1965, A classification for quartz rich igneous rock based on feldspar ratios. *U. S. Geol. Surv. Prof. Paper.* **525B**. 79-84.
- O'Nions, R. K., Hamilton, P. J., & Hooker, P. J., 1983, A Nd isotope investigation of sediments related to crustal development in the British Isles. *Earth Planet. Sci. Lett.* **63**. 229-240.
- Oldershaw, W., 1974, The Lochnagar granitic ring complex, Aberdeenshire. *Scott. J. Geol.* **10**. 297-310.

- Oyenhausen, C. von & Dechen, H. von., 1830, Der Ben Nevis am Loch Eil. Karsten's Archiv für Mineralogie, Geognosie, Bergbau und Huttenkunde. **2.** 38-54.
- Pankhurst, R. J., 1979, Isotope and trace element evidence for the origin and evolution of Caledonian granites in the Scottish Highlands. In: Atherton, M. P. and Tarney, J. (eds.) Origin of granite batholiths-Geochemical evidence. Shiva, 18-33.
- Pankhurst, R. J., 1974, Rb-Sr whole rock geochronology of Caledonian events in North-east Scotland. Bull. Geol. Soc. Am. **85.** 345-350.
- Pankhurst, R. J., 1970, The geochronology of the basic igneous complexes. Scott. J. Geol. **6.** 83-107.
- Parson, L. M., 1979, The state of strain adjacent to the Great Glen Fault. In: Harris, A. L., Holland, C. H. & Leake, B. E. (eds.), The Caledonides of the British Isles Reviewed. Spec. Pub. Geol. Soc. London, **NO. 8.** 287-289.
- Paterson, B. A., Rogers, G., Stephens, W. E., & Hinton, R. W., 1993, The longevity of acid-basic magmatism associated with a major transcurrent fault. Geol. Soc. Amer., Abstracts with Programs. **25.** 42.
- Paterson, B. A., Stephens, W. E., Rogers, G., Williams, I. S., Hinton, R. W. & Herd, D. A., 1992, The nature of zircon inheritance in two granite plutons. Trans. R. Soc. Edinburgh Earth Sci. **83.** 459-471.
- Paterson, I. B. & Harris, A. L., 1969, Lower Old Red Sandstone Igimbrites from Dunkeld, Perthshire. Inst. Geol. Sci. Rep. **No. 69/7.**
- Paterson, S. R. & Fowler, T. K., 1993a, Re-examining pluton emplacement mechanisms. J. Struct. Geol. **15.** 191-206.
- Paterson, S. R. & Fowler, T. K., 1993b, Extensional pluton-emplacement models: Do they work for large plutonic complexes. Geology **21.** 781-784.
- Paterson, S. R., Vernon, R. H. & Tobisch, O. T., 1989, A review of criteria for the implications of magmatic and tectonic foliations in granites. J. Struct. Geol. **11.** 349-363.
- Paton, J., 1954, The Ben Nevis Observatory 1883-1904. Weather **9.** p301.
- Peach, B. N., 1930, The Lochaber Water-power Scheme and its Geological Aspect. Trans. Instn. Min. Engrs. **78.** 212-223.
- Pearce, J. A., 1983, Role of the sub-continental lithosphere in magma genesis at active continental margins. In: Hawkesworth, C. J. & Norry, M. J. (eds.) Continental Basalts and Mantle xenoliths. Shiva Nantwich 230-249.
- Pearce, J. A., 1982, Trace element characteristics of lavas from destructive plate boundaries. In: Thorpe, R. S. (ed.), Andesites. 525-548.
- Pearce, J. A. & Norry, M. J., 1979, Petrogenetic implications of Ti, Zr, Y. & Nb variations in volcanic rocks. Cont. Min. Pet. **69.** 33-47.
- Pearce, J. A., Harris, N. B. W. & Tindle, A. G., 1984, Trace element discrimination diagrams for the tectonic interpretation of granitic rocks. J. Petrol. **25.** 956-983.
- Pearce, T. H., 1969, A contribution to the theory of variation diagrams. Contrib. Mineral. Petrol., **19.** 142-157.

- Peccerillo, A. & Wu, T. W., 1992, Evolution of calc-alkaline magmas in continental arc-volcanoes - evidence from Alicudi, Aeolian arc (South Tyrrhenian Sea, Italy). *J. Petrol.* **33**. 1295-1315.
- Peccerillo, A., 1985, Roman comagmatic province (central Italy): evidence for subduction related magma genesis. *Geology* **13**. 103-106.
- Peccerillo, A. & Taylor, S. R., 1976, Geochemistry of Eocene calc-alkaline volcanic rocks from the Kastamonu area. Northern Turkey. *Contrib. Mineral. Petrol.* **58**. 63-81.
- Phillips, W. E. A., Stillman, C. J. & Murphy, T., 1976, A Caledonian plate tectonic model. *J. Geol. Soc. Lond.* **132**. 579-609
- Piasecki, M. A. J., 1980, New light on the Moine rocks of the Central Highlands of Scotland. *J. Geol. Soc. Lond.* **137**. 41-59.
- Piasecki, M. A. J. & van Breemen, O., 1983, Field and isotopic evidence for a c 750Ma tectonothermal event in Moine rocks in the Central Highlands of the Scottish Caledonides. *Trans. Roy. Soc. Edin., Earth Sci.* **73**. 119-134.
- Pidgeon, R. T. & Compston, W., 1992, A SHRIMP ion microprobe study of inherited and magmatic zircons from four Scottish Caledonian granites. *Trans. R. Soc. Edinburgh Earth Sci.* **83**. 473-483.
- Pidgeon, R. T. & Aftalion, M., 1978, Cogenetic and inherited zircon U-Pb systems in Palaeozoic granites from Scotland and England. In: Bowes, D. R. & Leake, B. E. (eds.) *Crustal processes and evolution in N. W. Britain and adjacent regions*. *Geol. Soc. Spec. Issue* **10**. 183-220
- Pitcher, W. S., 1993, *The nature and origin of Granite*. Blackie Academic & Professional.
- Pitcher, W. S., 1982, Granite type and tectonic environment. In: Hsu, K. J. (ed.), *Mountain Building Processes*. Academic Press, London. 19-40.
- Pitcher, W. S., 1979a, The nature, ascent and emplacement of granitic magmas. *J. Geol. Soc. Lond.* **136**. 627-662.
- Pitcher, W. S., 1979b, Comments on the geological environments of granites. In: Atherton, M. P. and Tarney, J. (eds.) *Origin of granite batholiths-Geochemical evidence*. Shiva, 1-8.
- Pitcher, W. S. & Berger, A. R., 1972, The appinite suite: basic rocks genetically associated with granite. In Pitcher, W. S. & Berger, A. R. (eds.), *Geology of Donegal*. Wiley, New York.
- Piwinskii, A. J. & Wyllie, P. J., 1968, Experimental studies of igneous rock series: a zoned pluton in the Wallowa batholith, Oregon. *J. Geol.* **76**. 205-234.
- Plant, J, Simpson, M., Green, P. M., Watson, J. V. & Fowler, M. B., 1983, Metalliferous and mineralised Caledonian granites in relation to regional metamorphism and fracture systems in northern Scotland. *Trans. Instn. Min. Metall.* **B92**. 33-42.
- Powell, R. & Smith, F. W., 1973, Pressure-temperature estimates for a late metamorphic event in the Dalradian in the Scottish Highlands. *Nature* **244**. 70-71.
- Pringle, J., 1973, The discovery of Cambrian trilobites in the Highland Border rocks near Callander, Perthshire. *Advanc. Sci. Lond.* **1**. 252.
- Ragland, P. C., 1989, *Basic Analytical Petrology*. Oxford University Press, Oxford.
- Ramsay, J. G., 1989, Emplacement kinematics of a granite diapir: The Chindamora batholith, Zimbabwe. *J. Struct. Geol.* **11**. 191-209.

- Read, H. H., 1961, Aspects of Caledonian magmatism in Britain. *Lpool & Manchr Geol. J.* **2**. 653-683.
- Rhodes, J. M., 1981, Characteristics of primary basaltic magmas. In: *Basaltic Volcanism on the Terrestrial Planets*. Pergamon, New York. 409-432.
- Rice, C. M. & Davies, B., 1979, Copper mineralisation associated with an appinitic pipe in Argyll, Scotland. *Trans. Instn. Min. Metall.* **88**. B154-160.
- Richardson, S. W. and Powell, R., 1976, Thermal causes of the Dalradian metamorphism in the central Highlands of Scotland. *Scott. J. Geol.* **12**. 237-268.
- Richardson, S. H., Gurney, J. J., Erlank, A. J. & Harris, J. W., 1984, Origin of diamonds in old enriched mantle. *Nature* **310**. 198-202.
- Rickwood, P. C., 1989, Boundary lines within petrologic diagrams which use oxides of major and minor elements. *Lithos* **22**. 247-263.
- Roberts, J. L., 1966, Ignimbrite eruptions in the volcanic history of the Glencoe cauldron subsidence. *Geol. J.* **5**. 173-184.
- Robertson, J. K., 1971, Experimental studies on rocks from the Deboullie Stock, Northern Maine, including melting relations in the water deficient environment. *J. Geol.* **79**. 549-571.
- Robertson, S., 1994, Timing of Barrovian metamorphism and 'Older Granite' emplacement in relation to Dalradian deformation. *J. Geol. Soc. Lond.* **151**. 5-8.
- Rock, N. M. S., 1991, *Lamprophyres*, Blackie. 285 pages.
- Rock, N. M. S., 1984, Nature and origin of Calc-alkaline lamprophyres: minettes, vogesites, kersanites and spessartites. *Trans. Roy. Soc. Edin. Earth Sci.* **75**. 193-227.
- Rock, N. M. S. & Carroll, G. W., 1990, MINTAB: a general-purpose mineral recalculation and tabulation program for Macintosh microcomputers. *Am. Mineral.* **75**. 424-430.
- Rock, N. M. S. & Hunter, R. H., 1987, Late Caledonian dyke swarms of N. Britain: Spatial and temporal intimacy between lamprophyric and granitic magmatism around the Ross of Mull pluton: Inner Hebrides. *Geol. Rund.* **76**. 805-826.
- Rock, N. M. S., Gaskarth, J. W., Henney, P. J. & Shand, P., 1988, Late Caledonian dyke swarms of N. Britain: Some preliminary petrogenetic and tectonic implications of their province-wide distribution and chemical variation. *Canad. Mineral.* **26**. 3-22.
- Rock, N. M. S., Gaskarth, J. W. & Rundle, C. C., 1986, Late Caledonian dyke swarms in southern Scotland, a regional zone of primitive K-rich lamprophyres and associated vents. *J. Geol.* **94**. 505-522.
- Rogers, D. A., Marshall, J. E. A. & Astin, T. R., 1989, Devonian and later movements on the Great Glen Fault system, Scotland. *J. Geol. Soc. Lond.* **146**. 369-372.
- Rogers, G. & Dunning, G. R., 1991, Geochronology of appinitic and related granitic magmatism in the Western Highlands of Scotland: Constraints on the timing of transcurrent Fault Movement. *J. Geol. Soc. Lond.* **148**. 17-27.
- Rogers, G. & Saunders, A. D., Magnesian andesites from Mexico, Chile and the Aleutian Islands: implications for magmatism associated with ridge-trench collision. In: Crawford, A. J. (ed.), *Boninites and Related Rocks*. London Unwin & Hyman. 416-445.

- Rogers, G., Dempster, T. J., Bluck, B. J. & Tanner, P. W. G., 1989, A high precision U-Pb age for the Ben Vuirich granite: Implications for the evolution of the Dalradian Supergroup. *J. Geol. Soc. Lond.* **146**. 789-798.
- Rogers, G., Saunders, A. D., Terrell, D. J., Verma, S. P. & Marriner, G. F., 1985, Geochemistry of Holocene volcanic rocks associated with ridge subduction in Baja California, Mexico. *Nature* **315**. 389-392.
- Rollinson, H., 1993, Using geochemical data: evaluation, presentation, interpretation. Longman Singapore Ltd, Singapore.
- Romick, J. D., Kay, S. M. & Kay, R. W., 1992, The influence of amphibole fractionation on the evolution of calc-alkaline andesite and dacite tephra from the central Aleutians, Alaska. *Contrib. Mineral. Petrol.* **112**. 101-118.
- Roobol, M. J., & Smith, A. L. 1975, Mount Pelée, Martinique; Proceedings Symposium "Andean and Antarctic Volcanological Problems": International Association of Volcanology and Chemistry of the Earth's Interior. 190-202.
- Roobol, M. J., & Smith, A. L. 1976, Stratigraphic studies of Mount Pelée, Martinique: Transactions 7th Caribbean Geological Conference, Gaudeloupe, 1974, 399-406.
- Roobol, M. J., Smith, A. L. & Wright, J. V., 1987, Lithic breccias in pyroclastic flow deposits on St. Kitts, West Indies. *Bull. Volcanol.* **49**. 694-707.
- Rose, W. I., Pearson, T. & Bonis, S., 1976, Nuées Ardente eruption from the foot of a Dacitic Lava Flow, Santiaguito Volcano, Guatemala. *Bull. Volcanol.* **40**. 23-38.
- Sabine, P. A., 1968, The Strontian granite complex, Argyllshire. *Bull. Geol. Surv. GB.* **20**. 6-42.
- Sato, H, Fujii, T. & Nekada, S., 1992, Crumbling of dacite dome lava and generation of pyroclastic flows at Unzen Volcano. *Nature* **360**. 664-666.
- Saunders, A. D., Tarney, J., Marsh, N. G., & Wood, D. A., 1980, Ophiolites as ocean crust or marginal basin crust: a geochemical approach. In: Panayiotou, A. (ed.). *Proc. Int. Ophiolite Conf. Nicosia, Cyprus.* 193-204.
- Seal, J. S. C. & Weaver, S. D., 1971, Trace element data bearing on the origin of salic rocks from the Quaternary volcano Paka, Gregory Rift, Kenya. *Earth Planet. Sci. Lett.* **12**. 327-331.
- Schairer, J. F. & Bowen, J. L., 1935, Preliminary report on equilibrium relations between feldspathoids, alkali feldspar and silica. *Trans. Amer. Geophys. Union, 16th Ann. Meeting,* 325-328.
- Schmid, R., 1981, Descriptive nomenclature and classification of Pyroclastic Deposits and Fragments: Recommendations of the IUGS, subcommission on the systematics of Igneous Rocks. *Geol.* **9**. 41-43.
- Schmidt, M. W., 1992, Amphibole composition in tonalite as a function of pressure: an experimental calibration of the Al-in-hornblende barometer. *Contrib. Mineral. Petrol.* **110**. 304-310.
- Seegerstrom, K, 1950, Erosion studies at Paracutin, State of Michoacan, Mexico. *Bull. US. Geol. Surv. Prof. Pap.* **454B**. 1-23.
- Selley, R. C., 1966, Tertiary fumaroles on the Island of Raasay. *Geol. Mag.* **103**. 558-564.

- Shackleton, R. M., 1979, The British Caledonides: comments and summary. In: Harris, A. L., Holland, C. H. & Leake, B. E. (eds.), *The Caledonides of the British Isles Reviewed*. Spec. Pub. Geol. Soc. London, **NO. 8**. 299-304.
- Shaw, D. M., 1968, A review of K-Rb fractionation trends by covariance analysis. *Geochim. Cosmochim. Acta* **32**. 573-601.
- Siebert, L., 1984, Large volcanic debris avalanches: characteristics of source areas, deposits and associated eruptions. *J. Volcanol. Geotherm. Res.* **22**. 163-197.
- Sigurddson, H., 1981, Geologic observations in the crater of Soufrière volcano, St. Vincent. Univ. West Indies Seismic Res. Unit Spec. Publ. 1981/1.
- Simpson, P. R., Brown, G. C., Plant, J. & Ostle, D., 1979, Uranium mineralisation and granite magmatism in the British Isles. *Phil. Trans. R. Soc. Lond.* **A291**. 385-412.
- Smedley, P. L., 1988a, Trace element and isotopic variations in Scottish and Irish Dinantian volcanism: Evidence for an Ocean island Basalt - like mantle source. *J. Petrol.* **29**. 413-443.
- Smedley, P. L., 1988b, The geochemistry of Dinantian volcanism in south Kintyre and the evidence for provincialism in the Southern Scottish Mantle. *Contrib. Mineral. Petrol.* **99**. 374-384.
- Smedley, P. L., 1986, The relationship between calc-alkaline volcanism and within-plate continental rift volcanism: evidence from Scottish Palaeozoic lavas. *Earth Planet. Sci. Lett.* **76**. 113-128.
- Smith, A. L. & Roobol, M. J., 1990, Mount Pelée, Martinique; a study of an active island-arc volcano. *Geol. Soc. Am. Mem.* **175**. 1-105.
- Smith, D. I., 1977, The Great Glen Fault. In: Gill, G., (ed.), *The Moray Firth area geological studies*. Inverness Field Club.
- Smith, R. L., 1960, Ash-flows. *Geol. Soc. Am. Bull.* **71**. 795-842.
- Smith, R. L., Bailey, R. A. & Ross, C. S., 1970, Geologic map of the Jemez Mountains, New Mexico. Map I-571, U.S.G.S. Geol. Surv.
- Speer, A. J., 1984, Micas in Igneous Rocks. In: Bailey, S. W., (ed.) *Micas. Reviews in Mineralogy, Mineralogical Society of America* **13**. 299-356.
- Soper, N. J., 1986, The Newer Granite Problem: A geotectonic view. *Geol Mag.* **123**. 227-236.
- Soper, N. J. & Woodcock, N. H., 1990, Silurian collision and sediment dispersal patterns in southern Britain. *Geol. Mag.* **127**. 527-542.
- Soper, N. J. & Anderton, R., 1984, Did the Dalradian slides originate as extensional faults? *Nature* **307**. 357-360.
- Soper, N. J. & Hutton, D. H. W., 1984, Late Caledonian sinistral displacements in Britain: implications for a three-plate collision model. *Tectonics* **3**. 781-794.
- Soper, N. J., Strachen, R. A., Holdsworth, R. E. Gayer, R. A. & Greiling, R. O., 1992, Sinistral transpression and the Silurian closure of Iapetus. *J. Geol. Soc. Lond.* **149**. 871-880.

- Soper, N. J., Webb, B. C. & Woodcock, N. H., 1987, Late Caledonian (Acadian) transpression in Northwestern England: Timing, geometry and geotectonic significance. *Proc. Yorks. Geol. Soc.* **46**. 175-192.
- Sparks, R. S. J., Sigurdsson, H. & Carey, S. N., 1980a, The entrance of pyroclastic flows into the sea, I. Oceanographic and geologic evidence from Dominica, Lesser Antilles. *J. Volcanol. Geotherm. Res.* **7**. 87-96.
- Sparks, R. S. J., Sigurdsson, H. & Carey, S. N., 1980a, The entrance of pyroclastic flows into the sea, II. Theoretical considerations on subaqueous emplacement and welding. *J. Volcanol. Geotherm. Res.* **7**. 97-105.
- Sparks, R. S. J., Self, S. & Walker, G. P. L., 1973, Products of ignimbrite eruptions. *Geology* **1**. 115-118.
- Spencer, A. M., 1971, Late Precambrian glaciation in Scotland. *Mem Geol. Soc. Lond.* **6**.
- Stacey, J. S. & Kramers, J. D., 1975, Approximation of terrestrial lead isotope evolution by a two-stage model. *Earth Planet. Sci. Lett.* **26**. 207-221
- Steiger, R. H. & Jäger, E., 1977, Subcommittee on geochronology convention on the use of decay constants in geo- and cosmochronology. *Earth Planet. Sci. Lett.* **36**. 359-362.
- Steiner, J. C., Jahns, R. H. & Luth, W. C., 1975, Crystallisation of the alkali feldspars and quartz in the haplogranite system NaAlSi<sub>3</sub>O<sub>8</sub> - KAlSi<sub>3</sub>O<sub>8</sub> - SiO<sub>2</sub> - H<sub>2</sub>O at 4kb. *Bull. Geol. Soc. Amer.* **86**. 83-98.
- Stephens, W. E., Whitley, J. E., Thirlwall, M. F. & Stevenson B. G., 1985, The Criffell zoned pluton: correlated behaviour of Rare Earth Element abundances with isotopic systems. *Contrib. Mineral. Petrol.* **89**. 226-238.
- Stephens, W. E., & Halliday, A. N., 1984, Geochemical contrasts between late Caledonian granitoid plutons of northern, central and southern Scotland. *Trans. Roy. Soc. Edin. Earth Sci.* **75**. 259-273.
- Stevens, N. C., 1959, Ring structures of the Mt. Alford district, southeast Queensland. *J. Geol. Soc. Aust.* **6**. 37-49.
- Stoker, M. S., 1982, Old Red Sandstone sedimentation and deformation in the Great Glen Fault Zone, NW of Loch Linnhe. *Scott. J. Geol.* **18**. 147-156.
- Storetvedt, K. M., 1975, Possible large-scale sinistral displacement along the Great Glen Fault in Scotland (reply). *Geol. Mag.* **112**. 93-94.
- Stormer, J. C., & Nicholls, J., 1978, XLFAC: A program for the interactive testing of magmatic differentiation models. *Comput. Geosci.* **4**. 143-159.
- Sturt, B. A., Ramsay, D. M., Pringle, I. R. & Teggins, D. E., 1977, Precambrian gneisses in the Dalradian sequence of NE Scotland. *J. Geol. Soc. Lond.* **134**. 41-44.
- Sun, S. S., 1980, Lead isotope study of young volcanic rocks from mid-ocean ridges, ocean islands and island arcs. *Phil. Trans. R. Soc. Lond.* **A297**. 409-445.
- Sun, S. S. & Hanson, G. N., 1975, Evolution of the mantle: geochemical evidence from alkali basalts. *Geology* **3**. 297-302
- Swanson, D. A., Dzurisin, D., Holcomb, R. T., Iwatsubo, E. Y., Chadwick, W. W., Casadevall, T. J., Ewert, J. W. & Heliker, C. C., 1987, Growth of the lava dome at Mount St. Helens,

- Soper, N. J., Webb, B. C. & Woodcock, N. H., 1987, Late Caledonian (Acadian) transpression in Northwestern England: Timing, geometry and geotectonic significance. *Proc. Yorks. Geol. Soc.* **46**. 175-192.
- Sparks, R. S. J., Sigurdsson, H. & Carey, S. N., 1980a, The entrance of pyroclastic flows into the sea, I. Oceanographic and geologic evidence from Dominica, Lesser Antilles. *J. Volcanol. Geotherm. Res.* **7**. 87-96.
- Sparks, R. S. J., Sigurdsson, H. & Carey, S. N., 1980a, The entrance of pyroclastic flows into the sea, II. Theoretical considerations on subaqueous emplacement and welding. *J. Volcanol. Geotherm. Res.* **7**. 97-105.
- Sparks, R. S. J., Self, S. & Walker, G. P. L., 1973, Products of ignimbrite eruptions. *Geology* **1**. 115-118.
- Spencer, A. M., 1971, Late Precambrian glaciation in Scotland. *Mem Geol. Soc. Lond.* **6**.
- Stacey, J. S. & Kramers, J. D., 1975, Approximation of terrestrial lead isotope evolution by a two-stage model. *Earth Planet. Sci. Lett.* **26**. 207-221
- Steiger, R. H. & Jäger, E., 1977, Subcommittee on geochronology convention on the use of decay constants in geo- and cosmochronology. *Earth Planet. Sci. Lett.* **36**. 359-362.
- Steiner, J. C., Jahns, R. H. & Luth, W. C., 1975, Crystallisation of the alkali feldspars and quartz in the haplogranite system NaAlSi<sub>3</sub>O<sub>8</sub> - KAlSi<sub>3</sub>O<sub>8</sub> - SiO<sub>2</sub> - H<sub>2</sub>O at 4kb. *Bull. Geol. Soc. Amer.* **86**. 83-98.
- Stephens, W. E., Whitley, J. E., Thirlwall, M. F. & Stevenson B. G., 1985, The Criffell zoned pluton: correlated behaviour of Rare Earth Element abundances with isotopic systems. *Contrib. Mineral. Petrol.* **89**. 226-238.
- Stephens, W. E., & Halliday, A. N., 1984, Geochemical contrasts between late Caledonian granitoid plutons of northern, central and southern Scotland. *Trans. Roy. Soc. Edin. Earth Sci.* **75**. 259-273.
- Stevens, N. C., 1959, Ring structures of the Mt. Alford district, southeast Queensland. *J. Geol. Soc. Aust.* **6**. 37-49.
- Stoker, M. S., 1982, Old Red Sandstone sedimentation and deformation in the Great Glen Fault Zone, NW of Loch Linnhe. *Scott. J. Geol.* **18**. 147-156.
- Storetvedt, K. M., 1975, Possible large-scale sinistral displacement along the Great Glen Fault in Scotland (reply). *Geol. Mag.* **112**. 93-94.
- Stormer, J. C., & Nicholls, J., 1978, XLFAC: A program for the interactive testing of magmatic differentiation models. *Comput. Geosci.* **4**. 143-159.
- Sturt, B. A., Ramsay, D. M., Pringle, I. R. & Teggins, D. E., 1977, Precambrian gneisses in the Dalradian sequence of NE Scotland. *J. Geol. Soc. Lond.* **134**. 41-44.
- Sun, S. S., 1980, Lead isotope study of young volcanic rocks from mid-ocean ridges, ocean islands and island arcs. *Phil. Trans. R. Soc. Lond.* **A297**. 409-445.
- Sun, S. S. & Hanson, G. N., 1975, Evolution of the mantle: geochemical evidence from alkali basalts. *Geology* **3**. 297-302
- Swanson, D. A., Dzurisin, D., Holcomb, R. T., Iwatsubo, E. Y., Chadwick, W. W., Casadevall, T. J., Ewert, J. W. & Heliker, C. C., 1987, Growth of the lava dome at Mount St. Helens,

- Washington, (USA), 1981-1983. In Fink, J. H., (ed.) The emplacement of silicic domes and lava flows. Special. Paper. Geol. Am. **212**. 1-16.
- Tanner, P. W. G. & Leslie, A. G., 1994, A pre-D2 age for the 590Ma Ben Vuirich Granite in the Dalradian of Scotland. J. Geol. Soc. Lond. **151**. 209-212.
- Taubeneck, W. H., 1967, Notes on the Glencoe subsidence, Argyllshire, Scotland. Geol. Soc. Am. Bull. **78**. 1295-1316.
- Taylor, H. P., 1980, The effects of assimilation of country rocks by magmas on  $^{18}\text{O}/^{16}\text{O}$  and  $^{87}\text{Sr}/^{86}\text{Sr}$  systematics in igneous rocks. Earth Planet. Sci. Lett. **47**. 243-254.
- Taylor, P. N., Jones, N. W. & Moorbath, S., 1984, Isotopic assessment of relative contributions from crust and mantle sources to the magma genesis of Precambrian Granitoid rocks. Phil. Trans. R. Soc. Lond. **A310**. 605-625.
- Teall, J. J. H., 1888, British Petrography, with special reference to Igneous Rocks. London.
- Thirlwall, M. F., 1988, Geochronology of Late Caledonian Magmatism in northern Britain. J. Geol. Soc. Lond. **145**. 951-967.
- Thirlwall, M. F., 1986, Lead isotope evidence for the nature of the mantle beneath Caledonian Scotland. Earth Planet. Sci. Lett. **80**. 55-70.
- Thirlwall, M. F., 1983, Isotope geochemistry and origin of calc-alkaline lavas from a Caledonian continental margin volcanic arc. J. Volcanol. Geotherm. Res. **18**. 589-631.
- Thirlwall, M. F., 1982, Systematic variations in chemistry and Nd-Sr isotopes across a Caledonian calc-alkaline volcanic arc: implications for source materials. Earth Planet. Sci. Lett. **58**. 27-50.
- Thirlwall, M. F., 1981, Implications for Caledonian plate tectonic models of chemical data from volcanic rocks of the British Old Red Sandstone. J. Geol. Soc. Lond. **138**. 123-138.
- Thirlwall, M. F., 1979, The petrochemistry of the British Old Red Sandstone volcanic province. Unpublished thesis University of Edinburgh.
- Thirlwall, M. F. & Burnard, P., 1990, Pb-Sr-Nd isotope and chemical studies of the origin of undersaturated and oversaturated shoshonitic magmas from the Borralan pluton, Assynt, NW. Scotland. J. Geol. Soc. Lond. **145**. 259-270.
- Thirlwall, M. F. & Bluck, B. J., 1984, Sr-Nd isotope and geochemical evidence that the Ballantrae 'ophiolite', SW Scotland is polygenetic. In Gass, I. G., Lipard, S. J. & Shelton, A. W. (eds.) Ophiolites and oceanic lithosphere. Spec. Pub. Geol. Soc. Lond. **13**. 215-230.
- Thirlwall, M. F. & Jones, N. W., 1983, Isotope geochemistry and contamination mechanics of Tertiary lavas from Skye, north west Scotland. In: Hawkesworth, C. J. & Norry, M. J. (eds.) Continental Basalts and Mantle xenoliths. Shiva Nantwich.
- Thomas, P. R., 1979, New evidence for a Central Highland Root Zone. In: Harris, A. L., Holland, C. H. & Leake, B. E. (eds.), The Caledonides of the British Isles Reviewed. Spec. Pub. Geol. Soc. London **NO. 8**. 205-212.
- Thompson, R. N. & Fowler, M. B., 1986, Subduction related shoshonitic and ultrapotassic magmatism: a study of Siluro-Ordovician syenites from the Scottish Caledonides. Contrib. Mineral. Petrol. **94**. 507-522.
- Treagus, J. E., 1991, Fault displacements in the Dalradian of the Central Highlands. Scott. J. Geol. **27**. 135-145.

- Washington, (USA), 1981-1983. In Fink, J. H., (ed.) The emplacement of silicic domes and lava flows. Special. Paper. Geol. Am. **212**. 1-16.
- Tanner, P. W. G. & Leslie, A. G., 1994, A pre-D2 age for the 590Ma Ben Vuirich Granite in the Dalradian of Scotland. J. Geol. Soc. Lond. **151**. 209-212.
- Taubeneck, W. H., 1967, Notes on the Glencoe subsidence, Argyllshire, Scotland. Geol. Soc. Am. Bull. **78**. 1295-1316.
- Taylor, H. P., 1980, The effects of assimilation of country rocks by magmas on  $^{18}\text{O}/^{16}\text{O}$  and  $^{87}\text{Sr}/^{86}\text{Sr}$  systematics in igneous rocks. Earth Planet. Sci. Lett. **47**. 243-254.
- Taylor, P. N., Jones, N. W. & Moorbath, S., 1984, Isotopic assessment of relative contributions from crust and mantle sources to the magma genesis of Precambrian Granitoid rocks. Phil. Trans. R. Soc. Lond. **A310**. 605-625.
- Teall, J. J. H., 1888, British Petrography, with special reference to Igneous Rocks. London.
- Thirlwall, M. F., 1988, Geochronology of Late Caledonian Magmatism in northern Britain. J. Geol. Soc. Lond. **145**. 951-967.
- Thirlwall, M. F., 1986, Lead isotope evidence for the nature of the mantle beneath Caledonian Scotland. Earth Planet. Sci. Lett. **80**. 55-70.
- Thirlwall, M. F., 1983, Isotope geochemistry and origin of calc-alkaline lavas from a Caledonian continental margin volcanic arc. J. Volcanol. Geotherm. Res. **18**. 589-631.
- Thirlwall, M. F., 1982, Systematic variations in chemistry and Nd-Sr isotopes across a Caledonian calc-alkaline volcanic arc: implications for source materials. Earth Planet. Sci. Lett. **58**. 27-50.
- Thirlwall, M. F., 1981, Implications for Caledonian plate tectonic models of chemical data from volcanic rocks of the British Old Red Sandstone. J. Geol. Soc. Lond. **138**. 123-138.
- Thirlwall, M. F., 1979, The petrochemistry of the British Old Red Sandstone volcanic province. Unpublished thesis University of Edinburgh.
- Thirlwall, M. F. & Burnard, P., 1990, Pb-Sr-Nd isotope and chemical studies of the origin of undersaturated and oversaturated shoshonitic magmas from the Borralan pluton, Assynt, NW. Scotland. J. Geol. Soc. Lond. **145**. 259-270.
- Thirlwall, M. F. & Bluck, B. J., 1984, Sr-Nd isotope and geochemical evidence that the Ballantrae 'ophiolite', SW Scotland is polygenetic. In Gass, I. G., Lipard, S. J. & Shelton, A. W. (eds.) Ophiolites and oceanic lithosphere. Spec. Pub. Geol. Soc. Lond. **13**. 215-230.
- Thirlwall, M. F. & Jones, N. W., 1983, Isotope geochemistry and contamination mechanics of Tertiary lavas from Skye, north west Scotland. In Hawkesworth, C. J. & Norry, M. J. (eds.) Continental Basalts and Mantle xenoliths. Shiva Nantwich.
- Thomas, P. R., 1979, New evidence for a Central Highland Root Zone. In: Harris, A. L., Holland, C. H. & Leake, B. E. (eds.), The Caledonides of the British Isles Reviewed. Spec. Pub. Geol. Soc. London **NO. 8**. 205-212.
- Thompson, R. N. & Fowler, M. B., 1986, Subduction related shoshonitic and ultrapotassic magmatism: a study of Siluro-Ordovician syenites from the Scottish Caledonides. Contrib. Mineral. Petrol. **94**. 507-522.
- Treagus, J. E., 1991, Fault displacements in the Dalradian of the Central Highlands. Scott. J. Geol. **27**. 135-145.

- Treagus, J. E., 1987, The structural evolution of the Dalradian of the Central Highlands of Scotland. *Trans. R. Soc. Edin. Earth Science.* **78.** 1-15.
- Treagus, J. E., 1974, A structural cross-section of the Moine and Dalradian rocks of the Kinlochleven area, Scotland. *J. Geol. Soc. Lond.* **137.** 469-482.
- Tuttle, O. F. & Bowen, N. L., 1958, Origin of granite in the light of experimental studies in the system NaAlSi<sub>3</sub>O<sub>8</sub> - KAlSi<sub>3</sub>O<sub>8</sub> - SiO<sub>2</sub> - H<sub>2</sub>O. *Geol. Soc. Am. Mem.* **74.** 1-153.
- van Breemen, O. & Hawkesworth C. J., 1980, Sm-Nd isotope study of garnets and their metamorphic host rocks. *Trans. R. Soc. Edin. Earth Science.* **71.** 97-102.
- van Breemen, O., Aftalion, M., Pankhurst, R. J. & Richardson, S. W., 1979a, Age of the Glen Dessary syenite. Inverness-shire: Diachronous metamorphism across the Great Glen. *Scott. J. Geol.* **15.** 49-62.
- van Breemen, O., Aftalion, M. & Johnson, M. R. W., 1979b, Age of the Borralan complex, Assynt, and late movements along the Moine thrust zone. *J. Geol. Soc. Lond.* **136.** 489-496.
- Vincent, P. M., Bourdier, J. L. and Boudon, G., 1989, The primitive volcano of Mount Pelée: its construction and partial destruction by flank collapse. *J. Volcanol. Geotherm. Res.* **38.** 1-15.
- Wager, L. R. & Mitchell, R. L., 1951, The distribution of trace elements during strong fractionation of basic magma - a further study of the Skaergaard intrusion on East Greenland. *Geochim. Cosmochim. Acta.* **1.** 1-29.
- Walenczak, Z., 1959, Gallium content in feldspars of the granites and pegmatites of the Karkonosze and Strzegon (Lower Silesia). *Bull. Acad. Polon. Sci. Ser. Sci. Chim. Geol. Geograph.* **7.** 595.
- Walker, G. P. L., 1985, Origin of coarse lithic breccias near ignimbrite source vents. *J. Volcanol. Geotherm. Res.* **25.** 157-171.
- Walker, G. P. L., 1975, A new concept for the evolution of the British Tertiary intrusive centres. *J. Geol. Soc. Lond.* **131.** 121-141.
- Walker, G. P. L., 1973, Lengths of lava flows. *Phil. Trans. R. Soc. Lond.* **274.** 107-118.
- Walker, R. T., 1928, Mineralised Volcanic Explosion Pipes, concluding statement. *Engineering & Mining Journal.* **126.** 895-897.
- Walsh, J. N. & Clarke, E., 1982, The role of fractional crystallisation in the formation of granitic and intermediate rocks of the Beinn Chaisgidle Centre, Mull, Scotland. *Mineral. Mag.* **45.** 247-255.
- Waters, F. G., Cohen, A. S., O'Nions, R. K. & O'Hara, M. J., 1990, Development of Archaean lithosphere deduced from chronology and isotope chemistry of Scourie dykes. *Earth Planet. Sci. Lett.* **97.** 241-255.
- Watson, J., 1984, The ending of the Caledonian orogeny in Scotland. *J. Geol. Soc. Lond.* **141.** 193-214.
- Watson, J. & Dunning, F. W. 1979, Basement-cover relations in the British Caledonides. In: Harris, A. L., Holland, C. H. & Leake, B. E. (eds.), *The Caledonides of the British Isles Reviewed. Spec. Pub. Geol. Soc. London*, **NO. 8.** 67-92.
- Watson, E. B. & Capobianco, C. J., 1981, Phosphorous and the rare earth elements in felsic magmas: an assessment of the role of apatite. *Geochem. Cosmochim. Acta.* **45.** 2349-2358.

- Treagus, J. E., 1987, The structural evolution of the Dalradian of the Central Highlands of Scotland. *Trans. R. Soc. Edin. Earth Science.* **78.** 1-15.
- Treagus, J. E., 1974, A structural cross-section of the Moine and Dalradian rocks of the Kinlochleven area, Scotland. *J. Geol. Soc. Lond.* **137.** 469-482.
- Tuttle, O. F. & Bowen, N. L., 1958, Origin of granite in the light of experimental studies in the system NaAlSi<sub>3</sub>O<sub>8</sub> - KAlSi<sub>3</sub>O<sub>8</sub> - SiO<sub>2</sub> - H<sub>2</sub>O. *Geol. Soc. Am. Mem.* **74.** 1-153.
- van Breemen, O. & Hawkesworth C. J., 1980, Sm-Nd isotope study of garnets and their metamorphic host rocks. *Trans. R. Soc. Edin. Earth Science.* **71.** 97-102.
- van Breemen, O., Aftalion, M., Pankhurst, R. J. & Richardson, S. W., 1979a, Age of the Glen Dessary syenite. Inverness-shire: Diachronous metamorphism across the Great Glen. *Scott. J. Geol.* **15.** 49-62.
- van Breemen, O., Aftalion, M. & Johnson, M. R. W., 1979b, Age of the Borralan complex, Assynt, and late movements along the Moine thrust zone. *J. Geol. Soc. Lond.* **136.** 489-496.
- Vincent, P. M., Bourdier, J. L. and Boudon, G., 1989, The primitive volcano of Mount Pelée: its construction and partial destruction by flank collapse. *J. Volcanol. Geotherm. Res.* **38.** 1-15.
- Wager, L. R. & Mitchell, R. L., 1951, The distribution of trace elements during strong fractionation of basic magma - a further study of the Skaergaard intrusion on East Greenland. *Geochim. Cosmochim. Acta.* **1.** 1-29.
- Walenczak, Z., 1959, Gallium content in feldspars of the granites and pegmatites of the Karkonosze and Strzegon (Lower Silesia). *Bull. Acad. Polon. Sci. Ser. Sci. Chim. Geol. Geograph.* **7.** 595.
- Walker, G. P. L., 1985, Origin of coarse lithic breccias near ignimbrite source vents. *J. Volcanol. Geotherm. Res.* **25.** 157-171.
- Walker, G. P. L., 1975, A new concept for the evolution of the British Tertiary intrusive centres. *J. Geol. Soc. Lond.* **131.** 121-141.
- Walker, G. P. L., 1973, Lengths of lava flows. *Phil. Trans. R. Soc. Lond.* **274.** 107-118.
- Walker, R. T., 1928, Mineralised Volcanic Explosion Pipes, concluding statement. *Engineering & Mining Journal.* **126.** 895-897.
- Walsh, J. N. & Clarke, E., 1982, The role of fractional crystallisation in the formation of granitic and intermediate rocks of the Beinn Chaisgidle Centre, Mull, Scotland. *Mineral. Mag.* **45.** 247-255.
- Waters, F. G., Cohen, A. S., O'Nions, R. K. & O'Hara, M. J., 1990, Development of Archaean lithosphere deduced from chronology and isotope chemistry of Scourie dykes. *Earth Planet. Sci. Lett.* **97.** 241-255.
- Watson, J., 1984, The ending of the Caledonian orogeny in Scotland. *J. Geol. Soc. Lond.* **141.** 193-214.
- Watson, J. & Dunning, F. W. 1979, Basement-cover relations in the British Caledonides. In: Harris, A. L., Holland, C. H. & Leake, B. E. (eds.), *The Caledonides of the British Isles Reviewed. Spec. Pub. Geol. Soc. London*, **NO. 8.** 67-92.
- Watson, E. B. & Capobianco, C. J., 1981, Phosphorous and the rare earth elements in felsic magmas: an assessment of the role of apatite. *Geochem. Cosmochim. Acta.* **45.** 2349-2358.

- Webb, P. C., 1977, Analytical and theoretical Petrology of metamorphic rocks from the aureole of the Ben Nevis Granite, SW Highlands of Scotland. Unpublished thesis Oxford University.
- Weiss, S. F. & Troll, G., 1989, The Ballachulish Igneous Complex, Scotland: Petrography, Mineral Chemistry, and Order of Crystallisation in the Monzodiorite-Quartz Diorite Suite and in the Granite. *J. Petrol.* **30**. 1069-1115.
- Wells, M. K., 1954, The structure of the granophyric quartz-dolerite intrusion of Centre 2, Ardnamurchan, and the problem of net-veining. *Geol. Mag.* **91**. 293-307.
- Westbrook, G. K. & Borradaile, G. J., 1978, The geological significance of magnetic anomalies in the region of Islay. *Scott. J. Geol.* **14**. 213-224.
- Whalen, J. B., Currie, K. L. & Chappell, B. W., 1987, A-type granites: geochemical characteristics, discrimination and petrogenesis. *Contrib. Mineral. Petrol.* **95**. 407-419.
- White, A. J. R. & Chappell, B. W., 1988, Some supracrustal (S-Type) granites of the Lachlan Fold Belt. *Trans. Roy. Soc. Edinburgh.* **79**. 169-181.
- White, A. J. & Chappell, B. W., 1977, Ultrametamorphism and granitoid gneiss. *Tectonophysics* **43**. 7-22.
- Whitehouse, M. J., 1990, Isotopic evolution of the southern Outer Hebrides Lewisian gneiss complex: constraints on Late Archaean source regions and the generation of transposed Pb-Pb palaeoisochrons. *Chem. Geol. (Isotope Geoscience)* **86**. 1-20.
- Whitehouse, M. J., 1989, Sm-Nd evidence for diachronous crustal accretion in the Lewisian complex of northwest Scotland. *Tectonophysics*. **161**. 245-256.
- Whitehouse, M. J., 1988, Granulite facies Nd-isotopic homogenisation in the Lewisian Complex of northwest Scotland. *Nature* **331**. 705-707.
- Wilkin, R. T. & Bornhurst, T. J., 1993, Archaean appinites from the Northern Complex, Michigan. *J. Geol.* **101**. 107-114.
- Williams, D. N., 1985, *Scrambles in Lochaber*. Cicerone Press.
- Winchester, J. A. & Floyd, P. A., 1977, Geochemical discrimination of different magma series and their differentiation products using immobile elements. *Chem. Geol.* **24**. 325-343.
- Wilson, M., 1989, *Igneous Petrogenesis*. Unwin & Hyman. London.
- Wolff, J. A., 1986, Welded-tuff dykes, conduit closure and lava dome growth at the end of pyroclastic eruptions. *J. Volcanol. Geotherm. Res.* **28**. 379-384.
- Wones, D. R. & Eugster, H. P., 1965, Stability of biotite : Experiment, theory and application. *Am. Mineral.* **50**. 1228-1272.
- Wood, D. A., Joron, J. L., Treuil, M., Norry, M. & Tarney, J., 1989, Elemental and Sr isotope variations in basic lavas from Iceland and the surrounding ocean floor. *Contrib. Mineral. Petrol.* **70**. 319-339.
- Wright, A. E. & Bowes, D. R., 1968, Formation of explosion breccias. *Bull. Volc.* **32**. 15-32.
- Wright, T. L., 1974, Presentation and interpretation of chemical data for igneous rocks. *Contrib. Mineral. Petrol.* **48**. 233-248.

- Webb, P. C., 1977, Analytical and theoretical Petrology of metamorphic rocks from the aureole of the Ben Nevis Granite, SW Highlands of Scotland. Unpublished thesis Oxford University.
- Weiss, S. F. & Troll, G., 1989, The Ballachulish Igneous Complex, Scotland: Petrography, Mineral Chemistry, and Order of Crystallisation in the Monzodiorite-Quartz Diorite Suite and in the Granite. *J. Petrol.* **30**. 1069-1115.
- Wells, M. K., 1954, The structure of the granophyric quartz-dolerite intrusion of Centre 2, Ardnamurchan, and the problem of net-veining. *Geol. Mag.* **91**. 293-307.
- Westbrook, G. K. & Borradaile, G. J., 1978, The geological significance of magnetic anomalies in the region of Islay. *Scott. J. Geol.* **14**. 213-224.
- Whalen, J. B., Currie, K. L. & Chappell, B. W., 1987, A-type granites: geochemical characteristics, discrimination and petrogenesis. *Contrib. Mineral. Petrol.* **95**. 407-419.
- White, A. J. R. & Chappell, B. W., 1988, Some supracrustal (S-Type) granites of the Lachlan Fold Belt. *Trans. Roy. Soc. Edinburgh.* **79**. 169-181.
- White, A. J. & Chappell, B. W., 1977, Ultrametamorphism and granitoid gneiss. *Tectonophysics* **43**. 7-22.
- Whitehouse, M. J., 1990, Isotopic evolution of the southern Outer Hebrides Lewisian gneiss complex: constraints on Late Archaean source regions and the generation of transposed Pb-Pb palaeoisochrons. *Chem. Geol. (Isotope Geoscience)* **86**. 1-20.
- Whitehouse, M. J., 1989, Sm-Nd evidence for diachronous crustal accretion in the Lewisian complex of northwest Scotland. *Tectonophysics*. **161**. 245-256.
- Whitehouse, M. J., 1988, Granulite facies Nd-isotopic homogenisation in the Lewisian Complex of northwest Scotland. *Nature* **331**. 705-707.
- Wilkin, R. T. & Bornhurst, T. J., 1993, Archaean appinites from the Northern Complex, Michigan. *J. Geol.* **101**. 107-114.
- Williams, D. N., 1985, *Scrambles in Lochaber*. Cicerone Press.
- Winchester, J. A. & Floyd, P. A., 1977, Geochemical discrimination of different magma series and their differentiation products using immobile elements. *Chem. Geol.* **24**. 325-343.
- Wilson, M., 1989, *Igneous Petrogenesis*. Unwin & Hyman. London.
- Wolff, J. A., 1986, Welded-tuff dykes, conduit closure and lava dome growth at the end of pyroclastic eruptions. *J. Volcanol. Geotherm. Res.* **28**. 379-384.
- Wones, D. R. & Eugster, H. P., 1965, Stability of biotite : Experiment, theory and application. *Am. Mineral.* **50**. 1228-1272.
- Wood, D. A., Joron, J. L., Treuil, M., Norry, M. & Tarney, J., 1989, Elemental and Sr isotope variations in basic lavas from Iceland and the surrounding ocean floor. *Contrib. Mineral. Petrol.* **70**. 319-339.
- Wright, A. E. & Bowes, D. R., 1968, Formation of explosion breccias. *Bull. Volc.* **32**. 15-32.
- Wright, T. L., 1974, Presentation and interpretation of chemical data for igneous rocks. *Contrib. Mineral. Petrol.* **48**. 233-248.

- Wyman, D. A. & Kerrich, R., 1993, Archaean Shoshonitic Lamprophyres of the Abitibi Subprovince, Canada: Petrogenesis, Age and Tectonic Setting. *J. Petrol.* **34**. 1067-1110.
- Yardley, B. W. D., Vine, F. J. & Baldwin, C. T., 1982, The plate tectonic setting of NW Britain and Ireland in late Cambrian and early Ordovician times. *J. Geol. Soc. Lond.* **139**. 455-463.
- Yarr, T. R., 1991, A petrological study of the appinite suite associated with the Ardara Pluton, County Donegal, Ireland. Unpublished thesis University of St Andrews.
- Yoder, H. S. & Tilley, C. E., 1962, Origin of basalt magmas: an experimental study of natural and synthetic rock systems. *J. Petrol.* **3**. 342-532.
- Zindler, A. & Hart, S. R., 1986, Chemical Geodynamics. *Annual Reviews of Earth & Planetary Science* **14**. 493-571.
- Zhou, J. X. 1987, An occurrence of shoshonites near Kilmelford in the Scottish Caledonides and its tectonic implications. *J. Geol. Soc. Lond.* **144**. 699-706.

- Wyman, D. A. & Kerrich, R., 1993, Archaean Shoshonitic Lamprophyres of the Abitibi Subprovince, Canada: Petrogenesis, Age and Tectonic Setting. *J. Petrol.* **34**. 1067-1110.
- Yardley, B. W. D., Vine, F. J. & Baldwin, C. T., 1982, The plate tectonic setting of NW Britain and Ireland in late Cambrian and early Ordovician times. *J. Geol. Soc. Lond.* **139**. 455-463.
- Yarr, T. R., 1991, A petrological study of the appinite suite associated with the Ardara Pluton, County Donegal, Ireland. Unpublished thesis University of St Andrews.
- Yoder, H. S. & Tilley, C. E., 1962, Origin of basalt magmas: an experimental study of natural and synthetic rock systems. *J. Petrol.* **3**. 342-532.
- Zindler, A. & Hart, S. R., 1986, Chemical Geodynamics. *Annual Reviews of Earth & Planetary Science* **14**. 493-571.
- Zhou, J. X. 1987, An occurrence of shoshonites near Kilmelford in the Scottish Caledonides and its tectonic implications. *J. Geol. Soc. Lond.* **144**. 699-706.

# Appendix I

## Sample Location

Grid references quoted correspond to the 1:25.000 Mountainmaster of Ben Nevis and the Grey Corries, Outdoor Leisure 32; and should all be prefixed by the grid letters NN.

<u>Sample</u>	<u>Type</u>	<u>Grid Ref</u>	<u>Description</u>
OBN11A	FQD	171 771	Allt Daimh
OBN13	FQD	172 770	Allt Daimh
BN6	FQD	147 763	Quarry
BN172	FQD	140 756	Allt Mhuillin
84BN33	FQD	147 763	Allt Creige Duibhe
84BN34	FQD	147 762	Allt Creige Duibhe
84BN35	FQD	148 761	Allt Creige Duibhe
BN378FQD	FQD	194 763	Sgurr Finnisg-aig
BN378b	SFQD	194 763	Sgurr Finnisg-aig
SURGE	CQD	136 748	Surge Chamber
OBN1	CQD	130 728	Allt Carnach
OBN5	CQD	132 735	Meall an t Suidhe
BN68b	CQD	155 764	Creag Dhubh
BN174	CQD	141 756	Allt Mhuillin
BN177	CQD	145 754	Allt Mhuillin
84BN36	CQD	149 759	Allt Creige Duibhe
84BN37	CQD	149 759	Allt Creige Duibhe
84BN38	CQD	155 738	Allt Creige Duibhe
OBN35P	POG	155 736	Allt Mhuillin
BNQ	POG	157 762	Adit/Quarry
BNQ2	POG	157 762	Adit/Quarry
BN155	POG	178 763	Allt an t Sneachda
BN175	POG	145 751	Allt Mhuillin
BN321	POG	186 726	Allt Daimh
BN323/POG	POG	179 738	Allt Daimh
BN325	POG	177 746	Allt Daimh
BN327	POG	147 748	Allt Mhuillin
BN328	POG	151 743	Allt Mhuillin
BN374	POG	148 739	Coire Dubh
BN394	POG	182 763	Nameless burn
BN416	POG	180 750	Meall Beag
BN417	POG	186 742	Leac-an-t-Sneachda
BN418	POG	192 729	Aonach Mor
BN430	POG	184 733	Allt Daimh
84BN42	POG	148 749	Allt Mhuillin
BN366	MARG POG	198 730	Bealach
BN420	MARG POG	184 722	W. Seang Aonach Mor
BN419	MARG POG	193 723	E. Seang Aonach Mor
GLEN	IG	167 721	Allt Coire Eoghainn
OBN9	IG	144 721	Tourist path
OBN35G	IG	155 736	Allt Mhuillin
OBN36	IG	168 721	Allt Mhuillin
BN191	IG	155 703	Coire Ghaimhnean
BN194	IG	164 700	Coire Eoghainn
BN310	IG	176 716	Coire Leis
BN311	IG	175 713	Carn Mor Dearg Arete
BN313	IG	178 722	Carn Mor Dearg Arete
BN314	IG	174 736	Carn Dearg Meadhonach
BN315	IG	174 732	Carn Dearg Meadhonach-Carn Beag Dearg
BN316	IG	173 736	Carn Beag Dearg
BN322	IG	183 733	Allt Daimh
BN323	IG	179 738	Allt Daimh
BN324	IG	177 745	Allt Daimh
BN326	IG	159 732	Allt Mhuillin
BN362/1	IG	152 711	Coire Ghaimhnean
BN421A	IG	185 727	Allt Daimh
BN432	IG	185 726	Allt Daimh
83BN9	IG	172 720	Allt Mhuillin
83BN14	IG	156 736	Allt Mhuillin
83BN15	IG	172 716	Coire Leis
83BN16	IG	168 725	Allt Mhuillin
BN242	FF	171 712	Coire Leis
BN362/3	FF	152 711	Coire Ghaimhnean
OBN35I	sliver	155 736	Allt Mhuillin

<u>Sample</u>	<u>Type</u>	<u>Grid Ref</u>	<u>Description</u>
BN427	sliver	183 736	Allt Daimh
BN381	Felsite	180 767	Nameless burn
OBN46	Dyke	136 719	Tourist Path
BN118C	Dyke	134 716	Red Burn
BN188/5	Dyke	140 705	Allt Coire Ghaimhnean
BN323/d	Dyke	179 738	Allt Daimh
BN365	Dyke	205 732	Stob an Cul Choire
BN378	Dyke	194 763	Sgurr Finnisg-aig
BN383	Dyke	181 766	Nameless burn
BN401	Dyke	205 769	Allt Chaille-Rais
BN391	Lamprophyre	181 764	Nameless burn
BN400	Lamprophyre	205 770	Allt Chaille-Rais
BN170	Appinite	138 749	Surge chamber
BN405b	Appinite	195 752	Coire nan Each
BN412	Granite sill	197 727	An Cul Choire
BN431	QD SILL	189 727	Allt Daimh
TOWER	VP AND	164 714	Great Tower
BN20	VP AND	164 713	Summit plateau
BN206	VP AND	167 721	CIC hut
BN211	VP AND	165 722	Coire na Ciste
BN212	VP AND	164 721	Coire na Ciste
BN222	VP AND	167 713	Summit outcrop
BN234/b	VP AND	165 717	Coire na Ciste
BN245	VP AND	165 721	Coire na Ciste
BN247	VP AND	164 720	Coire na Ciste
BN263	VP AND	164 720	Coire Leis
BN267	VP AND	168 718	Coire na Ciste
BN269	VP AND	167 716	Coire na Ciste
BN277/1	VP AND	162 721	Ledge route
BN281	VP AND	162 718	Coire na Ciste
BN292	VP AND	168 717	Gardyloo
BN296/a	VP AND	168 718	Gardyloo
BN300	VP AND	171 714	Coire Leis
BN307	VP AND	168 735	Coire Leis
BN362/9	VP AND	152 711	Coire Ghaimhnean
83BN1	VP AND	167 711	summit
83BN2	VP AND	169 714	Eagle Ridge
83BN3	VP AND	166 713	summit
83BN4	VP AND	162 713	summit path
83BN5	VP AND	158 713	summit path
83BN6	VP AND	157 716	summit plateau
83BN7	VP AND	155 717	top of Red Burn
83BN8	VP AND	171 717	NE Buttress
83BN10	VP AND	167 721	CIC hut slabs
83BN11	VP AND	165 723	Carn Dearg slabs
BN362/10	VP AND	152 711	Coire Ghaimhnean
BN279/main	VP Dome	160 722	Ledge route
BN279/pipe	VP Feeder	160 722	Ledge route
CL	Clast	167 721	CIC Slabs
INT	Intrusion	166 691	CIC Slabs
BN259	Intrusion	165 728	Coire na Ciste slabs
BN197SEDI	Sediment	169 720	Allt Mhuillin
BN200s	Sediment	172 715	Coire Leis
BN215	Sediment	162 731	ledge route
BN277/br	VP Breccia	162 721	Ledge route
BN299/b	VP Breccia	172 715	Coire Leis
83BN12	VP Breccia	160 726	Eagle Ridge
BN256	VP Breccia	171 717	Coire Leis
BN288/a	VP BR Clast	160 726	Castle Coire
BN288/b	VP BR Clast	160 726	Castle Coire

### Key.

FQD - Fine Quartz Diorite  
 SFQD - Sgurr Finnisg-aig Quartz Diorite  
 CQD - Coarse Quartz Diorite  
 POG - Porphyritic Outer Granite  
 MARG POG - Marginal variant of POG  
 IG - Inner Granite

Sliver - Quartz diorite outcropping between the  
 POG and IG  
 FF - Fault Facies  
 VP AND - Andesite  
 VP Breccia - Volcanic breccia  
 VP BR Clast - Clast from VP Breccia

## **Appendix II**

### **Electron Microprobe Analysis**

The microprobe analysis of the major phases were made on a JEOL 733 Superprobe equipped with WDS operating at 15kV and 20nA. A focused beam was used for all minerals. Count times were 10s on peak and 5s on two background positions. The following standards were used; wollastonite (Si, Ca), corundum (Al), rutile (Ti), metal (Fe, Mn), periclase (Mg), Albite (Na) and Orthoclase (K). Apparent concentrations were corrected using standard ZAF techniques.

The majority of microprobe analyses were obtained from relatively fresh phenocrysts.

Volcanic amphiboles from the Ben Nevis Complex

Sample	BN210								
Rock Type	Andesite								
SiO2	43.15	42.87	42.01	42.37	41.18	42.37	45.63	41.93	40.61
TiO2	2.22	2.66	2.95	2.11	2.54	2.74	2.33	2.37	2.84
Al2O3	10.62	10.98	11.34	11.49	11.71	11.44	8.01	11.38	12.26
Fe2O3	7.29	6.69	6.97	7.84	4.94	3.57	6.15	7.33	4.16
FeO	4.18	5.24	4.2	5.21	7.27	6.16	4.89	3.11	8.5
MnO	0.14	0.22	0.16	0.15	0.09	0.04	0.23	0.1	0.2
MgO	15.24	14.77	14.52	13.91	13.63	15.05	15.3	15.45	12.93
CaO	11.63	11.71	11.08	11.36	11.75	11.86	10.92	11.49	11.71
Na2O	2.39	2.48	2.47	2.51	2.47	2.56	2.01	2.38	2.41
K2O	0.65	0.66	0.68	0.59	0.72	0.63	0.65	1.05	1.06
CalcTotal	97.51	98.28	96.38	97.54	96.3	96.42	96.12	96.59	96.68
Si	6.28	6.21	6.18	6.2	6.14	6.23	6.68	6.15	6.07
Al	1.82	1.88	1.97	1.98	2.06	1.98	1.38	1.97	2.16
Fe3	0.8	0.73	0.77	0.86	0.55	0.4	0.68	0.81	0.47
Fe2	0.51	0.64	0.52	0.64	0.91	0.76	0.6	0.38	1.06
Mg	3.3	3.19	3.18	3.03	3.03	3.3	3.34	3.38	2.88
Ca	1.81	1.82	1.75	1.78	1.88	1.87	1.71	1.81	1.87
Na	0.67	0.7	0.7	0.71	0.71	0.73	0.57	0.68	0.7
K	0.12	0.12	0.13	0.11	0.14	0.12	0.12	0.2	0.2
Ti	0.24	0.29	0.33	0.23	0.29	0.3	0.26	0.26	0.32
Mn	0.02	0.03	0.02	0.02	0.01	0.01	0.03	0.01	0.03
Total Cations	15.57	15.61	15.55	15.56	15.72	15.7	15.37	15.65	15.76

Volcanic amphiboles from the Ben Nevis Complex

| BN210<br>Andesite |
|-------------------|-------------------|-------------------|-------------------|-------------------|-------------------|-------------------|
| 44.53             | 41.8              | 42.28             | 41.39             | 41.44             | 41.26             | 42.46             |
| 2.51              | 2.51              | 2.25              | 3.03              | 2.77              | 2.19              | 1.71              |
| 8.65              | 11.31             | 11.02             | 10.97             | 10.7              | 11.35             | 10.58             |
| 5.42              | 5.2               | 3.83              | 4.05              | 6.12              | 5.2               | 6.16              |
| 5.92              | 5.54              | 7.65              | 6.73              | 5.39              | 5.39              | 6.6               |
| 0.31              | 0.08              | 0.24              | 0.05              | 0.13              | 0.05              | 0.26              |
| 15.1              | 14.76             | 13.94             | 14.25             | 14.18             | 14.53             | 13.43             |
| 11.32             | 11.61             | 11.72             | 11.68             | 11.42             | 11.61             | 11.31             |
| 2.28              | 2.56              | 2.5               | 2.32              | 2.27              | 2.3               | 2.17              |
| 0.73              | 0.84              | 0.71              | 0.64              | 0.56              | 0.93              | 0.77              |
| 96.77             | 96.21             | 96.14             | 95.11             | 94.98             | 94.81             | 95.45             |
| 6.53              | 6.19              | 6.29              | 6.21              | 6.21              | 6.19              | 6.36              |
| 1.5               | 1.97              | 1.93              | 1.94              | 1.89              | 2.01              | 1.87              |
| 0.6               | 0.58              | 0.43              | 0.46              | 0.69              | 0.59              | 0.69              |
| 0.73              | 0.69              | 0.95              | 0.84              | 0.68              | 0.68              | 0.83              |
| 3.3               | 3.26              | 3.09              | 3.19              | 3.17              | 3.25              | 3                 |
| 1.78              | 1.84              | 1.87              | 1.88              | 1.83              | 1.87              | 1.81              |
| 0.65              | 0.74              | 0.72              | 0.67              | 0.66              | 0.67              | 0.63              |
| 0.14              | 0.16              | 0.14              | 0.12              | 0.11              | 0.18              | 0.15              |
| 0.28              | 0.28              | 0.25              | 0.34              | 0.31              | 0.25              | 0.19              |
| 0.04              | 0.01              | 0.03              | 0.01              | 0.02              | 0.01              | 0.03              |
| 15.55             | 15.72             | 15.7              | 15.66             | 15.57             | 15.7              | 15.56             |

Plagioclase from the Ben Nevis Complex

Sample	OBN11a	BN68b	BN68b						
Rock Type	FQD	COQ	COQ						
SiO <sub>2</sub>	56.2	61	60.2	62	63	56.5	61	59.9	59.78
TiO <sub>2</sub>	0.16	0	0.05	0	0.01	0.12	0.13	0	0.03
Al <sub>2</sub> O <sub>3</sub>	27.3	24.5	25.4	24.4	24.8	26.8	24.4	24.41	24
FeO	0.18	0.16	0.11	0.11	0.17	0.22	1.27	0.1	0.03
MnO	0.01	0.01	0	0.04	0.01	0.06	0	0	0.01
MgO	0.05	0	0	0	0.01	0.01	0.01	0.08	0.09
CaO	9.29	5.72	6.79	5.5	4.84	8.72	5.63	6.14	5.99
Na <sub>2</sub> O	6.19	7.62	7.51	8.21	8.17	6.53	7.52	7.9	8.56
K <sub>2</sub> O	0.27	0.38	0.29	0.46	0.25	0.25	0.42	0.32	0.21
Total	99.7	99.5	100	101	101	99.1	100	98.85	98.7
Si	10.15	10.89	10.69	10.94	11	10.24	10.84	10.79	10.8
Al	5.81	5.16	5.32	5.07	5.1	5.72	5.11	5.18	5.11
Fe <sub>2</sub>	0.03	0.02	0.02	0.02	0.03	0.03	0.19	0.01	0.01
Mg	0.01	0	0	0	0	0	0	0.02	0.02
Ca	1.8	1.09	1.29	1.04	0.91	1.69	1.07	1.19	1.16
Na	2.17	2.64	2.59	2.81	2.77	2.29	2.59	2.76	3
K	0.06	0.09	0.07	0.1	0.06	0.06	0.1	0.07	0.05
Ti	0.02	0	0.01	0	0	0.02	0.02	0	0
Mn	0	0	0	0.01	0	0.01	0	0	0
Total Cat	20.04	19.89	19.97	19.98	19.86	20.06	19.93	20.03	20.16

Plagioclase from the Ben Nevis Complex

BN29 POG	BN210 Andesite	BN210 Andesite	BN210 Andesite						
64.81	62.99	61.79	61.72	59.64	60.62	62.42	57.43	59.18	60.98
0	0.01	0	0.01	0.05	0.06	0.02	0	0.07	0
22.85	24.04	23.7	23.95	24.5	25.23	24.2	25.71	24.44	23.74
0.13	0.19	0.15	0.22	0.2	0.21	0.22	0.35	0.29	0.15
0.05	0	0.03	0.01	0	0.03	0.01	0	0	0
0	0	0.01	0.02	0.03	0.02	0	0.05	0.02	0
3.18	4.76	4.94	4.97	6.68	6.49	4.95	7.73	6.04	5.16
8.92	7.4	8.13	8.1	7.88	7.98	8.36	6.95	8.22	8.28
0.32	0.38	0.54	0.55	0.41	0.32	0.33	0.52	0.25	0.7
100.27	99.88	99.3	99.57	99.42	101.21	100.52	98.73	98.52	99.02
11.37	11.13	11.03	11	10.73	10.71	11.01	10.44	10.73	10.96
4.73	5.01	4.99	5.03	5.19	5.26	5.03	5.51	5.22	5.03
0.02	0.03	0.02	0.03	0.03	0.03	0.03	0.05	0.05	0.02
0	0	0	0.01	0.01	0.01	0	0.01	0.01	0
0.6	0.9	0.95	0.95	1.29	1.23	0.94	1.51	1.17	0.99
3.03	2.53	2.82	2.8	2.75	2.74	2.86	2.45	2.89	2.89
0.07	0.09	0.12	0.12	0.1	0.07	0.07	0.12	0.06	0.16
0	0	0	0	0.01	0.01	0	0	0.01	0
0.01	0	0.01	0	0	0.01	0	0	0	0
19.82	19.68	19.94	19.95	20.09	20.06	19.94	20.09	20.13	20.05

Volcanic amphiboles of the Ben Nevis Complex

Sample	BN210								
Rock Type	Andesite								
SiO2	43.15	42.87	42.01	42.37	41.18	42.37	45.63	41.93	40.61
TiO2	2.22	2.66	2.95	2.11	2.54	2.74	2.33	2.37	2.84
Al2O3	10.62	10.98	11.34	11.49	11.71	11.44	8.01	11.38	12.26
Fe2O3	7.29	6.69	6.97	7.84	4.94	3.57	6.15	7.33	4.16
FeO	4.18	5.24	4.20	5.21	7.27	6.16	4.89	3.11	8.50
MnO	0.14	0.22	0.16	0.15	0.09	0.04	0.23	0.10	0.20
MgO	15.24	14.77	14.52	13.91	13.63	15.05	15.30	15.45	12.93
CaO	11.63	11.71	11.08	11.36	11.75	11.86	10.92	11.49	11.71
Na2O	2.39	2.48	2.47	2.51	2.47	2.56	2.01	2.38	2.41
K2O	0.65	0.66	0.68	0.59	0.72	0.63	0.65	1.05	1.06
Total	97.51	98.28	96.38	97.54	96.30	96.42	96.12	96.59	96.68
Si	6.28	6.21	6.18	6.20	6.14	6.23	6.68	6.15	6.07
Al	1.82	1.88	1.97	1.98	2.06	1.98	1.38	1.97	2.16
Fe3	0.80	0.73	0.77	0.86	0.55	0.40	0.68	0.81	0.47
Fe2	0.51	0.64	0.52	0.64	0.91	0.76	0.60	0.38	1.06
Mg	3.30	3.19	3.18	3.03	3.03	3.30	3.34	3.38	2.88
Ca	1.81	1.82	1.75	1.78	1.88	1.87	1.71	1.81	1.87
Na	0.67	0.70	0.70	0.71	0.71	0.73	0.57	0.68	0.70
K	0.12	0.12	0.13	0.11	0.14	0.12	0.12	0.20	0.20
Ti	0.24	0.29	0.33	0.23	0.29	0.30	0.26	0.26	0.32
Mn	0.02	0.03	0.02	0.02	0.01	0.01	0.03	0.01	0.03
Total Cations	15.57	15.61	15.55	15.56	15.72	15.70	15.37	15.65	15.76

## Volcanic amphiboles of the Ben Nevis Complex

| BN210<br>Andesite |
|-------------------|-------------------|-------------------|-------------------|-------------------|-------------------|-------------------|
| 44.53             | 41.80             | 42.28             | 41.39             | 41.44             | 41.26             | 42.46             |
| 2.51              | 2.51              | 2.25              | 3.03              | 2.77              | 2.19              | 1.71              |
| 8.65              | 11.31             | 11.02             | 10.97             | 10.70             | 11.35             | 10.58             |
| 5.42              | 5.20              | 3.83              | 4.05              | 6.12              | 5.20              | 6.16              |
| 5.92              | 5.54              | 7.65              | 6.73              | 5.39              | 5.39              | 6.60              |
| 0.31              | 0.08              | 0.24              | 0.05              | 0.13              | 0.05              | 0.26              |
| 15.10             | 14.76             | 13.94             | 14.25             | 14.18             | 14.53             | 13.43             |
| 11.32             | 11.61             | 11.72             | 11.68             | 11.42             | 11.61             | 11.31             |
| 2.28              | 2.56              | 2.50              | 2.32              | 2.27              | 2.30              | 2.17              |
| 0.73              | 0.84              | 0.71              | 0.64              | 0.56              | 0.93              | 0.77              |
| 96.77             | 96.21             | 96.14             | 95.11             | 94.98             | 94.81             | 95.45             |
| 6.53              | 6.19              | 6.29              | 6.21              | 6.21              | 6.19              | 6.36              |
| 1.50              | 1.97              | 1.93              | 1.94              | 1.89              | 2.01              | 1.87              |
| 0.60              | 0.58              | 0.43              | 0.46              | 0.69              | 0.59              | 0.69              |
| 0.73              | 0.69              | 0.95              | 0.84              | 0.68              | 0.68              | 0.83              |
| 3.30              | 3.26              | 3.09              | 3.19              | 3.17              | 3.25              | 3.00              |
| 1.78              | 1.84              | 1.87              | 1.88              | 1.83              | 1.87              | 1.81              |
| 0.65              | 0.74              | 0.72              | 0.67              | 0.66              | 0.67              | 0.63              |
| 0.14              | 0.16              | 0.14              | 0.12              | 0.11              | 0.18              | 0.15              |
| 0.28              | 0.28              | 0.25              | 0.34              | 0.31              | 0.25              | 0.19              |
| 0.04              | 0.01              | 0.03              | 0.01              | 0.02              | 0.01              | 0.03              |
| 15.55             | 15.72             | 15.70             | 15.66             | 15.57             | 15.70             | 15.56             |

Pyroxenes from the Ben Nevis Complex

Sample	OBN11a	BN68b	BN68b						
Rock Type	FQD	CGD	CGD						
SiO2	56.20	61.00	60.20	62.00	63.00	56.50	61.00	59.90	59.78
TiO2	0.16	0.00	0.05	0.00	0.01	0.12	0.13	0.00	0.03
Al2O3	27.30	24.50	25.40	24.40	24.80	26.80	24.40	24.41	24.00
FeO	0.18	0.16	0.11	0.11	0.17	0.22	1.27	0.10	0.03
MnO	0.01	0.01	0.00	0.04	0.01	0.06	0.00	0.00	0.01
MgO	0.05	0.00	0.00	0.00	0.01	0.01	0.01	0.08	0.09
CaO	9.29	5.72	6.79	5.50	4.84	8.72	5.63	6.14	5.99
Na2O	6.19	7.62	7.51	8.21	8.17	6.53	7.52	7.90	8.56
K2O	0.27	0.38	0.29	0.46	0.25	0.25	0.42	0.32	0.21
Total	99.70	99.50	100.00	101.00	101.00	99.10	100.00	98.85	98.70
Si	10.15	10.89	10.69	10.94	11.00	10.24	10.84	10.79	10.80
Al	5.81	5.16	5.32	5.07	5.10	5.72	5.11	5.18	5.11
Fe2	0.03	0.02	0.02	0.02	0.03	0.03	0.19	0.01	0.01
Mg	0.01	0.00	0.00	0.00	0.00	0.00	0.00	0.02	0.02
Ca	1.80	1.09	1.29	1.04	0.91	1.69	1.07	1.19	1.16
Na	2.17	2.64	2.59	2.81	2.77	2.29	2.59	2.76	3.00
K	0.06	0.09	0.07	0.10	0.06	0.06	0.10	0.07	0.05
Ti	0.02	0.00	0.01	0.00	0.00	0.02	0.02	0.00	0.00
Mn	0.00	0.00	0.00	0.01	0.00	0.01	0.00	0.00	0.00
Total Cat	20.04	19.89	19.97	19.98	19.86	20.06	19.93	20.03	20.16

## Pyroxenes from the Ben Nevis Complex

BN29	BN29	BN29	BN29	BN29	BN29	BN29	BN210	BN210	BN210
POG	POG	POG	POG	POG	POG	POG	Andesite	Andesite	Andesite
64.81	62.99	61.79	61.72	59.64	60.62	62.42	57.43	59.18	60.98
0.00	0.01	0.00	0.01	0.05	0.06	0.02	0.00	0.07	0.00
22.85	24.04	23.70	23.95	24.50	25.23	24.20	25.71	24.44	23.74
0.13	0.19	0.15	0.22	0.20	0.21	0.22	0.35	0.29	0.15
0.05	0.00	0.03	0.01	0.00	0.03	0.01	0.00	0.00	0.00
0.00	0.00	0.01	0.02	0.03	0.02	0.00	0.05	0.02	0.00
3.18	4.76	4.94	4.97	6.68	6.49	4.95	7.73	6.04	5.16
8.92	7.40	8.13	8.10	7.88	7.98	8.36	6.95	8.22	8.28
0.32	0.38	0.54	0.55	0.41	0.32	0.33	0.52	0.25	0.70
100.27	99.88	99.30	99.57	99.42	101.21	100.52	98.73	98.52	99.02
11.37	11.13	11.03	11.00	10.73	10.71	11.01	10.44	10.73	10.96
4.73	5.01	4.99	5.03	5.19	5.26	5.03	5.51	5.22	5.03
0.02	0.03	0.02	0.03	0.03	0.03	0.03	0.05	0.05	0.02
0.00	0.00	0.00	0.01	0.01	0.01	0.00	0.01	0.01	0.00
0.60	0.90	0.95	0.95	1.29	1.23	0.94	1.51	1.17	0.99
3.03	2.53	2.82	2.80	2.75	2.74	2.86	2.45	2.89	2.89
0.07	0.09	0.12	0.12	0.10	0.07	0.07	0.12	0.06	0.16
0.00	0.00	0.00	0.00	0.01	0.01	0.00	0.00	0.01	0.00
0.01	0.00	0.01	0.00	0.00	0.01	0.00	0.00	0.00	0.00
19.82	19.68	19.94	19.95	20.09	20.06	19.94	20.09	20.13	20.05

Pyroxenes from the Ben Nevis Complex

BN210 Andesite	BN140 Ignimbrite								
60.52	55.52	60.75	61.66	55.64	56.18	53.99	56.96	58.42	54.89
0.02	0.10	0.03	0.00	0.04	0.03	0.02	0.04	0.04	0.03
23.81	27.66	25.08	24.87	27.01	27.01	28.21	26.78	25.68	27.80
0.15	0.45	0.34	0.24	0.32	0.30	0.28	0.38	0.44	0.42
0.00	0.00	0.00	0.04	0.00	0.00	0.00	0.02	0.03	0.00
0.02	0.03	0.01	0.02	0.14	0.00	0.01	0.00	0.01	0.01
5.35	9.84	6.16	5.76	9.23	8.97	10.78	8.76	7.49	9.97
8.54	6.01	7.96	8.16	6.00	6.45	5.49	6.81	7.21	6.03
0.49	0.13	0.89	0.15	0.16	0.26	0.31	0.22	0.23	0.17
98.91	99.80	100.53	100.91	98.71	99.21	99.14	100.01	99.54	99.38
10.90	10.04	10.74	10.86	10.15	10.19	9.86	10.25	10.51	9.98
5.06	5.89	5.23	5.16	5.81	5.77	6.07	5.68	5.45	5.96
0.02	0.07	0.05	0.04	0.05	0.05	0.04	0.06	0.07	0.06
0.01	0.01	0.00	0.01	0.04	0.00	0.00	0.00	0.00	0.00
1.03	1.91	1.17	1.09	1.80	1.74	2.11	1.69	1.44	1.94
2.98	2.11	2.73	2.79	2.12	2.27	1.94	2.38	2.51	2.13
0.11	0.03	0.20	0.03	0.04	0.06	0.07	0.05	0.05	0.04
0.00	0.01	0.00	0.00	0.01	0.01	0.00	0.01	0.01	0.00
0.00	0.00	0.00	0.01	0.00	0.00	0.00	0.00	0.01	0.00
20.12	20.07	20.11	19.97	20.02	20.08	20.11	20.11	20.05	20.12

## Pyroxenes from the Ben Nevis Complex

| BN140<br>Ignimbrite |
|---------------------|---------------------|---------------------|---------------------|---------------------|---------------------|---------------------|---------------------|---------------------|---------------------|
| 57.78               | 56.12               | 54.70               | 53.63               | 56.93               | 56.93               | 58.75               | 54.96               | 55.08               | 57.11               |
| 0.05                | 0.04                | 0.02                | 0.08                | 0.06                | 0.02                | 0.03                | 0.00                | 0.06                | 0.05                |
| 26.09               | 27.18               | 28.07               | 28.26               | 26.09               | 26.68               | 25.89               | 27.85               | 28.03               | 26.59               |
| 0.44                | 0.37                | 0.32                | 0.47                | 0.42                | 0.42                | 0.30                | 0.63                | 0.52                | 0.49                |
| 0.02                | 0.00                | 0.00                | 0.00                | 0.01                | 0.00                | 0.00                | 0.00                | 0.01                | 0.00                |
| 0.06                | 0.02                | 0.00                | 0.07                | 0.00                | 0.01                | 0.00                | 0.06                | 0.04                | 0.00                |
| 8.25                | 9.29                | 10.32               | 11.33               | 8.50                | 8.62                | 7.75                | 10.66               | 10.93               | 8.68                |
| 6.87                | 6.29                | 5.35                | 5.30                | 6.18                | 6.40                | 6.90                | 5.78                | 4.23                | 6.66                |
| 0.28                | 0.13                | 0.14                | 0.19                | 1.32                | 0.20                | 0.28                | 0.15                | 0.16                | 0.23                |
| 99.84               | 99.48               | 98.96               | 99.39               | 99.57               | 99.28               | 99.90               | 100.10              | 99.07               | 99.81               |
| 10.39               | 10.16               | 9.97                | 9.79                | 10.33               | 10.29               | 10.52               | 9.94                | 10.00               | 10.29               |
| 5.53                | 5.80                | 6.03                | 6.08                | 5.58                | 5.68                | 5.46                | 5.94                | 6.00                | 5.65                |
| 0.07                | 0.06                | 0.05                | 0.07                | 0.06                | 0.06                | 0.05                | 0.10                | 0.08                | 0.07                |
| 0.02                | 0.01                | 0.00                | 0.02                | 0.00                | 0.00                | 0.00                | 0.02                | 0.01                | 0.00                |
| 1.59                | 1.80                | 2.02                | 2.22                | 1.65                | 1.67                | 1.49                | 2.07                | 2.13                | 1.68                |
| 2.40                | 2.21                | 1.89                | 1.88                | 2.18                | 2.24                | 2.39                | 2.03                | 1.49                | 2.33                |
| 0.07                | 0.03                | 0.03                | 0.05                | 0.31                | 0.05                | 0.06                | 0.03                | 0.04                | 0.05                |
| 0.01                | 0.01                | 0.00                | 0.01                | 0.01                | 0.00                | 0.00                | 0.00                | 0.01                | 0.01                |
| 0.00                | 0.00                | 0.00                | 0.00                | 0.00                | 0.00                | 0.00                | 0.00                | 0.00                | 0.00                |
| 20.07               | 20.06               | 19.98               | 20.12               | 20.11               | 20.01               | 19.97               | 20.12               | 19.75               | 20.07               |

Pyroxenes from the Ben Nevis Complex

BN140 Ignimbrite	BN140 Ignimbrite	BN140 Ignimbrite	BN140 Ignimbrite	BN140 Ignimbrite
56.57	52.95	61.15	58.18	60.20
0.02	0.05	0.05	0.06	0.01
26.45	29.09	25.27	26.16	24.81
0.05	0.46	0.38	0.34	0.33
0.04	0.00	0.00	0.05	0.04
0.09	0.04	0.02	0.00	0.04
9.12	11.96	6.30	7.70	6.21
6.45	4.53	7.14	6.75	7.84
0.32	0.08	0.24	0.18	0.28
99.52	99.16	100.56	99.42	99.76
10.26	9.68	10.80	10.46	10.76
5.66	6.27	5.26	5.55	5.23
0.01	0.07	0.06	0.05	0.05
0.03	0.01	0.01	0.00	0.01
1.77	2.34	1.19	1.48	1.19
2.27	1.61	2.45	2.35	2.72
0.08	0.02	0.06	0.04	0.06
0.00	0.01	0.01	0.01	0.00
0.01	0.00	0.00	0.01	0.01
20.08	20.00	19.82	19.95	20.02

Biotites from the Ben Nevis Complex

Sample	OBN11a								
Rock Type	FQD								
SiO2	36.8	36.9	37.3	37.3	37.6	38.0	37.3	37.9	37.9
TiO2	4.6	4.4	4.0	3.8	3.6	3.6	4.0	4.5	3.5
Al2O3	13.7	13.8	13.3	13.6	13.4	13.7	13.1	13.2	13.4
FeO (total)	15.7	15.8	16.4	16.2	15.0	16.2	15.5	15.9	16.1
MnO	0.1	0.0	0.0	0.2	0.2	0.1	0.1	0.1	0.3
MgO	13.4	13.9	13.9	14.0	14.5	14.3	14.6	14.6	14.3
CaO	0.0	0.0	0.0	0.0	0.0	0.0	0.1	0.0	0.0
Na2O	0.2	0.0	0.1	0.0	0.1	0.1	0.1	0.1	0.1
K2O	9.2	9.0	9.0	9.2	9.3	9.2	9.1	7.7	9.2
CalcTotal	93.6	93.8	94.0	94.3	93.8	95.2	93.8	93.9	94.8
Si	5.6	5.6	5.7	5.7	5.7	5.7	5.7	5.7	5.7
Al iv	2.4	2.4	2.3	2.3	2.3	2.3	2.3	2.3	2.3
Al vi	0.1	0.1	0.1	0.1	0.1	0.1	0.0	0.1	0.1
Fe2*	2.0	2.0	2.1	2.1	1.9	2.0	2.0	2.0	2.0
Mg	3.1	3.2	3.2	3.2	3.3	3.2	3.3	3.3	3.2
Ti	0.5	0.5	0.5	0.4	0.4	0.4	0.5	0.5	0.4
Mn	0.0	0.0	0.0	0.0	0.0	0.0	0.0	0.0	0.0
Ca	0.0	0.0	0.0	0.0	0.0	0.0	0.0	0.0	0.0
Na	0.0	0.0	0.0	0.0	0.0	0.0	0.0	0.0	0.0
K	1.8	1.7	1.7	1.8	1.8	1.8	1.8	1.5	1.8
Total Cat	15.5	15.5	15.6	15.6	15.6	15.6	15.6	15.4	15.6



Biotites from the Ben Nevis Complex

OBN5	BN68b	BN68b	BN68b	BN68b	BN68b	BN68b	BN242	BN242	BN170
COO	COO	COO	COO	COO	COO	COO	Fault facies	Fault facies	Appinite
37.3	36.2	35.9	36.4	36.3	35.9	35.8	36.0	36.0	37.8
5.0	3.1	2.9	2.6	3.1	3.2	2.9	4.8	4.8	3.8
13.0	17.3	16.7	17.0	16.7	16.8	17.2	14.2	14.2	14.0
13.8	17.5	17.3	16.6	17.5	17.5	17.7	16.2	16.2	17.9
0.0	0.2	0.1	0.1	0.1	0.1	0.2	0.5	0.5	0.1
14.7	11.5	11.4	11.6	11.7	11.2	11.6	13.0	13.0	13.8
0.0	0.0	0.0	0.0	0.0	0.0	0.0	0.0	0.0	0.0
0.2	0.1	0.1	0.1	0.1	0.1	0.2	0.3	0.3	0.1
9.3	9.0	9.7	9.7	9.7	9.6	9.6	8.6	8.6	9.5
93.3	94.9	93.9	94.1	95.1	94.4	95.0	93.7	93.7	97.0
5.7	5.5	5.5	5.5	5.5	5.5	5.4	5.5	5.5	5.6
2.3	2.5	2.5	2.5	2.5	2.5	2.6	2.5	2.5	2.4
0.0	0.6	0.5	0.6	0.5	0.5	0.5	0.1	0.1	0.1
1.8	2.2	2.2	2.1	2.2	2.2	2.2	2.1	2.1	2.2
3.3	2.6	2.6	2.6	2.6	2.5	2.6	3.0	3.0	3.1
0.6	0.3	0.3	0.3	0.3	0.4	0.3	0.6	0.6	0.4
0.0	0.0	0.0	0.0	0.0	0.0	0.0	0.1	0.1	0.0
0.0	0.0	0.0	0.0	0.0	0.0	0.0	0.0	0.0	0.0
0.1	0.0	0.0	0.0	0.0	0.0	0.1	0.1	0.1	0.0
1.8	1.7	1.9	1.9	1.9	1.9	1.9	1.7	1.7	1.8
15.5	15.5	15.6	15.6	15.6	15.6	15.6	15.5	15.5	15.6

Biotites from the Ben Nevis Complex

BN170 Appinite	BN140 Ignimbrite	BN140 Ignimbrite	BN140 Ignimbrite	BN140 Ignimbrite
37.9	36.6	36.4	37.3	37.6
3.9	3.2	2.5	3.8	3.6
14.3	14.5	15.4	13.6	13.4
17.9	15.3	14.7	16.2	15.0
0.2	0.4	0.3	0.2	0.2
12.9	14.2	15.2	14.0	14.5
0.1	0.1	0.1	0.0	0.0
0.1	0.1	0.2	0.0	0.1
9.4	9.0	8.1	9.2	9.3
96.7	93.4	92.9	94.4	93.7
5.7	5.6	5.5	5.7	5.7
2.3	2.4	2.5	2.3	2.3
0.2	0.2	0.3	0.1	0.1
2.2	2.0	1.9	2.1	1.9
2.9	3.2	3.4	3.2	3.3
0.4	0.4	0.3	0.4	0.4
0.0	0.1	0.0	0.0	0.0
0.0	0.0	0.0	0.0	0.0
0.0	0.0	0.0	0.0	0.0
1.8	1.8	1.6	1.8	1.8
15.6	15.6	15.6	15.6	15.6















## Appendix III

### X-ray Fluorescence Analysis

The sample is prepared first by removing all obvious weathered portions using a grinding wheel. Samples are then crushed in a Tema Tungsten carbide swing mill to a powder of much less than 240 mesh. Major elements were determined from a fused glass bead prepared from 0.5g of rock powder and 2.666g of Spectroflux 105 using ammonium nitrate as an oxidant. Weight loss was determined by weighing before and after fusing of the glass bead. X-Ray analysis was performed on a Philips PW1212 using a Rh tube for primary excitation essentially following the methods of Norrish & Hutton (1969). For major elements, matrix corrections were applied on an iterative basis using an on-line computer. Trace elements were analysed on pressed powder discs prepared by pressing to 12 tons, 6 grams of powder mixed with Moviol as a binder. The elements were excited in a Rh tube and analysed with either Li F200 or Li F220 crystals. All elements were determined by ratio to a monitor for which the composition is accurately known and for the trace elements a mass absorption correction based on major oxide composition was applied. Duplicate samples were run for both major and trace elements.

### XRF Analytical Precision

The precision estimates are based on six replicates on six separate beads or pressed powder pellets (trace elements and MnO) of a granodiorite and the standard deviation values are derived in the manner of Harvey et al. (1973). Precision estimates expressed as wt% for major element oxides and as ppm for trace elements.

Element	Error ( $1\sigma$ )	Element	Error ( $1\sigma$ )
SiO <sub>2</sub>	0.177	Y	1.5
TiO <sub>2</sub>	0.006	Sr	1.8
Al <sub>2</sub> O <sub>3</sub>	0.042	Rb	1.4
Fe <sub>2</sub> O <sub>3</sub>	0.144	Th	4.2
MnO	0.0003	Pb	0.8
MgO	0.035	Zn	0.7
CaO	0.01	Cu	0.8
Na <sub>2</sub> O	0.099	V	0.9
K <sub>2</sub> O	0.13	Ba	8.0
P <sub>2</sub> O <sub>5</sub>	0.011	Ce	2.0
Nb	2.0	La	1.3
Zr	6.9		

The Geochemistry of the Ben Nevis Complex

SAMPLE	0BN11A	0BN13	BN6	BN172	84BN33	84BN34	84BN35	BN378FQD	BN378b	SURGE
TYPE	FQD	FQD	FQD	FQD	FQD	FQD	FQD	FQD	SFQD	COQD
SiO2	58.04	58.02	61.49	59.10	58.80	62.16	59.76	59.31	63.09	52.97
TiO2	1.04	0.94	0.81	0.82	0.96	0.78	0.97	0.99	0.65	1.17
Al2O3	16.58	16.28	15.87	16.35	16.28	15.81	16.44	15.95	18.54	16.49
FeO*	6.61	6.08	5.04	5.62	5.94	4.97	5.88	5.99	4.45	8.17
MnO	0.09	0.08	0.07	0.08	0.11	0.08	0.09	0.08	0.07	0.11
MgO	3.95	4.21	3.21	3.64	4.14	3.17	3.94	3.15	1.66	6.18
CaO	5.77	5.23	4.15	4.63	4.49	3.84	5.13	4.30	3.55	7.36
Na2O	4.15	4.61	4.30	4.36	3.66	4.45	4.40	4.14	4.06	4.06
K2O	2.56	2.62	3.20	2.71	3.71	3.46	3.09	3.56	2.95	1.40
P2O5	0.42	0.34	0.27	0.30	0.33	0.26	0.33	0.32	0.26	0.45
Loss on Fusion	0.93	1.18	2.03	0.80	1.59	2.20	2.36	2.03	2.89	0.56
TOTAL	100.42	99.51	99.31	99.22	100.21	99.98	100.43	99.00	99.08	99.87
Nb	1	2	8	4	6	7	7	9	12	5
Zr	105	114	169	136	146	152	152	197	186	82
Y	13	12	15	14	15	14	14	17	18	16
Sr	1313	1179	1064	1066	1244	980	980	1134	827	1628
U	0	1	0	1	0	2	2	3	1	0
Pb	40	36	76	61	79	72	72	130	84	21
Th	4	4	7	6	6	8	8	8	10	2
Pb	12	10	12	13	20	15	15	24	16	5
Ga	21	21	26	21	21	21	21	23	21	22
Zn	55	46	57	46	63	57	57	71	65	61
Ni	36	65	55	45	48	40	40	5	50	90
Ce	62	55	73	64	66	69	69	63	89	58
Sc	13	13	12	9	14	8	8	6	14	19
V	135	127	93	102	128	94	94	78	118	185
Ba	1293	1287	1219	1308	1380	1154	1154	1113	1104	991
La	32	32	38	32	33	35	35	38	49	31

.310 .

The Geochemistry of the Ben Nevis Complex

OBN1	OBN5	BN68b	BN174	BN177	84BN36	84BN37	84BN38	OBN35P	BNQ	BNQ2
COQ	COQ	COQ	COQ	COQ	COQ	COQ	COQ	POG	POG	POG
60.16	58.16	65.15	58.30	55.53	60.71	61.60	61.68	68.77	67.98	68.23
0.87	0.85	0.68	1.08	1.03	0.86	0.81	0.83	0.44	0.47	0.47
16.23	16.38	16.38	14.76	15.41	16.13	15.94	16.19	15.01	14.70	14.98
5.73	6.33	4.50	6.74	7.75	5.51	5.21	5.21	2.79	2.92	2.98
0.08	0.10	0.06	0.09	0.11	0.09	0.07	0.08	0.05	0.05	0.05
4.04	4.77	2.26	5.21	5.66	3.89	3.29	3.37	1.61	1.67	1.59
4.69	5.68	2.36	5.16	7.13	4.26	4.07	4.51	2.21	2.15	2.51
4.37	4.37	3.62	3.76	3.77	4.53	4.28	4.29	4.20	4.22	4.12
3.07	2.39	3.76	3.16	1.70	3.25	3.49	3.41	4.10	3.92	4.06
0.30	0.36	0.34	0.35	0.36	0.29	0.26	0.28	0.16	0.15	0.16
1.81	1.44	2.02	1.40	0.08	1.94	2.43	2.73	2.52	2.49	3.30
100.50	99.98	100.51	100.02	99.87	100.54	99.82	100.25	100.76	99.51	99.75
7	5	16	11	3	7	8	8	6	11	10
165	114	126	96	60	171	185	206	142	146	144
14	15	41	23	16	15	16	15	11	13	13
985	1274	512	1135	1225	1063	927	1062	582	633	658
1	1	1	3	0	2	1	1	2	2	3
65	48	193	101	31	83	87	80	103	116	117
7	7	5	21	4	10	10	10	15	16	21
14	11	30	8	8	12	15	18	13	13	15
47	35	45	21	20	22	22	22	19	24	23
46	63	72	56	64	60	50	60	0	28	31
64	74	38	72	60	66	54	51	22	27	29
73	73	42	111	65	71	73	73	72	61	63
13	12	21	13	22	10	9	9	0	4	5
105	115	76	133	252	106	90	94	44	44	45
1260	1404	564	1197	890	1317	1186	1290	1146	978	974
38	40	23	59	32	40	42	38	42	40	38

- 311 -

The Geochemistry of the Ben Nevis Complex

BN155	BN175	BN321	BN323/POG	BN325	BN327	BN328	BN374	BN394	BN416	BN417
POG	POG	POG	POG	POG	POG	POG	POG	POG	POG	POG
66.81	67.38	68.66	70.87	68.71	66.38	68.85	66.59	68.00	67.81	67.88
0.51	0.49	0.47	0.36	0.44	0.50	0.44	0.40	0.43	0.46	0.49
14.87	14.84	14.53	14.11	14.51	14.91	14.70	15.95	15.86	14.77	15.19
3.20	2.94	2.77	2.12	2.69	3.16	2.68	2.52	2.56	2.87	3.21
0.04	0.04	0.06	0.06	0.04	0.06	0.04	0.05	0.05	0.05	0.05
1.74	1.73	1.25	0.87	1.37	1.48	1.40	1.31	1.42	1.56	1.60
2.38	2.18	2.12	1.08	2.14	2.13	2.13	2.63	2.22	2.17	2.36
3.87	4.02	5.14	5.47	4.03	5.38	3.89	4.45	4.52	3.94	4.29
4.20	4.09	4.36	4.12	4.19	4.18	4.32	4.06	3.98	4.18	4.22
0.17	0.16	0.19	0.18	0.13	0.20	0.13	0.12	0.13	0.15	0.18
2.82	1.72	3.46	2.84	3.26	2.78	3.09	2.96	2.75	2.23	2.84
99.00	100.08	100.26	100.34	99.05	99.58	99.68	99.06	100.27	99.76	100.67
8	9	10	10	13	11	11	9	9	11	12
167	155	162	122	143	150	156	153	152	148	171
14	14	14	13	14	13	12	17	11	14	15
625	608	615	438	581	689	620	855	769	635	690
2	2	4	6	6	2	3	3	3	3	4
111	111	131	139	132	109	116	96	98	125	117
17	21	18	17	21	18	23	15	12	18	21
14	13	15	16	15	11	18	18	17	16	21
19	19	24	24	24	25	18	19	19	18	18
0	0	30	26	27	24	27	29	33	30	34
25	24	28	23	26	22	26	26	28	30	28
65	67	70	56	63	44	56	61	52	53	71
1	1	2	1	1	3	5	4	4	6	5
47	44	38	28	38	45	40	38	40	46	50
1338	1240	1013	693	968	1098	1074	1180	1068	1032	1131
41	40	44	39	43	39	43	37	33	42	48

The Geochemistry of the Ben Nevis Complex

BN418	BN430	84BN42	BN366	BN419	BN420	GLEN	OBN9	OBN35G	OBN36	BN191
POG	POG	POG	MARG POG	MARG POG	MARG POG	IG	IG	IG	IG	IG
66.38	66.74	69.83	68.08	63.73	65.26	69.62	70.99	70.74	70.49	70.55
0.56	0.49	0.49	0.54	0.60	0.61	0.39	0.40	0.40	0.42	0.39
15.27	15.30	15.17	15.50	15.57	15.55	15.12	15.40	15.59	15.44	14.99
3.61	3.19	2.87	3.78	4.08	3.96	1.97	2.13	2.16	2.17	2.10
0.06	0.05	0.04	0.05	0.07	0.06	0.05	0.04	0.03	0.04	0.06
1.99	1.69	1.58	1.83	2.45	2.27	0.64	0.73	0.63	0.66	0.67
2.63	2.53	2.33	2.06	3.07	2.81	1.24	1.34	1.01	1.07	1.43
4.06	4.16	4.29	3.53	3.99	4.10	4.67	4.74	4.66	5.13	4.90
4.18	3.93	4.20	3.25	3.87	4.03	4.06	3.90	3.92	4.00	3.95
0.18	0.16	0.16	0.18	0.20	0.18	0.10	0.12	0.12	0.12	0.11
2.40	2.68	3.44	1.80	2.27	2.65	2.16	2.78	2.50	2.88	2.23
100.52	99.33	101.56	100.07	99.03	100.03	99.66	100.79	100.56	100.54	100.76
11	10	8	13	10	11	9	8	8	8	7
182	187	144	204	191	208	197	219	216	260	218
19	14	13	20	16	16	14	16	15	17	16
738	710	634	594	838	776	376	404	394	475	511
2	3	3	3	3	4	1	2	2	2	1
117	110	109	181	114	113	91	84	82	97	93
20	19	19	14	13	15	10	11	12	13	11
20	19	10	19	15	15	16	14	11	22	15
21	20	19	20	21	20	16	19	19	19	19
48	42	16	65	53	45	19	0	0	16	26
40	29	22	35	50	45	7	8	7	6	4
76	65	58	56	65	65	74	94	101	112	96
6	6	1	6	8	6	2	0	0	0	0
61	50	41	52	70	63	19	18	17	12	15
1153	1165	1117	910	1308	1226	1313	1488	1545	1431	1715
53	43	37	35	46	42	46	55	59	67	57

The Geochemistry of the Ben Nevis Complex

BN311	BN310	BN313	BN314	BN315	BN316	BN326	BN432	BN421A	83BN9	83BN14
g	g	g	g	g	g	g	g	g	g	g
70.74	70.01	70.40	70.15	70.20	69.91	69.70	70.19	71.95	70.04	70.05
0.44	0.36	0.36	0.37	0.39	0.39	0.38	0.38	0.31	0.39	0.40
15.41	15.08	15.26	14.64	15.10	14.89	15.11	15.28	14.41	14.90	15.19
2.07	2.09	2.09	1.95	2.15	2.16	2.09	2.18	1.66	2.06	2.14
0.04	0.06	0.54	0.05	0.07	0.07	0.07	0.05	0.04	0.05	0.05
0.67	0.71	0.65	0.60	0.42	0.43	0.33	0.70	0.50	0.69	0.66
1.32	1.29	1.41	1.12	1.24	1.30	1.62	1.51	1.05	1.47	1.57
4.93	4.76	4.68	4.35	5.91	5.94	5.91	4.65	4.26	4.78	4.80
4.14	3.91	3.96	4.34	3.96	3.98	3.91	3.95	4.15	3.94	3.94
0.11	0.10	0.11	0.10	0.14	0.14	0.14	0.10	0.06	0.10	0.11
3.60	2.39	3.32	2.82	2.83	2.83	2.76	3.06	3.09	3.03	2.63
100.30	99.79	99.99	99.09	100.57	100.22	100.27	99.78	99.39	99.23	100.11
11	8	10	10	10	10	10	10	11	8	8
226	219	213	196	217	220	218	218	169	210	196
18	16	15	17	16	16	14	16	20	17	16
520	507	527	407	509	497	541	533	390	494	532
2	0	3	0	2	1	0	2	2	1	3
101	97	98	106	98	97	94	94	99	91	87
12	10	11	11	13	13	12	13	13	11	12
14	10	13	14	15	12	14	17	15	13	13
23	23	24	23	24	23	24	19	17	19	20
21	31	22	23	27	34	34	36	26	10	13
7	7	7	6	9	8	7	7	8	6	5
99	93	87	88	101	95	102	88	75	90	92
0	3	0	0	1	0	1	1	2	0	0
12	20	21	14	19	22	17	20	15	14	15
1536	1464	1441	1436	1408	1483	1476	1531	1253	1536	1700
60	58	52	60	57	60	61	54	48	51	56

The Geochemistry of the Ben Nevis Complex

83BN15	83BN16	BN362/1	BN194	BN322	BN323	BN324	0BN351	BN427	BN412	0BN46
IG	IG	IG	IG	IG	IG	IG	SLIVER	SLIVER	GRANITE SILL	DYKE
69.61	70.39	70.09	67.21	67.91	66.67	68.19	61.33	62.74	74.76	56.23
0.39	0.41	0.40	0.51	0.46	0.47	0.50	0.78	0.66	0.22	0.96
15.29	15.41	15.52	15.43	15.27	15.35	14.87	16.57	16.15	13.15	16.24
2.22	2.17	2.12	3.19	3.01	3.21	3.06	4.95	4.51	1.29	6.99
0.06	0.05	0.03	0.06	0.06	0.07	0.05	0.07	0.07	0.02	0.10
0.87	0.73	0.61	1.47	1.35	1.48	1.65	3.15	2.49	0.36	6.00
1.19	1.49	1.25	1.39	2.71	2.70	1.94	3.22	3.96	0.72	5.81
4.70	4.55	4.96	4.55	5.61	5.70	4.15	4.69	4.37	3.29	4.00
3.86	3.90	3.92	3.62	3.34	3.26	4.35	2.98	3.06	5.39	2.31
0.13	0.13	0.11	0.18	0.18	0.19	0.14	0.28	0.23	0.03	0.27
2.33	2.98	2.90	0.76	2.35	1.78	3.01	0.31	1.23	4.96	0.73
99.72	100.02	99.92	100.29	100.71	100.39	100.10	100.41	99.84	99.63	100.22
8	7	11	7	6	6	11	4	7	19	2
211	213	262	172	83	91	172	101	138	94	145
16	15	18	15	11	8	14	12	13	18	18
462	493	450	671	775	828	635	964	991	148	810
3	1	2	2	1	2	4	2	0	18	0
93	85	92	85	78	74	121	72	62	207	63
13	12	13	11	8	10	21	8	7	29	5
17	14	19	12	11	11	20	13	16	33	14
18	19	18	19	25	25	18	20	22	17	20
51	14	29	11	28	29	38	46	59	17	58
5	5	6	13	22	23	29	29	34	11	57
95	100	107	77	44	35	62	54	54	47	51
0	1	3	1	5	5	3	7	9	2	20
18	18	18	42	47	42	45	84	84	13	132
1433	1686	1477	1598	1242	1226	1103	1163	1418	338	943
56	58	64	46	35	27	41	32	33	30	28

The Geochemistry of the Ben Nevis Complex

BN118C	BN188/5	BN323D	BN365	BN383	BN401	BN381	BN391	BN400	BN170	BN405b
DYKE	DYKE	DYKE	DYKE	DYKE	DYKE	FELSITE	APPINITE	APPINITE	APPINITE	APPINITE
62.53	64.65	62.15	64.66	63.89	65.48	75.92	54.18	51.77	59.40	57.38
0.66	0.54	0.67	0.52	0.63	0.58	0.13	0.77	0.82	0.75	0.98
16.59	15.82	16.31	15.53	15.46	15.40	15.10	16.32	15.40	7.88	20.82
5.54	4.98	4.60	4.18	4.06	3.88	0.55	8.34	9.11	9.61	7.67
0.04	0.03	0.08	0.06	0.07	0.06	0.03	0.12	0.14	0.21	0.09
2.59	1.96	2.71	2.17	2.50	2.02	0.12	4.37	6.29	10.18	1.85
3.83	2.56	4.05	2.83	2.81	2.83	0.32	6.49	7.95	8.53	1.06
4.92	4.15	5.97	4.35	4.54	4.16	4.64	4.24	3.02	1.48	2.15
2.66	3.33	2.79	3.47	4.32	3.85	3.77	3.41	2.98	1.21	4.47
0.29	0.22	0.27	0.18	0.22	0.18	0.02	0.41	0.33	0.78	0.15
1.86	1.93	1.50	1.90	1.90	1.97	4.84	2.18	0.53	0.02	1.11
100.16	99.42	100.62	99.34	100.70	100.14	99.51	99.47	99.93	100.44	99.83
1	5	4	8	11	11	13	6	2	10	23
117	138	130	145	210	202	63	179	76	53	264
8	9	11	12	14	15	11	21	16	32	72
1072	892	1087	755	761	822	23	1255	876	294	230
0	2	0	2	4	4	2	1	1	4	6
53	109	66	96	122	97	92	79	76	30	195
4	8	2	12	16	16	12	6	2	10	30
4	15	9	12	19	17	27	18	11	2	49
21	19	24	23	21	20	17	20	17	14	37
13	44	59	46	50	54	27	71	104	83	126
29	25	48	38	49	41	4	20	41	157	28
40	49	49	48	74	69	12	77	22	126	155
7	5	10	8	7	6	2	19	29	39	15
83	64	177	67	73	61	0	193	254	199	82
1313	1337	1455	1127	1115	1167	263	1182	867	516	934
25	24	34	34	42	42	6	46	16	61	79

The Geochemistry of the Ben Nevis Complex

BN431	TOWER	BN20	BN206	BN211	BN212	BN222	BN234B	BN245	BN247	BN263
MISC	VP AND									
64.03	64.45	64.00	68.99	64.91	63.78	63.65	65.36	61.66	62.89	67.00
0.53	0.62	0.56	0.44	0.51	0.71	0.60	0.52	0.65	0.88	0.52
16.79	15.96	15.65	15.44	16.32	16.48	16.70	15.80	11.29	16.89	16.18
4.32	4.44	3.97	2.32	3.69	4.19	4.28	3.62	4.50	6.49	3.57
0.05	0.05	0.05	0.05	0.07	0.07	0.06	0.07	0.07	0.10	0.34
1.94	2.23	2.30	0.82	1.98	1.64	2.35	2.26	3.12	2.95	1.77
3.26	3.43	3.48	1.68	3.24	3.31	3.95	3.21	4.32	1.01	3.06
4.61	4.46	4.19	4.51	3.83	4.82	3.87	4.10	3.93	0.99	3.64
2.87	2.93	2.84	3.90	3.21	3.06	3.09	3.15	3.69	4.38	3.19
0.17	0.19	0.20	0.14	0.21	0.27	0.23	0.18	0.31	0.14	0.18
1.29	1.34	0.62	2.54	0.70	0.59	2.26	1.48	3.02	1.02	2.66
99.98	100.16	99.26	99.51	100.27	100.53	99.38	99.76	99.94	99.94	99.80
4	7	3	8	5	6	4	4	5	14	5
126	159	124	252	184	190	132	94	149	208	114
10	12	8	17	13	14	10	7	8	33	9
952	924	890	545	932	971	1106	961	1399	100	917
1	0	0	2	0	0	1	1	1	2	0
72	63	51	80	51	53	63	53	67	120	80
5	8	6	14	7	7	6	6	9	14	4
12	11	10	20	16	17	72	16	14	11	14
19	20	20	19	21	21	26	23	24	22	24
45	48	27	23	52	58	66	49	61	88	47
18	41	29	7	8	8	35	33	63	56	26
30	53	49	113	77	76	62	50	62	98	51
7	7	5	1	3	3	7	7	8	9	8
71	71	65	24	73	71	66	60	82	106	69
1593	1306	1549	1594	1553	1528	1392	1411	1596	651	1407
25	35	27	66	41	41	29	30	37	51	31

The Geochemistry of the Ben Nevis Complex

BN267 VP AND	BN269 VP AND	BN277/1 VP AND	BN281 VP AND	BN296A VP AND	BN300 VP AND	BN307 VP AND	BN362/9 VP AND	83BN1 VP AND	83BN2 VP AND	83BN3 VP AND
63.55	64.51	64.40	64.16	64.79	60.69	64.41	64.82	69.31	68.19	66.27
0.59	0.60	0.52	0.62	0.55	0.71	0.60	0.58	0.42	0.44	0.55
16.04	16.24	16.13	16.71	16.31	16.52	16.26	16.61	15.41	15.62	15.89
4.26	3.95	4.07	4.36	3.75	5.49	4.01	4.38	2.32	2.66	3.64
0.07	0.10	0.06	0.05	0.07	0.09	0.05	0.09	0.06	0.06	0.06
2.47	3.05	2.05	2.63	1.42	3.35	1.72	2.25	0.80	1.01	1.92
2.77	3.98	3.55	3.26	3.25	4.86	3.48	3.15	1.59	2.10	3.54
5.11	3.64	4.44	3.74	4.48	3.53	4.69	4.27	4.58	4.49	4.43
2.89	2.53	2.96	2.60	3.70	3.10	2.85	2.47	4.20	3.81	3.29
0.23	0.18	0.17	0.21	0.24	0.31	0.19	0.21	0.13	0.13	0.18
1.27	0.54	1.60	0.39	2.56	1.68	1.46	1.46	2.85	2.60	1.91
99.37	100.59	99.54	100.34	99.46	99.76	99.46	99.63	100.04	99.59	100.97
3	8	3	8	7	7	5	7	8	8	5
119	181	91	175	141	137	113	165	256	256	150
10	14	8	16	12	12	9	11	18	18	10
646	910	1370	986	1195	1551	944	1045	564	643	925
1	1	0	1	1	0	1	0	2	0	0
50	89	54	79	70	60	52	63	51	68	72
5	8	5	6	8	6	6	7	16	15	7
12	14	12	5	15	11	21	17	26	13	37
19	27	24	26	25	25	25	21	19	21	22
46	97	57	24	53	86	57	73	35	43	65
26	35	28	45	22	52	27	36	7	7	28
56	79	47	77	73	66	47	45	117	114	61
5	9	9	8	7	13	7	8	3	0	5
74	94	69	67	66	98	82	83	15	20	58
1255	1158	1307	971	1422	1611	1358	2022	1627	1605	1364
28	41	31	51	42	41	27	32	68	64	32

The Geochemistry of the Ben Nevis Complex

83BN4	83BN5	83BN6	83BN7	83BN8	83BN10	83BN11	BN362/10	BN279MAIN	BN279PIPE	CL
VP AND	VP MISC	VP MISC	VP MISC	VP MISC						
62.42	65.81	63.02	65.30	60.07	66.61	65.04	63.49	61.64	61.50	73.44
0.58	0.58	0.67	0.54	0.77	0.42	0.52	0.74	0.74	0.74	0.27
15.62	16.28	16.82	16.20	16.41	16.00	16.16	16.78	15.78	15.99	14.12
4.30	4.03	4.37	3.81	5.51	2.94	3.82	4.28	5.29	5.36	1.24
0.07	0.06	0.08	0.06	0.10	0.05	0.05	0.06	0.08	0.09	0.03
2.61	1.96	1.72	1.91	3.18	1.38	1.95	1.43	2.74	4.14	0.30
3.39	3.74	4.25	3.67	4.56	3.15	3.33	2.96	4.72	4.89	0.48
4.46	4.61	3.91	4.55	4.86	4.09	4.05	4.79	4.39	3.77	4.53
2.93	3.01	3.53	3.09	3.26	3.28	2.91	3.50	2.48	2.22	5.02
0.22	0.21	0.20	0.18	0.33	0.14	0.21	0.27	0.27	0.27	0.04
0.31	2.39	2.34	2.11	1.94	2.12	1.50	2.41	0.83	0.35	4.59
99.00	100.70	99.56	100.11	100.04	99.08	99.24	99.12	99.51	100.57	99.86
5	5	2	2	6	1	3	10	8	8	11
187	132	115	117	156	87	106	276	161	166	154
12	10	9	8	13	7	8	17	13	15	16
953	1003	937	892	1344	1161	909	882	951	970	163
1	0	1	1	2	1	0	2	0	2	2
72	59	52	55	48	61	62	62	43	66	71
7	7	4	7	7	3	5	11	6	9	12
1	14	18	14	18	11	16	19	14	12	54
20	21	20	20	23	20	34	25	25	25	17
47	48	43	46	77	35	52	60	53	78	16
36	34	17	22	51	12	23	6	106	106	5
64	52	42	51	75	31	44	84	67	66	62
8	6	7	6	10	5	6	6	13	15	1
69	73	75	52	85	37	65	71	94	102	4
1273	1426	1471	1486	1415	1725	1337	1380	1213	980	1133
38	31	28	27	41	20	26	52	39	35	37

320

The Geochemistry of the Ben Nevis Complex

INT	BN259	BN197	BN200s	BN200S	BN215	BN256	BN277/br	BN292	BN299B	83BN12
VP MISC	VP MISC	VP MISC	VP MISC							
69.26	67.32	57.10	66.08	65.40	66.94	68.01	64.68	69.29	61.27	65.99
0.42	0.49	0.74	0.48	0.58	0.64	0.49	0.59	0.40	0.60	0.55
15.55	16.22	18.58	15.82	15.80	16.51	15.17	16.10	15.10	16.84	15.79
2.42	3.14	5.98	3.69	3.67	4.32	3.26	4.14	2.27	4.64	3.87
0.06	0.06	0.08	0.07	0.08	0.06	0.06	0.06	0.05	0.13	0.05
0.75	1.09	5.93	2.21	2.27	2.90	1.61	2.16	0.86	2.66	1.66
1.75	0.94	3.99	3.56	2.90	2.11	2.20	3.73	1.34	4.64	3.05
4.32	5.27	1.55	4.07	4.06	1.94	4.12	3.94	4.09	3.86	4.15
4.31	3.58	4.17	2.94	3.38	3.39	3.78	3.43	4.62	3.64	3.14
0.10	0.16	0.11	0.16	0.21	0.15	0.16	0.21	0.11	0.22	0.21
3.15	2.21	2.35	1.58	1.78	1.74	2.64	1.83	2.91	2.02	1.51
100.00	99.48	99.94	100.28	99.74	100.46	99.84	100.43	99.73	99.90	99.88
10	9	15	10	10	14	10	5	10	10	6
268	226	201	155	155	198	178	139	252	159	157
17	12	30	13	13	28	17	10	18	12	13
604	544	218	928	928	344	792	941	548	1114	894
2	3	2	2	2	3	1	1	1	0	1
61	83	157	85	85	117	82	51	84	68	71
14	11	13	9	9	12	9	7	13	8	11
36	14	22	11	11	14	17	15	24	11	13
18	19	30	23	23	23	42	25	23	25	22
51	48	99	60	60	73	45	84	36	100	49
7	8	49	22	22	37	15	36	9	22	27
102	82	65	65	65	80	78	62	0	64	66
2	2	14	6	6	10	3	7	119	10	5
21	44	112	55	55	74	41	69	17	63	63
1521	1184	1240	1601	1601	700	1353	1312	1396	1988	1334
61	53	41	41	41	46	48	39	68	42	38

# The Geochemistry of the Ben Nevis Complex

BN288A	BN288B
VP MISC	VP MISC
68.59	67.37
0.45	0.49
14.90	15.35
3.18	3.37
0.04	0.05
0.78	1.61
1.75	2.24
3.66	3.99
4.84	3.91
0.16	0.17
3.38	2.52
99.65	99.77
9	9
129	129
12	12
725	725
5	5
79	79
13	14
23	21
23	24
21	47
26	30
60	66
3	4
42	51
1086	1048
44	40

## Appendix IV

### Analytical Procedures for Radiogenic Isotope Geochemistry

Samples were crushed to much less than 240 mesh size according to the same procedure outlined in Appendix III.

#### **Sr and Nd Chemistry:**

##### Sample Dissolution:

Samples were dissolved in PFA teflon screw-top beakers (Savillex) using 10mls 40% HF and 1ml 14M HNO<sub>3</sub> on a hotplate overnight. The beakers were removed, cooled, and then the solution was dried down under lamps. The residue was then dissolved in 3 mls 14M HNO<sub>3</sub> overnight on a hotplate, and dried down as before. The residue was now dissolved in 8 mls 6M HCl overnight on a hotplate. After cooling, a weighed aliquot of about 1/3 the volume of the solution was taken, to which was added weighed quantities of <sup>145</sup>Nd and <sup>149</sup>Sm spikes for isotope dilution determination of Sm and Nd concentrations. The remaining 2/3 aliquot was used for the determination of the isotopic composition of both Sr and Nd. Both solutions (spiked and unspiked) were dried down and the final residues each taken up in 2 mls 2.5M HCl.

##### Column chemistry:

Sr and the REE were separated using standard cation exchange chromatography techniques. The sample was transferred to a centrifuge tube and any residue was centrifuged off. The solution was then loaded onto a preconditioned cation exchange column containing 10 mls Bio-Rad AG50W x 8, 200-400 mesh resin. The sample was washed in with 2 \* 1 ml 2.5M HCl. For unspiked samples 46 mls 2.5M HCl were then eluted. The Sr fraction was collected with a further 10 mls 2.5M HCl, and evaporated to dryness. Sr blanks were less than 5ng. For spiked samples the Sr fraction did not need to be collected, and so 56 mls 2.5M HCl were eluted.

The REE were separated by further eluting 20 mls 2.5M HCl and 10 mls 3M HNO<sub>3</sub>. The next 26 mls 3M HNO<sub>3</sub> were collected, and evaporated to dryness.

Sm and Nd were isolated from Ba and the other REE using 3 columns.

Column 1 (initial Ba clean-up): The residue from the REE fraction from the Sr columns was dissolved in 1 ml of a solution of 75% CH<sub>3</sub>COOH - 25% 5M HNO<sub>3</sub> (hereafter called 75/25). This was loaded onto a column containing 8ml of Bio-Rad AG1 x8, 200-400 mesh anion exchange resin which had been preconditioned with 5 mls of a solution of 90% CH<sub>3</sub>COOH - 10% 5M HNO<sub>3</sub> (90/10). The sample was washed in with 2 \* 1 ml 90/10 solution, and then eluted with 50 mls 90/10 solution. The REE's were collected with 15 mls

0.05M HNO<sub>3</sub>, and evaporated to dryness.

Column 2 (Sm and Nd separation): The residue from column 1 was dissolved in 1 ml of "orange cocktail". This cocktail consisted of 75% CH<sub>3</sub>OH - 25% orange cocktail mix: the mix is made of 1336 mls H<sub>2</sub>O - 406 mls CH<sub>3</sub>COOH - 256 mls 5M HNO<sub>3</sub>. The sample was loaded onto a column containing 8 ml of Bio-Rad AG1 x8, 200-400 mesh anion exchange resin which had been preconditioned with 5 mls "orange cocktail". This column was encased in a water jacket through which water kept at 25°C by a thermostatically-controlled water bath was circulated. The sample was washed in with 2 \* 1 ml "orange cocktail", and eluted with 10 mls "orange cocktail". For spiked samples the next 17 mls "orange cocktail" were collected which contained the Sm fraction; this was evaporated to dryness. A further 12 mls "orange cocktail" were then eluted. For unspiked samples 29 mls "orange cocktail" were eluted. The next 29 mls "orange cocktail" containing the Nd fraction were then collected, and the solution evaporated to dryness.

Column 3 (final Ba clean-up): The residue from the Nd fraction from column 2 (both spiked and unspiked) was dissolved in 1 ml 75/25 solution, and loaded onto a column containing 5 ml of Bio-Rad AG1 x8, 200-400 mesh anion exchange resin which had been preconditioned with 3 mls 90/10 solution. The sample was washed in with 2 \* 1 ml of 90/10 solution and eluted with 15 mls 90/10 solution. The Nd was collected with 10 mls 0.05M HNO<sub>3</sub>, and evaporated to dryness.

Sm and Nd blanks were less than 0.2ng.

## Mass Spectrometry

### Sr

Sr samples were run on a single collector VG 54E thermal ionisation mass spectrometer. Sr samples were dissolved in 1ml 1M H<sub>3</sub>PO<sub>4</sub> and were loaded onto a single outgassed Ta filament. A small current is passed through the filament to dry the sample which is then increased slowly until the H<sub>3</sub>PO<sub>4</sub> fumes off and the filament glows dull red. Sr beams were managed to give an intensity of 1.5 pA <sup>86</sup>Sr. Peak intensities were corrected for zero, dynamic memory and Rb interference (if necessary). The <sup>87</sup>Sr/<sup>86</sup>Sr ratio was corrected for mass fractionation using <sup>86</sup>Sr/<sup>88</sup>Sr = 0.1194. Repeat analysis of NBS 987 Sr standard gave <sup>87</sup>Sr/<sup>86</sup>Sr = 0.71023 ± 4 (2 s.d.). Decay constant (λ) for <sup>87</sup>Rb = 1.42 \* 10<sup>-11</sup> a<sup>-1</sup>.

### Nd

Nd analyses were performed on a VG Sector 54-30 thermal ionisation mass spectrometer with 8 Faraday collectors. Nd samples were dissolved in water and loaded on the Ta side filaments of an outgassed triple filament assembly with a Re centre filament. The sample was dried very carefully at 0.5A. For Nd isotopic composition runs beams were managed to give a <sup>144</sup>Nd intensity of 10pA with a centre filament current of 4 A. Data were

acquired in multi-dynamic mode (to avoid inter-collector gain calibration uncertainties) using a 5 collector peak jumping routine. The data were collected in 12 blocks of 10 collection routines/block, giving 120 ratios in total. Each collection routine comprised 4 cycles; after each cycle the magnet was switched to place a different isotope into any given collector. The integration time for each cycle within a collection routine was 5 seconds with a 2 second wait time between each cycle to allow the magnet to settle.  $^{143}\text{Nd}/^{144}\text{Nd}$  ratios were corrected for mass fractionation using  $^{146}\text{Nd}/^{144}\text{Nd} = 0.7219$ . Peak intensities were corrected for background and the  $^{144}\text{Nd}$  peak was corrected for Sm interference. During the course of this study the JM Nd standard gave  $^{143}\text{Nd}/^{144}\text{Nd} = 0.511500 \pm 10$  (2 s.d.). Decay constant ( $\lambda$ ) for  $^{147}\text{Sm} = 6.54 * 10^{-12} \text{ a}^{-1}$ .

For Nd isotope dilution runs the  $^{143}\text{Nd}$  beam intensity was 0.5 pA. The analyses were performed in static mode, with 3 blocks of 10 cycles being collected. The integration time for each cycle was 5 seconds. Peak intensities are corrected for zero and Sm interference (where necessary).

### Sm

Sm analyses were also performed on the Sector 54-30 instrument. Loading techniques were the same as those for Nd. Sm beams were managed to give a  $^{149}\text{Sm}$  beam intensity of 0.5 pA. The analyses were performed in static mode, with 3 blocks of 10 cycles being collected. The integration time for each cycle was 5 seconds. Peak intensities are corrected for background.

Measured Sm/Nd ratios are considered to be better than 0.15% (2 s.d.).